AD NUMBER

AD867307

NEW LIMITATION CHANGE

TO

Approved for public release, distribution unlimited

FROM

Distribution authorized to U.S. Gov't. agencies and their contractors; Administrative/Operational Use; Feb 1970. Other requests shall be referred to Air Force Materials Lab., Attn: MAMC, Wright-Patterson AFB, OH 45433.

AUTHORITY

AFML ltr, 29 Mar 1972

AFML-TR-69-84
PART III, VOLUME III

AD 867307

STABILITY CHARACTERIZATION OF REFRACTORY MATERIALS UNDER HIGH VELOCITY ATMOSPHERIC FLIGHT CONDITIONS

PART III, VOLUME III: EXPERMENTAL RESULTS OF HIGH VELOCITY HOT GAS/COLD WALL TESTS

LARRY KAUFMAN

HARVEY NESOR

ManLabs, Inc.

TECHNICAL REPORT AFML-TR-69-84, PART III, VOLUME III

FEBRUARY 1970

This document is subject to special export controls and each transmittal to foreign governments or foreign nationals may be made only with prior approval of the Air Force Materials Laboratory (MAMC), Wright-Patterson Air Force Base, Ohio 45433.

AIR FORCE MATERIALS LABORATORY
AIR FORCE SYSTEMS COMMAND
WRIGHT-PATTERSON AIR FORCE BASE, OHIO

364

NOTICE

When Government drawings, specifications, or other data are r any purpose other than in connection with a definitely related ment procurement operation, the United States Government y incurs no responsibility nor any obligation whatsoever; and the fa.. .at the Government may have formulated, furnished, or in any way supplied the said drawings, specifications, or other data, is not to be regarded by implication or otherwise as in any manner licensing the holder or any other person or corporation, or conveying any rights or permission to manufacture, use, or sell any patented invention that may in any way be related thereto.

This document is subject to special export controls and each transmittal to foreign governments or foreign nationals may be made only with prior approval of the Air Force Materials Laboratory (MAMC), Wright-Patterson Air Force Base, Ohio 45433.

Distribution of this report is limited for the protection of technology related to critical materials restricted by the Export Control Act.

Copies of this report should not be returned unless return is required by security considerations, contractual obligations, or notice on a specific document.

STABILITY CHARACTERIZATION OF REFRACTORY MATERIALS UNDER HIGH VELOCITY ATMOSPHERIC FLIGHT CONDITIONS

PART III, VOLUME III: EXPERMENTAL RESULTS OF HIGH VELOCITY HOT GAS/COLD WALL TESTS

LARRY KAUFMAN

HARVEY NESOR

FOREWORD

This report was prepared by ManLabs, Inc., Cambridge, Mass., with the assistance of Avco/SSD, Wilmington, Mass. (H. Hoercher, Project Director, supported by J. Recesso, R. Abate and R. Broughton) under Project 7312, "Metal Surface Deterioration and Protection," Task 731201, "Metal Surface Protection," and Project 7350, "Refractory Inorganic Nonmetallic Materials," Task Numbers 735001, "Refractory Inorganic Nonmetallic Materials: Nongraphitic," and 735002, "Refractory Inorganic Nonmetallic Materials: Graphitic," under AF33(615)-3859, and was administered by the Metals and Ceramics Division of the Air Force Materials Laboratory (MAMC), with J.D. Latva, J. Krochmal and N.M. Geyer acting as Project Engineers.

This report covers the period from April 1966 to July 1969.

ManLabs' personnel participating in this study included L. Kaufman, H. Nesor, H. Bernstein, J.R. Baron, G. Stepakoff, R. Hopper, R. Yeaton, S. Wallerstein, E. Sybicki, J. Davis, K. Meaney, K. Ross, J. Dudley, E. Offner, A. Macey, A. Silverman and A. Constantino.

The following reports will be issued under this contract.

Part/Volume	
I-I	Summary of Results
II-I	Facilities and Techniques Employed for Characterization of Candidate Materials
II-II	Facilities and Techniques Employed for Cold Gas/Hot Wall Tests
II-III	Facilities and Techniques Employed for Hot Gas/Cold Wall Tests
III-I	Experimental Results of Low Velocity Cold Gas/Hot Wall Tests
III-II	Experimental Results of High Velocity Cold Gas/Hot Wall Tests
III-III	Experimental Results of High Velocity Hot Gas/Cold Wall Tests
IV-I	Theoretical Correlation of Material Performance with Stream Conditions
IV-II	Calculation of the General Surface Reaction Problem

This report was released by the authors in December 1969.

This technical report has been reviewed and is approved.

W.G. RAMKE
Chief, Ceramics and Graphite Branch
Metals and Ceramics Divisions
Air Force Materials Laboratory

ABSTRACT

The oxidation of refractory borides, graphites and JT composites, hypereutectic carbide-graphite composites, refractory metals, coated refractory metals, metal oxide composites, and iridium coated graphites in air over a wide range of conditions was investigated over the spectrum of conditions encountered during reentry or high velocity atmospheric flight, as well as those employed in conventional furnace tests. Elucidation of the relationship between hot gas/cold wall (HG/CW) and cold gas/hot wall (CG/HW) surface effects in terms of heat and mass transfer rates at high temperatures was a principal goal.

Arc plasma exposures have been performed at Mach Numbers between 0.1 and 3.2 stagnation pressures between 0.01 and 1.0 atm., stagnation enthalpies up to 16,000 BTU/lb, cold wall heat flux up to 1200 BTU/ft^{2}sec, exposure times up to 23,400 seconds and surface temperatures between 2100° and 6500°F. Data include material recession, metallographic and X-ray analysis, radiated heat flux and normal total emittance. In addition, color motion picture coverage was provided. Materials forming solid oxides show lower recessions in the HG/CW tests at a stated surface temperature than in CG/HW tests. The reverse is true for ablating materials. Temperature gradients of 800° to 1500°F through 30-50 mil oxides are observed. The practical implications of this finding are substantial (if the gradients exist under free flight conditions). Since the temperature level experienced by the substrate is substantially below that predicted, strength and load carrying capacity of the substrate would be much higher than for the case where gradients are ignored. Long-time cyclic exposures of diboride composites in the Model 500 and ROVERS facilities for trajectories typified by FDL-7MC provide a striking illustration of the reuse capability of boride composites for lifting reentry applications.

A HfB_2+SiC composite was exposed for thirteen cycles at 0.07 atm (1 psi) stagnation pressure, a stagnation enthalpy of 10,200 BTU/lb and a cold wall heat flux of 495 BTU/ft^{2}sec. Each cycle was about 1800 seconds long with a total exposure time of 22,500 seconds at a surface temperature near 5300°R. Total material recession was 15 mils. A ZrB_2+SiC composite was exposed for four cycles at 1.0 atm (15 psi) stagnation pressure, a stagnation enthalpy of 5000 BTU/lb and a cold wall heat flux of 380 BTU/ft^{2}sec. Each cycle was 1800 seconds long, total exposure time was 7200 seconds. The surface temperatures were near 5000°R. Total material recession was 26 mils. Under similar conditions graphite and tungsten would exhibit recessions of 7 to 14 inches.

These results illustrate the reuse capability of boride composites for lifting reentry application, since they exceed the range of conditions for FDL-7MC. This capability is unrivaled by any other materials system.

Surface temperatures calculated from stream conditions and radiation equilibrium agree with observed temperatures on melting. When solid coatings are present, surface temperatures are below computed values. Silicon carbide bearing materials achieve lower temperatures than predicted from stream conditions and exhibit superior behavior.

This abstract is subject to special export controls, and each transmittal to foreign governments or foreign nationals may be made only with prior approval of the Air Force Materials Laboratory (MAMC), Wright-Patterson Air Force Base, Ohio 45433.

TABLE OF CONTENTS

LIST OF ILLUSTRATIONS

Figure		Page

Figure		Page

Figure		Page
111	Arc Plasma Test ZrB_2+SiC+C(A-10)	130
112	Arc Plasma Test ZrB_2+SiC+C(A-10)	130
113	Arc Plasma Test ZrB_2+SiC+C(A-10)	131
114	Arc Plasma Test ZrB_2+SiC+C(A-10)	131
115	Post Exposure Photographs of Arc Plasma Tests RVA(B-5)	132
116	Post Exposure Photographs of Arc Plasma Tests RVA(B-5)	133
117	Post Exposure Photograph of Arc Plasma Test RVA(B-5)	133
118	Arc Plasma Test RVA(B-5)	134
119	Arc Plasma Test RVA(B-5)	134
120	Arc Plasma Test RVA(B-5)	135
121	Arc Plasma Test RVA(B-5)	135
122	Post Exposure Photographs of Arc Plasma Tests PG(B-6)	136
123	Post Exposure Photographs of Arc Plasma Tests PG(B-6)	136
124	Post Exposure Photographs of Arc Plasma Tests PG(B-6)	137
125	Post Exposure Photographs of Arc Plasma Tests PG(B-6)	137
126	Arc Plasma Test PG(B-6)	138
127	Arc Plasma Test PG(B-6)	138
128	Arc Plasma Test PG(B-6)	139
129	Arc Plasma Test PG(B-6)	139
130	Post Exposure Photographs of Arc Plasma Tests BPG(B-7)	140
131	Post Exposure Photographs of Arc Plasma Tests BPG(B-7)	140
132	Post Exposure Photographs of Arc Plasma Tests BPG(B-7)	141
133	Post Exposure Photographs of Arc Plasma Tests BPG(B-7)	141
134	Arc Plasma Test BPG(B-7)	142
135	Arc Plasma Test BPG(B-7)	142

Figure		Page

Figure		Page

Figure		Page

Figure		Page

Figure		Page
230	Post Exposure Photographs of 5Mil WSi_2 Coated W, WSi_2/W(G-18)-1M, 2M, 3M, 4M, 5M, 11M, 12M, 13M, 14M, 9R and 10R	196
231	Post Exposure Photographs of 5 Mil WSi_2 Coated W, WSi_2/W(G-18)-6R, 7R and 8R	197
232	Post Exposure Photographs of 5M WSi_2 Coated W, WSi_2/W(G-18)-17M, 18M, 19M, 20M, 21M, 22M, 23R and 24R	197
233	Post Exposure Photographs of Tungsten and Molybdenum Samples Employed in Temperature Calibration Tests in the Model 500(M) and ROVERS (R) Facilities	198
234	Arc Plasma Test WSi_2/+(G-18)-4M	199
235	Arc Plasma Test WSi_2/W(G-18)-4M, Interface Showing W_5Si_3 Zone	199
236a	Arc Plasma Test WSi_2/W(G-18)-6R	200
236b	Arc Plasma Test WSi_2/W(G-18)-6R, Interface Showing W_5Si_3 Zone	200
237	Growth of W_5Si_3 Zone on WSi_2/W(G-18) as a Function of Flow Rate and Pressure	201
238	Post Exposure Photographs of 8 Mil Sn-Al-Mo Coated Ta-10W, Sn-Al/Ta-10W(G-19)-1M, 2M, 3M, 4M, 5M, 6R, 7R, 8R, 9R, 10R, 11R and 12R	202
239	Arc Plasma Test Sn-Al/Ta-W(G-19)-4M	203
240	Sn-Al/Ta-W(G-19)-4M, Interface of Sn-Al Coating (Top) and Ta-W Matrix	203
241	Arc Plasma Test Sn-Al/Ta-W(G-19)-1M	204
242	Arc Plasma Test Sn-Al/Ta-W(G-19)-1M, Interface of Melted Region and Matrix	204
243	Arc Plasma Test Sn-Al/Ta-W(G-19)-9R	205
244	Arc Plasma Test Sn-Al/Ta-W(G-19)-9R, Interface of Coating (Right) and Matrix	205
245	Sn-Al/Ta-W(G-19)-8R	206
246	Arc Plasma Test Sn-Al/Ta-W(G-19)-8R, Interface of Melted Ta-W(Right) and Matrix	206

Figure		Page

Figure		Page

Figure		Page

Figure		Page
337	Model KT-SiC(E-14)-1-8, Run #1, Sting #2	270
338	Model KT-SiC(E-14)-3-18, Run #1, Sting #3	271
339	Model Hf-20Ta-2Mo(I-23)-4-19, Run #1, Sting #4 . . .	272
340	Model W (Uncoated) (G-18)-X-11, Run #1, Sting #5 . .	273
341	a) Model RVA(B-5)-X-5, Run #1, Sting #6, b&c) Model JTA(D-13)-X-7, Run #1, Sting #7	274
342	Model Hf-20Ta-2Mo(I-23)-1-12, Run #2, Sting #1 . . .	275
343	Model $HfB_{2.1}$(A-2)-X-1, Run #2, Sting #2	276
344	Model HfB_2+SiC(A-4)-X-4, Run #2, Sting #3	277
345	Model PG(B-6)-X-6, Run #2, Sting #4, Model BPG(B-7)-X-16, Run #2, Sting #5	278
346	Model JT0981(F-16)-X-10, Run #2, Sting #6	279
347	Model Sn-Al/Ta-W(G-19)-3-22, Run #2, Sting #8 . . .	280
348	Geometrical Definitions for Analysis of Conduction Losses through a Hemispherical Shell	281
349	Temperature Response for Hemispherical Shells of 1020 Steel Exposed under Flux-Conductivity Conditions to Simulated Wave Superheater Tests	281

LIST OF TABLES

I. INTRODUCTION AND SUMMARY

A. Introduction

The response of refractory materials to high temperature oxidizing conditions imposed by furnace heating has been observed to differ markedly from the behavior in arc plasma "reentry simulators." The former evaluations are normally performed for long times at fixed temperatures and slow gas flows with well defined solid/gas-reactant/product chemistry. The latter on the other hand are usually carried out under high velocity gas-flow conditions in which the energy flux rather than the temperature is defined and significant shear forces can be encountered. Consequently, the differences in philosophy, observables and techniques used in the "material centered" regime and the "environment centered-reentry simulation" area differ so significantly as to render correlation of material responses at high and low speeds difficult if not impossible in many cases. Under these circumstances, expeditious utilization of the vast background of information available in either area for optimum matching of existing material systems with specific missions or prediction and synthesis of advanced material systems to meet requirements of projected missions is sharply curtailed.

In order to progress toward the elimination of this gap, an integrated study of the response of refractory materials to oxidation in air over a wide range of time, gas velocity, temperature and pressure has been designed and implemented. This interdisciplinary study spans the heat flux and boundary-layer-shear spectrum of conditions encountered during high velocity atmospheric flight as well as conditions normally employed in conventional materials centered investigations. In this context, significant efforts have been directed toward elucidating the relationship between hot gas/cold wall (HG/CW) and cold gas/hot wall (CG/HW) surface effects in terms of heat and mass transfer rates at high temperatures, so that full utilization of both types of experimental data can be made. The elucidation of mass transfer reactions has been studied in regimes where gaseous and solid oxide formation occurs.

The principal goal of this study is the coupling of the material-centered and environment-centered philosophies in order to gain a better insight into systems behavior under high-speed atmospheric flight conditions. This coupling function has been provided by an interdisciplinary panel composed of scientists representing the component philosophies. The coupling framework consists of an intimate mixture of theoretical and experimental studies specifically designed to overlap temperature/energy and pressure/velocity conditions. This overlap has provided a means for the evaluation of test techniques and the performance of specific materials systems under a wide range of flight conditions. In addition, it provides a base for developing an integrated theory of modus operandi capable of translating

reentry systems requirements such as velocity, altitude, configuration and life time into requisite materials properties as vaporization rates, oxidation kinetics, density, etc., over a wide range of conditions.

The correlation of heat flux, stagnation enthalpy, Mach No., stagnation pressure and specimen geometry with surface temperature through the utilization of thermodynamic, thermal and radiational properties of the material and environmental systems used in this study was of prime importance in defining the conditions for overlap between materials-centered and environment-centered tests.

Significant practical as well as fundamental progress along the above mentioned lines necessitated evaluation of refractory material systems which exhibit varying gradations of stability above 2700°F. Emphasis was placed on candidates for 3400° to 6000°F exploitation. Thus, borides, carbides, boride-graphite composites (JTA), JT composites, carbide-graphite composites, pyrolytic and bulk graphite, PT graphite, coated refractory metals/alloys, oxide-metal composites, oxidation resistant refractory metal alloys and iridium-coated graphites were considered (See Table 1). Similarly, a range of test facilities and techniques including oxygen pickup measurements, cold sample/hot gas and hot sample/cold gas devices at low velocities, as well as different arc plasma facilities capable of covering the 50-2500 BTU/ft^2sec flux range under conditions equivalent to speeds up to Mach 12 at altitudes up to 200,000 ft were employed. Stagnation pressures between 0.001 and 10 atmsopheres were covered. Splash and pipe tests were performed in order to evaluate the effects of aerodynamic shear. Based on the present results, this range of heat flux and stagnation enthalpy produced surface temperatures between 2000° and 6500°F.

B. Summary

The present report is one of a series (1 - 6)* and describes the results of Hot Gas/Cold Wall exposures performed at Avco/SSD and at the Wave Superheater Arc Tunnel of Cornell Aeronautical Laboratory. The testing at Avco/SSD was performed under the direction of H. Hoercher. J. Recesso, R. Broughton and R. Abate were actively engaged in performing these tests. Exposures were carried out in the Model 500, ROVERS and Ten Megawatt Arc Facilities. The range of conditions employed in these tests covered stagnation pressures between 0.002 and 4.0 atm., stagnation enthalpy between 2000 and 16,000 BTU/lb, cold wall heat flux between 100 and 1500 BTU/ft^2sec and exposure times between 20 seconds and 23,000 seconds. A full spectrum of diagnostic measurements including surface temperature and radiated heat flux was continuously monitored during the exposures. Complete color film coverage were reported for selected models. A complete description of the techniques employed in these tests has been presented (3).

---

*Underscored numbers in parentheses indicate references given at the end of this report.

Testing in the Cornell Wave Superheater was performed under the direction of S. Tate, D. Colosimo and K. Graves. The Wave Superheater offers the possibility of exposing samples at very high velocity for short times. The heat flux levels can be varied by changing the position of the specimen relative to the nozzle. In this manner variable heat flux/temperature levels can be attained. Multiple-sample runs can be made using samples in the size range programmed. CAL furnished data on gas enthalpy, heat flux, surface temperature, stagnation pressure as well as colored motion pictures of the test samples. A complete description of testing methods has been presented (3). All test samples were returned to ManLabs for post-mortem metallography conducted under the direction of H. Nesor.

Current results for boride-base materials indicate substantially lower recession rates in the HG/CW arc plasma tests than in the CG/HW furnace tests. This difference is most striking for $HfB_{2.1}$ (A-2) and ZrB_2(A-3) where an order of magnitude difference is observed at surface temperatures of 4000°F. This difference is reduced by the addition of SiC to the boride. Thus, the HG/CW and CG/HW results for HfB_2 + SiC(A-4) and (A-7) agree more closely than do the corresponding data for the pure diborides. Results of "in-depth" temperature measurements during arc plasma tests indicate that these differences are principally due to temperature gradients through the oxide. Direct measurements indicate that temperature gradients of 1500°F can exist through a 100 mil wall thickness of boride plus oxide.

Gradients have also been observed for $HfB_{2.1}$(A-2) and ZrB_2(A-3) in the high velocity CG/HW tests (5). In these tests the temperature of the CG/HW interface is lower than that of the substrate. Moreover, the rate of oxidation observed in these high velocity CG/HW tests agreed with results of CG/HW furnace tests (in which virtually no gradients exist) run at temperatures corresponding to the surface temperatures observed in the high velocity CG/HW tests. In the HG/CW arc plasma tests, however, the temperature is highest at the HG/CW interface. The rate of oxidation observed in the arc plasma tests at a stated HG/CW surface temperature is much less than that observed in furnace tests at the same surface temperature. Moreover, the gradients appear to exist for long periods of time. These findings are in general agreement with the deductions based on post-mortem metallography and comparison of arc plasma and furnace oxidation tests. The figure shown below offers a schematic representation of the behavior of oxide forming refractory materials in the CG/HW and HG/CW tests.

The central figure represents the oxide and matrix of a solid oxide forming material (i.e., $HfB_{2.1}$(A-2), ZrB_2(A-3) or Hf-20Ta-2Mo(I-23) in a CG/HW furnace test at 3900°R. The temperature distribution across the oxide and matrix zones is assumed to be constant. In the figure at the right, which represents the temperature gradients through a high velocity CG/HW sample (inductively heated), the temperature is lowest at the CG/HW surface. Conversely, in the figure at the left representing a HG/CW arc plasma test sample, the temperature is highest at the HG/CW surface. These schematic figures suggest, that if the observed recession is limited by the minimum temperature in the oxide (where diffusion rates

of oxygen and components of the substrate would be slowest) the present HG/CW and high velocity CG/HW results could be brought into line with the CG/HW furnace results where temperature gradients are largely absent.

SCHEMATIC REPRESENTATION OF

MINIMUM OXIDE TEMPERATURE LIMIT CRITERION

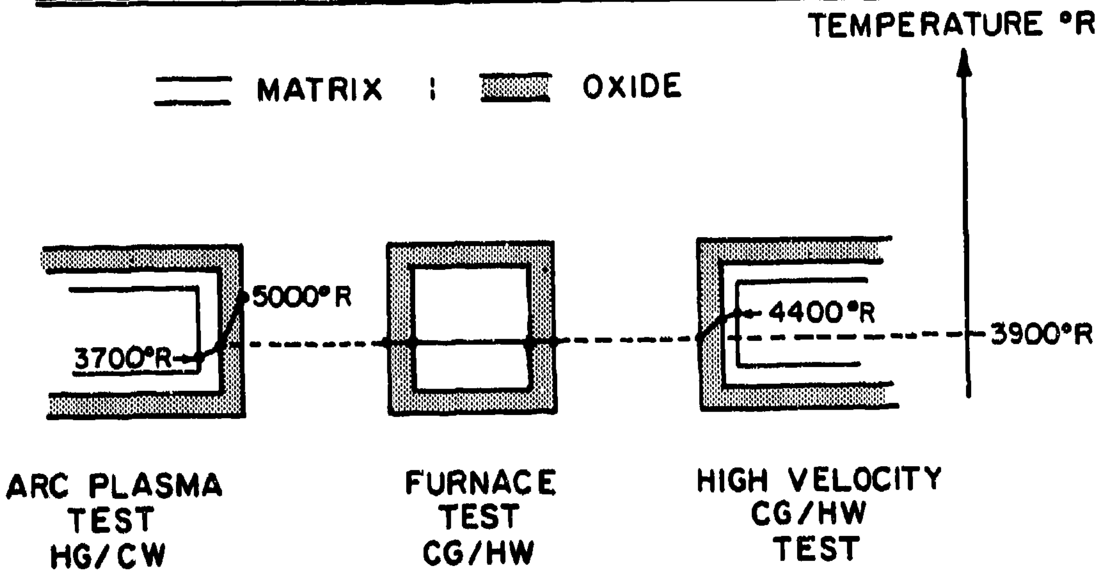

The practical implications of this finding are quite substantial since if thin layers of these solid oxides can result in such large gradients (and if the gradients exist under free flight conditions), the temperature level experienced by the substrate is substantially below the temperature at the HG/CW surface. Under such circumstances, the predicted strength and load carrying capacity of the substrate would be much higher than for the case where gradients are ignored.

As a direct illustration of the implications of these findings a number of long-time cyclic exposures of diboride composites have been performed in the Model 500 and ROVERS facilities to evaluate reuse capabilities for trajectories typified by FDL-7MC which is shown in the figure below. The results provide a striking illustration of the reuse capability of these materials for lifting reentry applications.

Sample $HfB_{2.1}$ + 20%SiC(A-7)-28R was exposed for thirteen cycles at 0.07 atm (1 psi) stagnation pressure, a stagnation enthalpy of 10,200 BTU/lb and a cold wall heat flux of 495 BTU/ft^{2}sec. Each cycle

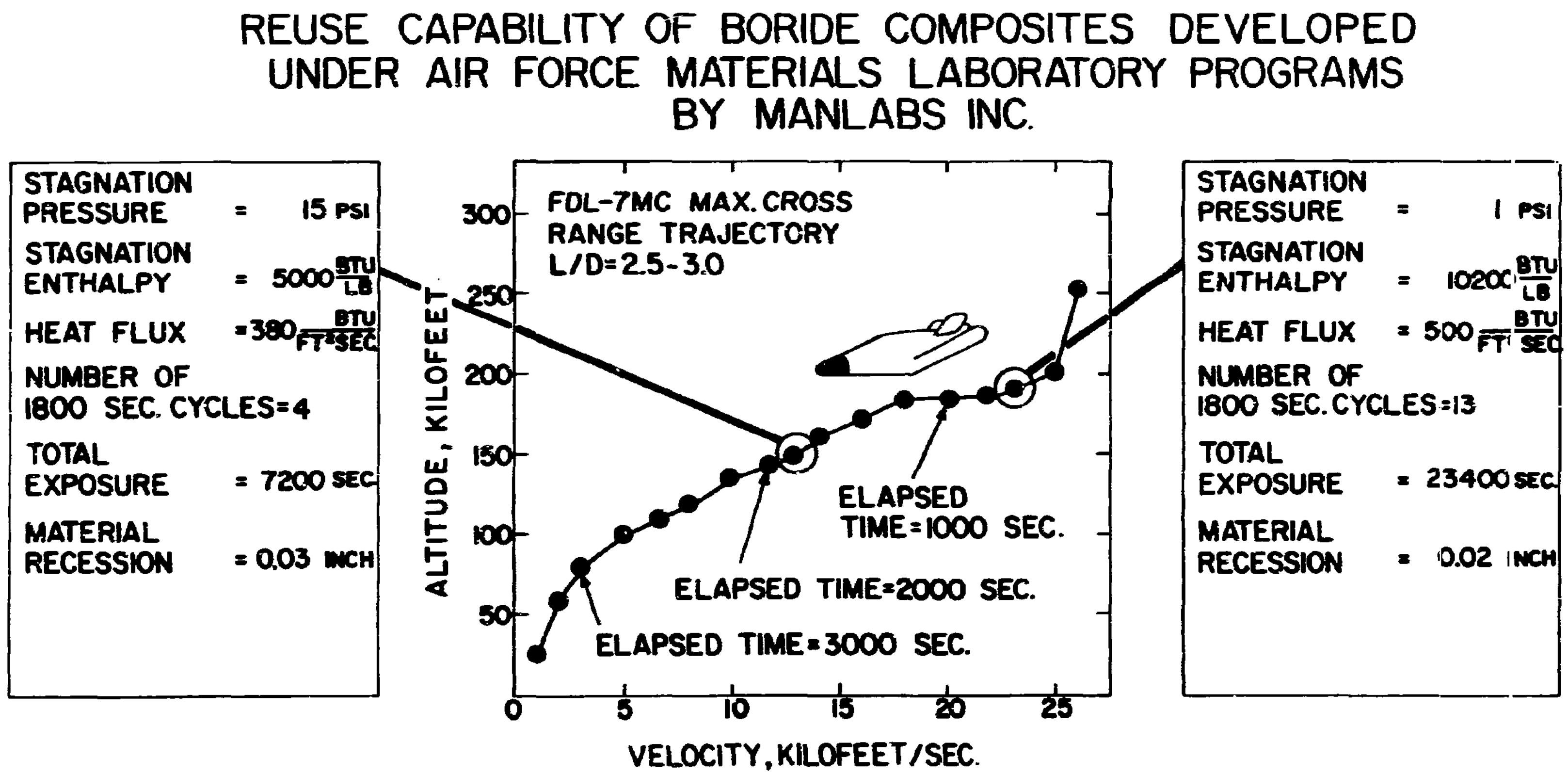

SCHEMATIC REPRESENTATION OF REUSE CAPABILITIES OF BORIDE COMPOSITES

was about 1800 seconds long with a total exposure time of 22,500 seconds. The surface temperature increased from one cycle to the next starting at 3500°R and holding near 5300°R for cycles 5 through 13. Total material recession was 15 mils after this extremely long exposure. Sample $ZrB_{2.1}$ + 20%SiC(A-8)-15M was exposed for four cycles at 1.0 atm (15 psi) stagnation pressure, a stagnation enthalpy of 5000 BTU/lb and a cold wall heat flux of 380 BTU/ft^{2}sec. Each cycle was 1800 seconds long, total exposure time was 7200 seconds. The surface temperatures were near 5000°R. Total material recession was 26 mils. Finally, sample ZrB_2+SiC+C (A-10)-26R (which is not illustrated on the accompanying figure) was exposed at 0.236 atmospheres (3 psi) stagnation pressure, a stagnation enthalpy of 7700 BTU/lb and a cold wall heat flux of 455 BTU/ft^{2}sec. This test covered eleven cycles of approximately 1800 seconds duration for a total exposure time of 18,900 seconds. Surface temperature held near 5100°R after the first cycle. Total material recession was 83 mils.

These results illustrate the reuse capability of boride composites for lifting reentry application, since their range of applicability exceeds the range of conditions and flight times of the FDL-7MC trajectory shown above. This capability is unrivaled by any other materials system.

The candidate ZrB_2(A-3) material did not exhibit any thermal stress failures at flux levels as high as 950 BTU/ft^{2}sec. However, Boride Z(A-5) exhibited thermal shock cracks after exposure at flux levels above 200-250 BTU/ft^{2}sec.

Boride composites HfB_2+20%SiC(A-4) and (A-7), and ZrB_2+ 20%SiC(A-8) were found to exhibit remarkable oxidation and thermal stress resistance in HG/CW arc plasma tests. Although these materials display temperature gradients in the oxides, the difference between the arc plasma and furnace oxidation depths are small. The adherent oxide which forms on these composites results in low recessions observed after exposures in the 3500°-4500°F temperature range. In addition, (A-4) exhibited no thermal shock failures at flux levels up to 1000 BTU/ft^{2}sec. Radiation equilibrium calculations performed for exposures of these materials showed that the ratio T(CALC)/T(OBS) for (A-2), (A-3) and (A-4) exceeds unity thus the observed temperature was 16% lower than expected for (A-2), 9% lower than expected for (A-3) and 22% lower than expected (based on radiation equilibrium) for (A-4). Similarly, the other boride composites containing SiC, i.e., HfB_2+20%SiC(A-7), ZrB_2+20%SiC(A-8) and HfB_2+ 35%SiC(A-9) yielded ratios of 1.25, 1.34 and 1.17. Moreover, exposure of hemispherical models exhibited lower surface temperatures than those observed for flat faced cylinders.

Examination of HfB_2+SiC(A-7) after 14,030 seconds exposure in eight-1800 second cycles at a stagnation pressure of 1.03 atmospheres a cold wall heat flux of 450 BTU/ft^{2}sec and an enthalpy level of 4180 BTU/lb, showed a total recession of 329 mils or about 0.32 inches. Under similar conditions graphite and tungsten would exhibit recessions of 14 to 28 inches. ZrB_2+20%SiC(A-8) displays all of the same features shown by HfB_2+SiC(A-7) although it is not as refractory as its hafnium base counterpart. However, the decrease in temperature resistance is compensated for by the reduced density and cost. Zirconium diboride is roughly one

half the density and one tenth the price of hafnium diboride. Measurements of the temperature gradients through oxide coatings formed on ZrB_2+SiC (A-8) yielded results which are smaller than exhibited by ZrB_2(A-3). This finding appears to be due to the higher thermal conductivity of the oxide formed on (A-8) (as compared with (A-3)). ZrB_2+SiC(A-8) exhibits the same tendency to develop low temperatures as (A-4) and (A-7). The behavior of HfB_2+35%SiC(A-9) was found to be similar to (A-4) and (A-7). The major difference is that (A-9) is less refractory than (A-4) and (A-7).

Recession rates observed for graphites in HG/CW arc plasma tests are substantially higher than thos observed in CG/HW furnace tests at 1-9 ft/sec in air flow rate. This indicates that the latter are supply limited. The results of high velocity CG/HW tests on graphite at air flow rates near 250 ft/sec approach the results obtained in the arc plasma exposures. Modest temperature gradients were measured through graphite samples during HG/CW tests. Limiting survival conditions for Si/RVC(B-8) determined under HG/CW conditions depart from the behavior in furnace tests and correspond to the failure characteristics observed for silicon carbide in HG/CW tests. In the arc plasma tests, Si/RVC(B-8) exhibits protective oxidation up to surface temperatures near 3800°F, some 700°F above the failure temperature in furnace tests. Graphite-type behavior occurs above this temperature. The recession rates of all of the graphites are inversely proportional to material density.

Hypereutectic carbides HfC+C(C-11) and ZrC+C(C-12) exhibited excellent oxidation resistance at surface temperatures below 5000°F and melted under very high temperature conditions in line with reported melting points. The present results are consistent with the eutectic temperatures but show little dependence on the melting point of the oxides. Current data indicate comparable oxidation rates in the CG/HW and HG/CW tests. No thermal shock failures were noted at flux levels up to 750 BTU/ft^{2}sec. In line with the oxidation behavior noted in furnace tests, the HG/CW arc plasma tests show a "puffy" oxide which forms at the lower temperatures investigated. This oxide has been noted in air oxidation tests performed in furnaces below 3400°F. Rapid oxidation occurs at the back of samples where the surface temperature is lower than at the front face. This is another characteristic of the HfC+C (C-11) oxidation which is in line with the furnace test results (4). The oxidation behavior of samples containing 13.6 w/o C does not appear to differ materially from samples fabricated from the billets which contain 14.0 to 15.6 w/o carbon. The behavior of ZrC+C(C-12) in the HG/CW arc plasma tests was found to be similar to that of HfC+C(C-11).

KT-SiC(E-14) exhibited rapid recession rates at surface temperatures above 3900°F. This is some 400°F above the limit observed in furnace tests and in line with the results obtained for Si/RVC(B-8).

Composites of borides, carbides and graphites including ZrB_2+SiC+C(A-10), JTA(C-ZrB_2-SiC)(D-13), JT0992(C-HfC-SiC)(F-15) and JT0981(C-ZrC-SiC)(F-16) exhibited HG/CW tests results which were comparable to their CG/HW behavior. At elevated temperatures, destruction of the protective oxide coatings leads to graphite-type recession behavior. ZrB_2+SiC+C(A-10) exhibits the best oxidation resistance in this group owing to the fact that is is a boride-base rather than a graphite base composite. It

also shows lower recession rates in the HG/CW tests than in the CG/HW tests as is the case for ZrB_2(A-3). Melting of ZrB_2+SiC+C(A-10) is encountered near 5000°F where substantial differences between low pressure and one atmosphere oxidation rates are observed. Thermal shock failures were not observed at flux levels up to 1010 BTU/ft^2sec. The low density (4.5 gms/cm^3), high strength, low modulus and good machinability exhibited by this composite, when coupled with its oxidation resistance up to 5000°F, offer an exceptional combination of properties.

In general, the behavior of the (A-10) composite is quite similar to that exhibited by (A-4), (A-7) and (A-8). Although (A-10) is not as refractory as (A-4) and (A-7) the lower density, cost, thermal stress resistance and machining characteristics of this composite provide compensating advantages for application in reusable lifting reentry spacecraft.

Extensive precautions were taken in order to insure that temperature measurements of the model surface are accurate. In general, the comparison of observed surface temperatures in HG/CW arc plasma tests with values calculated from stream conditions are in relatively good agreement. Moreover, a number of temperature measurements employing two color pyrometers yielded good results. Additional verification was obtained by measuring the melting points of tungsten and molybdenum in the arc facilities using pure nitrogen streams for comparison with accepted values. The relatively good agreement obtained in these tests should eliminate concern over the accuracy of surface temperature measurements due to interference of the arc with optical observations.

A substantial number of thermal shock failures of JTA(D-13) and JT0981(F-16) have been observed. For JTA(D-13), these failures occurred in random fashion at flux levels above 500 BTU/ft^2sec. The samples which failed by thermal shock were machined from 2-1/2" diameter x 2" long billets of JTA(D-13) in an orientation which corresponded to the hot pressing direction. Thus, the axis of the arc plasma test sample was parallel to that of the hot pressed cylinder. Under these conditions, residual strain present in the billets and in the samples could provide a source of the failures. However, a series of samples oriented with their axes perpendicular to the pressing direction showed no thermal shock failures at flux levels in excess of 500 BTU/ft^2sec. This finding has particular relevance to applications in which JTA(D-13) parts are exposed to severe environmental heat fluxes. JT0992(F-15) did not exhibit sensitivity to thermal shock.

The behavior of these composites is characterized by low recession rates at temperatures between 3000°F and 4000°F, best illustrated in ZrB_2+SiC+C(A-10) and JT0992(F-15) at temperatures up to 4500°F. Above 5000°F, the protection afforded by formation of ZrO_2 (or HfO_2) and SiO_2 is eliminated and oxidation rates which are characteristic of graphite are encountered.

Failure limits for the coated refractory metals WSi_2/W (G-18) and Sn-Al/Ta-10W(G-19) have been established in general agreement with furnace tests. Maximum survival conditions for WSi_2/W(G-18)

are 450 $BTU/ft^2 sec$ and 3100 BTU/lb at P_e = 1 atm. At lower pressures, failure was observed at 458 $BTU/ft^2 sec$ and 11,420 BTU/lb. Coating failure conditions were established for Sn-Al/Ta-10W(G-19) at lower flux and enthalpy levels. Modest temperature gradients were measured through WSi_2/W(G-18) arc plasma test samples.

Current results for W+Zr+Cu(G-20) indicate relatively good resistance to oxidation at 10,000 BTU/lb and 500 $BTU/ft^2 sec$ at 0.100 atm. However, at 1 atmosphere stagnation pressure, very rapid degradation was observed at much lower flux and enthalpy levels. This behavior indicates that the mechanism of degradation is sensitive to pressure in the 0.1-1.0 atmosphere range. The precise nature of the degradation mechanism which is operative is not clear at present. The results obtained for W+Ag (G-21) in the Model 500 tests at stagnation pressures of one atmosphere were comparable to the results for (G-20).

The silica-tungsten composites SiO_2+68.5 w/o W(H-22) and SiO_2+60 w/o W(H-23) exhibited similar recession behavior in the one atmosphere HG/CW arc plasma tests as encountered in the CG/HW furnace tests. At low pressures, higher recession rates were observed due to instability of SiO_2 relative to SiO. At temperatures above 4000°F, extensive flow of this composite was observed, in agreement with the furnace test findings. Samples exposed at one atmosphere showed sting hole cracking.

Arc plasma exposures of Hf-20Ta-2Mo(I-23) exhibited lower oxidation rates than in the CG/HW tests at comparable surface temperatures. In addition, several samples with indicated surface temperatures in excess of the melting point of the alloy did not melt. Current results indicate that gradients of 1500°F can exist through 100 mils of alloy and oxide. This behavior is the basis for the surface temperature in the 4000°-5000°F range which were not accompanied by melting of the alloy.

Hf-Ta-Mo(I-23) was exposed to seven cyclic exposures at a stagnation pressure of 1.05 atmospheres, a stagnation enthalpy of 3300 BTU/lb and a cold wall heat flux of 410 $BTU/ft^2 sec$. The observed surface temperature was 4230°F and a recession of 138 mils was observed after an exposure of 11,600 seconds in cycles of 1800 second duration. This behavior is not quite as good as that exhibited by ZrB_2+20%SiC(A-8) or ZrB_2+SiC+C(A-10) which were exposed under more severe conditions than (I-23)-27M and exhibited less recession. Nevertheless, Hf-20Ta-2Mo (I-23) is metallic and as such offers advantages as regards fabricability and resistance to thermal stress. On the other hand (A-8) and (A-10) possess higher strength and more temperature capability than (I-23). Hf-20Ta-2Mo(I-23) was also exposed to a 4 cycle exposure at a stagnation pressure of 0.132 atm, an enthalpy of 7600 BTU/lb and a cold wall heat flux of 398 $BTU/ft^2 sec$. Total exposure time was 7220 seconds yielding a recession of 55 mils. As indicated above, boride composites exposed to more severe conditions in the ROVERS facility exhibited less recession. However, the behavior of Hf-Ta-Mo(I-23)-38R is outstanding for a metallic structure.

Present results for Ir/C(I-24) are in general agreement with the CG/HW tests, which showed that iridium exhibits very low oxidation rates up to its melting temperature at 4430°F. The temperature of the iridium-carbon eutectic is 4175°F. Samples exposed to higher conditions exhibited melting of the coating and ablation of the graphite. The major drawback of this coating system is the low emittance of the iridium ($\epsilon = 0.30$). However, addition of HfO_2 raised the emittance to values near 0.50 and extended the range of conditions under which the coating can be used. Thus, the pure coating is destroyed at flux levels in excess of 310 BTU/ft^{2}sec. At flux levels below 300 BTU/ft^{2}sec the coating is hardly affected; however, at higher levels, melting followed by rapid ablation occurs. In contrast, when HfO_2 is added to increase the emittance, failure does not occur until the flux level reaches 510 BTU/ft^{2}sec. Thus, although Ir/C(I-24) has excellent temperature capability to temperatures near 4200°F, it has very low resistance to stream conditions. In fact if heat flux/enthalpy characteristics are used as a yardstick, Ir/C(I-24) ranks below Si/RVC(B-8), even though the latter has a temperature limit near 3200°F.

Temperature gradients have been measured through 100 and 400 mil walls of ZrB_2(A-3), $HfB_{2.1}$+20%SiC(A-7), ZrB_2+20%SiC(A-8), ZrB_2+SiC+C(A-10), RVA(B-5), WSi_2/W(G-18) and Hf-20Ta-2Mo(I-23). Calculations of the temperature gradients through the test cylinders described have been presented. These calculations are based on side losses due to radiation and conduction down the length of the model but no heat loss via conduction. In general, relatively good agreement between observed and calculated temperature gradients has been obtained in view of the simple model employed.

Measurements of total normal emittance have been provided for all of the candidate materials based on radiated heat flux observations during HG/CW exposures. Averaged values obtained for solid oxides formed during exposure are higher than normal emittance values observed for melting surfaces. Comparison of calculated surface temperatures based on stream conditions with those observed yields relatively good results. However, systematic differences worthy of note have been observed. Calculated temperatures are quite close to those observed when melting occurs, but when solid coatings are present, actual temperatures are below values computed from stream conditions and the assumption of radiation equilibrium. Moreover, materials containing silicon carbide achieve lower surface temperatures during exposure than predicted on the basis of stream conditions. As a consequence, the overall behavior of these materials under HG/CW conditions appears to be better than under CG/HW furnace test conditions.

The present results illustrate the difference between solid oxide formers and graphites. The latter group exhibit increasing oxidation rates with increasing pressure while the former show little pressure effect. When the solid oxide formers are exposed to stream conditions at one atm, which result in surface temperatures below their

melting points, they exhibit recession rates 100 to 1000 times less than graphites do under comparable conditions. Coated metals and silicon carbide degrade at temperatures comparable to those observed in CG/HW furnace tests. These limits are due to melting or rapid vaporization. However, at a given surface temperature, the solid oxide formers exhibit much lower recession rates under HG/CW arc plasma test conditions than in a CG/HW air oxidation furnace test. This may be due to large temperature gradients across the oxide which occur in the HG/CW arc plasma tests than in the CG/HW furnace tests due to artificial oxygen supply limits imposed by the air flow limitations of the latter tests.

Ten Megawatt Arc exposures of 1/2" diameter and 7/8" diameter cylinders of diboride materials have been employed in splash tests to establish thermal shock thresholds at stagnation pressures of 4.3 atm under Mach 2 flow conditions. The best results were obtained with HfB_2+SiC(A-4) and (A-7), which survived fluxes at 950 BTU/ft^2sec and 790 BTU/ft^2sec at 1/2" and 7/8" diameters respectively. Failures were noted at 970 BTU/ft^2sec and 840 BTU/ft^2sec for the 1/2" and 7/8" diameter cylinders. A limited number of ten megawatt arc pipe tests were conducted in order to evaluate the combined effects of exposure to heat flux and high shear. Unfortunately one design aspect of the test generated a substantial thermal stress condition which caused this failure mode to dominate. Si/RVC(B-8) was found to be more thermal stress resistant than boride composites while ZrB_2+SiC+C(A-10) proved most thermal stress resistant of all of the boride composites exposed in the pipe tests.

Sixteen samples were exposed to Mach 6 tests in the Cornell Aeronautical Laboratory Wave Superheater Tunnel, including $HfB_{2.1}$, ZrB_2, HfB_2+SiC, RVA, PG, BPG, JTA, KT-SiC, JT0992, JT0981, W, Sn-Al/Ta-10W and Hf-20Ta-2Mo. Stagnation pressure and enthalpy levels of one atmosphere and 2200 BTU/lb at a cold wall heat flux level of 600 BTU/ft^2sec were applied to one half inch hemispherical cap specimens. Total exposure time was 15 seconds. Radiometer measurements of surface temperature indicated that the heat up time was much shorter than calculated, but surface temperature levels achieved compared reasonably with computed levels near 4000°F. In contrast, a one inch hemispherical cap Hf-20Ta-2Mo alloy showed evidence for melting (melting temperature, 3850°F) while a one half inch diameter cap of the same material showed no signs of melting and little oxidation.

II. RESULTS OF HG/CW ARC PLASMA TESTING IN THE AVCO MODEL 500 AND ROVERS FACILITIES

A. Introduction

More than 700 arc plasma exposures (HG/CW) have been performed in the Avco-SSD Model 500 and ROVERS (Radiation Orbital Vehicle Re-entry Simulator) in air between Mach 0.1 and 3.2. Almost all of the candidate materials listed in Table 1 were tested. Detailed descriptions of the testing facilities and techniques employed are given in Part II-Volume III of this series (3). Stagnation pressures and enthalpies ranged between 0.01 and 1 atmosphere and 1,000 to 16,000 BTU/lb, respectively. Cold wall heat fluxes between 35 and 1200 BTU/ft^{2}sec were employed for times up to 1800 seconds per test with aggregate times of up to 23,400 seconds per sample for those undergoing multiple exposure tests. Surface temperatures ranging between 1700° and 7000°F were generated and radiated heat flux measurements were performed in order to obtain estimates of normal total emittance for the candidate materials. Post-mortem metallographic and x-ray studies have been employed to characterize material behavior. The HG/CW arc plasma exposures are compared with CG/HW air oxidation test results reported in Part III-Volume I of this series (4). The results of temperature gradient measurements through oxide films formed during exposure are presented for flat-faced, hemispherical tipped and shrouded samples of several of the candidate materials. These results are compared with theoretical calculations based on stream conditions and material properties. A theoretical correlation of material performance with stream conditions is presented in Part IV-Volume I of this series (7).

B. Presentation of Arc Plasma Test Conditions and Results

The test conditions and results are presented in Tables 2-39. A description of the facilities and techniques for performing measurements of stream conditions and sample temperatures is presented elsewhere (3). The tabulated information presented for each exposure includes the Mach number, stagnation pressure, P_e, stagnation enthalpy, i_e, initial diameter of the samples, cold wall heat flux, q_{cw}, and the observed surface temperature. The latter values were obtained by employing the emittance values for $\lambda = 0.65\mu$ which are contained in Tables 2-39 for each material. It should be noted that employing a constant value of emittance at $\lambda = 0.65\mu$ for the wide range of temperatures and pressures encountered in the present tests represents an over-simplification. However, the current values are employed as a first approximation to the problem at hand.

In addition to the foregoing, Tables 2-39 contain measurements of the surface radiation, q_r, and the total normal emittance, ϵ_N, computed on the basis of Eq. (1):

$$\epsilon_N = q_r(\text{BTU/ft}^2\text{sec})\ (0.47)^{-1}\ (T^\circ R/1000)^{-4} \qquad (1)$$

Measurements of surface radiation emitted from samples having 1/2 inch diameter faces requires special alignment of the optical system. Initial measurements in the ROVERS facility were performed with an optical system which was designed for measuring surface radiation from 3/4 inch diameter models. These measurements are expected to be lower than values obtained with an optical system specifically designed to measure radiation from 1/2 inch diameter samples. This system was employed for all measurements. In addition, comparison of test data obtained with 1/2 inch and 3/4 inch diameter samples has been performed and will be discussed below.

It should be pointed out that measurement of the surface brightness temperature carried out in the ROVERS facility is converted to true temperature by employing the emittance at 0.65μ and a transmissivity factor to correct for the window material. The correction factor is the product of the surface emittance and the transmissivity factor of the window. A transmissivity factor of 0.86 was used for the sapphire windows employed.

In addition to the foregoing set of "stream conditions" and surface radiation and temperature data, Tables 2-39 contain data on initial and final lengths, exposure time and recession rates for each sample. Also included are ratios of the calculated surface temperature, T_{CALC} and the observed surface temperature, T_{OBS}, which are based on radiation equilibrium as indicated by Eq. (2):

$$0.47\epsilon \; (T_{CALC}{}^{\circ}R/1000)^4 = h_e \; (i_e - i_w \, [T_{CALC}, P_e] \,) \qquad (2)$$

where h_e is the heat transfer coefficient, ϵ is the total normal emittance, and $i_w[T_{CALC}, P_e]$ (BTU/lb) is the enthalpy of air at T_{CALC} and P_e (6). In the first order calculations presented in Tables 2-39, the normal total emittance, ϵ_N, is assumed to be equal to the emittance at $\lambda = 0.65\mu$. Thus, these calculations ignore the measured q_r and normal emittance values. Part IV-Volume I of the present series (6) repeats the calculation including the measured emittance. The first order calculations are presented for comparison with results obtained earlier. Finally, the heat transfer coefficient, h_e, in Eq. (2) is calculated in two ways. The cold wall heat transfer coefficient is defined by Eq. (3) as:

$$h_e = q_{cw}/i_e \qquad (3)$$

while the Fay-Riddell heat transfer coefficient is given by Eq. (4) (6), as:

$$h_e = 0.0386 \; (1 + 0.17M^{-1})^{-1} \; (24 \; P_e/D)^{1/2} \; \text{lbs/ft}^2\text{sec} \qquad (4)$$

where M is the Mach No., and D is the diameter of a hemispherical tipped cylinder in inches. For flat faced samples an effective diameter was used, where (6)

$$D_{eff} = 2.5D_{cylinder} \tag{5}$$

Evaluation of the sample recession was performed by measuring the overall length of the test cylinders as well as the depth of the sting hole drilled in the back. The difference is the thickness. Measurement of the thickness after exposure is carried out by sectioning the sample and metallographic analysis. This procedure is preferable to measurements of the overall length before and after test. The latter are also made and are presented in Tables 2-39 for reference. Initially, measurements of the sting hole depth were not performed and final dimensions were obtained by sectioning the exposed cylinders and comparing the overall length of the sectioned sample with the initial length. As a consequence, some of the materials contained in Tables 2-39 show identical values of initial length and thickness*.

Figures 1-8 show the results graphically as compared with the behavior in furnace tests, while Figures 9-301 show post exposure photographs of the samples tested as well as typical photomicrographs.

1. $HfB_{2.1}$(A-2)

The results obtained for $HfB_{2.1}$(A-2) are contained in Table 2 and compared in Figure 1 with the results of CG/HW furnace tests in air at a flow rate of 1 ft/sec (4). The melting point of this material shown in Figure 1 is based on the work of E. Rudy (7). Figures 9-11 show post exposure macrographs of all of the samples after test. As indicated above, all of the samples were sectioned after exposure and examined metallographically. Typical sections are shown in Figures 12-23 illustrating the most severe test where minimal recession occurred (Figures 12-15) and the least severe test where rapid recession occurred (Figures 16-19) in the Model 500. Similarly Figures 20-23 show maximum "survival" and minimum "failure" conditions in the ROVERS arc. Figures 16, 17, 22 and 23 (when compared with the microstructural features of virgin material (1)) show that rapid recession coincides with melting of the boride. This conclusion is reinforced by Figure 1 where the measured recession results at high temperatures are compared with the published melting point (7).

---

*Tests where changes occurred due to arc or sample conditions are denoted by A and B. Thus, in Table 2, $HfB_{2.1}$(A-2)-18MA refers to melting at the beginning of the exposure, while (A-2)-18MB refers to the behavior after melting ceased. Multiple exposures such as $HfB_{2.1}$+20 v/o SiC(A-7)-23M in Table 6 are denoted by roman numerals I, II, etc. Finally, hemispherical capped cylinders and shrouded samples are denoted by MH and MS as shown in Table 6 for tests $HfB_{2.1}$ + 20 v/o SiC(A-7)-36MH and 44MS.

Figures 24-27 illustrate the excellent oxidation resistance of $HfB_{2.1}$(A-2) at temperatures in the 4500°F range. Although the mechanical integrity of the (A-2) samples was poor (see Section IV. C and Table 16 of Reference (1) for details) no thermal stress failures were noted below a heat flux of 770 BTU/ft^{2}sec. In particular dye penetrant tests of sample (A-2)-8R exhibited a band of high porosity near the center while sample (A-2)-9R was sound. At a heat flux of 772 BTU/ft^{2}sec, the former exhibited thermal shock failure while the latter did not. As indicated in Section II. B-4, 6 and 7, addition of silicon carbide materially improved the mechanical integrity and increased the resistance to thermal stress failures. This finding has been extensively documented in a companion study of fabrication characteristics and mechanical, thermal and physical properties (8, 14). The most striking feature of the present result for $HfB_{2.1}$(A-2) in the HG/CW tests is the difference between the recession rates encountered at a given surface temperature in these exposures and those observed at the same surface temperature in furnace tests (4). This difference is shown in Figure 1 which indicates that an oxidation depth of 20 mils in 30 minutes is obtained in an arc plasma test at 5000°F while the same oxidation depth can be produced at 3500°F in a furnace test. Alternatively a 100 mil oxidation depth is observed in a furnace test at 4000°F after 30 minutes while comparable oxidation depths are not obtained in arc plasma tests below 5500°F. The source of this difference is the temperature gradient through the oxide as indicated in Section I. B. Reference to Figure 1 also indicates no significant effect of oxygen pressure on the oxidation rate of this material in the pressure range between 0.002 and 1.0 atmospheres (air). This finding is in keeping with previous results (15, 16).

Table 2 shows the results of several test samples (A-2)-16M, 17M and 18M which were preoxidized at 1930°C (3500°F) for ten minutes to form a 10 mil oxide (4) and subsequently exposed under marginal survival conditions. These tests were performed to ascertain whether a high normal emittance coating (oxide = 0.50, bare boride = 0.40) could extend the operating range. Comparison of (A-2)-16M with (A-2)-1M and (A-2)-4M indicates little or no improvement. In addition, cyclic exposure of (A-2)-13M, 14M and 15M to three cycles which were each of 600 second duration (interrupted by cooling to room temperature) produced no accelerated oxidation over uninterrupted 1800 second tests (i.e., see (A-2)-1M)).

2. ZrB_2(A-3)

Table 3 summarizes the results obtained for ZrB_2(A-3). As before, Figures 28 and 29 show post exposure photographs of all samples, while Figures 30-39 illustrate "maximum severity survivals" and "minimum failures" in the Model 500 and ROVERS. The melting point (7) shown in Figure 1 as well as Figures 32, 33, 37 and 38 indicate that melting of the boride is the cause of rapid recession. The excellent long time oxidation resistance of this material at 4000°F is illustrated in Figures 40 and 41. Graphical comparison of CG/HW furnace test data (4) with the current results in Figure 1 shows evidence for temperature gradients and the

"minimimum oxide temperature limit criterion" discussed in Section I.B. Tests (A-3)-1MC, 2MC, 3MC and 4MC were designed to measure the temperature gradients through 100 mil wall thicknesses of oxide and boride. Thus, reference to Table 3 shows that nose thicknesses of 104, 101, 102 and 104 mils were machined in samples (A-3)-1MC, 2MC, 3MC and 4MC. In-depth temperature measurements were performed at these stations along the lines previously indicated (3). Figure 42 shows post exposure photographs of all these "in-depth temperature" tests, while Figure 43 shows a section through (A-3)-2MC which exhibited a 1500°F temperature gradient. Reference to Table 3 and Figure 43 shows that the final boride thickness was 87 mils. The time-temperature history at the "in-depth" station is documented in Table 40. This illustrates the long time stability of this effect which will be discussed in further detail in Section II.C. Figure 43 also shows the tungsten sting in place. Close examination illustrates the small contact area between sting and sample designed to minimize heat transfer by conduction. In view of the 9:1 length/diameter ratio of the "sighting hole" the "blackbody" assumption of Table 40 is justified. Additional experimental justification is presented in Section II.C. Comparison of the observed temperature gradients with calculations based on a simple one dimensional model which allows for side losses due to radiation (6) yields good agreement with observations. For the case of (A-3)-2MC shown in Figure 43 the computed surface and internal temperatures were 4170°F (4470°F observed) and 2910°F (2930°F observed), respectively.

Cyclic exposures of ZrB_2(A-3)-52M, 53M and 54M were performed along the lines previously indicated for $HfB_{2.1}$(A-2) to assess the effects of heating and cooling in three-600 second cycles. The results showed that at the lowest level ZrB_2(A-3) exhibited a recession equivalent to that observed in an 1800 second test. At higher levels ZrB_2(A-3) exhibited larger recessions for cyclic exposures than in the case of uninterrupted 1800 second tests. By contrast, the cyclic tests performed on HfB_2 did not result in larger recessions than the uninterrupted tests. The motion picture coverage indicated that the oxide formed on $HfB_{2.1}$(A-2) exhibited greater tenacity under these conditions than did the oxide formed on ZrB_2(A-3). The latter flaked off between cycles. As indicated in Section II.B.1, preoxidation of HfB_2(A-2) to form a 10 mil coating did not result in noticeable changes in behavior.

Reference to Table 3 shows that the ZrB_2(A-3) material employed in these tests did not exhibit any thermal stress failures at flux levels as high at 950 BTU/ft^{2}sec. In contrast to the $HfB_{2.1}$(A-2) material discussed in Section II.B.1, the (A-3) material was mechanically sound and did not exhibit the flaws shown by the (A-2) in the nondestructive tests prior to exposure (see Sections IV.B, C and Tables 15, 16 of Reference 1).

3. HfB_2 + SiC(A-4)

Table 4 contains the results obtained for HfB_2+SiC(A-4) which has the same composition as HfB_2+SiC(A-7) (1) but was prepared by

an alternate supplier (Table 1). Post exposure photographs of all test samples are shown in Figures 44 and 45. Figure 2 compares the furnace tests results (4) with the current HG/CW arc plasma data. Metallographic sections of "maximum severity survivals" and "minimum failure" tests in the Model 500 and ROVERS are shown in Figures 46-53. Figures 47, 52 and 53 show the "silicon carbide depletion zone" which is observed (4) when this composite is exposed to oxidizing environments at high temperature. The depletion depths for various exposures of (A-4) are shown in Table 15 and displayed in Figure 1. Thus, a ten mil depletion depth was observed in HfB_2+SiC(A-4)-2M (Figure 47) after 30 minutes in an arc plasma test where the surface temperature was 5020°F. By contrast Figure 1 of Reference (4) shows that a ten mil depletion depth is attained in 30 minutes near 3500°F in a CG/HW furnace test. Although these observations suggest the existence of temperature gradients in the boride-silicon carbide composites, the difference between the arc plasma and furnace oxidation depths are small (Figure 2). This finding is in contrast to the results obtained for $HfB_{2.1}$(A-2) and ZrB_2(A-3) shown in Figure 1. This subject will be discussed in greater detail in Sections II.B-5, II.B-7 and II.C. The adherent oxide which forms on this composite is shown clearly in Figures 47 and 53. Figures 54-57 show the low recessions observed after exposures in the 3500°-4500°F temperature range. Reference to Table 4 shows that no thermal shock failures were noted at the highest flux levels employed in these tests (1000 BTU/ft^2sec).

As indicated above (Section II.B) radiation equilibrium calculations were performed for each exposure to compare observed and computed temperatures as a general check on the internal consistency of the data. An extensive comparison of the data collected in the present study with the results obtained in other investigations is presented in Reference (6). Although the significance of these comparisons in terms of the ratio T(CALC)/T(OBS) will be discussed in some detail below (Section II.D) it is worth noting at this point that the average values of this ratio (for cases where melting does not occur) for (A-2), (A-3) and (A-4) are 1.16, 1.09 and 1.22, respectively. The significance of this result will become evident if one considers that on the average, the observed temperature was 16% lower than expected for (A-2), 9% lower than expected for (A-3) and 22% lower than expected (based on radiation equilibrium) for (A-4).

4. Boride Z (A-5)

Table 5 and Figures 1 and 58 show the results obtained for Boride Z(A-5). Samples Boride Z(A-5)-2M, 5M, 6M, 7R, 8R and 12R all showed thermal shock behavior. All of the remaining samples except 9R were observed to contain large cracks after sectioning. Samples Boride Z(A-5)-7R and 8R cracked after the exposures were completed. Consequently, the current results indicate that Boride Z(A-5) is very susceptible to thermal shock failure. Figures 59a and 59b show Boride Z(A-5)-4M and 8R which

exhibit thermal shock cracks after exposure at 348 BTU/ft^2sec and 3215 BTU/lb and 262 BTU/ft^2sec and 9200 BTU/lb, respectively. Thus, flux levels above 200-250 BTU/ft^2sec appear to result in thermal shock failures of Boride Z. By contrast ZrB_2(A-3) discussed in Section II.B.2 and ZrB_2+SiC(A-8) to be discussed in Section II.B.6 did not exhibit thermal shock failures at these levels.

5. HfB_2 + 20%SiC(A-7)

Tables 6, 7, 8 and 15 summarize the results observed for HfB_2+20%SiC(A-7). As indicated earlier, this material has the same composition as (A-4). This composite was exposed to extensive evaluation since it exhibited the most outstanding high temperature-long time oxidation resistance. Exposure (A-7)-28R details the 23,400 second exposure noted in Section 1B. As indicated earlier, multiple exposures are denoted by roman numerals, i.e., (A-7)-24MI, 24MII, 24MIII, 24MIV. Hemispherical capped samples and shrouded samples are designated by the suffix H and S respectively as can be seen by comparing the tables with Figures 60-62. The latter illustrate all of the samples after exposure. Thus, (A-7)-45MS is shown in Figure 60 (sample 45M) to consist of the (A-7) cylinder with a 437 mil diameter in a 875 mil shroud. The shroud material was ZrB_2+SiC+C(A-10). This material was employed because it is machinable and quite oxidation resistant. Reference to Figure 60 shows qualitatively that (A-7) is more resistant to oxidation than (A-10). Figure 61 shows the hemispherical samples (A-7)-36MH, 37MH, 38RH, 39RH, 48RH and 50RH. Finally a few of the hemispherical samples were shrouded in order to evaluate the effect of such shrouds on internal temperature distributions. Samples 49RHS and 51RHS shown in Figure 61 are examples of this configuration. Little effect was noted due to shrouding of hemispherical models. However, hemispherical models and shrouded flat faced models resulted in lower temperature levels. This aspect of the testing program will be discussed later.

Finally samples (A-7)-38RH and (A-7)-46RS were run twice. The second exposures are denoted as (A-7)-38RR and (A-7)-46RR. Sample (A-7)-39RH was run three times with the second and third exposures designated as (A-7)-39RRI and (A-7)-39RRII.

Figures 63-70 show the "maximum severity survival" and "minimum failure" conditions in the Model 500 and ROVERS facility. As in the case of $HfB_{2.1}$(A-2) and ZrB_2(A-3), rapid recession appears to result from melting. However, since the composite does not melt as sharply as the pure diboride, the transition in Figure 2 is not very sharp. The temperature limit appears to be 5000°F. Figures 71 and 72 show metallographic sections of (A-7)-28R exposed for thirteen cycles (each of 1800 second duration) at a stagnation pressure of 0.07 atm, an average heat flux of 495 BTU/ft^2sec and an enthalpy near 10,300 BTU/lb. Reference to Table 7 shows that the temperature increased progressively during

the first four cycles even though the stream conditions were constant. Cycle number five exhibited a large temperature increase which was maintained through the remaining eight exposures. This behavior is characteristic of all of the multicycle exposures of boride composite samples. The difference in temperature between cycles (A-7)-28RIII and (A-7)-28RV is real since it is reflected in the measured value of radiated flux as well as in the surface temperature. Physically, the increase in temperature appears to be connected with the presence of an oxide over the entire surface of the sample. Thus, in cycles (A-7)-28RI through (A-7)-28RIII little or no oxide is visible (see Film Description) and the observed surface temperature and radiated flux is low. Similarly, in cycle X the oxide has fallen off exposing the bare composite. Here again the surface temperature and radiation are low. Apparently then, the oxide sustains a large temperature gradient over a very small thickness (1500°F over 5-10 mils in the present case). Reference to Figure 72 indicates minimal depletion of SiC. The depletion depth was of the order of 1-2 mils.

Another interesting feature is the ratio T(CALC)/T(OBS) and its variation from one cycle to the next. This ratio is near 1.18 when the oxide is present. However, when the bare boride composite is exposed, the ratio is near 1.70. Thus, the boride composite exhibits surface temperatures which are much lower than expected on the basis of radiation equilibrium. When the oxide is present, calculated temperatures are closer to (but still 15% below) the observed values. Although the cause of this behavior is not known at present (6) part of the difference is undoubtedly due to conduction losses and side radiation (6). Thus, if the conduction between the oxide and the boride is very low the radiation equilibrium calculation applies well to the oxide layer. However, when the bare boride composite surface is exposed conduction losses coupled with side radiation (6) and other factors lead to much lower surface temperatures than expected.

Apart from these fine points, the gross behavior of HfB_2+20%SiC(A-7)-28R is quite remarkable. Table 7 and Figure 71 show that the total recession after the thirteen cycle exposure was 15 mils. This behavior is unrivaled by any other known material system.

Figures 73 and 74 show post exposure sections through (A-7)-52M after 14,030 seconds exposure in eight-1800 second cycles at a stagnation pressure of 1.03 atmospheres. The average cold wall heat flux was 450 BTU/ft^2sec at an enthalpy level of 4180 BTU/lb. Total recession was 329 mils or about 0.33 inches. Under similar conditions graphite and tungsten would exhibit recessions of 14 to 28 inches.

Figures 75-78 show post exposure metallographic sections through samples (A-7)-37MH and (A-7)-39RH which were employed for in-depth temperature measurements. Table 41 shows the

time temperature histories of the internal temperature measurements which will be discussed in Section II. C. However, several points are worth noting currently. First, the temperature gradients observed for (A-7) are not as large as those observed for (A-2). Part of the reason for this behavior is believed to be due to the fact that the oxide which forms on (A-7) is much more adherent than that which forms on (A-2). Consequently, this oxide has a higher thermal conductivity which reduces the temperature gradient (6). As a consequence, the difference between the recession rates observed in HG/CW arc plasma tests and CG/HW furnace tests is smaller for (A-7) than for (A-2). This can be observed by comparing Figures 1 and 2.

As indicated above, (A-4) and (A-7) exhibit lower temperatures than anticipated from radiation equilibrium considerations (i.e., T(CALC)/T(OBS) is much larger than unity). This conclusion was derived by considering flat faced cylinders in the earlier discussion. Consideration of the hemispherical capped specimen tests indicates an additional lowering of the surface temperature. Thus, the T(CALC)/T (OBS) ratios for tests (A-7)-38RH, 39RH, 48RH, 49RHS, 50RH and 51RHS are near 2.0. A graphical illustration of this phenomena is afforded by tests (A-7)-39RRI and 39RRII shown at the end of Table 8. As indicated above, these tests were re-runs of sample (A-7)-39RH. The sample is shown sectioned after exposure in Figures 77 and 78. Here, exposure at 965 BTU/ft^{2}sec and 7290 BTU/lb resulted in a surface temperature of 4285°F for the hemispherical model. By contrast, exposure of a flat faced sample (A-7)-34R to milder conditions (720 BTU/ft^{2}sec, 8040 BTU/lb) resulted in a surface temperature of 5005°F. Moreover, at 791 BTU/ft^{2}sec and 9030 BTU/lb, flat faced sample (A-7)-35R reached 5350°F and receded 315 mils in 90 seconds.

6. ZrB_2 + 20%SiC(A-8)

Tables 9, 10, 15 and 42 and Figures 1, 2 and 79-92 detail all of the results obtained for ZrB_2+20%SiC(A-8). This composite exhibits all of the same features shown by HfB_2+SiC(A-7) although it is not as refractory as its hafnium base counterpart. However, the decrease in temperature resistance is compensated for by the reduced density and cost. Zirconium diboride is roughly one half the density and one tenth the price of hafnium diboride. Reference to Tables 9 and 10 and the post exposure photographs shown in Figures 79 and 80 indicates that most of the tests were conducted with flat faced cylinders. A few tests were shrouded with ZrB_2+14%SiC+30%C(A-10). As in the case of (A-7), the ZrB_2+20%SiC (A-8) material is more oxidation resistant than (A-10) as indicated by samples 30M and 32R in Figure 80. In addition, it is interesting to note the results of (A-8)-29M in which a graphite shroud was employed (Tables 9 and 42). Although the boride exhibited minimal recession (8 mils in 1800 seconds) the graphite shroud which was one inch long ablated completely in 500 seconds.

Table 15 and Figure 1 show the depletion depths for ZrB_2+SiC(A-8) as a function of temperature. This material exhibited the lowest

depletion rate of all the boride composites as shown in Figure 1. In addition, the depletion rate in the current HG/CW tests was much less than the corresponding rates (for a given surface temperature) in CG/HW furnace tests (4). Metallographic sections were prepared for all of the exposures. Figures 83-88 show the "maximum severity survivals" and "minimum exposure failures" in the Model 500 and ROVERS tests.

Figures 89-92 illustrate the results of long exposure cyclic tests in the Model 500 and ROVERS. Test (A-8)-15M shown in Figures 89 and 90 was discussed previously in Section I. B. The sting section of (A-8)-16R shown in Figure 91 was cracked on removal from the sting. Both tests show excellent long time oxidation resistance. Reference to Table 42 shows that temperature gradients through one hundred and four hundred mil walls exist in these materials which are comparable to those observed in (A-7). However, the gradients appear to be smaller than exhibited by ZrB_2(A-3). This finding apparently results from the higher thermal conductivity of the oxide formed on (A-8) (as compared with (A-3))(6). Consideration of Tables 9 and 10 shows that ZrB_2+SiC(A-8) exhibits the same tendency to develop low temperatures as (A-4) and (A-7). Thus, tests in the ROVERS facility at flux levels below 500 BTU/ft^2sec and in the Model 500 facility at flux levels below 350 BTU/ft^2sec develop ratios of T(CALC)/T(OBS) which are of the order of 1.5. This feature of the boride composites which contain SiC permits a wider range of applicability than materials which exhibit (T(CALC)/T(OBS)) near unity.

7. $HfB_{2.1}$+35v/oSiC(A-9)

A limited set of exposures of $HfB_{2.1}$+35v/oSiC(A-9) was conducted in the Model 500 facility. The results are summarized in Tables 11 and 15 and in Figures 1 and 2. Figure 93 shows post exposure photographsof all the test samples while Figures 94-97 show "maximum severity survival" and "minimum failure" conditions in the Model 500. The nonuniform recession exhibited by (A-9)-5M is due to misalignment of the sample in the arc. These results show that the features of (A-9) are similar to (A-4) and (A-7)(i.e., T(CALC)/T(OBS) comparison, recession rate vs. temperature for HG/CW arc plasma tests and furnace exposures, depletion depth vs. temperature in HG/CW tests as a function of temperature, etc.). The major difference is that (A-9) is less refractory than (A-4) and (A-7). Thus, (A-9) exhibits melting in Model 500 exposures when the flux level exceeds 500 BTU/ft^2sec at enthalpy levels near 4000 BTU/lb. By contrast, (A-7)-23M receded 193 mils after 7200 seconds at flux levels near 600 BTU/ft^2sec and 4500 BTU/lb. Similar thermal stability is evidenced by (A-4)-2M and (A-4-2)-3M. A method for comparing the recession rate as a function of flux and enthalpy, rather than exclusively in terms of surface temperature as in Figures 1 and 2, is described in Reference (6).

8. ZrB_2+14%SiC+30%C(A-10)

This composite has been developed (8-14) in order to improve the thermal stress resistance of boride composites (by lowering

of the elastic modulus) without sacrificing oxidation resistance. Moreover, (A-10) is machinable with carbide tools while (A-8) is not. Tables 12-15 and 43 summarize the results of an extensive series of tests conducted on ZrB_2+SiC+C(A-10). Figures 1 and 6 display the results in graphical form. Reference to Figure 6 shows that at surface temperatures between 3000°and 5000°F. (A-10) exhibits a much slower rate of oxidation in HG/CW arc plasma tests than in CG/HW furnace tests. This result is undoubtedly a manifestation of the MOTEL criterion presented in Section I. B.

Figures 98-100 are post exposure photographs of all of the samples after testing. Shrouded samples shown in Figure 99 consisted of the test model jacketed in a cylinder of (A-10) with a 3/16 inch wall thickness. Utilization of the shrouds did not have a substantial effect on model behavior or temperature (6).

In general, the behavior of this composite is quite similar to that exhibited by (A-4), (A-7) and (A-8) discussed earlier in Sections II. B-3, 5 and 6. However, (A-10) is not as refractory as (A-4) and (A-7). Nevertheless, the lower density, cost, thermal stress resistance and machining characteristics of this composite provide compensating advantages.

The series of photographs of tests (A-10)-30R, 31R, 32R and 33R shown in Figure 100 are extremely revealing when examined along with the data shown in Table 14. Test (A-10)-30R exhibits the connection between oxide coating and surface temperature described in Section II. B. 4 for (A-7). During the first 428 seconds of this long test (1669 seconds total) the oxide slowly covered the face and the observed surface temperature of 3650°R was 75% lower than expected from radiation equilibrium. The radiated flux was 33 BTU/ft^2sec. However, once the thin oxide coating covered the surface, the temperature increased to 5455°R and the radiated flux level jumped to 196 BTU/ft^2sec. Under these circumstances the observed surface temperature was only 17% lower than expected on the basis of Eqs. 2 and 3. The total conversion of boride to oxide during the 1669 second exposure was 26 mils. However, reference to Table 14 shows that the total length of the sample actually increased by 10 mils. Thus, the oxide thickness was probably of the order of 36 mils. Figure 100 shows the oxide cover which separated from the sample on cooling. This cover was 35 mils thick. Test (A-10)-31R exposed at identical conditions as (A-10)-30R except that the flux was 596 BTU/ft^2sec instead of 551 BTU/ft^2sec, melted.

Figures 101-108 show the "maximum severity survival" and "minimum failure" tests in the Model 500 and ROVERS facilities. Figures 109-112 show sections through (A-10)-24M and (A-10)-26R which were exposed for times up to 21,600 seconds near 4500°F with total recession of the order of 100 mils. This behavior, which was discussed in Section I. B, shows striking evidence for the applicability of these composites in reusable lifting reentry spacecraft. The sting leg portion of sample (A-10)-26R was cracked on removal after completion of the test.

Table 43 details the results of in-depth temperature measurements. These tests will be discussed later in Section II.C. Comparison of the results with calculations based on side losses due to radiation is presented in a companion report in this series (6). Relatively good agreement between observed and calculated gradients has been obtained (6).

Reference to Table 14 shows that (A-10)-36RH and (A-10)-37RH (hemispherical capped models with in-depth temperature holes) were exposed at flux levels near 500 BTU/ft^{2}sec. Table 43 details the time-temperature history for these exposures. Reference to Table 14 indicates that the observed temperature for these exposures was 60% lower than calculated on the basis of Eqs. 2 and 3. This behavior (noted earlier with (A-7) and (A-8) in Sections II.B.4 and II.B.6), characterized by lower temperatures achieved with hemispherical models than with flat faced models is not understood at present. Nevertheless, the practical implications of this finding are substantial. For example, (A-10)-25R, 26R, 40R and 41R (which were flat faced models) exposed at conditions similar to (A-10)-37R and 38R (i.e., 500 BTU/ft^{2}sec, 7700 BTU/lb, 0.15 atm.) exhibited temperatures near 5000^{o}R in contrast to (A-10)-37R and 38R which exhibited temperatures near 3700^{o}R. Naturally the hemispherical models exhibited lower recession rates. Sample (A-10)-37RH is shown after sectioning in Figures 113 and 114.

Similarly, sample (A-10)-48RH was exposed to four exposures at ascending flux levels until evidence of melting was noted. Melting of this hemispherical capped model was not observed to occur until fluxes near 850 BTU/ft^{2}sec were attained. Flat faced models melted near 650 BTU/ft^{2}sec.

9. Pure Graphite Materials -RVA(B-5), PG(B-6) and BPG (B-7)

Figures 3, 4 and 115-137 compare the results of (HG/CW) Arc Plasma Tests with the results of (CG/HW) Air Oxidation Furnace Tests (4). Figures 3 and 4 also contain a number of results reported by Kendall et al. (17) and by Tanzilli (18) for comparison. The results of these studies are in general agreement with present findings. The general behavior indicated by Figures 3 and 4 is that the supply limited (oxidation rates observed to increase as air flow rate increases) oxidation rates observed in the furnace tests are much lower than observed in the one atmosphere (HG/CW) Arc Plasma Tests. Recession rates in the latter exposures are dependent on pressure and weakly temperature dependent. In general, the results are in keeping with the theoretical description (6). Thus, it appears that the oxidation of graphite observed in the arc plasma exposures is limited by diffusion of oxygen and oxidation products in the boundary layer. This is certainly the case at lower pressures. Reference to Figures 3 and 4 shows that little if any temperature dependence of the

recession rate is noted in the Mach 3.2 exposures at 0.01 to 0.03 atmospheres. However, at higher pressures the temperature dependence becomes more pronounced. The one atmosphere subsonic exposures exhibit a definite temperature dependence of the recession rate particularly in the temperature range between 2500°F and 3500°F. This result is in keeping with the observations derived from high velocity CG/HW tests (5) and theoretical studies (6). The pressure dependence of the recession rate appears to agree with the $P_e^{1/2}$ relation predicted by theory (6). The present results shown in Figures 3 and 4 (Tables 16-18) indicate that PG (B-6) and BPG(B-7) are comparable in oxidation resistance to RVA(B-5) in the (HW/CG) Arc Plasma Tests and the the "C" plane recedes more slowly than the "A" plane of PG(B-6) and BPG(B-7). This is readily evident in Figure 4 for the Mach 0.30-0.50 exposures at one atmosphere.

It should be noted that the observation of enhanced "A" plane recession indicates that while gaseous boundary layer diffusion exercises dominant control, surface reactions do exert some influence on the overall rate.

Reference to Tables 17 and 18 indicates that thermal shock delaminations were noted along the "C" plane for samples of PG (B-6) and BPG(B-7) exposed normal to the "C" axis. Thermal shock failures were not noted for RVA or PG(B-6) and BPG(B-7) when samples of the latter were exposed perpendicular to their "C" axes. This was evidently due to nonuniform heating of samples so exposed due to enhanced conductivity parallel to "C" planes. Motion picture footage clearly illustrated this behavior in which central bands of material which were parallel to the "C" plane and parallel to the cylinder axis heated up before the cylinder surface heated. Figures 123, 126, 131, 134 and 135 illustrate the thermal shock failures of (B-6) and (B-7). Photographs of (B-5), (B-6) and (B-7) samples exposed in the Model 500 illustrate "necking" of the test samples due to oxidation on the sides. This behavior is seen in Figures 115, 118, 122-126, 130 and 132-134.

Comparison of the T(CALC)/T(OBS) ratios obtained for (B-5), (B-6) and (B-7) with those noted for other materials will be performed in Section II. D. For the present however, reference to Tables 16-18 shows that this ratio is approximately 1.18 for these materials. Thus, observed temperatures are about 18% less than expected based on radiation equilibrium. In addition, the ratios are nearer unity for (B-6) and (B-7) when the "C" axis is parallel to the arc (i.e., when the basal planes of graphite are exposed). Table 44 details the results of two exposures of RVA(B-5) in which internal temperatures were recorded. Comparison of the results with calculated values yield relatively good results (6). Temperature gradients are modest due to the bare surface and high thermal conductivity of graphite. Section II. C will provide an additional discussion of these findings.

In comparing the behavior of the foregoing boride materials to the pure graphites RVA(B-5), PG(B-6) and BPG(B-7), it is

evident that the former group (i.e., the borides) exhibit substantially lower recession rates than the graphites at temperatures below the melting temperatures of the borides. This is the case at atmospheric pressures. Thus, at 5000°F and 1 atmosphere, graphite recessions of the order of 3000-6000 mils in 30 minutes are observed as compared to boride recessions in the 30-60 mils in 30 minute range. Even at 0.01 atmosphere stagnation pressures, graphites recede at rates of 1000 mils in 30 minutes. However, once the melting temperature of the borides is exceeded, their advantage is lost.

10. Siliconized RVC Graphite, Si/RVC(B-8)

Table 19 documents the results of the HG/CW arc plasma tests performed on Si/RVC(B-8). Figure 5 compares the results of these tests with CG/HW furnace tests, while post exposure photographs and "maximum severity survivals" are illustrated in Figures 138-142. The present results demonstrate that Si/RVC(B-8) exhibits protective oxidation for short periods of time up to surface temperatures near 3800°F. This is some 700°F above the coating failure temperature observed in the CG/HW furnace tests (4). Above this temperature coating-breakdown occurs and samples exhibit typical graphite behavior. As noted previously, graphite oxidation rates in the arc plasma tests are 20 times larger than the rates observed in the furnace indicating that the latter are supply limited. In particular, exposure Si/RVC(B-8)-5M (Table 19) shows coating burn-off after 735 seconds at 470 BTU/ft^{2}sec and 3720 BTU/lb corresponding to a surface temperature of 3790°F. At low pressure, Si/RVC(B-8)-7R showed protective behavior at 210 BTU/ft^{2}sec and 8850 BTU/lb corresponding to a surface temperature of 2740°F.

Exposures (B-8)-4M and (B-8)-5M discussed above represent short time survival conditions. Survival for 30 minutes was exhibited at slightly lower levels by (B-8)-18M at 362 BTU/ft^{2}sec. A surface temperature of 3110°F was observed in this test in accordance with the CG/HW furnace results (4). Reference to Table 19 indicates that T(CALC)/T(OBS) ratios for this material are high (approximately equal to 1.36) when the coating is intact. This result is in keeping with the behavior noted for other SiC bearing materials ((A-4), (A-7), (A-8), (A-9) and (A-10)) discussed above. Thus (6), Si/RVC(B-8) exhibits enhanced temperature resistance.

11. Special Graphites PT0178(B-9), POCO(B-10) and Glassy Carbon (B-11)

Tables 20 and 21 as well as Figures 3, and 143-155 display the results obtained for the fibrous graphite composite PT0178(B-9), fine grained graphite, Poco (B-10) and glassy carbon (B-11). As in the case of RVA(B-5), PG(B-6) and PG(B-7), the oxidation rates observed in the furnace tests are 20 times smaller than those observed in the arc plasma tests, indicating that the former are supply limited. In line with the high velocity CG/HW test results (5) and the theoretical findings (6), the recession rates of the graphites are inversely proportional to density (7). The motion picture coverage of test (B-11)-1M shown in Table 21 indicates melting during

the exposure. No post exposure examination could be made since the sample ablated completely. Since glassy carbon is not reported to melt at one atmosphere, the only possible explanation that can be advanced at present for this observation is based on surface contamination of the sample by tungsten from the arc or sting (Reference 5, pages 28 and 29).

Figures 143-146 indicate the extensive "necking" of PT0178(B-9) in the Model 500 tests which resulted from side wall oxidation. Although Poco Graphite (B-9) showed similar characteristics (see Figure 148) the necking was less pronounced.

Section II. D will present a complete discussion of the emittance and T(CALC)/T(OBS) ratios for these materials. For the present, it is sufficient to note that the T(CALC)/T(OBS) ratios for PT0178(B-9) and Glassy Carbon (B-11) are near unity while the average ratio for Poco Graphite (B-10) is near 1.15.

12. Arc Cast Hypereutectic Carbides HfC+C(C-11) and ZrC+C(C-12)

Tables 22 and 23 along with Figures 5 and 156-179 detail the results obtained for the arc cast hypereutectic carbides HfC+C(C-11) and ZrC+C(C-12). The melting points shown in Figure 5 are taken from the work of Rudy (7). Reference to Figure 5 indicates that the present results on melting of (C-11) and (C-12) are in keeping with Rudy's results. In addition, the values of T(CALC)/T(OBS) for (C-11) and (C-12) are found to lie near 1.0. Although the temperature range of the present HG/CW arc plasma tests were not overlapped with CG/HW furnace tests, Figure 5 indicates the two sets of results are comparable. This is due in part to the unusual oxidation characteristics of (C-11) and (C-12) (4). These materials do not form protective oxides below 3300°F. At lower temperatures they form porous flakey oxides which do not suppress the oxidation rate. Thus, arc plasma samples which are hotter at the front than at the back are expected to exhibit variable oxidation characteristics. This behavior is shown clearly in the post exposure photographs which constitute Figures 156, 157, 168 and 169. Thus, the post exposure pictures of (C-11)-17M and (C-12)-15M are quite reminiscent of the structures shown on page 64 of Reference (4). Figures 158, 170 and 178 illustrate the rapid oxidation of the sting leg region where a thick nonprotective oxide forms. Figures 171 and 179 show preferential oxidation along the graphite flakes in the hypereutectic structure. As indicated in Figure 5, HfC+C(C-11) is more refractory than ZrC+C(C-12) and is thus capable of withstanding higher flux and enthalpy levels before melting (6). Figures 158-178 illustrate the "maximum severity survival" and "minimum failure" condition in the Model 500 and ROVERS facilities. The latter are associated with melting of the carbide. This conclusion is based on the large number of survivals (recession rates of 100 mils or less in

30 minutes) observed for (C-11) above the melting point of HfO_2 near 5100°F, and the clear difference in resistance to stream conditions evidenced by (C-11) and (C-12) despite the fact that the melting points of HfO_2 and ZrO_2 are nearly equal.

The samples employed in tests HfC+C(C-11)-10R and 12R (Figures 160-163) were fabricated from billet 1422A (Table 8 of Reference 1) which is lowest in carbon. Consequently, these samples do not exhibit large graphite flakes. Nonetheless, the oxidation behavior of samples from Billet 1422A does not appear to differ materially from samples fabricated from the billets which are higher in carbon. Figure 163 shows the microstructure which is characteristic of billet 1422A.

Figures 170-175 show post exposure photomicrographs of ZrC+C(C-12)-15M, 10R and 7R. A recession of 64 mils was observed for (C-12)-15M after 1800 seconds at 3900°F. Figure 170 shows the "puffy" attack of the hypereutectic carbides. Figure 172 displays the structure of (C-12)-10R after 1800 seconds at 5030°F. A recession of 32 mils was observed subsequent to this exposure. At 4955°F (C-12)-7R exhibited a total recession of 209 mils in 1800 seconds at 5030°F. The apparent reversal in behavior of (C-12)-10R and (C-12)-7R indicates that these conditions are borderline relative to melting of ZrO_2 as shown in Figure 5. Both HfC+C(C-11) and ZrC+C(C-12) are resistant to thermal shock over the range of conditions employed.

Cyclic exposures of (C-11) and (C-12) were not carried out due to the problems associated with the poor low temperature oxidation behavior. Under these conditions it is expected that excessive side oxidation at cooler locations on the sample would lead to rapid oxidation.

13. JTA($C+ZrB_2+SiC$) (D-13)

The results of the present arc plasma testing programs for JTA(D-13) (which is predominantly a graphite in contrast to (A-10) which is mostly boride) is shown in Tables 24 and 25. Figure 6 compares the HG/CW results with furnace test data, while Figures 180-197 show post exposure photographs and metallographic sections of selected test samples. Experimental results obtained in HG/CW tests by Kendal et al. (17), Criscione et al. (19) and by Buckley and Stein (20) are included for comparison in Figure 6.

The ratio of T(CALC)/T(OBS) for most exposures of this material was near 1.10. Comparison of the temperature calculations and emittance values for this material will be compared with the results obtained for other candidate materials in Section II. D.

A substantial number of thermal shock failures were observed in these tests. These failures, noted in Table 24, occurred in random fashion at flux levels above 500 BTU/ft^{2}sec. The samples which failed by thermal shock were machined from 2-1/2" diameter x 2" long billets of JTA(D-13) in an orientation which corresponds to the hot pressing direction. Thus, the axis of the arc plasma test sample was parallel to that of the hot pressed cylinder. Under these conditions, residual strains present in the billets and in the samples could provide a source for the failures. In order to investigate this possibility a second series of samples were machined from additional billets. These sample cylinders were oriented with their axes perpendicular to the pressing direction. Nondestructive testing of these cylinders showed no nonuniformities or imperfections (see Page 19 of Reference 1). The above mentioned samples are designated as (D-13)-31MX through (D-13)-41MX in Table 24. Significantly, no thermal shock failures were noted for these samples even at flux levels in excess of 500 BTU/ft^{2}sec. This finding has particular relevance to applications in which JTA(D-13) parts are exposed to severe environmental heat fluxes. A preoxidized coating on (D-13)-43M, 44M and 45M had no noticeable effect.

Reference to Figure 6 shows that the results obtained for JTA(D-13) in HG/CW arc plasma tests and CG/HW furnace tests "dove tail." By contrast the HG/CW results for (A-10) lie below the CG/HW rates at temperatures up to 5000°F as shown in Figure 6. At 4500°F and one atmosphere stagnation pressure, JTA(D-13) behaves like a graphite exhibiting recession of 2-4 inches in thirty minutes, while (A-10) behaves like a boride and exhibits recessions of 10-20 mils in thirty minutes.

A post exposure metallographic section of JTA(D-13)-22M is shown in Figures 185 and 186 to illustrate a "maximum severity survival" in the Model 500. Rapid recession is illustrated by Figures 188 and 189 for JTA(D-13)-4M after rapid oxidation at 660 BTU/ft^{2}sec and 4320 BTU/lb (surface temperature equals 4560°F). ROVERS exposures at low pressure lead to protective oxidation at a surface temperature of 4665°F (500 BTU/ft^{2}sec and 9520 BTU/lb) as shown in JTA(D-13)-7R illustrated by Figures 190 and 191. At higher levels (770 BTU/ft^{2}sec, 7310 BTU/lb and surface temperature equal to 5305°F) rapid oxidation rates are observed as shown in Figures 192 and 193 for JTA(D-13)-8R.

Figures 194 and 195 show sample (D-13)-48MX after 4 cyclic exposures at a stagnation enthalpy of 4350 BTU/lb, stagnation pressure of 1.01 atm and a cold wall heat flux of 330 BTU/ft^{2}sec. Each exposure was 1800 seconds long making the total exposure time 7200 seconds. The average recession was 118 mils. This test can be compared with (A-10)-24 shown in Figure 109 which exhibited a recession of 104 mils after 12 cycles (1800 seconds each) totalling 21,600 seconds under comparable conditions.

Figures 196 and 197 show sample (D-13)-49RX after 4 cyclic exposures at a stagnation pressure of 0.057 atmospheres at a stagnation enthalpy of 9600 BTU/lb and a cold wall heat flux of 440 BTU/ft^2sec. Each exposure was 1800 seconds long making the total exposure time 7200 seconds. Total recession for this test was 45 mils. By comparison, (A-10)-26R exposed for 18,951 seconds at comparable heat flux and enthalpy and a higher pressure (0.238 atm) exhibited a recession of 83 mils as shown in Figure 111.

14. KT-SiC(E-14)

The behavior of KT-SiC in (HG/CW) exposures is compared with the (CG/HW) tests in Figure 5. Detailed results are contained in Table 26. Rapid oxidation rates are observed at temperatures above 4000°F, or 500°F higher than observed in (CG/HW) tests (4). Although a complete discussion of the emittance and calculated temperatures for this material will be postponed to Section II. D, it should be noted that the computed ratios T_{CALC}/T_{OBS} exceed unity with typical values near 1.5. This indicates that the observed surface temperature is substantially less than anticipated on the basis of radiation equilibrium. Thus, heat absorbtion due to vaporization or degradation of the heat transfer coefficient due to injection or blocking is operative. At 4500°F, significant vaporization of KT-SiC leads to rapid rates of recession.

Figure 5 shows a slightly higher failure temperature for KT-SiC(E-14) in the HG/CW Arc Plasma Tests at one atmosphere than in the CG/HW furnace tests. At lower pressures, higher oxidation rates are observed as expected. This is due to the instability of SiO_2 (relative to SiO) at low pressure (4).

Post exposure photographs of all samples are shown in Figures 198 and 199. Figures 200 and 201 show metallographic sections through sample (E-14)-4M after survival at 3670°F for 1835 seconds. At higher levels rapid ablation is illustrated. Figures 202 and 203 show KT-SiC(E-14)-5M after exposure for 165 seconds at 4440°F. A total recession of 425 mils was observed. Under these conditions recession occurs by ablation and vaporization.

Samples KT-SiC(E-14)-3R, 5R and 7R exhibited low oxidation rates but showed internal cracks on sectioning as indicated in Figure 204.

15. JT-0992(C-HfC-SiC)(F-15) and JT-0981(C-ZrC-SiC)(F-16)

The results obtained for the graphite composites JT-0992(C-HfC-SiC)(F-15) and JT-0981(C-ZrC-SiC)(F-16) are summarized

in Tables 27 and 28. These composites, like JTA($C-ZrB_2-SiC$)(D-13), are mainly graphite (1). Unlike the former, however, they do not contain boron and are therefore susceptible to rapid oxidation at temperatures below 2800°F. This fact is illustrated in Figure 6 which compares the current results of HG/CW arc plasma tests with furnace tests conducted under CG/HW conditions. Reference to Tables 27 and 28 shows that the ratio T(CALC)/T(OBS) is near 1.05 for (F-15) and 1.10 for (F-16). These findings and the results of the emittance measurements presented in Tables 27 and 28 will be discussed in Section II. D. Post exposure photographs and metallographic sections are shown in Figures 206-229. Photographs of all the exposures of (F-15) shown in Figures 206-208 and (F-16) shown in Figures 218-220 illustrate a large number of thermal shock failures particularly in the case of JT0981(F-16). As indicated earlier in Section II. B-13 (Table 24), JTA(D-13) also exhibited thermal shock failures when exposed to heat flux levels above 600 $BTU/ft^2 sec$. This failure mode was eliminated (for JTA) by orienting the pressing axis of the billets perpendicular to the arc (Section II. B-13). All of the samples of (F-15) and (F-16) discussed in Tables 27 and 28 were oriented so that the pressing axis was parallel to the arc since testing was completed before the effect of orientation was established for JTA(D-13).

After initial observation of thermal shock failures in exposures JTA(D-13)-23M and 24M (Table 24) and JT0981(F-16)-21M, 22M, 23M and 24M, a second set of samples was prepared and submitted for nondestructive testing as noted on p. 19 of Reference 1. The NDT results indicated that JTA(D-13)-1, 6 and 9 and JT0981(F-16)-1, 4, 9 and 11 gave extreme values in the ultrasonic velocity and eddy current measurements. No nonuniformities or surface cracks were disclosed by radiographic or dye penetrant methods. Reference to Tables 24 and 28 show that none of these extreme samples exhibited thermal shock failures.

If the results are taken at face value, it appears that JT0981 exhibits a high thermal shock failure rate at flux levels in excess of 400 $BTU/ft^2 sec$. The failure level for JTA appears to be in the vicinity of 600 $BTU/ft^2 sec$, while JT0992 exhibited only two random failures when exposed at flux levels up to 1145 $BTU/ft^2 sec$. Examination of the microstructures of the test cylinders with Mr. S. E. Slosarik, Applications Manager of the Aerospace and Nuclear Products Division of Union Carbide Corp., showed some preliminary evidence for carbon and carbide grain size differences between test cylinders which seemed to correlate with the occurrence of thermal shock failures. However, subsequent extensive metallographic investigation of this factor did not verify the hypothesis that fine grained structures exhibit a higher flux tolerance than coarse grain structures. Since all of the 1/2 inch diameter x 1 inch long cylinders were cut from one 2 inch diameter x 2-1/2 inch billet which

in turn were cut from 7 inch diameter x 7 inch pressings, grain size variations between test cylinders were not ancitipated. The axes of the test cylinders, billets and pressings were identical and thermal shock failures were found to occur by delaminations along planes perpendicular to the cylinder axis.

Reference to Figure 6 shows that the 30 minute oxidation depths exhibited by JT0992(F-15) and JT0981(F-16) in the (HW/CG) Arc Plasma Tests at Mach 0.3-0.5 and one atmosphere agree with the (CG/HW) Air Oxidation Furnace Tests (4). These rates are 30 times less than those encountered for RVA(B-5) Graphite at temperatures below 4000°F indicating some beneficial effect of the solid oxide formers contained in the composites. A substantial lowering of the 30 minute conversion depth was observed at stagnation pressures in the 0.01-0.03 atmosphere range at temperatures below 5500°F. Melting was observed at this temperature.

Figures 209-217 illustrate "maximum severity survivals" and "minimum failures" for JT0992(F-15). Figure 211 in this group illustrates the low temperature susceptibility to rapid oxidation of JT0992 (C-HfC-SiC)(F-15) which was noted earlier for HfC+C(C-11) and ZrC+C (C-12) in Section II. B-12. This low temperature attack (which is eliminated when boron is present) is clearly seen in Figure 211. Here, test (F-15)-2M exhibited a 34 mil recession on the hot face at a surface temperature of 3470°F after an 1173 second exposure at one atmosphere stagnation pressure. However, the oxidation depth increases along the sides of the model as the distance from the hot face increases (due to the fact that the temperature decreases) in accordance with Figure 6. Thus, oxidation depths of 100 mils are seen at a distance of 750 mils from the front face where the temperature level dropped below 2800°F.

Post exposure metallographic sections for JT0981(F-16) shown in Figures 221 and 222 present additional graphic evidence of the rapid low temperature oxidation. This behavior is absent at low pressure (0.075 atm) as shown in Figure 226. Figures 224 and 228 illustrate rapid recession at temperatures near 5000°F due to melting.

16. Molybdenum and Tungsten Melting Tests and Exposures of WSi_2/W(G-18) and Sn-Al/Ta-10W(G-19)

As indicated in Reference (3) extensive precautions have been taken in order to insure that temperature measurements of the model surface are accurate. In general, the comparison of observed surface temperatures in HG/CW arc plasma tests with values calculated from stream conditions are in relatively good agreement. Moreover, a number of temperature measurements employing two color pyrometers yielded good results (page 8 of Reference (3)). In order to obtain additional verification of the surface temperature measurements, the melting points of tungsten and molybdenum were measured in the arc facilities using pure nitrogen streams

for comparison with accepted values. The results of these tests are shown in Table 29 and in Figure 230. The relatively good agreement obtained in these tests should eliminate concern over the accuracy of surface temperature measurements due to interference of the arc with optical observations.

The results of arc plasma testing of the coated refractory metals WSi_2/W(G-18) and Sn-Al/Ta-10W(G-19) is shown in Tables 30-32 and 45. Both of these materials exhibit high ratios of T(CALC)/T(OBS) when the coating is intact. Thus, ratios near 1.55 are typical for (G-18) and 1.40 for (G-19). As indicated earlier, ratios which are larger than 1.0 indicate enhanced temperature resistance. This behavior will be discussed in Section IID. Modest temperature gradients observed for (G-18) are shown in Table 45. The results will be discussed in Section IIC. These data agree with computed results (6). Figure 6 compares the results for (G-18) and (G-19) obtained in the current HG/CW arc plasma tests with those obtained in CG/HW furnace tests. Post exposure photographs and metallographic sections of "maximum severity survivals" and "minimum failures" are shown in Figures 231-246.

It should be noted that (G-18)-19M and (G-18)-20M which were shrouded in cylinders of ZrB_2+SiC+C(A-10) as indicated in Table 30 and Figure 233 showed no sign of reaction with the shroud. This indicates compatability between the coated tungsten and boride composite under these conditions.

Figures 234 and 235 show post exposure metallographic sections through sample WSi_2/W(G-18)-4M which represent a "maximum severity survival" condition in the Model 500 at one atmosphere stagnation pressure. This test conducted at a flux level of 460 BTU/ft^2sec and 2785 BTU/lb survived the full 1800 second exposure as did tests (G-18)-21M and 22M at slightly lower flux levels and slightly higher enthalpies. In all three cases, the observed surface temperatures were below 3450^oF which corresponds to the survival limit noted in the furnace tests (4). In addition, in each case the calculated temperature based on Eqs. 2 and 3 was 40% to 60% higher than observed. This finding is in keeping with the behavior noted for SiC, SiC coated graphite and SiC bearing composites discussed earlier.

Raising the conditions slightly as in (G-18)-14M at 440 BTU/ft^2sec and 3485 BTU/lb results in coating burn-off and tungsten ablation. This test resulted in complete ablation of the sample in 1032 seconds. The initial length of 452 mils leads to a rate of about 0.44 mils/sec under these conditions or a 30 minute recession depth of 790 mils. These rates are in good agreement with calculated recession rates for tungsten ablation (6). It should be noted that once the WSi_2 coating is burned off (as in (G-18)-14M) the ratio T(CALC)/T(OBS) drops to unity. This finding offers strong support for the calculation and the conclusion that silicious materials act to lower the surface temperature. It also mitigates against errors due to conduction losses. Figure 235 shows the W_5Si_3 zone formed during Test (G-18)-4M. The width of this zone is seen to be 0.55 mils. Table 31 summarizes the W_5Si_3 zone widths measured after exposure of all the WSi_2/W(G-18) samples. The results are plotted in Figure 237 for comparison with

published values (21, 22) and complementary values obtained during CG/HW tests of this material (4, 5). Figure 236b shows a similar measurement of W_5Si_3 zone width for exposure (G-18)-6R in the Rovers arc.

Reference to Figure 237 shows that the zone width data obtained in arc plasma tests under HG/CW conditions at temperatures above 3050°F are in good agreement with the observations obtained using other exposure techniques; however, at lower temperatures, substantial discrepancies exist as shown in Figure 237. These differences cannot be attributed to errors in zone width measurement or temperature measurement. At present the source of these differences is unknown.

The data presented in Table 30 show that Mach 3.2 exposures at P_e = 0.082, i_e = 8310 BTU/lb and q_{cw} = 554 (Sample No. 6RB, Table 30) did not lead to failure. However, exposures 7RA-7RB and 8RA-8RB described in Table 30 clearly describe failure conditions. In the former case, the five mil coating of WSi_2 burned off after 300 seconds at a surface temperature of 3610°F generated by P_e = 0.158 atm, i_e = 8020 BTU/lb and q_{cw} = 781 BTU/ft^{2}sec. Subsequently, the surface temperature rose to 5420°F as the tungsten began to burn and 40 mils of tungsten were lost during the 50 second exposure of the bare tungsten. Exposures 8RA and 8RB repeat the 7RA-7RB conditions and extend the exposure time for oxidation of the bare tungsten surface. These exposures (7RB-8RB) indicate a recession rate of 0.80-0.95 mils/sec. The computed rate (6) is 0.35 mils/sec under these conditions. The comparsion of tungsten recession rates observed in this study with those reported in the literature (17) shown in Figure 7 is quite reasonable. These failure conditions are in agreement with the air oxidation, oxygen pickup and high velocity (CG/HW) tests which indicated failure of the WSi_2/W coating system at 3450°F to 3680°F. Table 30 illustrates the effects of the WSi_2 coating on the surface temperature. For these cases (in contrast to the aforementioned behavior of the boride, graphite and graphite composite materials) the T(CALC)/T(OBS) ratios are much larger than unity. Exposures 7RA-7RB and 8RA-8RB are particularly illuminating in this regard in that 7RB and 8RB, corresponding to the bare tungsten surface after WSi_2 burn-off, yield ratios much more typical of the borides and graphites. As indicated earlier, SiC(E-14), Table 26, exhibited high values of T(CALC)/T(OBS).

Exposures (G-18)-23R and (G-18)-24R bracket failure conditions at a stagnation pressure near 0.25 atm. In this case, (G-18)-24R survived a full 30 minute time period characteristic of a hot gas/cold wall exposure at a heat flux of 653 BTU/ft^{2}sec and an enthalpy of 7460 BTU/lb. Raising the stream conditions slightly to 699 BTU/ft^{2}sec and 8180 BTU/lb results in coating failure.

The behavior of Sn-Al/Ta-10W(G-19) shown in Table 32 and Figures 7 and 238-246 compares HG/CW arc plasma test results with furnace data obtained under CG/HW conditions. In addition, post exposure photographs of all samples are presented along with "maximum severity survival" and "minimum failure conditions".

The behavior of Sn-Al/Ta-10W(G-19) indicates failure at temperatures above 3000°F in agreement with the results of CG/HW tests (4, 5). Examination of Table 32 shows that the subsonic exposures (G-19)-2M, 3M and 4M resulted in protection at surface temperatures up to 3000°F. In the last case illustrated in Figures 239 and 240, flux-enthalpy conditions at 350 BTU/ft^{2}sec and 2980 BTU/lb were not sufficient to degrade the coating in 1830 seconds. These conditions lead to a computed temperature, T_{CALC} = 4590°F, on the basis of Eqs 23-25. However, at slightly higher conditions of 390 BTU/ft^{2}sec and 2880 BTU/lb (exposure (G-19)-1M) shown in Figures 241 and 242 which correspond to T_{CALC} = 4640°F, complete degradation of the coating occurs. As in the case of WSi_2/W(G-18) and KT-SiC(E-14) the ratios of T(CALC)/T(OBS) are much larger than unity when the coating is retained. When the coating is eliminated (i.e., (G-18)-1M, 5M and 6R), the T(CALC)/T(OBS) ratios are closer to unity. Table 32 contains the values of total normal emittance for Sn-Al-Mo coated Ta-10W as determined from measurements of surface radiation as $\epsilon_N = 0.59$. Values of $\epsilon_N = 0.44$ and $\epsilon_N = 0.17$ were measured for Ta_2O_5 and liquid tantalum. These values will be discussed in Section II. D.

The results contained in Table 32 lead to the following characterization of survival and failure conditions for Sn-Al/Ta-10W (G-19):

PASS

No.	P_e (atm)	Mach No.	q_{cw} (BTU/ft^{2}sec)	i_e (BTU/lb)
9R	0.010	3.2	158	10,520
7R	0.050	3.2	355	7,100
4M	1.0	0.29	350	2,980

FAIL

No.	P_e (atm)	Mach No.	q_{cw} (BTU/ft^{2}sec)	i_e (BTU/lb)
8R	0.011	3.2	200	11,440
6R	0.063	3.2	504	8,740
1M	1.0	0.32	390	2,880

These results show the expected decrease in coating stability with decreasing pressure. Rovers exposures Sn-Al/Ta-10W(G-19)-9R and 8R shown in Figures 243-246 illustrate survival and failure under low pressure conditions.

17. W+Zr+Cu(G-20) and W+Ag(G-21)

Table 33 summarizes the tests conducted on the tungsten composites W+Zr+Cu(G-20) obtained from Rocketdyne (23) and W+Ag(G-21) obtained from Wah Chang. The latter material was only exposed at one atmosphere stagnation pressure. CG/HW tests were not performed for these materials. Reference to Table 33 shows that values of T(CALC)/ T(OBS) near 1.3 were obtained for these materials. This result is not surprising in view of the fact that the heat resisting mechanism involves vaporization of Cu or Ag. This behavior will be discussed further in Section II.D. Figures 7 and 247-260 show the recession in thirty minutes as a function of temperature for the current set of tests as well as post exposure photographs of all exposures and examples of "maximum severity survivals" and "minimum failure conditions".

Arc plasma tests have been reported for W+Zr+Cu (G-20) by Schwarzkopf (23) who observed a gross recession of 91 mils after a 720 second exposure at a stagnation pressure of 0.121 atmospheres, a stagnation enthalpy of 10,520 BTU/lb and a cold wall heat flux of 535 BTU/ft^{2}sec at Mach 3.2. One half inch diameter flat faced samples were employed in these tests (Reference 23, pages 62-63). Reference to Table 33 and Figure 252 show the results of a comparable exposure, W+Zr+Cu (G-20)-9R, run at a stagnation pressure of 0.1 atm, a stagnation enthalpy of 10,680 BTU/lb, and cold wall heat flux of 585 BTU/ft^{2}sec at Mach 3.2. A gross recession of 17 mils was observed after 775 seconds. Total recession of 22 mils was observed. Exposure (G-20)-7R was performed at 0.075 atm, 9,280 BTU/lb and 489 BTU/ft^{2}sec resulted in a gross recession of 28 mils and a total recession of 43 mils after 1800 seconds. However, when the conditions were increased to 0.135 atm, 11,980 BTU/lb and 662 BTU/ft^{2}sec melting was observed initially followed by oxidation. The gross recession was 253 mils and the total recession was 257 mils after an exposure time of 500 seconds as shown in Figure 254. In the Model 500 tests at one atmosphere stagnation pressure extremely rapid degradation was observed at much lower flux and enthalpy levels. Thus, W+Zr+Cu(G-20)-1M exhibited a recession of 147 mils after 157 seconds at 1.03 atm, 2970 BTU/lb and 315 BTU/ft^{2}sec. This behavior indicates that the mechanism of degradation is sensitive to pressure in the 0.1-1.0 atmosphere range. The precise nature of the degradation mechanism which is operative is not clear at present. Figures 247-251 illustrate the behavior at one atmosphere stagnation pressure.

The results obtained for W+AG(G-21) in the Model 500 tests at stagnation pressures of one atmosphere were comparable to the results for (G-20). Figures 256-260 illustrate the high rate of oxidation at one atmosphere.

18. Silica-Tungsten Composites SiO_2+68.5 w/o W(H-22) and SiO_2+60 w/o W(H-23)

The current results for SiO_2+68.5 w/o W(H-22) and SiO_2+60 w/o W(H-23) are shown in Tables 34 and 35 and in Figure 8.

Post exposure macrographs as well as "maximum severity survivals" and "minimum failure exposures" are shown in Figures 261-272. The behavior of these materials is quite similar. Figure 8 shows good correspondence between the CG/HW furnace tests and the HG/CW arc plasma tests. In particular, exposures at one atmosphere which achieved surface temperatures in excess of 4000°F all exhibit viscous flow. Higher oxidation rates are observed at lower pressure due to instability of SiO_2 relative to SiO (Section VI of Reference 4). All samples exposed in the Model 500 showed sting hole cracking. In addition, all samples which flowed and mushroomed during exposure increased in front face diameter and were exposed to lower effective flux levels. Microstructural features shown in Figure 270 illustrate depletion of tungsten particles from the surface of the one atmosphere tests. The low pressure exposures showed no tungsten depletion, sting hole cracking or viscous flow. Test SiO_2 + 68.5 w/o W(H-22)-4M in Figure 262 shows rapid recession at a surface temperature of 5205°F and one atmosphere. At a lower temperature (Test (H-22)-2M, Figure 263) the recession rate is much lower but sting leg oxidation is observed due to the lack of SiO_2 viscosity (see Section III. K of (5)). Figures 261 and 265 show tests (H-22)-10R and (H-22)-7R which illustrate the zones depleted of tungsten particles. The latter figure shows the SiO_2 zone (depleted of tungsten) actually separated and "peeled back" from the sample.

Reference to Table 35 shows that tests SiO_2+60 w/oW (H-23)-6M, 7M, 15M, 16M, 17M, 18M, 19M and 20 M which achieved surface temperatures in excess of 4000°F all exhibit viscous flow. Higher oxidation rates are observed at lower pressure due to instability of SiO_2 relative to SiO (Section VI of Reference 3). All samples exposed in the Model 500 showed sting hole cracking. In addition, all samples which flowed and mushroomed during exposure increased in front face diameter and were exposed to lower effective flux levels. Figures 267-270 show exposures SiO_2+60 w/oW (H-23)-2M and 15M. Figure 270 shows the zone depleted of tungsten particles. Figures 271 and 272 show Rovers exposures SiO_2+60 w/o W(H-23)-8R. The low pressure exposures showed no tungsten depletion, sting hole cracking or viscous flow.

The T(CALC)/T(OBS) ratios shown in Tables 34 and 35 indicate values of 1.10 for SiO_2+68.5 w/o W(H-22) and 1.25 for SiO_2 + 60 w/o W(H-23). These values will be discussed further in Section II. D. However, the former appears low, while the latter seems consistent with values obtained for other silicon bearing materials. It appears difficult to blame the small difference in tungsten content between (H-22) and (H-23) for the disparity in T(CALC)/T(OBS) ratios.

19. Hf-20Ta-2Mo(I-23)

The results obtained for Hf-20Ta-2Mo(I-23) are summarized in Tables 36, 37, 38, 46 and 47. Figure 8 compares the HG/CW test data with results obtained in CG/HW furnace tests. Photographs of all test samples after exposure and metallographic sections of selected samples are displayed in Figures 273-293. Reference to Tables 36-38 indicates that the ratio T(CALC)/T(OBS) for this refractory metal alloy is near 1.20 when

melting does not occur. This characteristic will be discussed in Section II. D. As shown in Tables 46 and 47, temperature gradients of 1500°R or more exist through 100 and 400 mil wall thicknesses of this material during oxidation. Measurement of these gradients has been discussed in Section II. B. 4 of Reference 3. Large gradients have also been observed in high velocity CG/HW tests (5).

Reference to Figure 8 shows that Hf-20Ta-2Mo(I-23) exhibits the same characteristics shown by the diborides $HfB_{2.1}$(A-2) and ZrB_2(A-3) where the rate of recession in the CG/HW furnace test exceeds that in the HG/CW arc plasma test at a given surface temperature. As indicated above, the source of this behavior are the temperature gradients and operation of the MOTEL criterion discussed in Section I. B. Indeed, the gradients are so severe that surface temperatures up to 5000°F are observed over long periods of time even though the alloy melts at 3860°F (Reference 2, page 5) in furnace tests. This behavior is indicated in 24M, 44R and 1MC shown in Tables 36 and 37. Reference to Figure 8 does not indicate any effect of stagnation pressure on oxidation rate in the 0.01-1.0 atmosphere range covered by these tests. This result is in keeping with earlier observations (24). Figures 274 and 275 show post exposure photographs of (I-23)-45M, 46M, 47R and 48R which were shrouded in ZrB_2+SiC+C(A-10) cylinders. Post exposure examination showed no interaction indicating compatibility between (I-23) and (A-10).

Figures 276 and 277 show the low recession observed for test (I-23)-1M at an observed temperature of 4030°F on the front face of the sample at the air/oxide interface. This temperature is 170°F above the melting point of 3860°F observed for samples of this alloy. This result is due to the occurrence of temperature gradients in the HG/CW tests. Exposure Hf-20Ta-2Mo(I-23)-14M at 605 BTU/ft^2sec and 3965 BTU/lb corresponding to a surface temperature of 4620°F melted in 30 seconds. By contrast, (I-23)-15M (shown in Figures 278 and 279) at 515 BTU/ft^2sec and 3735 BTU/lb exhibited a surface temperature of 4645°F and did not melt. Nonetheless, (I-23)-15M showed melting of the oxide but not of the metal. This would imply a temperature gradient of more than 700°F through the oxide. In contrast to (I-23)-15M, exposure (I-23)-1M at 530 BTU/ft^2sec and 3295 BTU/lb exhibited a surface temperature of 4030°F. ROVERS exposures Hf-20Ta-2Mo(I-23)-12R and 9R are shown in Figures 280-283. The former shows protective oxidation at 378 BTU/ft^2sec and 12,710 BTU/lb (surface temperature equals 3755°F). Surprisingly, (I-23)-9R at 337 BTU/ft^2sec and 11,250 BTU/lb (surface temperature equals 4220°F) showed signs of melting. This could be due to the formation of a very thin oxide at low pressure which was not an effective insulator.

Figures 284 and 285 show post exposure photographs of several (I-23) samples which were employed for measurements of internal temperature. Sample (I-23)-3MC shows the results of a burn-through after 1455 seconds. The time-temperature history of this exposure which is documented in Table 46 shows that the internal temperature reached 3800°F

(melting point equals 3860°F) at this point. Sample (I-23)-1MC is shown after sectioning in Figure 285. The tungsten sting is in place in this figure to illustrate the small contact area for conduction losses.

Figures 286-293 illustrate samples exposed to multiple cycles and in the hemispherical configuration after sectioning.

Test (I-23)-27M was exposed to seven cyclic exposures at a stagnation pressure of 1.05 atmospheres, a stagnation enthalpy of 3300 BTU/lb and a cold wall heat flux of 410 BTU/ft^{2}sec. The observed surface temperature was 4230°F and a recession of 138 mils was observed after an exposure of 11,600 seconds in cycles of 1800 second duration. This behavior is not quite as good as that exhibited by ZrB_2+20%SiC(A-8)-17M shown in Figure 83 or ZrB_2+SiC+C(A-10)-24M shown in Figure 109. These samples ran for longer times under more severe conditions than did (I-23)-27M and exhibited less recession. Nevertheless, Hf-20Ta-2Mo(I-23) is metallic and as such offers advantages as regards fabricability and resistance to thermal stress. On the other hand (A-8) and (A-10) possess higher strength and more temperature capability (6) than (I-23).

Figure 288 illustrates the results obtained with Hf-Ta-Mo (I-23)-28R after a 4 cycle exposure at a stagnation pressure of 0.132 atm., an enthalpy of 7600 BTU/lb and a cold wall heat flux of 398 BTU/ft^{2}sec. Total exposure time was 7220 seconds yielding a recession of 55 mils. As indicated above, boride composites shown in Figures 71, 91 and 111 exposed to more severe conditions in the ROVERS facility exhibited less recession. However, the behavior of Hf-Ta-Mo(I-23)-28R is outstanding for a metallic structure.

The earlier discussions of cyclic boride exposures presented in Sections II.B.5, 6 and 8 made note of the fact that the temperature increased from one cycle to the next. Reference to Tables 37 and 38 indicates that although tests (I-23)-27M exhibited an increase in surface temperature during the first two cycles, the temperature was relatively stable from cycle III to cycle VII with T(CALC)/T(OBS) ratios near 1.08. Surface temperature held steady during cyclic exposure of (I-23)-28R with T(CALC)/T(OBS) ratios near 1.27.

Figures 290-293 show the results obtained with hemispherical capped samples of (I-23)-38MH and 39RH. Reference to Tables 37 and 38 show that T(CALC)/T(OBS) for these tests were 1.12 and 1.44, respectively. Although the latter value is higher than the typical ratios observed for this material (1.20) the former value is lower. In any case, the magnitude of temperature reduction observed with hemispherical caps is smaller than observed for (A-8), (A-8) and (A-10) (c.f., (A-7)-36MH, Table 6; (A-7)-48RH, Table 8; (A-10)-35MH, Table 13; and (A-10)-46RH, Table 14).

20. Iridium Coated Poco Graphite Ir/C (I-24)

Iridium coated Poco graphite samples furnished by Battelle Memorial Institute (25) were tested in the Model 500 and Rovers facilities. In view of the high cost of these samples an attempt was made to use them for several runs and to avoid sectioning (thus destroying the sample) where possible. Accordingly, techniques were employed for nondestructively measuring coating thickness (Reference (1), pages 7, 8, 24 and 25). Most of the coatings were of the order of 20 mils thick based on the NDT results and the observations made on sectioned samples. The sample numbers supplied by Battelle were retained in order to permit cross referencing with the fabrication report (25). In addition to the samples of Ir/C(I-24) listed in Reference (1), Battelle supplied two cylinders of iridium coated graphite in which an Iridium-50 v/o HfO_2 coating was applied to improve the oxidation resistance. Photographs of these samples are shown on page 101 of Reference (25). Fabrication is discussed on page 89 of Reference (25). In accordance with the Battelle designation, these samples are numbered Ir/C(I-24)-36 and 37.

The results obtained in arc plasma testing of Ir/C(I-24) are summarized in Table 39. Figure 8 shows the temperature dependence of the oxidation behavior, while Figures 294-301 display post exposure photographs of all test samples and sections through a failure and a survival. In line with the CG/HW tests reported earlier (4), iridium exhibits very low oxidation rates up to its melting temperature at 4430°F. The temperature of the iridium-carbon eutectic (4) is 4175°F. Reference to Figure 8 shows that samples exposed to higher conditions exhibited melting of the coating and ablation of the graphite. The major drawback of this coating system is the low emittance of the iridium (ϵ = 0.30). However, addition of HfO_2 raised the emittance to values near 0.50 and extended the range of conditions under which the coating can be used. Thus, examination of Table 39 shows that the pure coating is destroyed at flux levels in excess of 310 BTU/ft^{2}sec. At flux levels below 300 BTU/ft^{2}sec the coating is hardly affected; however at higher levels, melting followed by rapid ablation occurs.

However, when HfO_2 is added to increase the emittance, failure does not occur until the flux level reaches 510 BTU/ft^{2}sec (i.e., see tests 36MRA and 36MRB).

In summary, although Ir/C(I-24) has excellent temperature capability to temperatures near 4200°F, it has very low resistance to stream conditions. In fact (6), if heat flux/enthalpy characteristics are used as a yardstick, Ir/C(I-24) ranks below Si/RVC(B-8), described in Table 19, even though the latter has a temperature limit near 3200°F. The difference is caused by the fact that (B-8) has a higher emittance than (I-24), 0.69 vs. 0.36, and a higher T(CALC)/T(OBS) ratio, 1.36 vs. 1.21. These factors will be discussed in further detail in Section II. D.

C. Results of Temperature Gradient Measurements

As indicated above, temperature gradients have been measured through 100 and 400 mil walls of ZrB_2(A-3), $HfB_{2.1}$+20%SiC(A-7), ZrB_2+20%SiC(A-8), ZrB_2+SiC+C(A-10), RVA(B-5), WSi_2/W(G-18) and Hf-20Ta-2Mo(I-23). Tables 40-47 detail the time-temperature histories obtained in these tests. Figures 302-312 show the time-temperature data graphically. Calculations of the temperature gradients through the test cylinders described by Figures 302-312 are presented in Section VII of Reference (6). These calculations are based on side losses due to radiation and conduction down the length of the model but no heat loss via conduction. Thus, the model employed implies a modification of Eqs. (2) and (3) to reflect side losses.

The materials chosen for examination actually cover a wide range of characteristics. Thus RVA(B-5) represents an ablator with no coating. On the other hand WSi_2/W(G-18) provides an alternative situation where the bulk thermal conductivity is nearly three times that of RVA(B-5) at the temperature of interest. However, WSi_2/W(G-18) has a 5 mil WSi_2 coating which has a thermal conductivity approximately one third that of RVA(B-5). The remaining materials, (A-3), (A-7), (A-8), (A-10) and (I-23) have bulk thermal conductivities ranging between 0.5 to 0.8 that of tungsten. However, they all form oxide coatings which have very low thermal conductivities. Thus, the coating which forms on ZrB_2 (A-3), which is quite flakey, is estimated to have a thermal conductivity of 10^{-4} BTU/ft sec°R or 65 times less than RVA(B-5).

The thermal conductivity of the oxides formed on (A-7), (A-8), (A-10) and (I-23), which are more adherent, was estimated to be five times larger than the oxide formed on (A-3).

Examination of Figures 302-312 shows that with few exceptions, the internal temperatures remain fairly constant over long periods of time. The exceptions are cases in which fairly rapid degradation is occurring. Thus, the principal exception is test (I-23)-3MC discussed earlier in Section II.B.18 where the melting point was achieved at 1455 seconds. As a consequence, comparison of the computed values, which are based on a steady state condition, with the observed temperatures appears justified. This description is contained in Tables 23-28 of Reference (6) which compare the observed internal temperatures with calculated values for ZrB_2+SiC(A-8), ZrB_2(A-3), HfB_2+SiC(A-7), RVA(B-5), ZrB_2+SiC+C(A-10), WSi_2/W(G-18) and Hf-Ta-Mo(I-23). Data include measured front face and internal temperatures, T_f and T_d, the cold wall heat flux, q, the stagnation enthalpy, i_e, and the stagnation pressure, P_e. In addition, these tables show the radius, R, length, L, and oxide coating thickness, I. The latter was equated to the conversion depth for the oxide formers. For WSi_2/W, I was equated to the WSi_2 coating thickness and I=0 for RVA(B-5) graphite which ablates without coating formation. Values of the emittance, ϵ_S (see Section II.D) as well as suitable values of the thermal conductivities characteristic of each material for the coating k_F and the substrate k_S are also shown in Tables 23-28 of Reference (6).

The computed results are displayed in terms of the ratio of calculated front face temperature to observed front face temperature T_f(CALC)/T_f(OBS) and the ratio of computed in-depth temperature T_d(CALC) to computed front face temperature T_f(CALC). If the agreement is exact (e.g., Hf-Ta-Mo(I-23)-43R in Figure 311), the ratio of T_f(CALC)/T_f(OBS) would be 1.00. In the example, T_f(CALC) is 4440°R vs. 4530°R = T_f(OBS). Similarly the measured temperature at 109 mils is 3560°R vs. T_d(CALC) = 3380°R. In this case, the observed gradient is 960°R while the calculated gradient is 1060°R in 109 mils.

All of the runs shown in Tables 41-47 were performed on flat faced cylinders except those designated by a suffix H (hemisphere) or S (cylindrical shroud with a 200 mil wall). Photographs of these models have been presented. The shrouds and hemispherical caps did not alter the gradients observed for flat faced cylinders. Thus, all of the calculations were based on flat faced cylinders ignoring the hemispherical caps and the shrouds. Reference to Tables 23-28 of Reference (6) indicates relatively good agreement between calculation and observation, in view of the simple model employed and the complexities of the experiments.

The largest deviations occur at low surface temperatures (i.e., T_f < 3300°R) for the materials which form SiO_2 as an oxidation product. Thus, in cases where samples of HfB_2+SiC(A-7), ZrB_2+SiC(A-8), ZrB_2+SiC+C(A-10) or WSi_2/W(G-18) were exposed with shrouds or as large diameter hemispheres T_f (CALC) is considerably larger than T_f(OBS). However, this difference is smaller than obtained when T_f is computed on the basis of radiation equilibrium. The cause of this behavior is presently unknown (6). Reference to Tables 23-28 of Reference (6) shows that the calculated and observed ratios of T_d/T_f are in general agreement.

D. Average Values of Normal Total Emittance and T(CALC)/T(OBS) Ratios for the Candidate Materials

Tables 2-39 contain values of the radiated heat flux, q_r, observed during the arc plasma exposures. These values are employed to compute total normal emittance on the basis of Eq. 1. The resultant values are contained in Tables 2-39 along side each exposure. As noted earlier (3), the surface temperature which appears in Tables 2-39 and in Eq. 1 is measured optically (at λ = 0.65μ) and converted to a true temperature by employing specific values of the normal spectral emittance at λ = 0.65μ (5).

In addition to the measurements presented in Tables 2-39, two-color pyrometer measurements were performed during the course of exposures HfB_2+SiC(A-4)-2M, PG(B-6)-9M, BPG(B-7)-6M, JTA(D-13)-2M, HfB_2+35%SiC(A-9)-6M and Si RVC(B-8)-13M. The results were combined with the brightness temperatures in order to obtain spectral emittance values at λ = 0.65μ. The results were found to agree reasonably with the current values assumed for ϵ_N at λ = 0.65, (3, 5).

Table 48 summarizes the average of all the ϵ_N results for each material. Tests conducted on flat faced cylinders without shrouds were employed exclusively in taking the averages. Separate averaged ϵ_N values are presented for conditions where melting was observed and conditions whwere a coated surface was removed. Most of the results for the solid oxidized surfaces are between 0.6 ± 0.2. Lower values are obtained for those cases where melting occurs (i.e., $\epsilon_N = 0.32$ for tungsten (WSi_2/W) (G-18)).

In view of the relatively low values of ϵ_N observed for 0.500 inch diameter graphite samples, a series of exposures were performed employing samples which were 0.740 inch in diameter. In the latter case, the image fills a larger fraction of the Eppley thermopile viewing area (3). As shown in Table 16, larger values of ϵ_N were observed with the larger diameter samples. Similar experiments performed with ZrB_2 (A-3) and Hf-20Ta-2Mo(I-23) where solid oxides form (Tables 3 and 36) did not show this behavior. For such cases, difference in ϵ_N are not anticipated since changes in diameter are not encountered during exposure.

Table 48 summarizes averaged ratios of T(CALC)/T(OBS) derived on the basis of Eqs. 2 and 3 and the stream conditions and surface temperatures contained in Tables 2-39. Ideally, if radiation equilibria were the dominant factor and all measurements were accurate, these ratios should be unity. Although there are departures, it is satisfying to note that the differences are small compared to those obtained by considering the results of other studies (i.e., Figures 16-21 of Reference (6)). Reference to Table 48 shows that ratios of T(CALC)/T(OBS) are lower for cases where melting is observed than for cases where a solid oxide (or coating) is present. Moreover, Table 48 shows that large values of T(CALC)/T(OBS) are characteristic for some of the materials. The occurrence of ratios which are larger than unity implies resistance to energy absorption by the material. Thus, exposure of HfB_2+SiC(A-4) and HfC+C(C-11) to identical stream conditions (i.e., stagnation pressure, enthalpy and cold wall heat flux) would result in an observed surface temperature for the former which is 1.10/1.22 = 0.90, or 11% lower than the surface temperature reached by HfC+C(C-11). This conclusion would apply if stream conditions were not sufficient to produce melting of HfB_2 + SiC(A-4). At lower levels, KT-SiC(E-14), WSi_2/W(G-18) and Sn-Al/Ta-10W(G-19), which exhibit T(CALC)/T(OBS) ratios of 1.43, 1.54 and 1.41, respectively, demonstrate similar resistance to energy transfer. Although the origin of this resistance is not clear at present, it is probably due to blocking effects caused by evolution of gaseous oxides. These observations suggest a method of ranking the behavior of the refractory materials which differs from the present recession vs. temperature curves (Figures 1-8). In Reference (6), an alternative method of presentation which compares recession rate as a function of heat flux and enthalpy for the candidate materials is considered. This method does not require a knowledge of the spectral or the normal emittance and integrates the blocking effects characteristic of each material.

E. Summary

Present results for $HfB_{2.1}$(A-2) and ZrB_2(A-3) in the HG/CW arc plasma tests show a marked difference between the recession rates at a given surface temperature and those observed at the same surface temperature in furnace tests (4). As shown in Figure 1, an oxidation depth of 20 mils in 30 minutes is obtained in an arc plasma test at $5000^{\circ}F$ while the same oxidation depth can be produced at $3500^{\circ}F$ in a furnace test. Alternatively a 100 mil oxidation depth is observed in a furnace test at $4000^{\circ}F$ after 30 minutes while comparable oxidation depths are not obtained in arc plasma tests below $5500^{\circ}F$. The source of this difference is the temperature gradient through the oxide as indicated in Section I.B. Thus, oxidation occurs slowly until temperatures are high enough to cause melting of the boride. The excellent long-time oxidation resistance of this material at $4000^{\circ}F$ is illustrated in Figures 40 and 41.

Cyclic exposures of ZrB_2(A-3) and $HfB_{2.1}$(A-2) were performed to assess the effects of heating and cooling in three 600-second cycles. At the lowest level ZrB_2(A-3) exhibited a recession equivalent to that observed in an 1800 second test. At higher levels ZrB_2(A-3) exhibited larger recessions for cyclic exposures than in the case of uninterrupted 1800 second tests. By contrast, the cyclic tests performed on HfB_2 did not result in larger recessions than the uninterrupted tests. Motion picture coverage indicated that the oxide formed on $HfB_{2.1}$(A-2) exhibited greater tenacity under these conditions than did the oxide formed on ZrB_2(A-3). The latter flaked off between cycles. As indicated in Section II.B.1, preoxidation of HfB_2(A-2) to form a 10 mil coating did not result in noticeable changes in behavior.

Reference to Table 3 shows that the ZrB_2(A-3) material employed in these tests did not exhibit any thermal stress failures at flux levels as high at 950 BTU/ft^2sec. In contrast to the $HfB_{2.1}$(A-2) material discussed in Section II.B.1, the (A-3) material was mechanically sound and did not exhibit the flaws shown by the (A-2) in the nondestructive tests prior to exposure (see Sections IV.B, C and Tables 15, 16 of Reference 1). However, Boride Z(A-5) was found to be very susceptible to thermal shock failure. Figures 59a and 59b show Boride Z(A-5)-4M and 8R which exhibit thermal shock cracks after exposure at 348 BTU/ft^2sec and 3215 BTU/lb and 262 BTU/ft^2sec and 9200 BTU/lb, respectively. Thus, flux levels above 200-250 BTU/ft^2sec appear to result in thermal shock failures of Boride Z.

Boride composites HfB_2+20%SiC(A-4) and (A-7), ZrB_2+20% SiC(A-8) and HfB_2+35%SiC(A-9) were found to exhibit remarkable oxidation and thermal stress resistance in HG/CW arc plasma tests. Although these materials display temperature gradients in the oxides, the difference between the arc plasma and furnace oxidation depths are small (Figure 2). This finding is in contrast to the results obtained for $HfB_{2.1}$(A-2) and ZrB_2(A-3) shown in Figure 1. The adherent oxide which forms on these composites results in low recessions observed after

exposures in the 3500°-4500°F temperature range. In addition, (A-4) exhibited no thermal shock failures at flux levels up to 1000 BTU/ft²sec. Radiation equilibrium calculations performed for exposures of these materials showed that the ratio T(CALC)/T(OBS) for (A-2), (A-3) and (A-4) exceed unity. Thus, the observed temperature was 16% lower than expected for (A-2), 9% lower than expected for (A-3) and 22% lower than expected (based on radiation equilibrium) for (A-4). Similarly, the other boride composites containing SiC, i.e., HfB_2+20%SiC(A-7), ZrB_2+20%SiC(A-8) and HfB_2+35%SiC(A-9) yielded ratios of 1.25, 1.34 and 1.17. Moreover, exposure of hemispherical models exhibited lower surface temperatures than those observed for flat faced cylinders.

Figures 71 and 72 show metallographic sections of (A-7)-28R exposed for thirteen cycles (each of 1800 second duration) at a stagnation pressure of 0.07 atm, an average heat flux of 495 BTU/ft²sec and an enthalpy near 10,300 BTU/lb. Reference to Table 7 and Figure 71 show that the total recession after the thirteen cycle exposure was 15 mils. This behavior is unrivaled by any other known material system.

Figures 73 and 74 show post exposure sections through (A-7)-52M after 14,030 seconds exposure in eight 1800-second cycles at a stagnation pressure of 1.03 atmospheres. The average cold wall heat flux was 450 BTU/ft²sec at an enthalpy level of 4180 BTU/lb. Total recession was 329 mils or about 0.33 inches. Under similar conditions graphite and tungsten would exhibit recessions of 14 to 28 inches. ZrB_2+20%SiC(A-8) displays all of the same features shown by HfB_2+SiC(A-7) although it is not as refractory as its hafnium base counterpart. However, the decrease in temperature resistance is compensated for by the reduced density and cost. Zirconium diboride is roughly one half the density and one tenth the price of hafnium diboride. A few tests of (A-8) were shrouded and it is interesting to note the results of (A-8)-29M in which a graphite shroud was employed (Tables 9 and 42). Although the boride exhibited minimal recession (8 mils in 1800 seconds) the graphite shroud which was one inch long ablated completely in 500 seconds.

Table 15 and Figure 1 show the depletion depths for ZrB_2+SiC(A-8) as a function of temperature. This material exhibited the lowest SiC depletion rate of all the boride composites. In addition, the depletion rate in the current HG/CW arc plasma tests were observed to be less than depletion rates in CG/HW furnace tests at comparable surface temperatures.

Measurements of the temperature gradients through oxide coatings formed on ZrB_2+SiC(A-8) yielded results which are smaller than exhibited by ZrB_2(A-3). This finding appears to be due to the higher thermal conductivity of the oxide formed on (A-8) (as compared with (A-3)) (6). Consideration of Tables 9 and 10 shows that ZrB_2+SiC (A-8) exhibits the same tendency to develop low temperatures as (A-4) and (A-7). Thus, tests in the ROVERS facility at flux levels below 500 BTU/ft²sec and in the Model 500 facility at flux levels below

350 BTU/ft^{2}sec develop ratios of T(CALC)/T(OBS) which are of the order of 1.50. This feature of the boride composites which contain SiC permits a wider range of applicability than materials which exhibit (T(CALC)/T(OBS)) near unity.

The behavior of HfB_2+35%SiC(A-9) was found to be similar to (A-4) and (A-7) as regards the T(CALC)/T(OBS) comparison, recession rate vs. temperature for HG/CW arc plasma tests and furnace exposures, depletion depth vs. temperature in HG/CW tests as a function of temperature, etc. The major difference is that (A-9) is less refractory than (A-4) and (A-7).

Recession rates observed for graphites in HG/CW arc plasma tests are substantially higher than those observed in CG/HW furnace tests at 1-9 ft/sec air flow rate (4). This indicates that the latter are supply limited. As indicated earlier (5), the results of high velocity CG/HW tests on graphite at air flow rates near 250 ft/sec approach the results obtained in the arc plasma exposures. Modest temperature gradients were measured through graphite samples during HG/CW tests. Limiting survival conditions for Si/RVC(B-8) determined under HG/CW conditions depart from the behavior in furnace tests and correspond to the failure characteristics observed for silicon carbide in HG/CW tests. In the arc plasma tests, Si/RVC (B-8) exhibits protective oxidation up to surface temperatures near 3800°F, some 700°F above the failure temperature in furnace tests. Graphite-type behavior occurs above this temperature. At one atmosphere stagnation pressure, coating burn-off occurs after 735 seconds at 470 BTU/ft^{2}sec and 3720 BTU/lb. At a stagnation pressure of 0.01 atmospheres protective behavior was observed in a 30 minute exposure at 210 BTU/ft^{2}sec and 8850 BTU/lb.

The recession rates of all of the graphites are inversely proportional to material density. Glassy Carbon (B-11) appeared to melt during exposure. No post exposure examination could be made since the sample was completely destroyed. Since glassy carbon is not reported to melt at one atmosphere, the only explanation of such an observation must be made on the basis of surface contamination of the sample by tungsten or copper (from the arc electrodes) and melting of the alloy. This conclusion is based on the findings at Lockheed (5).

Hypereutectic carbides HfC+C(C-11) and ZrC+C(C-12) exhibited excellent oxidation resistance at surface temperatures below 5000°F and melted under very high temperature conditions in line with reported melting points. The present results are consistent with the eutectic temperatures but show little dependence on the melting point of the oxides. Current data indicate comparable oxidation rates in the CG/HW and HG/CW tests. No thermal shock failures were noted at flux levels up to 750 BTU/ft^{2}sec. In line with the oxidation behavior noted in furnace tests, the HG/CW arc plasma tests show a "puffy" oxide which forms at the lower temperatures investigated. This oxide has been noted in air oxidation tests

performed in furnaces below 3400°F (4). Rapid oxidation occurs at the back of samples where the surface temperature is lower than at the front face. This is another characteristic of the HfC+C(C-11) oxidation which is in line with the furnace test results (4). The oxidation behavior of samples containing 13.6 w/oC does not appear to differ materially from samples fabricated from the billets which contain 14.0 to 15.6 w/o carbon. The behavior of ZrC+C(C-12) in the HG/CW arc plasma tests was found to be similar to that of HfC+C(C-11).

KT-SiC(E-14) exhibited rapid recession rates at surface temperatures above 3900°F. This is some 400°F above the limit observed in furnace tests and in line with the results obtained for Si/RVC (B-8).

Composites of borides, carbides and graphites including ZrB_2+SiC+C(A-10), JTA(C-ZrB_2-SiC)(D-13), JT0992(C-HfC-SiC)(F-15) and JT0981(C-ZrC-SiC)(F-16) exhibited HG/CW test results which were comparable to their CG/HW behavior. At elevated temperatures, destruction of the protective oxide coating leads to graphite-type recession behavior. ZrB_2+SiC+C(A-10) exhibits the best oxidation resistance in this group owing the fact that it contains the largest percentage of boride. In addition, it exhibits lower recession rates in the HG/CW tests than in the CG/HW tests as is the case for ZrB_2(A-3). Melting of ZrB_2+SiC+C(A-10) is encountered near 5000°F where substantial differences between low pressure and one atmosphere oxidation rates are observed. Thermal shock failures were not observed at flux levels up to 1010 BTU/ft^{2}sec. The low density (4.5 gms/cm^3), high strength, low modulus and good machinability exhibited by this composite, when coupled with its oxidation resistance up to 5000°F, offer an exceptional combination of properties.

In general, the behavior of the (A-10) composite is quite similar to that exhibited by (A-4), (A-7) and (A-8) discussed earlier in Sections II.B-3, 5 and 6. However, (A-10) is not as refractory as (A-4) and (A-7). However, the lower density and cost as well as the thermal stress resistance and machining characteristics of this composite provide compensating advantages. Figures 109-112 show sections through (A-10)-24M and (A-10)-26R after exposure for times up to 21,600 seconds near 4500°F with total recessions of the order of 100 mils. This behavior, which was discussed in Section I.B shows striking evidence for the applicability of this material in reusable lifting reentry spacecraft.

Exposures of hemispherical models of (A-10) indicate that the observed temperature was 60% lower than expected. This behavior (noted earlier with (A-7) and (A-8) in Sections II.B.4 and II.B.6), characterized by lower temperatures achieved with hemispherical models than with flat faced models is not understood at present. Nevertheless, the practical implications of this finding are substantial. For example, (A-10)-25R, 26R, 40R and 41R (which were flat faced models) exposed at conditions similar to (A-10)-37R and 38R (i.e., 500 BTU/ft^{2}sec, 7700 BTU/lb, 0.15 atm) exhibited temperatures near 5000°R in contrast to (A-10)-37R and 38R which exhibited temperatures near 3700°R. Naturally the hemispherical models exhibited lower recession rates. Sample (A-10)-37RH is shown after sectioning in Figures 113 and 114.

Similarly, sample (A-10)-48RH was exposed to four exposures at ascending flux levels until evidence of melting was noted. Melting of this hemispherical capped model was not observed to occur until fluxes near 850 BTU/ft^{2}sec were attained. Flat faced models melted near 650 BTU/ft^{2}sec.

Figures 194 and 195 show sample (D-13)-48MX after 4 cyclic exposures at a stagnation enthalpy of 4350 BTU/lb, stagnation pressure of 1.01 atm and a cold wall heat flux of 380 BTU/ft^{2}sec. Each exposure was 1800 seconds long making the total exposure time 7200 seconds. The average recession was 118 mils. This test can be compared with (A-10)-24 shown in Figure 109 which exhibited a recession of 104 mils after 12 cycles (1800 seconds each) totalling 21,600 seconds under comparable conditions.

Figures 196 and 197 show sample (D-13)-49RX after 4 cyclic exposures at a stagnation pressure of 0.57 atmospheres at a stagnation enthalpy of 9600 BTU/lb and a cold wall heat flux of 440 BTU/ft^{2}sec. Each exposure was 1800 seconds long making the total exposure time 7200 seconds. Total recession for this test was 45 mils. By comparison, (A-10)-26R exposed for 18,951 seconds at comparable heat flux and enthalpy and a higher pressure (0.238 atm) exhibited a recession of 83 mils as shown in Figure 111.

As indicated in Reference (3) extensive precautions have been taken in order to insure that temperature measurements of the model surface are accurate. In general, the comparison of observed surface temperatures in HG/CW arc plasma tests with values calculated from stream conditions are in relatively good agreement. Moreover, a number of temperature measurements employing two color pyrometers yielded good results (page 8 of Reference (3)). In order to obtain additional verification of the surface temperature measurements, the melting points of tungsten and molybdenum were measured in the arc facilities using pure nitrogen streams for comparison with accepted values. The results of these tests are shown in Table 29 and in Figure 230. The relative good agreement obtained in these tests should eliminate concern over the accuracy of surface temperature measurements due to interference of the arc with optical observations.

A substantial number of thermal shock failures of JTA(D-13) and JT0981(F-16) have been observed. For JTA(D-13), these failures occurred in random fashion at flux levels above 500 BTU/ft^{2}sec. The samples which failed by thermal shock were machined from 2-1/2" diameter x 2" long billets of JTA(D-13) in an orientation which corresponded to the hot pressing direction. Thus, the axis of the arc plasma test sample was parallel to that of the hot pressed cylinder. Under these conditions, residual strain present in the billets and in the samples could provide a source of the failures. However, a series of samples oriented with their axes prependicular to the pressing

direction showed no thermal shock failures at flux levels in excess of 500 BTU/ft^{2}sec. This finding has particular relevance to applications in which JTA(D-13) parts are exposed to severe environmental heat fluxes. JT0992(F-15) did not exhibit sensitivity to thermal shock.

The behavior of these composites is characterized by low recession rates at temperatures between 3000°F and 4500°F, best illuatrated in ZrB_2+SiC+C(A-10) and JT0992(F-15) at temperatures up to 4500°F. Above 5000°F, the protection afforded by formation of ZrO_2 (or HfO_2) and SiO_2 is eliminated and oxidation rates which are characteristic of graphite are encountered.

Failure limits for the coated refractory metals WSi_2/W (G-18) and Sn-Al/Ta-10W(G-19) have been established in general agreement with furnace tests. Maximum survival conditions for WSi_2/W (G-18) are 450 BTU/ft^{2}sec and 3100 BTU/lb at P_e = 1 atm. At lower pressures, failure was observed at 458 BTU/ft^{2}sec and 11,420 BTU/lb. Coating failure conditions were established for Sn-Al/Ta-10W(G-19) at lower flux and enthalpy levels. Modest temperature gradients were measured through WSi_2/W(G-18) arc plasma test samples.

Current results for W+Zr+Cu(G-20) indicate relatively good resistance to oxidation at 10,000 BTU/lb and 500 BTU/ft^{2}sec at 0.100 atm in agreement with the findings of Schwarzkopf (5). However, in the Model 500 tests at 1 atmosphere stagnation pressure, very rapid degradation was observed at much lower flux and enthalpy levels. Thus W + Zr+Cu(G-20)-1M exhibited a recession of 147 mils after 157 seconds at 1.03 atm, 2970 BTU/lb and 315 BTU/ft^{2}sec. This behavior indicates that the mechanism of degradation is sensitive to pressure in the 0.1-1.0 atmosphere range. The precise nature of the degradation mechanism which is operative is not clear at present. The results obtained for W+Ag(G-21) in the Model 500 tests at stagnation pressures of one atmosphere were comparable to the results for (G-20).

The silica-tungsten composites SiO_2+68.5 w/o W(H-22) and SiO_2+60 w/oW (H-23) exhibited similar recession behavior in the one atmosphere HG/CW arc plasma tests as encountered in the CG/HW furnace tests. At low pressures, higher recession rates were observed due to instability of SiO_2 relative to SiO. At temperatures above 4000°F, extensive flow of this composite was observed, in agreement with the furnace test findings. Samples exposed at one atmosphere showed sting hole cracking.

Arc plasma exposures of Hf-20Ta-2Mo(I-23) exhibited lower oxidation rates than in the CG/HW tests at comparable surface temperatures. In addition, several samples with indicated surface temperatures in excess of the melting point of the alloy did not melt. Current results indicate that gradients of 1500°F can exist through 100 mils of alloy and

oxide. This behavior is the basis for the surface temperature in the 4000°-5000°F range which were not accompanied by melting of the alloy.

Test (I-23)-27M was exposed to seven cyclic exposures at a stagnation pressure of 1.05 atmospheres, a stagnation enthalpy of 3300 BTU/lb and a cold wall heat flux of 410 BTU/ft^{2}sec. The observed surface temperature was 4230°F and a recession of 138 mils was observed after an exposure of 11,600 seconds in cycles of 1800 second duration. This behavior is not quite as good as that exhibited by ZrB_2+20%SiC (A-8)-17M shown in Figure 83 or ZrB_2+SiC+C(A-10)-24M shown in Figure 109. These samples ran for longer times under more severe conditions than did (I-23)-27M and exhibited less recession. Nevertheless, Hf-20Ta-2Mo(I-23) is metallic and as such offers advantages as regards fabricability and resistance to thermal stress. On the other hand (A-8) and (A-10) possess higher strength and more temperature capability (6) than (I-23).

Figure 288 illustrates the results obtained with Hf-Ta-Mo (I-23)-28R after a 4 cycle exposure at a stagnation pressure of 0.132 atm, an enthalpy of 7600 BTU/lb and a cold wall heat flux of 398 BTU/ft^{2}sec. Total exposure time was 7220 seconds yielding a recession of 55 mils. As indicated above, boride composites shown in Figures 71, 91 and 111 exposed to more severe conditions in the ROVERS facility exhibited less recession. However, the behavior of Hf-Ta-Mo(I-23)-38R is outstanding for a metallic structure.

Present results for Ir/C(I-24) are in general agreement with the CG/HW tests (4), which showed that iridium exhibits very low oxidation rates up to its melting temperature at 4430°F. The temperature of the iridium-carbon eutectic is 4175°F. Reference to Figure 8 shows that samples exposed to higher conditions exhibited melting of the coating and ablation of the graphite. The major drawback of this coating system is the low emittance of the iridium (ϵ = 0.30). However, addition of HfO_2 raised the emittance to values near 0.50 and extended the range of conditions under which the coating can be used. Thus, examination of Table 39 shows that the pure coating is destroyed at flux levels in excess of 310 BTU/ft^{2}sec. At flux levels below 300 BTU/ft^{2}sec the coating is hardly affected. However, at higher levels melting followed by rapid ablation occurs.

In contrast, when HfO_2 is added to increase the emittance, failure does not occur until the flux level reaches 510 BTU/ft^{2}sec (i.e., Table 39 - 36MRA and 36MRB). Thus, although Ir/C(I-24) has excellent temperature capability to temperatures near 4200°F, it has very low resistance to stream conditions. In fact (6), if heat flux/enthalpy characteristics are used as a yardstick, Ir/C(I-24) ranks below Si/RVC (B-8), described in Table 19, even though the latter has a temperature limit near 3200°F. The difference is caused by the fact that (B-8) has a higher emittance than (I-24), 0.69 vs. 0.36, and a higher T(CALC)/T(OBS) ratio, 1.36 vs. 1.21.

Temperature gradients have been measured through 100 and 400 mil walls of ZrB_2(A 3), $HfB_{2.1}$+20%SiC(A-7), ZrB_2+20% SiC(A-8), ZrB_2+SiC+C(A-10), RVA(B-5), WSi_2/W(G-18) and Hf-20Ta-2Mo(I-23). Tables 40-47 detail the time-temperature histories obtained in these tests. Figures 302-312 show the time-temperature data graphically. Calculations of the temperature gradients through the test cylinders described by Figures 302-312 are presented in Section VII of Reference (6). These calculations are based on side losses due to radiation and conduction down the length of the model but no heat loss via conduction. In general, relatively good agreement between observed and calculated temperature gradients has been obtained in view of the simple model employed.

Measurements of total normal emittance have been provided for all of the candidate materials based on radiated heat flux observations during HG/CW exposures. Averaged values obtained for solid oxides formed during exposure are higher than normal emittance values observed for melting surfaces. Comparison of calculated surface temperatures based on stream conditions with those observed yields relatively good results. However, systematic differences worthy of note have been observed. Calculated temperatures are quite close to those observed when melting occurs, but when solid coatings are present, actual temperatures are below values computed from stream conditions and the assumption of radiation equilibrium. Moreover, materials containing silicon carbide achieve lower surface temperatures during exposure than predicted on the basis of stream conditions. As a consequence, the overall behavior of these materials under HG/CW conditions appears to be better than under CG/HW furnace test conditions.

The present results illustrate the difference between solid oxide formers and graphites. The latter group exhibit increasing oxidation rates with increasing pressure while the former show little pressure effect. When the solid oxide formers are exposed to stream conditions at one atm, which result in surface temperatures below their melting points, they exhibit recession rates 100 to 1000 times less than graphites do under comparable conditions. Coated metals and silicon carbide degrade at temperatures comparable to those observed in CG/HW furnace tests. These limits are due to melting or rapid vaporization. However, at a given surface temperature, the solid oxide formers exhibit much lower recession rates under HG/CW arc plasma test conditions than in a CG/HW air oxidation furnace test. This may be due to large temperature gradients across the oxide which occur in the HG/CW tests. Conversely, graphites exhibit higher recession rates in the HG/CW arc plasma tests than in the CG/HW furnace tests due to artificial oxygen supply limits imposed by the air flow limitations of the latter tests.

III. RESULTS OF HG/CW ARC PLASMA SPLASH TESTS IN THE AVCO TEN MEGAWATT FACILITY

A limited number of tests were conducted early in the program to establish thermal stress failure thresholds at low enthalpy levels. Although this phenomena is quite complex, the tests were conducted in order to determine flux thresholds for shock failure for cylinders of borides and boride composites with different diameters. Subsequent results obtained for hemispherical caps (vs. flat faced cylinders) which are reported in Section IIB indicate that these thresholds will depend upon sample shape as well as sample diameter. Descriptions of the facilities, techniques and samples employed in these tests have been presented in Sections IID-1 and IID-2 of reference (3) and Section VIE of reference (1).

A. Results of Ten Megawatt Arc Exposures

1. Calculation of Transient Thermal Gradients in Boride Cylinders

Since the present series of exposures were of relatively short duration (maximum of twenty seconds) a series of one dimensional heat transfer calculations were performed for hafnium diboride and zirconium diboride in order to compute the transient thermal gradients through the cylinders. The values of density, ρ, specific heat, c_p, and thermal conductivity, k, employed in these calculations are shown in Figure 313, while the results are shown in Figures 314a and 314b and in Table 49. The calculations were performed for one inch thick samples employing the properties of diboride compounds (12). Figure 314 and Table 49 indicate that temperature gradients of 2100°F in 250 mils can exist at a flux level of 1000 BTU/ft^{2}sec and an enthalpy of 2000 BTU/lb at two seconds. These gradients are most severe near the front (hot face) of the cylinder. After twenty seconds, the thermal gradients are reduced to 800°F in 250 mils. Reference to Table 50 indicates that the ratio of the computed temperature for radiation equilibrium (Eqs. 2, 3) divided by the observed surface temperature is approximately 1.3.

2. Test Results

Table 50 summarizes the results of the present tests. Headings include stream conditions, sample diameter, cold wall heat flux, maximum observed surface temperature and computed surface temperatures based on radiation equilibrium (Eqs. 2 and 3). In addition, exposure time, recession depth, degradation mode and metallographic features are summarized. The result of pre- and post-exposure nondestructive test data are given in reference (1). Cases where samples are numbered A and B (i.e., $HfB_{2.1}$ + 20%SiC(A-4)(HF-25A and 25B)) indicate situations where a sample was run consecutively under two different conditions. Samples ZrB_2 (HF-17) and $HfB_{2.1}$(A-6)(HF-20) were the only models exhibiting cracks prior to testing. Neither sample failed because of these flaws. Figures 315-317 show post exposure photographs of the 10MW samples. Reference to Figure 315 shows obvious thermal shock failure of $HfB_{2.1}$(A-2)(HF-1), $HfB_{2.1}$(A-6)(HF-20),

$HfB_{2.1}$ + 20%SiC(A-4)(HF-25,26,36 and 38). Similarly, Figure 316 shows that $HfB_{2.1}$ + 20%SiC(A-7)(HF-19B and 33) and ZrB_2(A-3)(HF-5,6 and 7B) failed by thermal shock. Finally, Figure 317 shows thermal shock failures for ZrB_2(A-3)(HF-13,14 and 15), ZrB_2(ManLabs-Avco)(HF-22), Boride Z(A-5)(HF-11 and 12) and ZrB_2 + 20%SiC(A-8)(HF-23B). The occurrence of clear thermal shock failures appears to depend on material and sample diameter. Table 51 summarizes the results and states tentative fracture thresholds for the boride samples tested. For example, HfB_2 + SiC(A-7) survived a flux of 948 BTU/ft^2sec in the one half inch diameter size but fractured at 840 BTU/ft^2sec in the 7/8 inch diameter size. Boride Z(A-5) did not survive the lowest fluxes employed. This is in line with the results of Model 500 and ROVERS exposures discussed in Section IIB-4. In line with the above mentioned effect of sample size, specimens of ZrB_2 + SiC(A-8) have been tested under AF33(615)3671 at flux levels of 2200-2400 BTU/ft^2sec, stagnation pressures of 17-18 atm and enthalpies near 1450 BTU/lb. Surface temperatures between 3700°F and 4000°F were noted for symmetrical wedge models of a sharp leading edge. The models were two inches long, one half inch wide and one quarter inch thick. Thirty and forty-five degree wedge angles were employed with a 30 mil radius of curvature. Three samples of ZrB_2 + SiC (A-8) were exposed for 15 seconds and survived with little erosion and no thermal shock failures (8).

Subsequent to exposure, samples were examined nondestructively by dye penetrant techniques and then sectioned for metallographic investigation. This procedure showed the presence of fine cracks which were not evident after exposure. The observations made after sectioning confirmed the NDT results shown in reference (1) and Table 50. Figures 318-323 show post exposure sections of $HfB_{2.1}$ (A-2)(HF-2), $HfB_{2.1}$(A-6)(HF-21), HfB_2 + 20%SiC(A-4)(HF-37), HfB_2 + 20%SiC(A-7)(HF-32 and 18) and ZrB_2(ManLabs-Avco)(HF-17) which did not thermal shock. As indicated in Table 50, all of the 7/8 inch diameter samples contain cracks. As indicated in Table 50 and in Figures 318-323, most of these cracks are between 100 and 400 mils from the front face of the samples. Reference to Figure 314 and Table 49 indicates thermal gradients of 1400°F in 500 mils in the vicinity of the fracture point.

IV. HOT GAS/COLD WALL ARC PLASMA PIPE TESTS IN THE AVCO TEN MEGAWATT FACILITY

A. Introduction

The purpose of this phase of the program was to examine experimentally the performance of selected candidate materials in high shear, turbulent flow steady-state heating environments. In particular, these tests attempted to simulate conditions at points beyond the sonic point where turbulent boundary layer flow prevails over the major heating period. A description of the experimental and calibration techniques employed is given elsewhere (see pp. 21-24 of Reference 3).

Pipes of selected materials which were 1-1/4" long with a 75 mil wall were exposed.* The candidate materials tested were $HfB_{2.1}$+20%SiC(A-7), $ZrB_{2.1}$+20%SiC(A-8), ZrB_2+SiC+C(A-10), Si/RVC(B-8)*, KT-SiC(E-14) and Hf-20Ta-2Mo(I-23). One pair of pipe samples of each material was tested at the initial test conditions of 3960 BTU/lb, q_{cw} = 480 BTU/ft^{2}sec, γ = 26.8 lbs/ft^2. Based on visual inspection of the results, conditions for the second pair of pipe samples were either increased to 6000 BTU/lb, 590 BTU/ft^{2}sec and 26.4 lbs/ft^2 or decreased to 3520 BTU/lb, 410 BTU/ft^{2}sec and 24.4 lbs/ft^2.

B. Results of Pipe Tests

Table 52 and Figures 324-326 summarize the results of these exposures. The material designation, sample number, position in the stream, heat flux, enthalpy and shear stress are given in Table 52. As indicated earlier (3), two pipes were run simultaneously. In each case the pipe closest to the exit plane of the arc is designated as occupying the UP position. The pipe farthest from the exit plane is designated as occupying the DOWN position. The down section is regarded as the test section. The purpose of the upstream section is to allow damping of flow irregularities and weak shock waves arising from the supersonic expansion processes in the pipe (3).

Table 52 also contains information covering pre and post exposure weight and dimensions for each sample. Visual observations and description of motion picture film coverage are also summarized. Reference to Table 52 and Figures 324-326 indicate that Si/RVC(B-8) was the only candidate material to survive the starting and "high" test condition. Post exposure examination indicated that the coating was burned off but that the pipes remained intact.

All other candidate materials completely failed the starting condition except for ZrB_2+SiC+C(A-10). The upstream pipe survived as

---

*The wall thickness of the Si/RVC(B-8) pipes were 140 mils. The pipe lengths were 1.5 inches.

shown in Figure 325. Thus, $ZrB_2+SiC+C$(A-10) was also exposed to the "high" condition at 590 BTU/ft^{2}sec, 6000 BTU/lb and 26.4 lbs/ft^2 shear stress. Under these conditions the downstream sample survived while the upstream sample thermal shocked.

The Hf-Ta-Mo(I-23) pipes exposed to the starting conditions of 480 BTU/ft^{2}sec, 3960 BTU/lb and 26.4 lbs/ft^2 shear stress melted badly as indicated in Figure 326. However, the Hf-Ta-Mo(I-23) pipe which occupied the upstream position in the "low test condition" did not fail.

Post test examination of the pipes reinforced the observations made during the exposures which indicated that heat conduction at the "O" ring resulted in severe temperature gradients (see Figure 64 of Reference (3)). As a result of this feature of the tests, it is difficult to make any firm quantitative conclusions about the results.

Qualitatively, the results indicate the fact that the thermal stress resistance of graphite exceeds that of the boride composites, and that $ZrB_2+SiC+C$(A-10) is more resistant to thermal stress failure than HfB_2+SiC(A-7) and ZrB_2+SiC(A-8) which do not contain graphite and have higher moduli of elasticity than (A-10) (11).

V. RESULTS OF TESTS CONDUCTED IN THE CORNELL AERONAUTICAL LABORATORY WAVE SUPERHEATER

A limited number of samples were exposed in the CAL Wave Superheater. A description of the nondestructive tests performed on the models employed is contained in Section IV. D of Reference (1). Section IV. D of Reference (3) describes the facilities and techniques employed in performing the exposures.

Analysis of the result obtained from models exposed in the Mach 6 Wave Superheater Hypersonic Tunnel are consistent with the behavior of these materials in the HG/CW tests in the Model 500 and ROVERS facilities. Limited recession was observed due to the short exposure time (15 seconds) and moderate temperatures (4000°F) encountered in these tests. Analytical and experimental studies of the relative importance of conduction losses for hemispherical shells have been performed in order to determine the origin of the unexpected behavior of 1/2" and 1" hemispherical cap models of Hf-20Ta-2Mo(I-23) and KT-SiC(E-14) in these tests. Surprisingly, it was noted that the 1" diameter caps attained a higher temperature level than the 1/2" diameter caps. Although the origin of this result is not definitely established, experimental simulation of these tests produced a similar result in torch tests on steel samples, and analysis has defined appropriate shell thickness/shell diameter ratios required to avoid such effects.

A. Description of Tests

Sixteen refractory material models were exposed (HG/CW) to the high velocity flow of air in the Mach 6 Wave Superheater Hypersonic Tunnel. Data were taken in two 15 second tests of eight models, each at a velocity of 10^4ft/sec, a stagnation pressure (at the model nose) of one atmosphere, and a tunnel flow rate of 2.5 lb/sec. The models were designed to permit their surface temperature to approach the radiation/aerodynamic heating equilibrium value during each exposure to the test stream at $q(R)^{1/2} = 90$ BTU/ft$^{3/2}$ sec. As indicated earlier (3), the models were expected to reach temperatures in excess of 4000°R.

All sixteen models tested were hollow hemispherical cylinders. The "elox" process was used to bore from the aft end to provide a uniform material thickness which was nominally 1/8 inch. The diameter of the bore was a nominal 1/4 inch for the thirteen 1/4 inch nose radius models and 3/4 inch for the three 1/2 inch nose radius models. The purpose of the shell or "thimble" design was to promote faster wall temperature response so as to approach the radiation equilibrium wall temperature as rapidly as possible. A sketch showing the typical model features and the typical attachment to their stings is presented in Figure 327. Eight models and a single 1/4 inch nose radius steady-heating copper calorimeter were mounted in the tunnel by a multiple sting arrangement as shown in Figure 328. Tables 53 and 54 list the initial dimensions and sting positions occupied by each model.

Motion picture coverage of the tests was provided as indicated earlier (3). Table 55 lists the camera settings employed for the motion picture coverage. The methods employed for establishing heat flux, enthalpy and stagnation pressure were described in Section III of Reference (3). Tables 56 and 57 summarize the results.

As indicated above, model surface temperatures in excess of 4000°R were anticipated. Calculations based on a transient heat flux calculation were presented in Section III. C of Reference (3). The results of these calculations are reproduced in Tables 58 and 59 and are shown graphically in Figures 329 and 330.

The models were not, in themselves, instrumented. The calorimeter had one chromel/alumel thermocouple welded to the back face of the thermal element. The models were observed individually by miniature radiometers. In addition to individual model radiometers, one ManLabs Milletron two-color pyrometer and one microphotographic camera (Photosonics #4) were arranged to observe the stagnation point of the model on sting number one. Two Photosonics cameras (#2 and #3) were arranged to observe all models from the right (pilot's view) during both runs. To obtain test conditions, the normal complex of Wave Superheater cycle instrumentation data were recorded as well as the tunnel throat and nozzle exit static pressure, and the test section cabin pressures. All data were recorded on EFB or ERB 16 mm film and a CEC optical galvonometer paper recorder.

Eight hemisphere-cylinder models and one calorimeter, as listed in Tables 53 and 54 were exposed in each (CAL 67-473 and 67-747) test. Tabulated camera settings are presented in Table 55. The facility functioned normally in both tests. However, the model instrumentation suffered some difficulties. In particular, the two-color Milletron gave no deflection, the microphotographic film was blank, and the test section windows became cloudy during the first test. The JT0992(F-15), KT-SiC(E-14) (one inch diameter) and Hf-20Ta-2Mo(I-23) models were lost during the first test, but the latter two were recovered from the floor of the test cabin, and some (but not all) measurements were made on these (see Tables 53 and 54).

The nozzle, sting assembly and windows were removed and the models replaced in preparation for the second test. The Milletron two color pyrometer was switched to a lower scale to improve its sensitivity. The second set of models, the nozzle and the cleaned test section windows were installed. The facility functioned normally for the second test. Again, however, there were difficulties in obtaining model data. The windows clouded early and a heavy dust deposit was found throughout the test cabin, which has never before been observed. This dust appeared to be asbestos. The recorded data show no deflection on any of the nine radiometers. The dust was also deposited on the lenses of the miniature radiometers. The microphotographic film was blank for the second tests, also.

The miniature radiometer data are presented in Figure 331. Model pre and post-test measurements are included for convenience in the model identification and location data of Tables 53 and 54. No data were obtained from the Milletron two-color pyrometer or the microphotography in either test. No data were obtained from the miniature radiometer during the second test.

The one inch diameter Hf-20Ta-2Mo(I-23) model which was exposed in the first run (473) has a melting temperature of 3860°F. The post-test examination of this model revealed evidence of the melt having formed during the test. Since it is evident that the model I-23-4 surface temperature was at least 3860°F during the test, a comparison of this result with that of Figure 331 (T_W MAX = 2750°F) produces the conclusion that the radiometer data are in error. This is indeed unfortunate because it invalidates the only temperature data obtained. The failure of this data can be attributed most probably to the dust in the test cabin. X-ray analysis of the dust indicated that it was asbestos. By contrast, the one half inch diameter Hf-20Ta-2Mo(I-23) model exposed in the second rung (474) showed no signs of melting.

Because of the relatively small heat absorption capacity of the models, at the rate of heating produced by the stream, the surface temperature should have approached the equilibrium value for the heat balance between aerodynamic heating and radiation dissipation (see Tables 58 and 59). For a one inch diameter model at an emittance of 0.55, equilibrium temperature is 4700°R. For a 1/2 inch diameter model it is 5000°R (Figure 330). Figures 332 and 333 compare the calculated time-temperature histories with the values contained in Figure 331. The latter have been "corrected" to true temperature by employing the values of normal total emittance measured in the Avco Arc Plasma Tests (i.e., Table 48). In comparing the observed and computed time/temperature histories, it should be noted that coating of the radiometers by asbestos dust as the exposure proceeded undoubtedly reduced the radiation received. Thus, the one inch diameter hemispherical cap sample Hf-20Ta-2Mo(I-23)-4-19 must have reached 4310°R during the exposure even though the maximum radiometer temperature was 3650°R. Secondly, the computations were performed for ZrB_2 which has different thermophysical and radiative properties than the samples shown in Figures 332 and 333. However, the product of $\rho C_p K$ (density x specific heat x thermal conductivity) for these materials is quite similar so that substitution of the specific values in each case would not alter the results. However, the value of normal emittance employed would have an important bearing. Thus, tungsten and RVA graphite having values of $\epsilon_N = 0.32$ and 0.52 differ most from the $\epsilon_N = 0.55$ employed in the calculations. Reference to Figures 332 and 333 indicates that the models were heated more rapidly than anticipated but did not reach the anticipated radiation equilibrium temperature levels. Although the later discrepancy may be due to coating of the radiometers, the observation that (T_{CALC}/T_{OBS}) is more than unity is in line with the results of the Avco

exposures where (T_{CALC}/T_{OBS}) is approximately 1.17 for RVA, 1.43 for KT-SiC, 1.04 for JT0992 at one atmosphere stagnation pressures. Bare tungsten yields (T_{CALC}/T_{OBS}) at 1.15 at P_e = 0.16 atm (see Table 30).

B. Metallographic Examination of the Test Models after Exposure

Figures 334 and 335 show post exposure photographs of all the models. In addition, Tables 53 and 54 summarize the dimensional changes which were very minor due to the short exposure time. The zirconium diboride (A-3)-1-2 model in the sting 1 position showed no recession and little change in structure. This finding is in general agreement with the results obtained at Mach 0.3 and P_e = 1 atm presented earlier for 1800 second exposures (Figure 1). Unfortunately no radiometer measurements were obtained for this model but it is doubtful that the surface temperature exceeded 4000°F. The KT-SiC models which were positioned at the sting 2 and sting 3 positions in run 67-473 exhibited recessions of 18 mils and 2 mils during the fifteen second exposures. In this case, the smaller model (488 mil diameter) reached a lower surface temperature than the larger model (944 mil diameter) as indicated in Figures 331-333. The cap of the larger model fractured on cooling (Figure 334). The observed recession rates of 0.1-1 mils per second or 180-1800 mils in 30 minutes are higher than indicated in Figure 5 for KT-SiC exposed at P_e = 1 atm at Mach 0.3. The RVA(B-5), PG(B-6) and BPG(B-7) samples which were exposed at the sting 6 position in Run 67-473 and sting 4 and 5 positions in Run 67-474 exhibited recessions of 30, 8 and 32 mils in the present runs which is comparable to the results shown in Figures 3 and 4; however, the tungsten model, Run 67-473 sting 5 showed virtually no recession. Recession rates near 1 mil/sec were anticipated on the basis of results at P_e = 1 atm and a Mach Number of 0.9 and the present results for bare tungsten shown in Figure 7. The Sn-Al/Ta-10W coated model, sting 8 Run 67-474, exhibited melting of the Sn outer layer but no degradation of the inner layer. However, this model probably attained a much lower surface temperature than the other models due to high values of (T_{CALC}/T_{OBS}).

The models which formed solid oxides on exposure (i.e., Hf-20Ta-2Mo(I-23) sting 1 Run 67-474 and sting 4 Run 67-474, ZrB_2(A-3) sting 1 Run 67-473, $HfB_{2.1}$(A-3) sting 2 Run 674, HfB_2+SiC(A-4) sting 3 Run 67-474) showed little recession in line with the temperature and time of exposure. Similar behavior was noted for JTA(D-13) sting 7 Run 67-473; JT0981(F-16) sting 6 Run 67-474 exhibited a recession comparable to the pure graphites.

The thermal shock failures noted for JT0992(F-16) sting 8, Run 67-473 and ZrB_2(A-3)-24-3 sting 7 Run 67-474 are surprising since these materials have survived flux levels in excess of the current values without failing. However, they were not tested as hollow shells. It is possible that the defects present in the later model (1) may have contributed to failure. Although HfB_2(A-2) samples have exhibited thermal shock failures at levels above 770 BTU/ft²sec, no failures were observed below this level in the Avco tests (Table 2) nor were any obvious defects noted for this sample as a result of nondestructive tests (1).

Figures 334 and 335 shows post exposure photographs of these models. Post exposure longitudinal sections are shown in Figures 336-347. Figure 336 shows Model ZrB_2(A-3)-1-2 which experienced a negligible recession during exposure and no change in surface structure was observed. Figures 337 and 338 illustrate KT-SiC(E-14)-1-8 and 3-18. Both models exhibit melting of the silicon binder and depletion through the nose section. Figure 339 shows Hf-20Ta-2Mo(I-23)-4-19 which melted during exposure. Model W (uncoated) (G-18)-X-11 presented in Figure 340 showed no change in structure as did RVA(B-5)-X-5 and JTA(D-13)-X-7 which are illustrated in Figure 341. This set of figures covers all of the models in Run No. 1. JT0992(F-15)-X-9 which occupied Sting 8 in Run No. 1 thermal shocked.

Figure 342 displays Model Hf-20Ta-2Mo(I-23)-I-12 and shows no melting (in contrast to the one inch model exposed in Run No. 1 shown in Figure 339). The one half inch diameter Hf-20Ta-2Mo(I-23) model is coated with suboxide containing tantalum stringers throughout. Figures 343-346 show models, $HfB_{2.1}$(A-2)-X-1, HfB_2+SiC(A-4)-X-4, PG(B-6)-X-6, BPG(B-7)-X-16 and JT0981(F-16)-X-10 which exhibited very minor changes during exposure. Model $HfB_{2.1}$(A-2)-X-1 (Figure 343) exhibited a thermal shock failure at the end of Run No. 2 when the cap broke off. Model HfB_2+SiC(A-4)-X-4 (Figure 344) shows no SiC depletion at the surface. Models PG(B-6)-X-6 and BPG(B-7)-X-16 experienced recessions of 8 and 32 mils respectively, (Figure 345). Model JT0981(F-16)-X-10 shown in Figure 346 exhibited a conversion depth of 19 mils and a very light oxide. Sting position 7 of Run No. 2 was occupied by ZrB_2(A-3)-23-3 which thermal shocked during exposure. The last position (Sting 8) in Run No. 2 was filled by Model Sn-Al/Ta-10W(G-19)-3-22 shown in Figure 347a. Melting and removal of the Sn cover of the duplex coating (page 55, Reference 1) is shown in Figure 347b.

C. Analysis of the Relative Conduction Losses for Spherical Shells

In the discussion of the Wave Superheater exposures presented above, the observation that the one inch diameter models Hf-20Ta-2Mo(I-23)-4-19 (Sting 4 Run 1) and KT-SiC(E-14)-3-18 (Sting 3 Run 1) achieved higher temperatures than one half inch diameter models of the same material (Hf-20Ta-2Mo(I-23)-1-12 (Sting 1 Run 2) and KT-SiC(E-14)-1-8) Sting 2 Run 1) was noted. This was deemed to be unusual since the heat flux to the larger model is 70% of that experienced by the smaller model. One possible source of this difference was considered to be the losses due to conduction through the models. In particular, the models are hollow shells. Consequently to consider the relative conduction losses it is necessary to introduce the ratio of shell thickness to model diameter as an additional factor.

A suitable analysis of the problem has been performed (3) based on the relative importance of conduction and aerodynamic heating for a model represented by the sketch shown in Figure 348, where the aerodynamic heating is given as a function of Θ by $q[\Theta] = q_0 \cos \Theta$. In

order to obtain experimental data on the relative conduction losses for spherical shells, one inch and one half inch diameter models having a wall thickness of 1/8" were fabricated from SAE1020 steel. This material was employed since its thermal conductivity is approximately one third that of KT-SiC(E-14) at temperatures between 500° and 2000°R. As a consequence, the heat flux level for this experiment was maintained at 1/3 the level of the Wave Superheater exposures described in Section V.B.

Accordingly, models were exposed in an oxyacetylene torch situated in the Wave Superheater Hypersonic Tunnel for convenience in utilizing the required test equipment. Separate copper calorimeters were employed to determine cold wall heat flux. Heat fluxes of 150 BTU/ft^{2}sec and 220 BTU/ft^{2}sec were applied to the one inch and one-half inch diameter models, respectively. Thermocouples which were spring mounted in contact with the inner wall directly behaind the stagnation point were employed to measure the thermal response of the models. The results are shown in Figure 349. These data indicate that the larger model reached 1900°F in 11.4 seconds; the smaller models reached 1900°F in 13.8 + 1.0 seconds. At shorter times, the rise rate for the smaller models is greater than for the larger models as expected. At longer times, the larger model does heat up more rapidly than the smaller model does. However, it is surprising that the crossover occurs at low temperatures near 600°F where the magnitudes of dT/dO are smaller than the values assumed in the foregoing calculation. Finally, it should be noted that the k/q matching is partially satisfied for KT-SiC but not satisfactory for Hf-20Ta-2Mo.

REFERENCES

1. Kaufman, L. and Nesor, H., "Stability Characterization of Refractory Materials under High Velocity Atmospheric Flight Conditions," AFML-TR-69-84, Part II Volume I: Facilities and Techniques Employed for Characterization of Candidate Materials, ManLabs, Inc., Cambridge, Mass. (September 1969).

2. Kaufman, L. and Nesor, H., "Stability Characterization of Refractory Materials under High Velocity Atmospheric Flight Conditions," AFML-TR-69-84, Part II Volume II: Facilities and Techniques Employed for Cold Gas/Hot Wall Tests, ManLabs, Inc., Cambridge, Mass. (September 1969).

3. Kaufman, L. and Nesor, H., "Stability Characterization of Refractory Materials under High Velocity Atmospheric Flight Conditions," AFML-TR-69-84, Part II Volume III: Facilities and Techniques Employed for Hot Gas/Cold Wall Tests, ManLabs, Inc., Cambridge, Mass. (September 1969).

4. Kaufman, L. and Nesor, H., "Stability Characterization of Refractory Materials under High Velocity Atmospheric Flight Conditions," AFML-TR-69-84, Part III Volume I: Experimental Results of Low Velocity Cold Gas/Hot Wall Tests, ManLabs, Inc., Cambridge, Mass. (September 1969).

5. Perkins, R., Kaufman, L. and Nesor, H., "Stability Characterization of Refractory Materials under High Velocity Atmospheric Flight Conditions," AFML-TR-69-84, Part III, Volume II: Experimental Results of High Velocity Cold Gas/Hot Wall Tests, ManLabs, Inc., Cambridge, Mass. (September 1969).

6. Kaufman, L. Nesor, H., Bernstein, H. and Baron, J.R., "Stability Characterization of Refractory Materials under High Velocity Atmospheric Flight Conditions," AFML-TR-69-84, Part IV Volume I: Theoretical Correlation of Material Performance with Stream Conditions, ManLabs, Inc., Cambridge, Mass. (September 1969).

7. Rudy, E., "Ternary Phase Equilibria in Transition Metal-Boron-Carbon-Silicon Systems: Part V. Compendium of Phase Diagram Data," AFML-TR-65-2, Part V, June 1969.

8. Clougherty, E. V., "Research and Development of Refractory Oxidation-Resistant Diborides, Part II Volume I: Summary," AFML-TR-68-190 Part II Volume I, December 1969.

9. Clougherty E.V., Hill, R.H., Rhodes, W.R., and Peters, E.T., "Research and Development of Refractory Oxidation-Resistant Diborides, Part II Volume II: Processing and Characterization," AFML-TR-68-190 Part II Volume II, November 1969.

10. Clougherty, E.V. and Peters, E.T., "Research and Development of Refractory Oxidation-Resistant Diborides, Part II Volume III: Thermochemical Stability Characteristics," AFML-TR-68-190, Part II Volume II, November 1969.

11. Rhodes, W.H., Clougherty, E.V., and Kalish, D., "Research and Development of Refractory Oxidation-Resistant Diborides, Part II Volume IV; Mechanical Properties," AFML-TR-68-190 Part II Volume IV, November 1969.

12. Clougherty, E.V., Wilkes, K.E., and Tye, R.P., "Research and Development of Refractory Oxidation-Resistant Diborides, Part II Volume V: Physical, Thermal, Electrical and Optical Properties," AFML-TR-68-190, Part II Volume V, November 1969.

13. Clougherty, E.V., Niesz, D.E., Mistretta, A.L., "Research and Development of Refractory Oxidation-Resistant Diborides, Part II Volume VI: Thermal Stress Resistance," AFML-TR-68-190, Part II Volume VI, November 1969.

14. Clougherty, E.V., "Research and Development of Refractory Oxidation-Resistant Diborides, Part II Volume VIII: Application Evaluations and Design Considerations," AFML-TR-68-190, Part II Volume VII, November 1969.

15. Kaufman, L., Clougherty, E.V. and Berkowitz-Mattuck, J.B., Trans. Met. AIME (1967) 239, 458.

16. Kaufman, L. and Clougherty, E.V., "Investigation of Boride Compounds for Very High Temperature Applications," RTD-TDR-63-4096, Part III, March 1966.

17. Kendall, E.G., Slaughter, J.I. and Riley, W.C., "A New Class of Hypereutectic Carbide Composites," Aerospace Corp., June 1965, TDR-469 (52500-10)-11 (SSD-TR-65-78).

18. Tanzilli, R.A., "Evaluating of Graphite Composites in Reentry Environments," AFML-TR-65-328, October 1965.

19. Criscione, J.M., et al., "High Temperature Protective Coatings for Graphite," ML-TDR-64-173, Part II, October 1964.

20. Buckley, J.D. and Stein, B.A., "Preliminary Investigation of the Dynamic Oxidation of JT Graphite Composites at Surface Temperatures between 4000°F and 5000°F," Summary of the Eleventh Refractory Composites Working Group Meeting, AFML-TR-66-179, July 1966.

21. Bartlett, R.W. and Gage, P/R., "Investigation of Mechanisms for Oxidation Protection and Failure of Intermetallic Coatings for Refractory Metals", ASD-TDR-63-753 Part II, July 1964.

22. Perkins, R. and Packer, C.M., "Coatings for Refractory Metals in Aerospace Environments", AFML-TR-65-351, September 1965.

23. Schwartzkopf, P., "Evaluation of Tungsten Composites for Hypersonic Vehicles", AFML-TR-67-272, Rocketdyne Division of North American Aviation, Inc., Canoga Park, California, June 1967.

24. Berkowitz-Mattuck, J.B., Kaufman, L., Clougherty, E.V. and Hopper, R., Trans. Met. Soc. AIME (1967) 239, 750.

25. Wright, T.R., Braeckel, T.R., Kizer, D.E., et al., "The Fabrication of Iridium and Iridium-Alloy Coatings on Graphite by Plasma-Arc Deposition and Gas-Pressure Bonding", AFML-TR-68-6, Battelle Memorial Institute, Columbus, Ohio, February 1968.

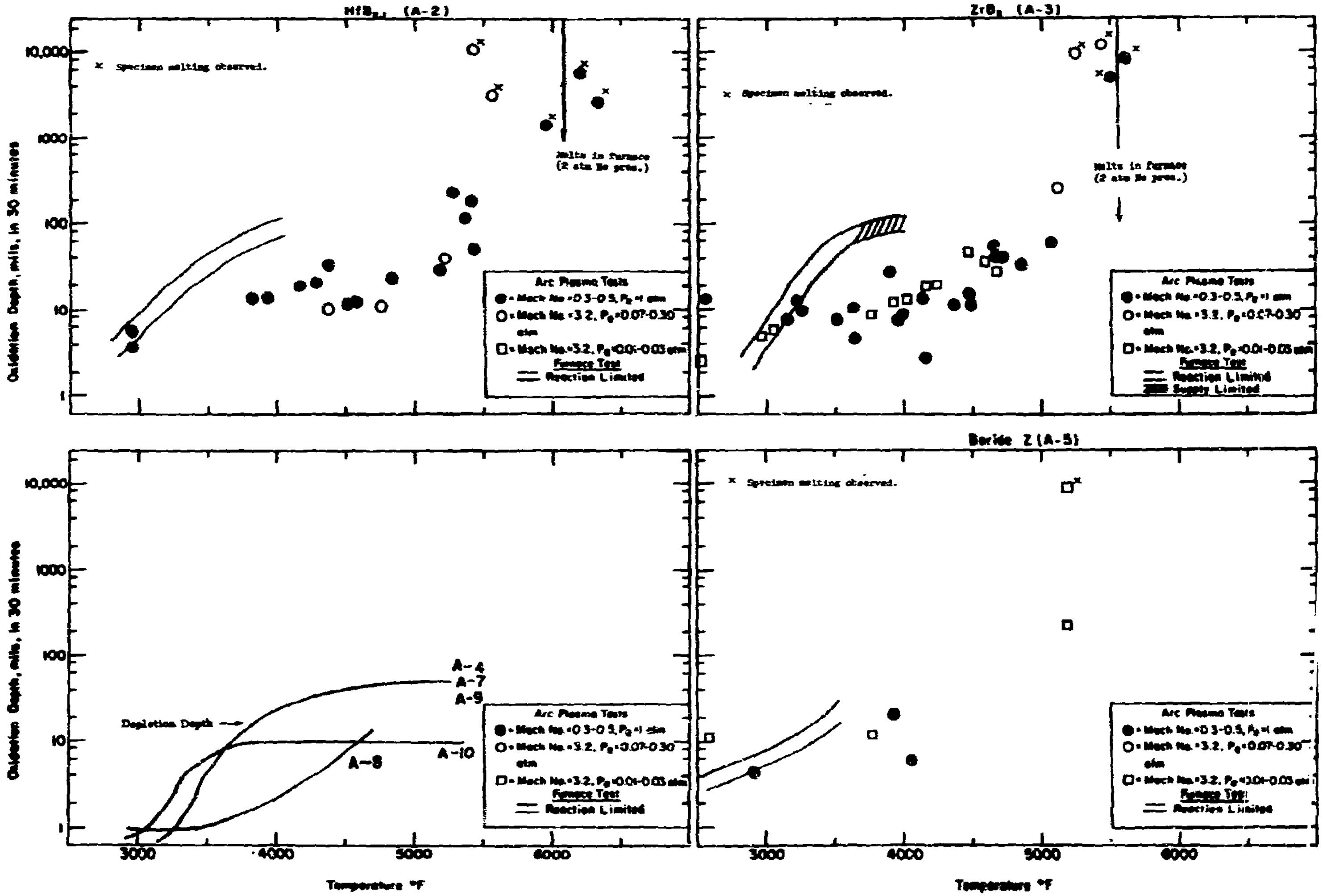

Figure 1. Comparison of Arc Plasma (HG/CW) Tests with Furnace Oxidation (CG/HW) Tests at 1.8 ft/sec for $HfB_{2.1}$(A-2), ZrB_2(A-3) and Boride Z(A-5) Plus Typical SiC Depletion Depths for Diboride-Silicon Carbide Composites.

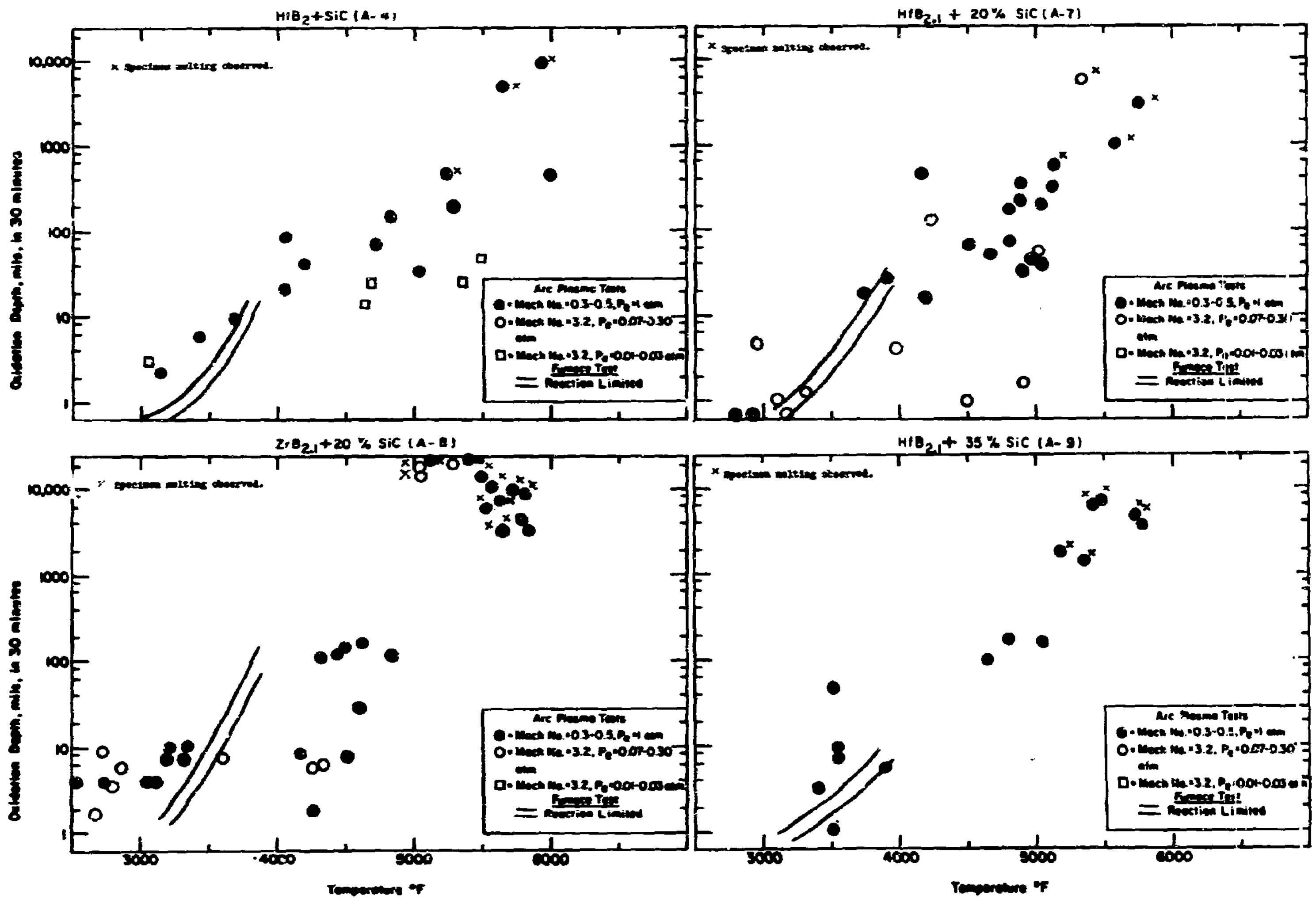

Figure 2. Comparison of Arc Plasma (HG/CW) Tests with Furnace Oxidation (CG/HW) Tests at 1.8 ft/sec for HfB_2+SiC(A-4), $HfB_{2.1}$+20v/oSiC(A-7), $ZrB_{2.1}$+20v/oSiC(A-8), and $HfB_{2.1}$+35v/oSiC(A-9).

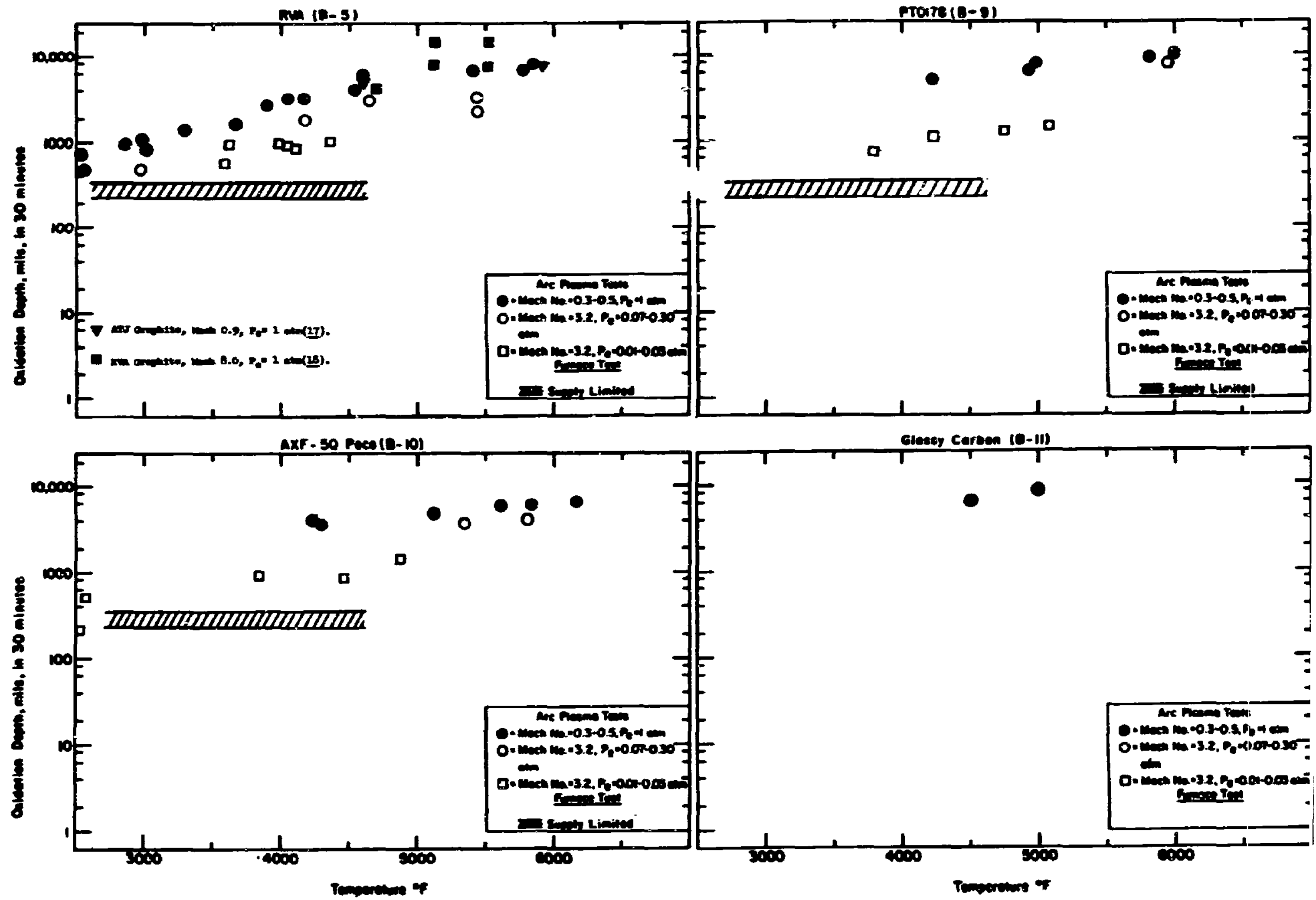

Figure 3. Comparison of Arc Plasma (HG/CW) Tests with Furnace Oxidation (CG/HW) Tests at 1.8 ft/sec for RVA(B-5), PTO178(B-9), AXF-5Q Poco(B-10) and Glassy Carbon (B-11).

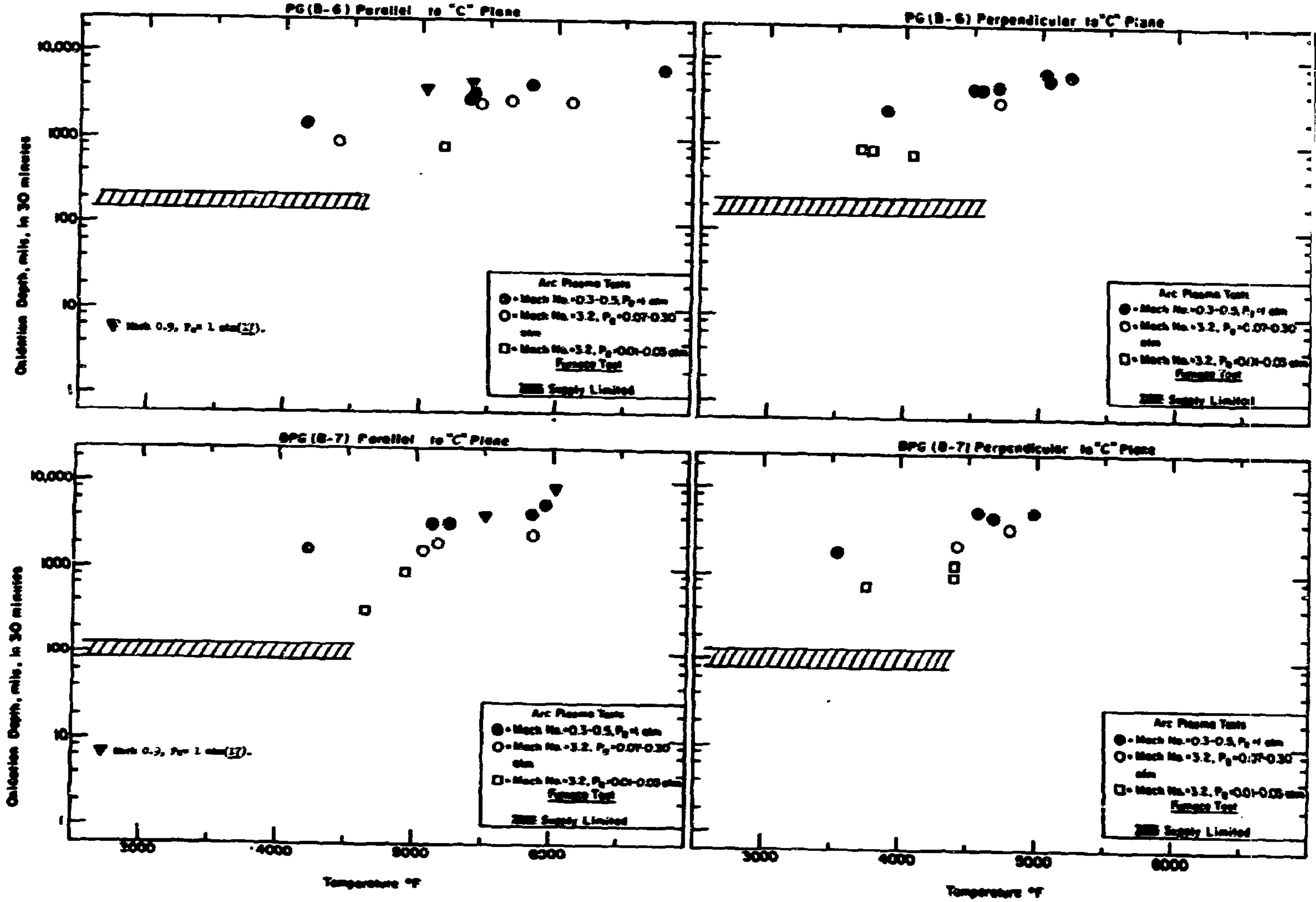

Figure 4. Comparison of Arc Plasma (HG/CW) Tests with Furnace Oxidation (CG/HW) Tests at 1.8 ft/sec for PG(B-6) and BPG(B-7).

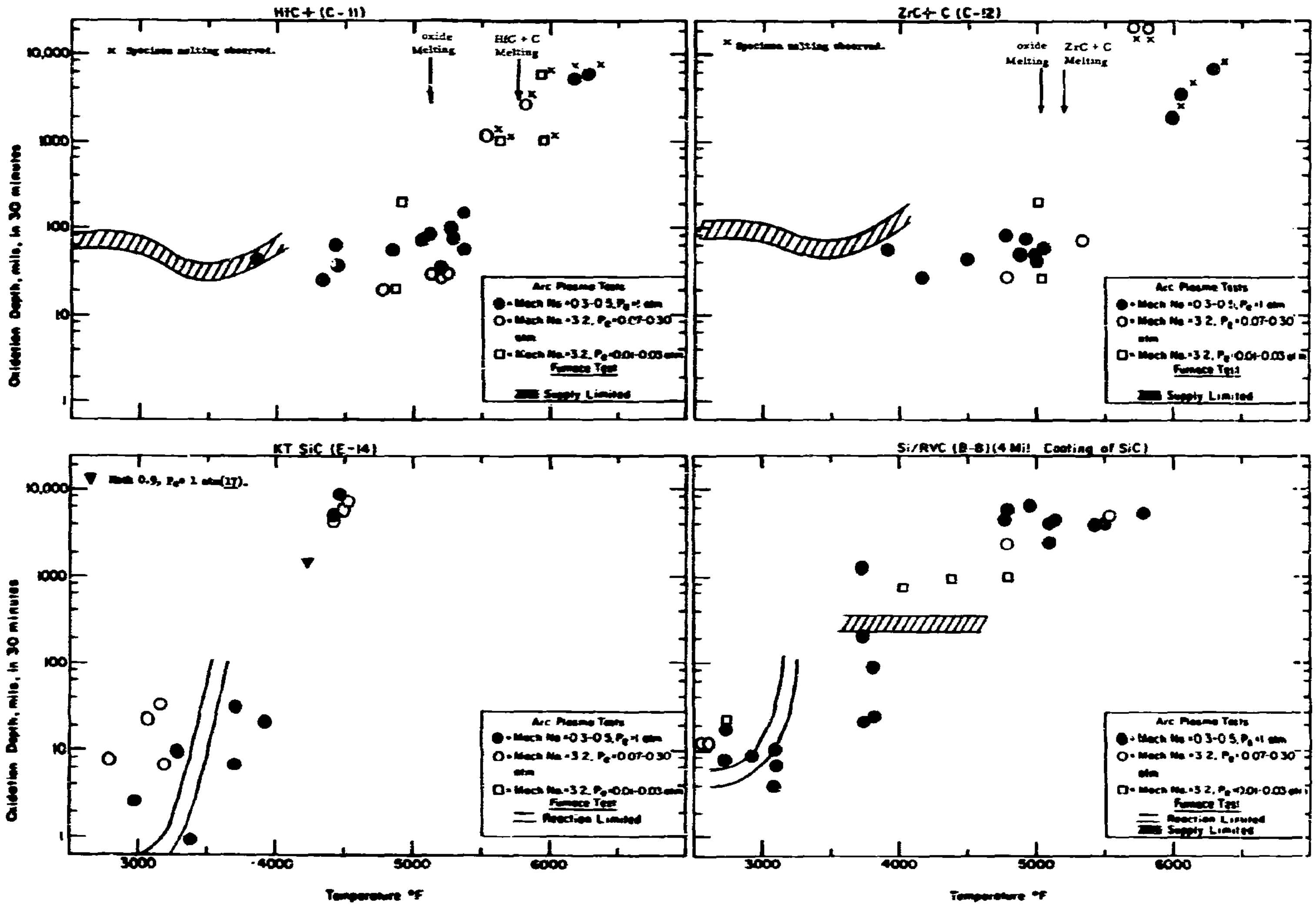

Figure 5. Comparison of Arc Plasma (HG/CW) Tests with Furnace Oxidation (CG/HW) Tests at 1.8 ft/sec for HfC+C(C-11), ZrC+C(C-12), KT-SiC(E-14), and Si/RVC(B-8).

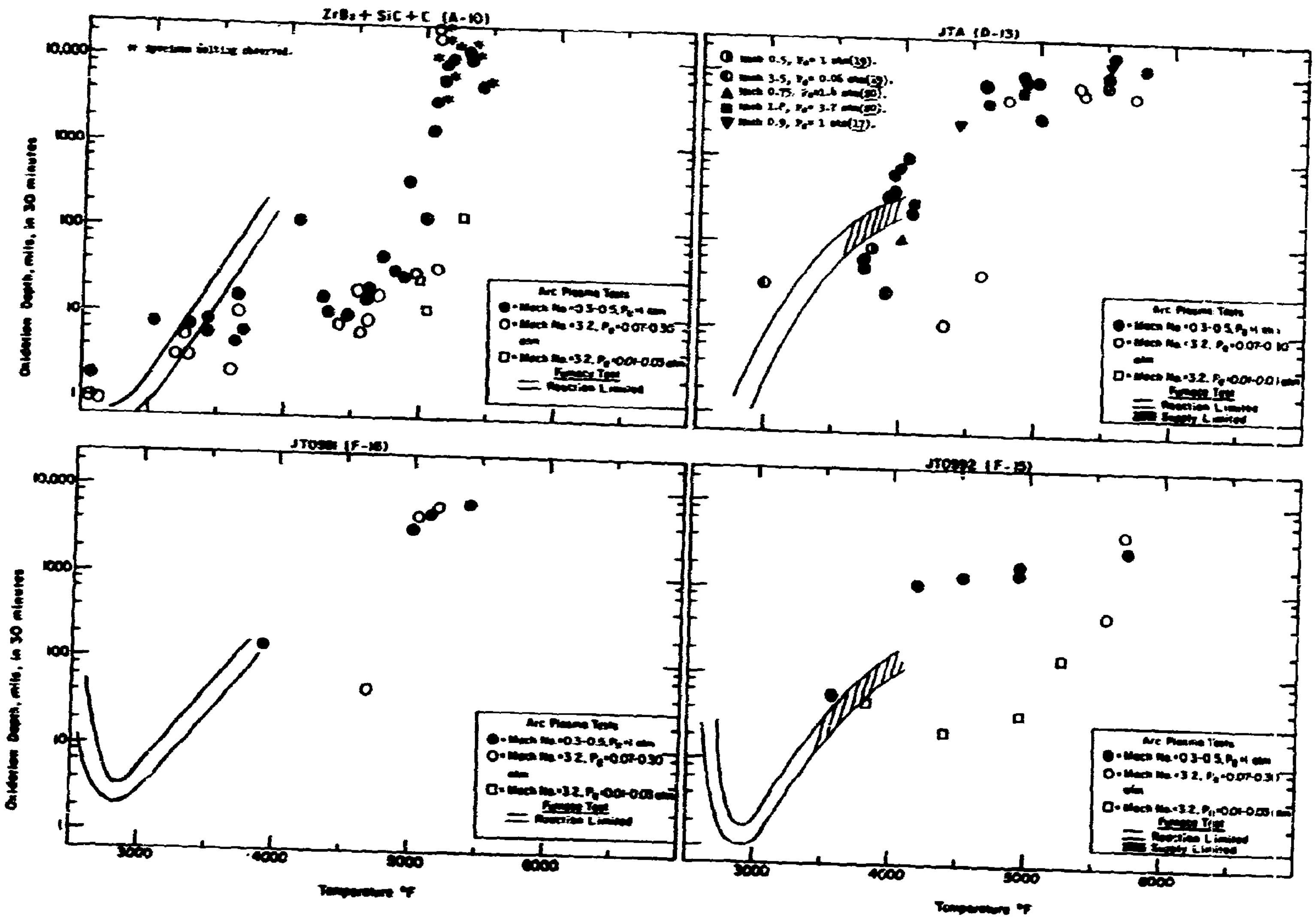

Figure 6. Comparison of Arc Plasma (HG/CW) Tests with Furnace Oxidation (CG/HW) Tests at 1.8 ft/sec for ZrB_2+SiC+C(A-10), JTA(D-13), JT 0981(F-16), and JT 0992(F-15).

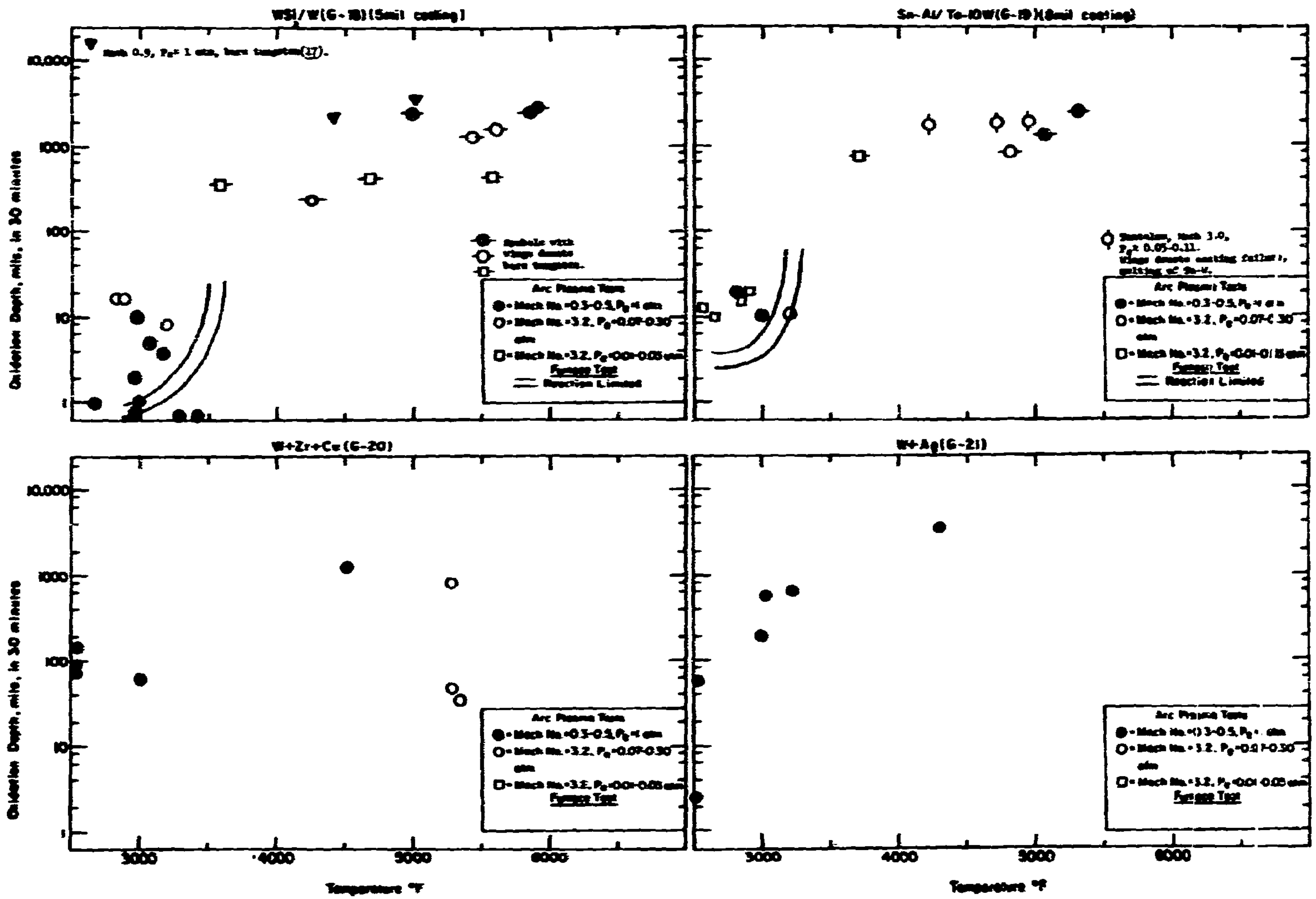

Figure 7. Comparison of Arc Plasma (HG/CW) Tests with Furnace Oxidation (CG/HW) Tests at 1.8 ft/sec for WSi_2/W(G-18), Sn-Al/Ta-10W(G-19), W+Zr+Cu(G-20), and W+Ag(G-21).

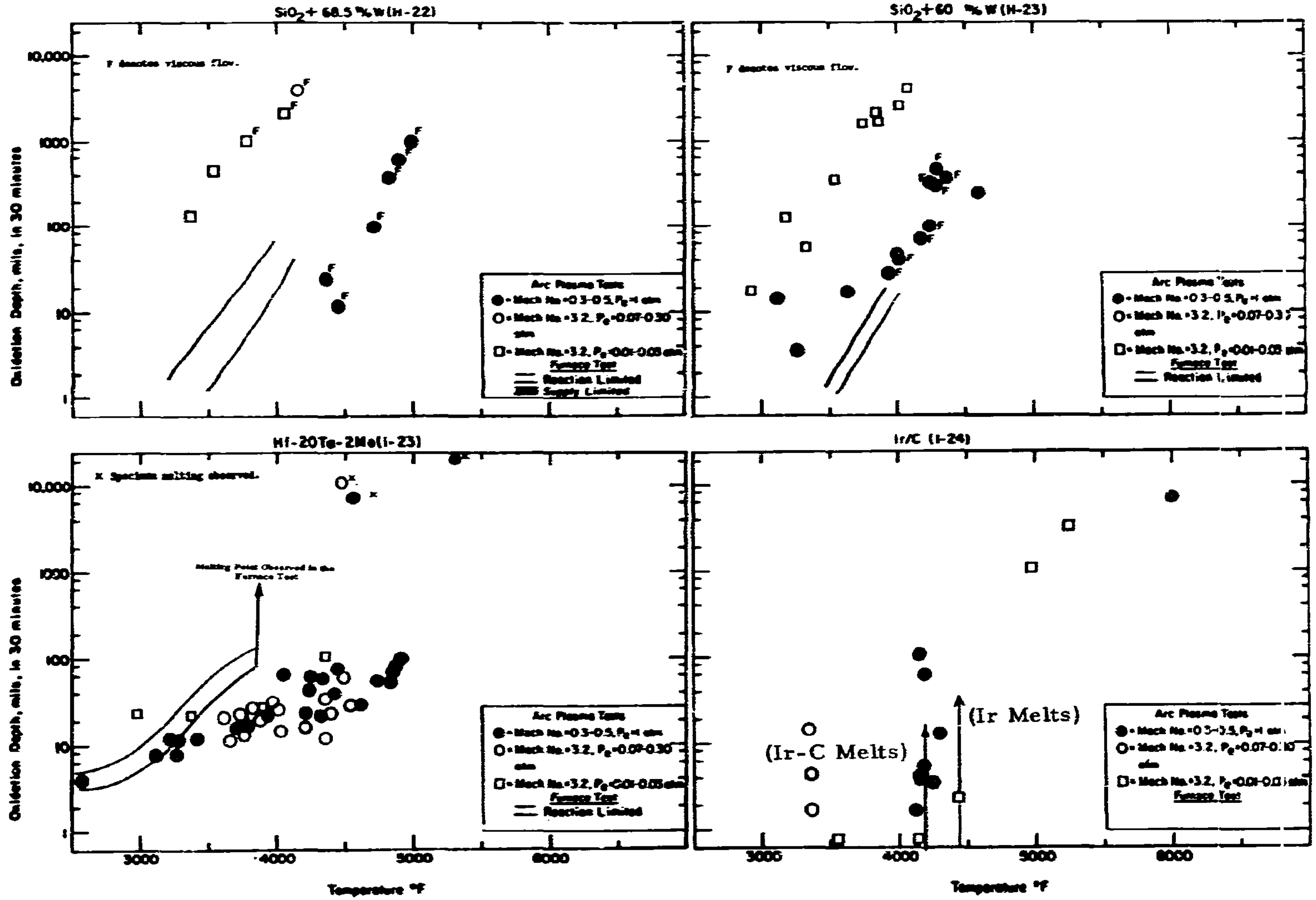

Figure 8. Comparison of Arc Plasma (HG/CW) Tests with Furnace Oxidation (CG/HW) Tests at 1.8 ft/sec for SiO_2+68.5w/oW(H-22), SiO_2+60w/oW(H-23), Hf-20Ta-2MO(I-23), and Ir/C(I-24).

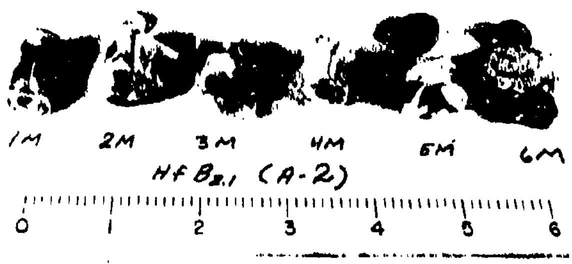

Plate 1-4225

Figure 9. Post Exposure Photographs of Arc Plasma Tests $HfB_{2,1}$(A-2)-1M, 2M, 3M, 4M, 5M and 6M. Samples 1M, 2M, 3M and 4M were Cracked During Removal of Tungsten Sting. Samples 5M and 6M Showed Initial Thermal Shock Delaminations and Were Cracked After*Sting Removal. Samples 3M and 5M Melted. Scale is One Inch. Hot Face is Pointing Up.

Plate 1-4250

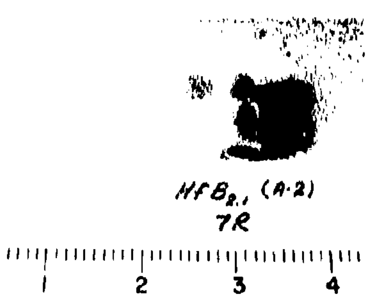

Plate 1-4254

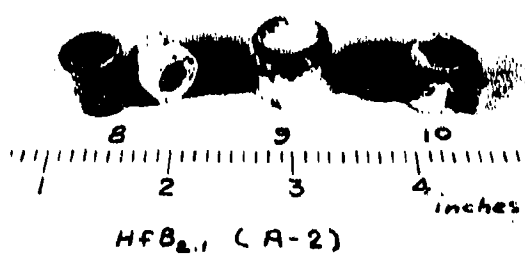

Figure 10. Post Exposure Photographs of Arc Plasma Tests $HfB_{2,1}$(A-2)-7R, 8R, 9R and 10R. Sample 8R showed an Initial Thermal Shock Failure While Samples 9R and 10R exhibited Melting. Scale is One Inch. Hot Face is Pointing Up.

*Distance between numbered divisions is equal to one inch.

Plate No. 1-8750

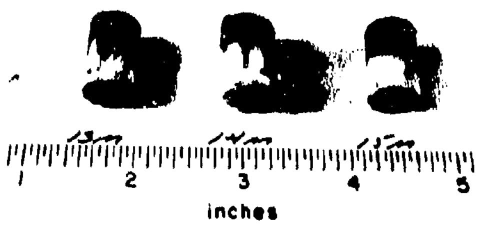

Plate No. 1-9521

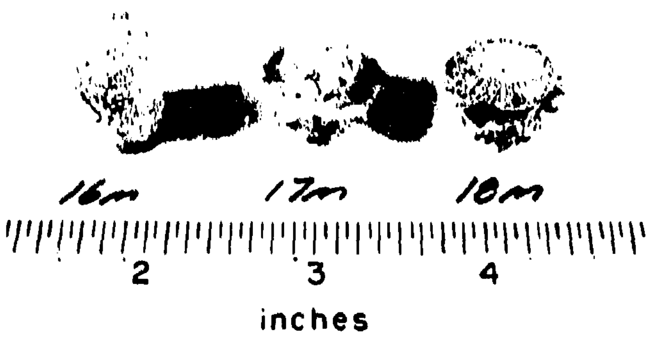

Plate No. 1-4992

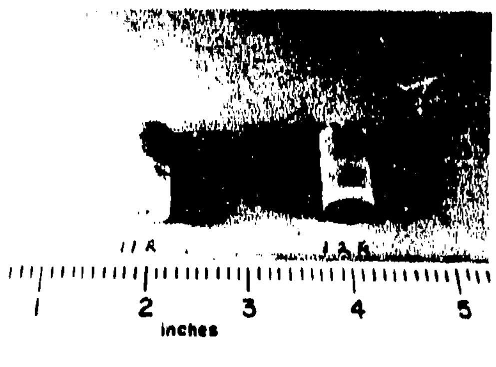

Figure 11. Post Exposure Photographs of Arc Plasma Tests $HfB_{2.1}$(A-2)-13M, 14M, 15M, 16M, 17M and 18M, 11R and 12R.

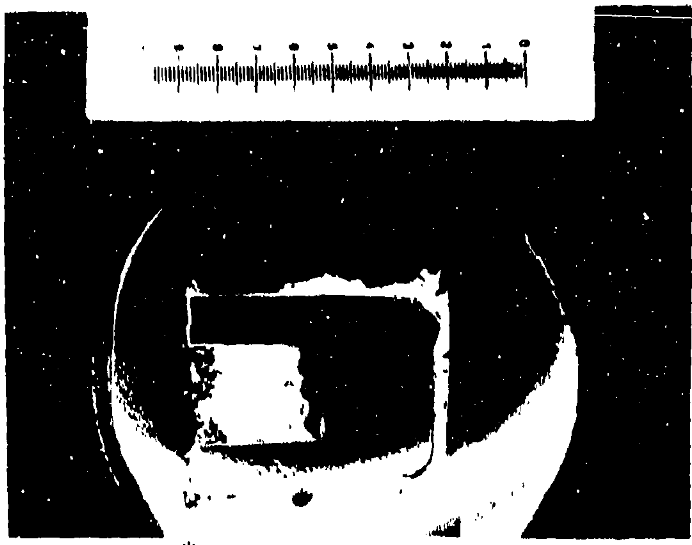

One Inch Scale* X 2.5

Figure 12. Arc Plasma Test $HfB_{2.1}$(A-2)-4M, Surface Temperature 5270°F, Stagnation Enthalpy 5570 BTU/lb, Stagnation Pressure 1 atm, Cold Wall Heat Flux 760 BTU/ft^2, Exposure Time 1830 Seconds, Initial Thickness 557 Mils, Final Thickness 286 Mils. Hot Face at Right.

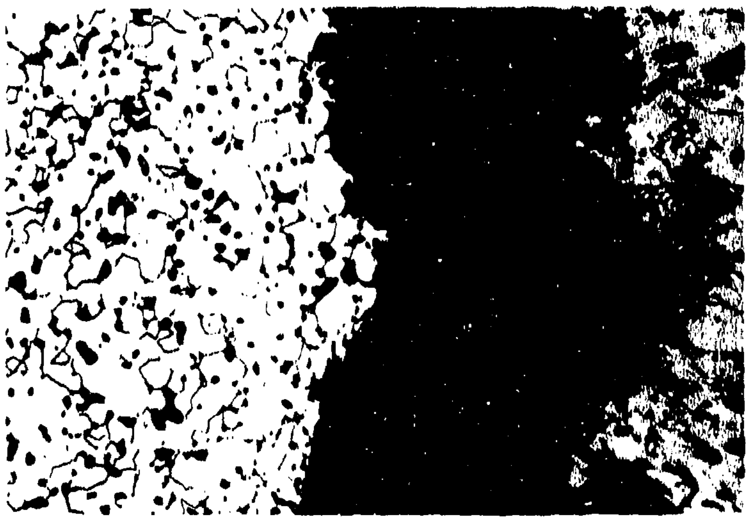

Etched with 10 Glycerine 5 HNO_3 3HF X160

Figure 13. Arc Plasma Test $HfB_{2.1}$ (A-2)-4M, Hot Face, Showing Boride at Left, Oxide at Right with 10 Mil Separation.

*Distance between numbered divisions is equal to one hundred mils.

$HfB_{2.1}$ Oxide

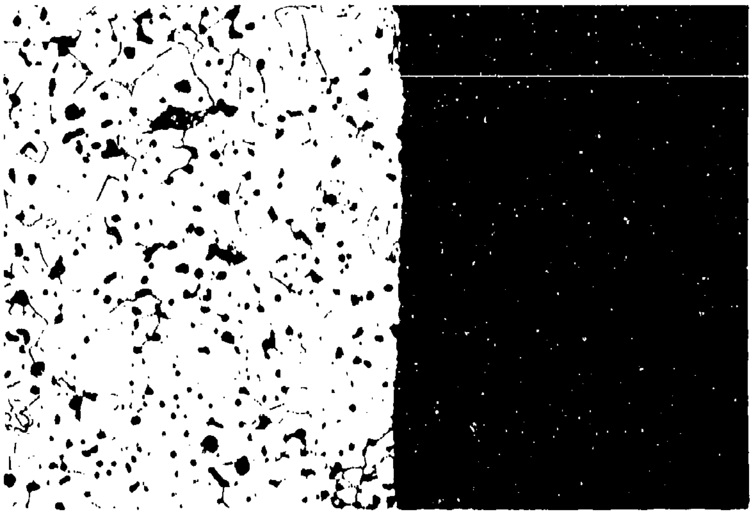

Plate 1-4240

Etched with 10 Glycerine $5HNO_3$ 3HF X250

Figure 14. Arc Plasma Test $HfB_{2.1}$ (A-2)-4M, Side Face of Test Sample Showing Adherent Oxide.

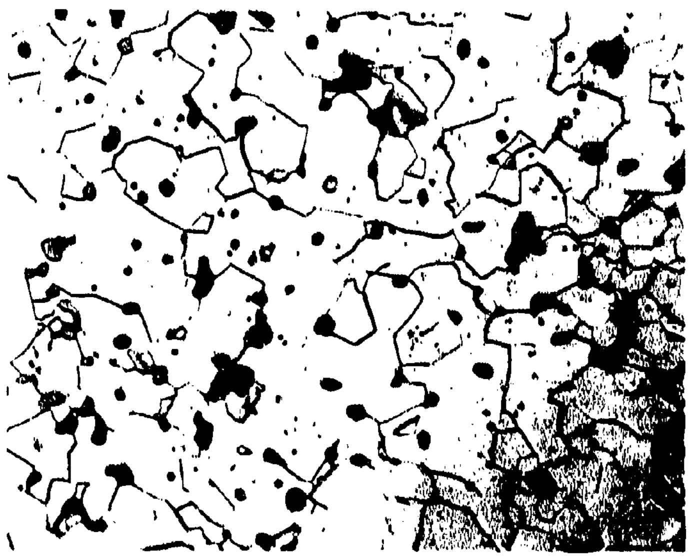

Plate 1-4241

Etched with 10 Glycerine $5HNO_3$ 3HF X500

Figure 15. Arc Plasma Test $HfB_{2.1}$ (A-2)-4M, Matrix Sting Leg Showing Matrix Grain Size.

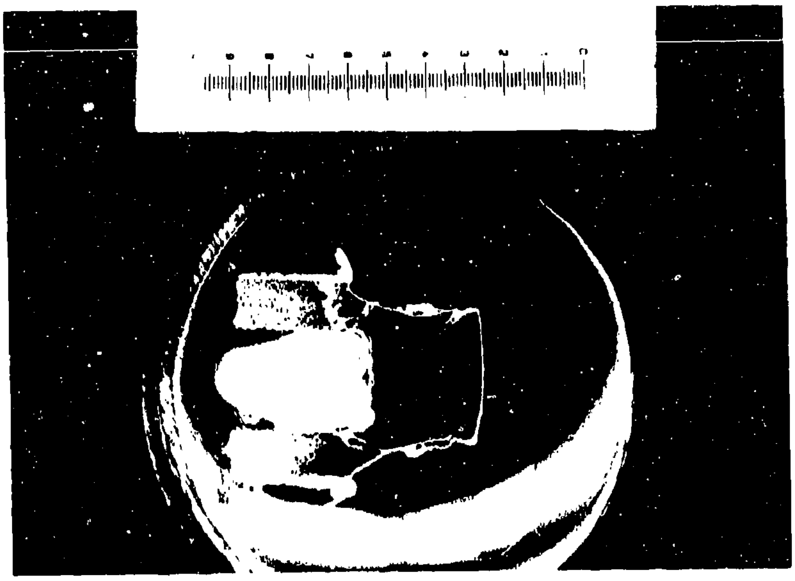

Plate 1-4233

One Inch Scale X 2.5

Figure 16. Arc Plasma Test $HfB_{2.1}$(A-2)-3M, Surface Temperature 6010°F, Stagnation Enthalpy 6585 BTU/lb, Stagnation Pressure 1 atm, Cold Wall Heat Flux 1060 BTU/ft^{2}sec, Exposure Time 82 Seconds, Initial Thickness 542 Mils, Final Thickness 281 Mils. Melting Observed. Hot Face on Right.

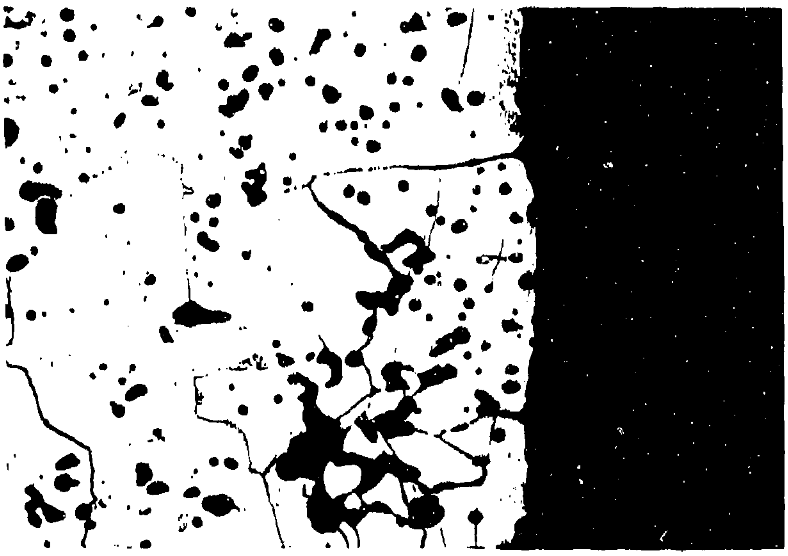

Plate 1-4234

Etched with 10 Glycerine $5HNO_3$ 3HF X250

Figure 17. Arc Plasma Test $HfB_{2.1}$(A-2)-3M, Hot Face, Showing Boride with Extremely Large Grain Size at Left.

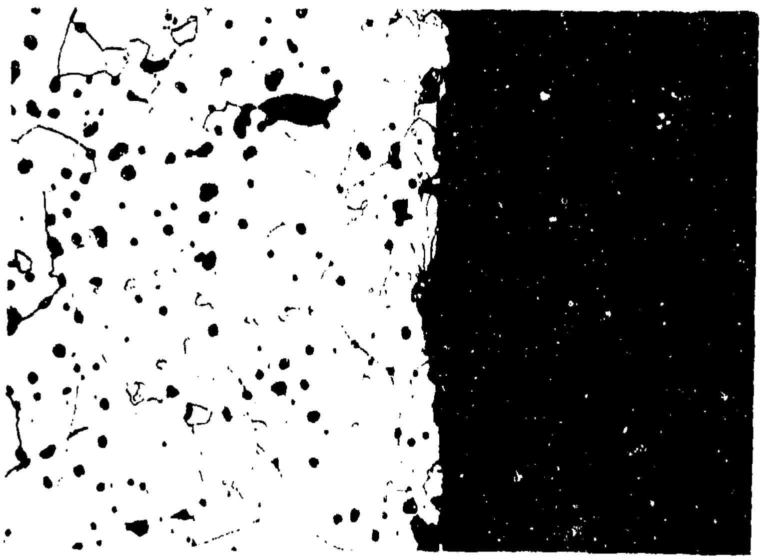

Plate 1-4236

Etched with 10 Glycerine $5HNO_3$ 3HF X250

Figure 18. Arc Plasma Test $HfB_{2.1}$(A-2)-3M, Side Face Showing Adherent Oxide and Boride at Left.

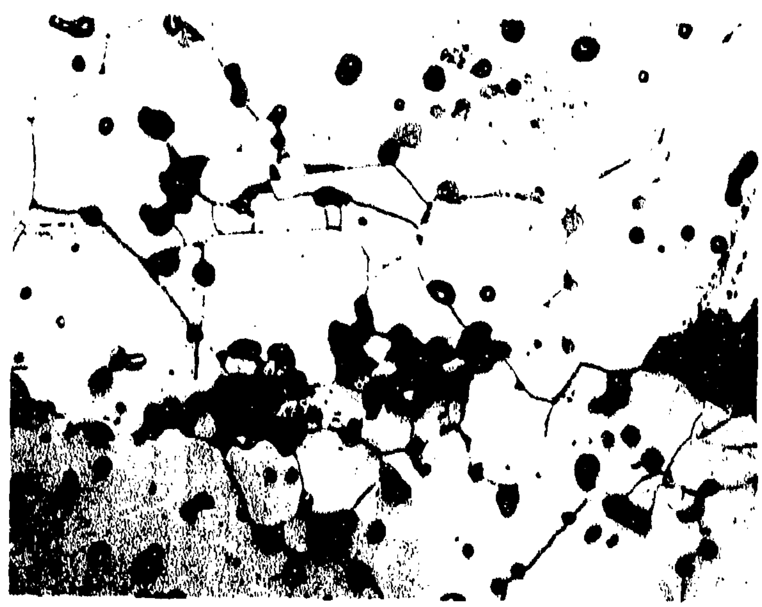

Plate 1-4237

Etched with 10 Glycerine $5HNO_3$ 3HF X500

Figure 19. Arc Plasma Test $HfB_{2.1}$(A-2)-3M, Matrix Sting Leg.

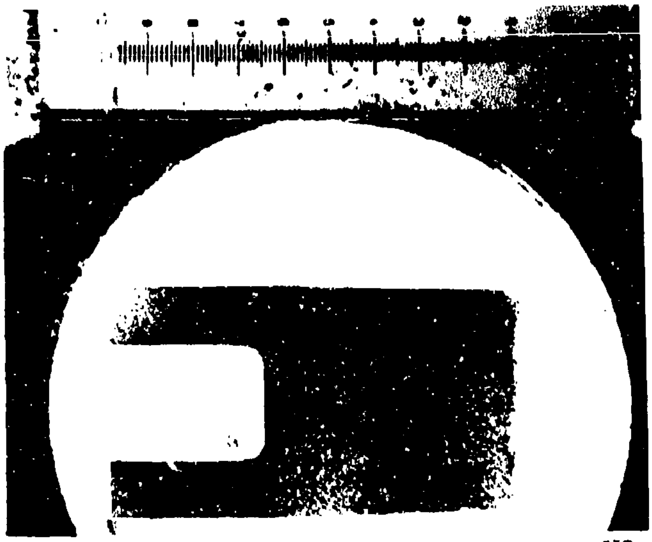

Plate No. 1-4993

X2.81

Figure 20. Arc Plasma Test $HfB_{2.1}$(A-2)-11R, Surface Temperature 5040°F, Exposure Time 1800 Seconds, Stagnation Pressure 0.097 atm, Stagnation Enthalpy 10730 BTU/lb, Cold Wall Heat Flux 651 BTU/ft^2sec., Initial Length 605 Mils, Final Length 566 Mils. Hot Face at Right. One Inch Scale.

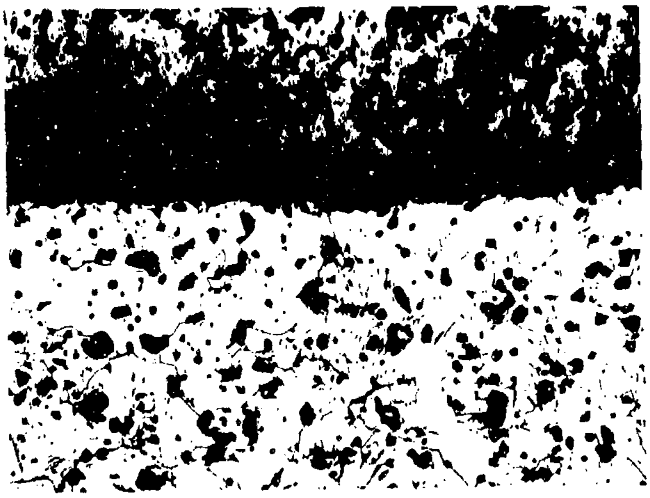

Plate No. 1-4994

Etched with 10 Glycerine $5HNO_3$ 3HF X250

Figure 21. Arc Plasma Test $HfB_{2.1}$(A-2)-11R. Interface of Oxide (Top) and Matrix.

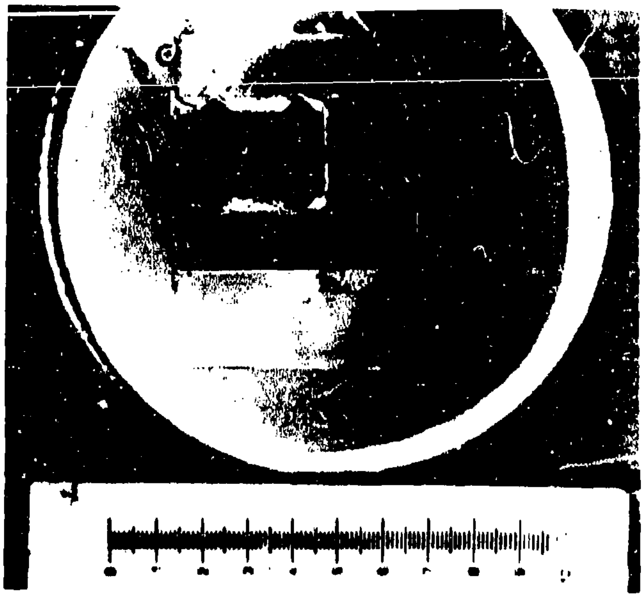

Plate No. 1-4264

X2.81

Figure 22. Arc Plasma Test $HfB_{2.1}$(A-2)-10R, Surface Temperature 5290°F, Exposure Time 60 Seconds, Stagnation Pressure 0.158 atm, Stagnation Enthalpy 7260 BTU/lb, Cold Wall Heat Flux 781 BTU/ft^{2}sec, Initial Length 558 Mils, Final Length 174 Mils. Hot Face at Right. One Inch Scale.

Plate No. 1-4265

Etched with 10 Glycerine $5HNO_3$ 3HF X250

Figure 23. Arc Plasma Test $HfB_{2.1}$(A-2)-10R. Rapid Melting was Observed. Interface of Melted Region (Right) and Matrix.

Plate No. 1-4226

X2.44

Figure 24. Arc Plasma Test $HfB_{2.1}$ (A-2)-1M, Surface Temperature $4060^{\circ}F$, Exposure Time 1800 Seconds, Stagnation Pressure 1.06 Atm., Stagnation Enthalpy 3270 BTU/lb, Cold Wall Heat Flux 520 BTU/ft^2 sec, 21 Mils Recession. Hot Face at Right. One Inch Scale.

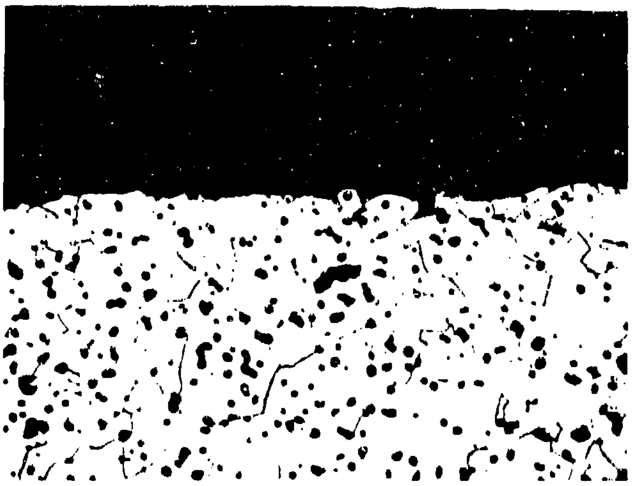

Plate No. 1-4227

Etched with 10 Glycerine $5HNO_2$ 3H F X250

Figure 25. Arc Plasma Test $HfB_{2.1}$ (A-2)-1M, Hot Surface.

X2.82

Plate No. 1-4996

Figure 26. Arc Plasma Test $HfB_{2.1}$ (A-2) - 12R, Surface Temperature 4640°F, Exposure Time 1800 Seconds, Stagnation Pressure 0.095 Atm., Stagnation Enthalpy 9830 BTU/lb, Cold Wall Heat Flux 573 BTU/ft^2 sec, 11 Mils Recession. Hot Face Down. One Inch Scale.

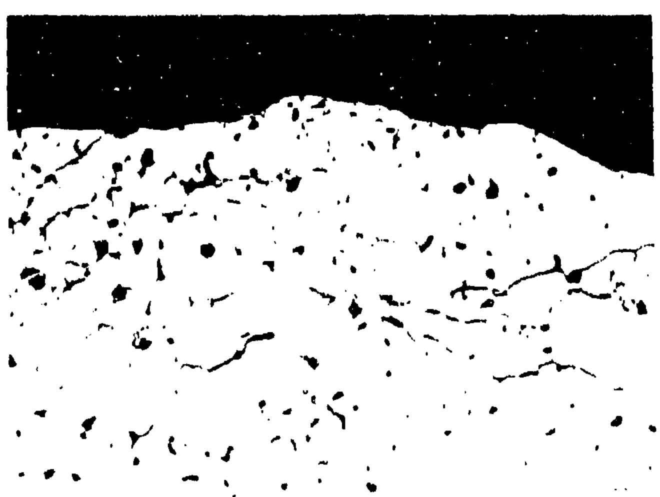

Plate No. 1-4997

Etched with 10 Glycerine $5HNO_3$ 3HF

Figure 27. Arc Plasma Test $HfB_{2.1}$(A-2) -12R, Hot Surface.

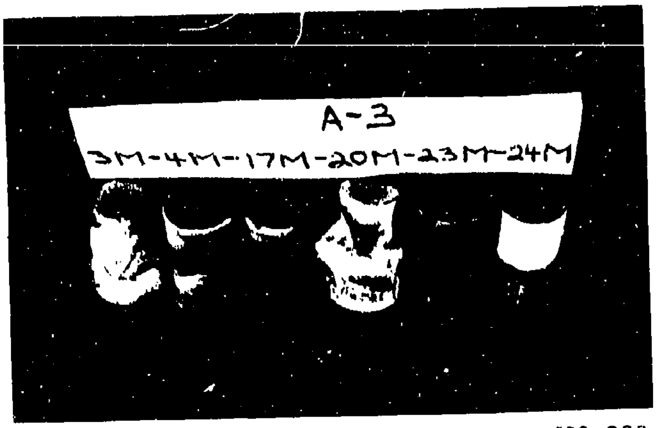

Plate No.
1-2803

X0.938

Figure 28. Post Exposure Photographs of Arc Plasma Tests ZrB_2 (A-3)-3M, 4M, 17M, 20M, 23M and 24M. Samples 3M and 20M Exhibited Melting. Sting End of 8M was Cracked During Removal from Sting. Hot Face is Pointing Up.

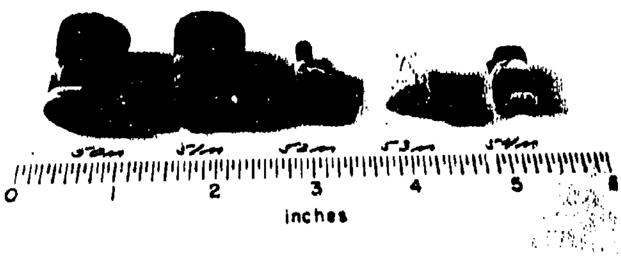

Plate No.
1-8734

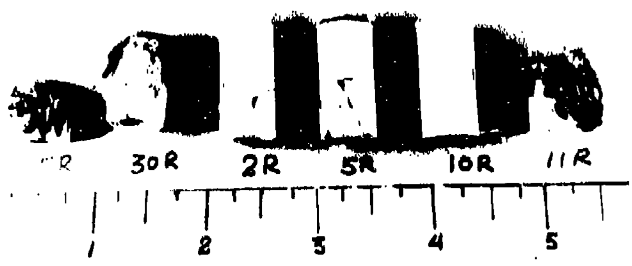

Plate No.
1-3595-A

Figure 29. Post Exposure Photographs of Arc Plasma Tests ZrB_2 (A-3)-50M, 51M, 52M, 53M, 54M, 15R, 30R, 2R, 5R, 10R and 11R. Samples 15R, 30R and 11R Exhibited Melting. Sting Ends of 30R, 2R and 5R were Cracked During Removal from Sting. Scale is One Inch. Hot Face is Pointing Up.

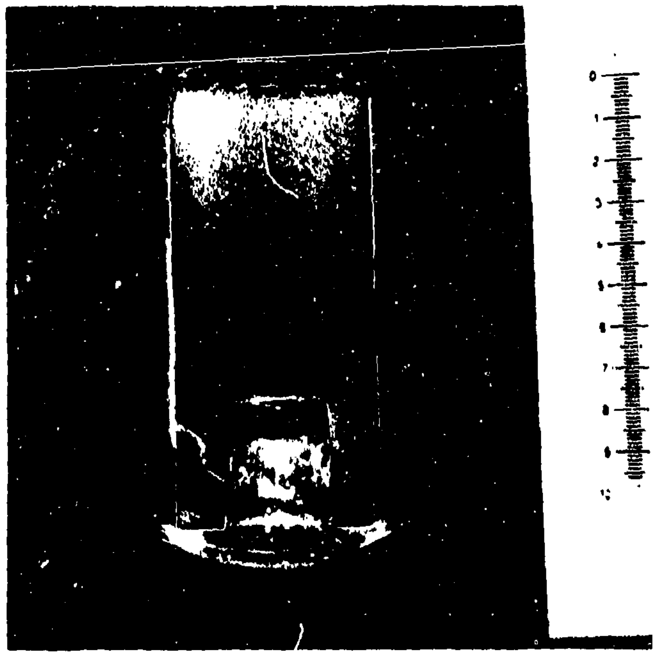

Plate No.
1-2810

X2.60

Figure 30. Arc Plasma Test ZrB_2(A-3)-4M, Surface Temperature 4505°F, Stagnation Enthalpy 3990 BTU/lb, Stagnation Pressure 1.07 Atm., Cold Wall Heat Flux 560 BTU/ft^2 sec, Exposure Time 1860 Seconds, Initial Length 1062 Mils, Final Length 1048 Mils, Hot Face Up. One Inch Scale

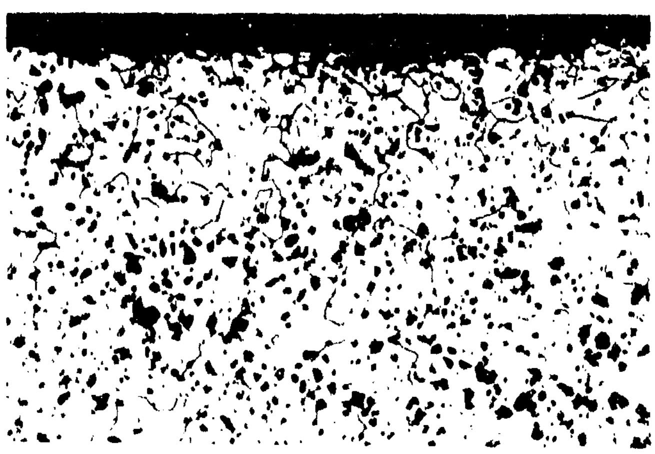

Plate No.
1-2811

Etched with 10 Glycerine
$5HNO_3 3HF$

X250

Figure 31. Arc Plasma Test ZrB_2(A-3)-4M, Hot Face at Top.

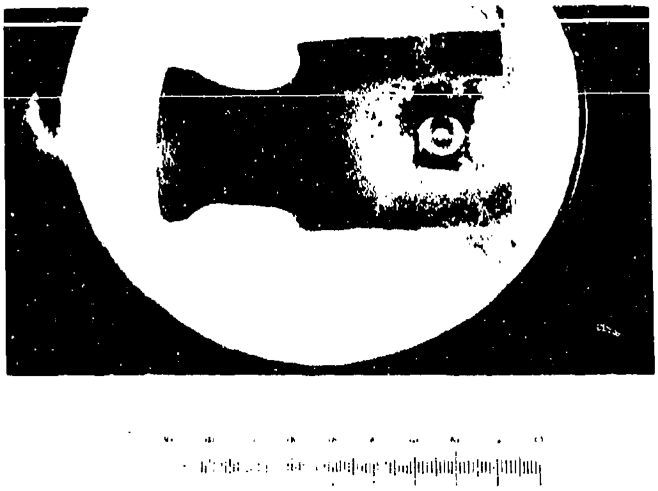

Plate No. 1-2814

X2.50

Figure 32 Arc Plasma Test ZrB_2(A-3)-20M, Surface Temperature 5530°F Exposure Time 90 Seconds, Stagnation Pressure 1.11 Atm. Stagnation Enthalpy 4665 BTU/lb, Cold Wall Heat Flux 840 BTU/ft^2 sec, 204 Mils Recession, Hot Face at Left. One Inch Scale.

Plate No. 1-2816

Etched with 10 Glycerine $5HNO_3$ 3HF X250

Figure 33. Arc Plasma Test ZrB_2 (A-3)-20M, Hot Surface.

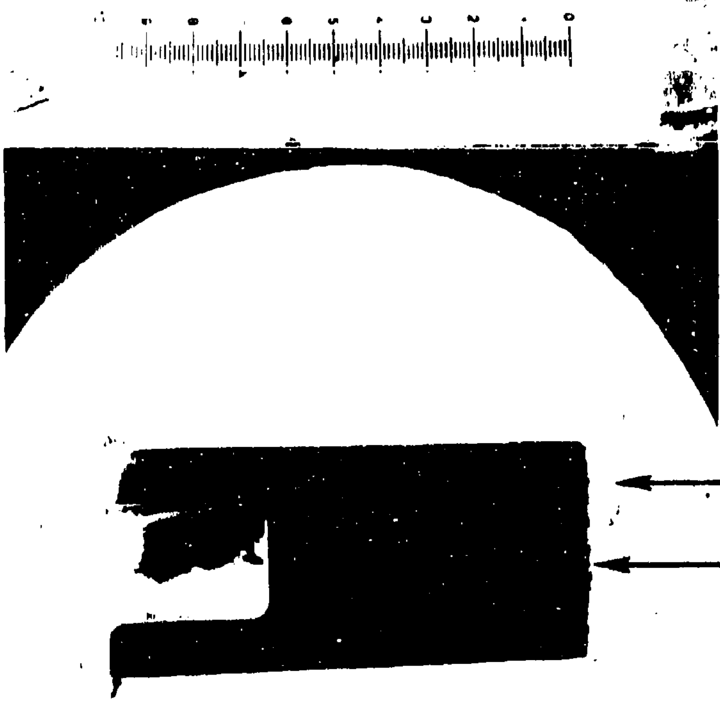

Plate 1-3602

X3

Figure 34. Arc Plasma Test ZrB_2(A-3)-10R, Surface Temperature 4345°F, Stagnation Enthalpy 9530 BTU/lb, Stagnation Pressure 0.021 atm., Cold Wall Heat Flux 520 BTU/ft^{2}sec, Exposure Time 1802 Seconds, Initial Length 1045 Mils, Final Length 1027 Mils. Hot Face at Right.

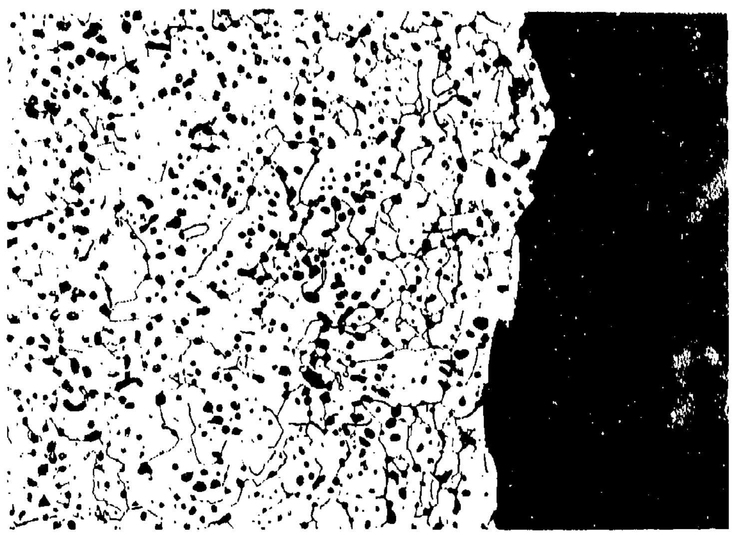

Plate 1-3603

Etched with 10 Glycerine $5HNO_3$ 3HF X250

Figure 35. Arc Plasma Test ZrB_2(A-3)-10R, Hot Face, Showing Boride at Left.

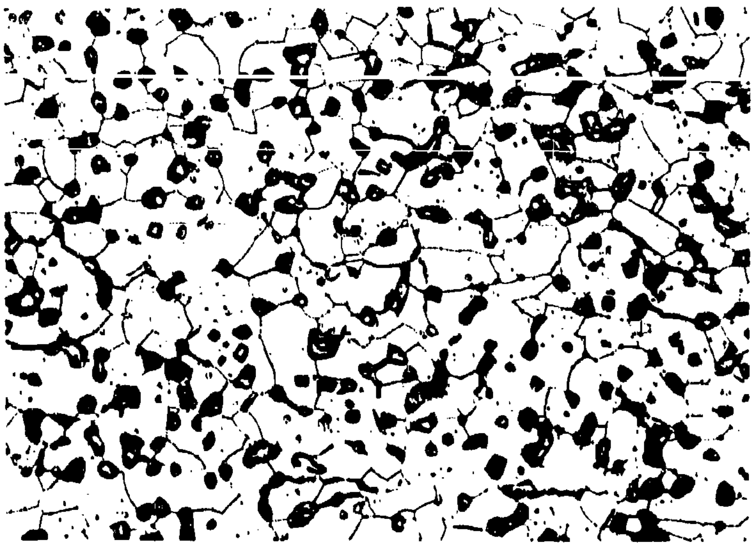

Plate 1-3604

Etched with 10 Glycerine $5HNO_3$ 3HF X500

Figure 36. Arc Plasma Test ZrB_2(A-3)-10R, Matrix Sting Leg, Showing Matrix Grain Size.

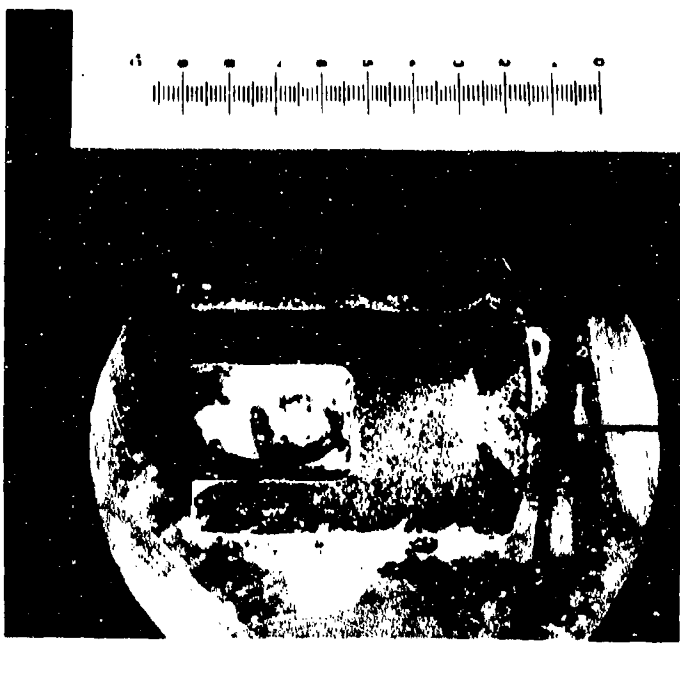

X3

Figure 37. Arc Plasma Test ZrB_2(A-3)-11R, Surface Temperature 5435°F, Stagnation Enthalpy 9270 BTU/lb, Stagnation Pressure 0.187 atm, Cold Wall Heat Flux 950 BTU/ft^2 sec, Exposure Time 51 Seconds, Initial Length 1063 Mils, Final Length 728 Mils. Hot Face at Right Illustrates Melting. One Inch Scale.

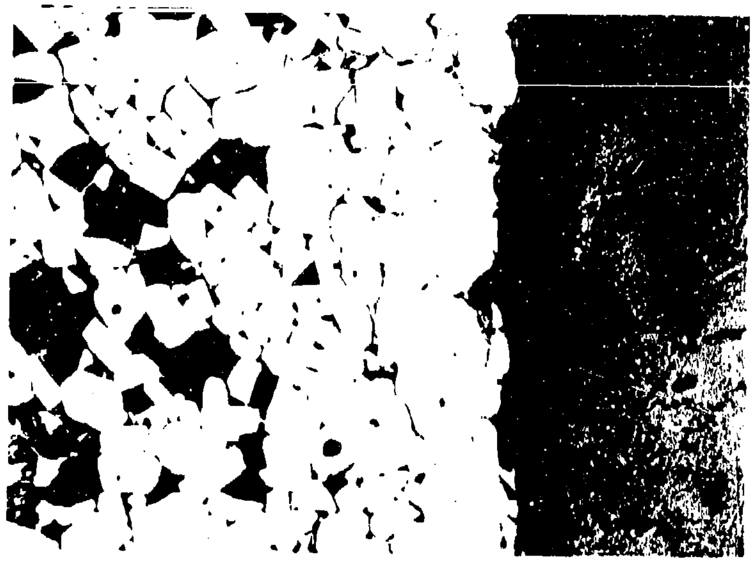

Plate 1-3606

Etched with 10 Glycerine $5HNO_3$ 3HF X250

Figure 38. Arc Plasma Test ZrB_2 (A-3)-11R, Hot Face, Showing Solidified Grain Structure in Core Region of Hot Face (See Figures 141 and 143).

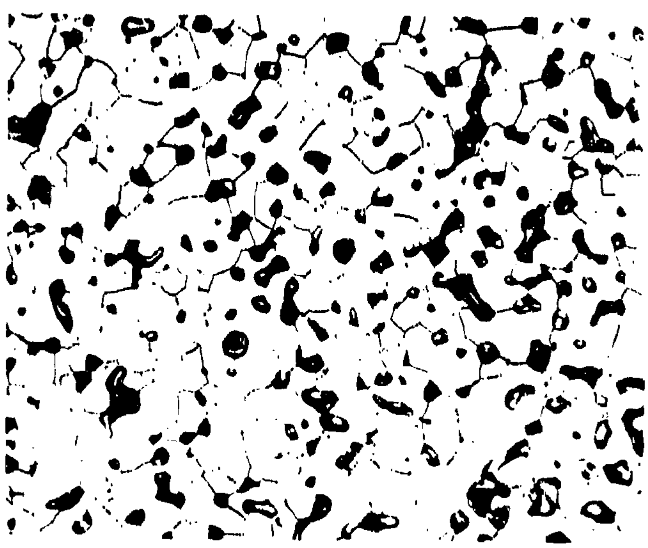

Plate 1-3595

Etched with 10 Glycering $5HNO_3$ 3HF X500

Figure 39. Arc Plasma Test ZrB_2(A-3)-11R, Matrix Sting Leg, Showing Matrix Grain Size.

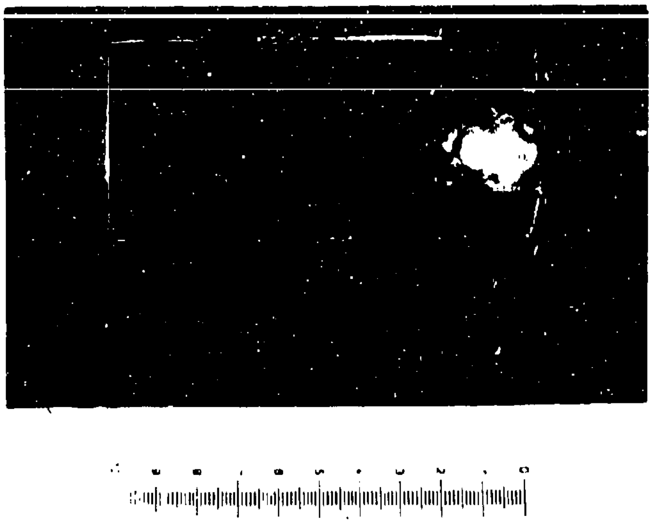

Plate No. 1-2821

X2.55

Figure 40. Arc Plasma Test ZrB_2(A-3)-23M, Surface Temperature 3990°F, Exposure Time 1860 Seconds, Stagnation Pressure 1.06 Atm., Stagnation Enthalpy 3345 BTU/lb, Cold Wall Heat Flux 460 BTU/ft^{2}sec, 8 Mils Recession. Hot Face at Left. One Inch Scale.

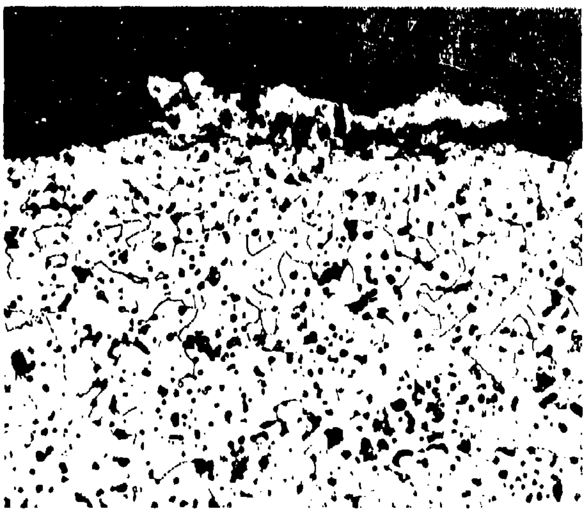

Plate No. 1-2822

X250

Etched with 10 Glycerine $5HNO_3$ 3HF

Figure 41. Arc Plasma Test ZrB_2(A-3)-23M, Hot Surface.

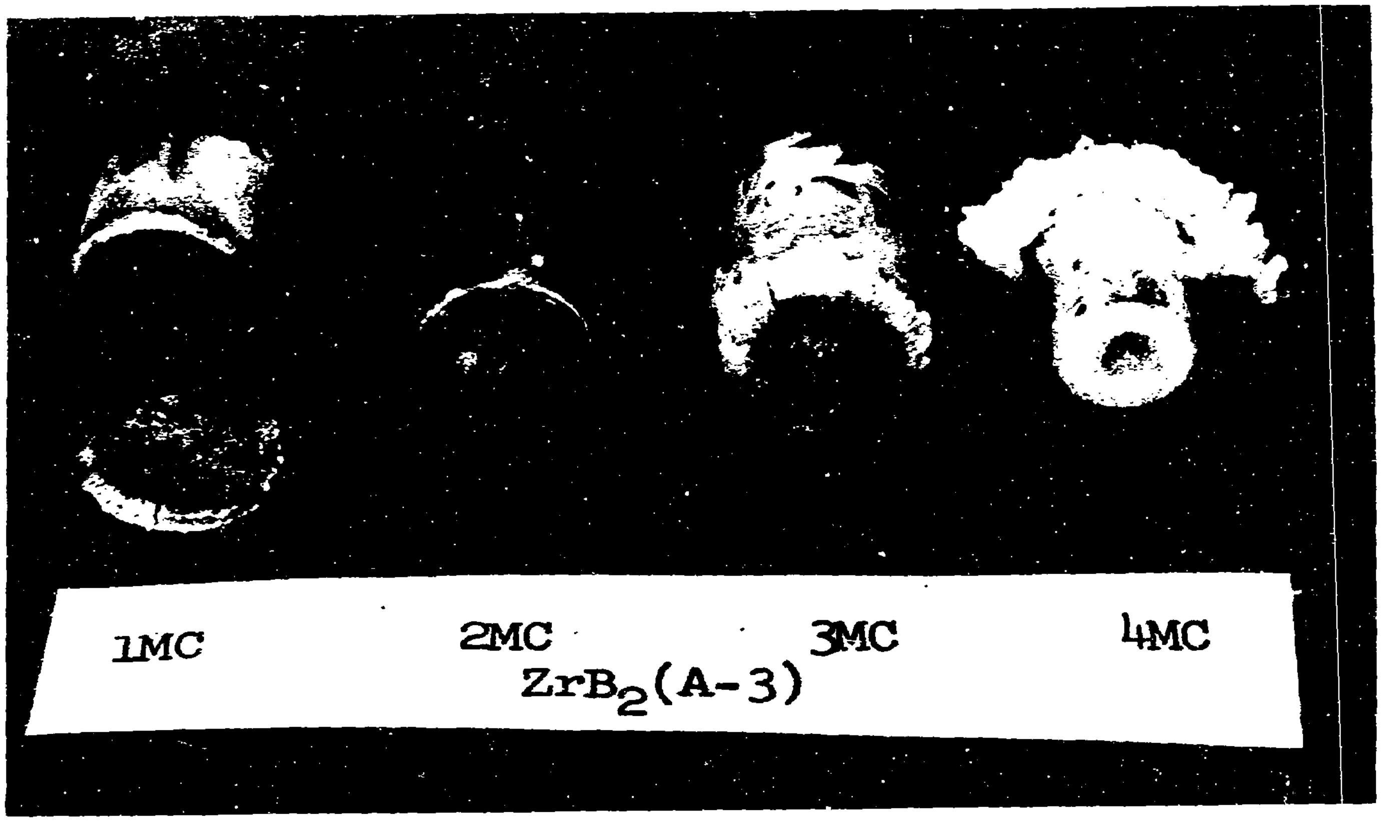

Figure 42. Post Exposure Photographs of Samples ZrB_2(A-3)-1MC, 2MC, 3MC and 4MC.

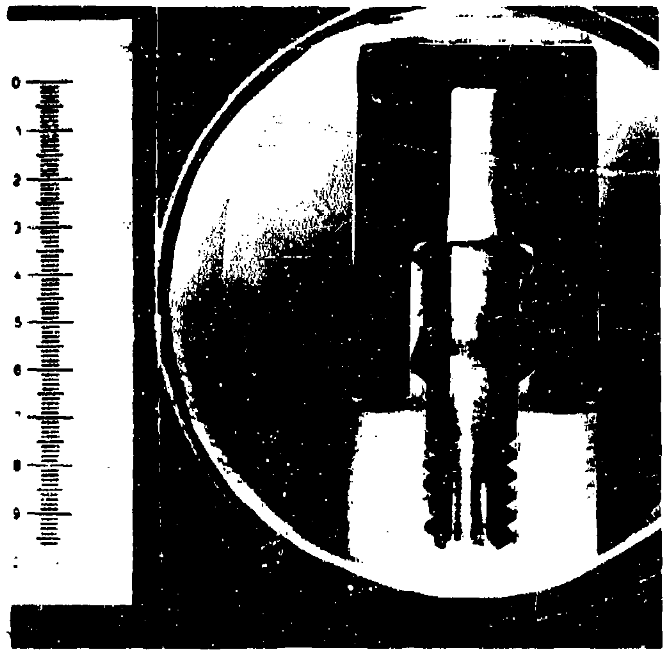

Plate No.
1-9213

X3.00

Figure 43. Arc Plasma Test ZrB_2(A-3)-2MC, Surface Temperature 4470°F, Internal Temperature 2940°F, Exposure Time 1800 Seconds, Stagnation Pressure 1.05 Atm., Stagnation Enthalpy 3230 BTU/lb, Cold Wall Heat Flux 365 BTU/ft^{2}sec, 14 Mil Recession. Hot Face Up. One Inch Scale.

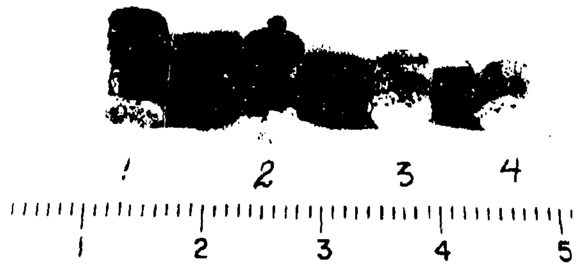

Plate No. 1-4269

Figure 44. Post Exposure Photographs of Arc Plasma Tests HfB_2+ SiC(A-4)-1M, 2M, 3M and 4M. Samples 3M and 4M Exhibited Melting. Hot Face is Pointing Down. Tungsten Sting was not Removed from Sample 2M and is Protruding from Sting Hole

Plate No. 1-5313

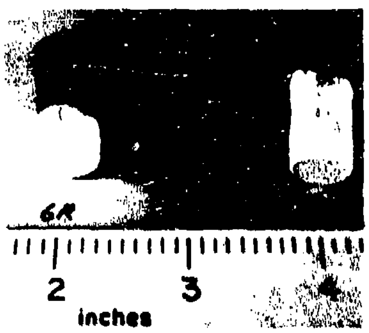

Plate No. 1-6423

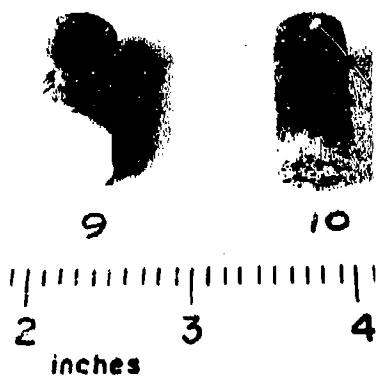

Plate No. 1-6609

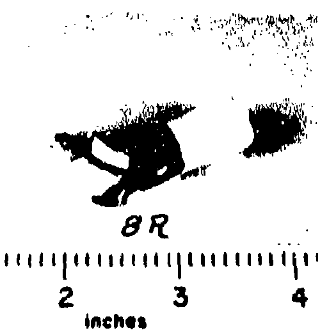

Plate No. 1-4411

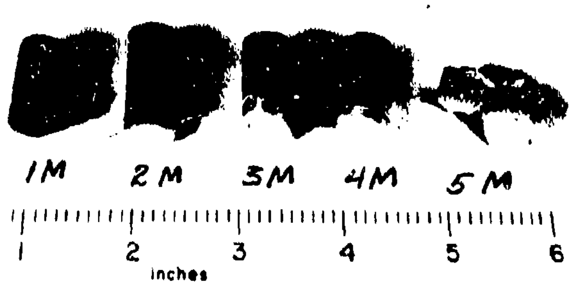

Figure 45. Post Exposure Photographs of Arc Plasma Tests HfB_2+ SiC(A-4)-2-6R, 7R, 9R, 10R, 8R, 1M, 2M, 3M, 4M and 5M.

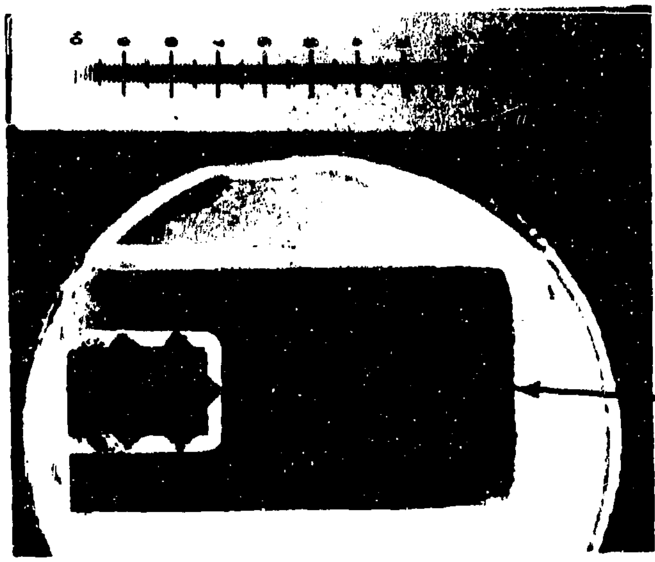

Plate 1-4438

Oxide on Surface of Model

X3

Figure 46. Arc Plasma Test HfB_2+SiC(A-4)-2M, Surface Temperature 5020°F, Exposure Time 1830 Seconds, Stagnation Pressure One Atm., Stagnation Enthalpy 5105 BTU/lb, Cold Wall Heat Flux 670 BTU/ft^2sec, Initial Thickness 675 Mils, Final Thickness 643 Mils. Hot Face at Right, One Inch Scale. Tungsten Sting is Seen in the Sting Hole.

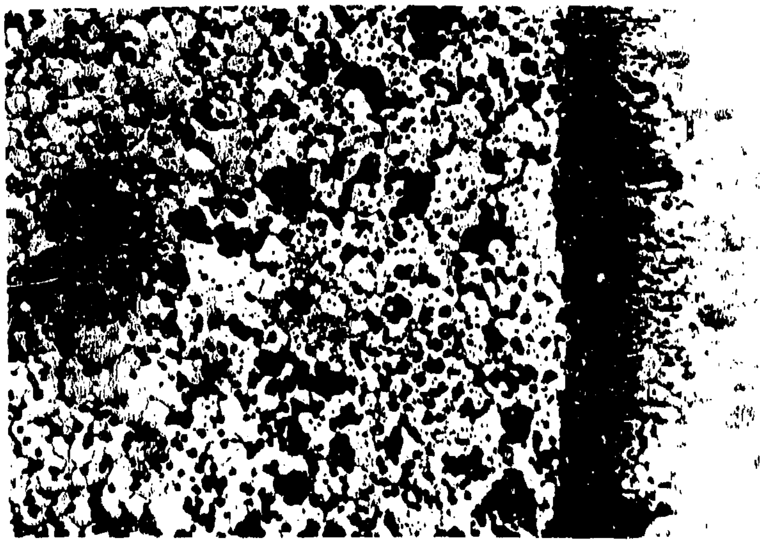

Plate 1-4439

X250

Figure 47. Arc Plasma Test HfB_2+SiC(A-4)-2M, Hot Face, Showing Boride at Left, Oxide at Right and Ten Mil Boride Zone Depleted of Silicon Carbide in Center. Note Adherence of Oxide.

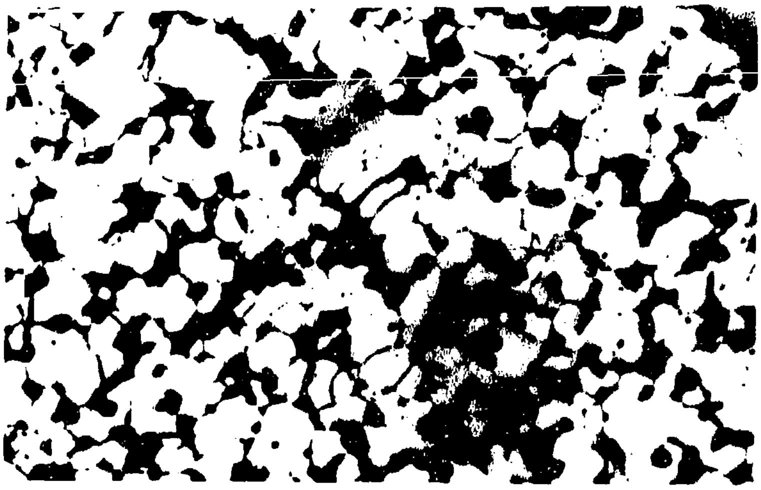

Plate 1-4441

Etched with 10 Glycerine $5HNO_3$ 3HF X500

Figure 48. Arc Plasma Test HfB_2+SiC(A-4)-2M, Matrix Sting Leg, Showing HfB_2 and SiC Grain Structure.

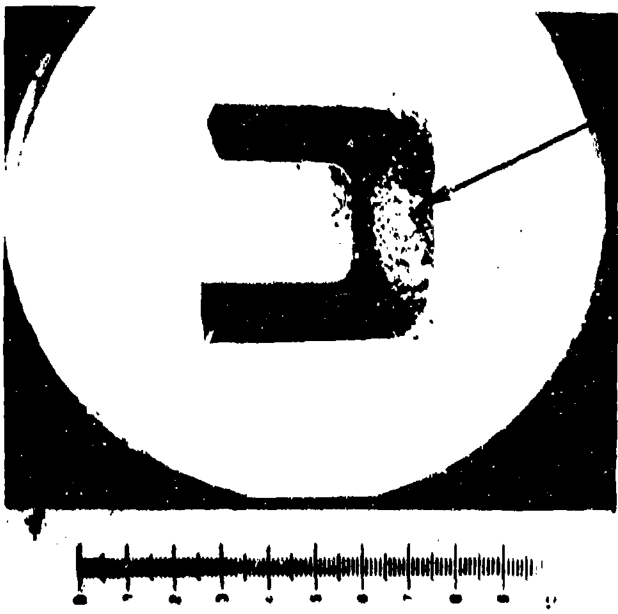

Surface at Hot Face Showing Melting Cup

Plate 1-4446

X3

Figure 49. Arc Plasma Test HfB_2+SiC(A-4)-4M, Surface Temperature 5160°F, Exposure Time 1608 Seconds, Stagnation Pressure One Atm., Stagnation Enthalpy 5410 BTU/lb, Cold Wall Heat Flux 900 BTU/ft^2 sec, Initial Thickness 644 Mils, Final Thickness 175 Mils. Hot Face on Right Illustrates Melting. One Inch Scale.

Zone Depleted of SiC

Oxide

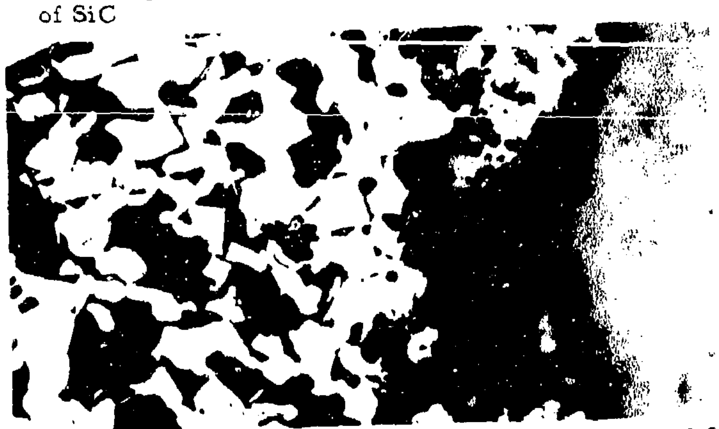

Plate 1-4447

X250

Figure 50. Arc Plasma Test HfB_2+SiC(A-4) Showing Hot Face.

(a)

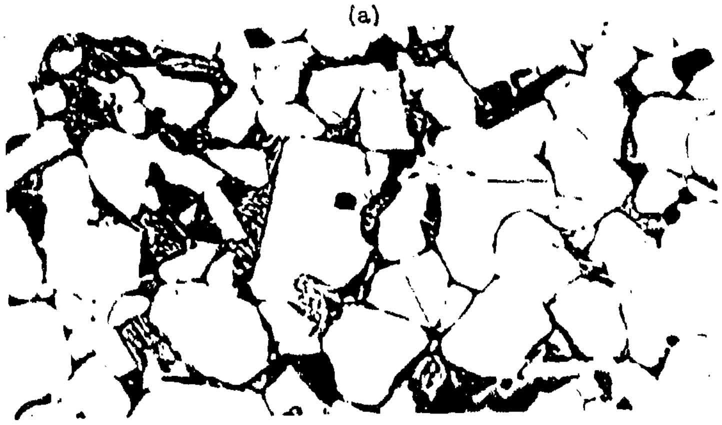

Plate 1-4449

Etched with 10 Glycerine $5HNO_3$ 3HF X500

(b)

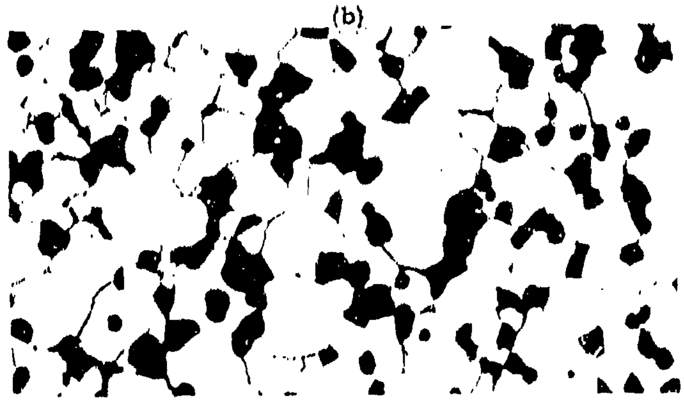

Plate 1-4448

Etched with 10 Glycerine $5HNO_3$ 3HF X500

Figure 51. Arc Plasma Test HfB_2 + SiC (A-4)-4M, (a) Matrix Near Top of Sting Hole, (b) Matrix at Sting Leg Showing Diboride Plus Silicon Carbide.

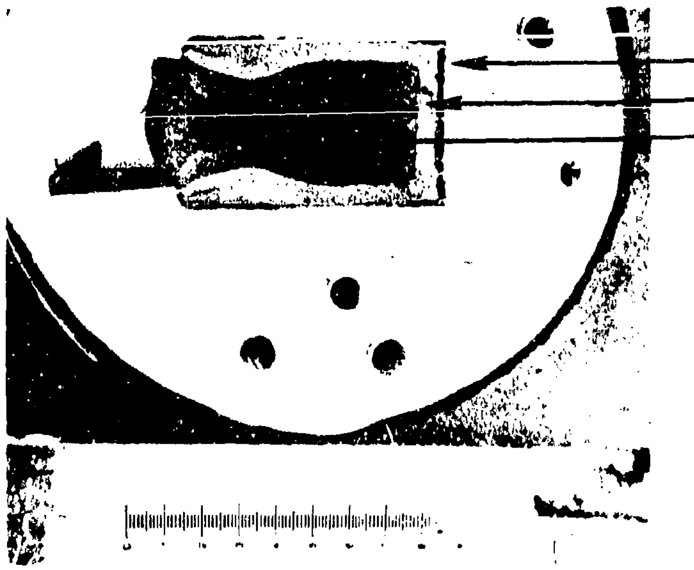

Plate No. 1-6610

X2.3

Figure 52. Arc Plasma Test HfB_2+20%SiC(A-4)-2-8R, Surface Temperature 5480°F, Exposure Time 1800 Seconds, Stagnation Pressure 0.027 Atm, Stagnation Enthalpy 13540 BTU/lb, Cold Wall Heat Flux 700 BTU/ft^2sec. Initial Length 781 Mils, Final Length 738 Mils. Hot Face at Right. One Inch Scale. Rear Broke on Removal After Test.

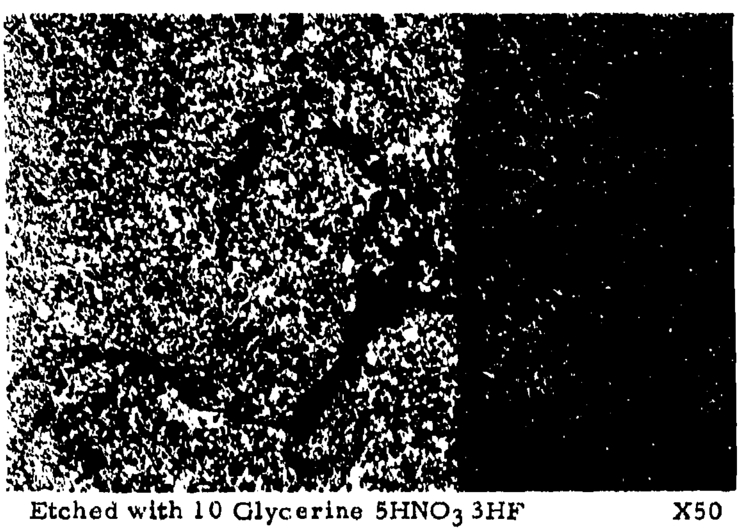

Plate No. 1-6611A

Etched with 10 Glycerine $5HNO_3$ 3HF X50

Figure 53. Arc Plasma Test HfB_2+20%SiC(A-4)-2-8R. Oxide at Right, Depletion Zone Center. Matrix at Left.

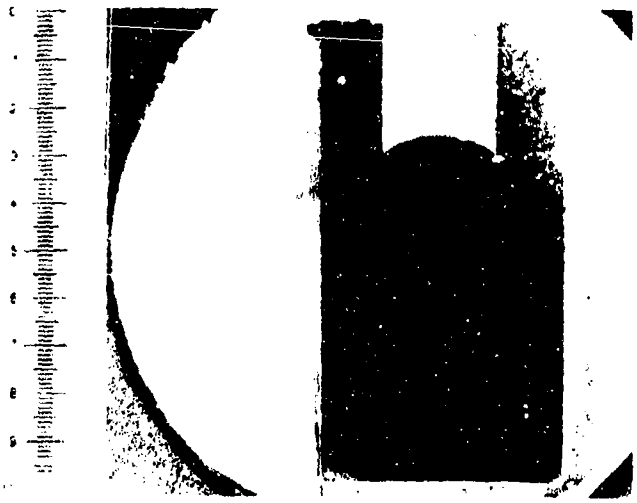

Plate No. 1-4435

X2.9

Figure 54. Arc Plasma Test HfB_2 + SiC(A-4)-1M, Surface Temperature 3450°F, Exposure Time 1830 Seconds, Stagnation Pressure 1.08 Atm., Stagnation Enthalpy 3915 BTU/lb, Cold Wall Heat Flux 570 BTU/ft^2sec, 6 Mil Recession. Hot Face Down. One Inch Scale.

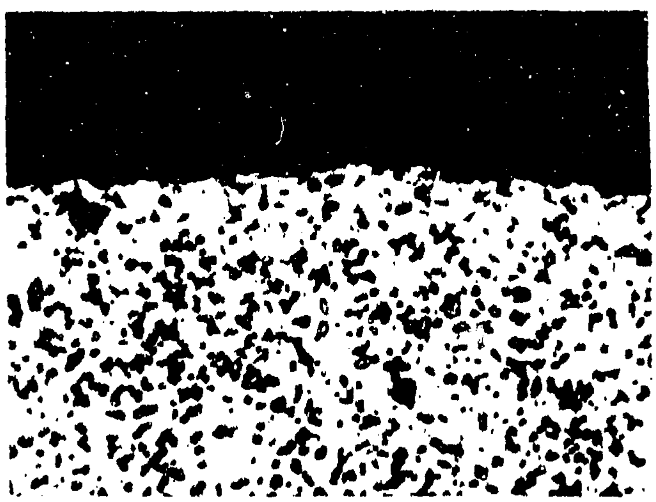

Plate No. 1-4436

Etched with 10 Glycerine $5HNO_3$ 3HF X250

Figure 55. Arc Plasma Test HfB_2 + SiC(A-4)-1M, Hot Surface Showing Oxide (Top) and Depletion Zone (Center).

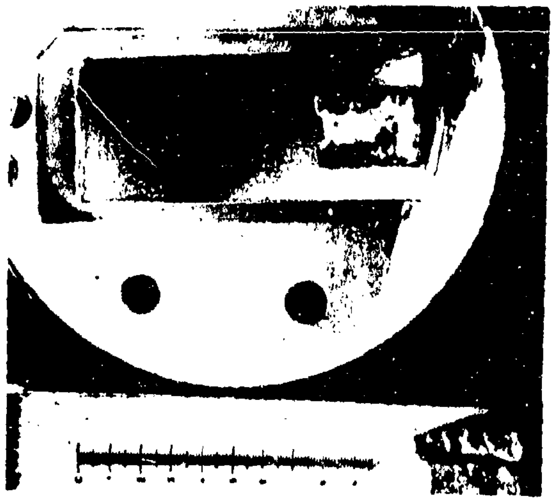

Plate No. 1-6424

X1.88

Figure 56. Arc Plasma Test HfB_2 + SiC (A-4)-2-9R, Surface Temperature 4680°F, Exposure Time 1800 Seconds, Stagnation Pressure 0.023 Atm., Stagnation Enthalpy 8920 BTU/lb, Cold Wall Heat Flux 402 BTU/ft^2 sec, 23 Mils Recession. Hot Face at Left. One Inch Scale.

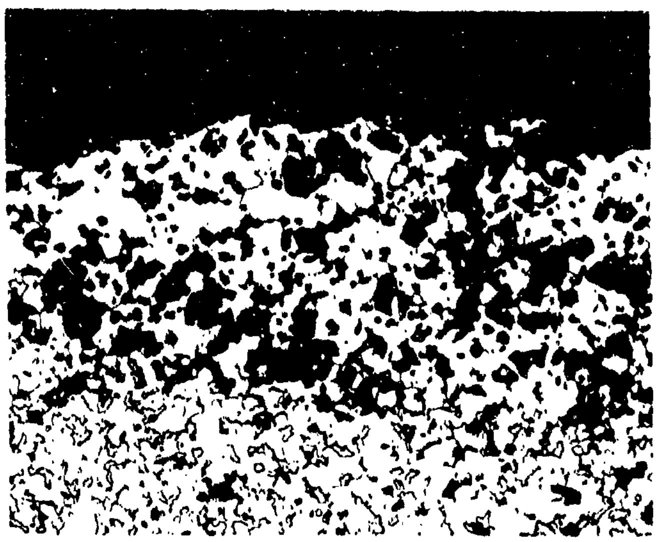

Plate No. 1-6425

Etched with 10 Glycerine $5HNO_3$ 3HF X250

Figure 57. Arc Plasma Test HfB_2 + SiC(A-4)-2-9R, Hot Surface Showing Depletion Zone at Top.

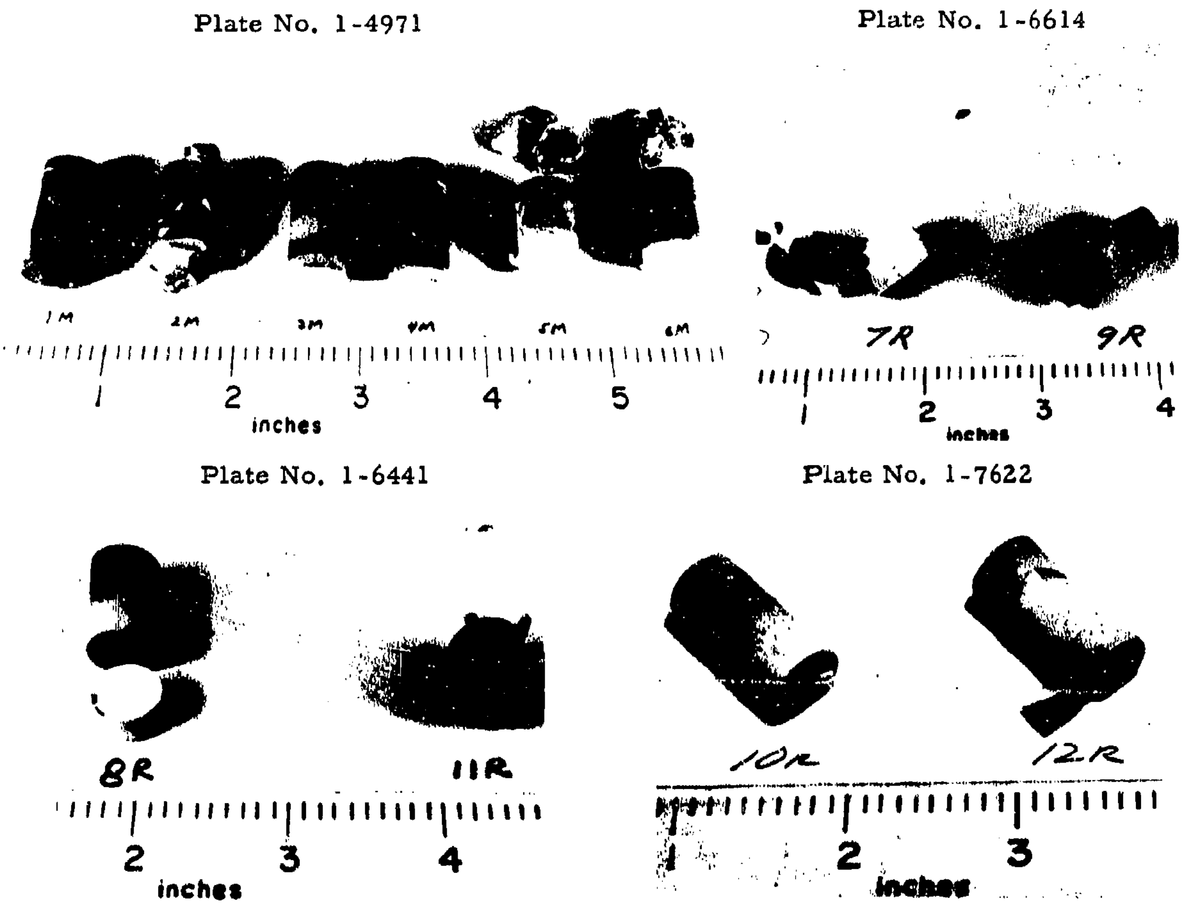

Figure 58. Post Exposure Photographs of Arc Plasma Tests Boride Z(A-5)-1M, 2M, 3M, 4M, 5M, 6M, 7R, 9R, 8R, 11R, 10R and 12R.

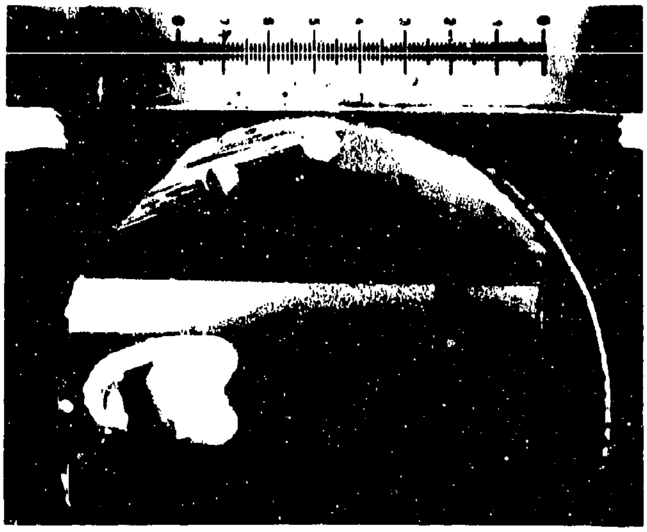

Plate No. 1-4981

X2.81

Figure 59a. Arc Plasma Test Boride Z(A-5)-4M, Surface Temperature 2920°F, Exposure Time 1830 Seconds, Stagnation Pressure 1.05 Atm, Stagnation Enthalpy 2500 BTU/lb, Cold Wall Heat Flux 350 BTU/ft^{2}sec, Initial Length 663 Mils, Final Length 659 Mils. Hot Face at Right. Specimen Thermal Shocked. One Inch Scale

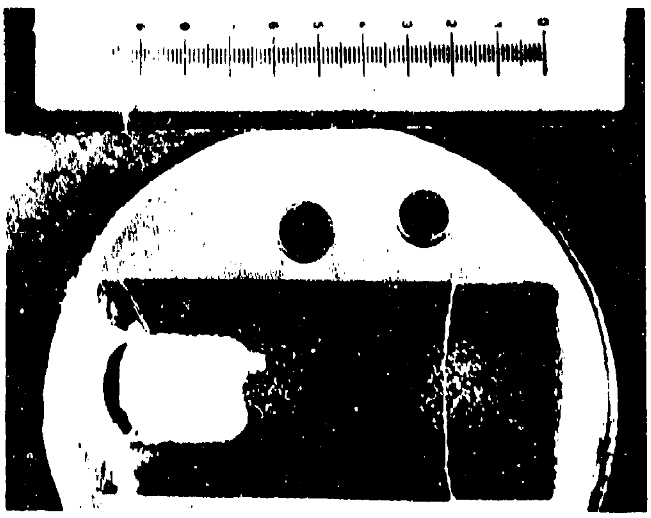

Plate No. 1-6442

X2.75

Figure 59b. Arc Plasma Test Boride Z(A-5)-8R, Surface Temperature 3790°F, Exposure Time 1800 Seconds, Stagnation Pressure 0.018 Atm, Stagnation Enthalpy 9200 BTU/lb, Cold Wall Heat Flux 262 BTU/ft^{2}sec, Inital Length 690 Mils, Final Length 680 Mils. Hot Face at Right. Specimen Thermal Shocked. One Inch Scale.

Plate No. 1-6574

Plate No. 1-7396

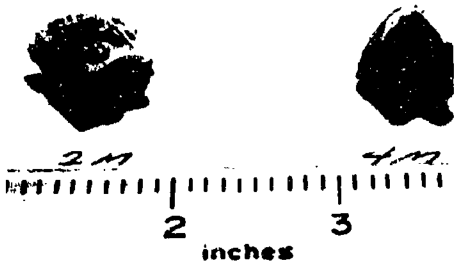

Plate No. 1-9526

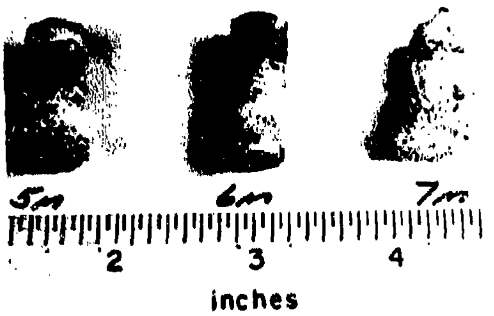

Plate No. 1-9586

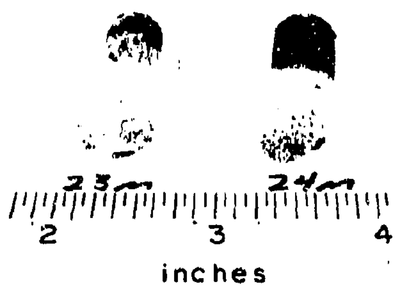

Plate No. 2-0190

Plate No. 2-0666

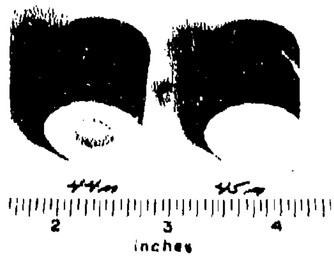

Figure 60. Post Exposure Photographs of Arc Plasma Tests $HfB_{2.1}$ + 20%SiC(A-7)-1M, 3M, 2M, 5M, 6M, 7M, 23M, 24M, 25M, 30M, 31M, 32M, 44M and 45M.

Plate No. 2-0583

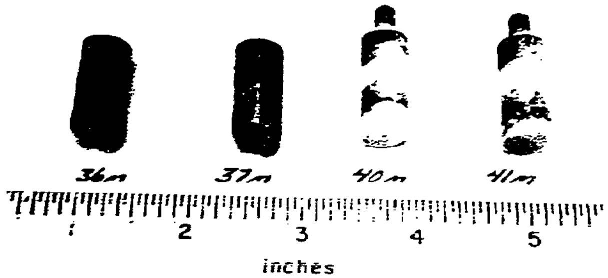

Plate No. 2-0581

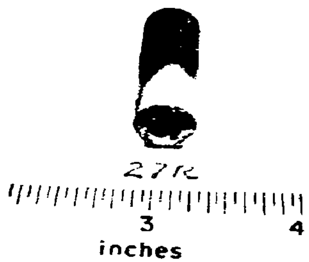

Plate No. 2-0191

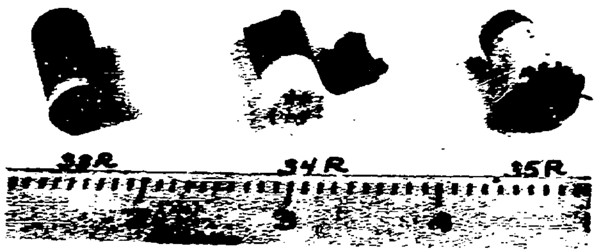

Plate No. 2-0667

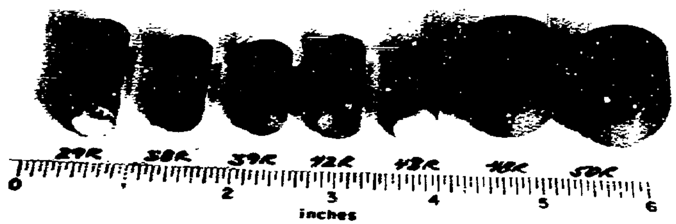

Plate No. 2-0703

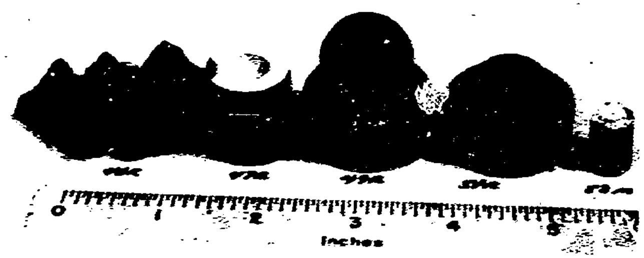

Figure 61. Post Exposure Photographs of Arc Plasma Tests HfB_2+20%SiC(A-7)-36M, 37M, 40M, 41M 27R, 33R, 34R, 5R, 29R, 38R, 39R, 42R, 43R, 48R, 50R, 46R, 47R, 49R, 51R and 52M.

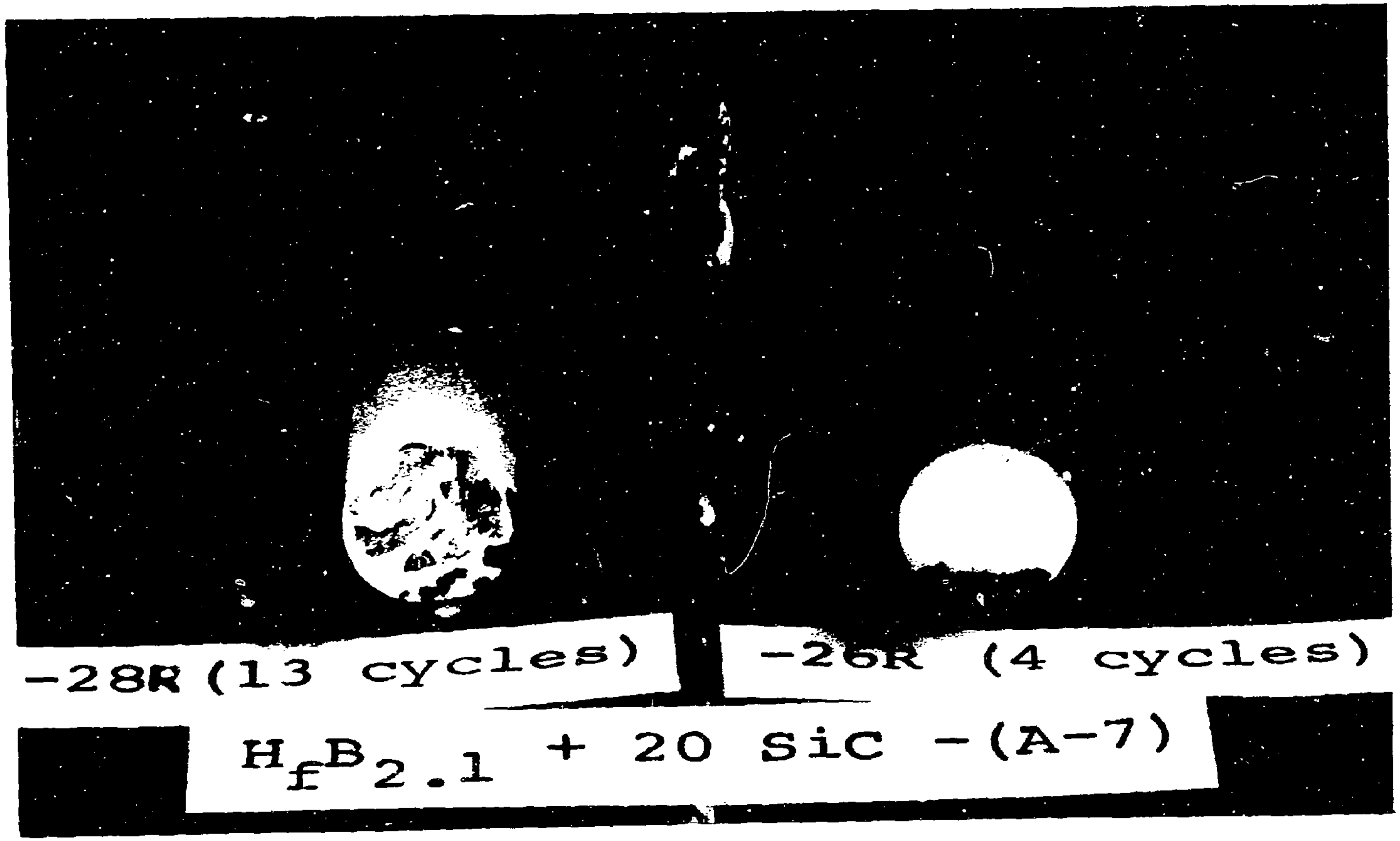

Figure 62. Post Exposure Photographs of Arc Plasma Tests $HfB_{2.1}$ + 20%SiC(A-7)-28R and 26R.

Plate No. 1-7397

X2.75

Figure 63. Arc Plasma Test $HfB_{2.1}$ + 20 v/o SiC(A-7)-2M, Surface Temperature 4800°F, Exposure Time 1745 Seconds, Stagnation Pressure 1.08 Atm. Stagnation Enthalpy 5055 BTU/lb, Cold Wall Heat Flux 715 BTU/ft^2 sec, 157 Mils Recession, Hot Face at Left. One Inch Scale.

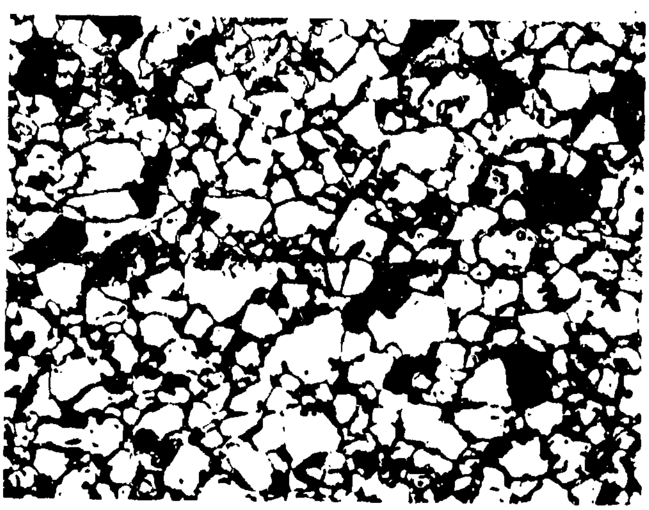

Plate No. 1-7398

Etched with 10 Glycerine $5HNO_3$ 3HF X250

Figure 64. Arc Plasma Test $HfB_{2.1}$ + 20 v/o SiC(A-7)-2M, Interface Between Depleted Zone and Matrix.

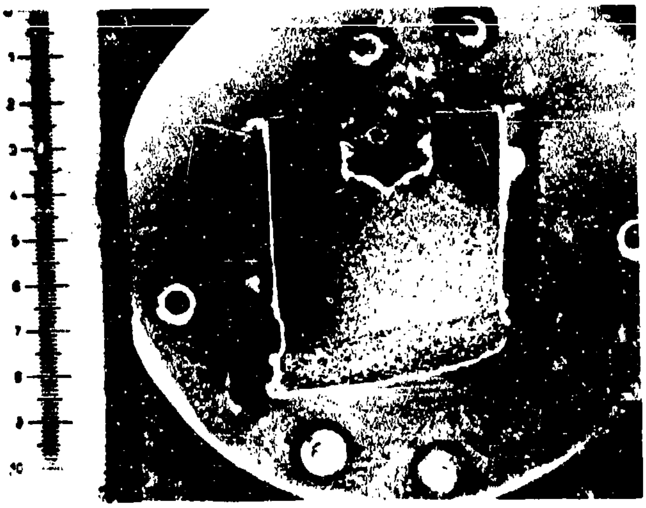

Plate No. 1-6575

X2.75

Figure 65. Arc Plasma Test $HfB_{2.1}$ + 20 v/o SiC(A-7)-1M Surface Temperature 5760°F, Exposure Time 56 Seconds, Stagnation Pressure 1.11 Atm. Stagnation Enthalpy 3915 BTU/lb, Cold Wall Heat Flux 810 BTU/ft^2 sec, 110 Mils Recession, Hot Face Down. One Inch Scale.

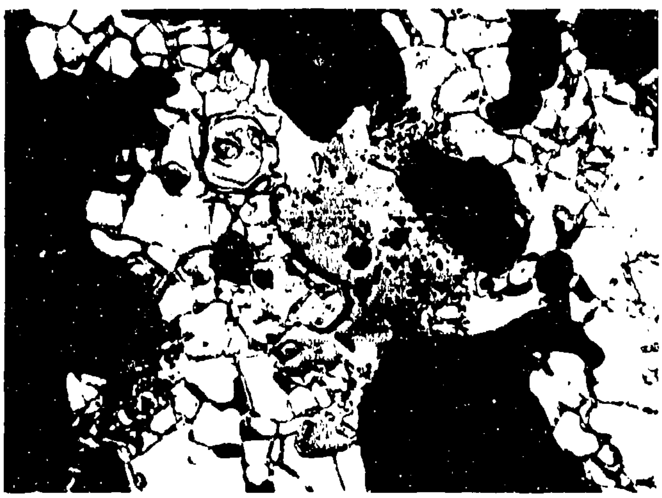

Plate No. 1-6576

Etched with 10 Glycerine 5HNO_3 3HF X 250

Figure 66. Arc Plasma Test $HfB_{2.1}$ + 20 v/o SiC(A-7)-1M, Hot Surface.

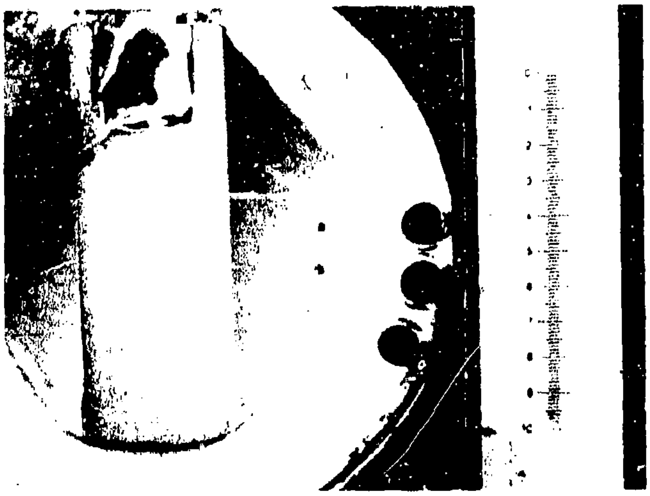

Plate No. 2-0211

X2.25

Figure 67. Arc Plasma Test $HfB_{2.1}$+20%SiC(A-7)-34R, Surface Temperature 5005°F, Exposure Time 1200 Seconds, Stagnation Pressure 0.160 Atm., Stagnation Enthalpy 8040 BTU/lb, Cold Wall Heat Flux 720 BTU/ft^{2}sec., Initial Length 920 Mils, Final Length 889 Mils, Hot Face Down. One Inch Scale. Oxide Broke Off on Handling.

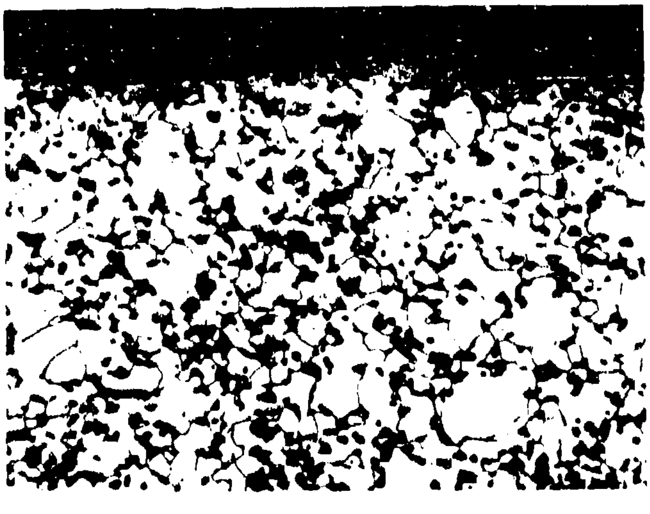

Plate No. 2-0212

Etched with 10 Glycerine $5HNO_3 3HF$ X250

Figure 68. Arc Plasma Test $HfB_{2.1}$+20%SiC(A-7)-34R. Hot Interface Up.

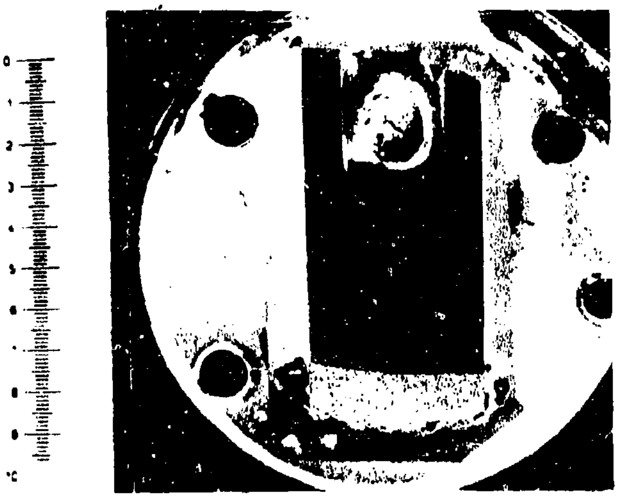

Plate No.
2-0214

X2.60

Figure 69. Arc Plasma Test $HfB_{2.1}$+20%SiC(A-7)-35R, Surface Temperature 5350°F, Exposure Time 90 Seconds, Stagnation Pressure 0.180 Atm., Stagnation Enthalpy 9030 BTU/lb, Cold Wall Heat Flux 791 BTU/ft^{2}sec, Initial Length 921 Mils, Final Length 606 Mils, Depletion Depth 130 Mils. Hot Face Down. One Inch Scale.

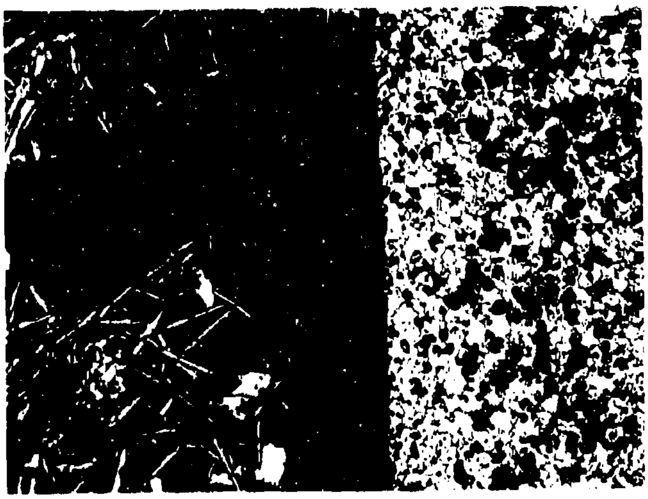

Plate No.
2-0215

Etched with 10 Glycerine 5$HNO_3$3HF

X250

Figure 70. Arc Plasma Test $HfB_{2.1}$+20%SiC(A-7)-35R. Side Interface, Depleted Matrix at Right, Melted Material at Left. Hot Face Up.

Plate No. 2-0675

X 2.35

Figure 71. Arc Plasma Test $HfB_{2.1}$ + 20 v/o SiC(A-7)-28R Average Surface Temperature 4650°F, Exposure Time 22, 400 Seconds (13 cyclic exposures each of approximately 1800 seconds), Stagnation Pressure 0.07 Atm. Stagnation Enthalpy 10300 BTU/lb, Cold Wall Heat Flux 495 BTU/ft^2sec, 15 Mils Recession, Hot Face Up. One Inch Scale.

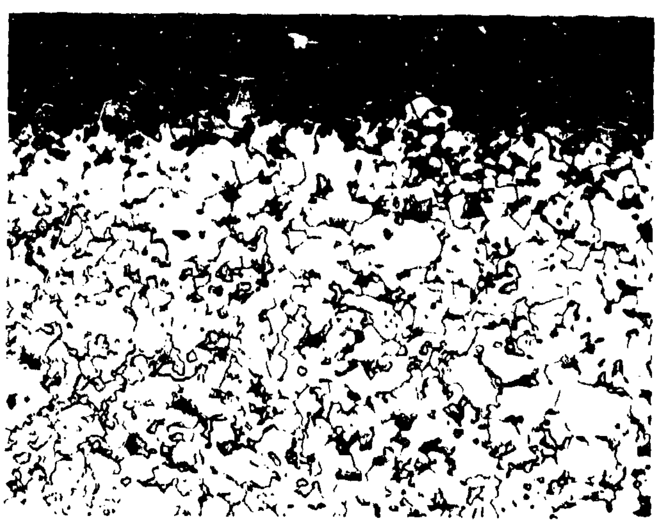

Plate No. 2-0676

Etched with 10 Glycerine $5HNO_3$ 3HF X250

Figure 72. Arc Plasma Test $HfB_{2.1}$ + 20 v/o SiC(A-7)-28R, Hot Surface.

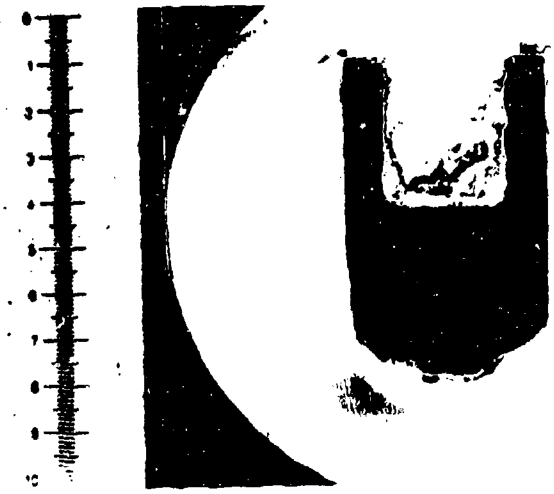

Plate No.
2-0681

Figure 73. Arc Plasma Test $HfB_{2.1}$+20 v/o SiC(A-7)-52M. Surface Temperature 4600°F, Exposure Time 14,030 Seconds (8 Cyclic Exposures Each of Approximately 1800 Seconds), Stagnation Pressure 1.03 Atm., Stagnation Enthalpy 4180 BTU/lb, Cold Wall Heat Flux 450 BTU/ft^2sec, 329Mils Recession, Hot Face Down, One Inch Scale.

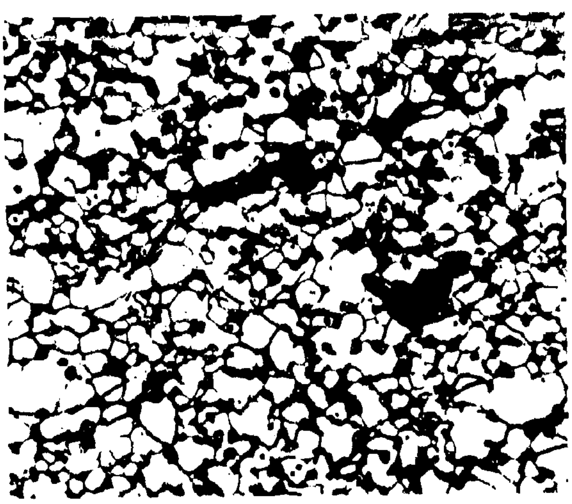

Plate No.
2-0682

Etched with 10 Glycerine
$5HNO_3 3HF$

X250

Figure 74. Arc Plasma Test $HfB_{2.1}$+20 v/o SiC(A-7)-52M Hot Surface.

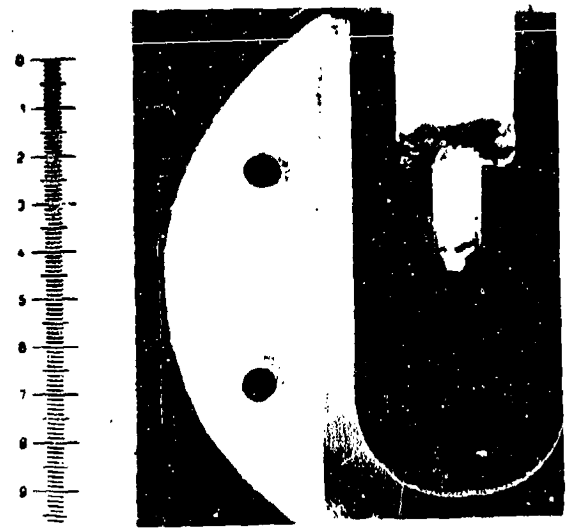

Plate No. 2-0677

X 2.95

Figure 75. Arc Plasma Test $HfB_{2.1}$ + 20 v/o SiC(A-7)-37MH Surface Temperature 3765°F, Exposure Time 1080 Seconds, Stagnation Pressure 1.02 Atm. Stagnation Enthalpy 3640 BTU/lb, Cold Wall Heat Flux 495 BTU/ft^{2}sec, 10 Mils Recession, Hot Face Down. One Inch Scale.

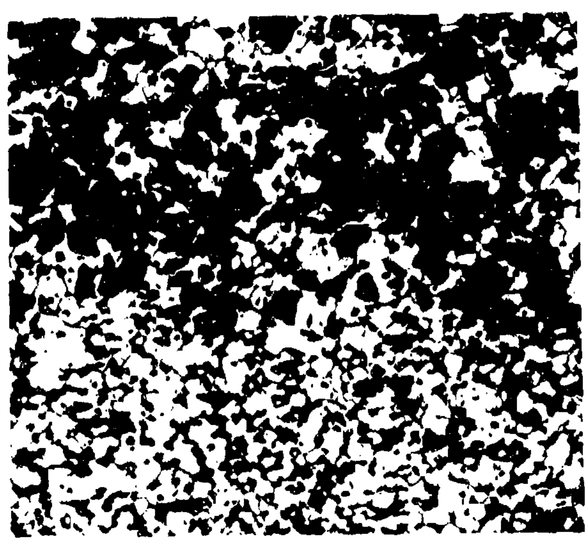

Plate No. 2-0678

Etched with 10 Glycerine $5HNO_3$ 3HF X 250

Figure 76. Arc Plasma Test $HfB_{2.1}$ + 20 v/o SiC(A-7)-37MH, Hot Surface.

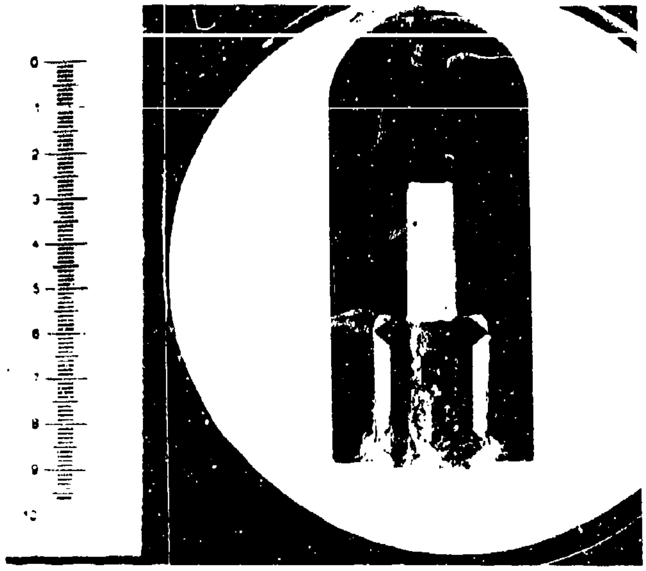

Plate No. 2-0679

X2.78

Figure 77. Arc Plasma Test $HfB_{2.1}$+20 v/oSiC(A-7)-39RH Surface Temperature 2710°F, Exposure Time 1812 Seconds, Stagnation Pressure 0.162 Atm., Stagnation Enthalpy 6540 BTU/lb, Cold Wall Heat Flux 487 BTU/ft^2sec, Second Exposure: Surface Temperature 2955°F, Exposure Time 1800 Seconds, Stagnation Pressure 0.053 Atm., Stagnation Enthalpy 8810 BTU/lb, Cold Wall Heat Flux 885 BTU/ft^2sec. Third Exposure: Surface Temperature 4285°F, Exposure Time 375 Seconds, Stagnation Pressure 0.105 Atm., Stagnation Enthalpy 7290 BTU/lb, Cold Wall Heat Flux 965 BTU/ft^2sec, 24 Mils Recession, Hot Face Up, One Inch Scale.

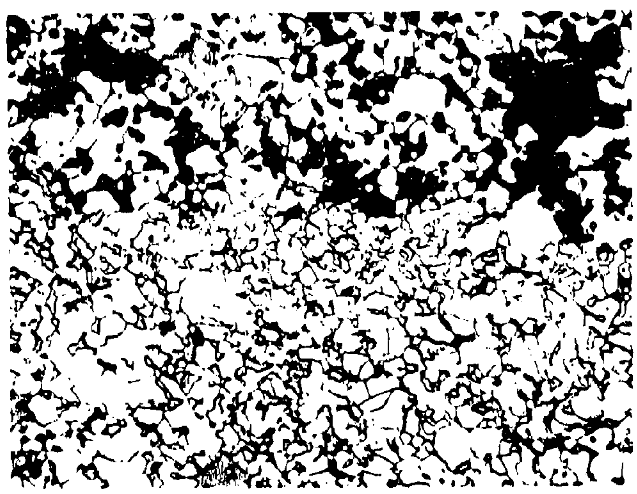

Plate No. 2-0680

Etched with 10 Glycerine $5HNO_3 3HF$ X250

Figure 78. Arc Plasma Test $HfB_{2.1}$+20 v/oSiC(A-7)-39RH, Hot Surface.

Plate No. 1-6563

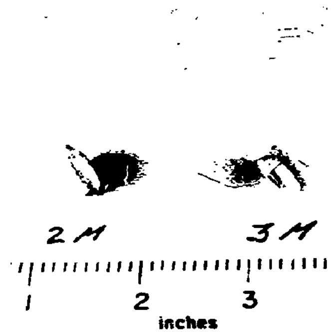

Plate No. 1-7387

Plate No. 1-9527

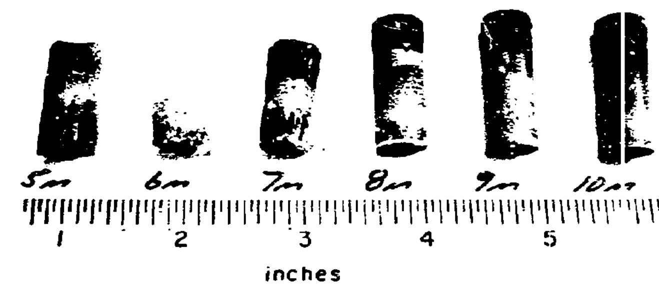

Plate No. 1-6582

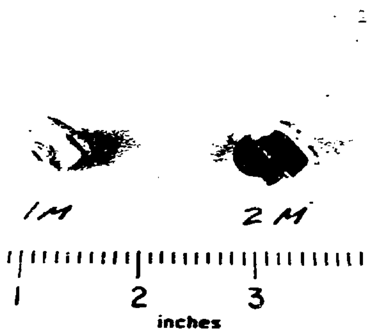

Plate No. 1-7411

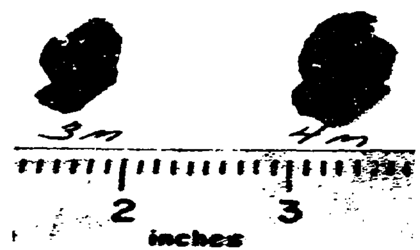

Plate No. 1-9522

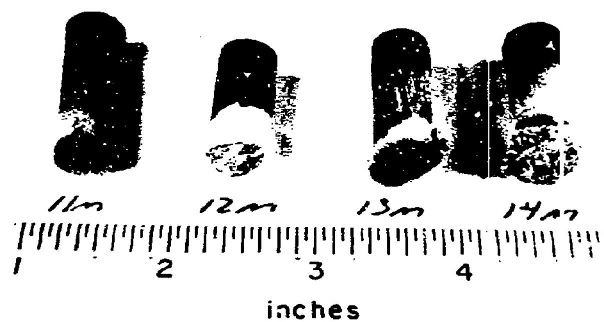

Figure 79. Post Exposure Photographs of Arc Plasma Tests ZrB_2+20%SiC(A-8)-1M, 2M, 3M, 4M, 5M, 6M, 7M, 8M, 9M, 10M, 11M, 12M, 13M, 14M, 40M, 41M, 42M and 43M.

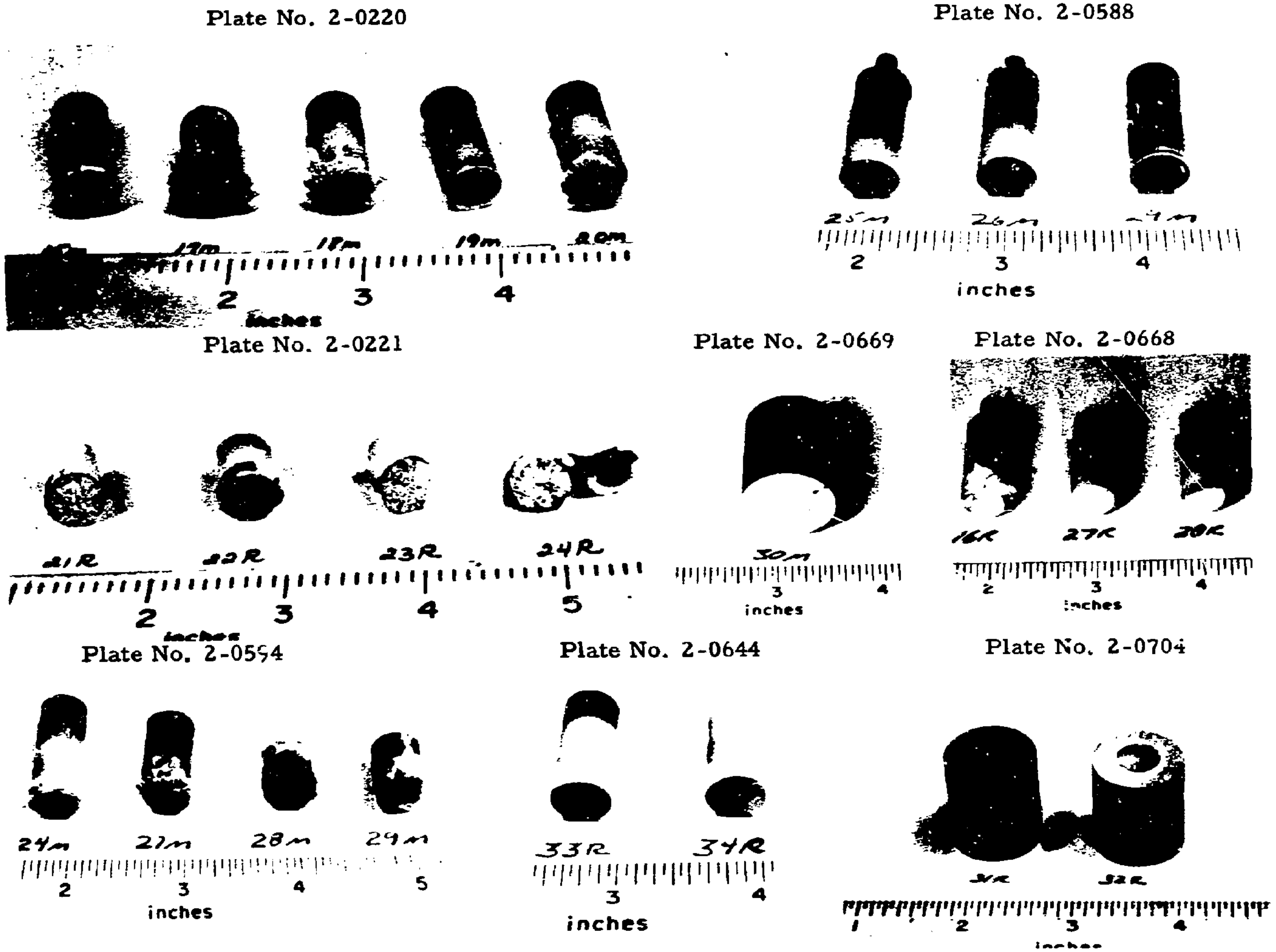

Figure 80. Post Exposure Photographs of Arc Plasma Tests ZrB_2+20%SiC(A-8)-15M, 17M, 18M, 19M, 20M, 25M, 26M, 29M, 30M, 21R, 22R, 23R, 24R, 16R, 27R, 28R, 24M, 27M, 28M, 29M, 33R, 34R, 31R, 32R.

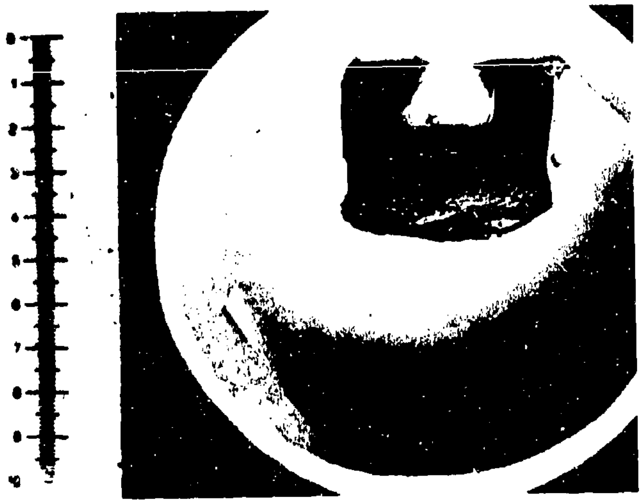

Plate No. 1-7415

X2.75

Figure 81. Arc Plasma Test ZrB_2 + 20 v/o SiC(A-8)-4M, Surface Temperature 5445°F, Exposure Time 327 Seconds, Stagnation Pressure 1.06 Atm. Stagnation Enthalpy 3915 BTU/lb, Cold Wall Heat Flux 515 BTU/ft^2 sec, 142 Mils Recession. Hot Face Down. One Inch Scale.

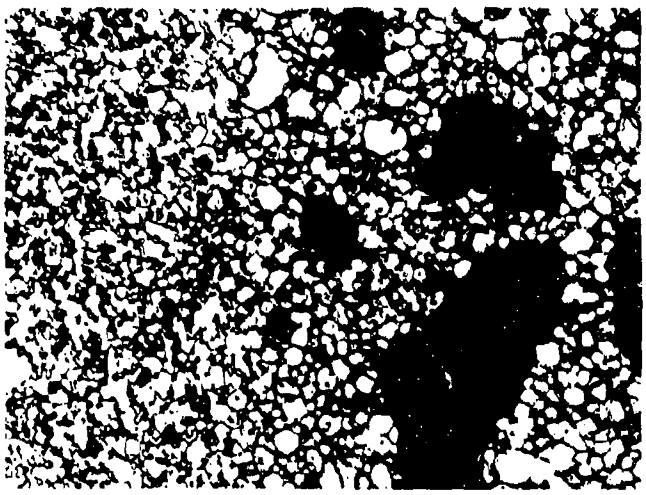

Plate No. 1-7416

Etched with 10 Glycerine $5HNO_3$ 3HF X250

Figure 82. Arc Plasma Test ZrB_2+ 20 v/o SiC(A-8)-4M, Hot Surface.

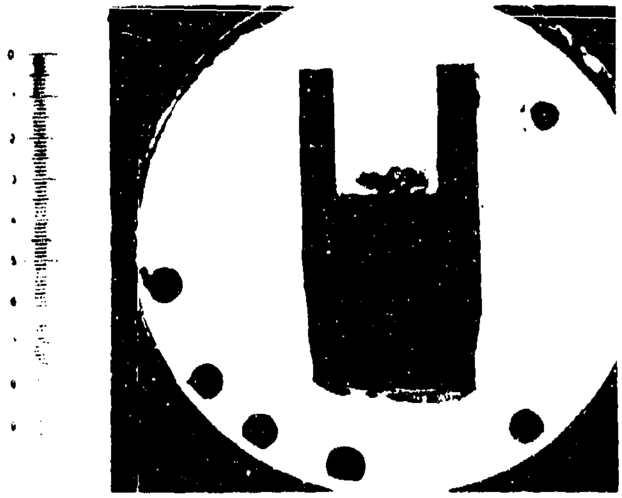

Plate No.
2-0225

X2.55

Figure 83. Arc Plasma Test $ZrB_{2.1}$+20%SiC(A-8)-17M, Surface Temperature 4880°F, Exposure Time 1800 Seconds, Stagnation Pressure 1.01 Atm., Stagnation Enthalpy 5700 BTU/lb, Cold Wall Heat Flux 503 BTU/ft^2sec, Initial Length 604 Mils, Final Length 494 Mils, Recession Depth 110 Mils. Hot Face Down. One Inch Scale.

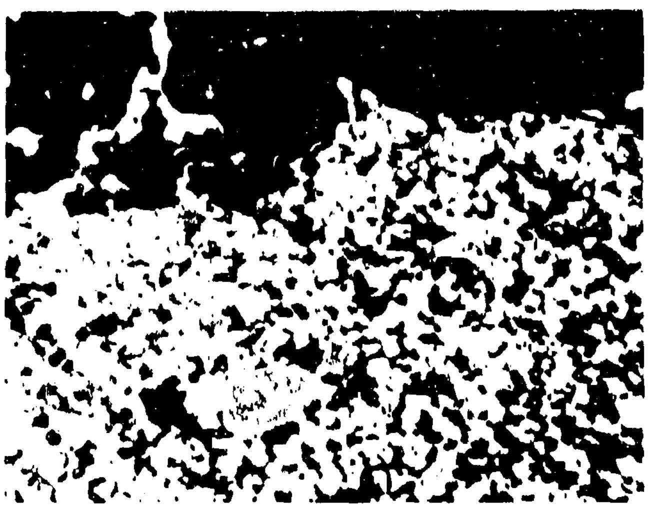

Plate No.
2-0686

Etched with 10 Glycerine
$5HNO_3 3HF$

X 250

Figure 84. Arc Plasma Test $ZrB_{2.1}$+20%SiC(A-8)-17M, Hot Interface at Top.

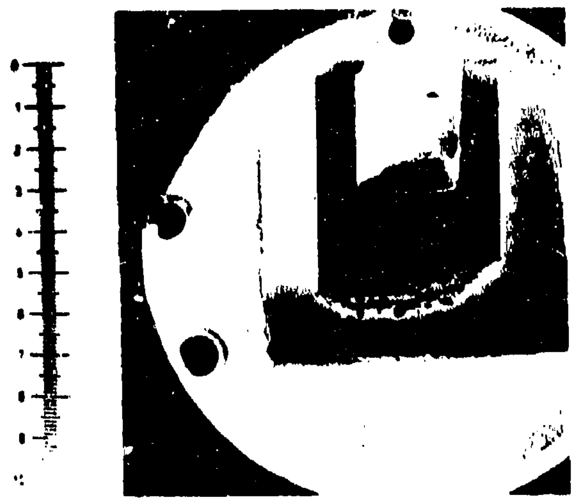

Plate No.
2-0237

X2.55

Figure 85. Arc Plasma Test $ZrB_{2.1}$+20%SiC(A-8)-21R, Surface Temperature 5280°F, Exposure Time 433 Seconds, Stagnation Pressure 0.095 Atm., Stagnation Enthalpy 10300 BTU/lb., Cold Wall Heat Flux 575 BTU/ft^2sec., Initial Length 838 Mils, Final Length 271 Mils. Hot Face Down. One Inch Scale.

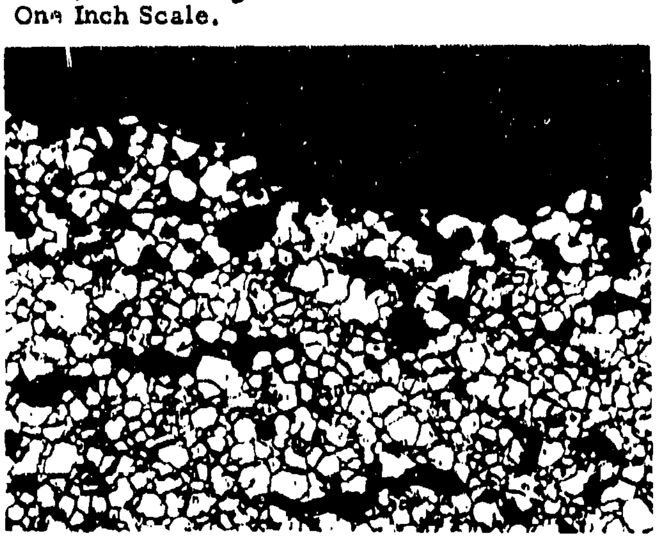

Plate No.
2-0238

Etched with 10 Glycerine 5$HNO_3$3HF X250

Figure 86. Arc Plasma Test $ZrB_{2.1}$+20%SiC(A-8)-21R, Hot Interface at Top.

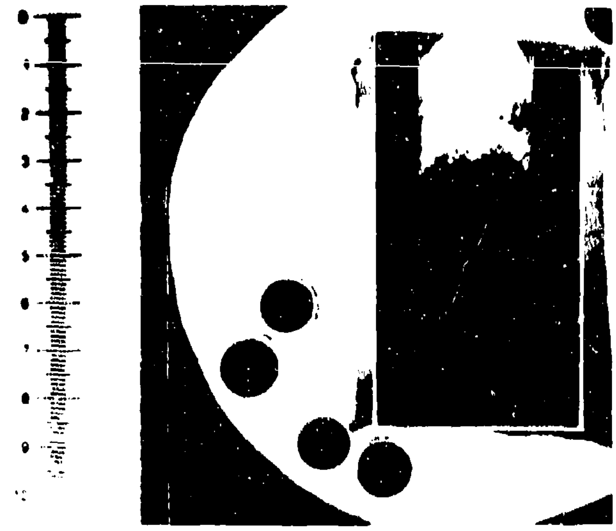

Plate No. 2-0648

X 2.95

Figure 87. Arc Plasma Test $ZrB_{2.1}$+20%SiC(A-8)-34R, Surface Temperature 4265°F, Exposure Time 1800 Seconds, Stagnation Pressure 0.063 Atm., Stagnation Enthalpy 10160 BTU/lb, Cold Wall Heat Flux 480 BTU/ft^{2}sec, Initial Length 503 Mils, Final Length 496 Mils, Total Recession 7 Mils. Hot Face Down. One Inch Scale.

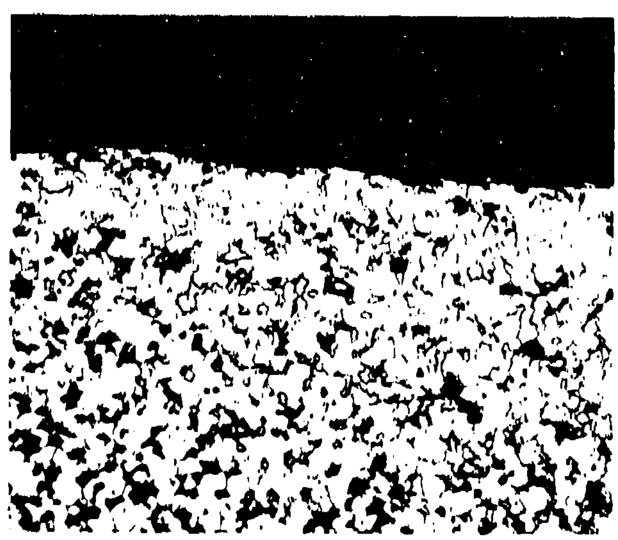

Plate No. 2-0687

Etched with 10 Glycerine $5HNO_3 3HF$ X250

Figure 88. Arc Plasma Test $ZrB_{2.1}$+20%SiC(A-8)-34R. Hot Interface at Top.

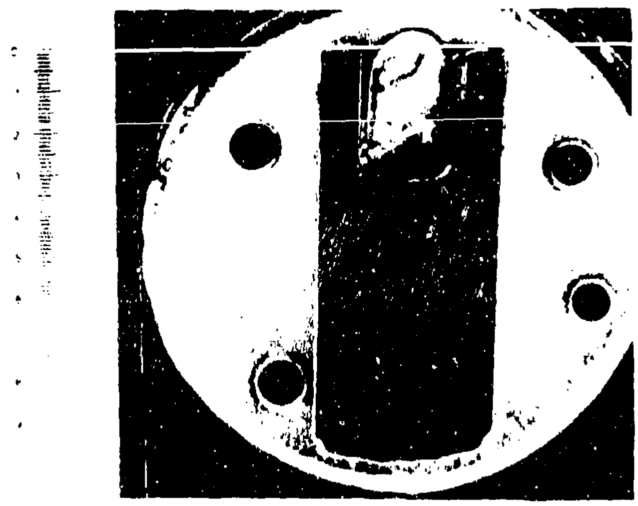

Plate No. 2-0222

X2.50

Figure 89. Arc Plasma Test $ZrB_{2.1}$+20v/o SiC(A-8)-15M Average Surface Temperature 4350°F, Exposure Time 7200 Seconds, (4 cyclic exposure each of 1800 seconds) Stagnation Pressure 1.00 Atm. Stagnation Enthalpy 5000 BTU/lb, Cold Wall Heat Flux 385 BTU/ft^2sec, 26 Mils Recession, Hot Face Down. One Inch Scale.

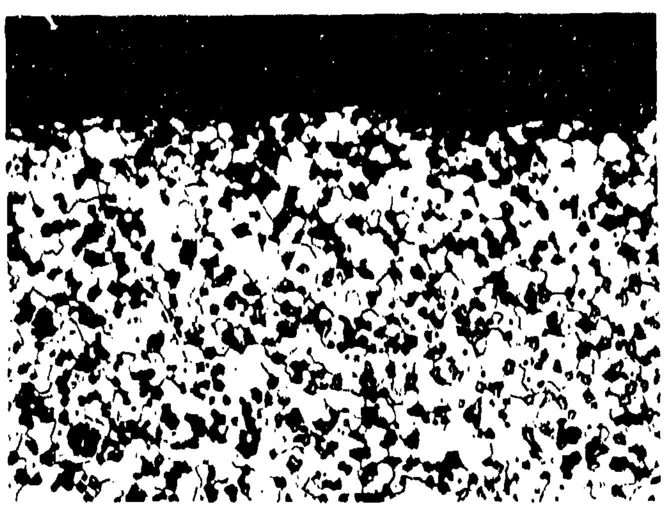

Plate No. 2-0223

Etched with 10 Glycerine $5HNO_3$ 3HF X 250

Figure 90. Arc Plasma Test $ZrB_{2.1}$+20v/o SiC(A-8)-15M, Hot Surface.

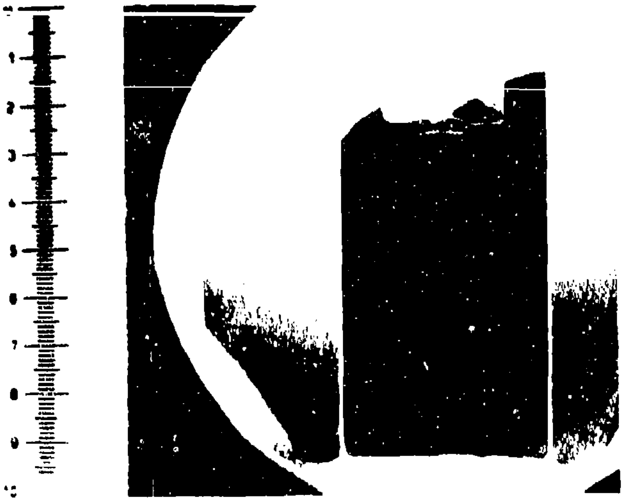

Plate No. 2-0683

X2.95

Figure 91. Arc Plasma Test $ZrB_{2.1}$+20v/o SiC(A-8)-16R Average Surface Temperature 4270°F, Exposure Time 7200 Seconds, (4 cyclic exposures, each of 1800 seconds) Stagnation Pressure 0.159 Atm. Stagnation Enthalpy 7000 BTU/lb, Cold Wall Heat Flux 450 BTU/ft^2sec, 27 Mils Recession, Hot Face Down. One Inch Scale.

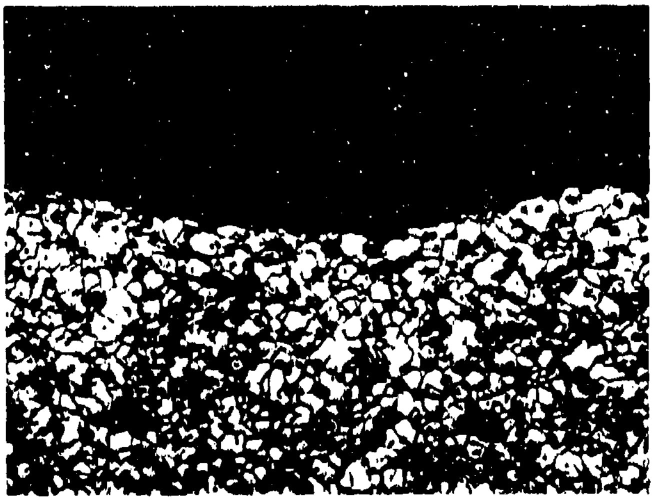

Plate No. 2-0684

Etched with 10 Glycerine $5HNO_3$ 3HF X250

Figure 92. Arc Plasma Test $ZrB_{2.1}$+20v/o SiC(A-8)-16R, Hot Surface.

Plate No. 1-6592

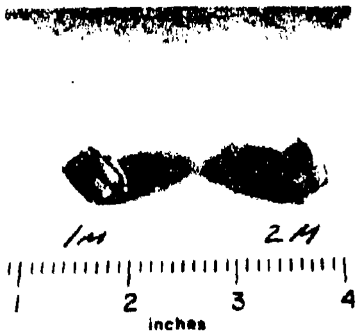

Plate No. 1-9528

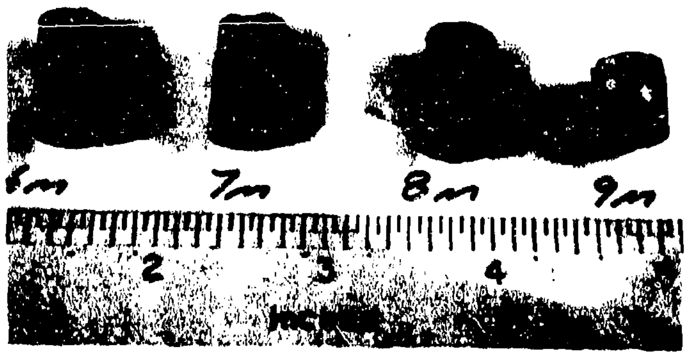

Plate No. 1-9529

Plate No. 1-7404

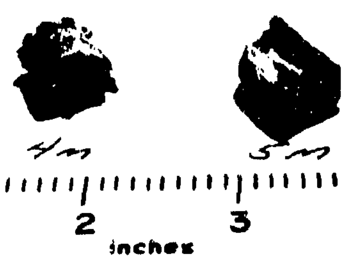

Plate No. 1-9523

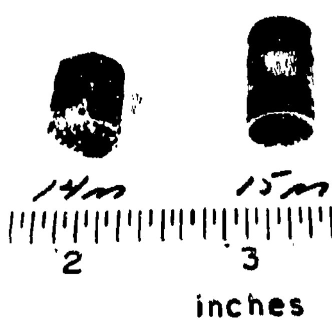

Figure 93. Post Exposure Photographs of Arc Plasma Tests HfB_2+ 35%SiC(A-9)-1M, 2M, 4M, 5M, 6M, 7M, 8M, 9M, 10M, 11M, 12M, 13M, 14M and 15M.

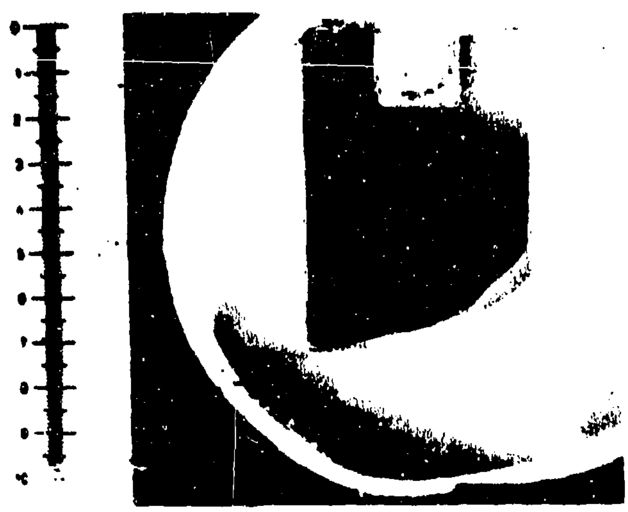

Plate No. 1-7408

X2.75

Figure 94. Arc Plasma Test $HfB_{2.1}$ + 35 v/o SiC(A-9)-5M, Surface Temperature 3540°F, Exposure Time 1800 Seconds, Stagnation Pressure 1.07 Atm, Stagnation Enthalpy 3665 BTU/lb, Cold Wall Heat Flux 530 BTU/ft^2 sec, 50 Mils Recession, Hot Face Down. One Inch Scale.

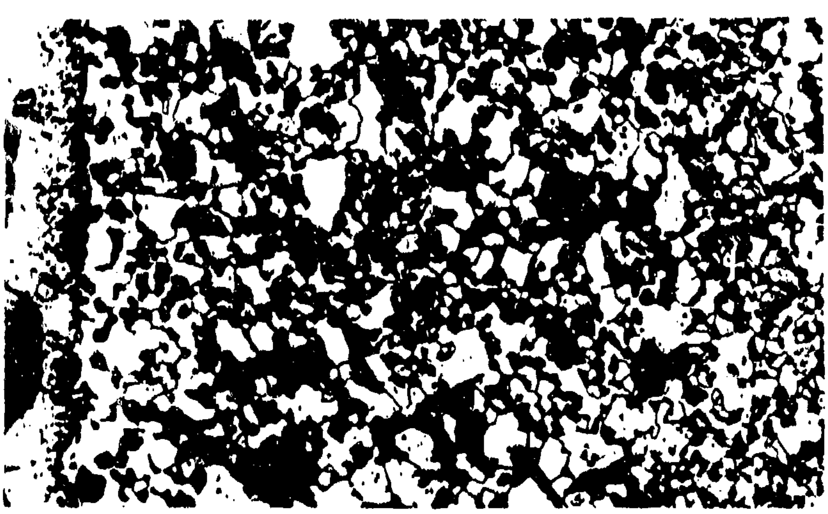

Plate No. 1-7409

Etched with 10 Glycerine $5HNO_3$ 3HF X250

Figure 95. Arc Plasma Test $HfB_{2.1}$ + 35 v/o SiC(A-9)-5M, Hot Surface at Left, Depletion Zone in Center, Matrix at Right.

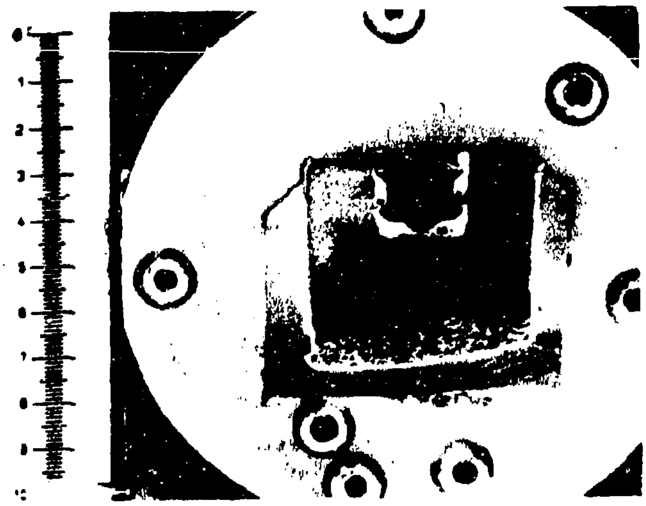

Plate No. 1-6598

X2.75

Figure 96. Arc Plasma Test $HfB_{2.1}$ + 35 v/o SiC(A-9)-2M, Surface Temperature 5840°F, Exposure Time 133 Seconds, Stagnation Pressure 1.12 Atm. Stagnation Enthalpy 4700 BTU/lb, Cold Wall Heat Flux 730 BTU/ft^2 sec, 231 Mils Recession. Hot Face Down. One Inch Scale.

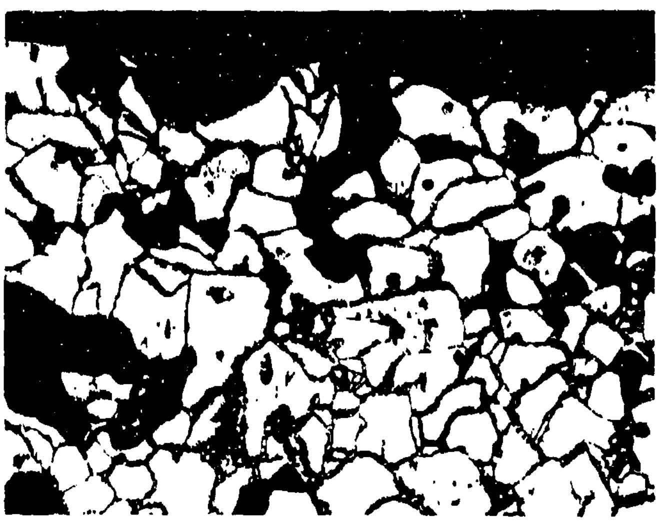

Plate No. 1-6599

Etched with 10 Glycerine $5HNO_3$ 3HF X250

Figure 97. Arc Plasma Test $HfB_{2.1}$ + 35 v/o SiC(A-9)-2M, Hot Surface.

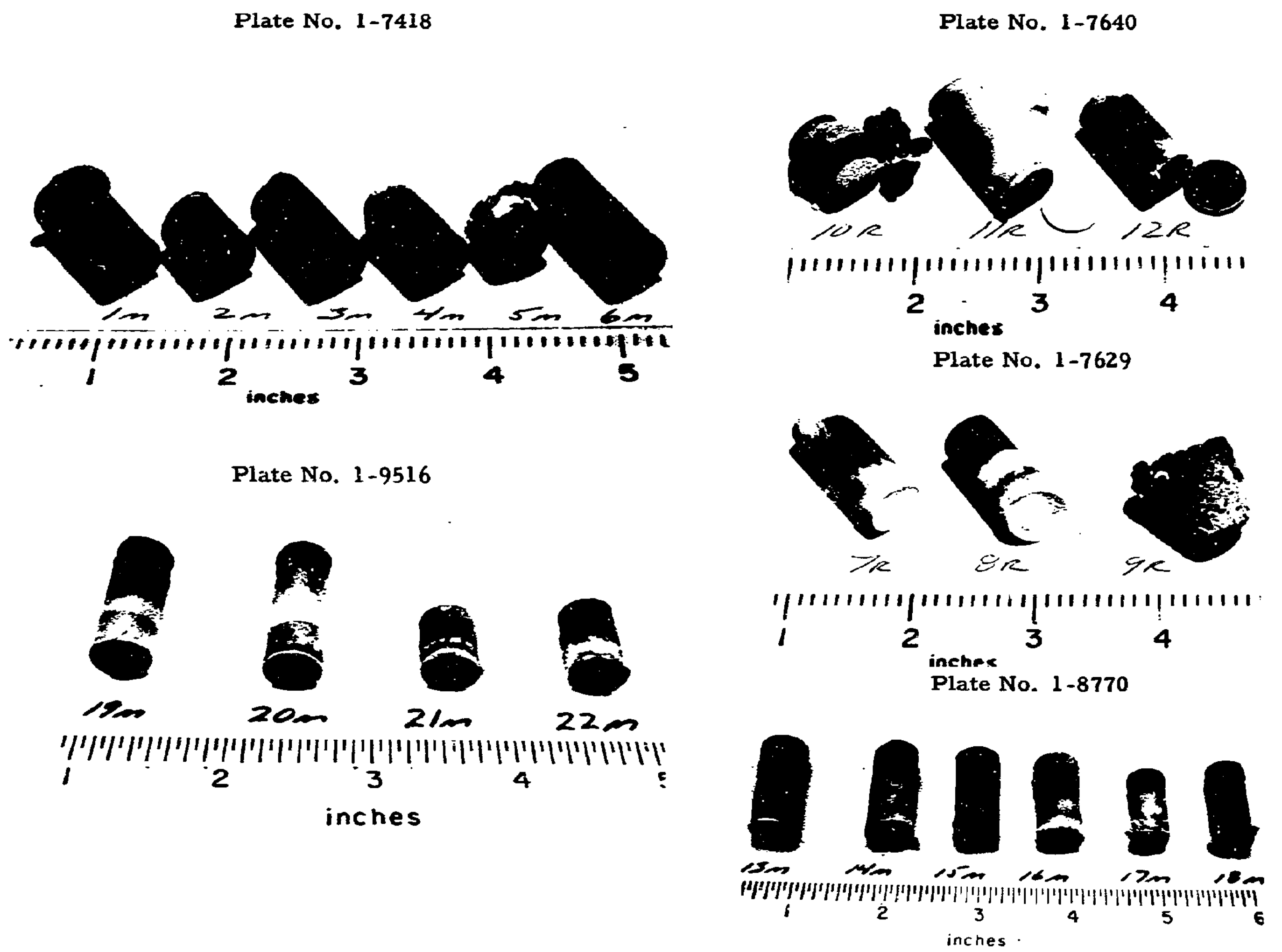

Figure 98. Post Exposure Photographs of Arc Plasma Tests ZrB_2+SiC+C(A-10)-10R, 11R, 12R, 7R, 8R, 9R, 1M, 2M, 3M, 4M, 5M, 6M, 13M, 14M, 15M, 16M, 17M, 18M, 19M, 20M, 21M and 22M.

Plate No. 2-0670

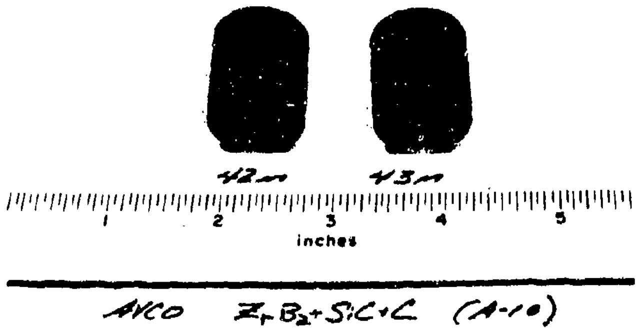

Plate No. 2-0705

Figure 99. Post Exposure Photographs of Arc Plasma Tests ZrB_2+SiC+C(A-10)-42M, 43M, 26R, 44R, 45R, 47R and 49R.

Plate No. 2-0594

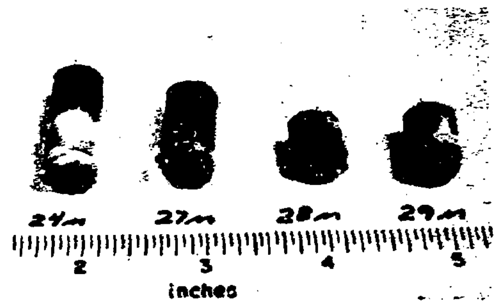

Plate No. 2-0255

Plate No. 2-0607

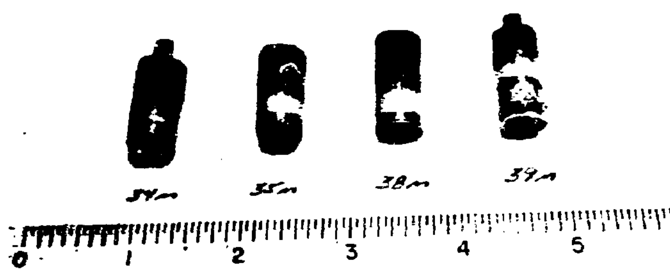

Plate No. 2-0671

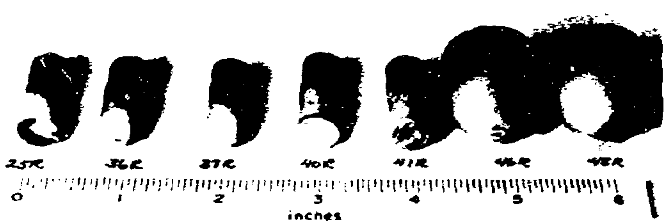

Figure 100. Post Exposure Photographs of Arc Plasma Tests ZrB_2+SiC+C(A-10)-24M, 27M, 28M, 29M, 30R, 31F., 32R, 33R, 34M, 35M, 38M, 39M, 23M, 25R, 36R. 37R, 40R, 41R, 46R and 48R.

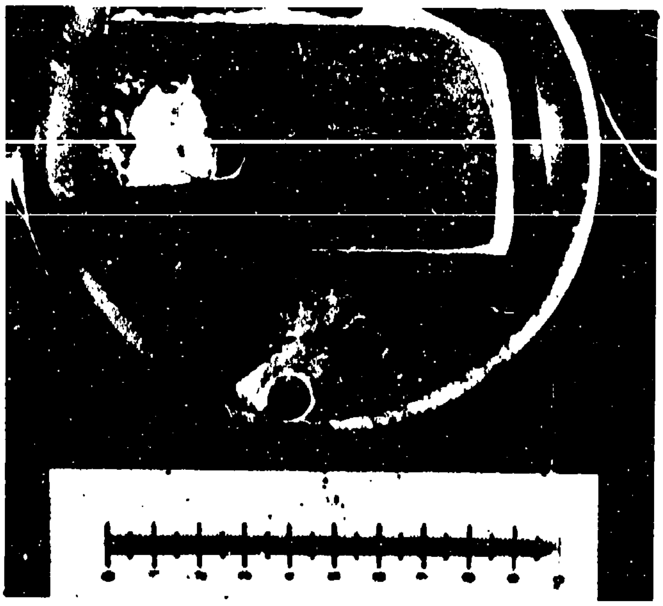

Plate No. 1-7428

X2.75

Figure 101. Arc Plasma Test ZrB_2+SiC+C(A-10)-4M, Surface Temperature 4870°F, Exposure Time 1800 Seconds, Stagnation Pressure 1.06 Atm, Stagnation Enthalpy 4075 BTU/lb, Cold Wall Heat Flux 620 BTU/ft²sec, Initial Length 850 Mil, Final Length 504 Mil. Hot Face at Right. One Inch Scale.

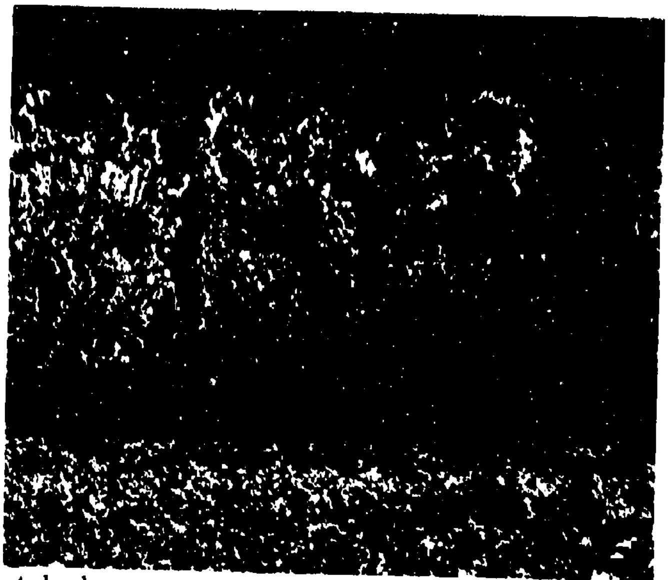

Plate No. 1-7429A

Unetched X75

Figure 102. ZrB_2+SiC+C(A-10)-4M. Interface of Oxide (Top) and Matrix.

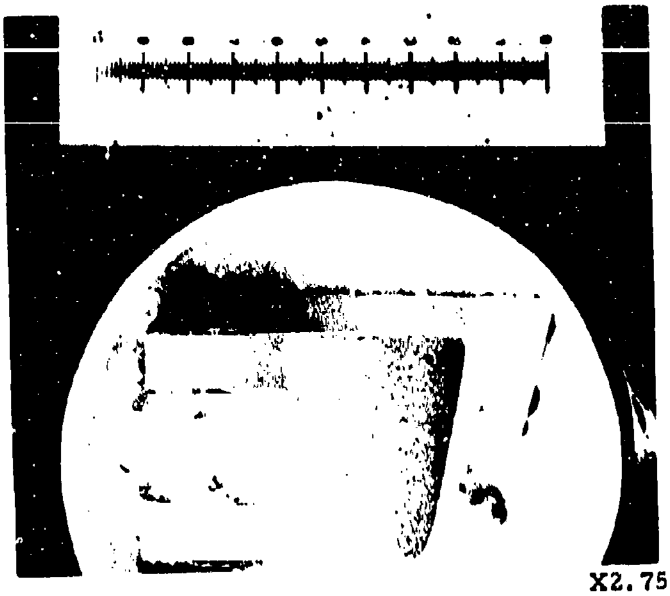

Plate No. 1-7422

X2.75

Figure 103. Arc Plasma Test ZrB_2+SiC+C(A-10)-2M, Surface Temperature 5110°F, Exposure Time 182 Seconds, Stagnation Pressure 1.07 Atm, Stagnation Enthalpy 4755 BTU/lb, Cold Wall Heat Flux 665 BTU/ft^2sec, Initial Length 848 Mil, Final Length 346 Mil, Hot Face at Right, One Inch Scale.

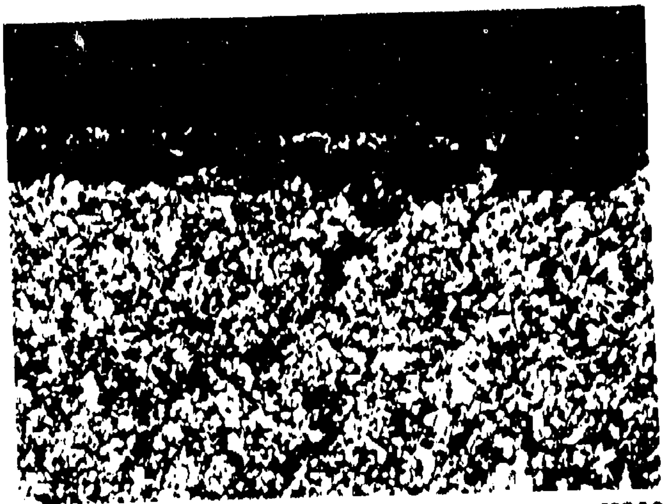

Plate No. 1-7423

Unetched X250

Figure 104. ZrB_2+SiC+C(A-10)-2M. Melted Interface.

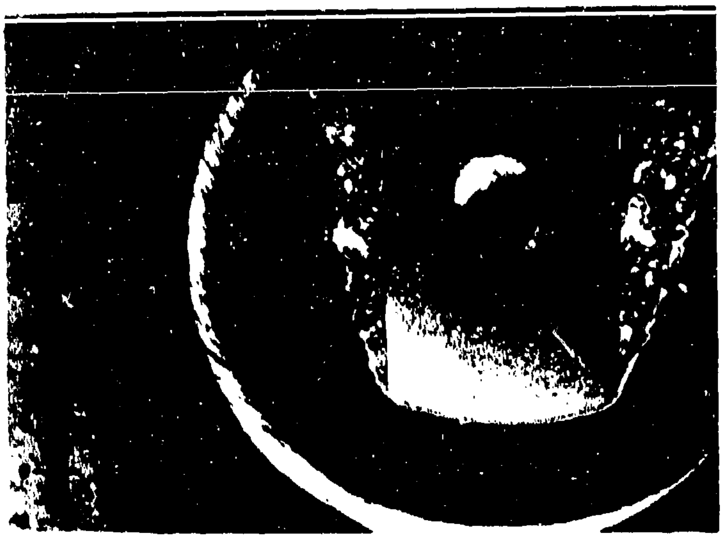

Plate No. 1-7637

X3

Figure 105. Arc Plasma Test ZrB_2+SiC+C(A-10)-9R, Surface Temperature 5065°F, Exposure Time 32 Seconds, Stagnation Pressure 0.222 Atm, Stagnation Enthalpy 10260 BTU/lb, Cold Wall Heat Flux 1010 BTU/ft^{2}sec, Initial Length 852 Mil, Final Length 277 Mil. Hot Face at Bottom, One Inch Scale. Melted Material on Sides.

Plate No. 1-7638

Unetched X250

Figure 106. ZrB_2 + SiC+C(A-10)-9R. Melted Interface.

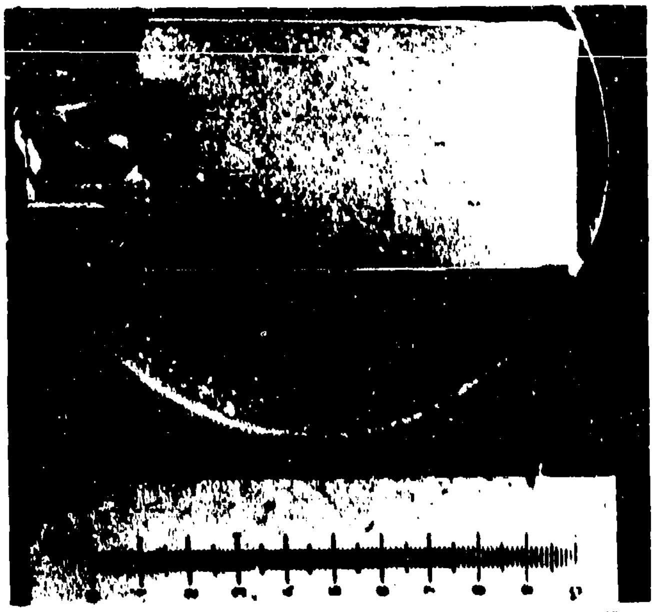

Plate No. 1-7644

X3

Figure 107. Arc Plasma Test ZrB_2+SiC+C(A-10)-11R, Surface Temperature 5075°F, Exposure Time 1800 Seconds, Stagnation Pressure 0.084 Atm, Stagnation Enthalpy 10540 BTU/lb, Cold Wall Heat Flux 696 BTU/ft^2sec, Initial Length 852 Mil, Final Length 816 Mils. Hot Face at Right. One Inch Scale. Rear Broke on Removal after Test.

Plate No. 1-7645

Unetched X250

Figure 108. Arc Plasma Test ZrB_2 + SiC+C(A-10)-11R. Hot Interface.

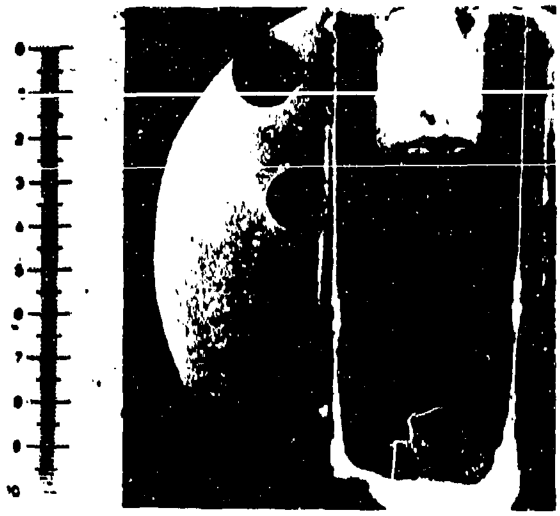

Plate No. 2-0595

X2.70

Figure 109. Arc Plasma Test ZrB_2+SiC+C(A-10)-24M Average Surface Temperature 4415°F, Exposure Time 21,600 Seconds (12 cyclic exposures each of 1800 seconds), Stagnation Pressure 1.02 Atm. Stagnation Enthalpy 4250 BTU/lb, Cold Wall Heat Flux 400 BTU/ft^{2}sec, 104 Mils Recession, Hot Face Down. One Inch Scale.

Plate No. 2-0596

Unetched X 250

Figure 110. Arc Plasma Test ZrB_2+SiC+C(A-10)-24M,Hot Surface.

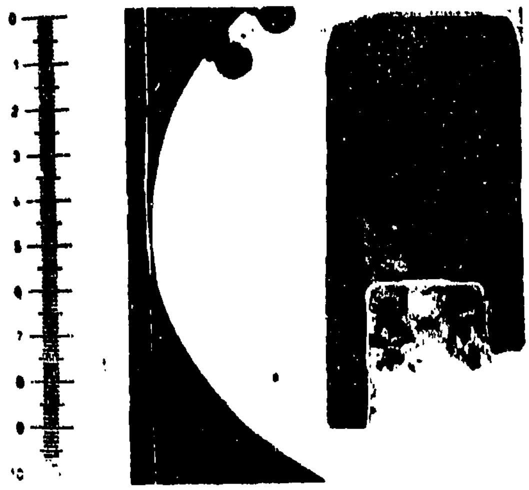

Plate No.
2-0688

Figure 111. Arc Plasma Test ZrB_2+SiC+C(A-10)-26R. Average Surface Temperature 4650°F, Exposure Time 18951 Seconds (11 Cyclic Exposures Each of Approximately 1800 Seconds), Stagnation Pressure 0.238 Atm., Stagnation Enthalpy 7750 BTU/lb, Cold Wall Heat Flux 460 BTU/ft^{2}sec, 83 Mils Recession, Hot Face Up. One Inch Scale.

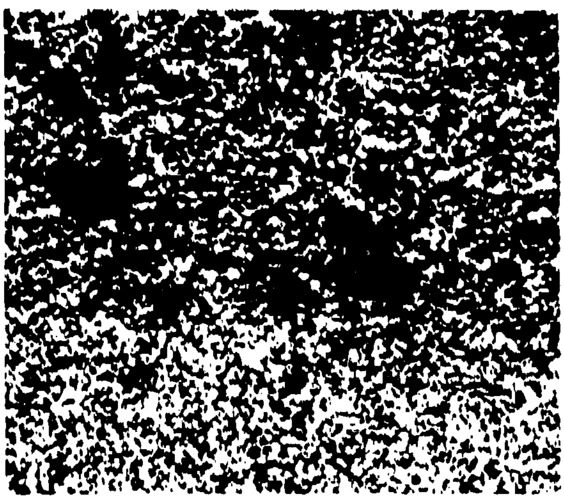

Plate No.
2-0689

Unetched X250

Figure 112. Arc Plasma Test ZrB_2+SiC+C(A-10)-26R, Hot Surface.

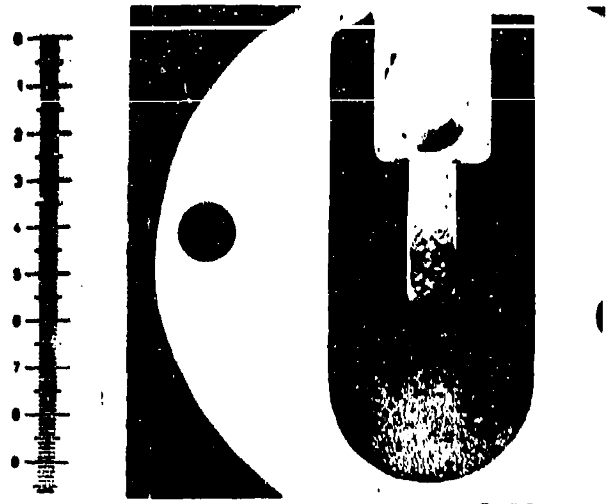

Plate No. 2-0690

X2.88

Figure 113. Arc Plasma Test ZrB_2+SiC+C(A-10)-37RH Surface Temperature 3235°F, Exposure Time 1800 Seconds, Stagnation Pressure 0.144 Atm. Stagnation Enthalpy 7710 BTU/lb, Cold Wall Heat Flux 482 BTU/ft^2sec, 3 Mils Recession, Hot Face Down. One Inch Scale.

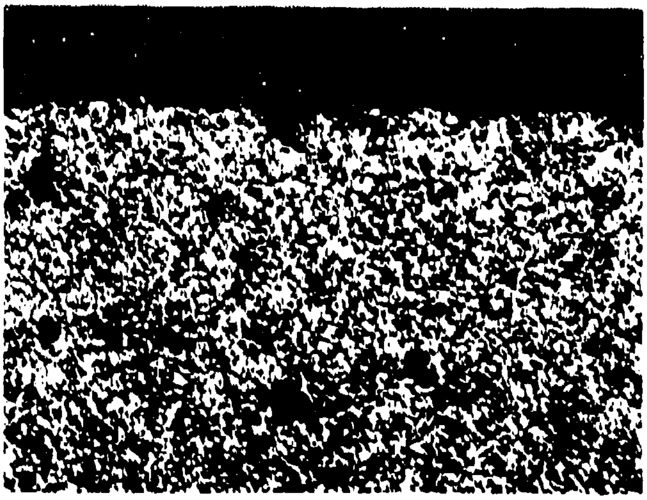

Plate No. 2-0691

Unetched X 250

Figure 114. Arc Plasma Test ZrB_2+SiC+C(A-10)-37RH, Hot Surface.

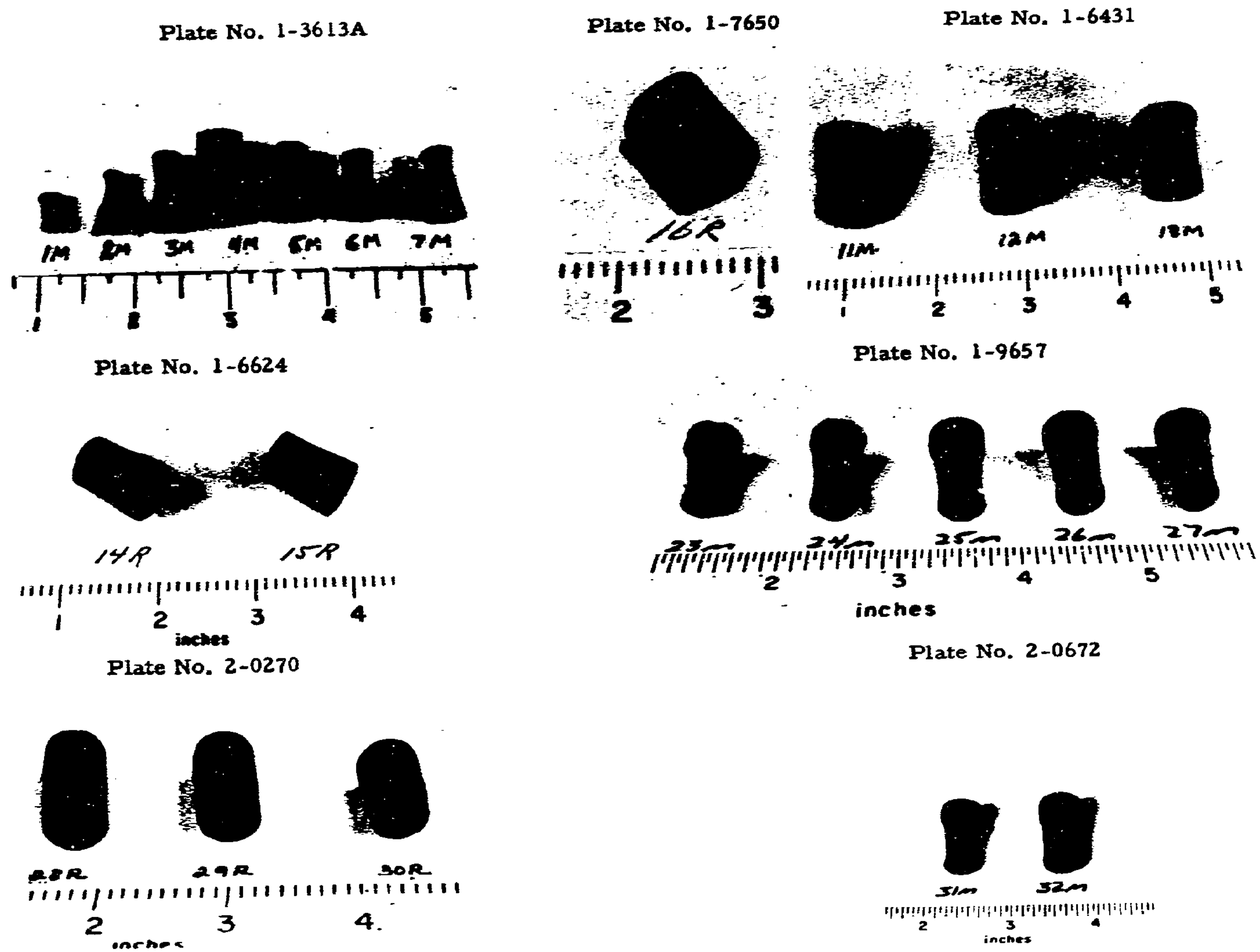

Figure 115. Post Exposure Photographs of Arc Plasma Tests RVA(B-5)-1M, 2M, 3M, 4M, 5M, 6M, 7M, 16R, 11M, 12M, 13M, 14R, 15R, 23M, 24M, 25M, 26M, 27M, 28R, 29R, 30R, 31M, 32M.

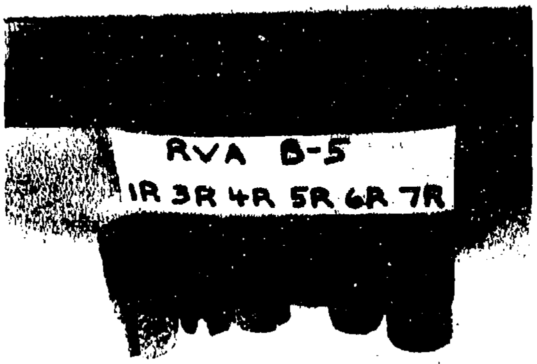

Plate 1-3429

Figure 116. Post Exposure Photographs of Arc Plasma Tests RVA (B-5)-1R, 3R, 4R, 5R and 7R. Hot Face is Pointing Up. Samples 1R and 3R Show Exposed Thermocouple Holes While 5R Shows Sting Hole Exposed Due to Side Ablation.

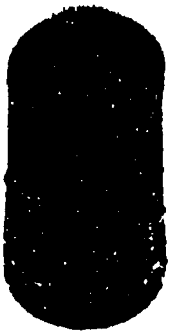

Plate 1-3432

X3.1

Figure 117. Post Exposure Photograph of Arc Plasma Test RVA (B-5)-2R Hot Face is Pointing Up.

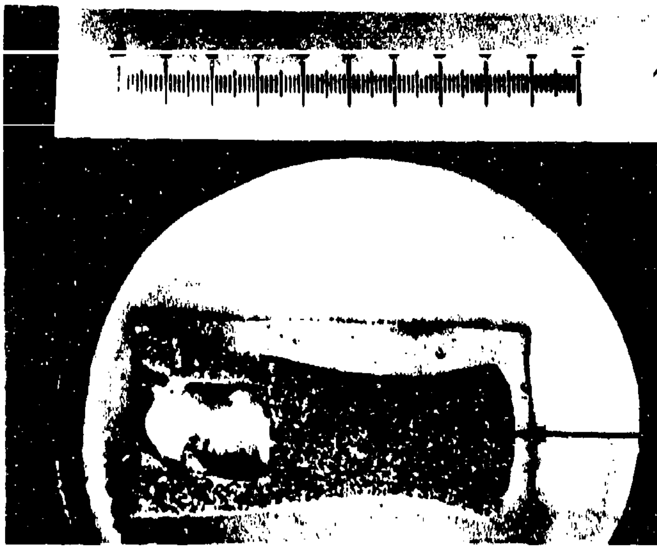

Plate 1-3697

Surface of Hot Face

X3

Figure 118. Arc Plasma Test RVA(B-5)-5M, Surface Temperature 5720°F, Exposure Time 58 Seconds, Stagnation Pressure 1 Atm, Stagnation Enthalpy 6455 BTU/lb, Cold Wall Heat Flux 1030 BTU/ft^{2}sec, Initial Length 1028 Mils, Final Length 830 Mils, Hot Face at Right. One Inch Scale. Side Ablation is Illustrated.

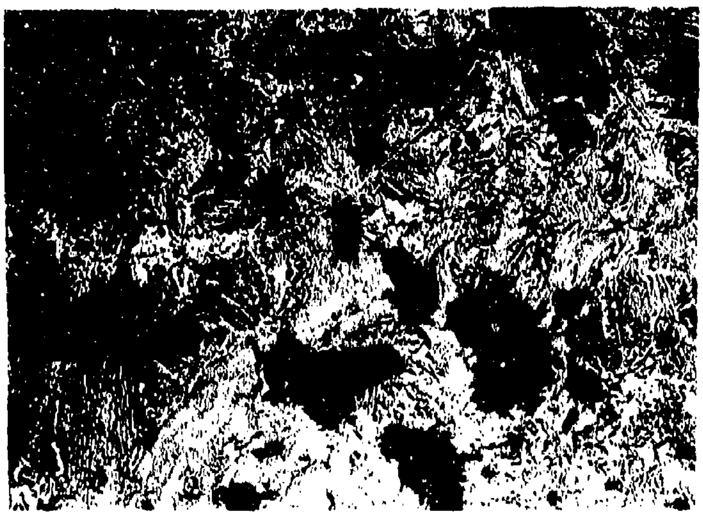

Plate 1-3619

X150

Figure 119. Arc Plasma Test RVA(B-5)-5M, Matrix Area. Little Difference Noted between Interface and Matrix.

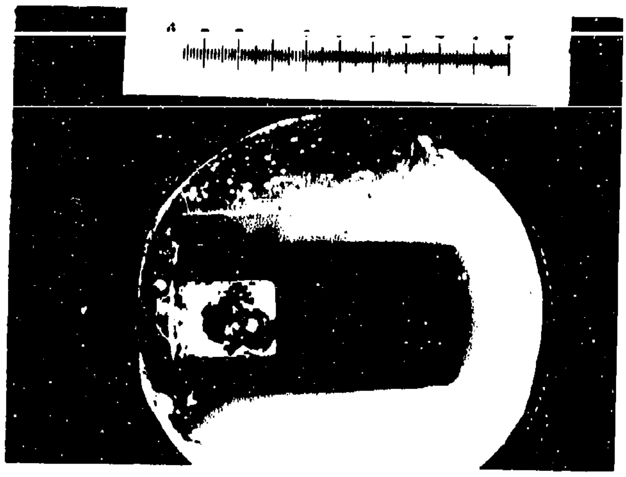

Plate 1

X2.1

Figure 120. Arc Plasma Test RVA(B-5)-7R, Surface Temperature 5430°F, Exposure Time 108 Seconds, Stagnation Pressure 0.299 Atm, Stagnation Enthalpy 10950 BTU/lb, Cold Wall Heat Flux 979 BTU/ft^2sec. Initial Length 1044 Mils, Final Length 839 Mils. Hot Face at Right. One Inch Scale.

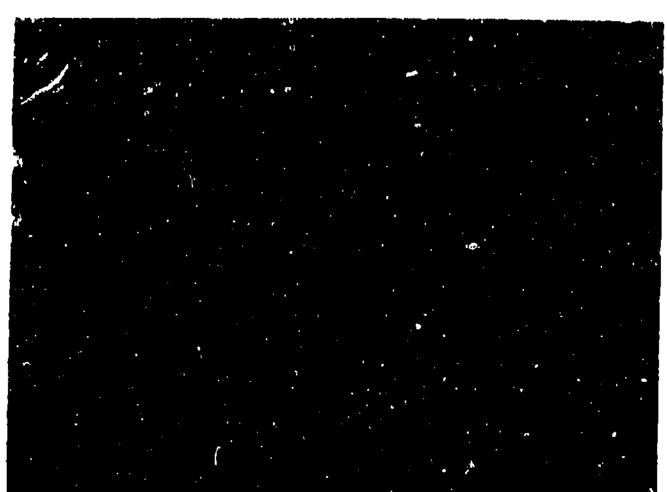

Plate 1

X150

Figure 121. Arc Plasma Test RVA(B-5)-7R, Matrix Area. Little Difference Noted between Interface and Matrix.

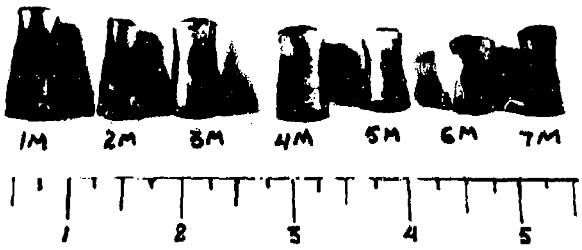

Plate 1-3630-A

Figure 122. Post Exposure Photographs of Arc Plasma Tests PG(B-6)-1M, 2M, 3M,4M, 5M, 6M, 7M, "C" Axis Perpendicular to Arc. Hot Face Pointing Up. One Inch Scale. Samples 3M and 7M Show "C" Plane Delaminations.

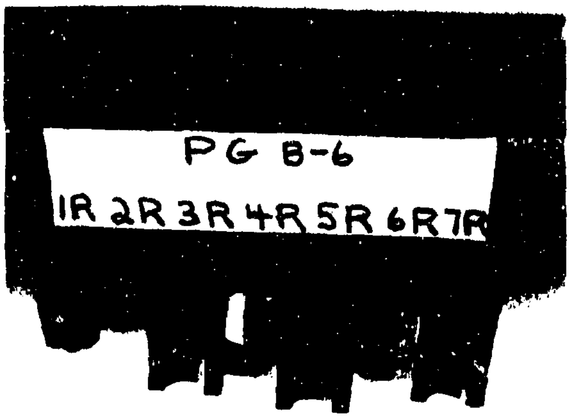

Plate 1-3446

Figure 123. Post Exposure Photographs of Arc Plasma Tests PG (B-6)-1R, 2R, 3R, 4R, 5R, 6R and 7R, "C" Axis Perpendicular to Arc. Hot Face Pointing Up. One Inch Scale. Samples 3R, 5R and 7R Show "C" Plane Delaminations. Sample PG(B-6)-5R Delaminated on "C" Plane During Installation Due to Interference Between Stinghole and Sting.

Plate No. 1-4270

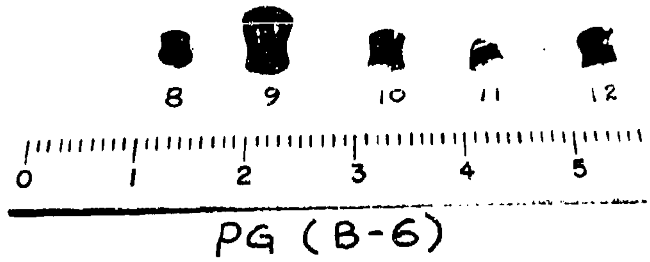

Figure 124. Post Exposure Photographs of Arc Plasma Tests PG (B-6)-8M, 9M, 10M, 11M and 12M, "C" Axis Parallel to Arc. Hot Face Pointing Down. One Inch Scale.

Plate No. 1-4271

Plate No. 1-4932

Figure 125. Post Exposure Photographs of Arc Plasma Tests PG (B-6)-8R, 9R, 10R, 11R and 12R, "C" Axis Parallel to Arc. Hot Face Pointing Down in All Cases. One Inch Scale.

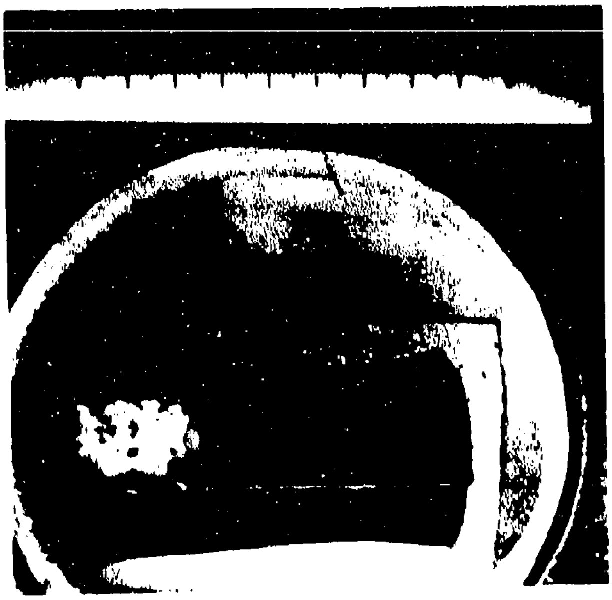

Plate 1-3634

X3

Figure 126. Arc Plasma Test PG(B-6)-3M, "C" Axis Perpendicular to Arc. Sample Delaminated on "C" Plane after Exposure. Surface Temperature 4530°F, Exposure Time 61 Seconds, Stagnation Pressure 1 Atm, Stagnation Enthalpy 4580 BTU/lb, Cold Wall Heat Flux 670 BTU/ft^{2}sec, Initial Length 999 Mils, Final Length 856 Mils. Hot Face at Right. One Inch Scale.

Plate 1-3635

X50

Figure 127. Arc Plasma Test PG(B-6)-3M, Matrix Area. Little Difference Noted between Matrix and Interface Areas.

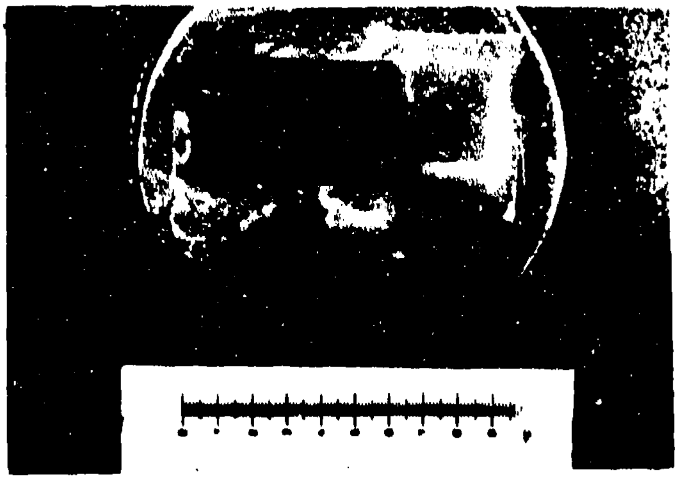

Plate 1-3453

Figure 128. Arc Plasma Test PG(B-6)-4R, "C" Axis Perpendicular to Arc. Surface Temperature 4650°F, Exposure Time 300 Seconds, Stagnation Pressure 0.187 atm, Stagnation Enthalpy 3440 BTU/lb, Cold Wall Heat Flux 852 BTU/ft^2, Initial Length 1084 Mils, Final Length 628 Mils. Hot Face at Right. One Inch Scale.

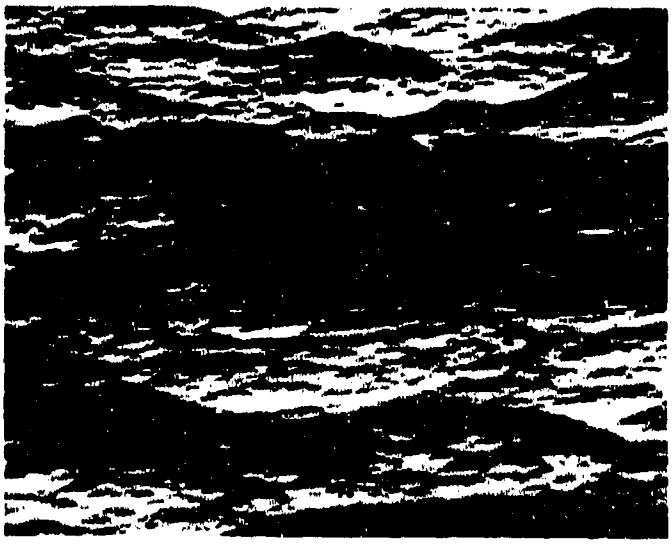

Plate 1-3454

Figure 129. Arc Plasma Test PG (B-6)-4R, Matrix Area. Little Difference Noted between Interface and Matrix Areas.

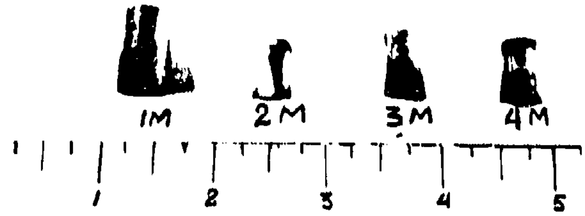

Plate 1-3622

Figure 130. Post Exposure Photographs of Arc Plasma Tests BPG (B-7)-1M, 2M, 3M and 4M, "C" Axis Perpendicular to Arc. Hot Face Pointing Up. One Inch Scale. Sample 3M Delaminated on "C" Plane, While Samples 1M and 3M show Incipient Delaminations.

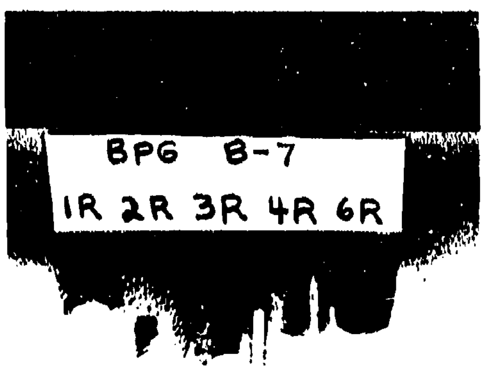

Plate 1-3416

Figure 131. Post Exposure Photographs of Arc Plasma Tests BPG (B-7)-1R, 2R, 3R, 4R and 6R, "C" Axis Perpendicular to Arc. Hot Face Pointing Up. One Inch Scale. Samples 1R and 2R Delaminated on "C" Plane During Test. Sample 3R, Showing Thermocouple Hole Delaminated on "C" Plane When Installed Due to Interference Fit of Sting and Tungsten Holder. Sample BPG (B-7)-5R Ablated Completely.

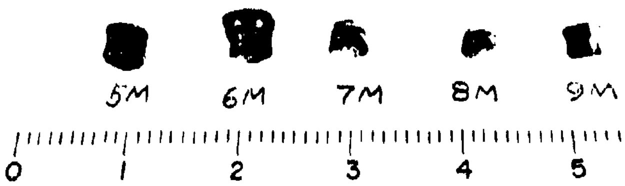

Plate No.
1-4272

Figure 132. Post Exposure Photographs of Arc Plasma Tests BPG(B-7)-5M, 6M, 7M, 8M and 9M, "C" Axis Parallel to Arc. Hot Face Pointing Down. One Inch Scale.

Plate No. 1-4273 Plate No. 1-4274 Plate No. 1-4939

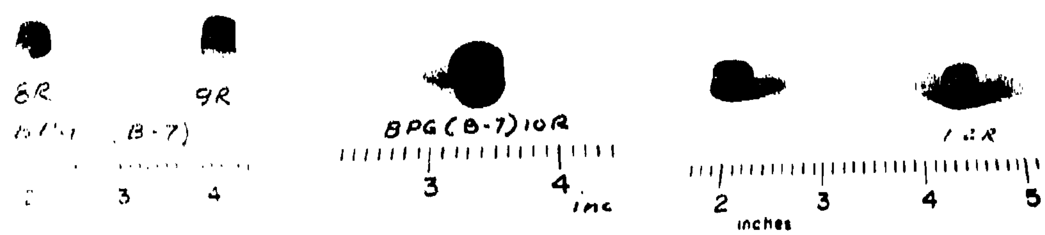

Figure 133. Post Exposure Photographs of Arc Plasma Tests BPG(B-7)-8R, 9R, 10R, 11R and 12R, "C" Axis Parallel to Arc. Hot Face Pointing Down except BPG(B-7)-10R, 11R and 12R Where It is Pointing Up. One Inch Scale.

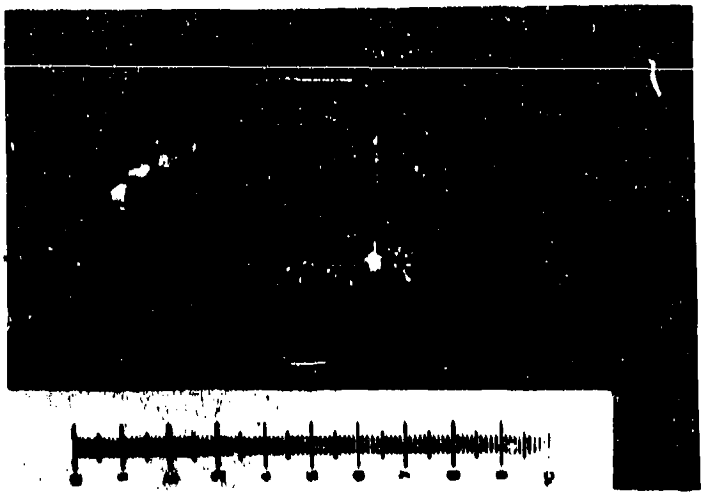

Plate 1-3701

X3

Figure 134. Arc Plasma Test BPG(B-7)-4M, "C" Axis Perpendicular to Arc. Incipient Delamination on "C" Plane. Side Ablation Present. Surface Temperature 4940°F, Exposure Time 75 Seconds, Stagnation Pressure 1 Atm, Stagnation Enthalpy 6500 BTU/lb, Cold Wall Heat Flux 760 BTU/ft²sec. Initial Length 799 Mils, Final Length 575 Mils. Hot Face at Right. One Inch Scale.

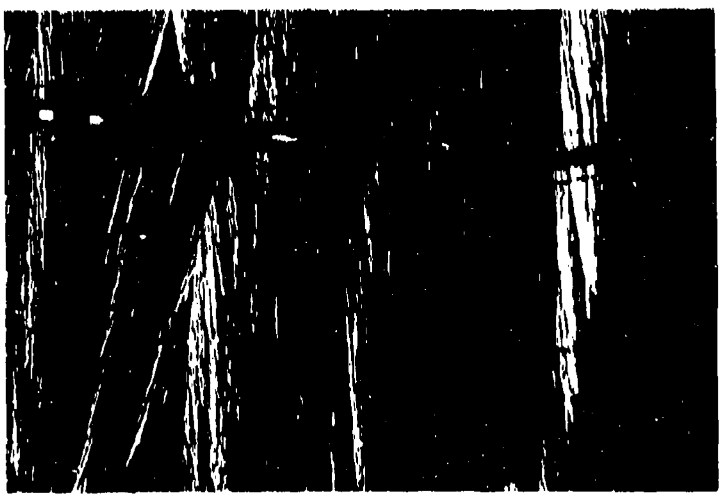

Plate 1-3628

Figure 135. Arc Plasma Test BPG(B-7)-4M, Interface Area Showing Cracks Extending along "C" Plane.

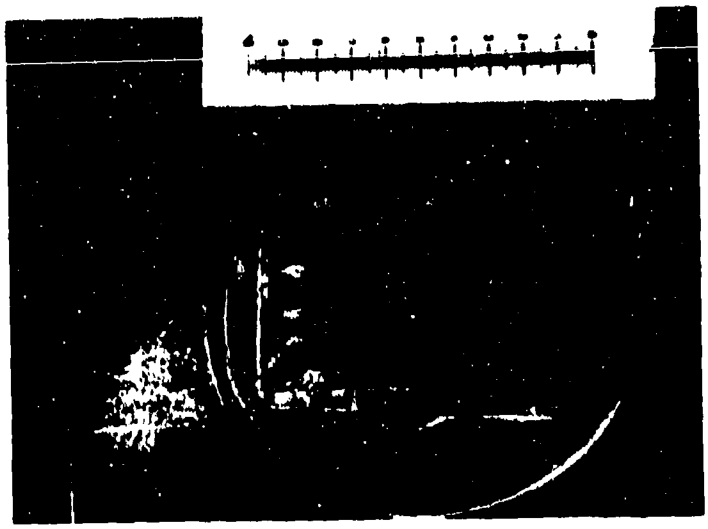

Plate 1-3427

Surface of
Hot Face

X2.1

Figure 136. Arc Plasma Test BPG(B-7)-6R, "C" Axis Perpendicular to Arc, Surface Temperature 3810°F, Exposure Time 600 Seconds, Stagnation Pressure 0.017 Atm, Stagnation Enthalpy 13890 BTU/lb, Cold Wall Heat Flux 321 BTU/ft²sec. Initial Length 785 Mils. Final Length 547 Mils. Hot Face at Right. One Inch Scale.

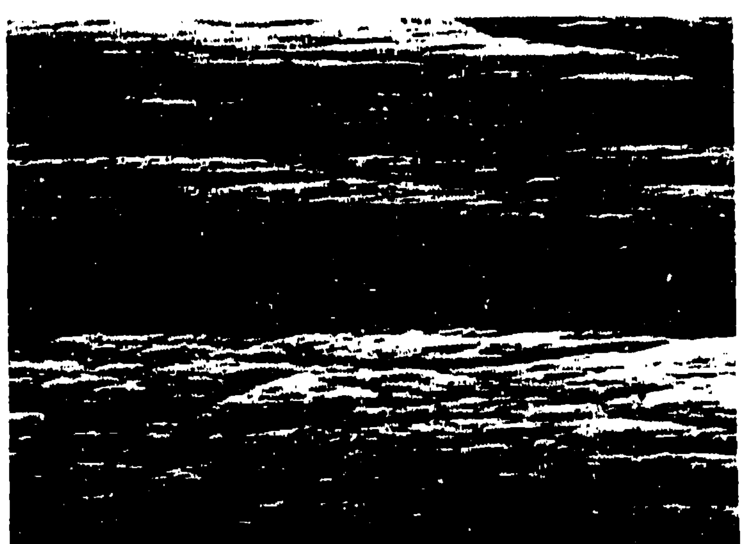

Plate 1-3428

X50

Figure 137. Arc Plasma Test BPG(B-7)-6R, Matrix Area. Little Difference between Interface and Matrix Areas.

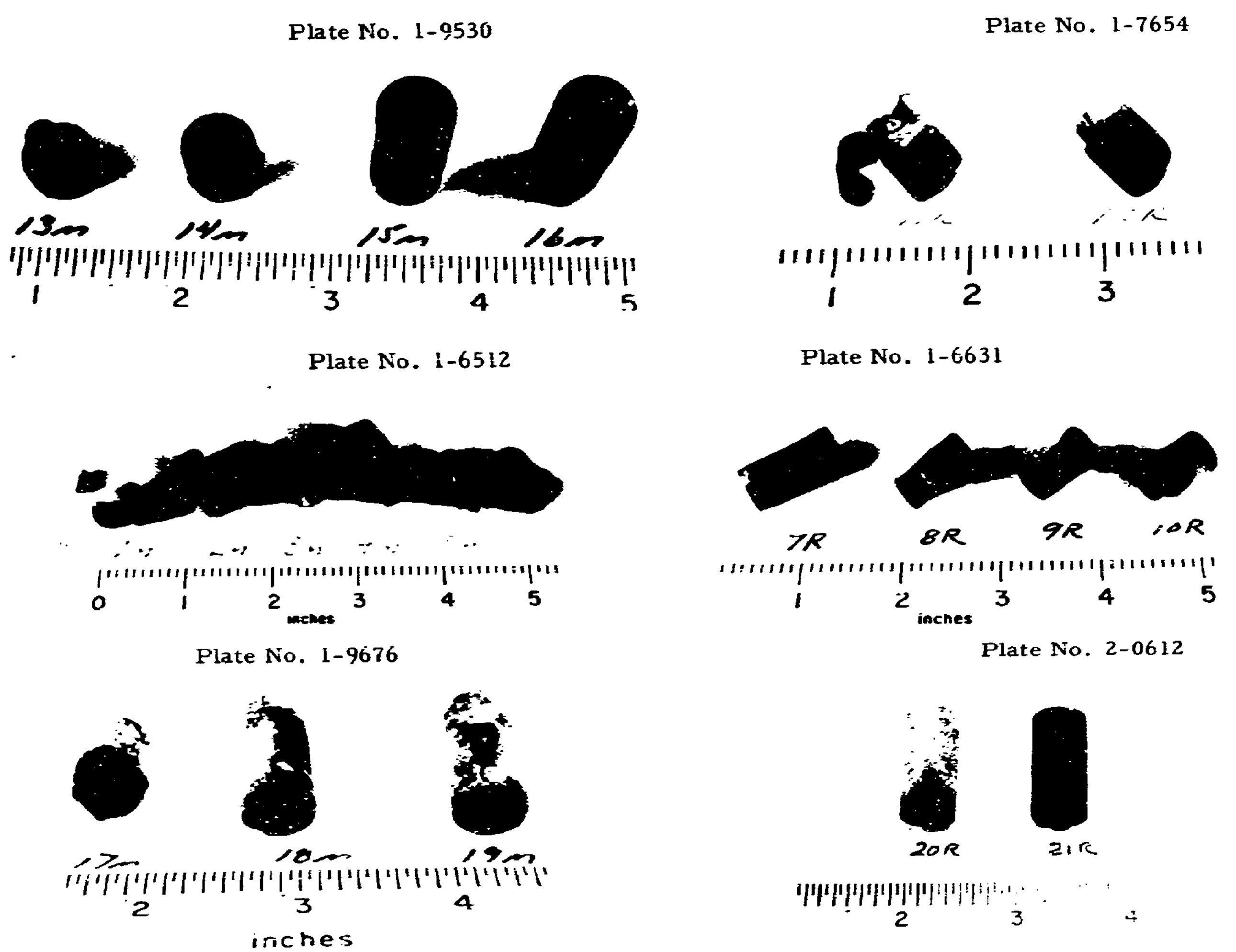

Figure 138. Post Exposure Photographs of Arc Plasma Tests Si/RVC(B-8)-1M, 2M, 3M, 4M, 5M, 6M, 7R 8R, 9R, 10R, 11R, 12R, 13M, 14M, 15M, 16M, 17M, 18M, 19M, 20R and 21R.

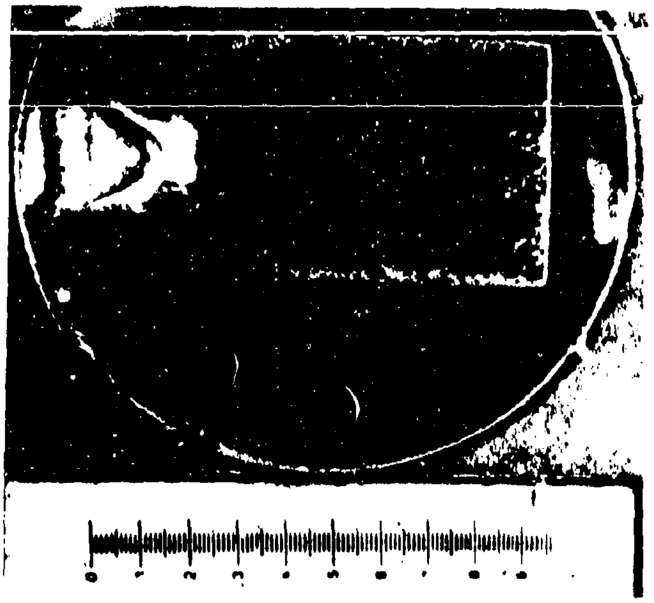

Plate No. 1-6632

X2.94

Figure 139. Arc Plasma Test Si/RVC(B-8)-7R, Surface Temperature 2740°F, Exposure Time 1800 Seconds, Stagnation Pressure 0.013 Atm, Stagnation Enthalpy 8850 BTU/lb, Cold Wall Heat Flux 210 BTU/ft^{2}sec, Initial Length 735 Mils, Final Length 714 Mils. Hot Face at Right. One Inch Scale.

Plate No. 1-6633

Unetched

X250

Figure 140. Arc Plasma Test Si/RVC(B-8)-7R, SiC Coating (Top) Did Not Fail.

Plate No. 1-6522

X2.69

Figure 141. Arc Plasma Test Si/RVC(B-8)-4M, Surface Temperature 3770°F, Exposure Time 240 Seconds, Stagnation Pressure 1.06 Atm, Stagnation Enthalpy 3270 BTU/lb, Cold Wall Heat Flux 475 BTU/ft^{2}sec, Intial Length 739 Mils, Final Length 727 Mils. Hot Face at Right. One Inch Scale.

Plate No. 1-6523

Unetched X250

Figure 142. Arc Plasma Test Si/RVC(B-8)-4M. SiC Coating (Top). Did Not Fail.

Plate No. 1-6394

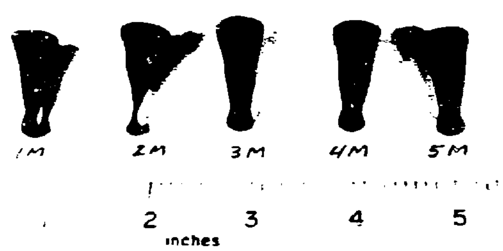

Plate No. 1-6410

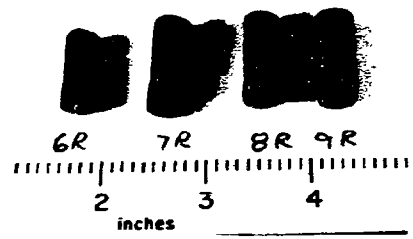

Plate No. 1-7661

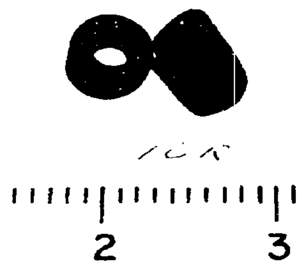

Figure 143. Post Exposure Photographs of Arc Plasma Tests PT0178(B-9)-1M, 2M, 3M, 4M, 5M, 6R, 7R, 8R, 9R and 10R.

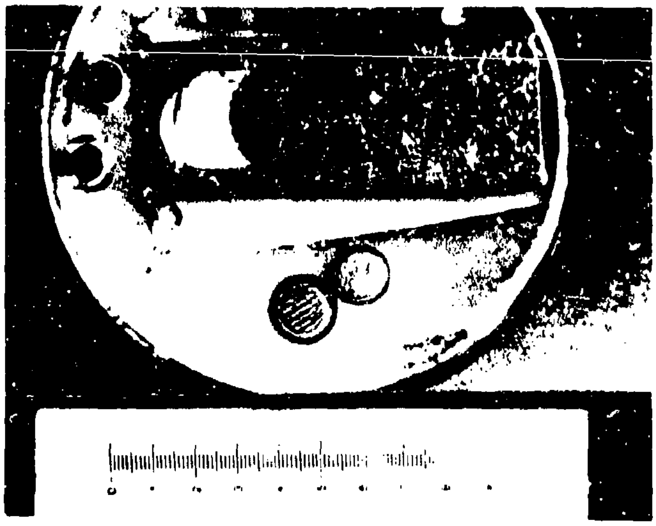

Plate No. 1-6420

X2.56

Figure 144. Arc Plasma Test PT0178(B-9)-9R, Surface Temperature 5040°F, Exposure Time 400 Seconds, Stagnation Pressure 0.030 Atm, Stagnation Enthalpy 16050 BTU/lb, Cold Wall Heat Flux 763 BTU/ft^{2}sec, Initial Length 1091 Mils, Final Length 675 Mils, Hot Face at Right. One Inch Scale.

Plate No. 1-6421

Unetched X250

Figure 145. Arc Plasma Test PT0178(B-9)-9R. Interface Showing Random Orientation of Fibers.

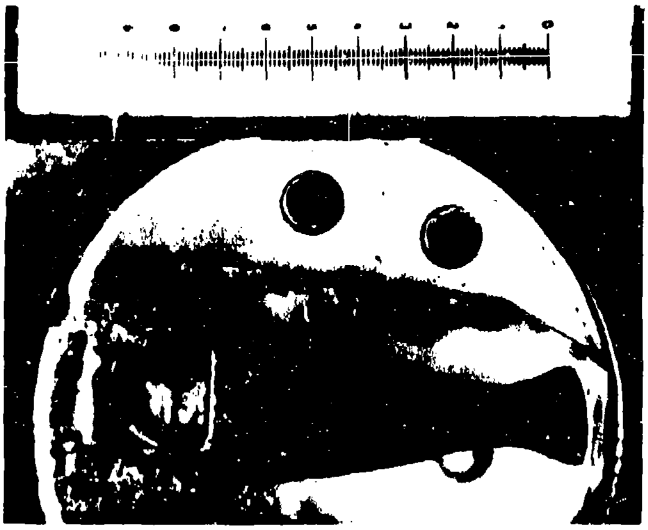

Plate No. 1-6407

X2.87

Figure 146. Arc Plasma Test PT0178(B-9)-5M, Surface Temperature 5985°F, Exposure Time 54 Seconds, Stagnation Pressure 1.07 Atm, Stagnation Enthalpy 5590 BTU/lb, Cold Wall Heat Flux 940 BTU/ft^{2}sec, Initial Length 1080 Mils, Final Length 801 Mils. Hot Face at Right. One Inch Scale.

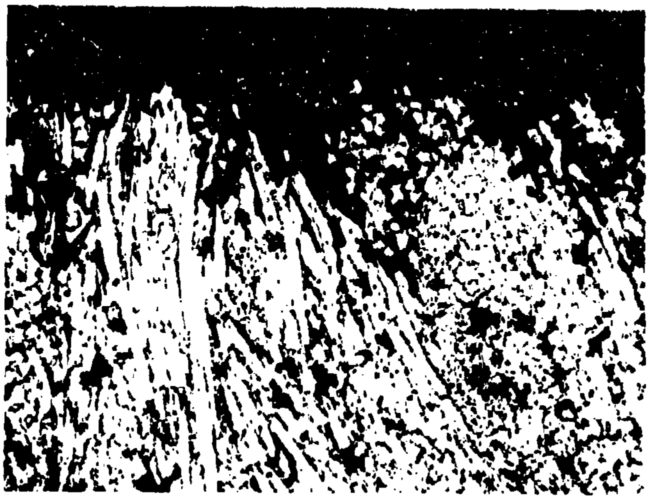

Plate No. 1-6408

Unetched X250

Figure 147. Arc Plasma Test PT0178(B-9)-5M. Interface Showing Random Orientation of Fibers.

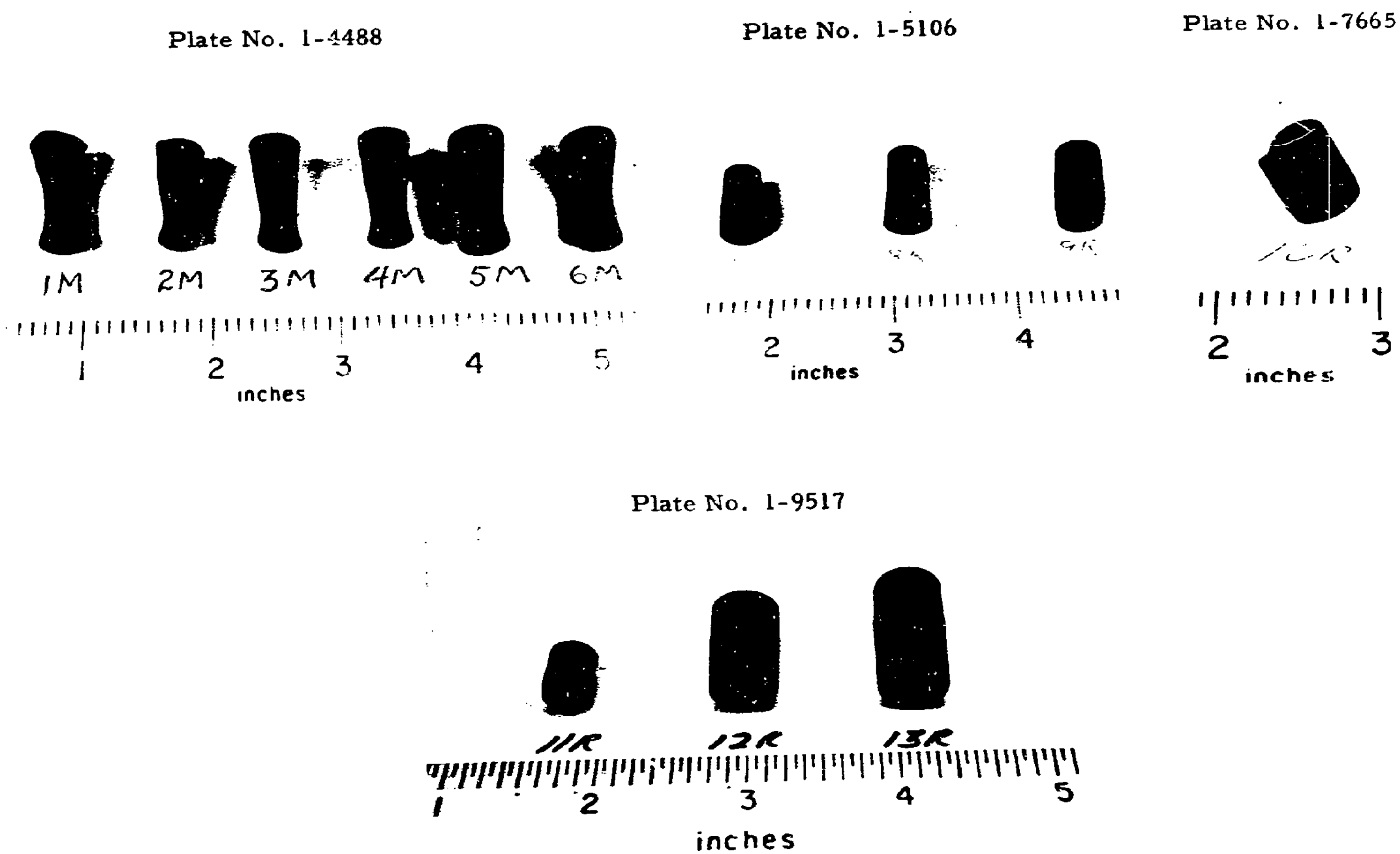

Figure 148. Post Exposure Photographs of Arc Plasma Tests Poco Graphite(B-10)-1M, 2M, 3M, 4M, 5M, 6M, 7R, 8R, 9R, 10R, 11R, 12R and 13R.

Plate No. 1-7666

X2.94

Figure 149. Arc Plasma Test POCO(B-10)-10R, Surface Temperature 5350°F, Exposure Time 250 Seconds, Stagnation Pressure 0.218 Atm, Stagnation Enthalpy 10890 BTU/lb, Cold Wall Heat Flux 1102 BTU/ft^{2}sec, Initial Length 836 Mils, Final Length 308 Mils. Hot Face at Right. One Inch Scale.

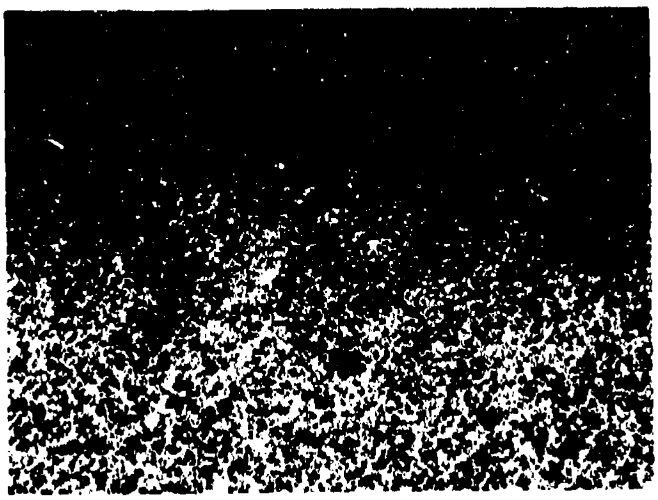

Plate No. 1-7667

Unetched X250

Figure 150. POCO(B-10)-10R. Hot Interface.

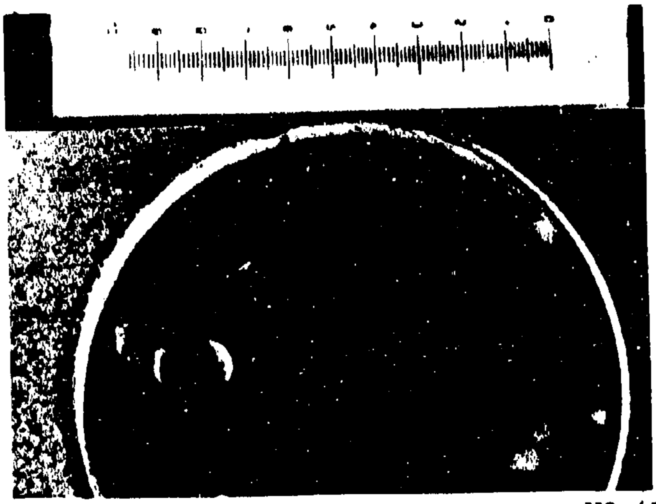

Plate No. 1-4497

X2.69

Figure 151. Arc Plasma Test POCO(B-10)-5M, Surface Temperature 6120°F, Exposure Time 44 Seconds, Stagnation Pressure 1.11 Atm, Stagnation Enthalpy 9195 BTU/lb, Cold Wall Heat Flux 1060 BTU/ft^{2}sec, Initial Length 841 Mils, Final Length 679 Mils. Hot Face at Right. One Inch Scale.

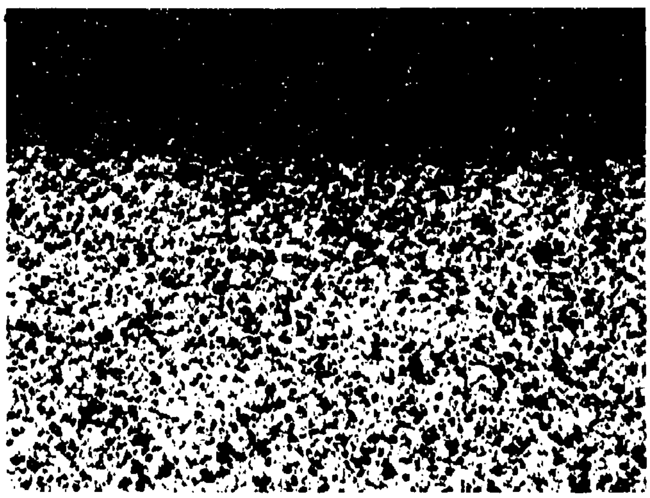

Plate No. 1-7762

Unetched X250

Figure 152. Arc Plasma Test POCO (B-10)-5M. Hot Interface.

Plate No. 1-8061

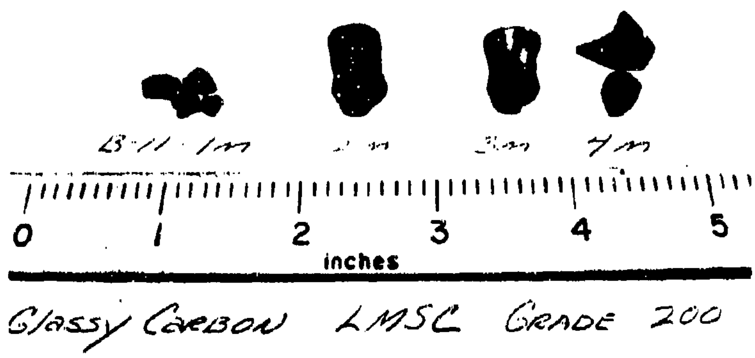

Figure 153. Post Exposure Photographs of Arc Plasma Tests
Glassy Carbon(B-11)-1M, 2M, 3M and 4M.

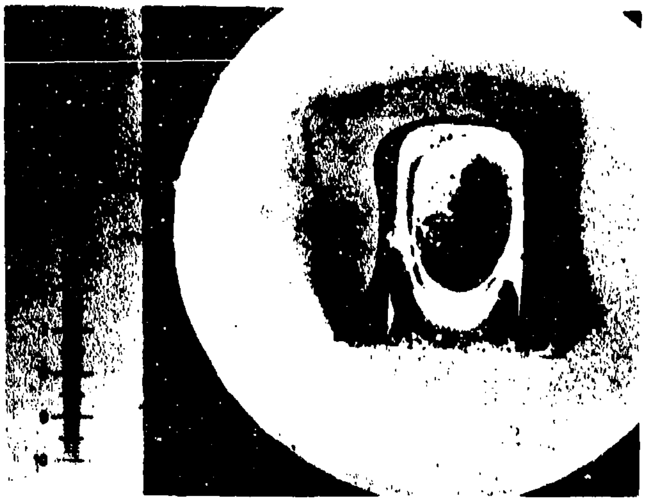

Plate No. 1-8065

X2.62

Figure 154. Arc Plasma Test Glassy Carbon (B-11)-3M, Surface Temperature 4540°F, Exposure Time 54 Seconds, Stagnation Pressure 1.03 Atm, Stagnation Enthalpy 3785 BTU/lb, Cold Wall Heat Flux 360 BTU/ft^2 sec, 125 Mils Recession, Hot Face Up. One inch Scale.

Plate No. 1-8063

Unetched X160

Figure 155. Arc Plasma Test Glassy Carbon (B-11)-3M, Hot Surface Down.

Plate No. 1-7438

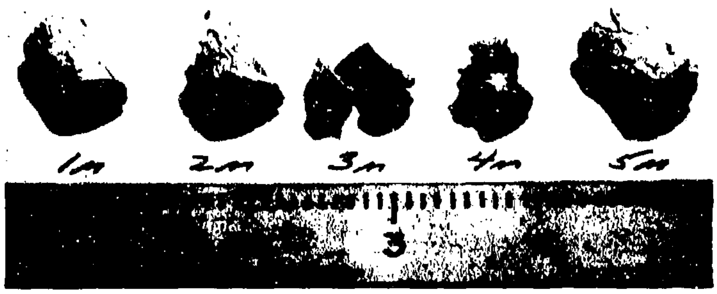

Plate No. 2-0615

Plate No. 2-0625

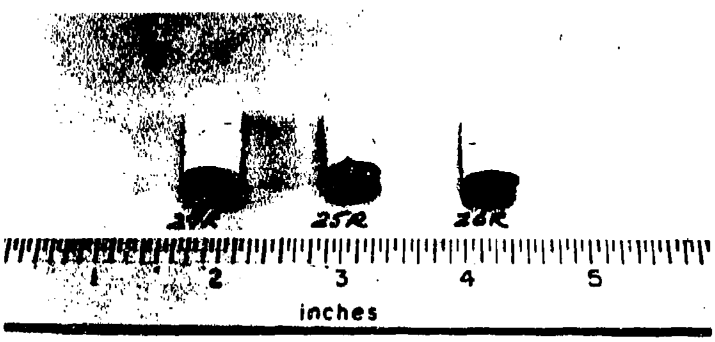

Figure 156. Post Exposure Photographs of Arc Plasma Tests HfC+C(C-11)-1M, 2M, 3M, 4M, 5M, 21M, 22M, 23M, 24R, 25R and 26R.

Plate No. 1-7669

Plate No. 1-8056

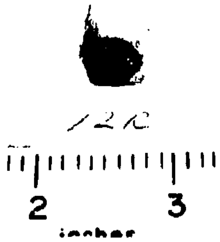

Plate No. 1-8760

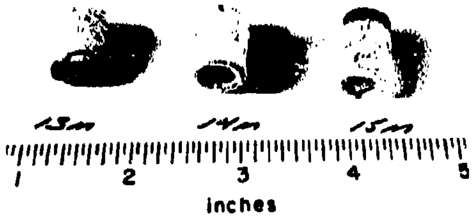

Plate No. 1-9493

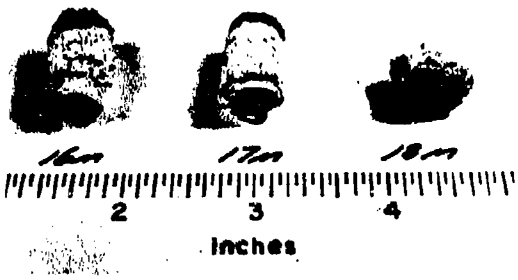

Plate No. 1-9520

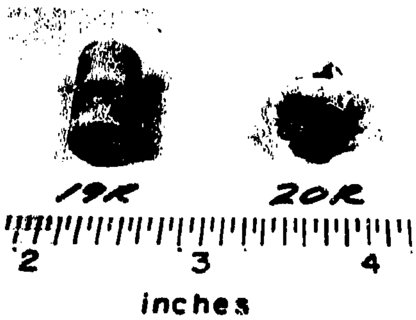

Figure 157. Post Exposure Photographs of Arc Plasma Tests HfC+C(C-11)-7R, 8R, 9R, 10R, 11R, 12R, 13M, 14M, 15M, 16M, 17M, 18M, 19R and 20R

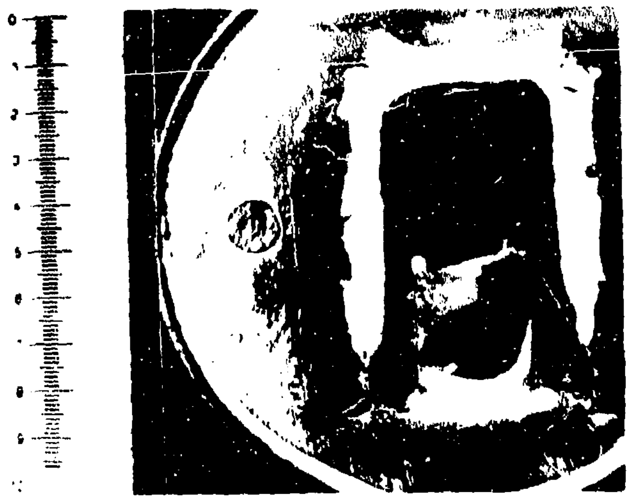

Figure 158. Arc Plasma Test HfC + C(C-11)-15M, Surface Temperature 3865°F, Exposure Time 1800 Seconds, Stagnation Pressure 1.01 Atm. Stagnation Enthalpy 2830 BTU/lb, Cold Wall Heat Flux 235 BTU/ft^2 sec, 47 mils Recession, Hot Face Up. One Inch Scale.

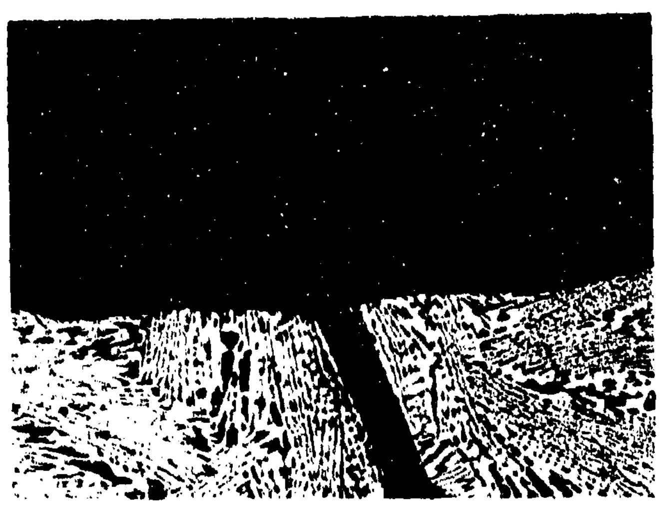

Figure 159. Arc Plasma Test HfC + C (C-11)-15M, Hot Surface Oxide at Top.

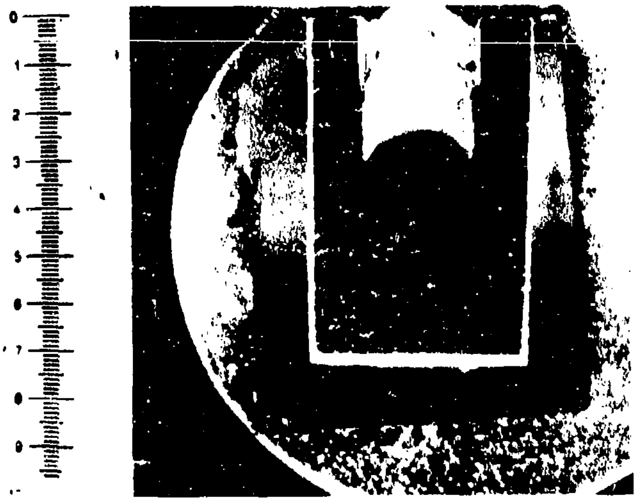

Plate No. 1-7676

X2.90

Figure 160. Arc Plasma Test HfC + C(C-11)-10R, Surface Temperature 4875°F Exposure Time 1800 Seconds, Stagnation Pressure 0.066 Atm. Stagnation Enthalpy 11,850 BTU/lb, Cold Wall Heat Flux 614 BTU/ft^2 sec, 20 Mil Recession, Hot Face Down, One Inch Scale.

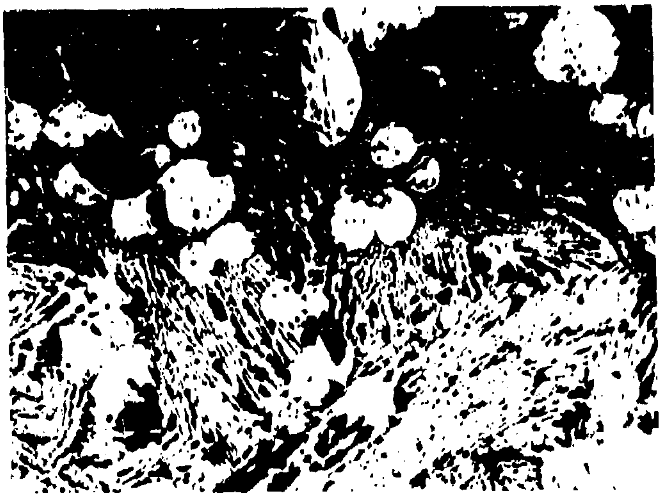

Plate No. 1-7677

Unetched X250

Figure 161. Arc Plasma Test HfC + C(C-11)-10R, Hot Surface, Oxide on Top.

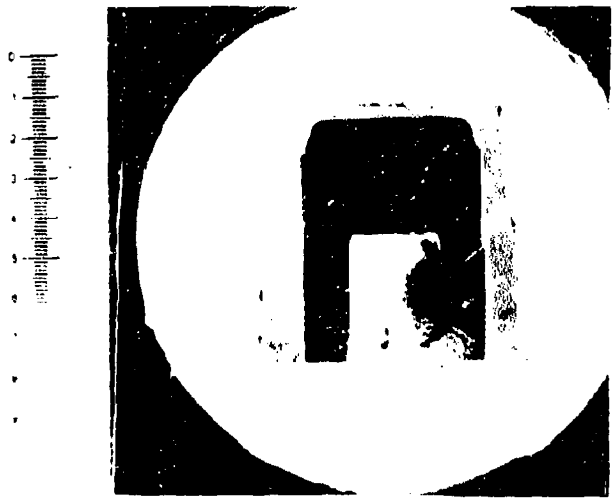

Plate No. 1-8057

X2.5

Figure 162. Arc Plasma Test HfC + C (C-11)-12R, Surface Temperature 5545°F, Exposure Time 180 Seconds, Stagnation Pressure 0.017 Atm. Stagnation Enthalpy 15,420 BTU/ft^2 sec, Cold Wall Heat Flux 756 BTU/ft^2 sec. 110 Mils Recession, Hot Face Up. One Inch Scale.

Plate No. 1-8059

Unetched X50

Figure 163. Arc Plasma Test HfC + C (C-11)-12R., Hot Surface.

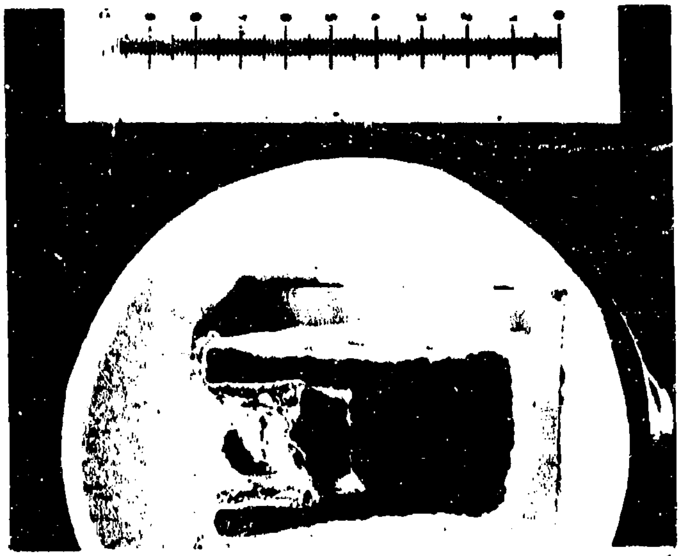

Plate No. 1-7439

X2.69

Figure 164. Arc Plasma Test HfC+C(C-11)-1M, Surface Temperature 5250°F, Exposure Time 1185 Seconds, Stagnation Pressure 1.07 Atm, Stagnation Enthalpy 4670 BTU/lb, Cold Wall Heat Flux 635 BTU/ft^{2}sec, Initial Length 407 Mils, Final Length 348 Mils. Hot Face at Right. One Inch Scale. White Oxide Clearly Visible.

Plate No. 1-7440

Unetched X250

Figure 165. HfC+C(C-11)-1M. Interface of Oxide (Top) and Carbide Matrix.

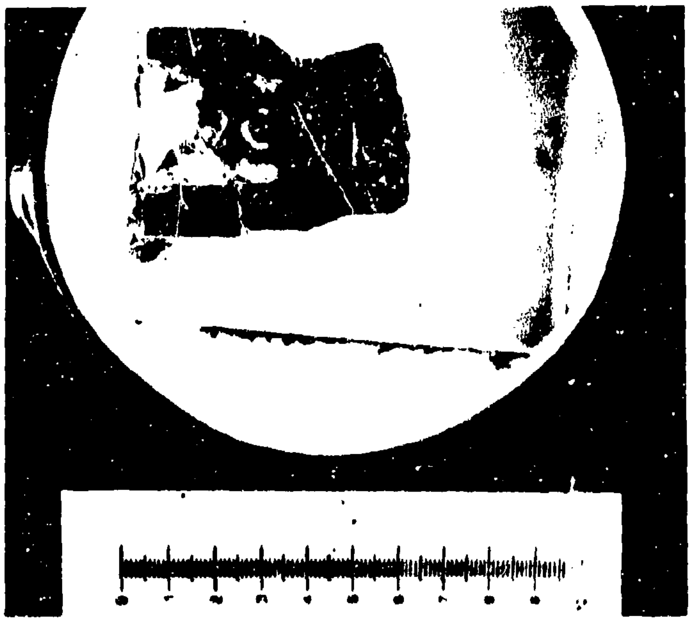

Plate No. 1-7448

X2.65

Figure 166. Arc Plasma Test HfC+C(C-11)-4M, Surface Temperature 6250°F, Exposure Time 45 Seconds, Stagnation Pressure 1.08 Atm, Stagnation Enthalpy 5200 BTU/lb, Cold Wall Heat Flux 755 BTU/ft^{2}sec, Initial Length 404 Mils, Final Length 256 Mils. Hot Face at Right. One Inch Scale.

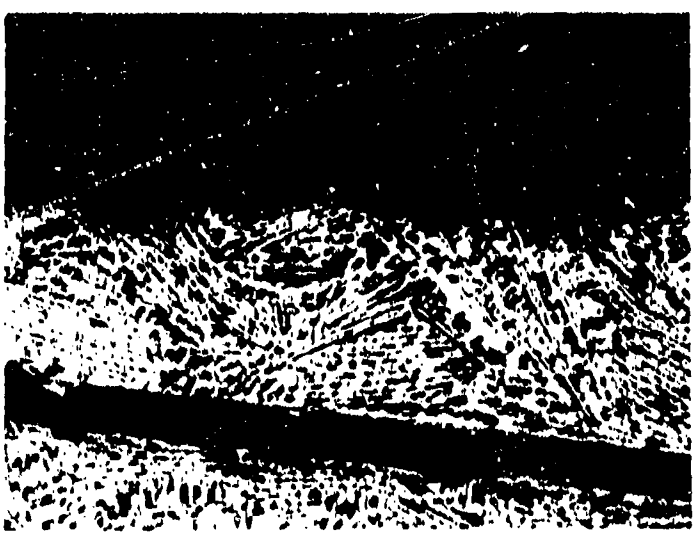

Plate No. 1-7449

Unetched X250

Figure 167. HfC+C(C-11)-4M. Interface of Oxide (Top) and Carbide Matrix.

Plate No. 1-7454

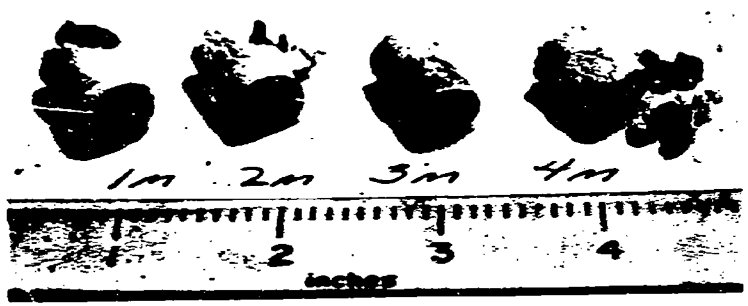

Plate No. 1-7467

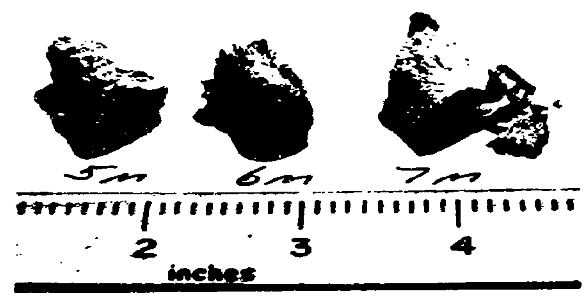

Figure 168. Post Exposure Photographs of Arc Plasma Tests ZrC+C(C-12)-1M, 2M, 3M, 4M, 5M, 6M and 7M.

Plate No. 1-7683

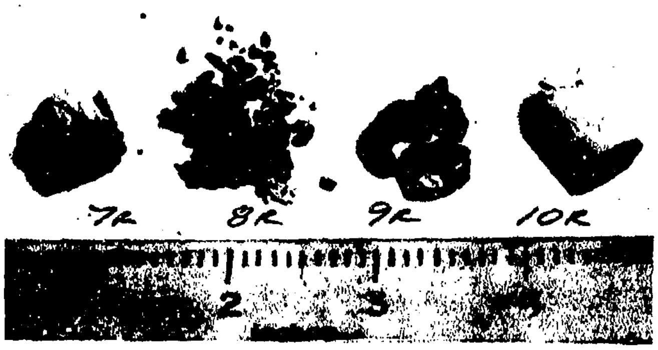

Plate No. 1-7822

Plate No. 1-8789

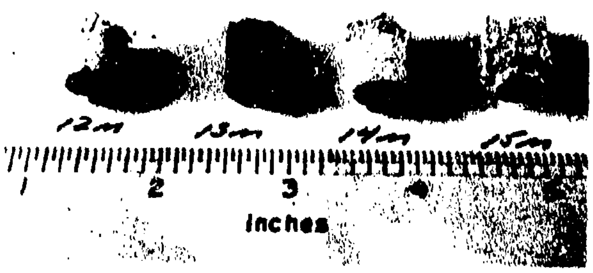

Plate No. 1-9489

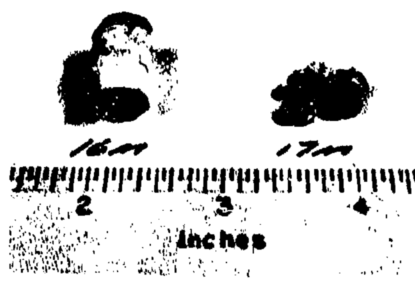

Plate No. 1-9519

Figure 169. Post Exposure Photographs of Arc Plasma Tests ZrC+C(C-12)-7R, 8R, 9R, 10R, 11R, 12M, 13M, 14M, 15M, 16M, 17M and 18R

Plate No. 1-8796

X2.90

Figure 170. Arc Plasma Test ZrC + C(C-12)-15M, Surface Temperature 3900°F, Exposure Time 1800 Seconds, Stagnation Pressure 1.01 Atm. Stagnation Enthalpy 2750 BTU/lb, Cold Wall Heat Flux 235 BTU/ft^2 sec. 64 Mils Recession, Hot Face Up. One Inch Scale.

Plate No. 1-8797

Unetched X250

Figure 171. Arc Plasma Test ZrC + C(C-12)-15M, Hot Surface Oxide on Top.

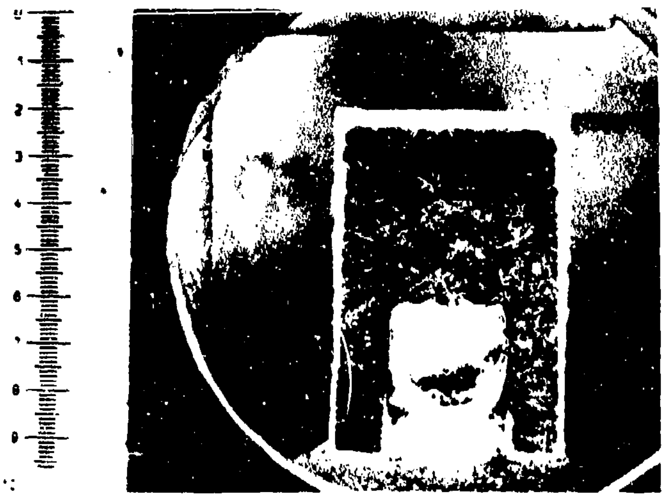

Plate No. 1-7688

X2.90

Figure 172. Arc Plasma Test ZrC + C(C-12)-10R, Surface Temperature $5030^{\circ}F$, Exposure Time 1800 Seconds, Stagnation Pressure 0.093 Atm. Stagnation Enthalpy 11,030 BTU/lb, Cold Wall Heat Flux 548 BTU/ft^2 sec, 32 Mils Recession, Hot Face Up. One Inch Scale.

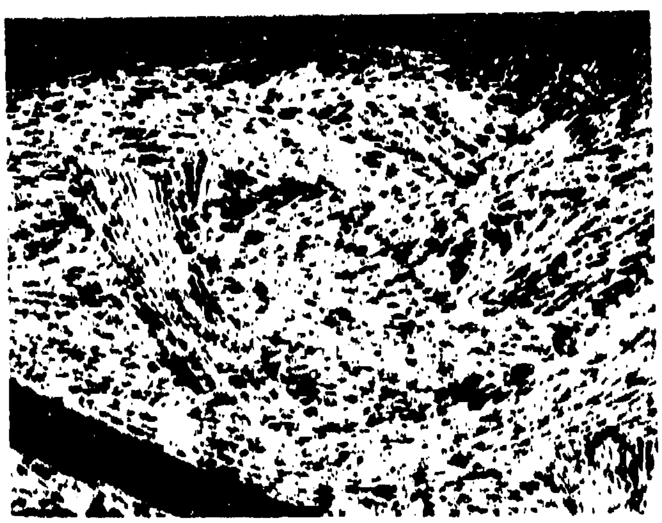

Plate No. 1-7689

Unetched X250

Figure 173. Arc Plasma Test ZrC+C(C-12)-10R, Hot Surface Oxide at Top.

Plate No. 1-7684

X2.90

Figure 174. Arc Plasma Test ZrC+C(C-12)-7R, Surface Temperature 4955° F, Exposure Time 1800 Seconds, Stagnation Pressure 0.084 Atm. Stagnation Enthalpy 11,100 BTU/lb, Cold Wall Heat Flux 775 BTU/ft^2 sec, 209 Mils Recession, Hot Face Down. One Inch Scale.

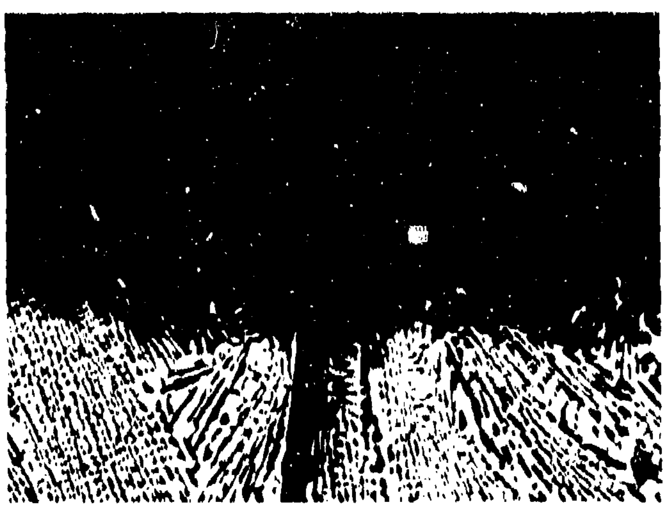

Plate No. 1-7685

Unetched X250

Figure 175. Arc Plasma Test ZrC+C(C-12)-7R, Hot Surface Oxide at Top.

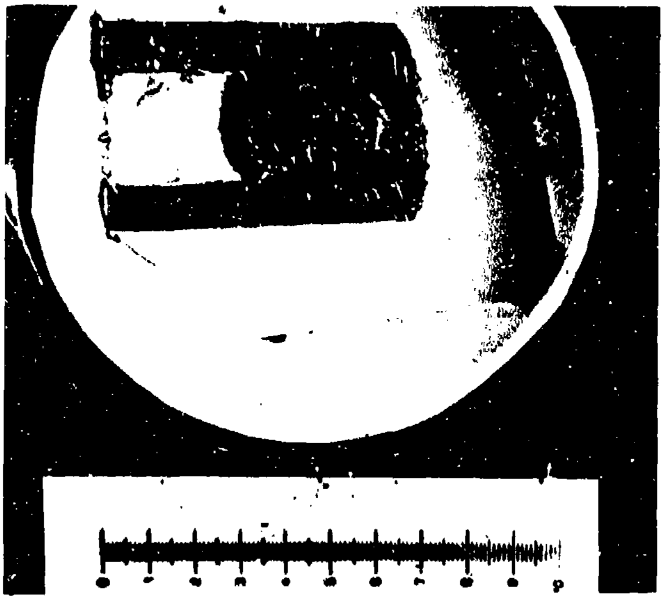

Plate No. 1-7461

X2.75

Figure 176. Arc Plasma Test ZrC+C(C-12)-3M, Surface Temperature 5970°F, Exposure Time 23 Seconds, Stagnation Pressure 1.08 Atm, Stagnation Enthalpy 4580 BTU/lb, Cold Wall Heat Flux 660 BTU/ft^{2}sec, Initial Length 404 Mils, Final Length 379 Mils. Hot Face at Right. One Inch Scale.

Plate No. 1-7462

Unetched X250

Figure 177. Arc Plasma Test ZrC+C(C-12)-3M. Interface of Melted Oxide (Top) and Carbide Matrix.

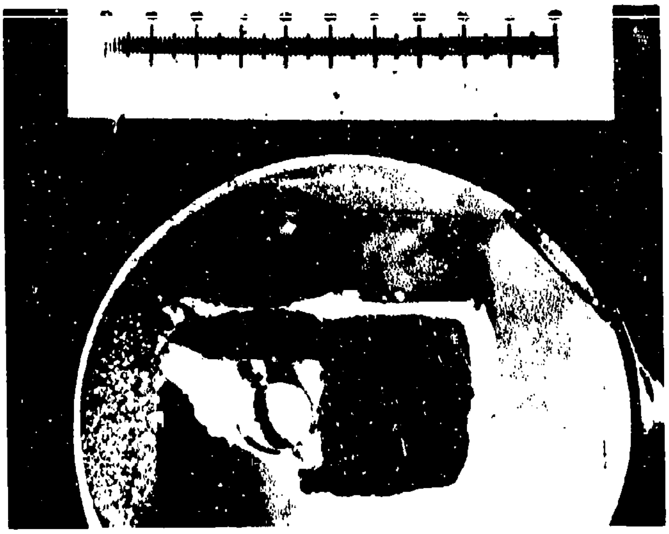

Plate No. 1-7468

X2.69

Figure 178. Arc Plasma Test ZrC+C(C-12)-5M, Surface Temperature $4860^{o}F$, Exposure Time 1800 Seconds, Stagnation Pressure 1.07 Atm, Stagnation Enthalpy 4460 BTU/lb, Cold Wall Heat Flux 620 BTU/ft^2sec, Initial Length 407 Mil, Final Length 341 Mils. Hot Face at Right. One Inch Scale. White Oxide Clearly Visible. Rear Broke on Removal after Test.

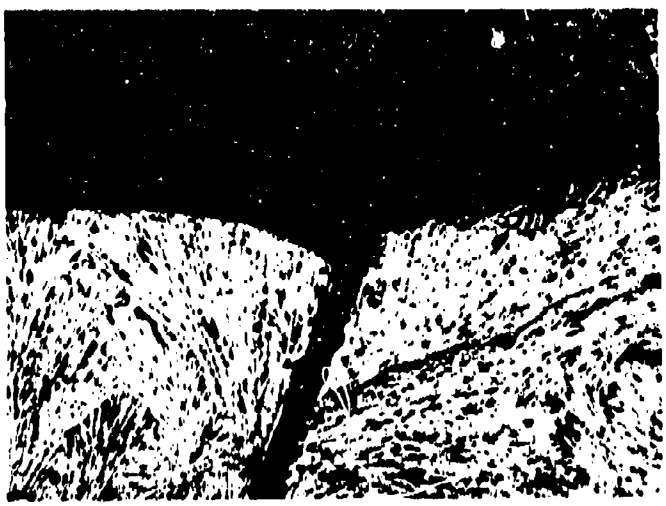

Plate No. 1-7469

Unetched X250

Figure 179. ZrC+C(C-12)-5M. Interface of Oxide (Top) and Carbide Matrix.

Plate 1-2782

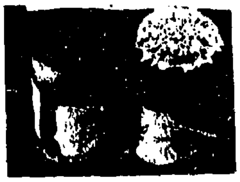

X0.88
(D-13)-21M and 22M
Hot Face Pointing Up

Plate 1-3510

(D-13)-23M X0.88
Hot Face On Right

Plate 1-3511

(D-13)-24M X0.88

Hot Face On Right

Figure 180. Post Exposure Photographs of Arc Plasma Tests JTA(C-ZrB_2-SiC) (D-13)-21M, 22M, 23M and 24M, Showing Thermal Shock Delaminations of JTA(D-13)-23M and 24M.

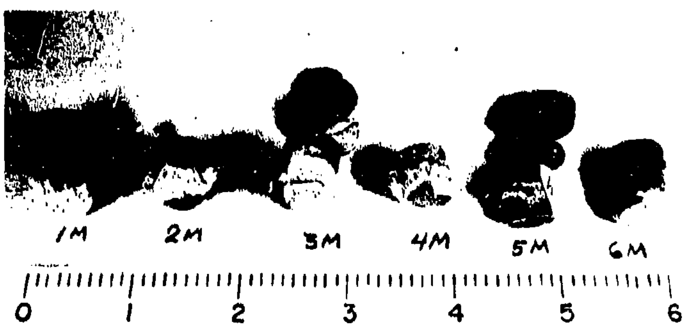

Plate 1-4275

Figure 181. Post Exposure Photographsof Arc Plasma Tests JTA(C-ZrB_2-SiC) (D-13)-1M, 2M, 3M, 4M, 5M and 6M. Hot Face Pointing Down. Samples 3M and 5M Show Thermal Shock Failures. Sample 2M is Propped on Support. One Inch Scale.

Plate 1-4277

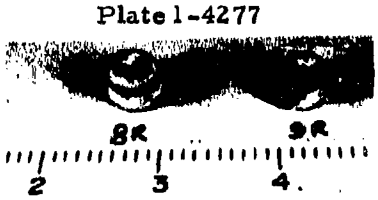

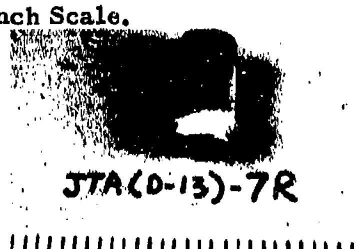

Plate -14276

Figure 182. Post Exposure Photographs of Arc Plasma Tests JTA(D-13)-8R and 9R (Hot Face Up) and 7R (Hot Face Down). One Inch Scale.

Plate No. 1-3068

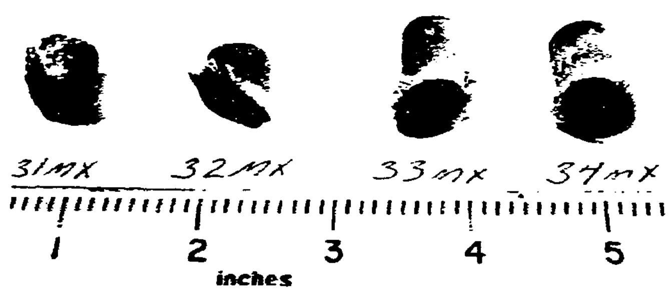

Plate No. 1-8082

Plate No. 1-8101

Plate No. 1-9525

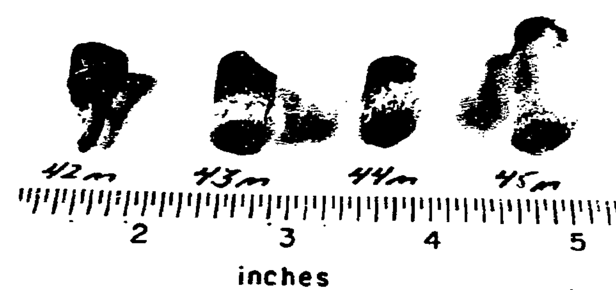

Figure 183. Post Exposure Photographs of Arc Plasma Tests JTA(D-13)-31MX, 32MX, 33MX, 34MX, 35MX, 36MX, 37MX, 38MX, 39MX, 40MX, 41MX, 42M, 43M, 44M and 45M

Plate No. 1-4944

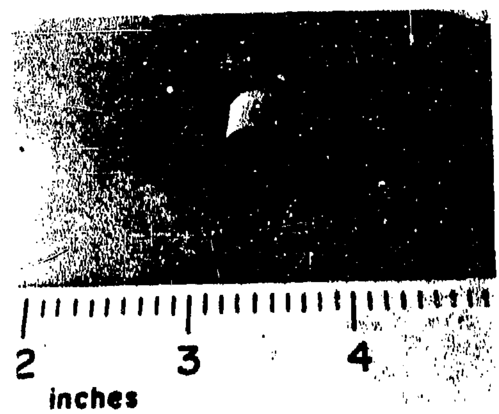

Plate No. 2-0418

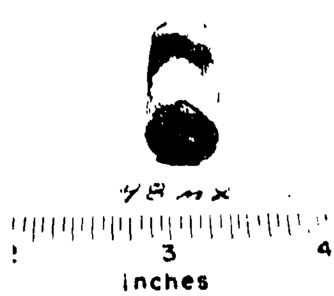

Plate No. 2-0277

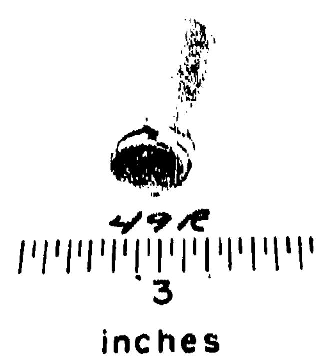

Figure 184. Post Exposure Photographs of Arc Plasma Tests JTA(D-13)-10R, 48MX and 49RX.

Plate 1-2786

X2.5

Figure 185. Arc Plasma Test JTA(C-ZrB_2-SiC)(D-13)-22M, Surface Temperature 3750°F, Exposure Time 1830 Seconds, Stagnation Pressure 1 Atm, Stagnation Enthalpy 3075 BTU/lb, Cold Wall Heat Flux 460 BTU/ft^2sec. Initial Length 1050 Mils, Final Length 977 Mils. Hot Face at Right, One Inch Scale.

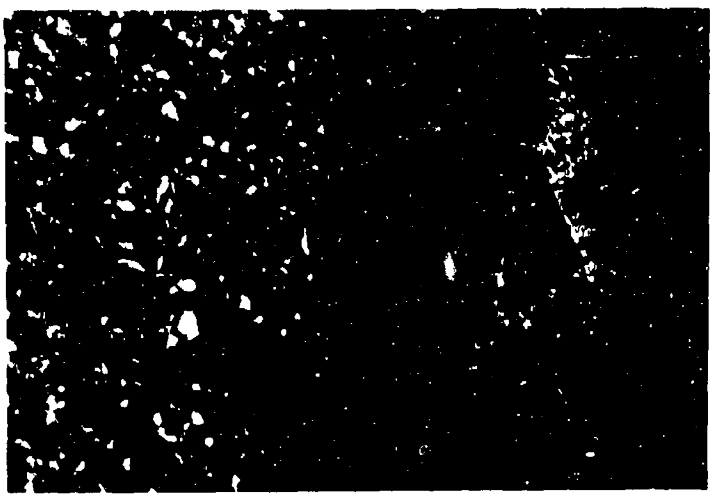

Plate 1-4466

X50

Figure 186. Arc Plasma Test JTA(C-ZrB_2-SiC)(D-13)-22M, Interface of Hot Face Showing Matrix on Left and Oxide on Right with Gap in Center.

Plate No.
1-2789

500X

Figure 187. Arc Plasma Test JTA(C-ZrB_2-SiC)(D-12)-22M, Matrix Sting Leg Showing White ZrB_2 Grains and Light Grey SiC Grains in Dark Grey Graphite Matrix.

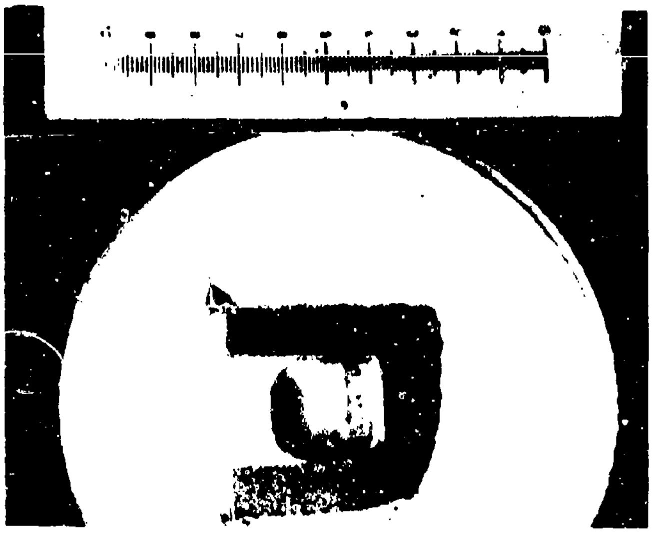

Plate No. 1-4511

X2.75

Figure 188. Arc Plasma Test JTA(D-13)-4M, Surface Temperature 4560°F, Exposure Time 214 Seconds, Stagnation Pressure 1.08 Atm, Stagnation Enthalpy 4320 BTU/lb, Cold Wall Heat Flux 660 BTU/ft^{2}sec, Initial Length 645 Mil, Final Length 125 Mil. Hot Face at Right. One Inch Scale.

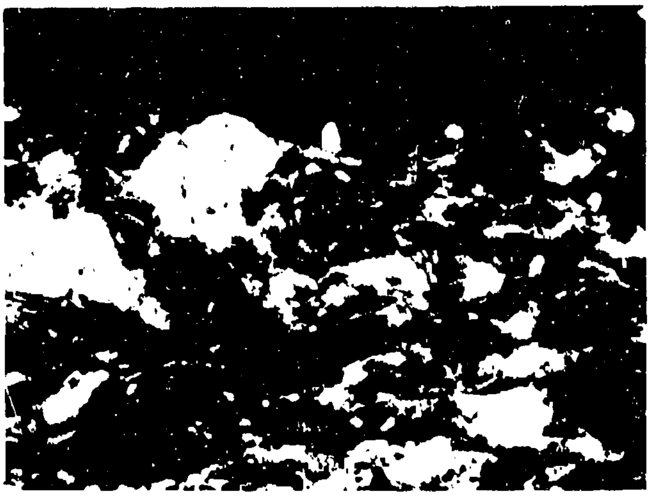

Plate No. 1-4512

Graphite

Boride

Unetched X250

Figure 189. Arc Plasma Tests JTA(D-13)-4M. Melted Interface.

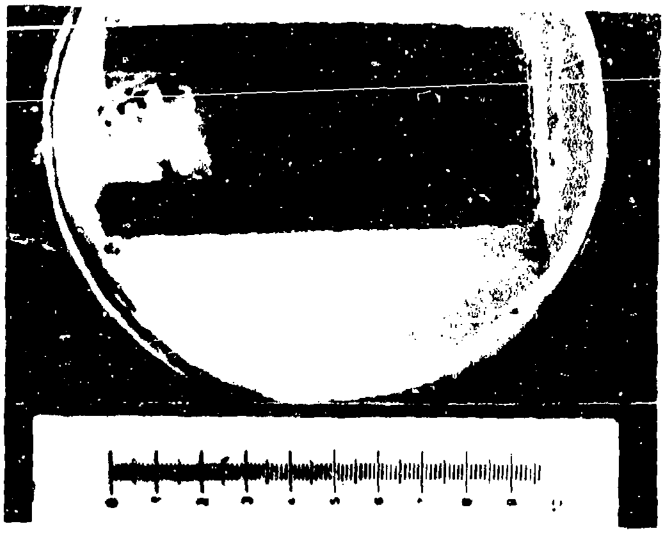

Plate No. 1-4520

X2.69

Figure 190. Arc Plasma Test JTA(D-13)-7R, Surface Temperature 4665°F, Exposure Time 1800 Seconds, Stagnation Pressure 0.074 Atm, Stagnation Enthalpy 9520 BTU/lb, Cold Wall Heat Flux 500 BTU/ft^2sec, Initial Length 681 Mil, Final Length 637 Mil, Hot Face At Right. One Inch Scale. White Oxide Clearly Visible.

Plate No. 1-4521

Boride

Graphite

Unetched

X250

Figure 191. Arc Plasma Test JTA(D-13)-7R. Oxide Detached at Top Interface.

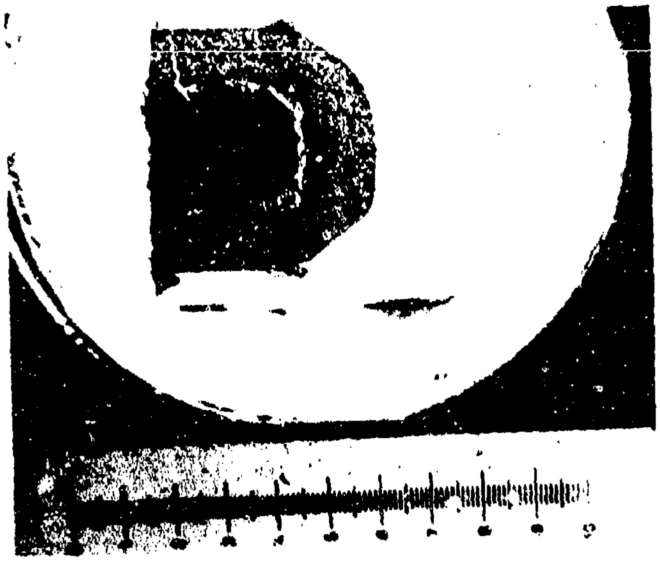

Plate No. 1-4523

X3.13

Figure 192. Arc Plasma Test JTA(D-13)-8R, Surface Temperature 5305°F, Exposure Time 180 Seconds, Stagnation Pressure 0.164 Atm, Stagnation Enthalpy 7310 BTU/lb, Cold Wall Heat Flux 770 BTU/ft^{2}sec, Initial Length 713 Mil, Final Length 132 Mil. Hot Face at Right. One Inch Scale.

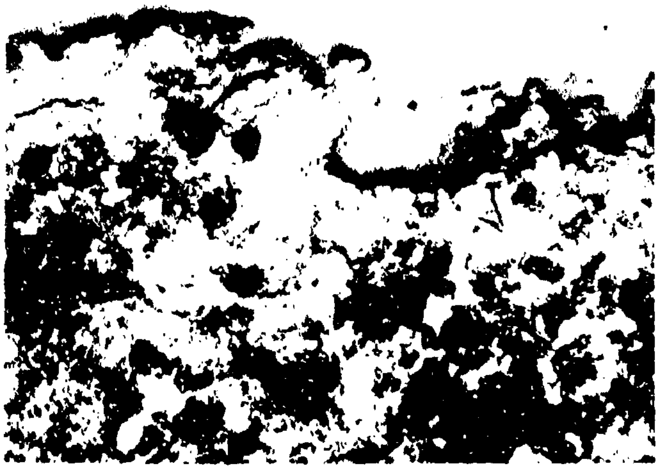

Plate No. 1-4525

Unetched X250

Figure 193. Arc Plasma Test JTA(D-13)-8R. Melted Interface.

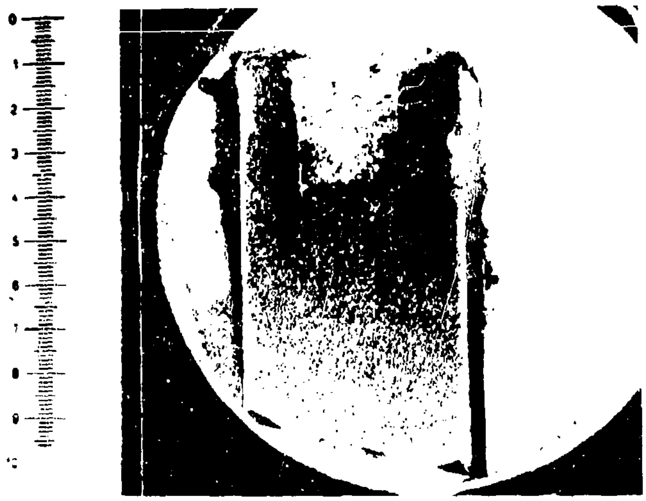

Plate No. 2-0419

X2.70

Figure 194. Arc Plasma Test JTA(D-13)-48MX Surface Temperature 4050°F, Exposure Time 7200 Seconds (4 cyclic exposures each of 1800 seconds), Stagnation Pressure 1.01 Atm. Stagnation Enthalpy 4350 BTU/lb, Cold Wall Heat Flux 380 BTU/ft^{2}sec, 118 Mils Recession, Hot Face Down, One Inch Scale.

Plate No. 2-0420

Unetched X 250

Figure 195. Arc Plasma Test JTA(D-13)-48MX, Hot Surface.

Plate No. 2-0278

X2.60

Figure 196. Arc Plasma Test JTA(D-13)-49RX Surface Temperature $4425^{o}F$, Exposure Time 7200 Seconds (4 cyclic exposures each of 1800 seconds), Stagnation Pressure 0.057 Atm. Stagnation Enthalpy 9600 BTU/lb, Cold Wall Heat Flux 440 BTU/ft^2sec, 45 Mils Recession, Hot Face Down, One Inch Scale.

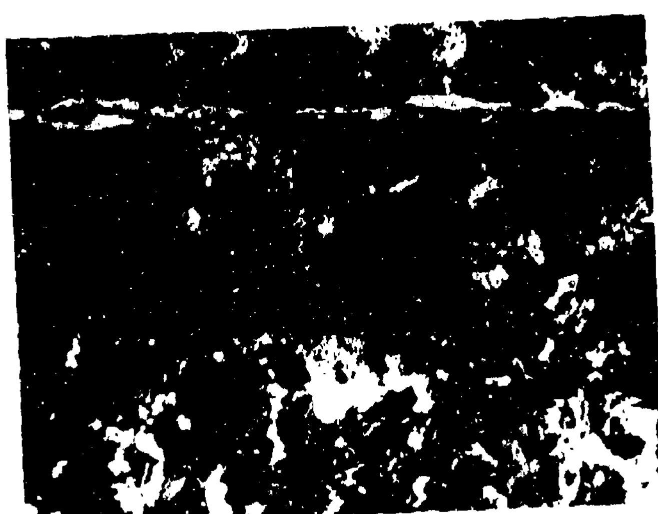

Plate No. 2-0279

Unetched X 250

Figure 197. Arc Plasma Test JTA(D-13)-49RX, Hot Surface.

Plate No. 1-4950

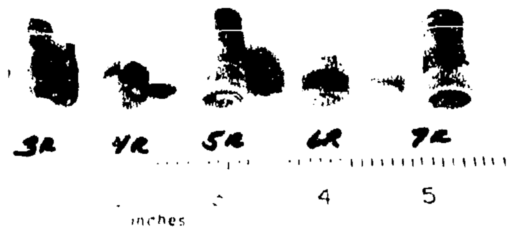

Plate No. 1-2791

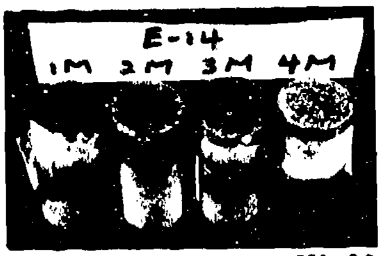

X0.88

Plate No. 1-4278

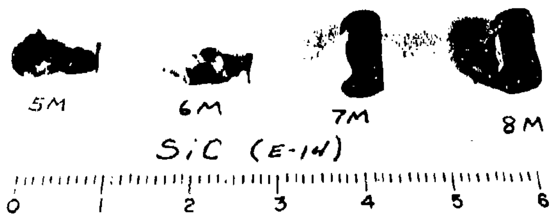

One Inch Scale

Figure 198. Post Exposure Photographs of Arc Plasma Tests KT-SiC(E-14)-3R, 4R, 5R, 6R, 7R, 1M, 2M, 3M, 4M, 5M, 6M, 7M and 8M. Hot Face Pointing Up. Sample 6M Ablated Completely While 7M and 8M showed Longitudinal Cracks.

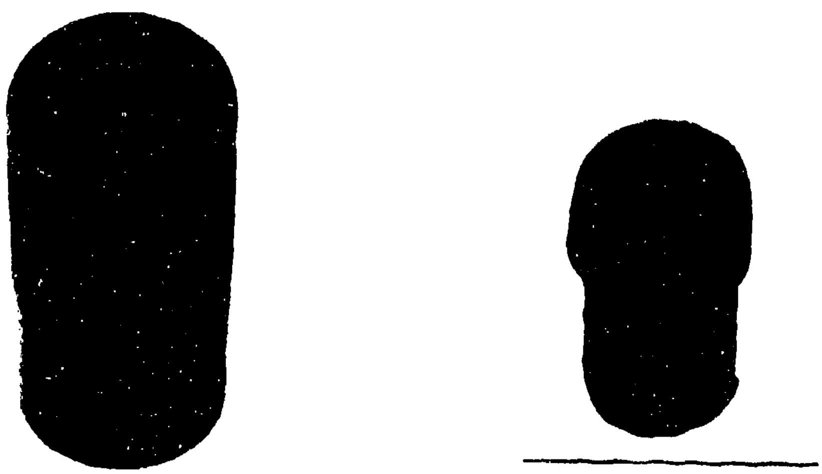

KT-SiC(E-14)-1R X3 KT-SiC(E-14)-2R X2.5

Figure 199. Post Exposure Photographs of Arc Plasma Tests KT-SiC (E-14)-1R and 2R. Hot Face Pointed Up. Sample KT-SiC (E-14)-2R Ablated Completely and is Shown Mounted on Tungsten Sting.

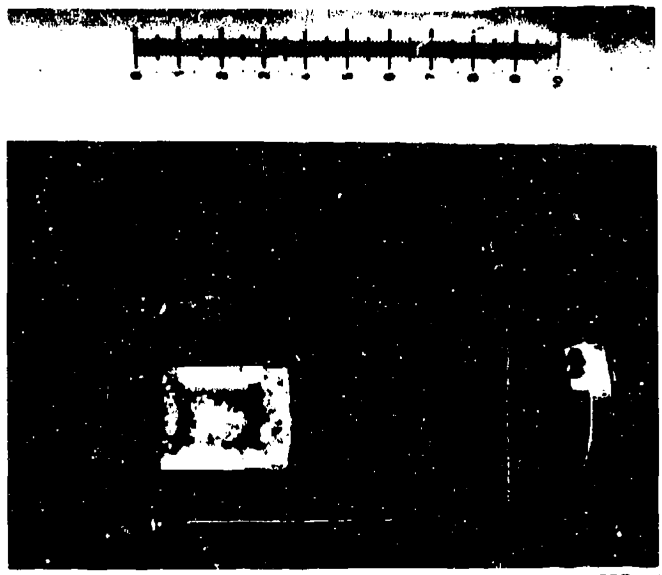

Plate No.
1-2801

X2.55

Figure 200. Arc Plasma Test KT-SiC(E-14)-4M, Surface Temperature 3670°F, Exposure Time 1835 Seconds, Stagnation Enthalpy 4155 BTU/lb, Stagnation Pressure 1 Atm, Cold Wall Heat Flux 600 BTU/ft^{2}sec, Initial Length 841 Mils, Final Length 834 Mils. Hot Face at Right. One Inch Scale.

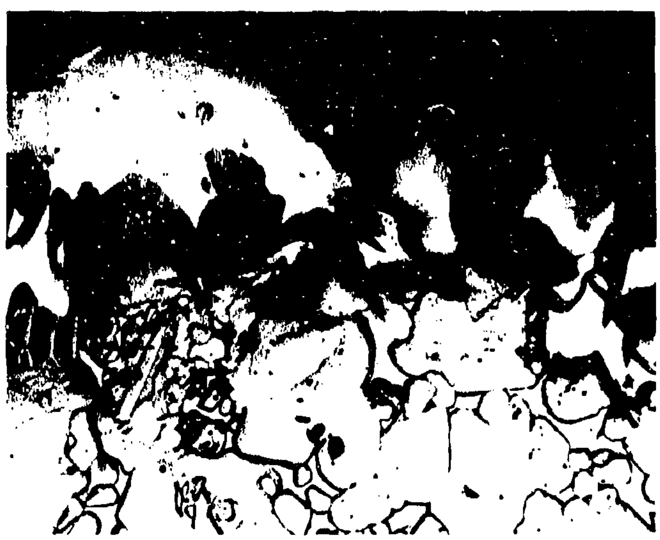

Plate No.
1-2802

X250

Figure 201. Arc Plasma Test KT-SiC(E-14)-4M, Hot Face Showing Light Grey, SiC Grains and White Silicon Binder Phase.

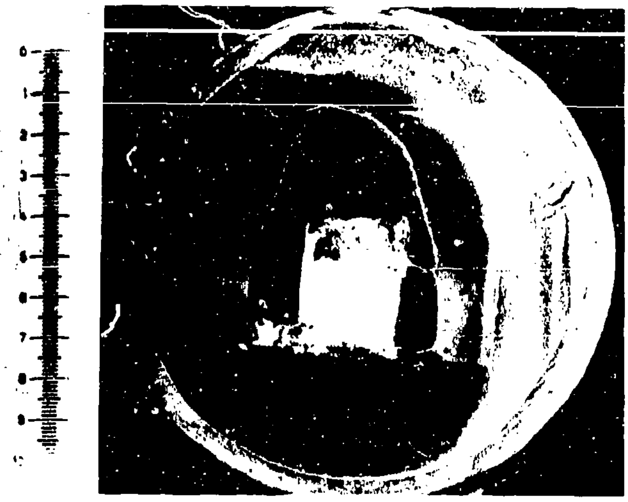

Plate No. 1-4738

X2.50

Figure 202. Arc Plasma Test KT-SiC(E-14)-5M, Surface Temperature 4440°F, Exposure Time 165 Seconds, Stagnation Pressure 1.08 Atm. Stagnation Enthalpy 4910 BTU/lb, Cold Wall Heat Flux 810 BTU/ft^2 sec, 425 Mil Recession, Hot Face Up. One Inch Scale.

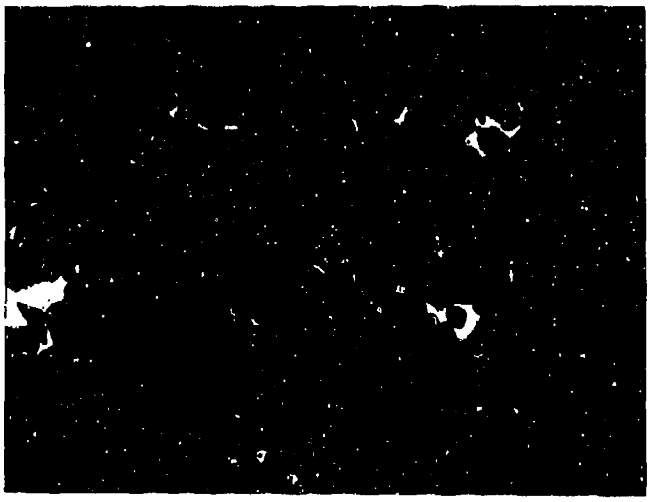

Plate No. 1-4739

Etched Electrolytically with 5% KOH Solution X 250

Figure 203. Arc Plasma Test KT-SiC(E-14)-5M, Hot Surface.

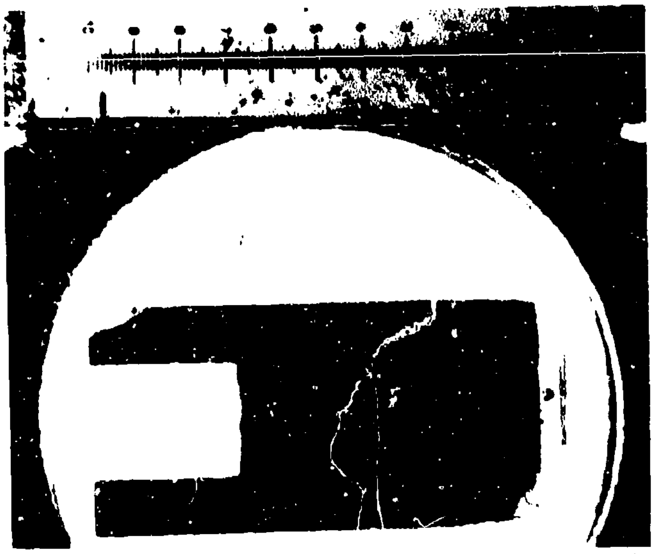

Plate No. 1-4957

X2.81

Figure 204. Arc Plasma Test KT-SiC(E-14)-7R, Surface Temperature 3060°F, Exposure Time 1800 Seconds, Stagnation Pressure 0.097 Atm, Stagnation Enthalpy 10880 BTU/lb, Cold Wall Heat Flux 652 BTU/ft^2sec, Initial Length 679 Mils, Final Length 655 Mils. Hot Face at Right. One Inch Scale. Specimen Cracked by Thermal Shock.

Plate No. 1-4958

Electrolytic Etch 5%KOH X250

Figure 205. Arc Plasma Test KT-SiC(E-14)-7R. Hot Interface.

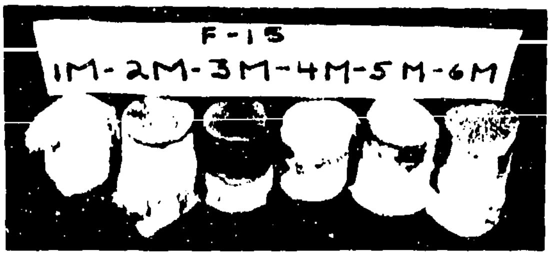

Plate 1-2762

X0.88

Figure 206. Post Exposure Photographs of Arc Plasma Tests JT0992 (C-HfC-SiC) (F-15)-1M, 2M, 3M, 4M, 5M and 6M. Hot Face Pointed Up.

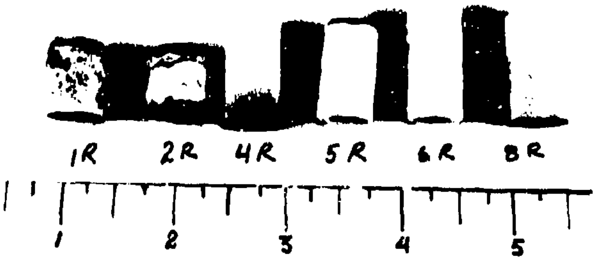

Plate 1-3642

Figure 207. Post Exposure Photographs of Arc Plasma Tests JT0992 (C-HfC-SiC) (F-15) (Billet 2/G/6)-1R, 2R, 4R, 5R, 6R and 8R. One Inch Scale. Hot Face Pointed Up.

Plate 1-3504

(F-15)-3R X0.88

Plate 1-3505

(F-15)-7R X0.88

Figure 208. Post Exposure Photographs of Arc Plasma Tests JT0992 (C-HfC-SiC) (F-15) (Billet 2/G/6)-3R and 7R. Hot Face at Right Pointed toward Left in 3R and Hot Face at Right in 7R Illustrating Thermal Shock Failures.

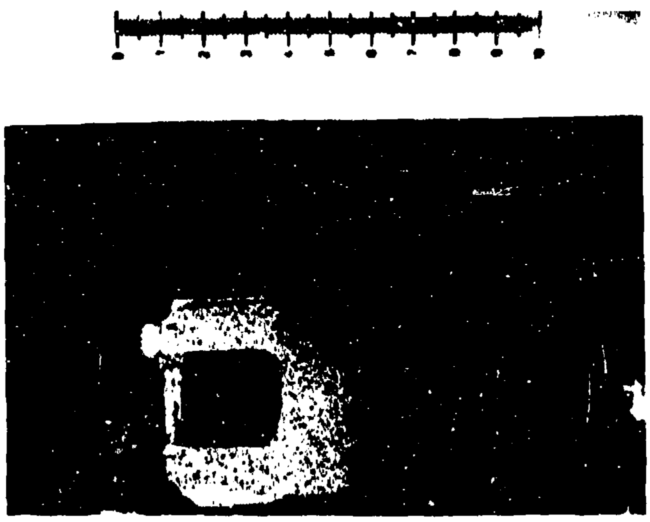

Plate No. 1-2769

X2.6

Figure 209. Arc Plasma Test JT0992(F-15)-3M, Surface Temperature 4930°F, Exposure Time 300 Seconds, Stagnation Pressure 1.10 Atm, Stagnation Enthalpy 4285 BTU/lb, Cold Wall Heat Flux 770 BTU/ft^{2}sec, Initial Length 1054 Mil, Final Length 692 Mil. Hot Face at Right. One Inch Scale. Some Side Recession.

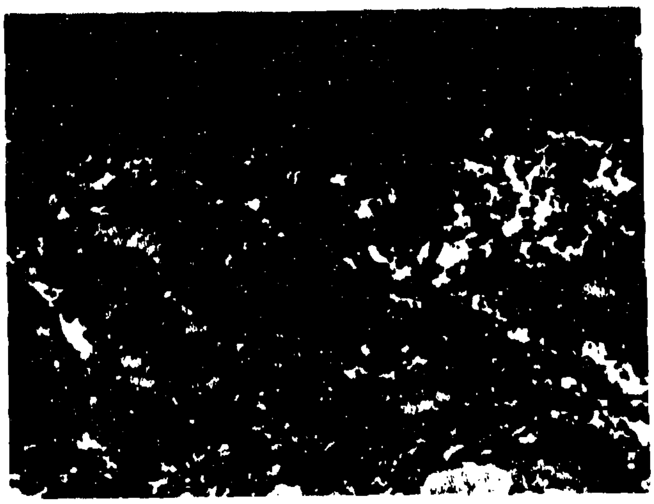

Plate No. 1-2770

Unetched X250

Figure 210. Arc Plasma Test JT0992(F-15)-3M. Melted Interface.

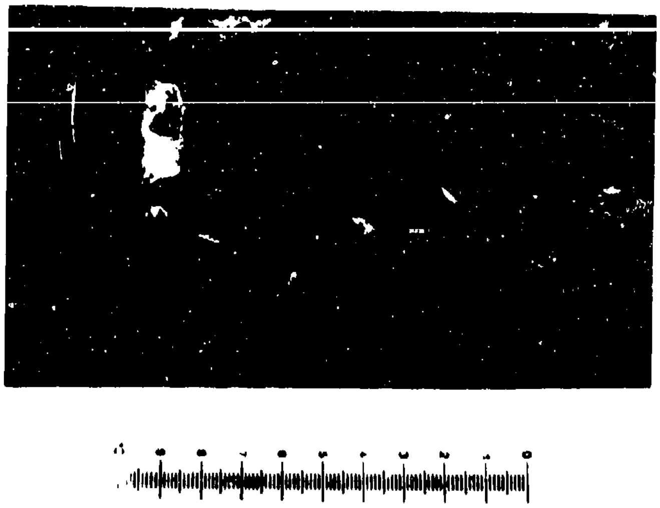

Plate No. 1-2766

X2.5

Figure 211. Arc Plasma Test JT0992(F-15)-2M, Surface Temperature 3470°F, Exposure Time 1173 Seconds, Stagnation Pressure 1.07 Atm, Stagnation Enthalpy 2105 BTU/lb, Cold Wall Heat Flux 430 BTU/ft^{2}sec, Initial Length 1033 Mil, Final Length 999 Mil. Hot Face at Right. One Inch Scale. Severe Recession at Sides and Rear.

Plate No. 1-2767

Unetched X250

Figure 212. Arc Plasma Test JT0992(F-15)-2M. Oxide (Top). Detached from Matrix at Hot Interface.

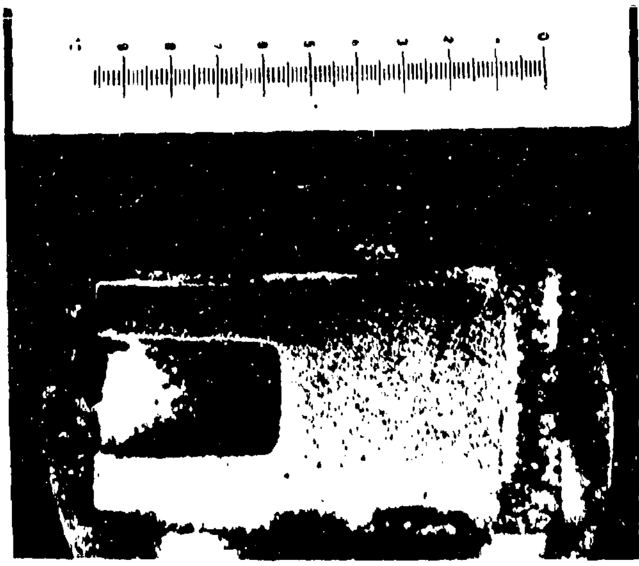

Figure 213. Arc Plasma Test JT0992(C-HfC-SiC)(F-15)-5R, Surface Temperature 5225°F, Exposure Time 1200 Seconds, Stagnation Pressure 0.027 atm, Stagnation Enthalpy 14550 BTU/lb, Cold Wall Heat Flux 500 BTU/ft^{2}sec, Initial Length 988 Mils, Final Length 865 Mils. Hot Face at Right. One Inch Scale.

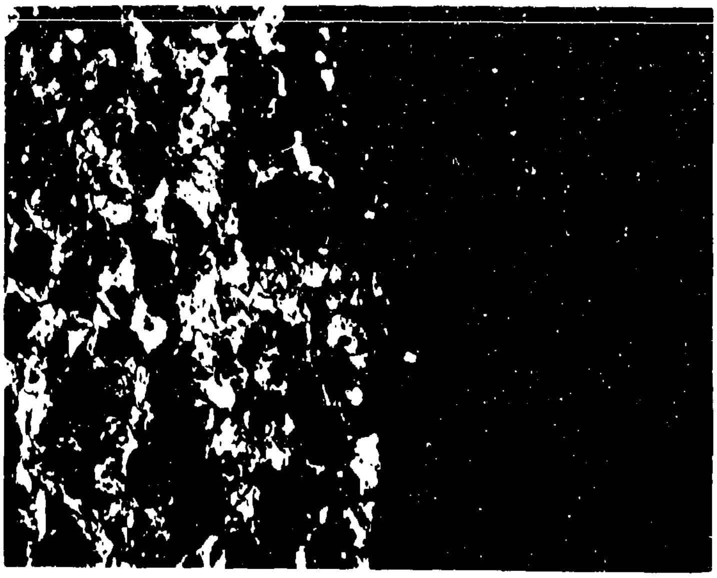

Plate 1-3653

X250

Figure 214. Arc Plasma Test JT0992(C-HfC-SiC)(F-15)-5R, Hot Face Interface. Matrix at Left Containing White HfC Grains and Light Grey SiC Grains in a Dark Grey Graphite Matrix. Oxide Skin is Out of Focus.

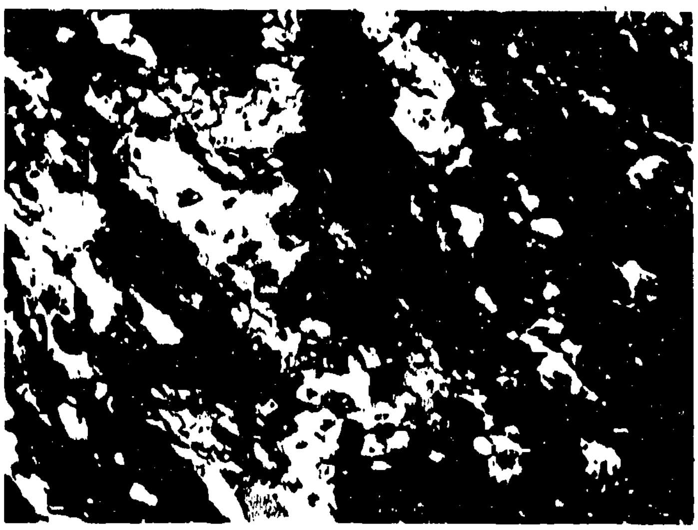

Plate 1-3655

X500

Figure 215. Arc Plasma Test JT0992 (C-HfC-SiC)(F-15)-5R, Sting Leg Matrix Showing White HfC Grains and Light Grey SiC Grains in a Dark Grey Graphite Matrix.

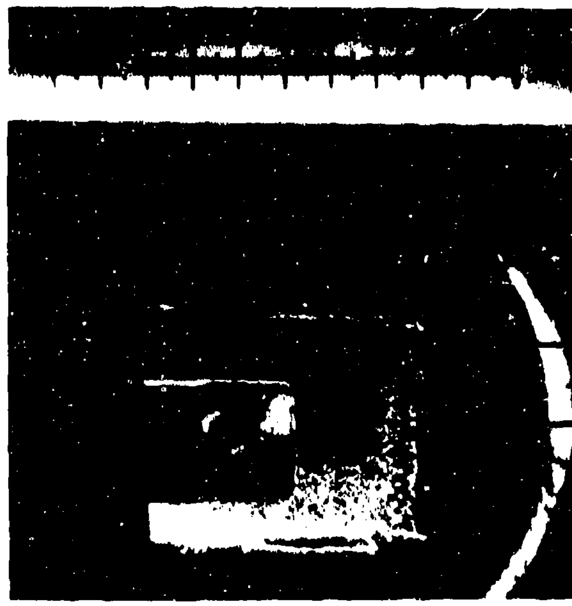

Figure 216. Arc Plasma Test JT0992(C-HfC-SiC)(F-15)-2R, Surface Temperature 5630°F, Exposure Time 110 Seconds, Stagnation Pressure 0.287 Atm, Stagnation Enthalpy 9390 BTU/lb, Cold Wall Heat Flux 1145 BTU/ft^{2}sec. Initial Length 994 Mils, Final Length 594 Mils. Hot Face at Right. One Inch Scale.

Figure 217. Arc Plasma Test JT0992 (C-HfC-SiC) (F-15)-2R, Hot Face Interface Zone, Matrix on Left, Zone Depleted of Carbides on Right.

Plate 1-3506

(F-16)-21M X0.88

Hot Face at Center Facing Right

Plate 1-3507

(F-16)-22M X0.88

Hot Face to Left

Plate 1-3508

(F-16)-23M X0.88

Hot Face to Right

Plate 1-3509

(F-16)-24M X0.88

Hot Face to Right

Figure 218. Post Exposure Photographs of JT0981 (C-ZrC-SiC) (F-16)-21M, 22M, 23M and 24M Showing Thermal Shock Failures. (F-16)-22M Experienced Low Temperature (3870°F) Oxidation for 1830 Seconds Prior to Failure.

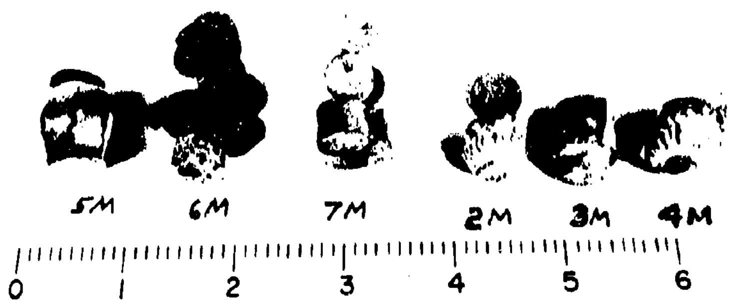

Plate 1-4280

Figure 219. Post Exposure Photographs of JT0981 (C-ZrC-SiC) (F-16)-2M, 3M, 4M, 5M, 6M and 7M. Samples 2M, 6M and 7M Exhibited Thermal Shock Failures While 5M Experienced Low Temperature (3910°F) Oxidation. One Inch Scale.

Plate No. 1-4281

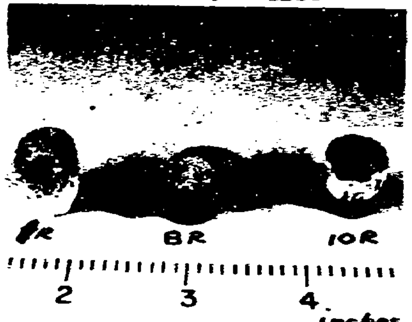

Hot Face Pointing Up

Plate No. 1-4282

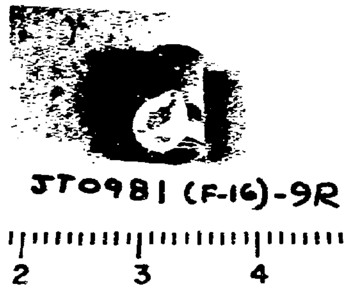

Hot Face Pointing Down

Plate No. 1-4966

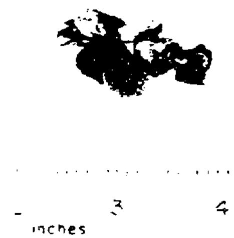

Figure 220. Post Exposure Photographs of JT0981(C-ZrC-SiC)(F-16)-1R, 8R, 10R, 9R and 11R. Samples 8R and 11R Exhibited Thermal Shock Failures. One Inch Scale.

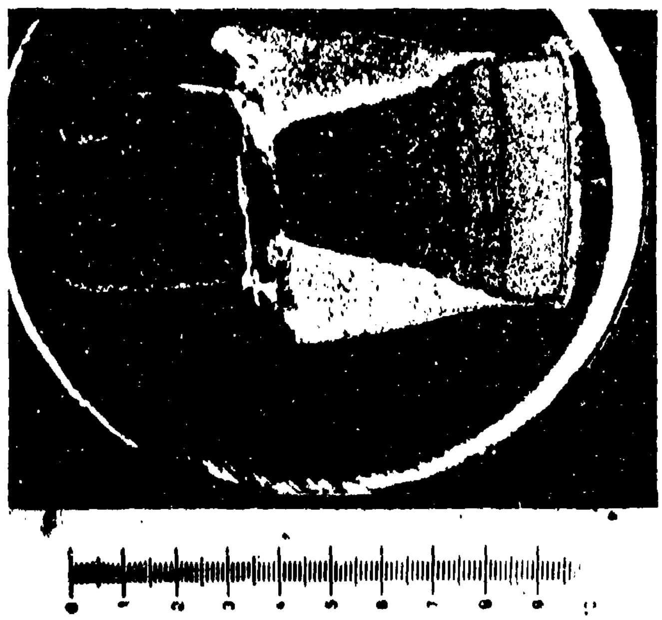

Plate No.
1-4183

X3

Figure 221. Arc Plasma Test JT0981(C-ZrC-SiC)(F-16)-22M, Surface Temperature 3870°F, Exposure Time 1830 Seconds, Stagnation Pressure 1 Atm., Stagnation Enthalpy 3230 BTU/lb, Cold Wall Heat Flux 460 BTU/ft^{2}sec, Initial Length 1055 Mils. Hot Face at Right. One Inch Scale. Exposure Illustrates Extensive Side Face Oxidation Occurring at Low Temperature where Protective Oxide Formation does not Occur.

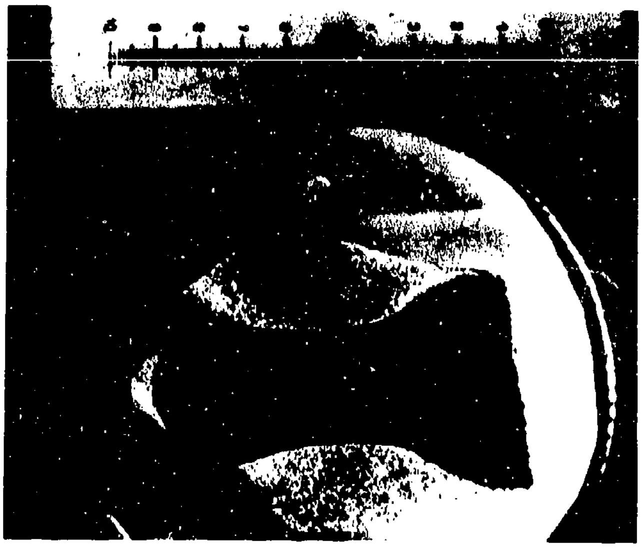

Plate No. 1-4614

X2.69

Figure 222. Arc Plasma Test JT0981(F-16)-5M, Surface Temperature 3910°F, Exposure Time 1830 Seconds, Stagnation Pressure 1.06 Atm, Stagnation Enthalpy 2485 BTU/lb, Cold Wall Heat Flux 390 BTU/ft^{2}sec, Initial Length 692 Mil, Final Length 586 Mil. Hot Face at Right. One Inch Scale. Severe Side Recession.

Unetched X250

Figure 223. Arc Plasma Test JT0981(F-16)-5M. Interface of Oxide and Matrix.

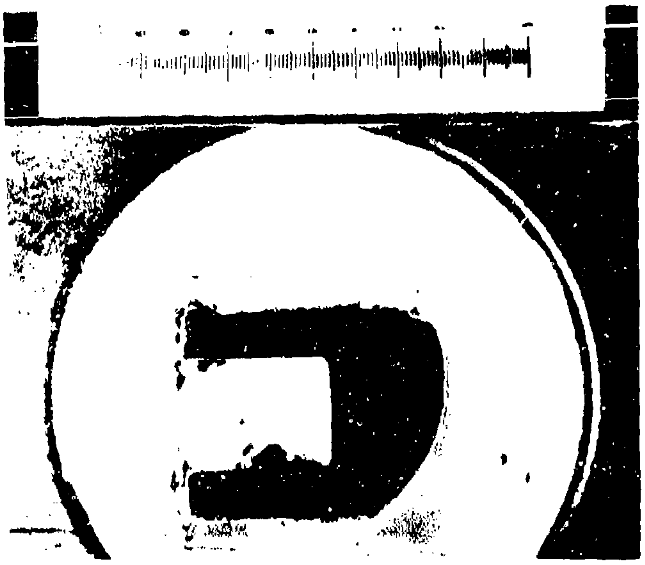

Plate No. 1-4610

X2.69

Figure 224. Arc Plasma Test JT0981(F-16)-4M, Surface Temperature 4990°F, Exposure Time 148 Seconds, Stagnation Pressure 1.08 Atm, Stagnation Enthalpy 3475 BTU/lb, Cold Wall Heat Flux 640 BTU/ft^{2}sec, Initial Length 565 Mil, Final Length 266 Mil. Hot Face at Right. One Inch Scale. Some Side Recession.

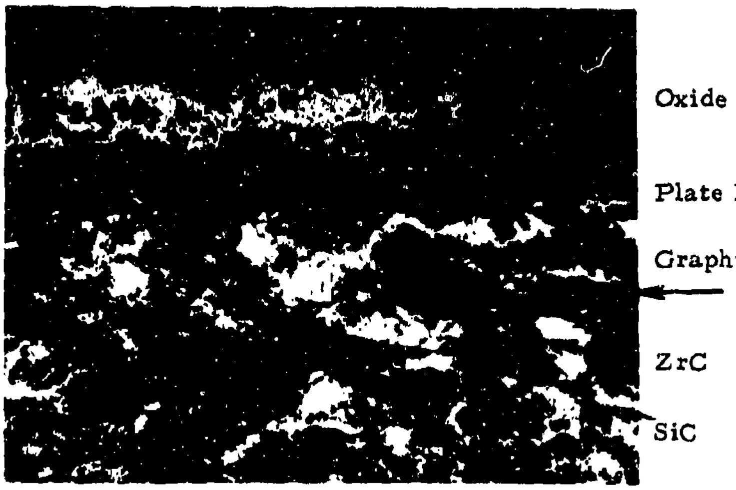

Oxide

Plate No. 1-4612

Graphite

ZrC

SiC

Unetched X250

Figure 225. Arc Plasma Test JT0981(F-16)-4M. Interface of Oxide and Matrix.

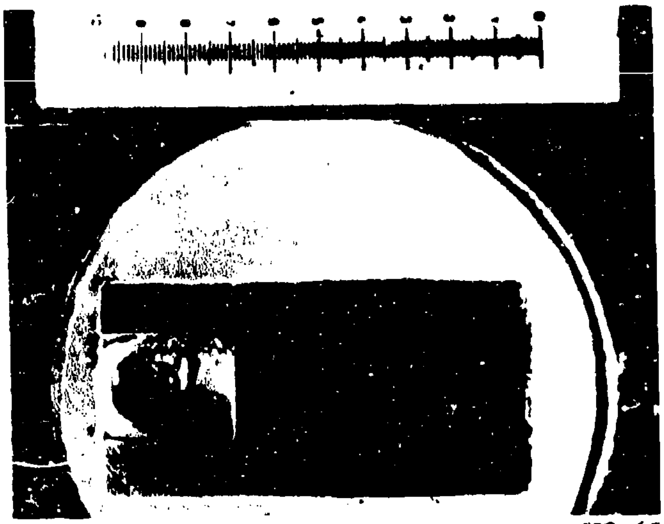

Plate No. 1-4636

X2.69

Figure 226. Arc Plasma Test JT0981(F-16)-9R, Surface Temperature 4695°F, Exposure Time 1800 Seconds, Stagnation Pressure 0.075 Atm, Stagnation Enthalpy 9120 BTU/lb, Cold Wall Heat Flux 523 BTU/ft^{2}sec, Initial Length 696 Mil, Final Length 655 Mil. Hot Face at Right. One Inch Scale.

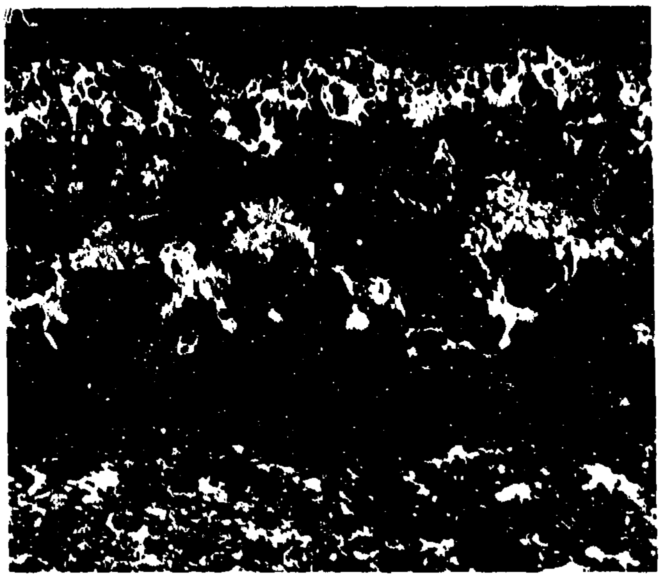

Plate No. 1-4637A

Unetched X75

Figure 227. JT0981(F-16)-9R. Oxide (Top). Detached from Matrix.

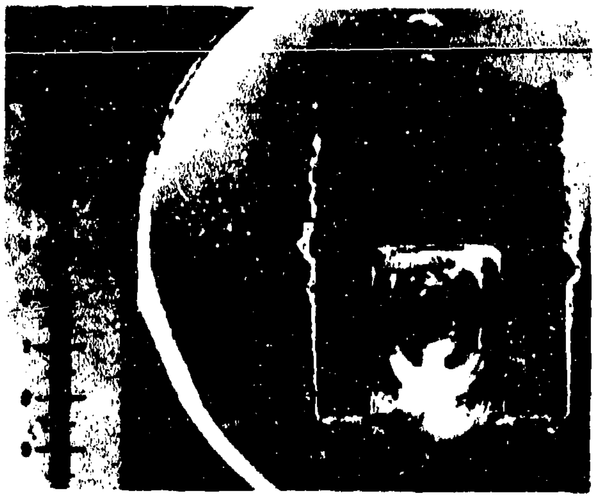

Plate No. 1-4624

X3.06

Figure 228. Arc Plasma Test JT0981(F-16)-1R, Surface Temperature 5065°F, Exposure Time 150 Seconds, Stagnation Pressure 0.179 Atm, Stagnation Enthalpy 7430 BTU/lb, Cold Wall Heat Flux 747 BTU/ft^{2}sec, Initial Length 694 Mil, Final Length 338 Mil. Hot Face at Top. One Inch Scale.

Plate No. 1-4626

Unetched X250

Figure 229. Arc Plasma Test JT0981(F-16)-1R. Melted Interface at Top.

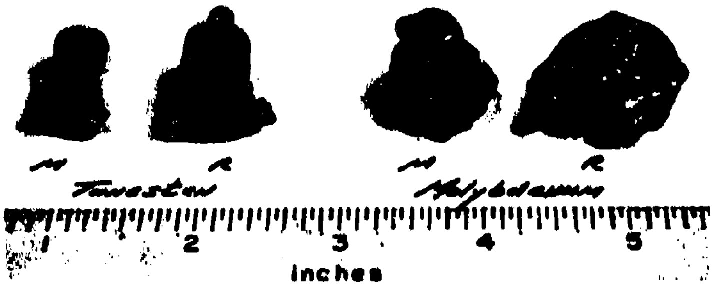

Figure 230. Post Exposure Photographs of Tungsten and Molybdenum Samples Employed in Temperature Calibration Tests in the Model 500 (M) and ROVERS (R) Facilities.

Plate No. 1-6453

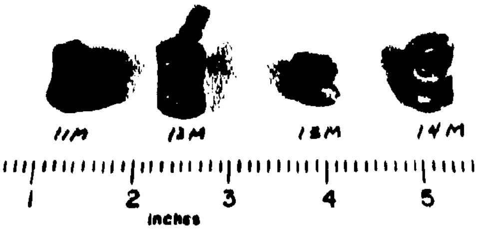

Plate No. 1-5417

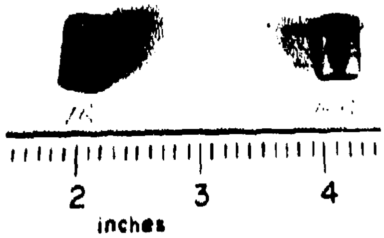

Plate No. 1-4283

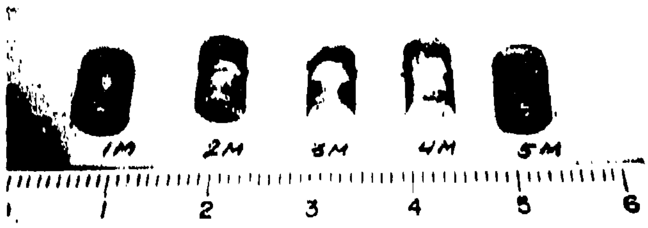

Figure 231. Post Exposure Photographs of 5 Mil WSi_2 Coated W; WSi_2/W(G-18)-1M, 2M, 3M, 4M, 5M, 11M, 12M, 13M, 14M, 9R and 10R. Hot Face Pointed Down. One Inch Scale.

Plate No. 1-4284

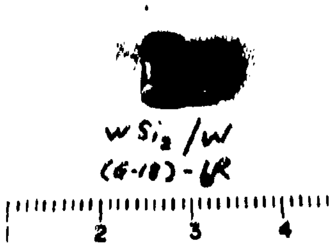

Plate No. 1-4285

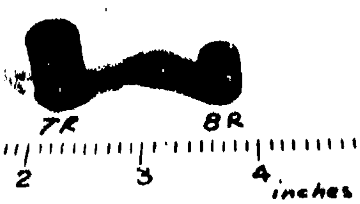

Figure 232. Post Exposure Photographs of 5 Mil WSi_2 Coated W; WSi_2/W(G-18)-6R, 7R and 8R. Hot Face Pointed Up. One Inch Scale.

Plate No. 2-0629

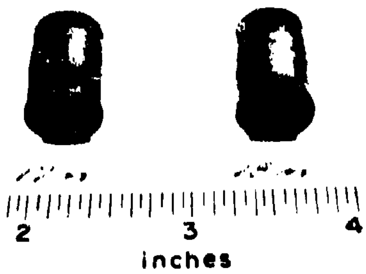

Plate No. 2-0713

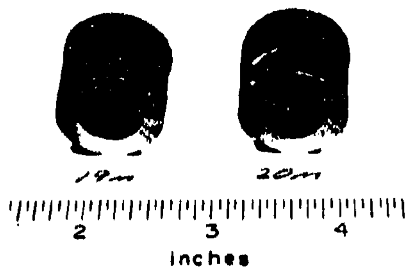

Plate No. 2-0634

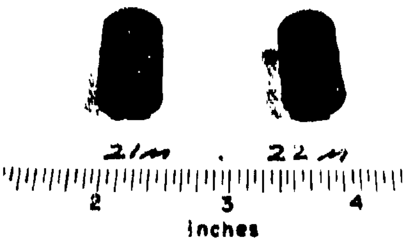

Plate No. 2-0639

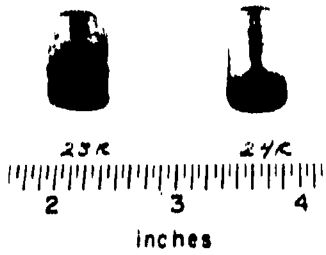

Figure 233. Post Exposure Photographs of 5 Mil WSi_2 Coated W WSi_2/W(G-18)-17M, 18M, 19M, 20M, 21M, 22M, 23R and 24R.

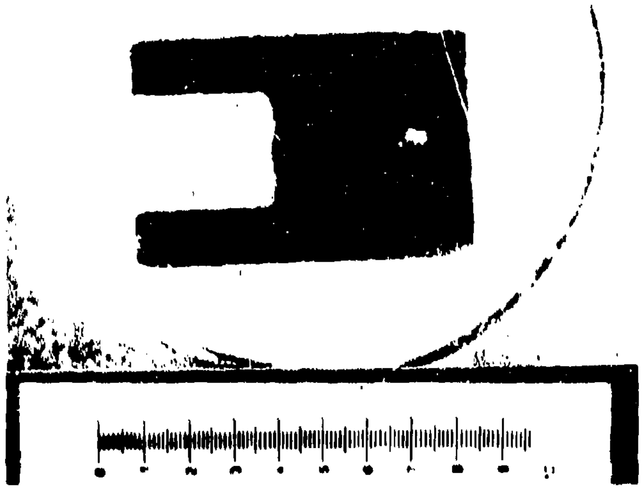

Plate No. 1-5363

X2.81

Figure 234. Arc Plasma Test WSi_2/W(G-18)-4M, Surface Temperature 3210°F, Exposure Time 1830 Seconds, Stagnation Pressure 1.05 Atm, Stagnation Enthalpy 2785 BTU/lb, Cold Wall Heat Flux 460 BTU/ft^{2}sec, Initial Length 449 Mil, Final Length 442 Mil. Hot Face at Right. One Inch Scale. No Coating Failure.

Plate No. 1-5364

Etched with Murakami's Reagent 0.394 Mils per Small Division (X200)

Figure 235. Arc Plasma Test WSi_2/W(G-18)-4M. Interface Showing W_5Si_3 Zone.

Plate No. 1-5411

Figure 236a. Arc Plasma Test WSi_2/W(G-18)-6R, Surface Temperature 2830°F, Exposure Time 1800 Seconds, Stagnation Pressure 0.082 Atm, Stagnation Enthalpy 8310 BTU/lb, Cold Wall Heat Flux 554 BTU/ft²sec, Initial Length 455 Mils, Final Length 434 Mils. Hot Face at Right. One Inch Scale Arc Conditions are for Most of Test (See Table 39). Coating Intact.

Plate No. 1-5412

Etched with Murakami's Reagent,0.394 Mils per Small Division (X200)

Figure 236b. Arc Plasma Test WSi_2/W(G-18)-6R. Interface Showing W_5Si_3 Zone.

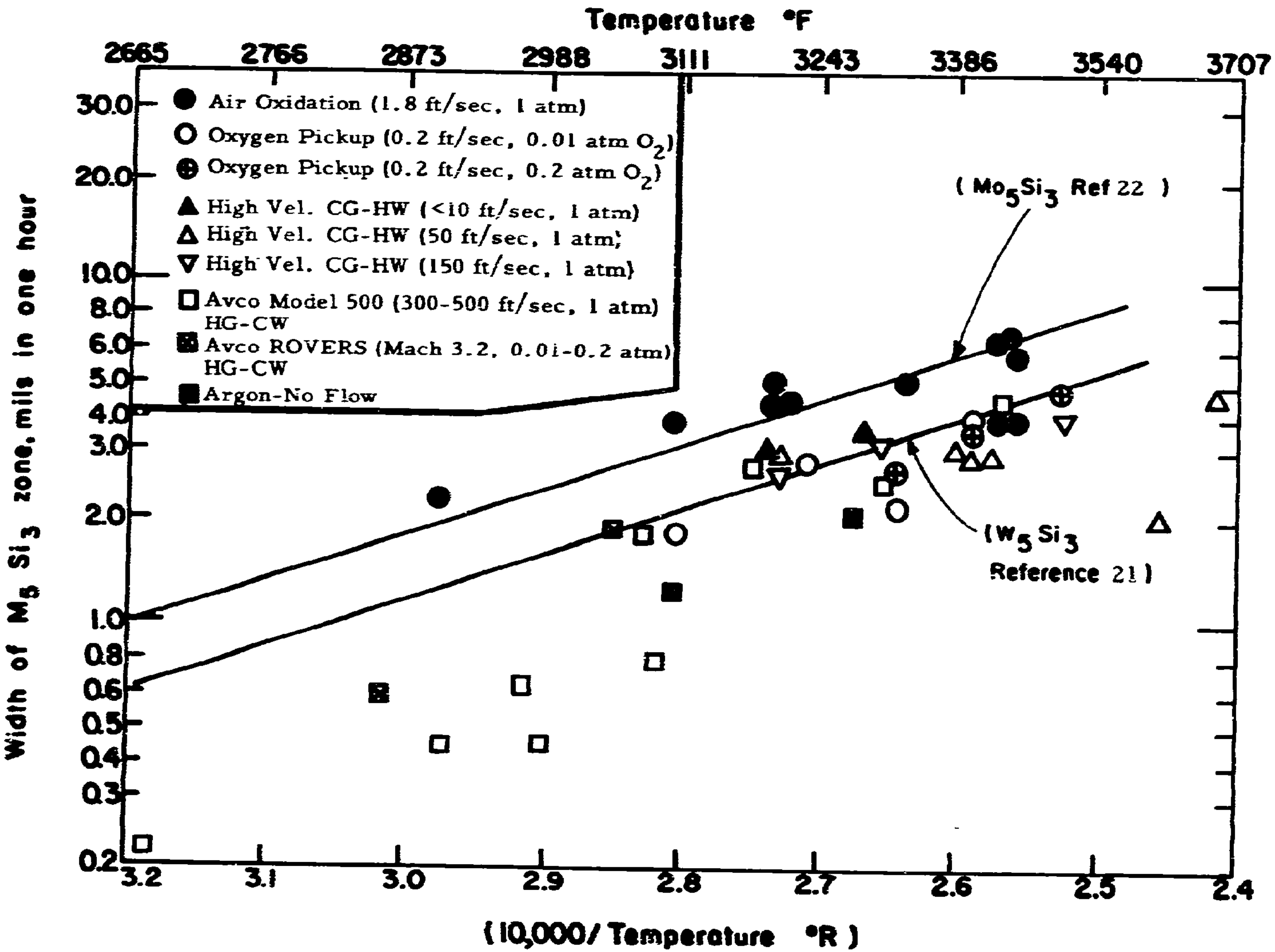

Figure 237. Growth of W_5Si_3 Zone on WSi_2/W(G-18) as a function of Flow Rate and Pressure Compared with the results of Bartlett and Gage (21) for W_5Si_3 and Perkins and Packer for Mo_5Si_3 (22).

Plate No. 1-5105

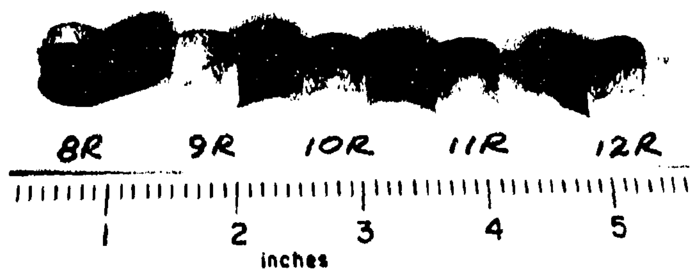

Plate No. 1-4286

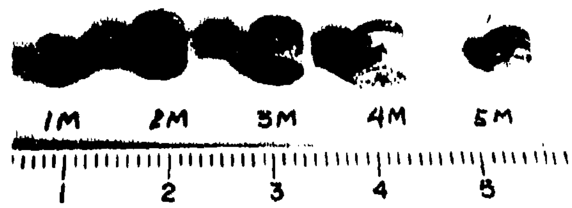

Plate No. 1-4287

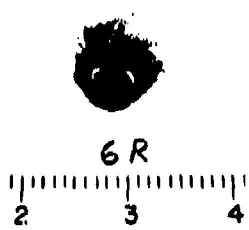

Plate No. 1-4288

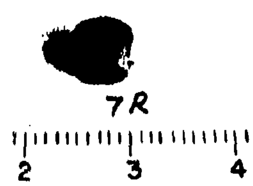

Figure 238. Post Exposure Photographs of 8 Mil Sn-*Al*-Mo Coated Ta-10W; Sn-*Al*/Ta-10W(G-19)-1M, 2M, 3M, 4M, 5M, 6R, 7R, 8R, 9R, 10R, 11R and 12R Arc Plasma Test Samples. Hot Face Pointing Down. Samples 1M and 5M Illustrate Coating Failure and Melting of Ta_2O_5. Samples 6R and 8R Illustrate Coating Failures and Melting of Tantalum. One Inch Scale.

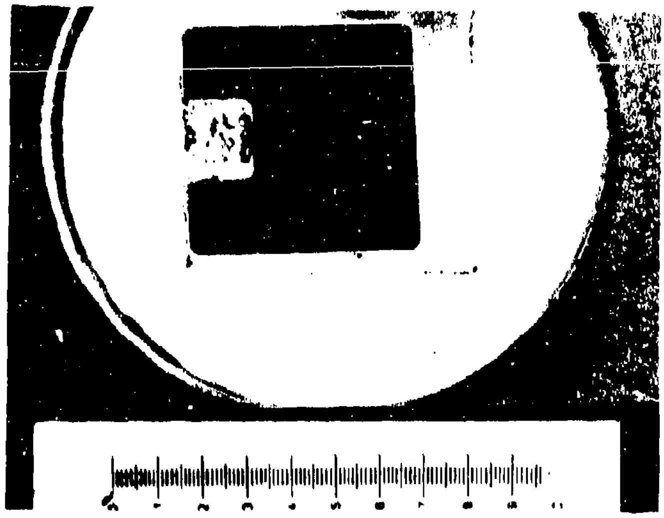

Plate No. 1-5040

X2.69

Figure 239. Arc Plasma Test Sn-Al/Ta-W(G-19)-4M, Surface Temperature 3000°F, Exposure Time 1830 Seconds, Stagnation Pressure 1.05 Atm, Stagnation Enthalpy 2980 BTU/lb, Cold Wall Heat Flux 350 BTU/ft^{2}sec, Initial Length 378 Mil, Final Length 367 Mil. Hot Face at Right. One Inch Scale. Coating Did not Fail.

Plate No. 1-5041

Unetched X250

Figure 240. Sn-Al/Ta-W(G-19)-4M. Interface of Sn-Al Coating (Top) and Ta-W Matrix.

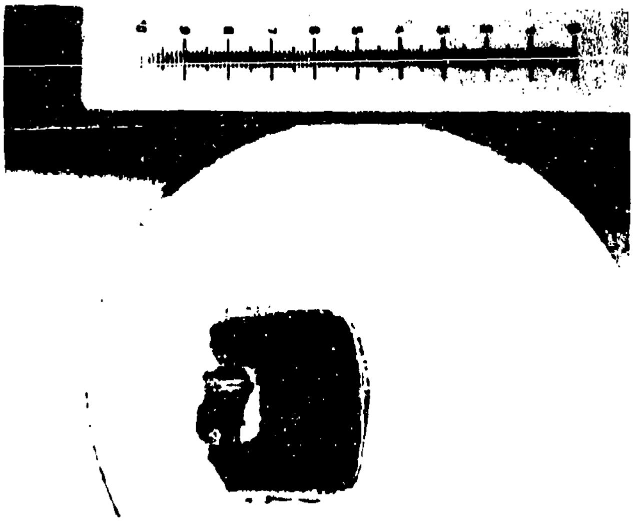

Plate No. 1-5031

X2.75

Figure 241. Arc Plasma Test Sn-Al/Ta-W(G-19)-1M, Surface Temperature 5090°F, Exposure Time 140 Seconds, Stagnation Pressure 1.06 Atm, Stagnation Enthalpy 2880 BTU/lb, Cold Wall Heat Flux 390 BTU/ft^{2}sec, Initial Length 368 Mil, Final Length 244 Mil. Hot Face at Right. One Inch Scale. Coating Failed.

Plate No. 1-5032

Unetched X250

Figure 242. Arc Plasma Test Sn-Al/Ta-W(G-19)-1M. Interface of Melted Region and Matrix.

Plate No. 1-5019

X3.18

Figure 243. Arc Plasma Test Sn-Al/Ta-W(G-19)-9R, Surface Temperature 2950°F, Exposure Time 1800 Seconds, Stagnation Pressure 0.010 Atm, Stagnation Enthalpy 10520 BTU/lb, Cold Wall Heat Flux 158 BTU/ft^{2}sec, Initial Length 362 Mil, Final Length 342 Mil. Hot Face at Top. One Inch Scale. Coating Did Not Fail.

Plate No. 1-5020

Unetched X250

Figure 244. Arc Plasma Test Sn-Al/Ta-W(G-19)-9R. Interface of Coating (Right) and Matrix.

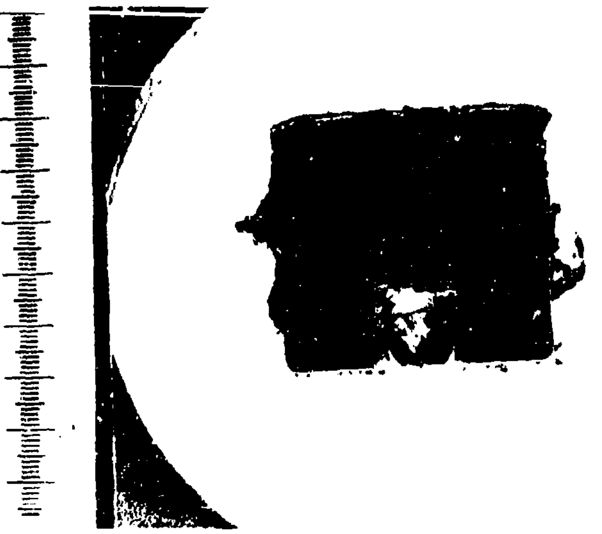

Plate No. 1-5016

X3.18

Figure 245. Sn-Al/Ta-W(G-19)-8R, Surface Temperature 3670°F, Exposure Time 400 Seconds, Stagnation Pressure 0.011 Atm, Stagnation Enthalpy 11440 BTU/lb, Cold Wall Heat Flux 200 BTU/ft^{2}sec, Initial Length 361 Mil, Final Length 322 Mil. Hot Face at Top. One Inch Scale. Coating Failed.

Plate No. 1-5018

Unetched X250

Figure 246. Arc Plasma Test Sn-Al/Ta-W(G-19)-8R. Interface of Melted Ta-W (Right) and Matrix.

Plate No. 1-9531

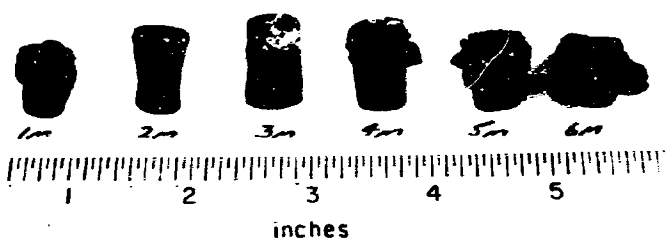

Plate No. 1-9518

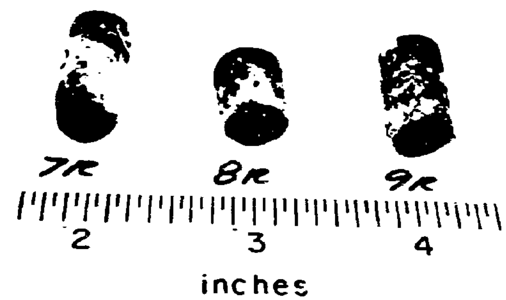

W+Zr+Cu (G-20)

Figure 247. Post Exposure Photographs of Arc Plasma Tests W+Zr+Cu(G-20)-1M, 2M, 3M, 4M, 5M, 6M, 7R, 8R and 9R.

X2.87

Plate No. 1-9729

Figure 248. Arc Plasma Test W+Zr+Cu(G-20)-6M, Surface Temperature 2420°F, Exposure Time 1800 Seconds, Stagnation Pressure 1.01 Atm., Stagnation Enthalpy 1830 BTU/lb, Cold Wall Heat Flux 155 BTU/ft^2sec, Initial Length 427 Mils, Final Length 262 Mils. Hot Face Up. One Inch Scale.

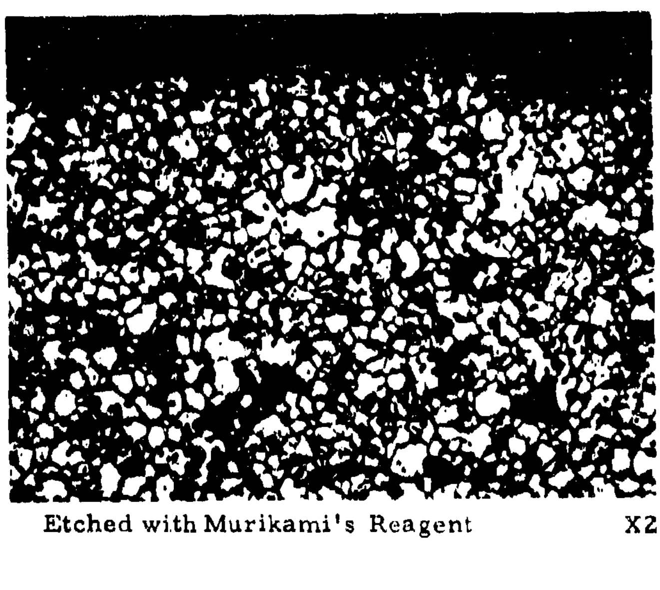

Plate No. 1-9731

Etched with Murikami's Reagent X250

Figure 249. Arc Plasma Test W+Zr+Cu(G-20)-6M, Hot Interface at Top.

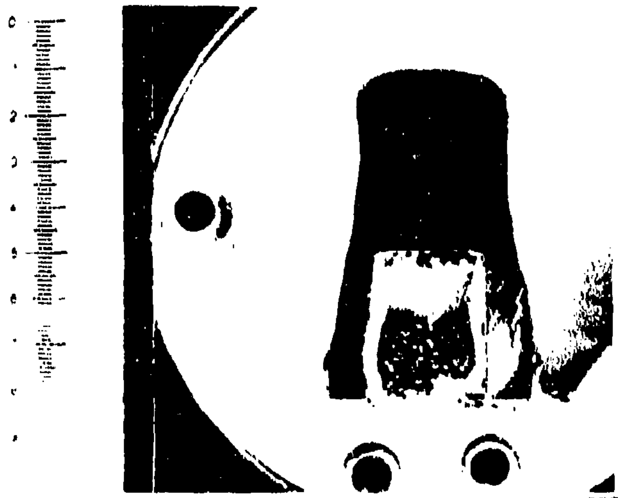

Plate No.
1-9712

X2.87

Figure 250. Arc Plasma Test W+Zr+Cu(G-20)-2M, Surface Temperature 3345°F, Exposure Time 324 Seconds, Stagnation Pressure 1.01 Atm., Stagnation Enthalpy 3030 BTU/lb, Cold Wall Heat Flux 170 BTU/ft^{2}sec, Initial Length 500 Mils, Final Length 388 Mils. Hot Face Up. One Inch Scale.

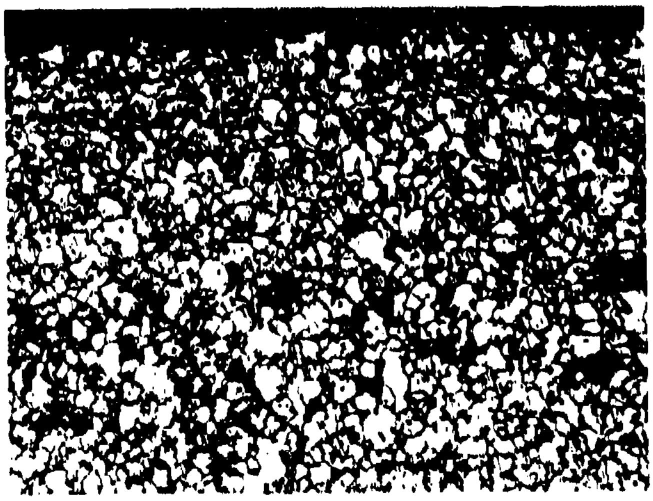

Plate No.
1-9713

Etched with Murikami's Reagent X250

Figure 251. Arc Plasma Test W+Zr+Cu(G-20)-2M, Hot Interface at Top.

Plate No.
1-9748

X2.80

Figure 252. Arc Plasma Test W+Zr+Cu(G-20)-9R, Surface Temperature 5300°F, Exposure Time 775 Seconds, Stagnation Pressure 0.100 Atm., Stagnation Enthalpy 10680 BTU/lb, Cold Wall Heat Flux 584 BTU/ft^{2}sec, Initial Length 433 Mils, Final Length 411 Mils. Hot Face Up. One Inch Scale.

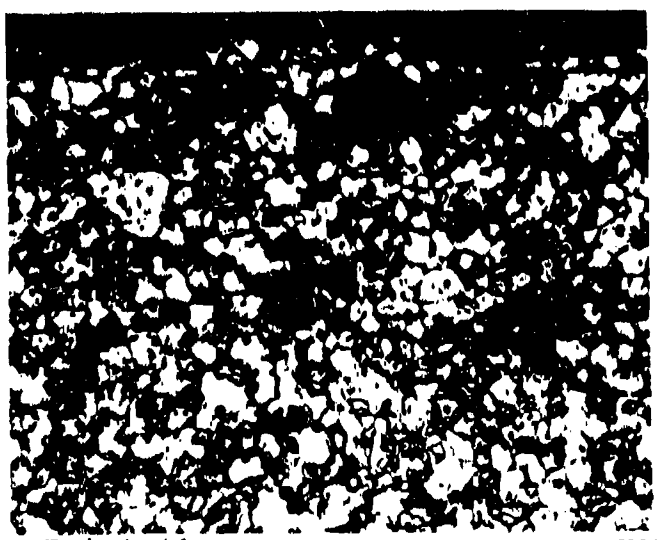

Plate No.
1-9749

Etched with Murikami's Reagent X250

Figure 253. Arc Plasma Test W+Zr+Cu(G-20)-9R. Hot Interface at Top.

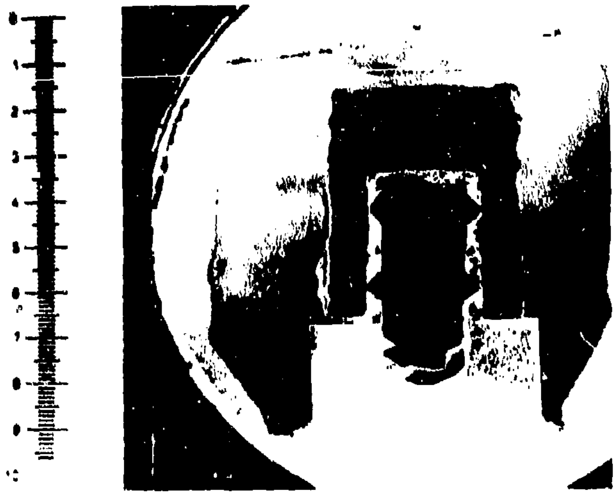

Plate No.
1-9742

X2.80

Figure 254. Arc Plasma Test W+Zr+Cu(G-20)-8R, Surface Temperature 5205°F, Exposure Time 500 Seconds, Stagnation Pressure 0.135 Atm., Stagnation Enthalpy 11980 BTU/lb, ColdWall Heat Flux 662 BTU/ft²sec. Initial Length 438 Mils, Final Length 181 Mils. Hot Face Up. One Inch Scale. Sting Shown in Place.

Plate No.
1-9743

Etched with Murikami's Reagent X250

Figure 255. Arc Plasma Test W+Zr+Cu(G-20)-8R Hot Interface at Top.

Plate No. 1-9532

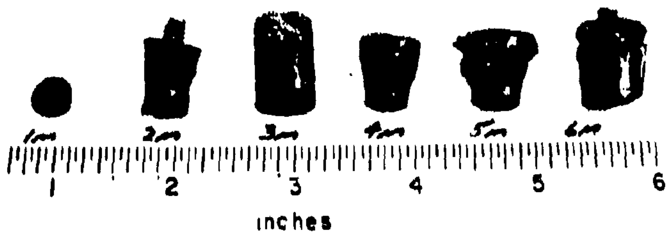

Figure 256. Post Exposure Photographs of Arc Plasma Tests W + Ag(G-21)-1M, 2M, 3M, 4M, 5M and 6M.

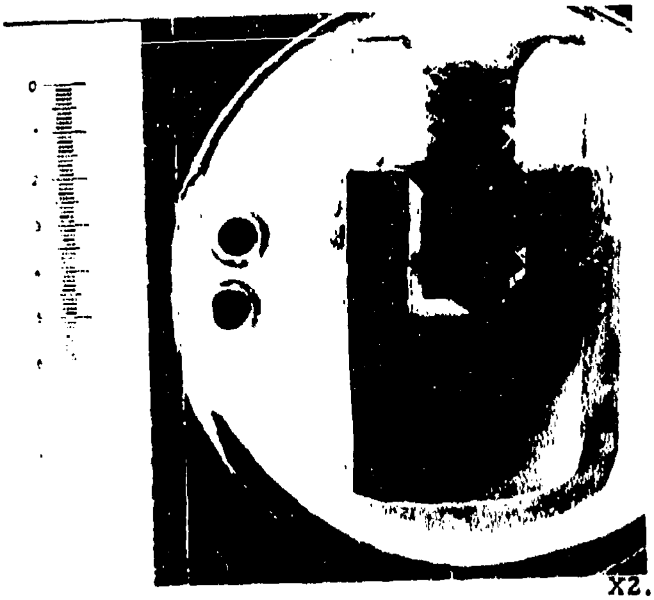

Plate No. 1-9773

X2.80

Figure 257. Arc Plasma Test W+Ag(G-21)-6M, Surface Temperature 2545°F, Exposure Time 1800 Seconds, Stagnation Pressure 1.01 Atm., Stagnation Enthalpy 2000 BTU/lb, Cold Wall Heat Flux 160 BTU/ft^{2}sec, Initial Length 445 Mils, Final Length 387 Mils. Hot Face Down. One Inch Scale

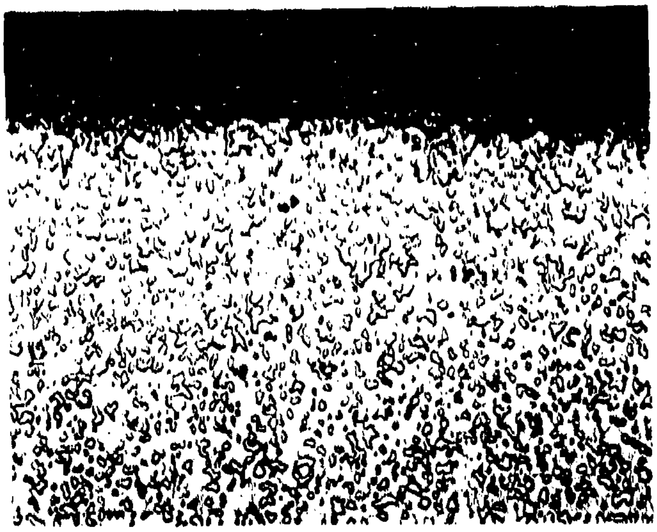

Plate No. 2-0693

Etched with Murikami's Reagent X250

Figure 258. Arc Plasma Test W+Ag(G-21)-6M. Hot Interface at Top.

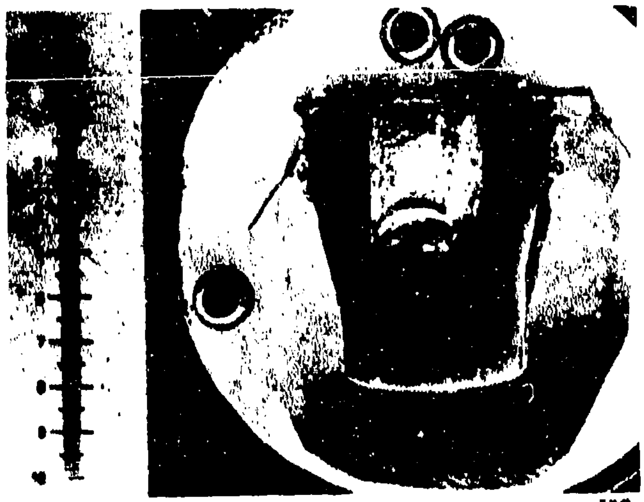

Plate No.
1-9768

X2.80

Figure 259. Arc Plasma Test W+Ag(G-21)-5M, Surface Temperature $3050^{\circ}F$, Exposure Time 460 Seconds, Stagnation Pressure 1.01, Stagnation Enthalpy 2760 BTU/lb, Cold Wall Heat Flux 210 BTU/ft^2sec., Initial Length 439 Mils, Final Length 301 Mils. Hot Face Down. One Inch Scale.

Plate No.
1-9769

Etched with Murikami's Reagent X250

Figure 260. Arc Plasma Test W+Ag(G-21)-5M. Hot Interface at Top.

Plate No. 1-7743

Plate No. 1-7691

Plate No. 1-7827

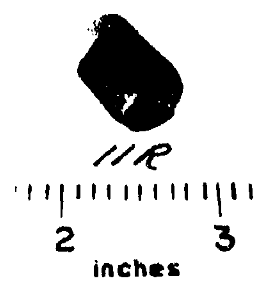

Figure 261. Post Exposure Photographs of Arc Plasma Tests SiO_2+ 68.5w/o(H-22)-1M, 2M, 3M, 4M, 5M, 6M, 7R, 8R, 9R, 10R and 11R.

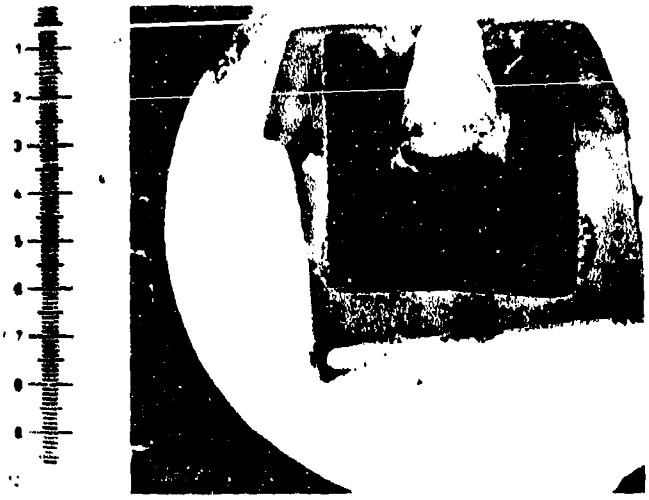

Plate No. 1-7753

X3.00

Figure 262. Arc Plasma Test SiO_2 + 68.5 w/o W(H-22)-4M, Surface Temperature 5205°F, Exposure Time 1800 Seconds, Stagnation Pressure 1.08 Atm. Stagnation Enthalpy 5500 BTU/lb Cold Wall Heat Flux 780 BTU/ft^2 sec, 428 Mil Recession, Hot Face Down. One Inch Scale.

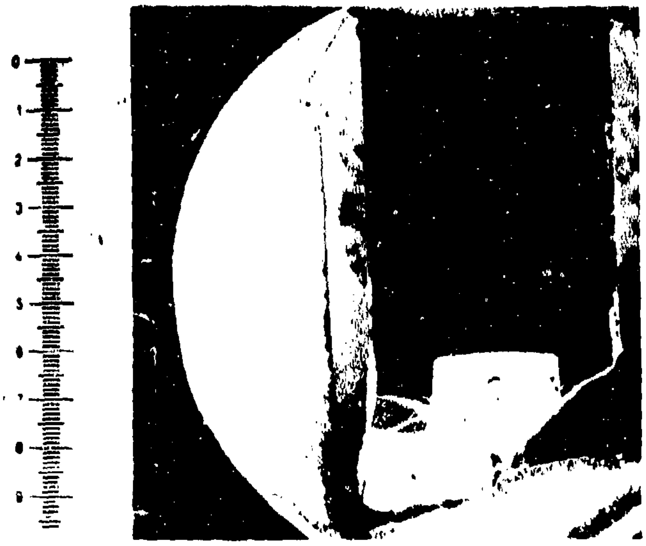

Plate No. 1-7747

X3.00

Figure 263. Arc Plasma Test SiO_2 + 68.5 w/o W(H-22)-2M, Surface Temperature 4505°F, Exposure Time 1557 Seconds, Stagnation Pressure 1.07 Atm, Stagnation Enthalpy 4110 BTU/lb, Cold Wall Heat Flux 580 BTU/ft^2 sec, 19 Mil Recession, Hot Face Up, One Inch Scale.

Plate No. 1-7701

X3.00

Figure 264. Arc Plasma Test SiO_2 + 68.5 w/o W(H-22)-10R, Surface Temperature 3750°F, Exposure Time 600 Seconds, Stagnation Pressure 0.009 Atm. Stagnation Enthalpy 13,100 BTU/lb, Cold Wall Heat Flux 230 BTU/ft^2 sec, 331 Mils Recession, Hot Face Up. One Inch Scale.

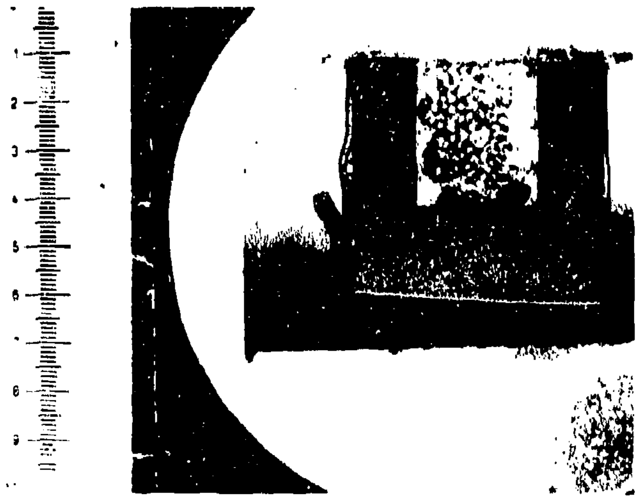

Plate No. 1-7692

X3.00

Figure 265. Arc Plasma Test SiO_2 + 68.5 w/o W(H-22)-7R, Surface Temperature 4175°F, Exposure Time 230 Seconds, Stagnation Enthalpy 10,580 BTU/lb, Cold Wall Heat Flux 526 BTU/ft^2 sec, 507 Mil Recession, Hot Face Down, One Inch Scale.

Plate No. 1-6602

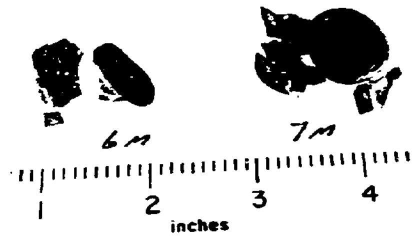

Plate No. 1-4756

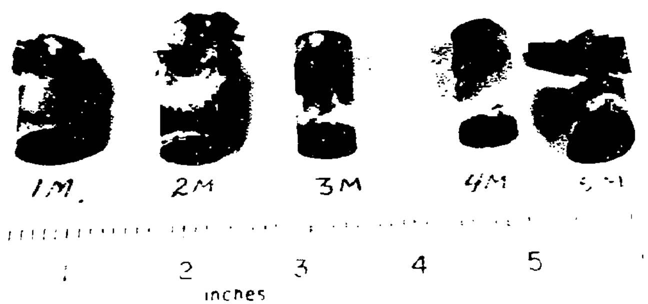

Plate No. 1-5317

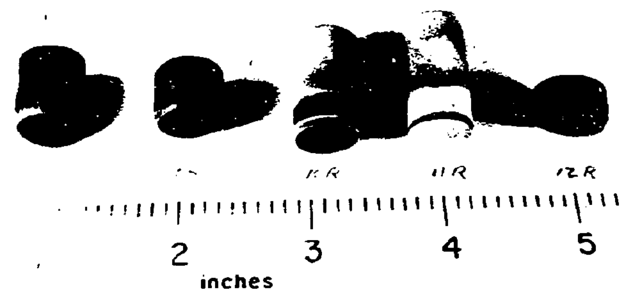

Plate No. 1-6531

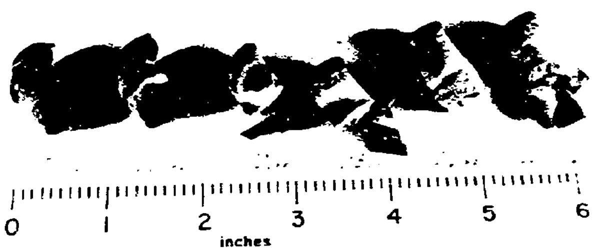

Plate No. 1-9503

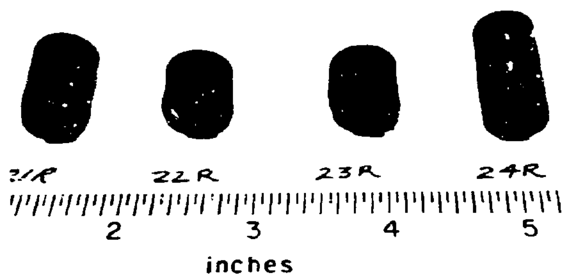

Figure 266. Post Exposure Photographs of Arc Plasma Tests SiO_2+60w/oW(H-23)-1M, 2M, 3M, 4M, 5M, 6M, 7M, 8R, 9R, 10R, 11R, 12R, 15M, 16M, 17M, 18M, 19M, 20M, 21R, 22R, 23R and 24R.

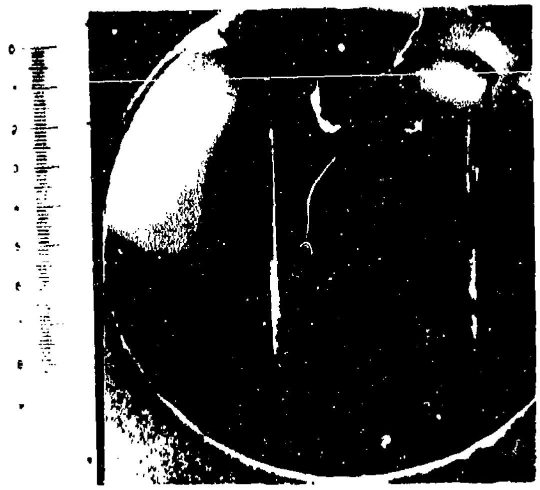

Plate No. 1-4760

X2.5

Figure 267. Arc Plasma Test SiO_2 + 60w/oW(H-23)-2M, Surface Temperature 3675°F, Exposure Time 1830 Seconds, Stagnation Pressure 1.06 Atm, Stagnation Enthalpy 3380 BTU/lb, Cold Wall Heat Flux 405 BTU/ft^{2}sec, Initial Length 700 Mil, Final Length 683 Mil. Hot Face at Bottom. One Inch Scale. Rear Broke on Removal after Test.

Plate No. 1-4762

Unetched

X125

Figure 268. Arc Plasma Test SiO_2+60w/oW(H-23)-2M. Hot Interface.

Figure 269. Arc Plasma Test SiO_2+60w/oW(H-23)-15M, Surface Temperature 4210°F, Exposure Time 1286 Seconds, Stagnation Pressure 1.08 Atm, Stagnation Enthalpy 5440 BTU/lb. Cold Wall Heat Flux 855 BTU/ft^{2}sec, Initial Length 686 Mil, Final Length 318 Mils. Hot Face at Right. One Inch Scale. Specimen Broke on Removal after Test. Viscous Flow Observed.

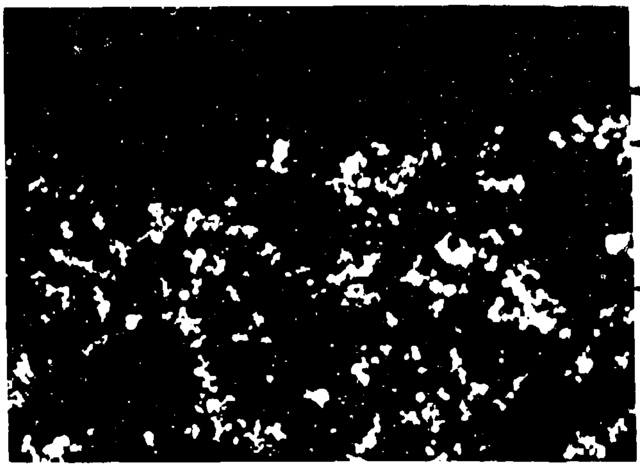

Figure 270. Arc Plasma Test SiO_2 + 60w/oW(H-23)-15M. Top Surface After Viscous Flow.

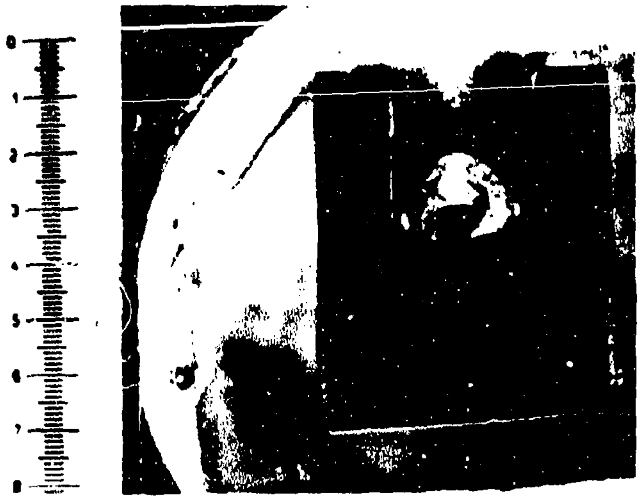

Plate No. 1-5318

X3.38

Figure 271. Arc Plasma Test SiO_2+60w/oW(H-23)-8R, Surface Temperature 3870°F, Exposure Time 325 Seconds, Stagnation Pressure 0.023 Atm, Stagnation Enthalpy 10860 BTU/lb, Cold Wall Heat Flux 475 BTU/ft^2sec, Initial Length 699 Mil, Final Length 320 Mil. Hot Face at Bottom. One Inch Scale.

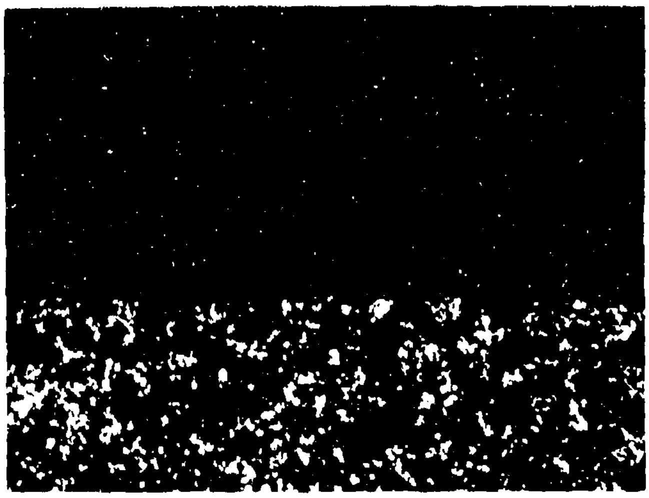

Plate No. 1-5319

Unetched X125

Figure 272. Arc Plasma Test SiO_2 + 60w/oW(H-23)-8R. Hot Interface Showing Some SiO_2 Reaction.

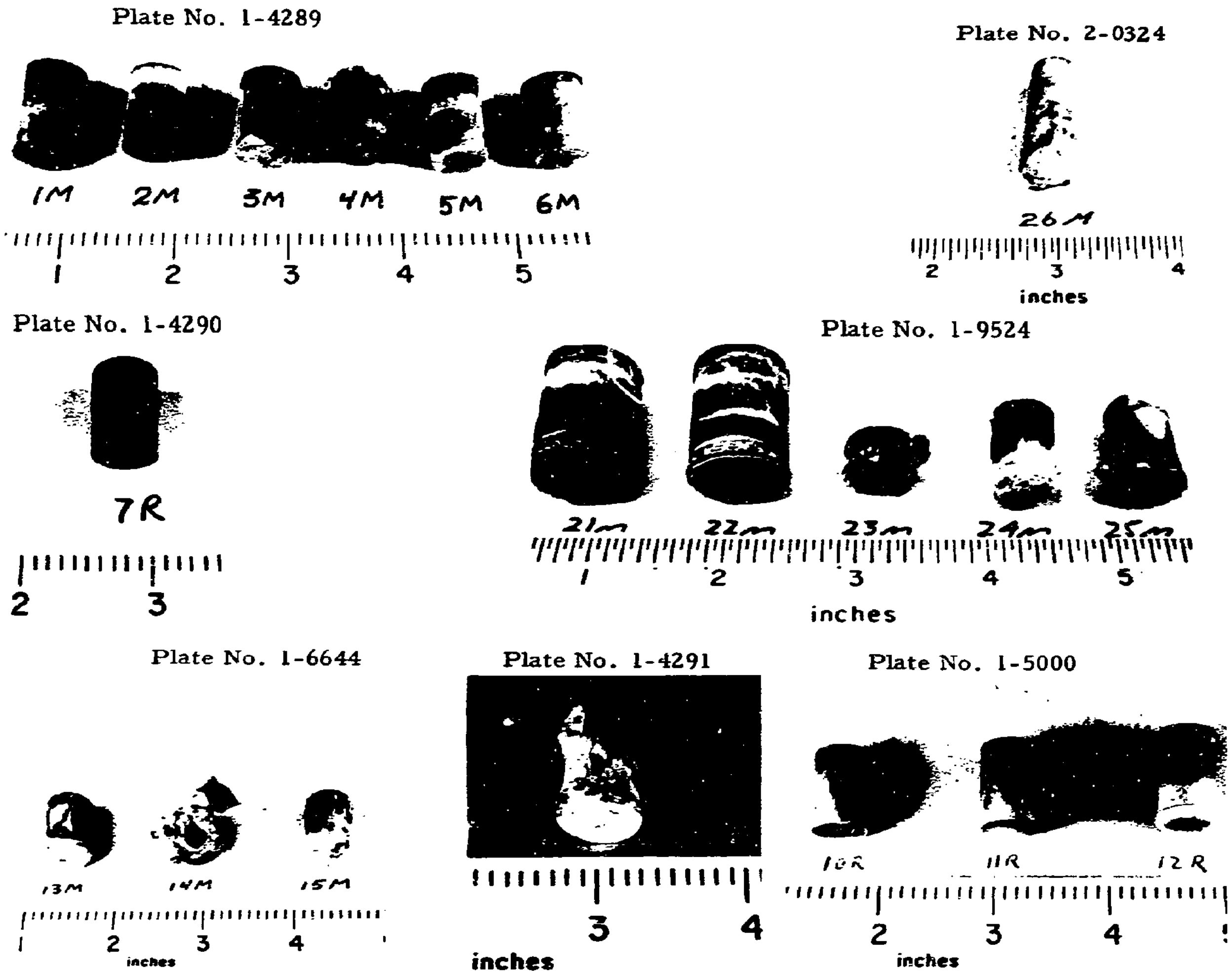

Figure 273. Post Exposure Photographs of Arc Plasma Tests Hf-Ta-Mo(I-23)-1M, 2M, 3M, 4M, 5M, 6M, 26M, 7R, 21M, 22M, 23M, 24M, 25M, 13M, 14M, 15M, 9R, 10R, 11R, 12R (8R Melted completely).

Plate No. 2-0706

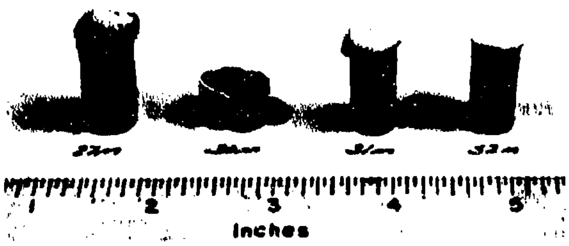

Plate No. 2-0674

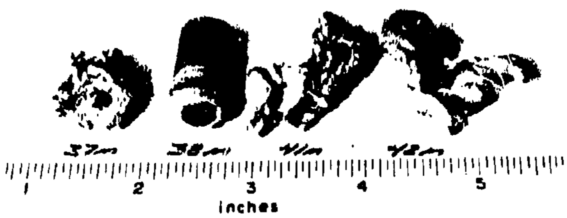

Plate No. 2-0707

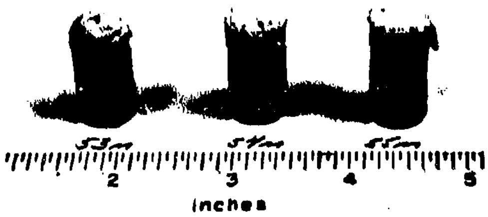

Plate No. 2-0708

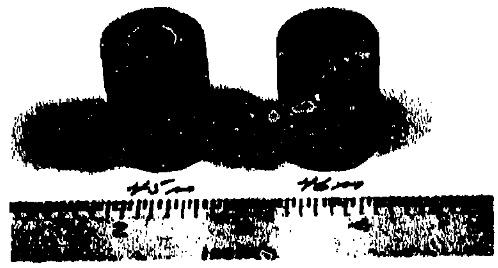

Figure 274. Post Exposure Photographs of Arc Plasma Tests Hf-Ta-Mo (I-23)-27M, 30M, 31M, 32M, 37M, 38M, 41M, 42M, 53M, 54M, 55M, 45M, 46M.

Plate No. 2-0649

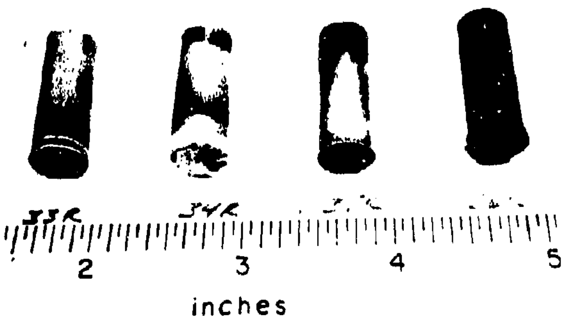

Plate No. 2-0673

Plate No. 2-0709

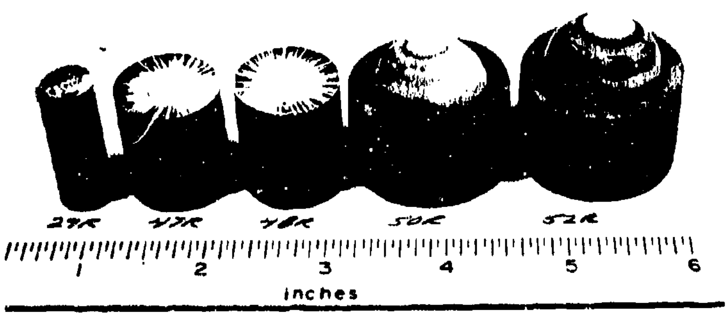

Figure 275. Post Exposure Photographs of Arc Plasma Tests Hf-Ta-Mo(I-23)-33R, 34R, 35R, 36R, 28R, 39R, 40R, 43R, 44R, 49R, 51R, 29R, 47R, 48R, 50R and 52R.

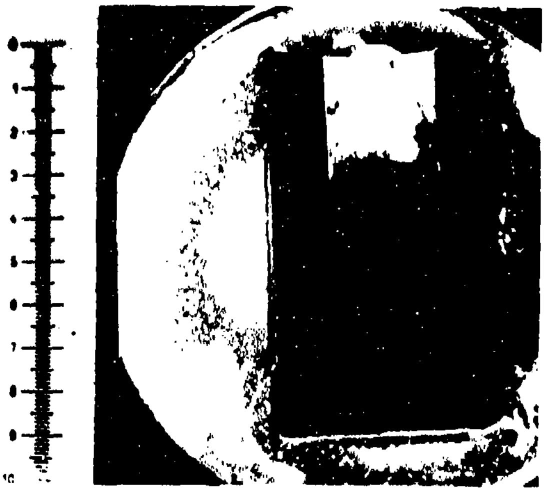

Plate No. 1-4785

X2.7

Figure 276. Arc Plasma Test Hf-Ta-Mo(I-23)-1M, Surface Temperature 4030°F, Exposure Time 1830 Seconds, Stagnation Pressure 1.08 Atm, Stagnation Enthalpy 3295 BTU/lb, Cold Wall Heat Flux 530 BTU/ft^{2}sec, Initial Length 578 Mil, Final Length 553 Mil. Hot Face at Bottom. One Inch Scale.

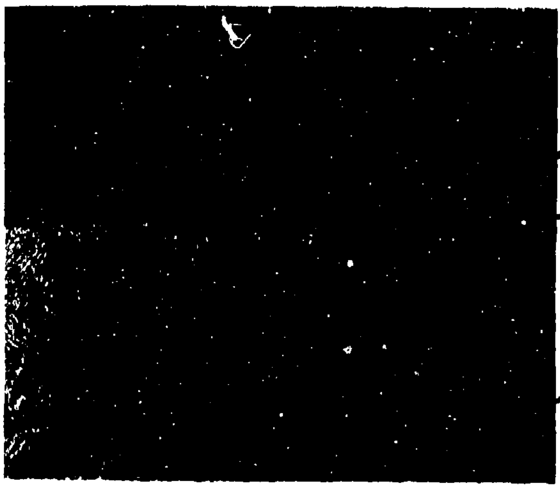

Oxide

Subscale

Plate No. 1-4786A

Matrix

Etched with 15 Glycerine 5 HNO_3 5HCl 3HF X75

Figure 277. Arc Plasma Test Hf-Ta-Mo(I-23)-1M. Interface Showing Oxide, Subscale and Matrix.

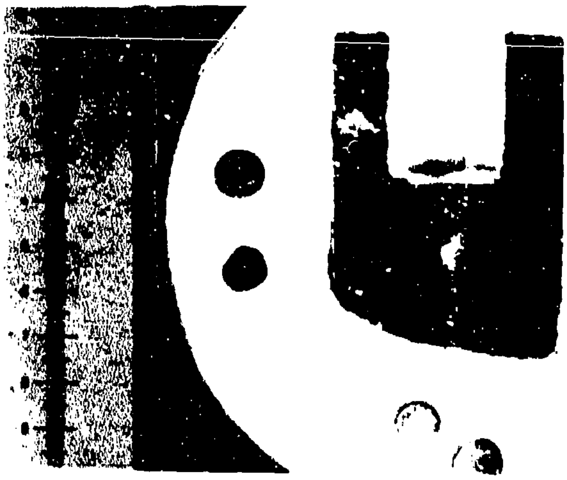

Plate No. 1-6652

X2.87

Figure 278. Arc Plasma Test Hf-Ta-Mo(I-23)-15M, Surface Temperature 4645°F, Exposure Time 1830 Seconds, Stagnation Pressure 1.06 Atm, Stagnation Enthalpy 3735 BTU/lb, Cold Wall Heat Flux 515 BTU/ft^{2}sec, Initial Length 421 Mil, Final Length 353 Mil. Hot Face at Bottom. One Inch Scale.

Plate No. 1-6653A

Etched with 15 Glycerine 5$HNO_3$5HCl 3HF X75

Figure 279. Arc Plasma Test Hf-Ta-Mo(I-23)-15M. Interface Showing Oxide, Subscale, Matrix. Some Melting of Oxide Has Occurred.

Plate No. 1-5007

X2.81

Figure 280. Arc Plasma Test Hf-Ta-Mo(I-23)-12R, Surface Temperature 3755°F, Exposure Time 1800 Seconds, Stagnation Pressure 0.018 Atm, Stagnation Enthalpy 12710 BTU/lb, Cold Wall Heat Flux 378 BTU/ft^{2}sec, Initial Length 560 Mil, Final Length 534 Mil. Hot Face at Bottom. One Inch Scale. Oxide and Subscale Clearly Visible at Hot Face.

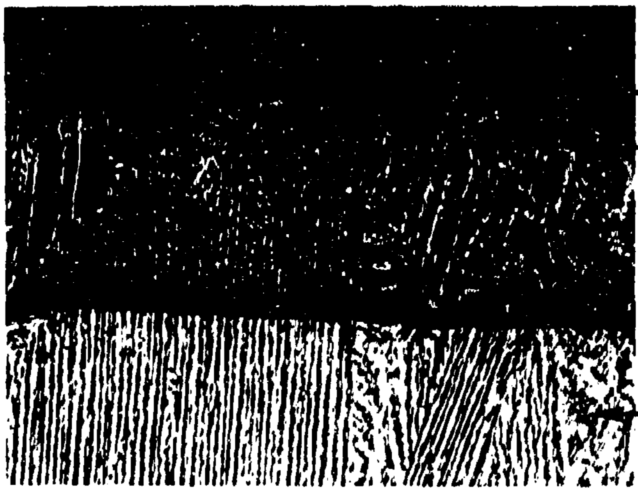

Plate No. 1-5008A

Etched with 15 Glycerine $5HNO_3HCl$ 3HF X75

Figure 281. Arc Plasma Test Hf-Ta-Mo(I-23)-12R, Interface Showing Oxide, Subscale and Matrix.

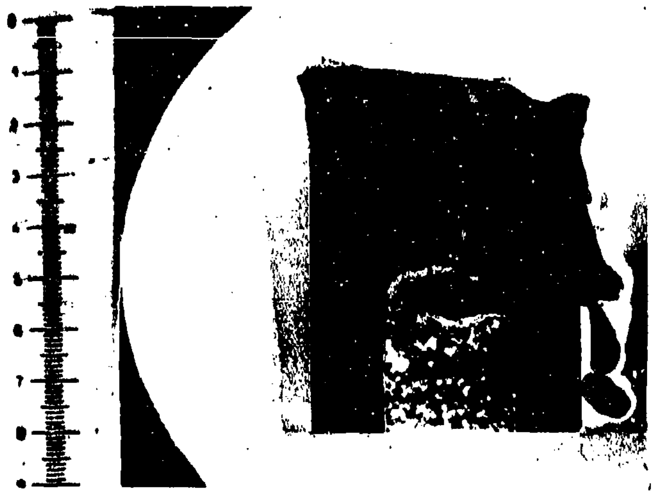

Plate No. 1-4807

X3.18

Figure 282. Arc Plasma Test Hf-Ta-Mo(I-23)-9R, Surface Temperature 4220°F, Exposure Time 1800 Seconds, Stagnation Pressure 0.022 Atm, Stagnation Enthalpy 11250 BTU/lb, Cold Wall Heat Flux 337 BTU/ft2sec, Initial Length 432 Mil, Final Length 326 Mil. Hot Face at Top. One Inch Scale. Oxide and Subscale Clearly Visible at Hot Face. Some Melting has Occurred.

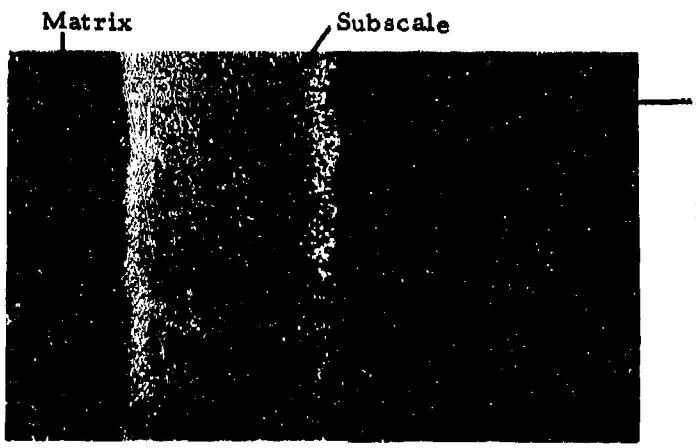

Plate No. 1-4808

Etched with 15 Glycerine $5HNO_3$ 5HCl 3HF X50

Figure 283. Arc Plasma Test Hf-Ta-Mo(I-23)-9R. Interface Showing Oxide, Subscale and Matrix. Some Melting of Oxide has Occurred.

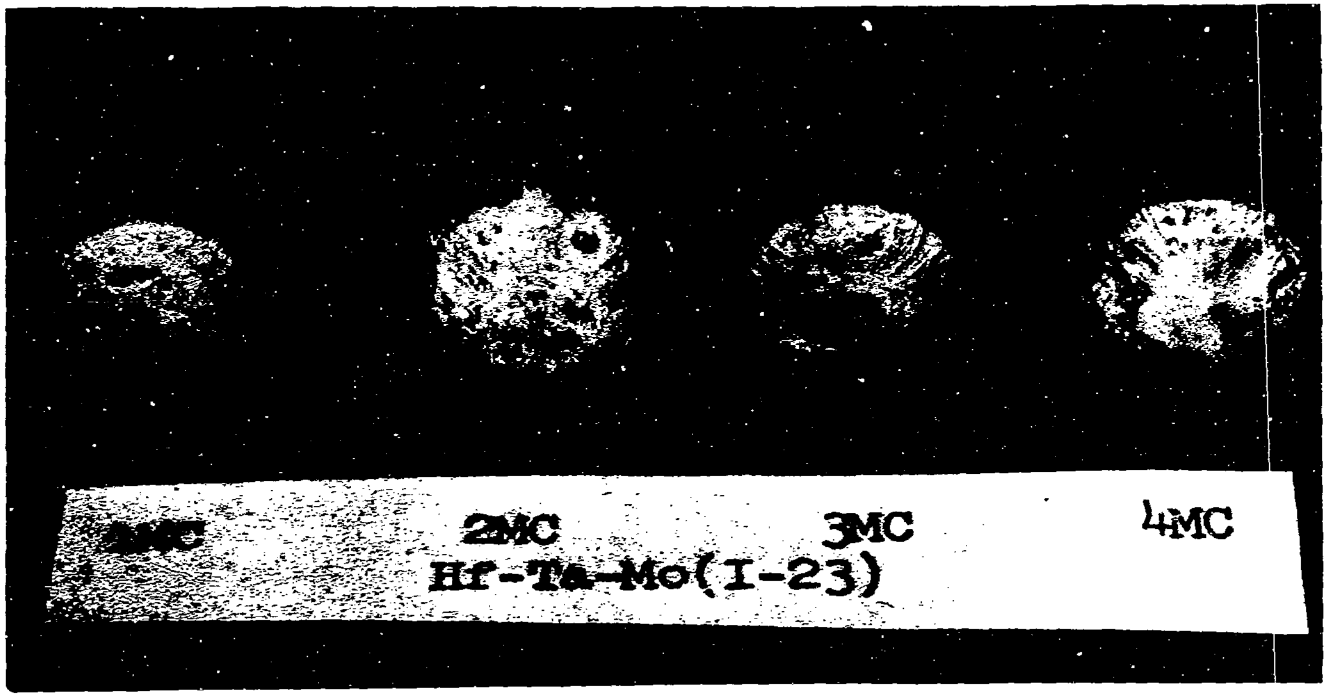

Figure 284. Post Exposure Photographs of Samples Hf-Ta-Mo(I-23) - 1MC, 2MC, 3MC and 4MC

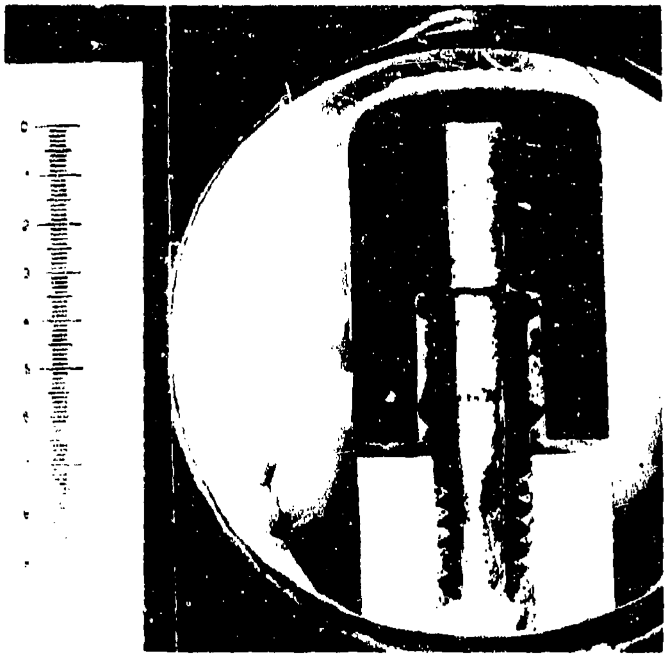

Plate No. 1-9224

X3.00

Figure 285. Arc Plasma Test Hf-20Ta-2Mo(I-23)-1MC, Surface Temperature 4760°F, Internal Temperature 3530°F, Exposure Time 1800 Seconds, Stagnation Pressure 1.05 Atm, Stagnation Enthalpy 3220 BTU/lb, Cold Wall Heat Flux 425 BTU/ft^2 sec, 46 Mil Recession, Hot Face Up. One Inch Scale.

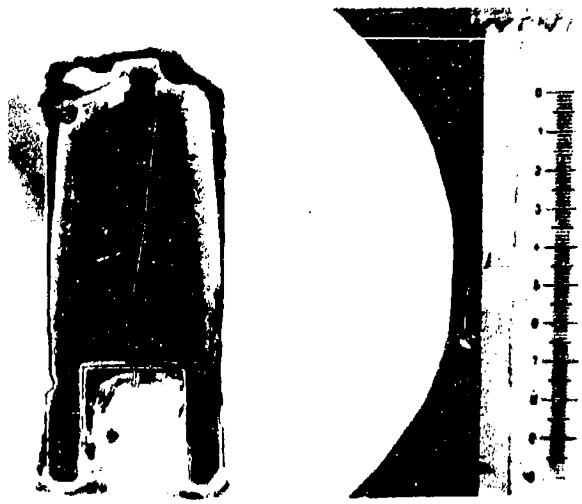

Plate No.
2-0694

X2.35

Figure 286. Arc Plasma Test Hf-Ta-Mo(I-23)-27M. Average Surface Temperature 4230°F, Exposure Time 11,600 Seconds (7 cyclic exposures each of approximately 1800 seconds), Stagnation Pressure 1.05 atm., Stagnation Enthalpy 3300 BTU/lb, Cold Wall Heat Flux 410 BTU/ft^{2}sec, 138 Mils Recession, Hot Face Up. One Inch Scale.

Plate No.
2-0695

Etched with 15 Glycerine 5$HNO_3$5HCl X250

Figure 287. Arc Plasma Test Hf-Ta-Mo(I-23)-27M, Hot Surface.

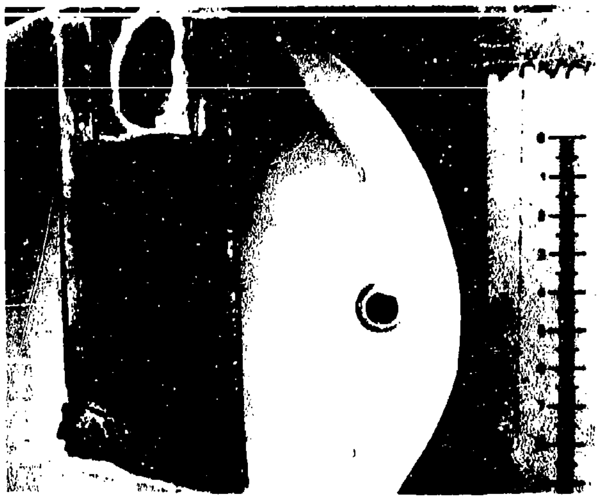

Plate No.
2-0696

X2.35

Figure 288. Arc Plasma Test Hf-Ta-Mo(I-23)-28R. Average Surface Temperature 4200°F, Exposure Time 7220 Seconds (4 cyclic exposures each of approximately 1800 seconds), Stagnation Pressure 0.132 Atm., Stagnation Enthalpy 7600 BTU/lb, Cold Wall Heat Flux 398 BTU/ft^{2}sec, 55 Mils Recession, Hot Face Down, One Inch Scale.

Plate No.
2-0697

Etched with 15 Glycerine
5HNO$_3$5HCl3HF

X250

Figure 289. Arc Plasma Test Hf-Ta-Mo(I-23)-28R, Hot Surface.

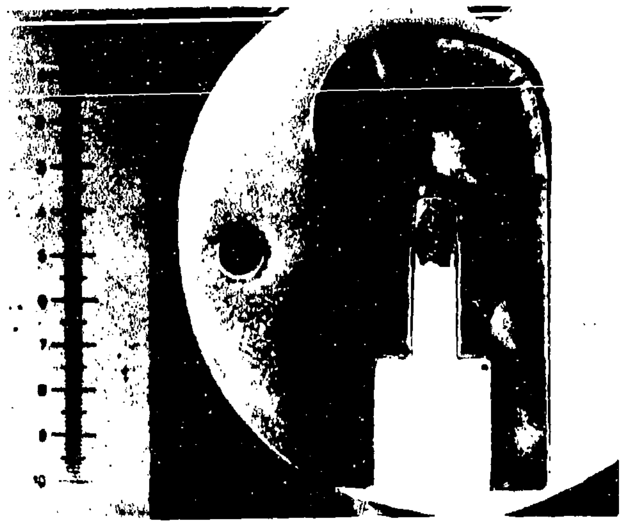

Plate No. 2-0699

X2.75

Figure 290. Arc Plasma Test Hf-Ta-Mo(I-23)-38MH Surface Temperature 4230°F, Exposure Time 1800 Seconds, Stagnation Pressure 1.02 Atm., Stagnation Enthalpy 3220 BTU/lb, Cold Wall Heat Flux 435 BTU/ft^{2}sec, 48 Mils Recession, Hot Face Up. One Inch Scale

Plate No. 2-0700

Etched with 10 Glycerine
$5HNO_3 5HCl 3HF$

X250

Figure 291. Arc Plasma Test Hf-Ta-Mo(I-23)-38MH, Hot Surface.

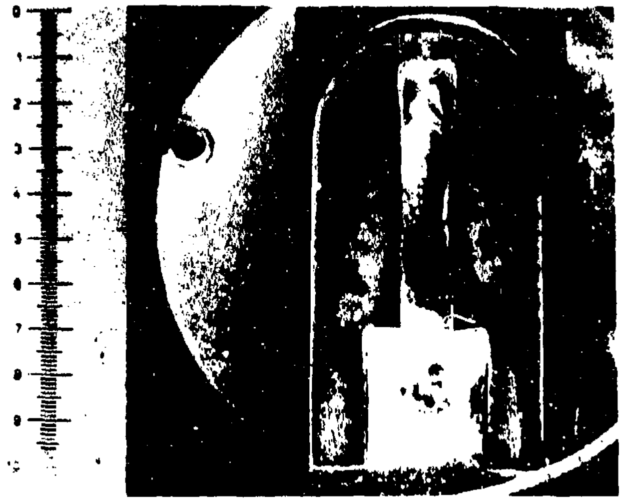

Plate No.
2-0701

X2.80

Figure 292. Arc Plasma Test Hf-Ta-Mo(I-23)-39RH. Surface Temperature 3620°F, Exposure Time 1800 Seconds, Stagnation Pressure 0.137 atm., Stagnation Enthalpy 6740 BTU/lb, Cold Wall Heat Flux 412 BTU/ft^{2}sec, 22 Mils Recession, Hot Face Up. One Inch Scale.

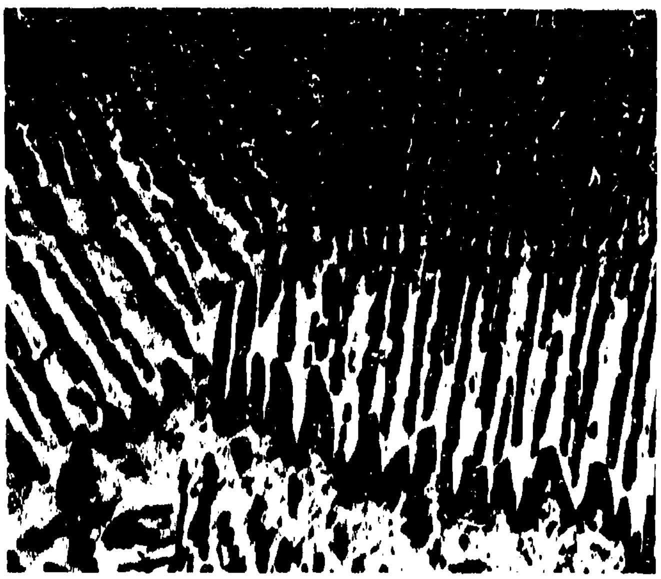

Plate No.
2-0702

Etched with 10 Glycerine
$5HNO_3 5HCl 3HF$

X250

Figure 293. Arc Plasma Test Hf-Ta-Mo(I-23)-39RH, Hot Surface.

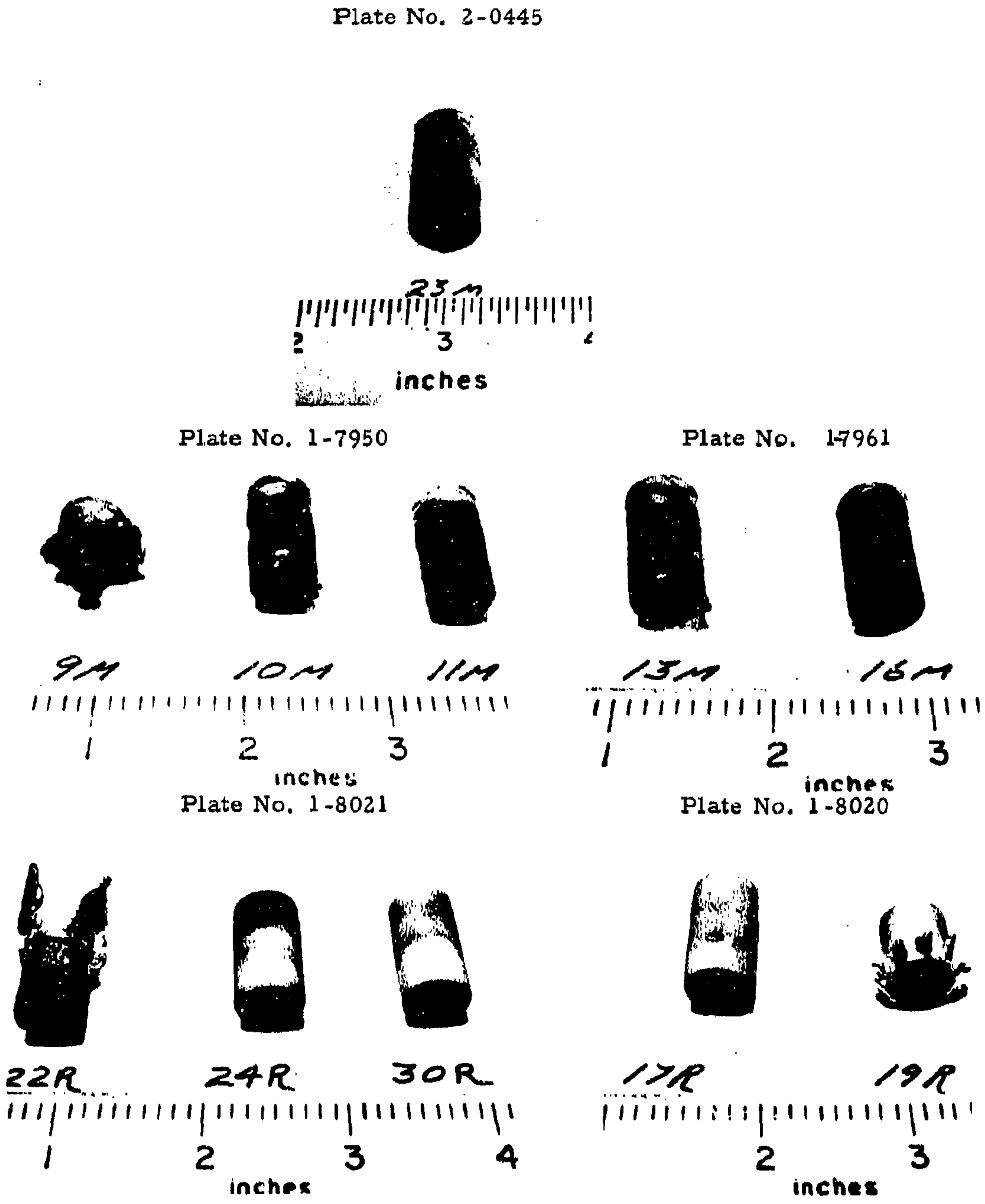

Figure 294. Post Exposure Photographs of Arc Plasma Tests IrC/C (I-24)-23M, 9M, 10M, 11M, 13M, 16M, 17R, 19R, 22R, 24R and 30R.

Plate No. 2-0710

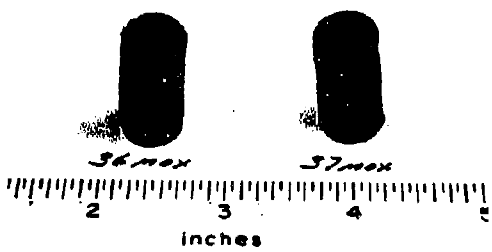

Plate No. 2-0711

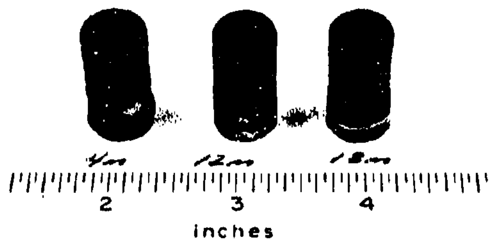

Plate No. 2-0712

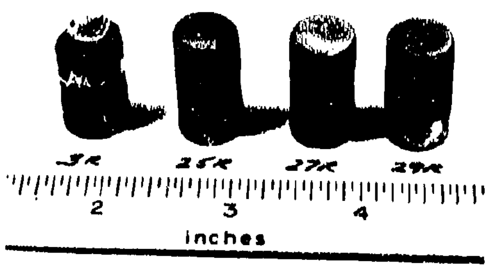

Figure 295. Post Exposure Photographs of Arc Plasma Tests Ir/C (I-24)-36MOX, 37MOX, 4M, 12M, 18M, 3R, 25R, 27R and 29R.

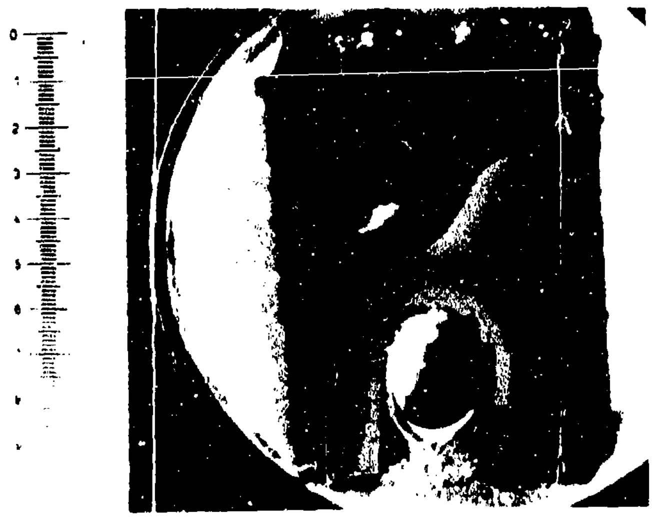

Plate No. 1-7962

X2.80

Figure 296. Arc Plasma Test Ir/C(I-24)-13M, Surface Temperature 4535°F, Exposure Time 1800 Seconds, Stagnation Pressure 1.02 Atm. Stagnation Enthalpy 3140 BTU/lb, Cold Wall Heat Flux 310 BTU/ft^2 sec, 16 Mil coating melted off. Hot Face Up. One inch Scale.

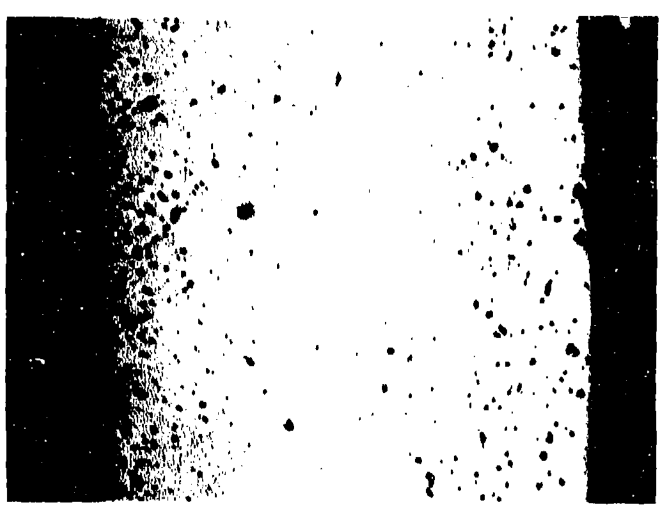

Plate No. 1-7966

Unetched X 200

Figure 297. Arc Plasma Test Ir/C(I-24)-13M, Location in Iridium Coating at Center of Side Wall.

Plate No. 1-7971

Etched Electrolytically in 20% HCl in Saturated Aqueous Solution of NaCl X500

Figure 298. Arc Plasma Test Ir/C(I-24)-13M, Location in Iridium Coating at Back of Sting Leg.

Plate No. 1-7970

Etched Electrolytically in 20% HCl in Saturated Aqueous Solution of NaCl. X500

Figure 299. Arc Plasma Test Ir/C (I-24)-13M, Location in Iridium Coating at Back Quarter of Side Wall.

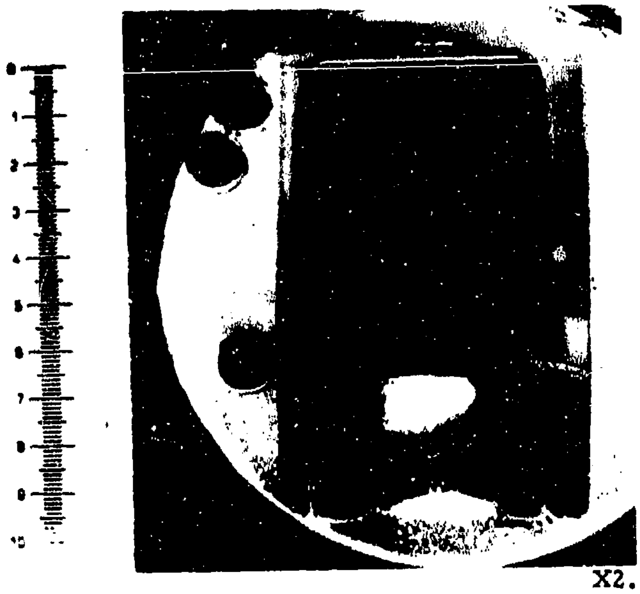

Plate No.
2-0446

X2.87

Figure 300. Arc Plasma Test Ir/C(I-24)-23M. Surface Temperature 4155°F, Exposure Time 1800 Seconds, Stagnation Pressure 1.01 Atm., Stagnation Enthalpy 2750 BTU/lb, Cold Wall Heat Flux 288 BTU/ft^{2}sec. Coating Survived Hot Face Up. One Inch Scale.

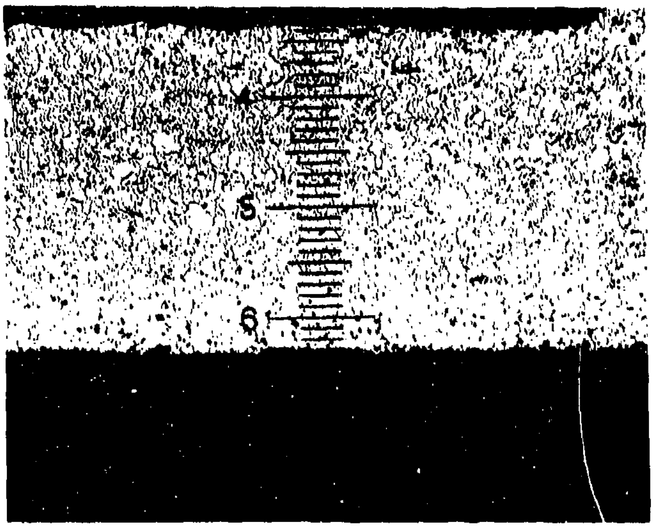

Plate No.
2-0447

Etched Electrolytically in 20% HCl in a Saturated Solution of NaCl in Water

X89

Figure 301. Arc Plasma Test Ir/C(I-24)-23M. Hot Interface at Top. One Division Equals 0.788 Mils. Coating Thickness Equals 23.6 Mils.

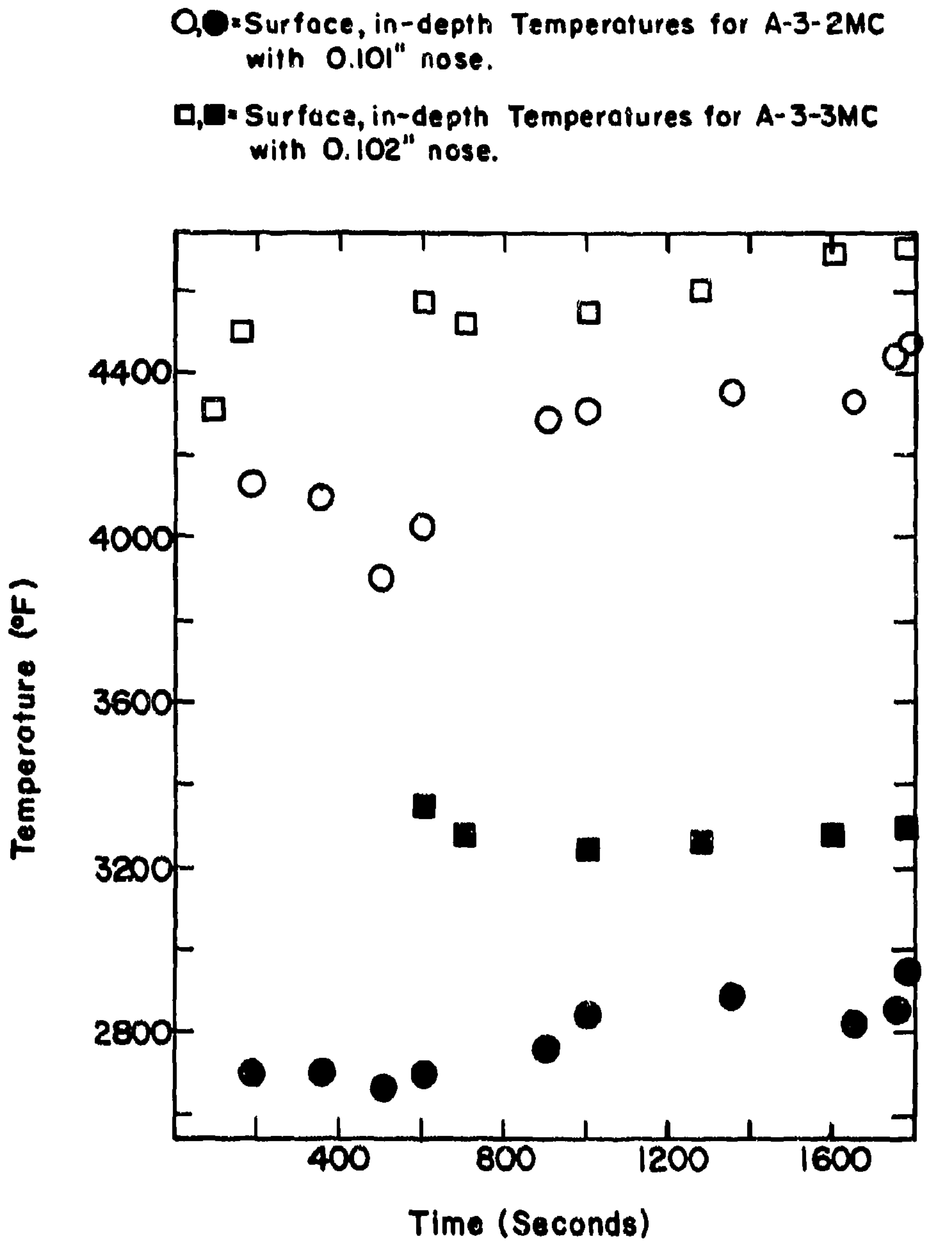

Figure 302. Time-Temperature Histories of Surface and In-Depth Temperatures for ZrB_2(A-3).

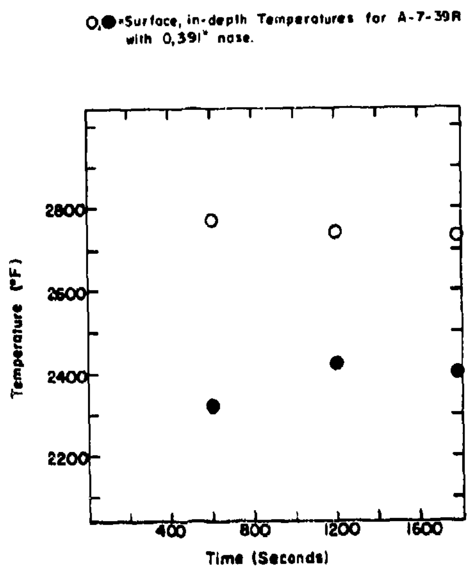

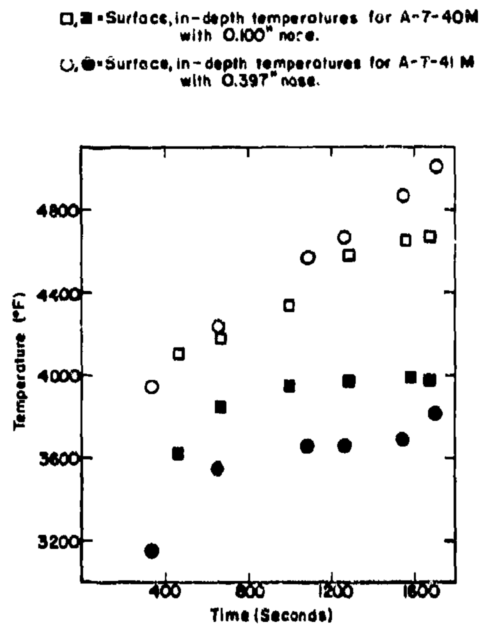

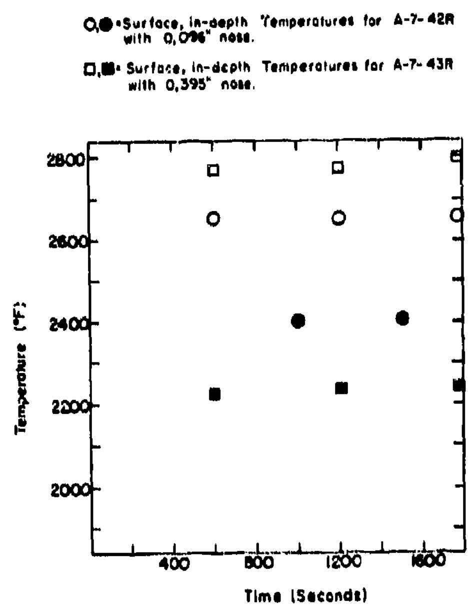

Figure 303. Time-Temperature Histories of Surface and In-Depth Temperatures for HfB_2+SiC(A-7).

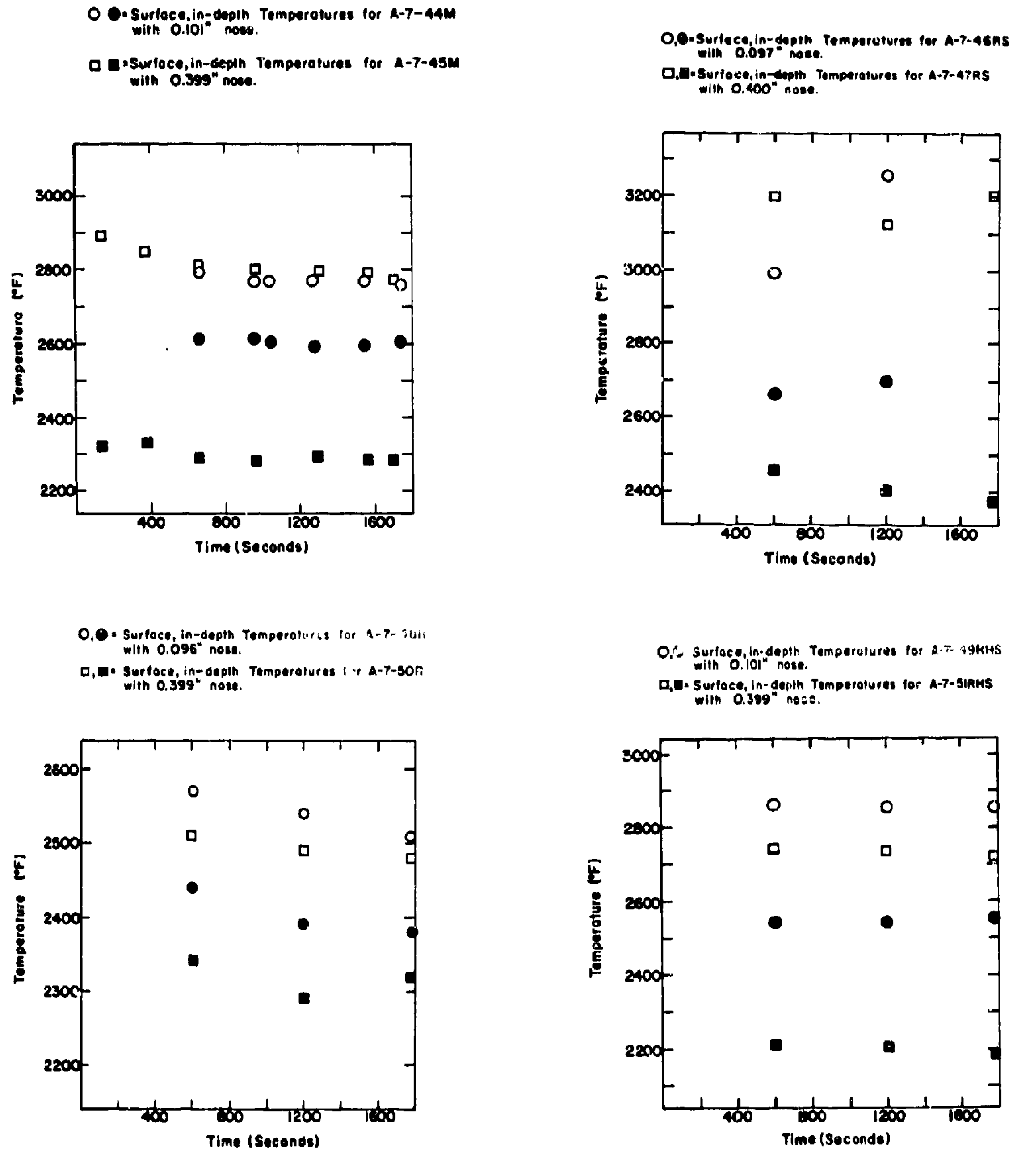

Figure 304. Time-Temperature Histories of Surface and In-Depth Temperatures for HfB_2+SiC(A-7).

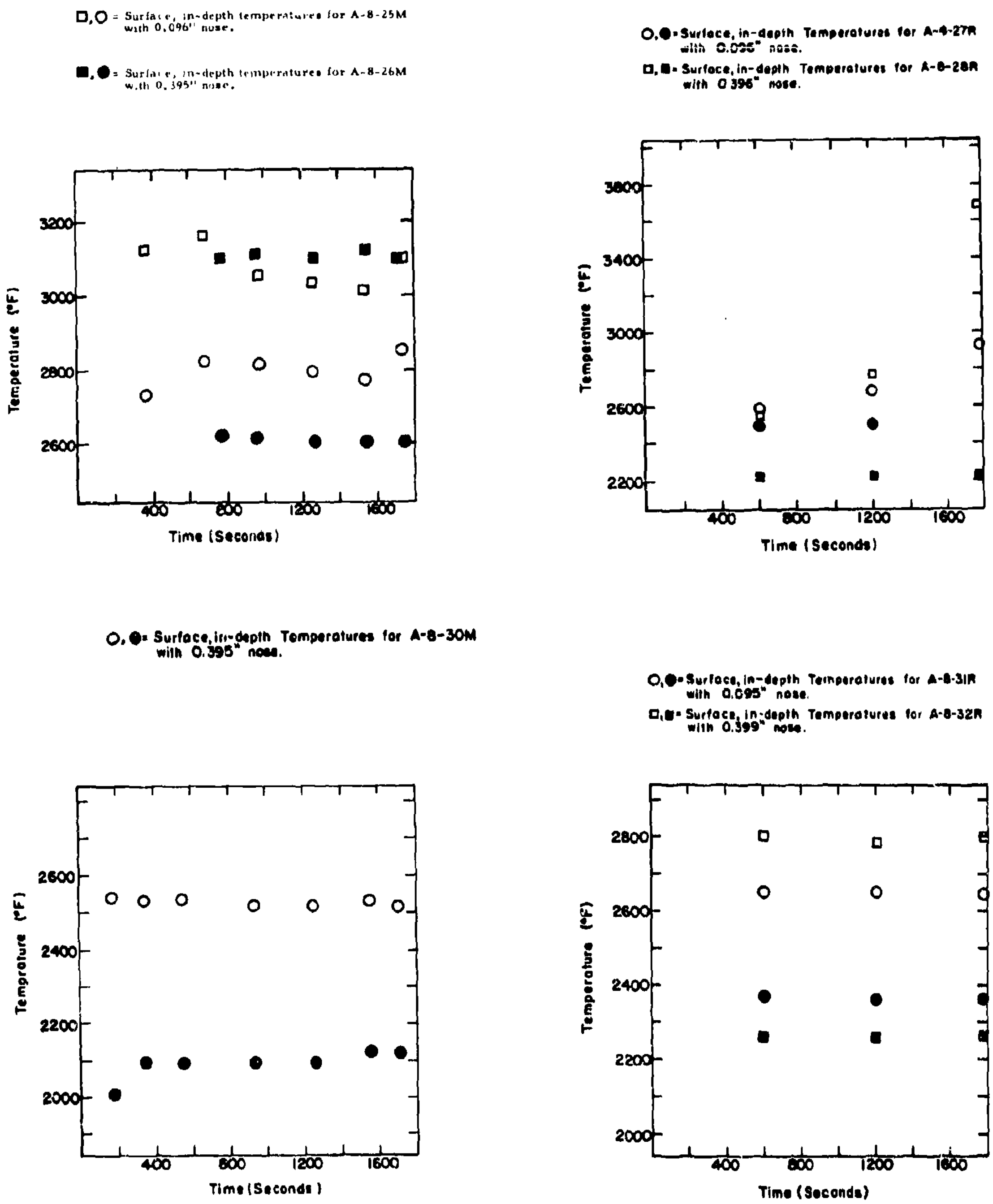

Figure 305. Time-Temperature Histories of Surface and In-Depth Temperatures for ZrB_2+SiC(A-8).

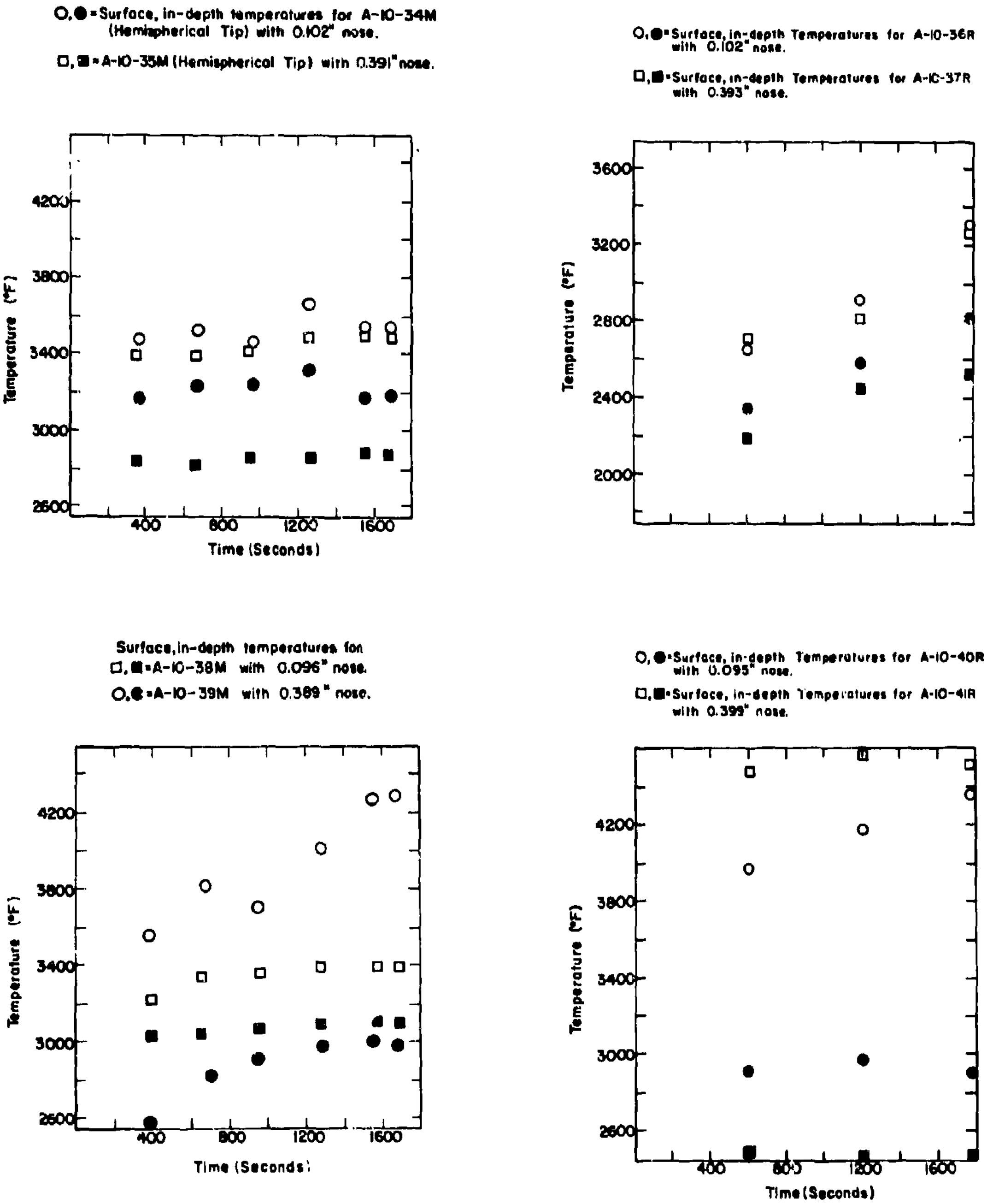

Figure 306. Time-Temperature Histories of Surface and In-Depth Temperatures for ZrB_2+SiC+C(A-10).

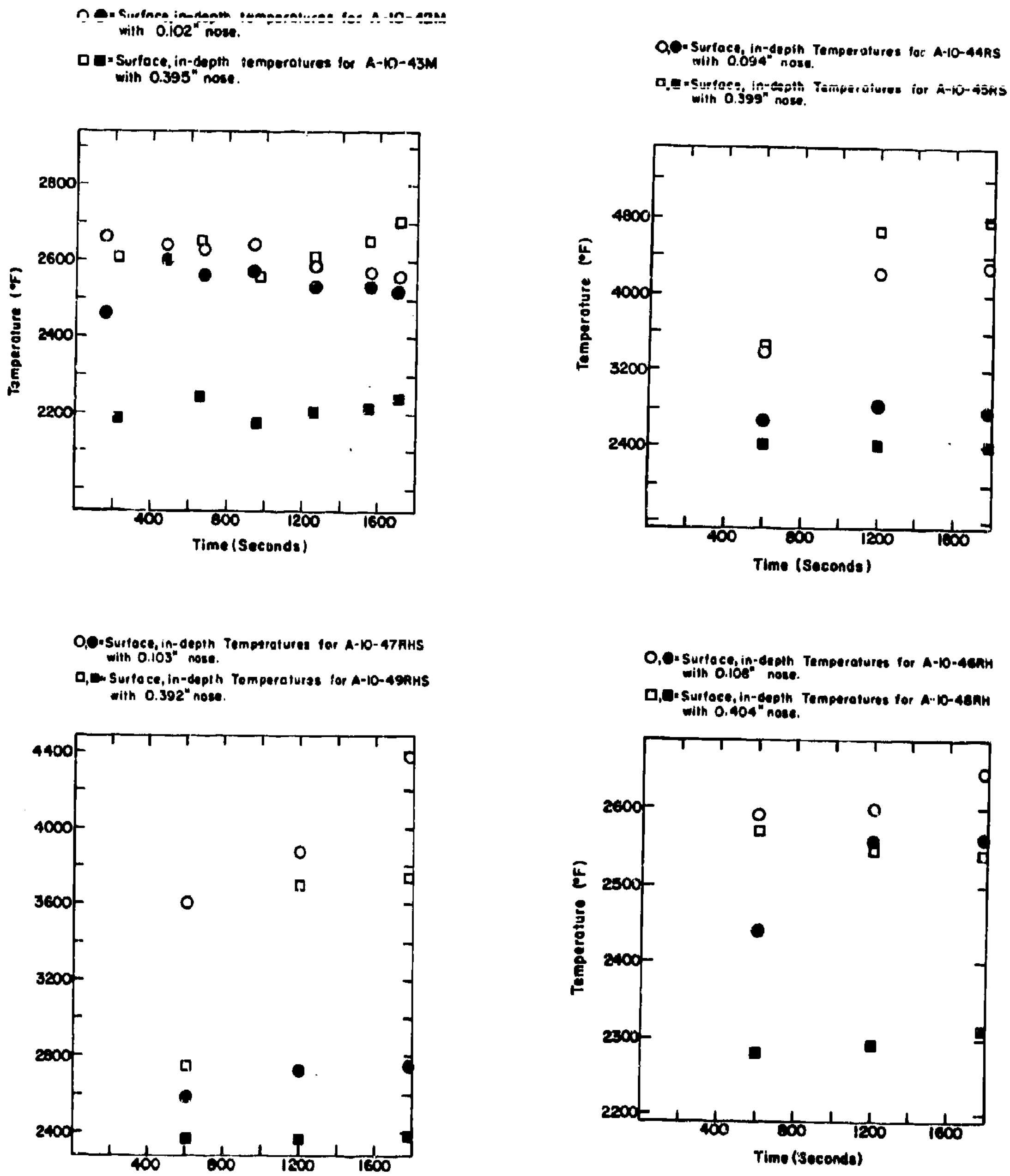

Figure 307. Time-Temperature Histories of Surface and In-Depth Temperatures for ZrB_2+SiC+C(A-10).

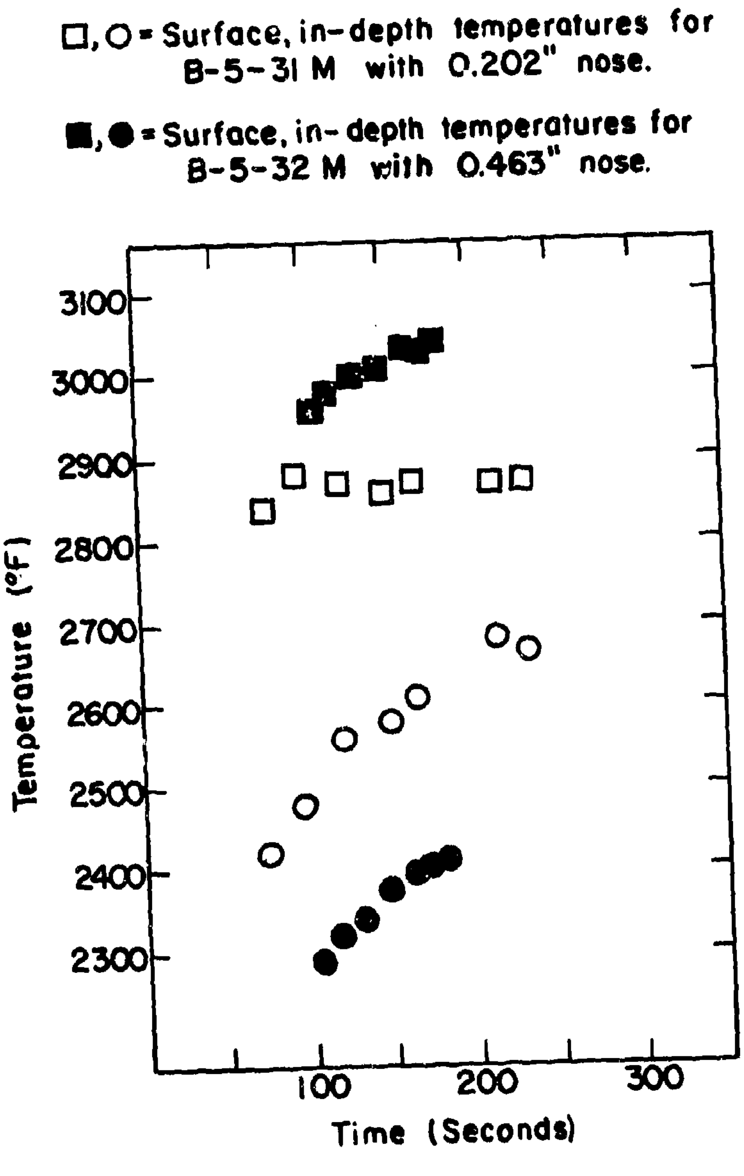

Figure 308. Time-Temperature Histories of Surface and In-Depth Temperatures for RVA(B-5).

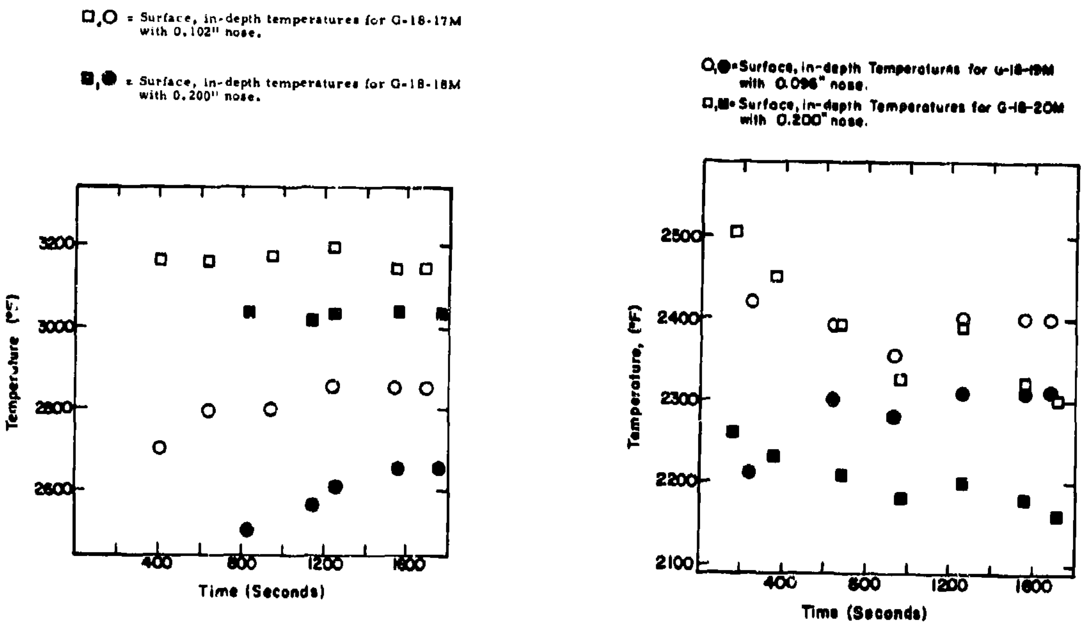

Figure 309. Time-Temperature Histories of Surface and In-Depth Temperatures for WSi_2/W(G-18).

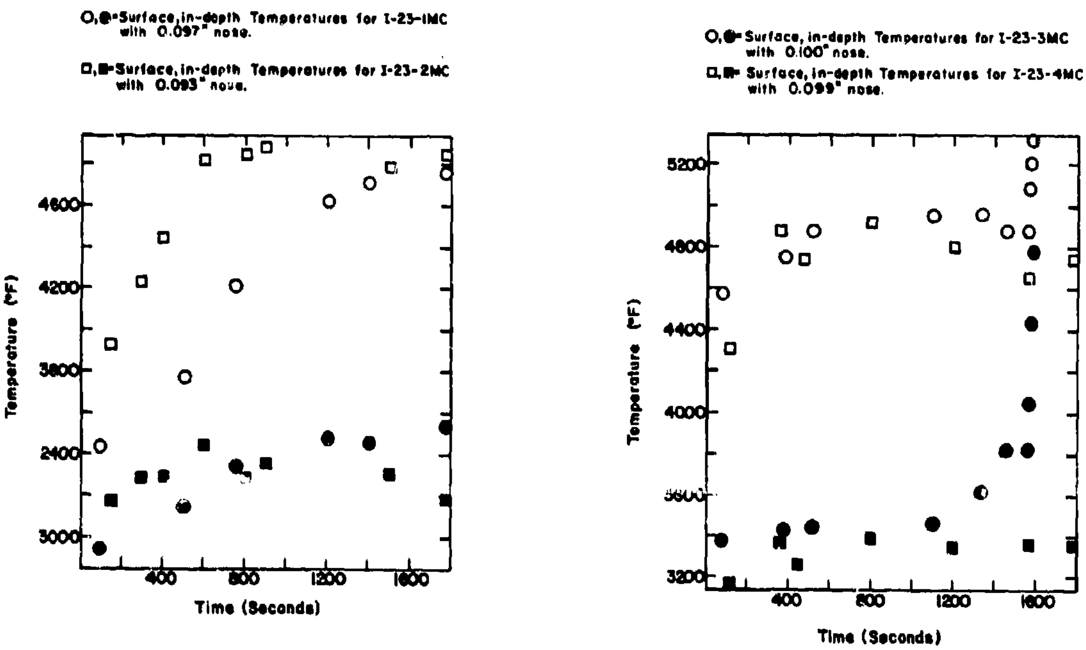

Figure 310. Time-Temperature Histories of Surface and In-Depth Temperatures for Hf-Ta-Mo(I-23).

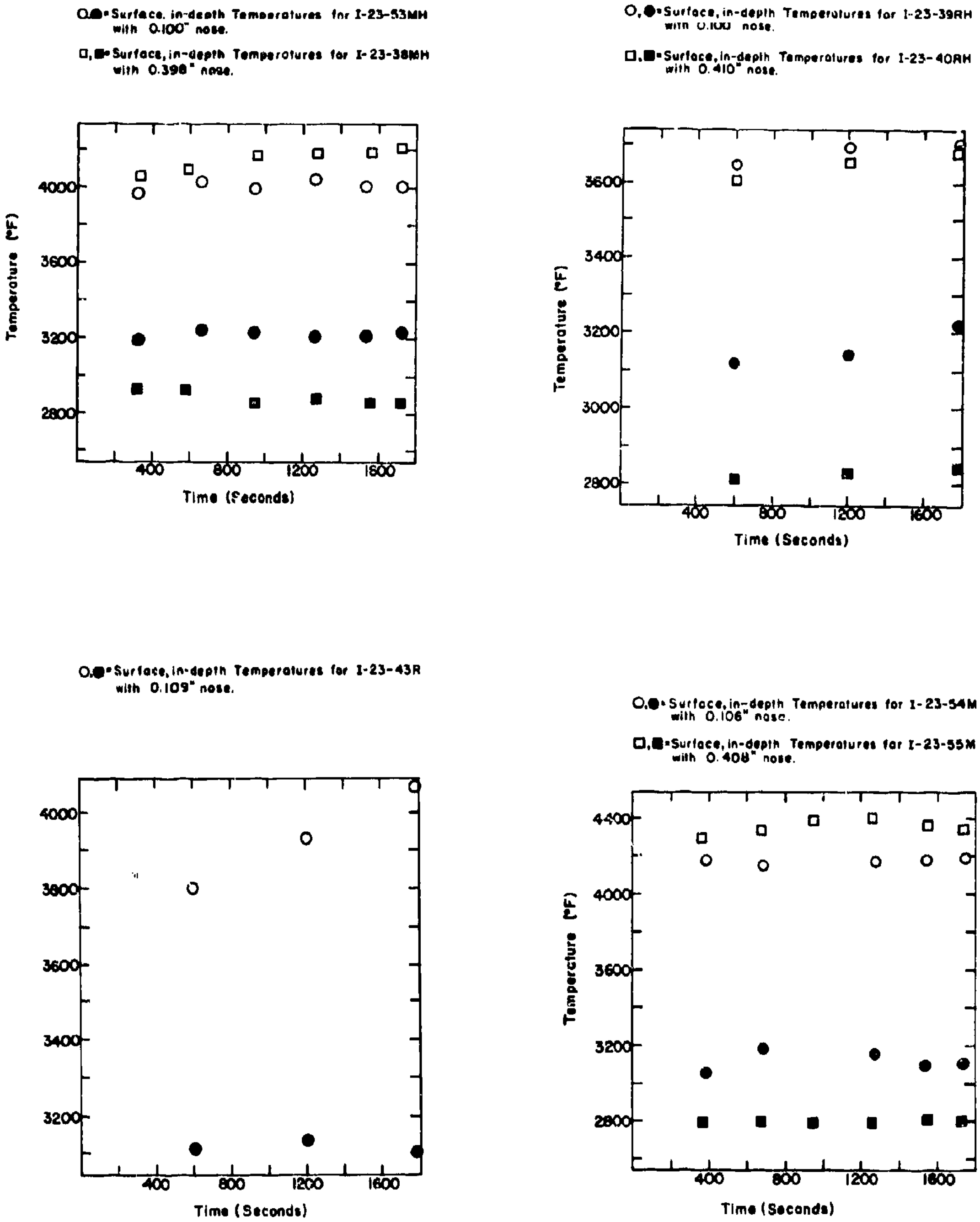

Figure 311. Time-Temperature Histories of Surface and In-Depth Temperatures for Hf-Ta-Mo(I-23).

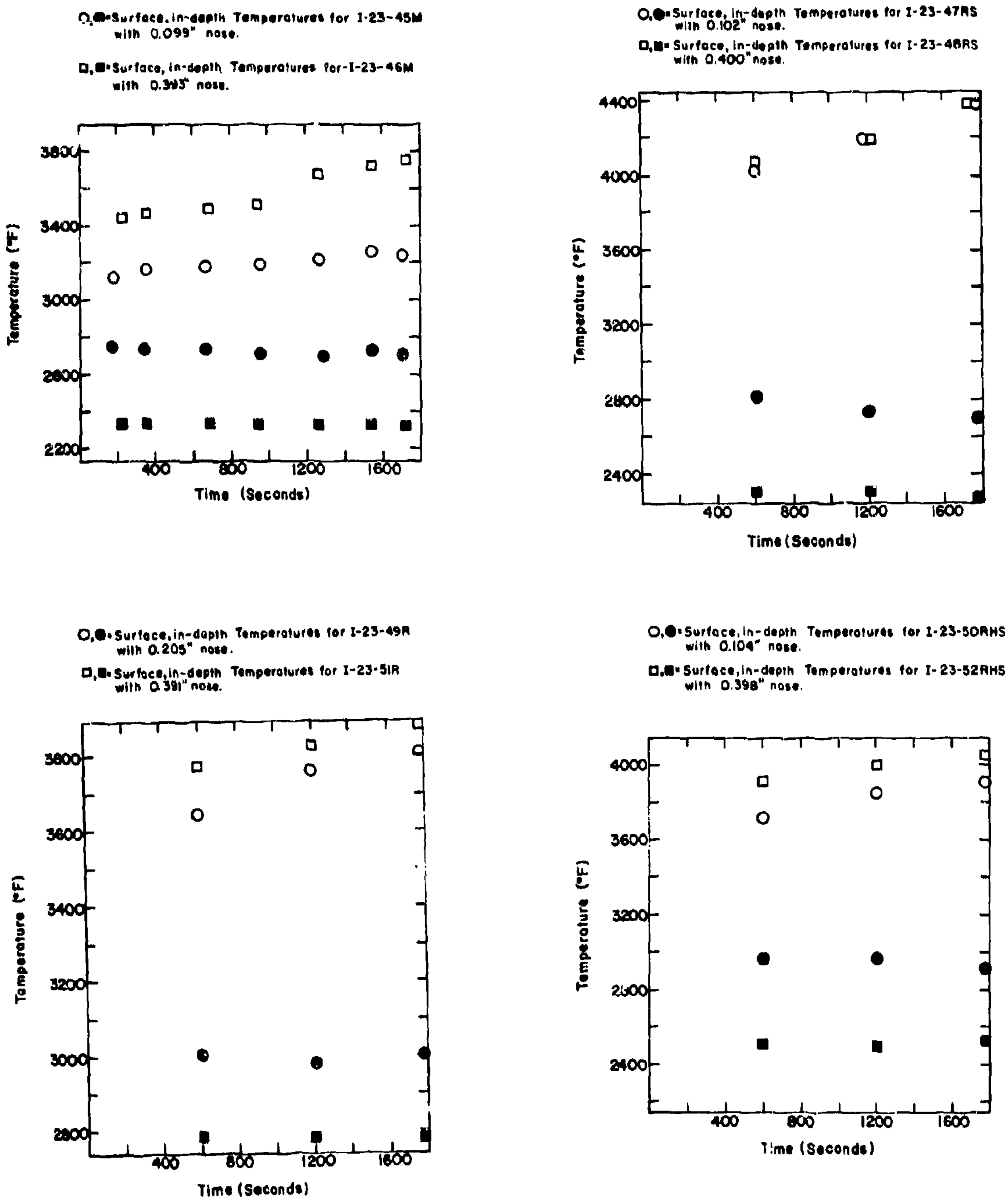

Figure 312. Time-Temperature Histories of Surface and In-Depth Temperatures for Hf-Ta-Mo(I-23).

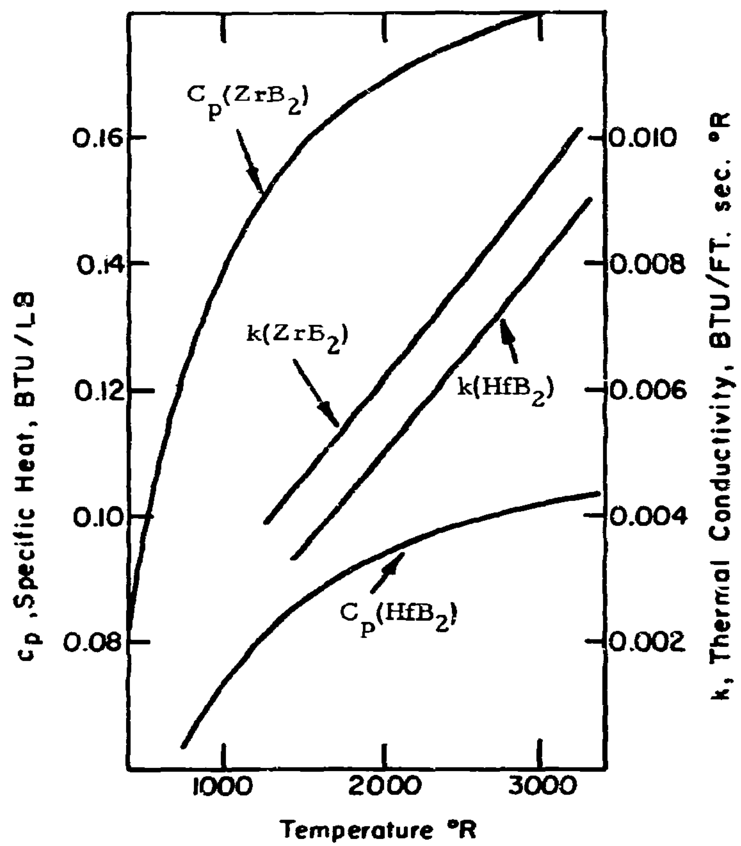

Figure 313. Thermal Properties of ZrB_2 (Density = 375 lbs/ft^3) and HfB_2(Density = 625 lbs/ft^3) as a Function of Temperature.

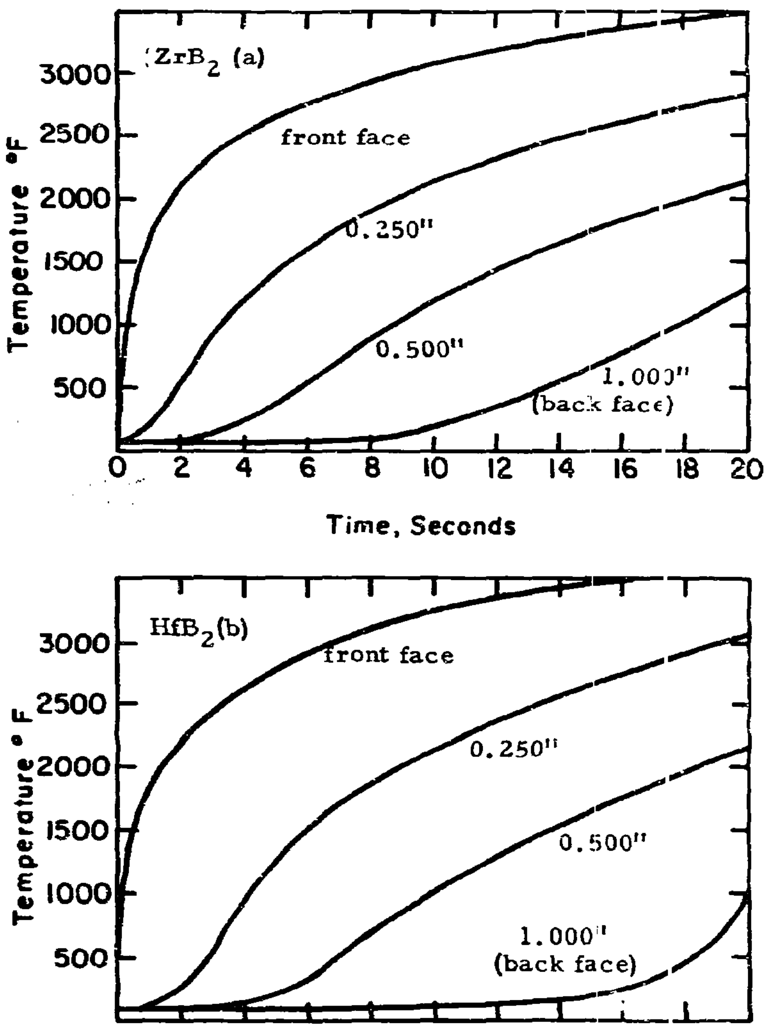

Figure 314 (a)(b). Calculated Thermal Gradients for ZrB_2 and HfB_2, q = 1000 BTU/ft^{2}sec, i_e = 2000 BTU/lb.

Plate No. 1-7169

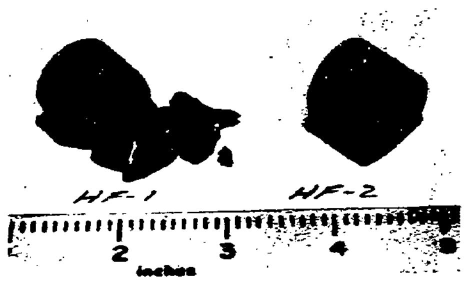

$HfB_{2.1}$ (A-2)

Plate No. 1-6694

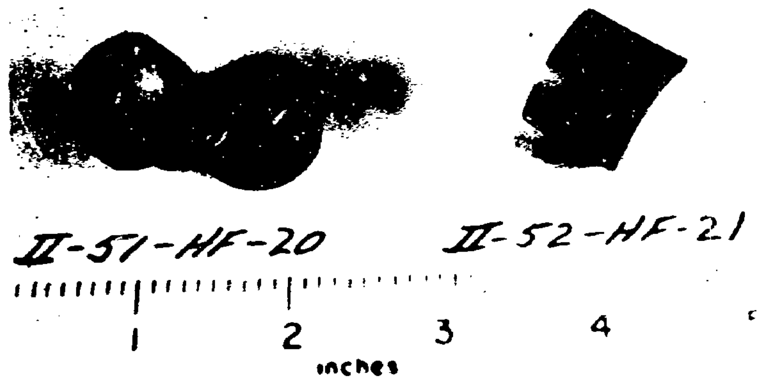

$HfB_{2.1}$ (A-6)

Plate No. 1-6707

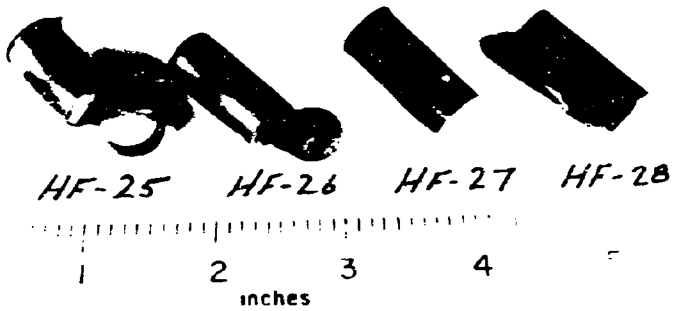

Plate No. 1-7205

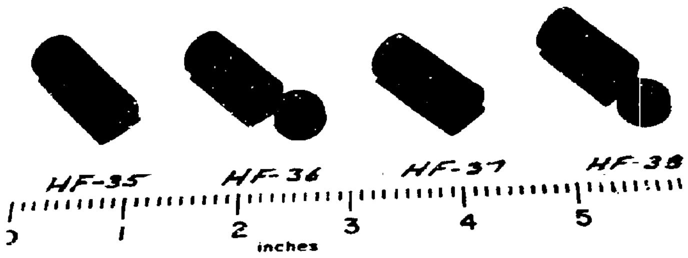

HfB_2 + 20% SiC (A-4)

Figure 315. Post Exposure Photographs of 10 MW Arc Exposures $HfB_{2.1}$(A-2) and (A-6), and HfB_2 + 20% SiC (A-4).

Plate No. 1-6690

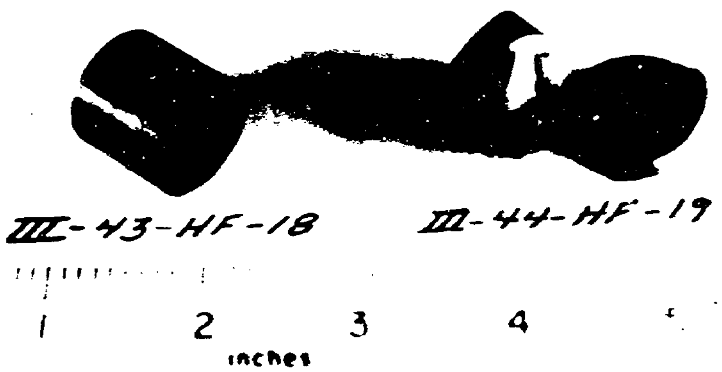

Plate No. 1-7191

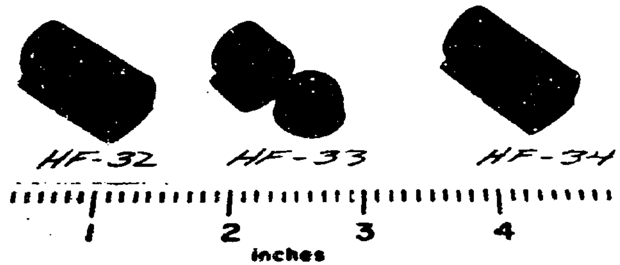

$HfB_{2.1}$ + 20%SiC (A-7)

Plate No. 5115

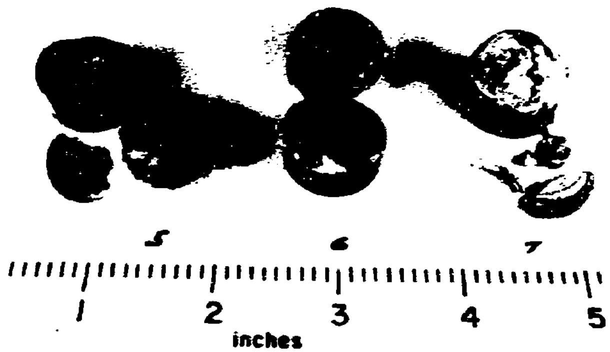

Plate No. 5126

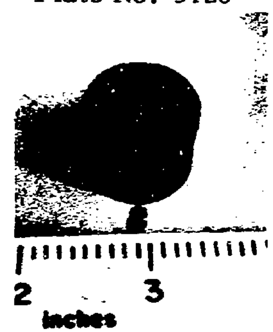

ZrB_2 (A-3)

Figure 316. Post Exposure Photographs of 10 MW Arc Exposures $HfB_{2.1}$+ 20%SiC(A-7) and ZrB_2(A-3).

Plate No. 1-6685

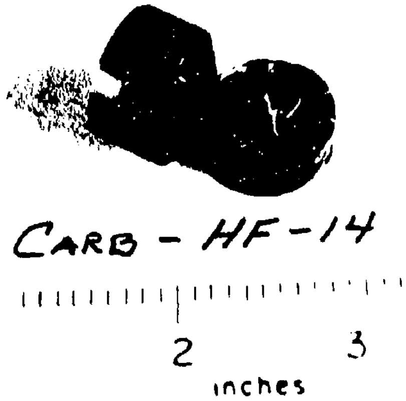

Plate No. 5127

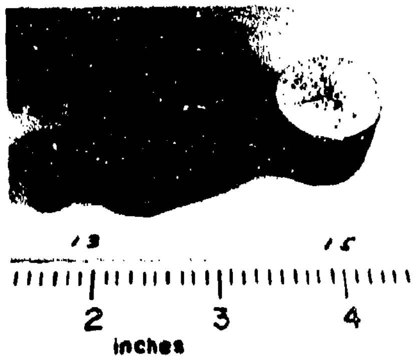

ZrB_2 (A-3)

Plate No. 1-6698

Plate No. 1-7176

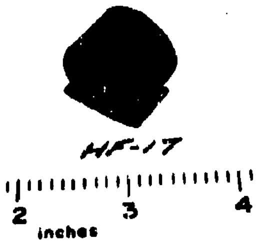

ZrB_2 (ManLabs-Avco)

Plate No. 1-6681

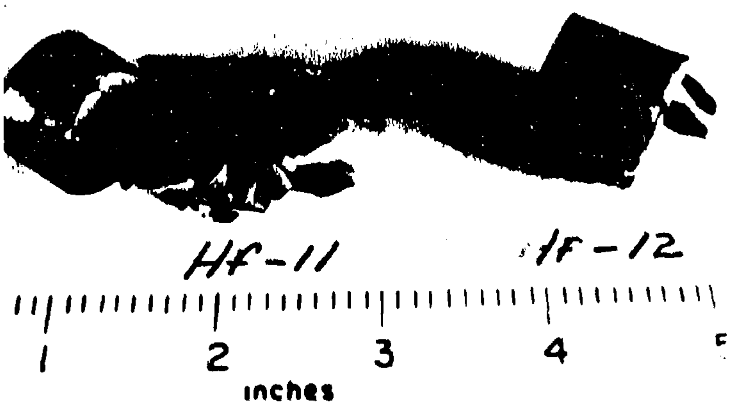

Boride Z (A-5)

Plate No. 1-6702

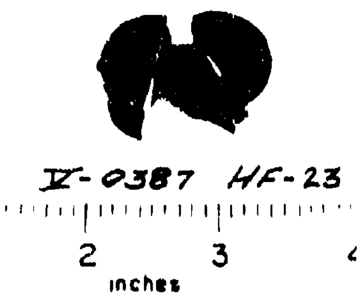

ZrB_2 + 20% SiC(A-8)

Figure 317. Post Exposure Photographs of 10MW Arc Exposures ZrB_2(A-3) and (ManLabs-Avco), Boride Z(A-5) and ZrB_2 + 20%SiC(A-8).

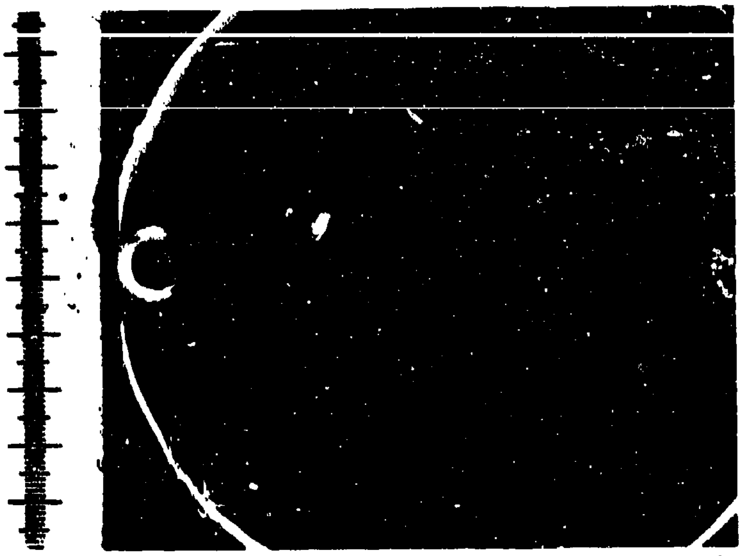

Plate No. 1-7173

X3.4

Figure 318. 10 MW Arc Test $HfB_{2.1}$(A-2)-HF-2, Surface Temperature 3305°F, Exposure Time 20.1 Seconds, Stagnation Pressure 4.3 Atm, Stagnation Enthalpy 1930 BTU/lb, Cold Wall Heat Flux 695 BTU/ft^{2}sec. Hot Face at Top. One Inch Scale. Fine Cracks Observed.

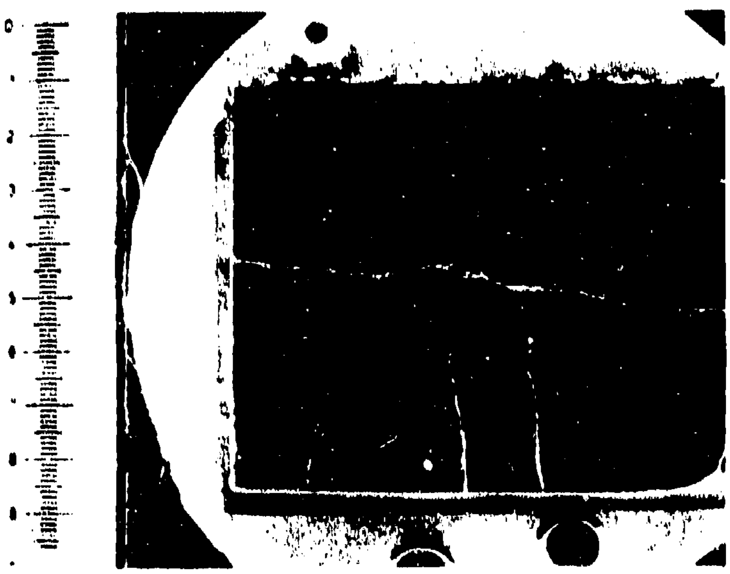

Plate No. 1-7188

X3.3

Figure 319. 10 MW Arc Test $HfB_{2.1}$(A-6)-HF-21, Surface Temperature 3470°F, Exposure Time 20.1 Seconds, Stagnation Pressure 4.3 Atm, Stagnation Enthalpy 2030 BTU/lb, Cold Wall Heat Flux 733 BTU/ft^{2}sec. Hot Face at Bottom. One Inch Scale. Large Cracks Observed.

Plate No. 1-7212

X2.87

Figure 320. 10MW Arc Test $HfB_{2.1}$+20%SiC(A-4)-HF-37, Surface Temperature 4790°F, Exposure Time 20.2 Seconds, Stagnation Pressure 4.3 Atm, Stagnation Enthalpy 2540 BTU/lb, Cold Wall Heat Flux 940 BTU/ft^{2}sec. Hot Face at Top. One Inch Scale.

Plate No. 1-7192

X3.4

Figure 321. 10MW Arc Test $HfB_{2.1}$+20%SiC(A-7)-HF-32, Surface Temperature 4610°F, Exposure Time 20.1 Seconds, Stagnation Pressure 4.3 Atm, Stagnation Enthalpy 2710 BTU/lb, Cold Wall Heat Flux 948 BTU/ft^{2}sec. Hot Face at Right. One Inch Scale.

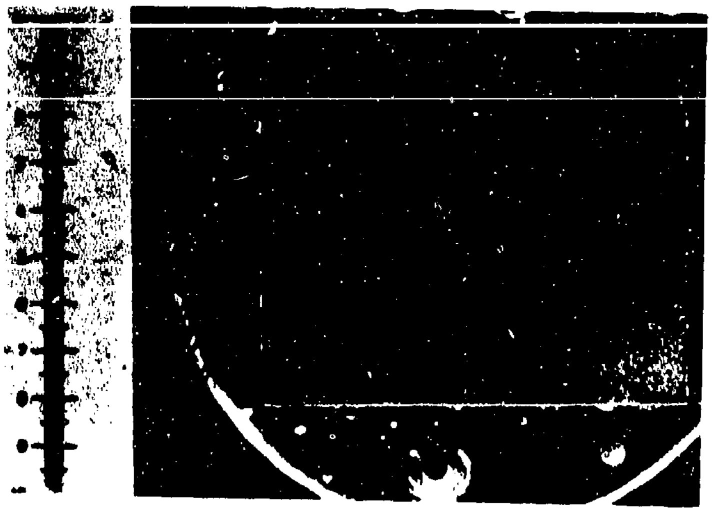

Plate No. 1-7202

X2.87

Figure 322. 10 MW Arc Test $HfB_{2.1}$+20%SiC(A-7)-HF-18, Surface Temperature 3500°F, Exposure Time 20.1 Seconds, Stagnation Pressure 4.3 Atm, Stagnation Enthalpy 2200 BTU/lb, Cold Wall Heat Flux 787 BTU/ft^2sec. Hot Face at Top. One Inch Scale. Fine Cracks Observed.

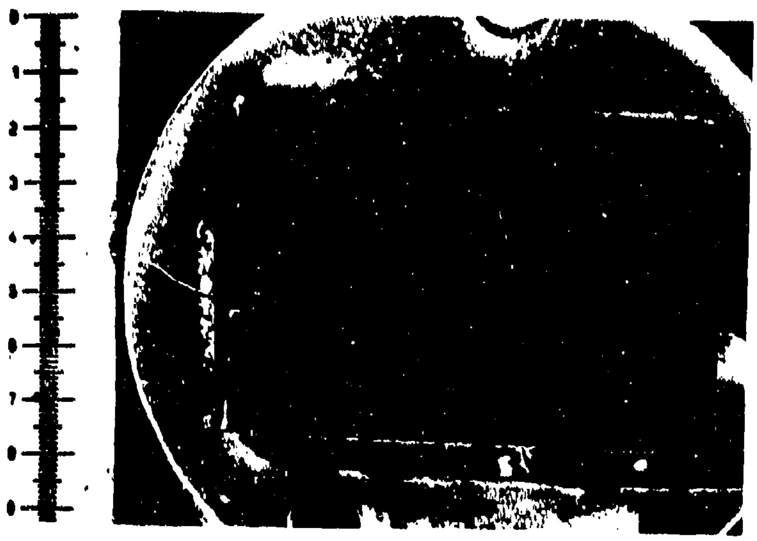

Plate No. 1-7177

X3.4

Figure 323. 10MW Arc Test ZrB_2 (ManLabs-Avco)-HF-17, Surface Temperature 3425°F, Exposure Time 20.1 Seconds, Stagnation Pressure 4.3 Atm, Stagnation Enthalpy 1964 BTU/lb, Cold Wall Heat Flux 714 BTU/ft^2sec. Hot Face at Bottom. One Inch Scale. Fine Cracks Observed.

Plate No. 2-0731

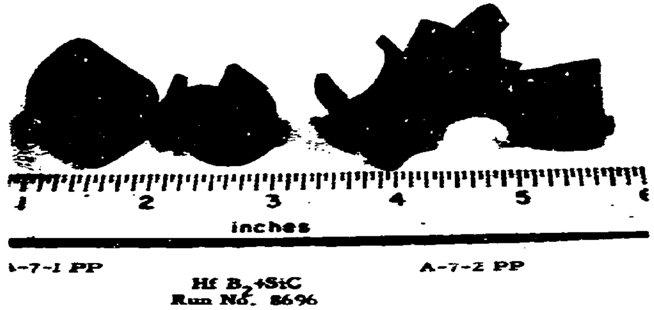

Plate No. 2-0732

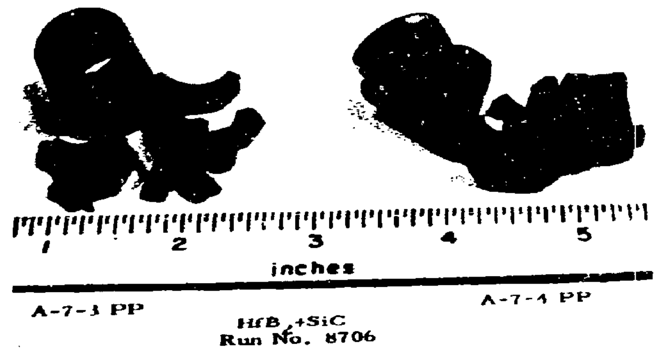

Plate No. 2-0733

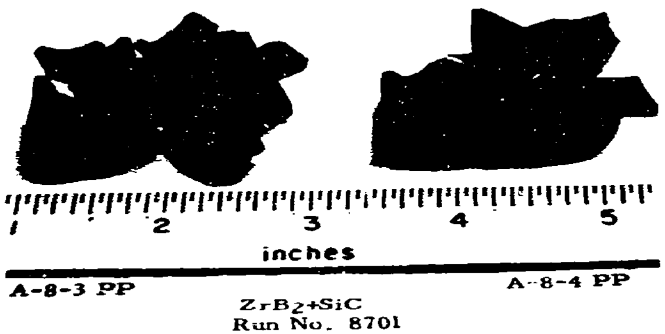

Plate No. 2-0734

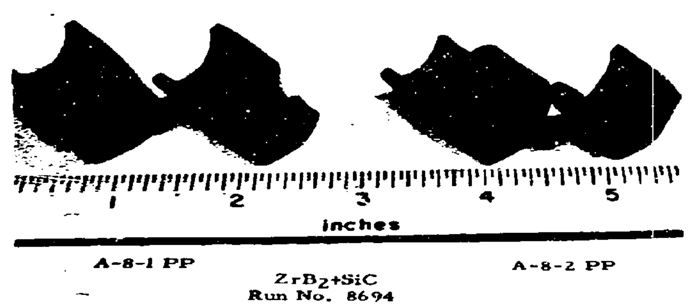

Figure 324. Post-exposure Photographs of $HfB_{2.1}$+20%SiC(A-7) and $ZrB_{2.1}$+20%SiC(A-8) Supersonic Pipe Test Samples Run in Avco 10-Megawatt Arc Facility.

Plate No. 2-0735

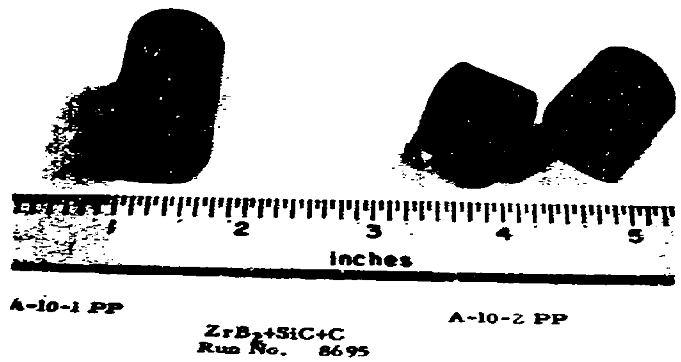

Plate No. 2-0736

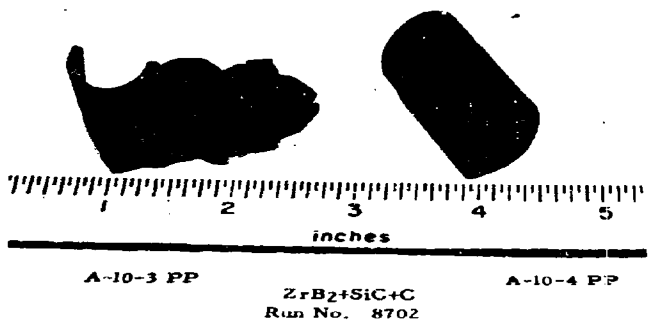

Plate No. 2-0737

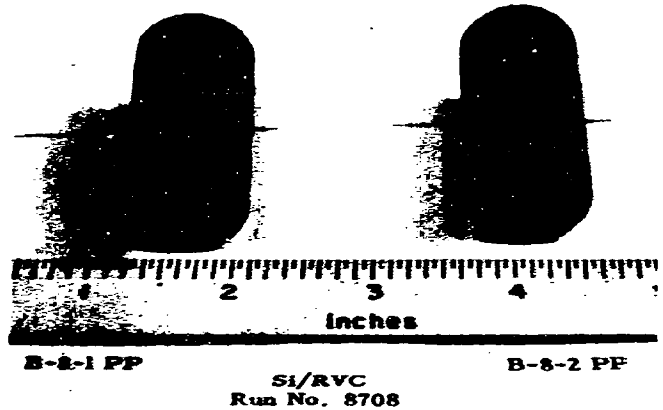

Plate No. 2-0738

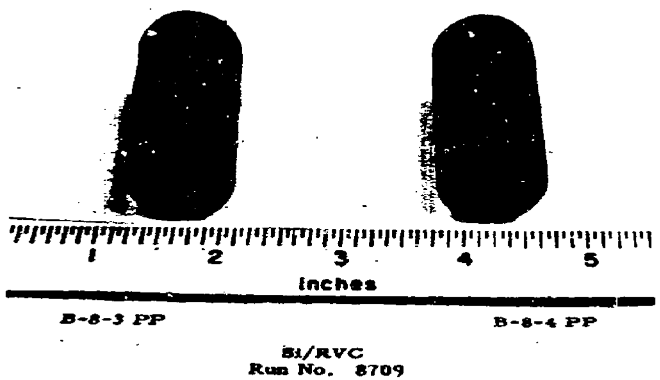

Figure 325. Post-exposure Photographs of ZrB_2+SiC+C(A-10) and Si/RVC(B-8) Supersonic Pipe Test Samples Run in Avco 10-Megawatt Arc Facility.

Plate No. 2-0739

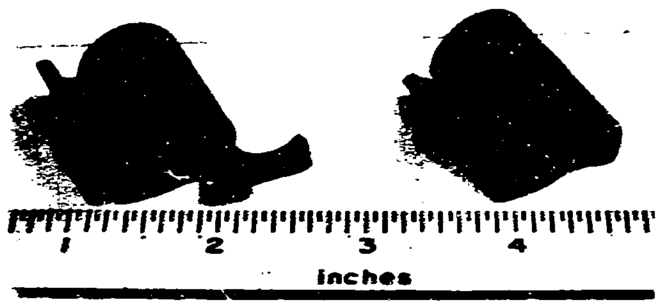

E-14-3 PP | E-14-4 PP

Kt-SiC
Run No. 8698

Plate No. 2-0740

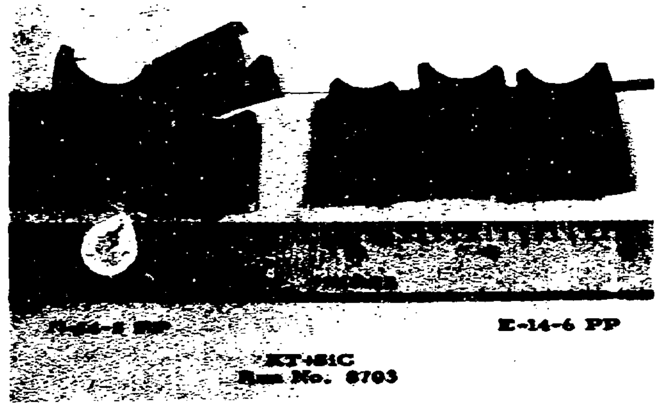

Plate No. 2-0741

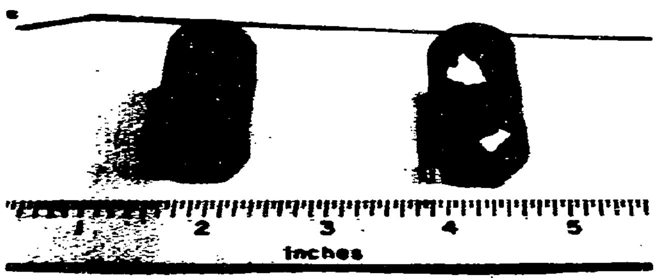

I-23-1 PP | I-23-2 PP

Hf+Ta+Mo
Run No. 8697

Plate No. 2-0742

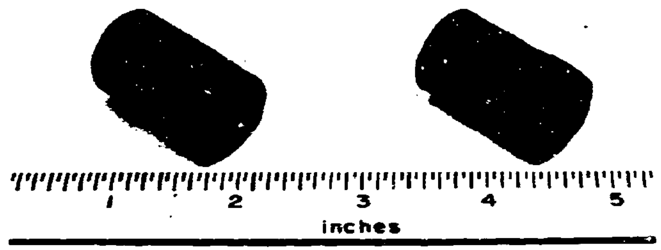

I-23-3 PP | I-23-4 PP

Hf+Ta+Mo
Run No. 8707

Figure 326. Post-exposure Photographs of KT-SiC(E-14) and Hf-Ta-Mo(I-23) Supersonic Pipe Test Samples Run in Avco 10-Megawatt Arc Facility.

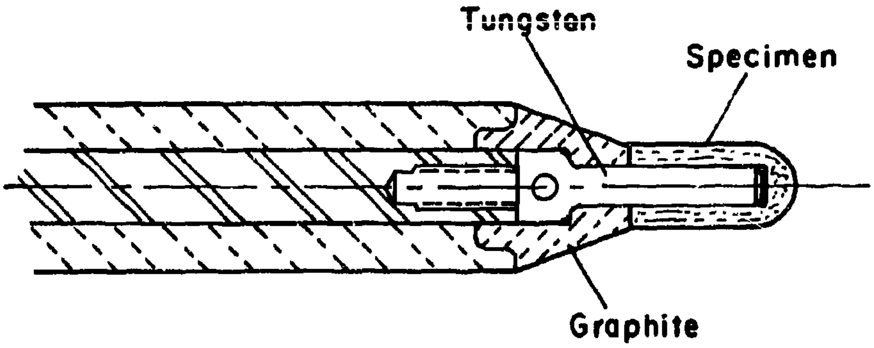

One Half Inch Diameter Specimens

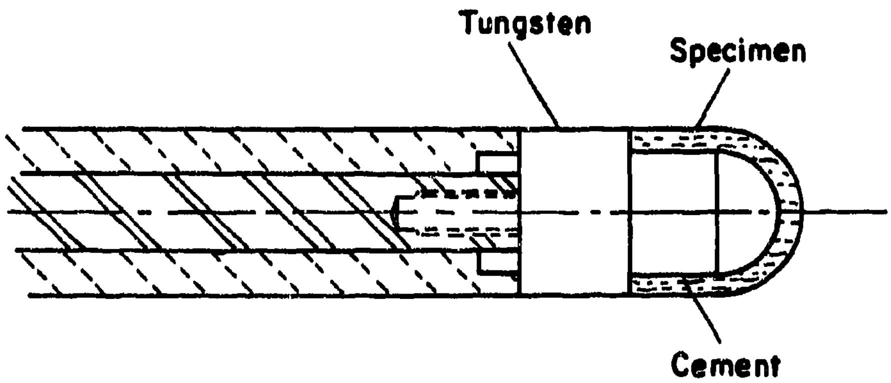

One Inch Diameter Specimens

Figure 327. Details of Specimen Holders Employed in Wave Superheater Tests.

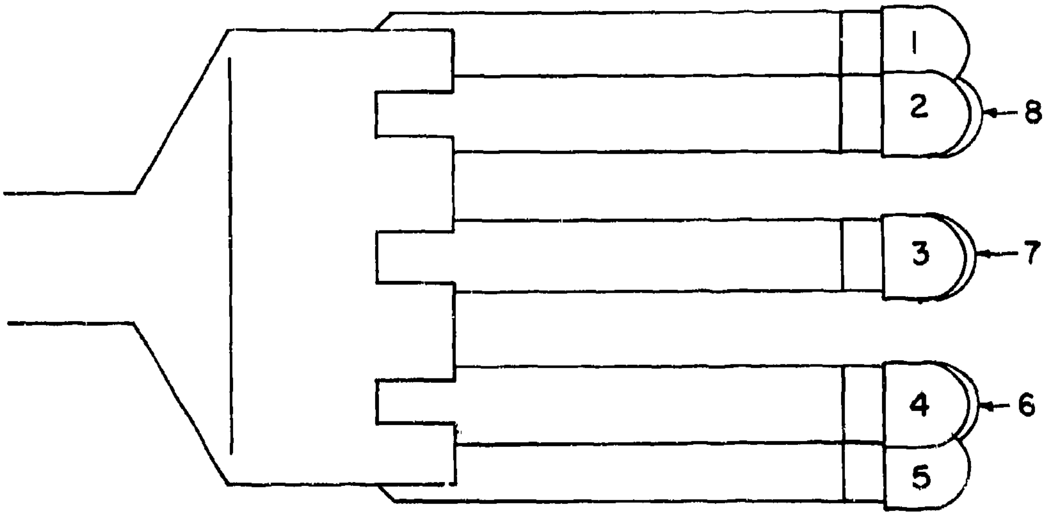

(a) View From Right Side
(Camera View)

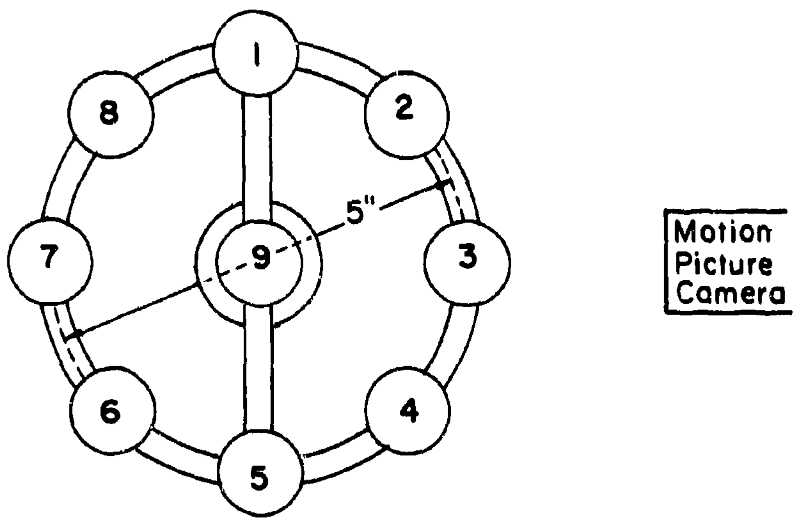

(b) Pilot's View (Looking Upstream)

Figure 328. Orientation of Calerimeter and Models in Wave Superheater Exposures.

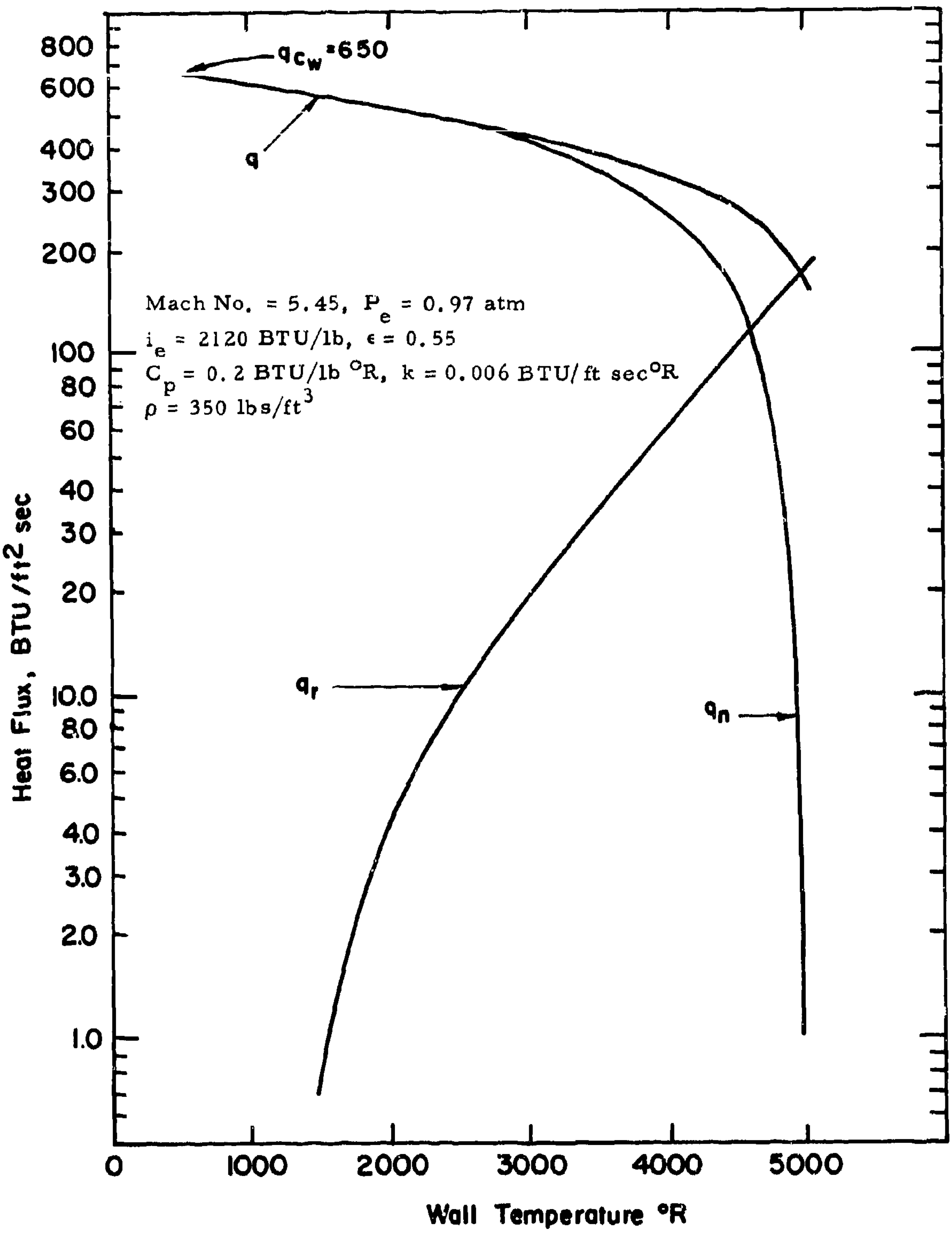

Figure 329. Calculated Heat Flux As A Function of Wall Temperature for A One-Half Inch Diameter Hemispherical Cap Shell of Zirconium Diboride One-Eighth Inch Thick in the Mach 6 Test Section of the Cornell Wave Superheater.

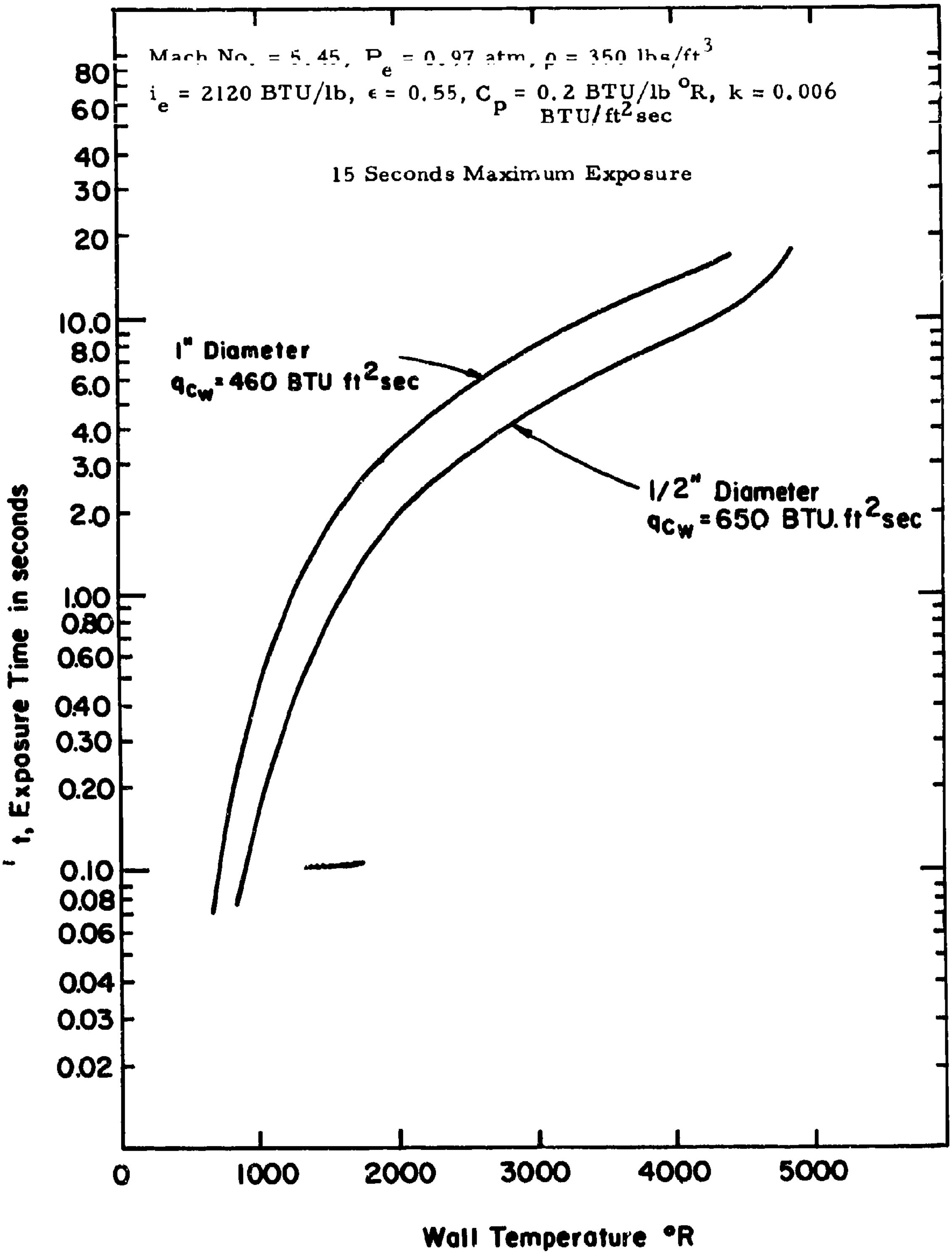

Figure 330. Calculated Wall Temperature As A Function of Time for A One Inch and a One-Half Inch Diameter Hemispherical Cap Shell of Zirconium Diboride One-Eighth Inch Thick in the Mach 6 Test Section of the Cornell Wave Superheater.

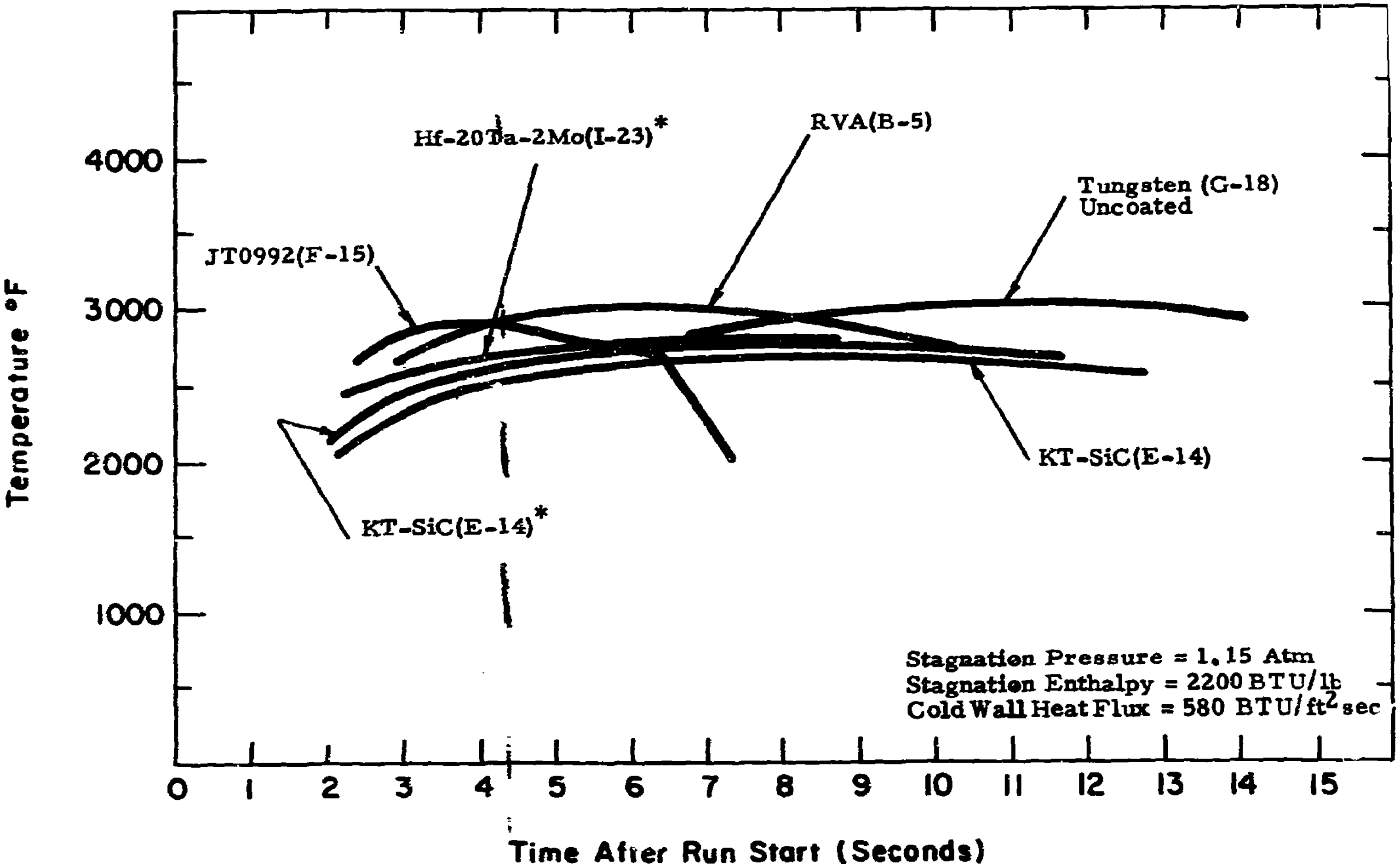

Figure 331. Brightness Temperature of Models as a Function of Time in the Wave Superheater at Mach 5.5 (Run 473). All Samples Were 1/2 Inch Diameter Hemispherical Caps except These Noted by an Asterisk Which Were One Inch Diameter Caps.

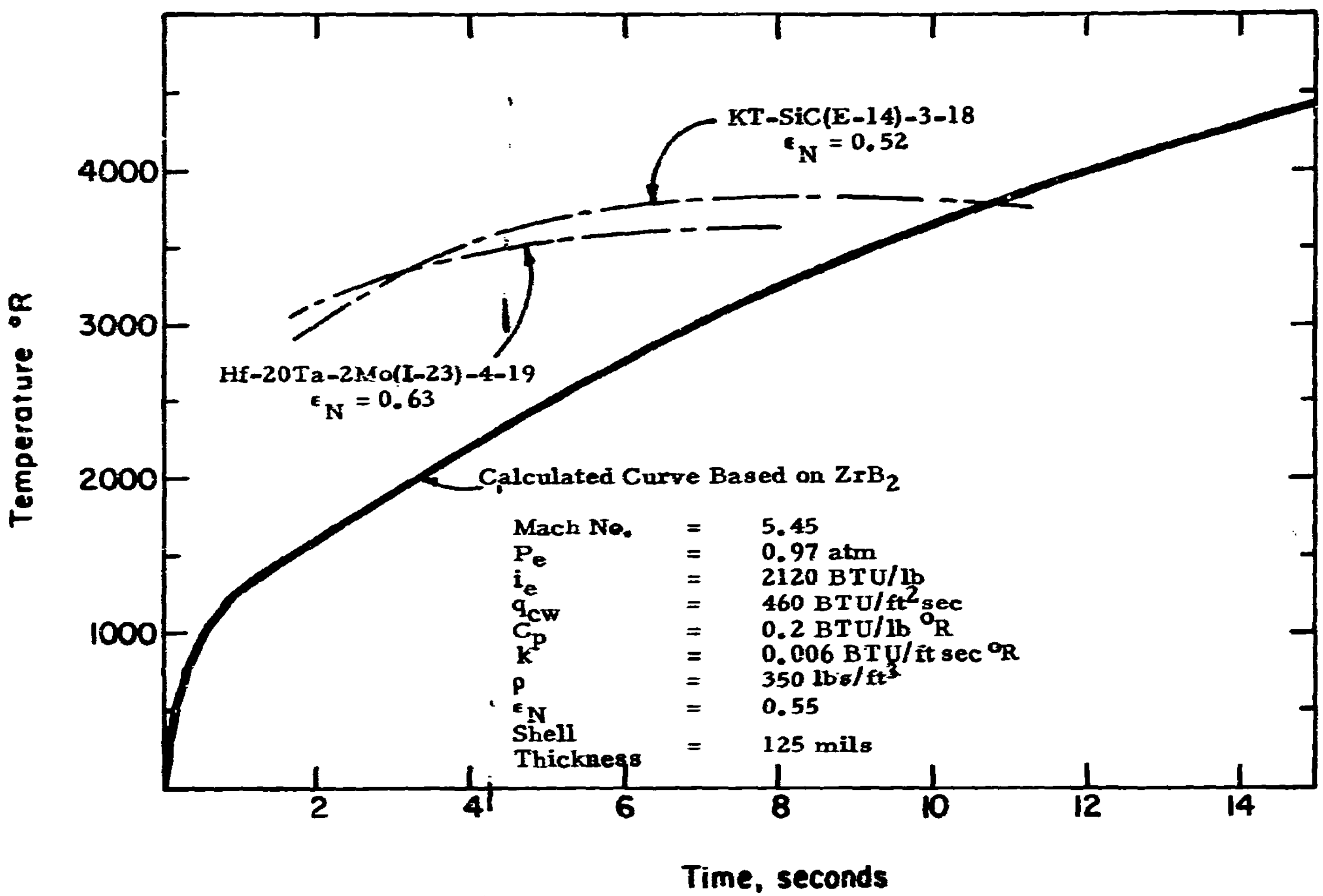

Figure 332. Comparison of Observed Time-Temperature Histories with Computed Values for One Inch Diameter Hemispherical Cap Models.

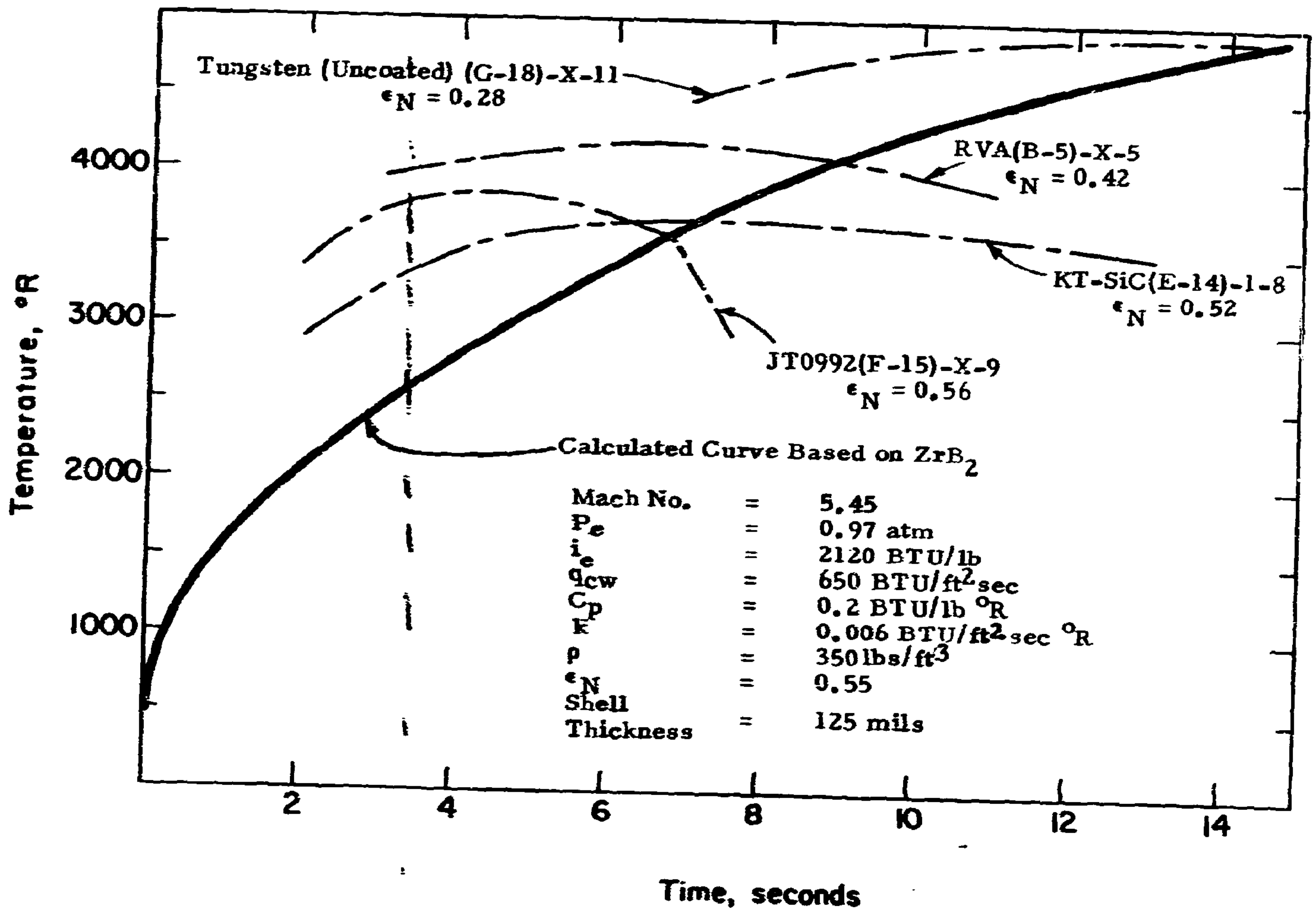

Figure 333. Comparison of Observed Time-Temperature Histories with Computed Values for One Half Inch Diameter Hemispherical Cap Models.

Plate 1-4483

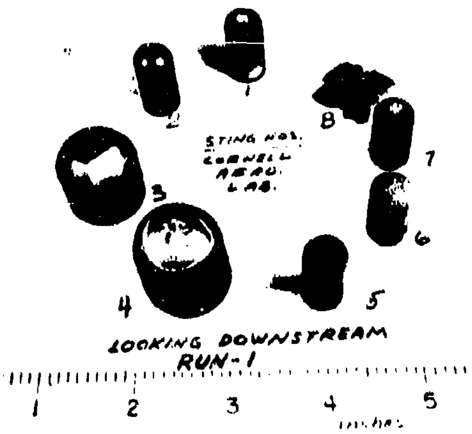

Sting Number	Material
1	ZrB_2(A-3)-1-2
2	KT-SiC(E-14)-1-8
3	KT-SiC(E-14)-3-18*
4	Hf-20Ta-2Mo(I-23)-4-19*
5	W(Uncoated)(G-18)-X-11
6	RVA(B-5)-X-5
7	JTA(D-13)-X-7
8	JT0992(F-15)-X-9

*Denotes one inch diameter cap. All other models are one half inch diameter.

Figure 334. CAL Run 67-473, Mach Number 5.45, Stagnation Pressure 1.15 atm, Stagnation Enthalpy 2200 BTU/lb, Cold Wall Heat Flux 580 BTU/ft^{2}sec, Exposure Time 15 Seconds.

Plate 1-4884

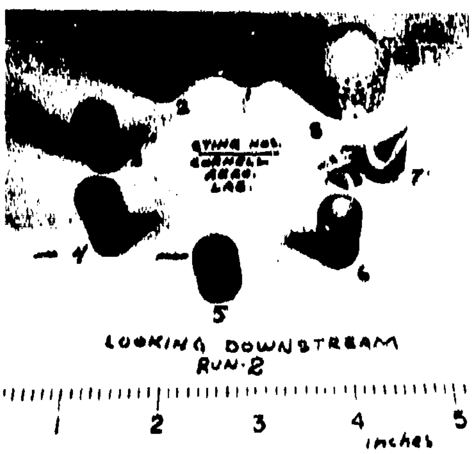

Sting Number	Material
1	Hf-20Ta-2Mo(I-23)-1-12
2	HfB_2(A-2)-X-1
3	HfB_2+SiC(A-4)-X-4
4	PG(B-6)-X-6
5	BPG(B-7)-X-16
6	JT0981(F-16)-X-10
7	ZrB_2(A-3)-24-3
8	Sn-Al/Ta-10W(G-19)-3-22*

*Denotes one inch diameter cap. All other models are one half inch diameter.

Figure 335. CAL Run 67-474, Mach Number 5.45, Stagnation Pressure 1.15 atm, Stagnation Enthalpy 2180 BTU/lb, Cold Wall Heat Flux 635 BTU/ft^{2}sec, Exposure Time 15 Seconds.

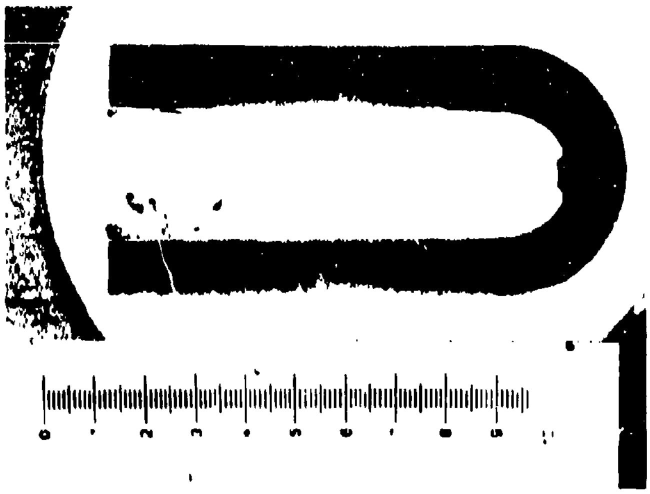

Plate No. 1-4691
a) One Inch Scale

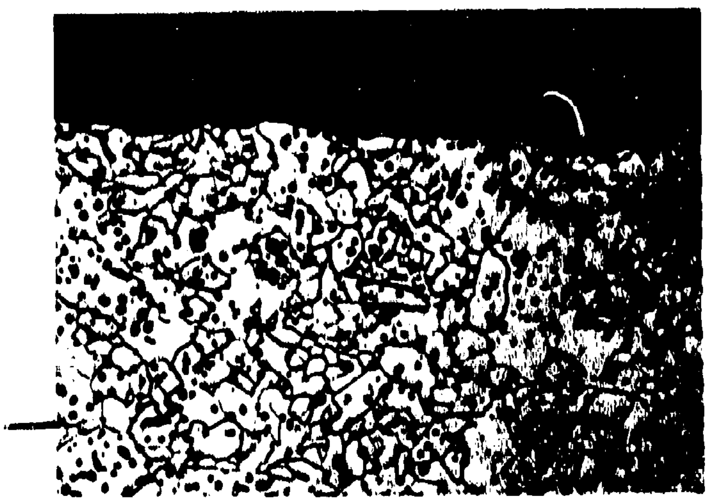

Plate No. 1-4692
b) X250, Etched with 10 Glycerine $5HNO_3$ 3HF. Hot Interface at Top.

Figure 336. Model ZrB_2(A-3)-1-2, Run #1, Sting #1.

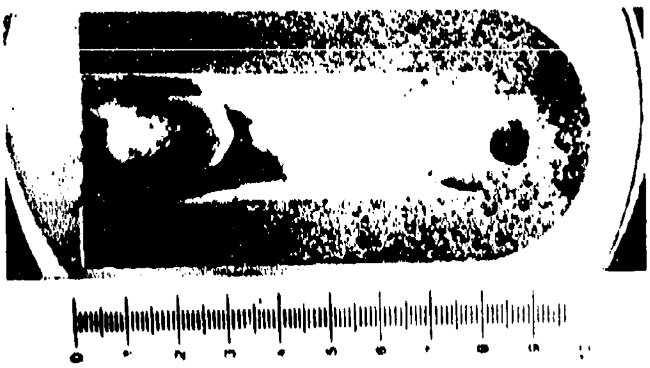

Plate No. 1-4708

a) One Inch Scale

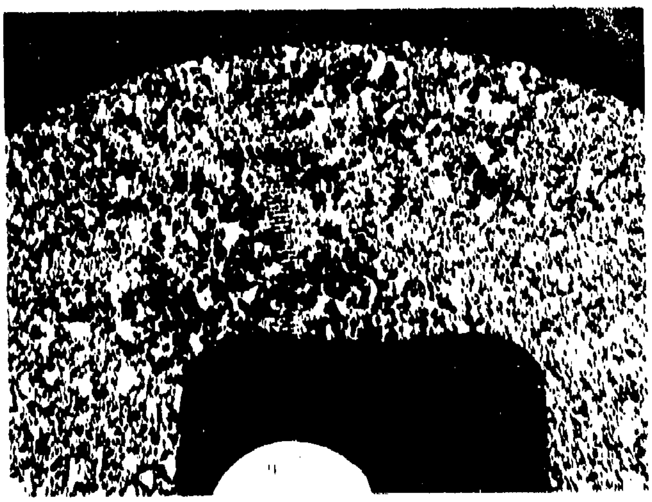

Plate No. 1-7767

b) 1.97 Mils per Small Division, Etched Electrolytically in 5% KOH, Hot Face at Top

Plate No. 1-5334

c) X250, Etched. Hot Interface at Top

Figure 337. Model KT-SiC(E-14)-1-8, Run #1, Sting #2.

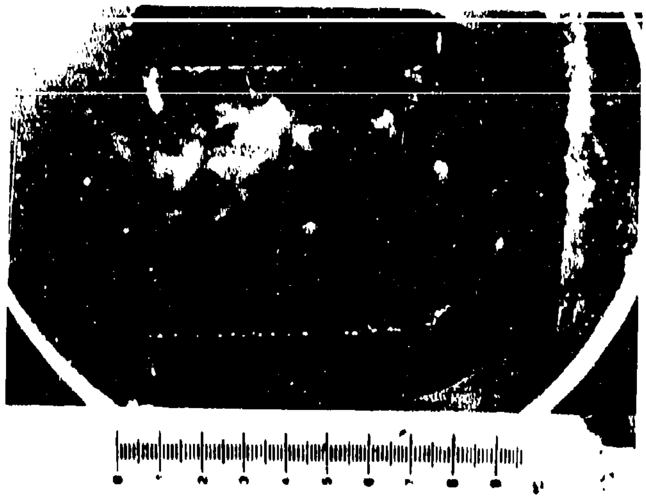

Plate No. 1-4709

a) One Inch Scale

Plate No. 1-7768

b) 1.97 Mils per Small Division, Etched Electrolytically in 5% KOH. Hot Face at Top

Plate No. 1-4710

c) X250, Etched, Hot Interface at Top.

Figure 338. Model KT-SiC(E-14)-3-18, Run #1, Sting #3.

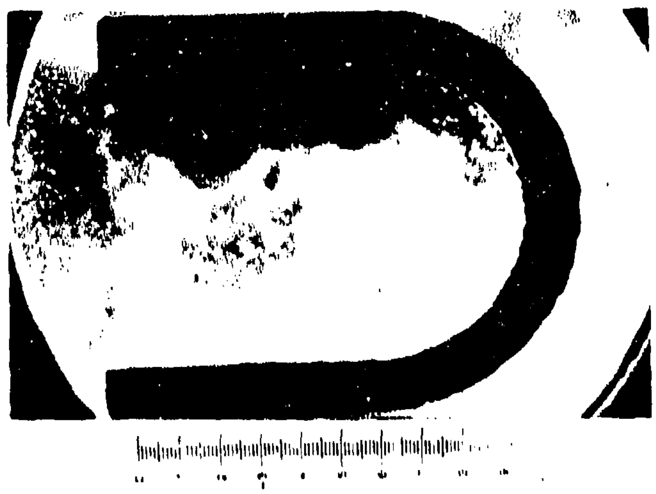

Plate No. 1-4719

a) One Inch Scale

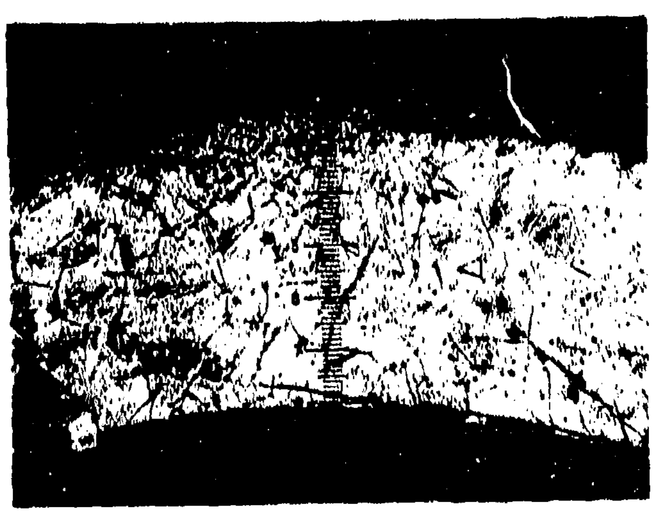

Plate No. 1-7766

b) 1.97 Mils per Small Division, Etched with 15 Glycerine $5HNO_3$ $5HCl$ 3HF, Hot Face at Top

Figure 339. Model Hf-20Ta-2Mo(I-23)-4-19, Run#1, Sting #4.

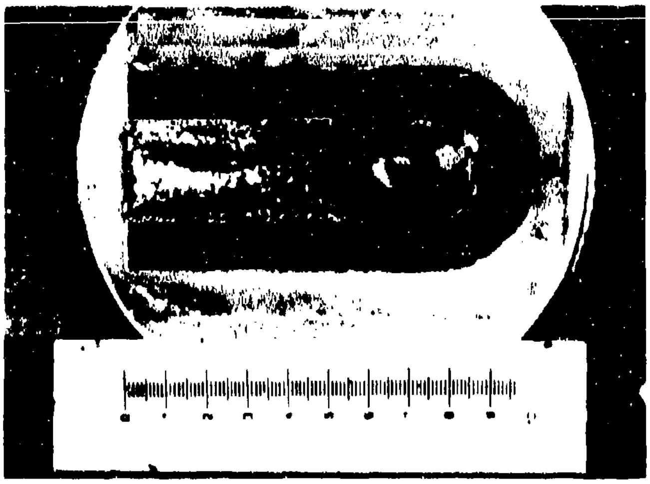

Plate No. 1-4716
a) One Inch Scale

Plate No. 1-5335
b) X200, Etched with Murakami's Reagent Hot Interface at Top

Figure 340. Model W(Uncoated) (G-18)-X-11, Run #1, Sting #5.

Plate No. 1-4698
a) One Inch Scale

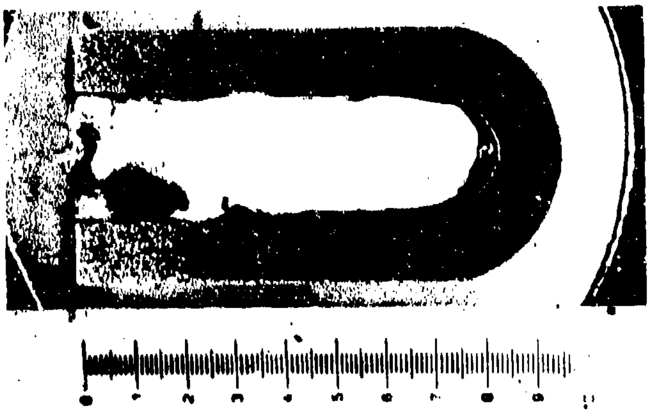

Plate No. 1-4705
b) One Inch Scale

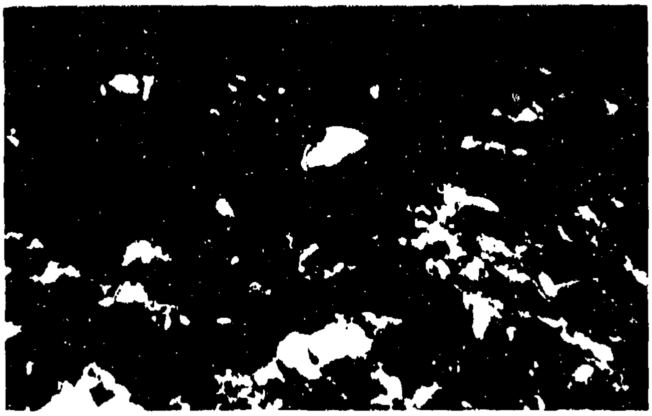

Plate No. 1-4706
c) X250, Unetched.
Hot Interface at Top

Figure 341. a) Model RVA(B-5)-X-5, Run #1, Sting #6.
b & c) Model JTA(D-13)-X-7, Run #1, Sting #7.

Plate No. 1-4718

a) One Inch Scale

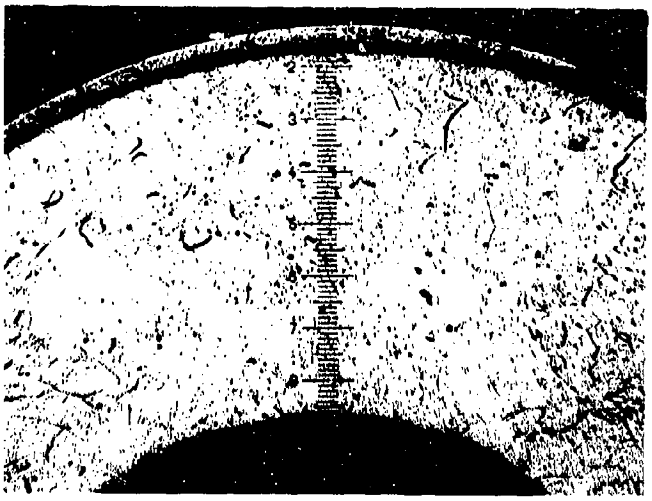

Plate No. 1-7765

b) 1.97 Mils per Small Division, Etched with 15 Glycerine $5HNO_3$ $5HCl$ 3HF. Hot Face at top.

Plate No. 1-7763

c) X500, Etched, Interface of Suboxide (Top) and Matrix.

Figure 342. Model Hf-20Ta-2Mo(I-23)-1-12, Run #2, Sting #1.

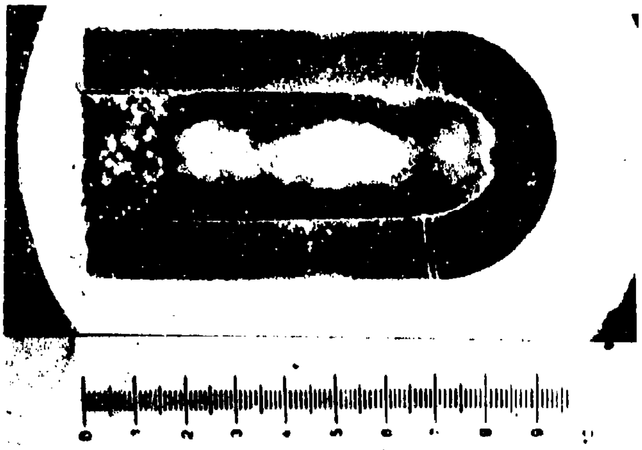

Plate No. 1-4688
a) One Inch Scale

Plate No. 1-4689
b) X250, Etched with 10 Glycerine $5HNO_3$ 3HF. Hot Interface at Top

Figure 343. Model $HfB_{2.1}$(A-2)-X-1, Run #2, Sting #2.

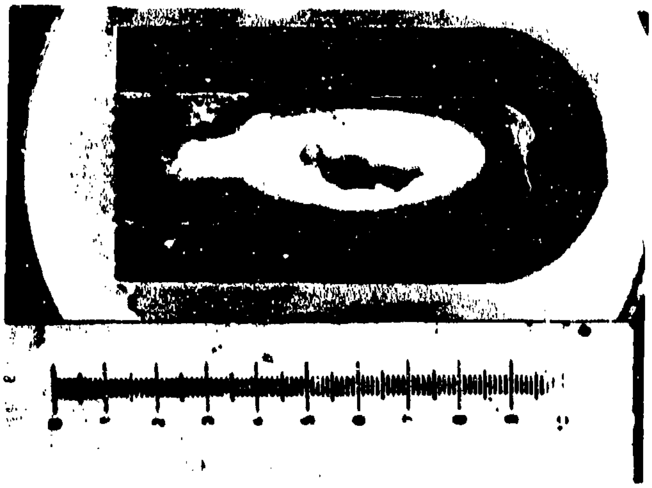

Plate No. 1-4694
a) One Inch Scale

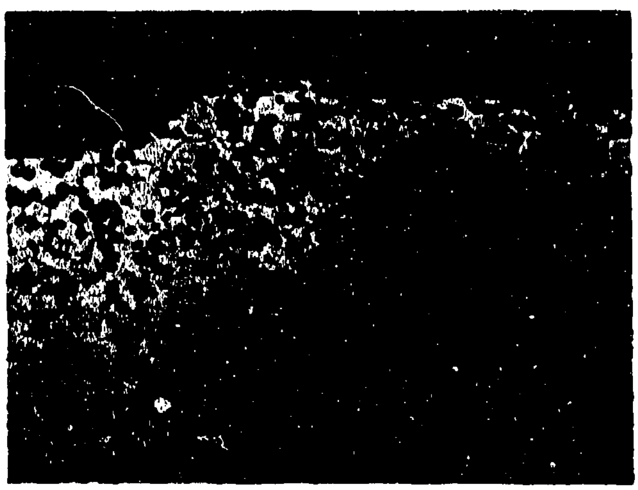

Plate NO. 1-4695
b) X250, Etched with 10 Glycerine $5HNO_3$ 3HF. Hot Interface at Top

Figure 344. Model HfB_2 + SiC(A-4)-X-4, Run #2, Sting #3.

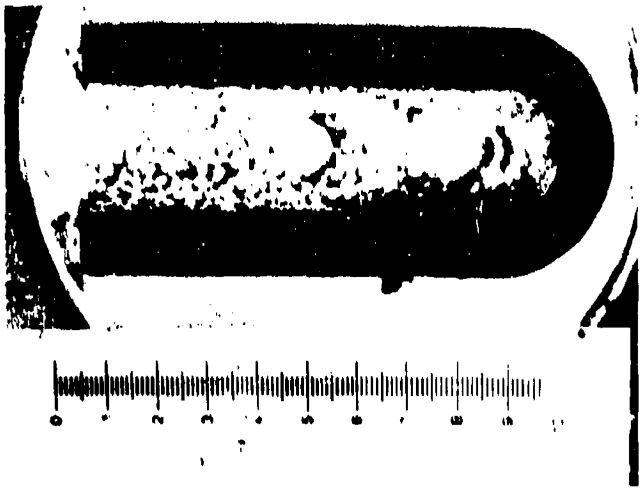

Plate No. 1-4701
a) One Inch Scale

Plate No. 1-4703
b) One Inch Scale

Figure 345. a) Model PG(B-6)-X-6, Run #2, Sting #4.
b) Model BPG(B-7)-X-16, Run #2, Sting #5.

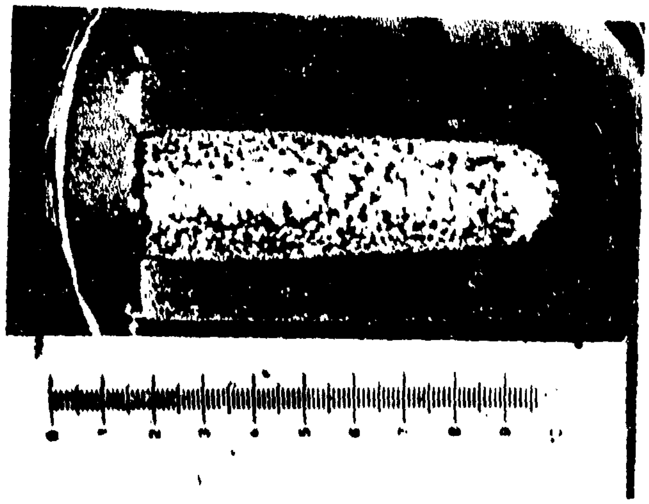

Plate No. 1-4713
a) One Inch Scale

Plate No. 1-4714
b) X250, Unetched.
Hot Interface at Top.

Figure 346. Model JT0981(F-16)-X-10, Run #2, Sting #6.

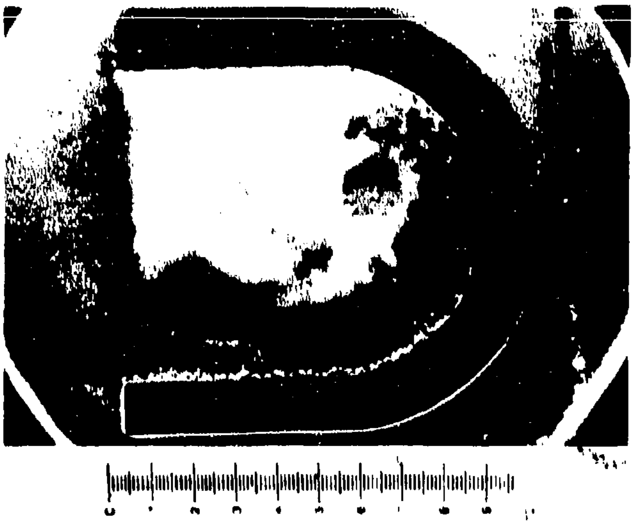

Plate No. 1-4717
a) One Inch Scale

Plate No. 1-5341
b) X250, Unetched.
Hot Interface at Top.

Figure 347. Model Sn-Al/Ta-W(G-19)-3-22, Run #2, Sting #8.

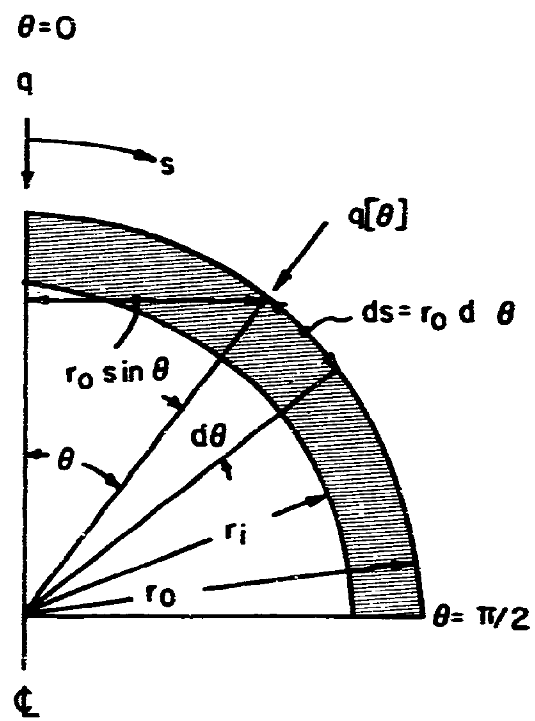

Figure 348. Geometrical Definitions for Analysis of Conduction Losses Through a Hemispherical Shell.

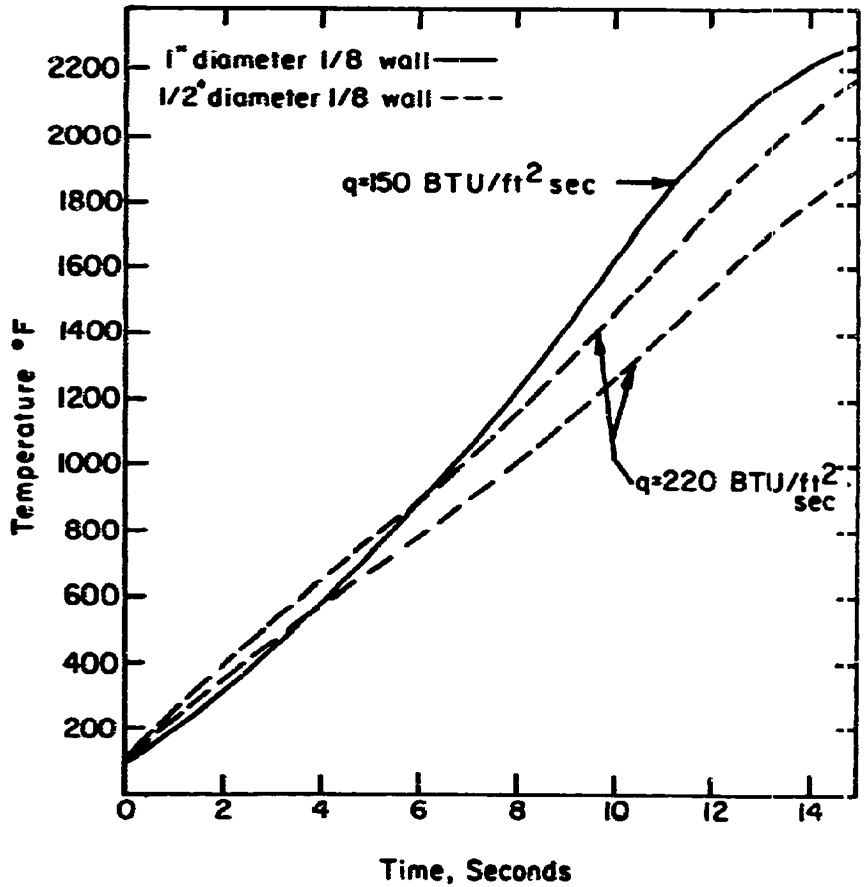

Figure 349. Temperature Response for Hemispherical Shells of 1020 Steel Exposed under Flux-Conductivity Conditions to Simulated Wave Superheater Tests.

TABLE 1

LIST OF CANDIDATE MATERIALS

Material	Code	Supplier
$HfB_{2.1}$	A-2	Carborundum Co., Niagara Falls, New York
ZrB_2	A-3	Carborundum Co., Niagara Falls, New York
HfB_2 + 20v/o SiC	A-4	Carborundum Co., Niagara Falls, New York
Boride Z	A-5	Carborundum Co., Niagara Falls, New York
$HfB_{2.1}$	A-6	ManLabs-Avco AF33(615)-3671
$HfB_{2.1}$ + 20v/o SiC	A-7	ManLabs-Avco AF33(615)-3671
$ZrB_{2.1}$ + 20 v/o SiC	A-8	ManLabs-Avco AF33(615)-3671
$HfB_{2.1}$ + 35 v/o SiC	A-9	ManLabs-Avco AF33(615)-3671
ZrB_2 + 14v/o SiC + 30 v/o C	A-10	ManLabs-Avco AF33(615)-3671
RVA	B-5	Union Carbide Corp., New York, New York
PG	B-6	General Electric Co., Detroit, Michigan
BPG	B-7	High Temperature Materials, Lowell, Mass.
Si/RVC	B-8	Union Carbide Corp., New York, New York
PT0178	B-9	Union Carbide Corp., New York, New York
Poco Graphite (AXF-5Q)	B-10	Poco Graphite Inc., Garland, Texas
Glassy Carbon	B-11	Lockheed M&SC, Palo Alto, California
HfC + C	C-11	Battelle Memorial Institute, Columbus, Ohio
ZrC + C	C-12	Battelle Memorial Institute, Columbus, Ohio
JTA (C-ZrB_2-SiC)	D-13	Union Carbide Corp., New York, New York
KT-SiC	E-14	Carborundum Co., Niagara Falls, New York
JT0992 (C-HfC-SiC)	F-15	Union Carbide Corp., New York, New York
JT0981 (C-ZrC-SiC)	F-16	Union Carbide Corp. New York, New York
WSi_2/W	G-18	General Electric Co., Cleveland, Ohio (Type MK-W)
		TRW, Cleveland, Ohio (WSi_2 coating)
Sn-Al/Ta-W	G-19	National Research Corp., Newton, Mass. (Ta-10W)
		GT&E, Hicksville, New York (Sn-Al coating)
		Rocketdyne, Canoga Park, California
W-Zr-Cu	G-20	Wah Chang Corp., Albany, Oregon
W-Ag	G-21	Bjorksten Research Labs, Madison, Wisconsin
SiO_2 + 68.5 w/o W	H-22	General Electric Co., Willoughby, Ohio
SiO_2 + 60 w/o W	H-23	General Electric Co., Willoughby, Ohio
SiO_2 + 35 w/o W	H-24	Wah Chang Corp., Albany, Oregon
Hf-20Ta-2Mo	I-23	Battelle Memorial Institute, Columbus, Ohio
Ir/Graphite	I-24	General Technologies Corp., Reston, Virginia

TABLE 2

SUMMARY OF ARC PLASMA EXPOSURES OF $HfB_{2.1}$(A-2)

Material: Sample No. Assumed Emittance at λ = 0.65μ	Mach No.	P_o atm	i_e BTU/lb	D (in)	q_{cw} BTU/ft² sec	T_B °R obs	q_r Surface Radiation BTU/ft² sec	ϵ_N Computed Normal Emittance	Initial Length/Thickness (mils)	Final Length*/Thickness (mils)	Exposure Time (seconds)	Calculated Temperature Ratio T(CALC)/T(OBS): Cold Wall Heat Transfer Coefficient	Fay and Riddell Heat Transfer Coefficient
$HfB_{2.1}$(A-2) ϵ = 0.50													
-1M	0.32	1.06	3270	0.500	820	4610	73	0.34	959/629	962/608	1800	1.13	1.19
-2M	0.36	1.08	5020	0.500	730	5645	208	0.44	930/585	973/516	1830	1.08	1.12
-3M	0.38	1.09	6185	0.500	1060	6640	363	0.37	868/542	.../281	82	1.00	1.06
-4M	0.38	1.09	5570	0.500	760	5885	129	0.23	890/557	667/286	1830	1.08	1.10
-5M	0.37	1.09	4735	0.500	900	6400	94	0.12	925/593	.../145	221	0.94	1.03
	220 mil disk thermal shocked off initially								220 mil disk thermal shocked off				
-6M	0.39	1.10	5635	0.500	910	5840	169	0.31	889/562	.../282	1830	1.09	1.15
	160 mil disk thermal shocked off initially								160 mil disk thermal shocked off initially				
-7R†	3.2	0.074	9470	0.500	492	5000	111	0.38	923/612	929/599	1800	1.24	1.28
-8R†	3.2	0.158	7260	0.500	772	....	...		903/563	.../560	14		
	thermal shock failure								thermal shock failure				
-9R†	3.2	0.158	7030	0.496	772	5995	299	0.49	902/553	732/412	60	1.02	1.13
-10R†	3.2	0.158	7260	0.500	781	5870	263	0.47	902/528	534/174	60	1.06	1.17
-11R†	3.2	0.097	10730	0.500	651	5640	329	0.69	940/605	962/566	1800	1.17	1.22
-12R†	3.2	0.095	9830	0.500	573	5245	197	0.55	936/594	957/583	1800	1.23	1.27
-13M-1	0.30	1.05	2765	0.500	465	4660	74	0.33	801/809	-/-	600	1.11	1.04
-13M-2	0.30	1.05	2765	0.500	465	4670	87	0.39	-/-	-/-	600	1.11	1.04
-13M-3	0.30	1.05	2765	0.500	465	4975	124	0.43	-/-	807/489	600	1.04	0.98
-14M-1	0.30	1.05	3870	0.500	510	5180	105	0.33	874/874	-/-	600	1.11	1.07
-14M-2	0.30	1.05	3870	0.500	510	5380	130	0.33	-/-	-/-	600	1.05	1.02
-14M-3	0.30	1.05	3870	0.500	510	5500	195	0.45	-/-	611/854	600	1.03	1.00
-15M-1	0.21	1.03	2835	0.500	365	3390	41	0.66	808/809	-/-	600	1.48	1.41
-15M-2	0.21	1.03	2835	0.500	365	3555	37	0.49	-/-	-/-	600	1.41	1.35
-15M-3	0.21	1.03	2835	0.500	365	3635	51	0.48	-/-	809/805	600	1.38	1.32
-16M*	0.21	1.03	4930	0.507	585	5865	291	0.52	828/803	849/482	1800	1.03	0.99
-17M*	0.30	1.05	4520	0.507	725	6700	431	0.46	859/825	364/356	90	0.92	0.86
-18MA*	0.33	1.07	4690	0.504	665	6685	483	0.45	826/806	-/-	70	0.92	0.88
-18MB*	0.33	1.07	4690	0.504	665	5695	287	0.58	-/-	308/208	1730	1.08	1.04

*Preoxidized 10 minutes at 1930°C.

†Transmissivity factor equals 0.86 for sapphire window.

*Final length refers to measurement after exposure, thickness refers to measurement after sectioning.

Material Sample No.	T °F	Gross Recession Mils	Material Recession Mils	Degradation Mode	Exposure Time seconds	Recession Rate* (Mils) (30 Min)	Description of Motion Picture Film Coverage
$HfB_{2.1}$ (A-2)							
-1M	4150	-3	21	Oxidation	1800	21	little activity, uniform oxidation, crack formed in oxide coating
-2M	5185	-43	29	Oxidation	1830	29	front face showed cold core, hot oxide rim, sunburst formation
-3M	6200	...	261	Melting	82	5742	uniform melting undercutting of sides
-4M	5425	225	271	Oxidation	1830	266	sunburst formation, oxide melting
-5M	5940	...	(220)	Th. Shock + Melting	221	1792	oxidation, thermal shock of disk followed by uniform melting
-6M	5380	...	(120)	Th. Shock+Oxid.	1830	118	initial oxidation followed by thermal shock
-7R	4540	-6	13	Oxidation	1800	13	speckled surface on heating, little activity
-8R	....	...	...	Th. Shock	14	....	thermal shock failure
-9R	5535	170	141	Melting	60	4028	melting from center to edges
-10R	5410	360	384	Melting	60	11520	rapid melting and recession
-11R	5180	-82	39	Oxidation	1800	39	oxide melting, uniform oxidation
-12R	4785	-21	11	Oxidation	1800	11	oxide melting, uniform oxidation
-13M-1	4200			Oxidation	600		Speckled front face, center appeared hotter than edges.
-13M-2	4210			Oxidation	600		Initial oxide breaking off in spots, center core still apparent.
-13M-3	4515	-6	20	Oxidation	600	20	Center core, oxide breaking off edges, some melting of oxide.
-14M-1	4640			Oxidation	600		Speckled front face, center core hotter than edges.
-14M-2	4920			Oxidation	600		Initial oxide breaking off front face.
-14M-3	5040	-37	20	Oxidation	600	20	Slight melting of oxide layer which appeared to be barely hanging onto front face.
-15M-1	2930			Oxidation	600		Little activity, hotter center core.
-15M-2	3095			Oxidation	600		Little activity, uniform appearance.
-15M-3	3175	-1	4	Oxidation	600	4	Little activity.
-16M	5405	-24	51	Oxidation	1800	51	Pre-oxide flaking off sides, edge melting, sunburst formation.
-17M	6240	195	169	Melting	90	3380	Oxide melted, burned off, material melted.
-18MA	6225	...	...	Melting	70	...	Oxide melted, burned off, material melted, solidified
-18MB	5235	224	304	Oxidation	1730	304	in sunburst.

*Recession rates converted to 30 minutes on linear basis.

TABLE 3

SUMMARY OF ARC PLASMA EXPOSURES OF ZrB_2(A-3)

Material Sample No. Assumed Emittance at λ = 0.65μ	Mach No.	P_e atm	i_e BTU/lb	D (in)	q_{cw} BTU/ft²sec	T °R obs	q_r Surface Radiation BTU/ft² sec	ϵ_N Computed Normal Emittance	Initial Length/Thickness (mils)	Final Length*/Thickness (mils)	Exposure Time (seconds)	Calculated Temperature Ratio T(CALC)/T(OBS) Cold Wall Heat Transfer Coefficient	Fay and Riddell Heat Transfer Coefficient
ZrB_2(A-3) ϵ = 0.57													
-3M	0.52	1.17	5945	0.492	860	6125	210	0.32	1063/1063	742/733	84	1.06	1.06
-4M	0.33	1.07	3990	0.492	560	4965	114	0.40	1062/1062	1061/1048	1860	1.14	1.10
-17M	0.35	1.07	3215	0.492	348	4170	31	0.22	1052/1052	1063/1047	1860	1.20	1.22
-20M	0.42	1.11	4665	0.492	840	6035	177	0.28	1059/1059	877/855	90	1.03	0.97
-24M	0.35	1.07	5375	0.492	750	5355	208	0.54	1057/1057	1076/1028	1860	1.17	1.13
-23M	0.32	1.06	3345	0.493	460	4475	51	0.27	1048/1048	1055/1040	1860	1.18	1.15
-10R†	3.2	0.021	9530	0.491	520	4835	103*	0.40	1045/1045	1057/1027	1802	1.30	1.09
-2R†	3.2	0.014	14860	0.491	327	5000	152*	0.52	1052/1052	1042/1004	1800	1.17	1.12
-5R†	3.2	0.012	13470	0.491	256	5120	132*	0.41	1062/1062	----/1025	1800	1.08	1.06
-30R†	3.2	0.063	9380	0.491	458	5655	328*	0.68	1066/1066	896/850	1464	1.09	1.05
-11R†	3.2	0.187	9270	0.491	950	5940	171*	0.29	1063/1063	722/720	51	1.21	1.12
-15R†	3.2	0.168	8500	0.491	790	5780	289*	0.54	1069/1069	579/589	98	1.18	1.10
-50M	0.30	1.05	3368	0.750	388	4670	110	0.49	733/720	732/717	1800	1.09	1.06
-51M	0.32	1.06	4535	0.750	475	4875	170	0.64	718/713	737/703	1800	1.18	1.13
-52M-1	0.30	1.05	2765	0.426	465	5000	215	0.69	297/291	---/---	600	1.00	0.98
-52M-2	0.30	1.05	2765	0.426	465	4975	195	0.68	---/---	---/---	600	1.02	0.97
-52M-3	0.30	1.05	2765	0.426	465	5320	222	0.59	---/---	---/245	600	0.96	0.91
-53M-1	0.30	1.05	3070	0.426	510	5285	185	0.50	308/310	---/---	600	1.05	1.03
-53M-2	0.30	1.05	3070	0.426	510	5610	152	0.33	---/---	---/---	600	0.99	0.97
-53M-3	0.30	1.05	3070	0.426	510	5565	264	0.54	---/---	353/231	600	0.99	0.98
-54M-1	0.21	1.03	2835	0.426	365	4375	83	0.48	303/289	---/---	600	1.13	1.09
-54M-2	0.21	1.03	2835	0.426	365	4555	45	0.22	---/---	---/---	600	1.08	1.04
-54M-3	0.21	1.03	2835	0.426	365	4760	85	0.35	---/---	332/280	600	1.04	1.00
-1MC	0.31	1.06	4540	0.491	475	5150	113	0.34	421/104	---/ 71	1800	1.09	1.11
-2MC	0.29	1.05	3230	0.491	365	4930	176	0.63	422/101	---/ 87	1800	1.03	1.02
-3MC	0.31	1.06	3380	0.491	460	5170	236	0.70	429/102	448/ 71	1800	1.03	0.99
-4MC	0.33	1.07	4560	0.491	610	6340	404	0.53	424/104	---/ 0	64	0.93	0.90

†Transmissivity factor equals 0.86 for sapphire window.
*Surface radiation values may be low due to requirements for critical alignment caused by utilization of one-half inch diameter sample.

* Final Length is based on measurement prior to sectioning, thickness refers to length after sectioning.

Material Sample No.	T °F	Gross Recession mils	Material Recession mils	Degradation Mode	Exposure Time seconds	Recession Rate* (mils)/(30 min)	Description of Motion Picture Film Coverage
ZrB_2 (A-3)							
-3M	5665	321	330	Melting	84	7062	boride melting
-4M	4505	1	14	Oxidation	1860	15	solid oxide, little activity, few liquid drops, sunburst
-17M	3710	-11	5	Oxidation	1860	5	
-20M	5575	182	204	Melting	90	4080	boride melting
-24M	4095	-19	29	Oxidation	1860	28	oxide melting, sunburst formation
-23M	4015	-7	8	Oxidation	1860	8	oxide solid, little activity noted
-10R	4375	-12	18	Oxidation	1802	18	uniform oxidation
-2R	4640	10	48	Oxidation	1800	48	uniform oxidation, some liquid bubbles
-5R	4660	---	37	Oxidation	1800	37	uniform oxidation, little activity
-30R	5195	170	216	Oxid. + Melting	1464	266	Initial oxidation followed by uniform melting
-11R	5480	341	335	Melting	51	11825	uniform melting, rapid recession
-15R	5320	490	480	Melting	98	8816	uniform melting, recession
-50M	4210	1	3	Oxidation	1800	3	Hot oxide spot developed in center, then rest of front face giving mottled appearance.
-51M	4415	-19	10	Oxidation	1800	10	Little activity, mottled appearance of oxide.
-52M-1	4620			Oxidation	600		Slight melting at edges, heavy oxide flaked off front face.
-52M-2	4515			Oxidation	600		Initial oxide broke away, new oxide formed and broke away, edges melting.
-52M-3	4060		46	Oxidation	600	46	Sunburst formed, slight melting, no further flaking.
-53M-1	4825			Oxidation	600		Melting, sunburst formation.
-53M-2	5150			Oxidation	600		Initial oxide broke away, melting and sunburst formation followed.
-53M-3	5105	-45	79	Oxidation	600	79	Oxide broke off again, melting and sunburst formation followed as before.
-54M-1	3915			Oxidation	600		Sunburst formation, oxide melting.
-54M-2	4095			Oxidation	600		Little activity.
-54M-3	4300	-29	9	Oxidation	600	9	No film coverage.
- 1MC	4690	---	33	Oxidation	1800	33	Speckled front face, some oxide melting.
- 2MC	4470	---	14	Oxidation	1800	16	Oxide chipping and melting off front face giving mottled appearance.
- 3MC	4710	-19	31	Oxidation	1800	31	Oxide chipping and melting, uniform oxide buildup with some melting at edges.
- 4MC	5880	---	104	Melting	64	2870	Rapid melting.

*Recession rate converted to 30 minutes on linear basis.

TABLE 4

SUMMARY OF ARC PLASMA EXPOSURES OF HfB_2 + SiC(A-4)

Material Sample No. Assumed Emittance at λ = 0.65μ	Mach No.	P_e atm	i_e BTU/lb	D (in)	q_{cw} BTU/ft^2 sec	T °R obs	q_r Surface Radiation BTU/ft^2 sec	ϵ_N Computed Normal Emittance	Initial Length/thickness (mils)	Final Length*/thickness (mils)	Exposure Time (seconds)	Calculated Temperature Ratio T(CALC)/T(OBS): Cold Wall Heat Transfer Coefficient	Calculated Temperature Ratio T(CALC)/T(OBS): Fay and Riddell Heat Transfer Coefficient
HfB_2 + SiC (A-4) ϵ = 0.60													
-1M	0.35	1.08	3915	0.505	570	3910	51	0.47	966/686	968/680	1830	1.44	1.38
-2M	0.36	1.08	5105	0.505	670	5480	208	0.49	999/675	986/643	1830	1.10	1.08
-3M	0.38	1.09	6510	0.505	930	6080	260	0.40	989/674	610/277	139	1.09	1.06
-4M	0.36	1.08	5410	0.505	900	5620	203	0.43	959/644	507/175	1608	1.14	1.07
-2-1M	0.42	1.11	6245	0.477	935	6405	390	0.49	1108/776	848/505	1100	1.03	1.00
-2-2M	0.31	1.06	3435	0.487	510	3630	58	0.71	1107/790	1111/787	1830	1.48	1.41
-2-3M	0.35	1.08	5365	0.474	680	5250	192	0.54	1109/772	944/639	1830	1.16	1.15
-2-4M	0.38	1.09	5565	0.477	915	5650	333	0.69	1112/787	947/600	1830	1.14	1.09
-2-5M	0.38	1.09	6715	0.477	1005	6370	434	0.56	1103/770	534/211	120	1.05	1.00
-2-6R⁺	3.2	0.023	11400	0.478	506	5650	271	0.56	1102/780	1117/767	1800	1.10	0.98
-2-7R⁺	3.2	0.026	17040	0.475	610	5760	355	0.68	1109/791	1116/767	1800	1.16	1.09
-2-8R⁺	3.2	0.027	13540	0.478	700	5940	408	0.70	1103/781	1087/738	1800	1.15	0.97
-2-9R⁺	3.2	0.023	8920	0.475	402	5140	211	0.64	1105/765	1113/742	1800	1.14	1.01
-2-10R⁺	3.2	0.022	7560	0.488	314	3540	59	0.80	1099/773	1100/770	1800	1.55	1.38

⁺Transmissivity factor equals 0.86 for sapphire window.

*Final length is based on measurement prior to sectioning; thickness refers to length after sectioning.

Material Sample No.	T °F	Gross Recession mils	Material Recession mils	Degradation Mode	Exposure Time seconds	Recession Rate* mils/sec / mils/30 min	Description of Motion Picture Film Coverage
HfB_2 + SiC (A-4)							
-1M	3450	-2	6	Oxidation	1830	----/6	surface activity, liquid bubbles at edges
-2M	5020	13	32	Oxidation	1830	----/31	liquid oxide formation
-3M	5620	389	397	Melting	139	----/5141	liquid oxide, composite melting
-4M	5160	459	469	Oxid + Melt	1608	----/525	liquid oxide, sunburst formation, melting, some flaking off of oxide
-2-1M	5945	260	271	Oxidation	1100	----/444	initial oxide melting, erosion at angle to face, solid oxide formed
-2-2M	3170	-4	3	Oxidation	1830	----/3	
-2-3M	4790	165	133	Oxidation	1830	----/131	initial oxide melting, erosion at angle to face, solid oxide formed
-2-4M	5190	165	187	Oxidation	1830	----/184	heated from top towards bottom, liquid oxide, erosion at angle, sunburst formation
-2-5M	5810	569	559	Melting	120	----/8385	rapid oxide melting, recession at angle, sunburst formation
-2-6R	5190	-15	13	Oxidation	1800	----/13	
-2-7R	5300	-7	24	Oxidation	1800	----/24	
-2-8R	5480	16	43	Oxidation	1800	----/43	
-2-9R	4680	-8	23	Oxidation	1800	----/23	
-2-10R	3080	-1	3	Oxidation	1800	----/3	

*Recession rate converted to 30 minutes on linear basis.

TABLE 5

SUMMARY OF ARC PLASMA EXPOSURES OF BORIDE Z (A-5)

Material Sample No. Assumed Emittance at $\lambda = 0.65\mu$	Mach No.	P_e atm	i_e BTU/lb	D (in)	q_{cw} BTU/ft²sec	T °R obs	q_r Surface Radiation BTU/ft²sec	ϵ_N Computed Normal Emittance	Initial Length/thickness (mils)	Final Length*/thickness (mils)	Exposure Time (seconds)	Calculated Temperature Ratio T(CALC)/T(OBS) Cold Wall Heat Transfer Coefficient	Calculated Temperature Ratio T(CALC)/T(OBS) Fay and Riddell Heat Transfer Coefficient
Boride Z (A-5) $\epsilon = 0.60$													
-1M	0.30	1.05	3660	0.490	370	4515	116	0.59	723/679	725/676	970	1.14	1.16
-2M	0.54	1.19	4525	0.485	890	----	---	----	695/670	---/653	11	---	----
-3M	0.32	1.06	3005	0.482	410	4405	---	----	674/639	680/617	1830	1.14	1.11
-4M	0.30	1.05	2500	0.490	350	3380	39	0.64	705/663	705/659	1830	1.40	1.35
-5M	0.36	1.08	5075	0.485	700	5605	356	0.77	736/690	----/505	33	1.08	1.06
-6M	0.42	1.11	4875	0.485	660	5710	335	0.67	719/695	----/603	40	1.05	1.04
-7R+	3.2	0.025	12120	0.491	539	5630	359	0.76	1037/703	768/469	1800	1.14	1.01
-8R+	3.2	0.018	9200	0.482	262	4250	112	0.73	1028/690	1051/680	1800	1.26	1.19
-9R+	3.2	0.011	10410	0.482	192	3080	43	1.02	1036/675	1037/665	1800	1.64	1.61
-11R+	3.2	0.031	14450	0.490	701	5620	250	0.55	1030/697	530/210	100	1.22	1.09
-10R+	3.2	0.017	11620	0.485	389	5490	312	0.73	1027/697	1045/---	1800	1.08	0.98
-12R+	3.2	0.011	13860	0.490	316	5335	306	0.80	1032/670	1058/---	1800	1.07	1.00

+Transmissivity factor equals 0.86 for sapphire window.

* Final Length is based on measurement prior to sectioning, thickness refers to length after sectioning.

Material Sample No.	T °F	Gross Recession mils	Material Recession mils	Degradation Mode	Exposure Time seconds	Recession Rate* (mils)/(30 min)	Description of Motion Picture Film Coverage
Boride Z (A-5)							
-1M	4055	-2	3	Oxidation	970	6	little oxidation
-2M	----	---	17	Th. Shock	11	-----	immediate thermal shock failure
-3M	3945	-6	22	Oxidation	1830	22	little oxidation
-4M	2920	0	4	Oxidation	1830	4	little oxidation
-5M	5145	---	185	Th. Shock	33	-----	specimen cracked, liquid oxide formed, spallation
-6M	5250	---	92	Th. Shock	40	-----	specimen cracked, liquid oxide formed, spallation
-7R	5170	269	234	Oxidation	1800	234	
-8R	3790	-23	10	Oxidation	1880	10	
-9R	2620	-1	10	Oxidation	1800	10	
-11R	5160	500	487	Melting	100	8770	
-10R	5030	-18	---	Th. Shock+Oxid	1800	----/----	radial crack 1/4" from face, little activity
-12R	4875	-26	---	Th. Shock+Oxid	1800	----/----	thermal shock of front face on heat-up, chipped non-uniformly, radial crack 1/4" from front, little activity

*Recession rates converted to 30 minutes on linear basis.

TABLE 6

SUMMARY OF ARC PLASMA EXPOSURES OF HfB_2 + 20% SiC (A-7)

Material Sample No. Assumed Emittance at $\lambda = 0.65\mu$	Mach No.	P_e atm	i_e BTU/lb	D (in)	q_{cw} BTU/ft^2sec	T ^oR obs	q_r Surface Radiation BTU/ft^2sec	ϵ_N Computed Normal Emittance	Initial Length/ Thickness (mils)	Final Length'/ Thickness (mils)	Exposure Time (seconds)	Calculated Temperature Ratio T(CALC/T(OBS) Cold Wall Heat Transfer Coefficient	Fay and Riddell Heat Transfer Coefficient
$HfB_{2.1}$ + 20v/o SiC(A-7)													
ϵ = 0.60													
-1M	0.42	1.11	9690	0.488	810	6220	336	0.48	540/523	---/413	56	1.02	1.00
-2M	0.36	1.08	5055	0.488	715	5260	224	0.62	535/520	---/363	1740	1.16	1.12
-3MA	0.39	1.09	2970	0.488	665	6055	318	0.50	552/544	---/444+	200	0.89	0.82
-3MB	0.39	1.09	2970	0.488	665	5205	198	0.57	---/---	420/363	1600	1.04	0.95
-4M	0.36	1.08	5200	0.488	755	5340	230	0.60	537/536	---/309	1800	1.16	1.12
-5MA*	0.15	1.01	5010	0.435	655	6405	335	0.42	936/926	---/---	50	0.93	0.86
-5MB*	0.15	1.01	5010	0.435	655	5490	112	0.26	---/---	710/640	1750	1.09	1.00
-6M*	0.71	1.34	3390	0.430	750	5595	246	0.53	912/909	849/811	264	1.02	0.98
-7MA*	0.15	1.01	6210	0.431	740	6595	318	0.36	916/921	---/---	30	0.96	0.90
-7MB*	0.15	1.01	6210	0.431	740	5560	57	0.13	---/---	592/539	1750	1.13	1.06
-23MI	0.33	1.06	4380	0.429	627	5420	209	0.51	923/922	---/---	1800	1.07	1.04
-23MII	0.33	1.06	4550	0.429	583	5470	214	0.51	---/---	---/---	1800	1.06	1.05
-23MIII	0.33	1.06	4530	0.429	583	5500	212	0.49	---/---	---/---	1600	1.05	1.04
-23MIV	0.33	1.06	4370	0.429	603	5700	250	0.50	---/---	789/729	1800	1.01	0.99
-24MI	0.36	1.07	3980	0.427	550	5170	198	0.59	895/883	---/---	1800	1.08	1.07
-24MII	0.36	1.08	3970	0.427	553	5365	233	0.60	---/---	---/---	1800	1.04	1.03
-24MIII	0.36	1.07	3950	0.427	561	5400	226	0.57	---/---	---/---	1800	1.04	1.02
-24MIV	0.36	1.08	3950	0.427	571	5365	214	0.55	---/---	792/728	1800	1.05	1.03
-25MI	0.24	1.03	4890	0.426	498	4945	169	0.60	925/921	---/---	1800	1.15	1.16
-25MII	0.27	1.04	4700	0.426	505	5090	156	0.49	---/---	---/---	1418	1.11	1.12
-25MIII	0.28	1.04	4960	0.426	487	5215	193	0.55	---/---	---/---	1800	1.0A	1.12
-25MIV	0.27	1.04	4910	0.426	495	5390	219	0.55	---/---	---/---	1800	1.05	1.08
-25MV	0.27	1.04	4610	0.426	498	5435	197	0.48	---/---	---/---	1800	1.03	1.05
-25MVI	0.26	1.04	4350	0.426	513	5435	211	0.51	---/---	---/---	1800	1.03	1.02
-25MVII	0.27	1.04	4780	0.426	508	5435	196	0.48	---/---	---/---	1800	1.04	1.06
-25MVIII	0.26	1.04	4420	0.426	507	5500	226	0.52	---/---	---/---	1800	1.03	1.02
-25MIX	0.27	1.04	4520	0.426	518	5585	235	0.51	---/---	---/---	1800	1.01	1.01
-25MX	0.26	1.04	4500	0.426	493	5700	262	0.53	---/---	---/---	1800	0.98	0.99
-25MXI	0.26	1.04	4500	0.426	483	5710	262	0.52	---/---	469/332	1800	0.97	0.98
-30M	0.25	1.03	5030	0.437	587	5375	216	0.55	666/664	322/321	1800	1.09	1.08
-31M	0.15	1.01	5580	0.438	487	4650	110	0.50	686/685	---/260	1800	1.23	1.23
-32M	0.21	1.02	5740	0.438	618	5615	253	0.54	687/687	576/516	1800	1.07	1.06
-36MH	0.21	1.02	3500	0.437	513	4370	85	0.19	699/107⁰	---/94⁰	1081	1.23	1.16
-37MH	0.21	1.02	3640	0.438	495	4225	80	0.53	690/405⁰	---/395⁰	1080	1.28	1.21
-40M	0.26	1.04	4390	0.438	495	4665	125	0.56	689/96⁰	---/82⁰	1800	1.19	1.19
-41M	0.27	1.04	4400	0.438	502	5000	150	0.51	687/392⁰	---/335⁰	1800	1.12	1.12
-44MS	0.26	1.04	4360	0.437	493	3250	36	0.69	684/93⁰	684/93	1800	1.71	1.71
-45MS	0.26	1.04	4580	0.437	522	3345	46	0.78	690/395⁰	690/395	1800	1.69	1.68

* Preoxidized samples

' Final length refers to sample length prior to sectioning; thickness refers to section length.

+ Estimated.

⁰ Nose to in-depth temperature measurement station.

Material Sample No.	T ^oF	Gross Recession (mils)	Material Recession (mils)	Degradation Mode	Exposure Time seconds	Recession Rate* mils/30 min	Description of Motion Picture Film Coverage
$HfB_{2.1}$ + 20% SiC (A-7)							
-1M	5760	---	110	Melting	56	3530	Sunburst formed, rapid melting at angle.
-2M	4800	---	157	Melt. + Oxid.	1740	162	Gradual heatup, rapid melting, solidified in sunburst.
-3MA	5595	---	100+	Melting	200	900+	Sunburst formed, oxide melting.
-3MB	4745	---	81+	Oxidation	1600	91+	Solidified sunburst, little change.
-4M	4880	---	227	Melt. + Oxid.	1800	227	Rapid melting, solidified in sunburst, little change.
-5MA	5945	---	---	Melting	50	----	Rapid melting, rapid recession.
-5MB	5030	236	286	Oxidation	1750	286	Solidified in sunburst.
-6M	5135	63	98	Oxid. + Melt.	264	668	Rotating and vibrating of sample, continuous oxide melting.
-7MA	6135	---	---	Melting	50	----	Rapid melting.
-7MB	5100	326	382	Oxidation	1750	382	Solidified in sunburst.
-23MI	4960	---	---	Melt. + Oxid.	1800	----	Rapid melting, solidified in sunburst, little activity.
-23MII	5010	---	---	Oxidation	1600	----	Intact from cycle I.
-23MIII	5040	---	---	Oxidation	1800	----	Intact from cycle II.
-23MIV	5240	134	193	Oxidation	1800	48	Intact from cycle III, some oxide chipped away.
-24MI	4710	---	---	Melt. + Oxid.	1800	----	Melting, solidified in sunburst, little activity.
-24MII	4905	---	---	Oxidation	1800	----	Intact from cycle I.
-24MIII	4940	---	---	Oxidation	1800	----	Intact from cycle II.
-24MIV	4905	103	153	Oxidation	1800	39	Intact from cycle III.
-25MI	4485	---	---	Melt. + Oxid.	1800	----	Considerable melting, solidified after several minutes.
-25MII	4630	---	---	Melt. + Oxid.	1418	----	Oxide melting and chipping, sunburst formed, some oxide melting.
-25MIII	4755	---	---	Melt. + Oxid.	1800	----	Same behavior as cycle II.
-25MIV	4930	---	---	Oxidation	1800	----	Slight melting and spalling of oxide, little change.
-25MV	4975	---	---	Oxidation	1800	----	No change from cycle IV.
-25MVI	4975	---	---	Oxidation	1800	----	Slight melting and spalling of oxide, little change.
-25MVII	4975	---	---	Oxidation	1800	----	No change from cycle VI.
-25MVIII	5040	---	---	Oxidation	1800	----	No change from cycle VII, oxide buildup on sides.
-25MIX	5125	---	---	Oxidation	1800	----	Slight melting and chipping of oxide at edges.
-25MX	5240	---	---	Oxidation	1800	----	No change from cycle IX.
-25MXI	5250	456	589	Oxidation	1800	53	Slight melting of oxide at edges.
-30M	4915	344	343	Melt. + Oxid.	1800	343	Melting, solidified in sunburst, some slight oxide melting.
-31M	4190	---	425	Melt. + Oxid.	1800	425	Slow melting, eventually solidified, some oxide melting.
-32M	5155	111	171	Melt. + Oxid.	1800	171	Melting, solidified in sunburst.
-36MH	3910	---	13	Oxidation	1081	22	Hot spot 1/8" diam. at nose, little activity.
-37MH	3765	---	10	Oxidation	1080	17	
-40M	4205	---	14	Oxidation	1800	14	Very slight oxide melting spread from edges inward.
-41M	4540	---	62	Oxidation	1800	62	Slow oxide melting from edges inward.
-44MS	2790	0	0	Oxidation	1800	0	
-45MS	2885	0	0	Oxidation	1800	0	Little visible.

+ Estimated

+ Estimated

* Converted to 30 minutes on a linear basis.

TABLE 7

SUMMARY OF ARC PLASMA EXPOSURES OF HfB_2 + 20% SiC (A-7)

Material Sample No. Assumed Emittance at λ = 0.65μ	Mach No.	P_e atm	i_e BTU/lb	D (in)	q_{cw} BTU/ft²sec	T °R obs	q_r Surface Radiation BTU/ft² sec	ϵ_N Computed Normal Emittance	Initial Length/Thickness (mils)	Final Length*/Thickness (mils)	Exposure Time (seconds)	Calculated Temperature Ratio T(CALC)/T (OBS) Cold Wall Heat Transfer Coefficient	Calculated Temperature Ratio T(CALC)/T (OBS) Fay and Riddell Heat Transfer Coefficient
$HfB_{2.1}$ + 20% SiC(A-7) ϵ = 0.60													
-26RI	3.2	0.085	10710	0.438	547	3900	26	0.41	1001/686	---/---	1800	1.82	1.81
-26RII	3.2	0.085	10890	0.438	547	3750	37	0.40	---/---	---/---	1800	1.70	1.70
-26RIII	3.2	0.085	10840	0.438	547	3750	49	0.53	---/---	---/---	1800	1.70	1.70
-26RIV	3.2	0.085	10800	0.438	547	3785	59	0.61	---/---	1005/681	1400	1.69	1.69
-27RI	2.2	0.209	7220	0.438	596	5455	76	0.18	1001/686	---/---	1800	1.15	1.14
-27RII	2.2	0.205	7360	0.438	604	5440	224	0.54	---/---	---/---	1800	1.16	1.14
-27RIII	2.2	0.197	7100	0.438	604	5370	212	0.54	---/---	---/---	1800	1.17	1.14
-27RIV	2.2	0.196	7150	0.438	596	5360	210	0.54	---/---	988/677	1800	1.17	1.15
-28RI	3.2	0.066	10320	0.427	499	3535	32	0.44	1206/898	---/---	1800	1.76	1.73
-28RII	3.2	0.066	10530	0.427	499	3660	34	0.40	---/---	---/---	1800	1.71	1.69
-28RIII	3.2	0.072	10200	0.427	489	3650	32	0.38	---/---	---/---	1800	1.70	1.69
-28RIV	3.2	0.072	10500	0.427	498	3840	60	0.59	---/---	---/---	1800	1.63	1.62
-28RV	3.2	0.072	10200	0.427	498	5180	136	0.40	---/---	---/---	1800	1.20	1.19
-28RVI	3.2	0.072	10300	0.427	498	5285	160	0.44	---/---	---/---	1800	1.18	1.17
-28RVII	3.2	0.062	9420	0.427	498	5285	154	0.42	---/---	---/---	1800	1.17	1.12
-28RVIII	3.2	0.062	10470	0.427	498	5415	152	0.38	---/---	---/---	1800	1.15	1.13
-28RIX	3.2	0.065	10210	0.427	487	6065	158	0.25	---/---	---/---	1479	1.02	1.01
-28RX	3.2	0.065	10790	0.427	489	3766	77	0.82	---/---	---/---	1800	1.66	1.65
-28RXI	3.2	0.065	10440	0.427	498	5190	113	0.33	---/---	---/---	1800	1.20	1.18
-28RXII	3.2	0.070	9980	0.427	480	5275	124	0.34	---/---	---/---	1800	1.17	1.16
-28RXIII	3.2	0.070	9880	0.427	480	5310	151	0.40	---/---	1210/883	1150	1.16	1.15
-29RI	2.2	0.165	7380	0.427	552	3470	47	0.69	1182/877	---/---	1800	1.79	1.76
-29RII	2.2	0.165	7510	0.427	552	3750	44	0.47	---/---	---/---	1800	1.66	1.64
-29RIII	2.2	0.167	7560	0.427	541	4410	72	0.40	---/---	---/---	1800	1.40	1.39
-29RIV	2.2	0.167	7810	0.427	549	4760	175	0.73	---/---	---/---	1800	1.31	1.31
-29RV	2.2	0.167	8290	0.427	555	4250	88	0.57	---/---	---/---	1800	1.48	1.49
-29RVI	2.2	0.166	7630	0.427	552	4525	94	0.48	---/---	---/---	1800	1.37	1.36
-29RVII	2.2	0.166	7650	0.427	547	4910	179	0.66	---/---	---/---	1800	1.27	1.26
-29RVIII	2.2	0.168	7720	0.427	555	4760	153	0.63	---/---	---/---	1800	1.31	1.30
-29RIX	2.2	0.168	7840	0.427	561	4795	221	0.89	---/---	---/---	1800	1.31	1.30
-29RX	2.2	0.168	7580	0.427	547	4760	151	0.63	---/---	---/---	1800	1.30	1.29
-29RXI	2.2	0.168	7850	0.427	552	4410	118	0.66	---/---	1167/828	1800	1.41	1.41
-33R	3.2	0.105	9840	0.427	590	3435	37	0.57	957/650	957/645	1542	1.88	1.85
-34R	3.2	0.160	8040	0.427	720	5465	198	0.47	1229/920	1242/889	1200	1.21	1.15
-35R	3.2	0.180	9030	0.427	791	5810	270	0.50	1224/921	931/606	90	1.17	1.13

*Final length refers to measurement after exposure, thickness refers to section length.

Material Sample No.	T °F	Gross Recession (mils)	Material Recession (mils)	Degradation Mode	Exposure Time seconds	Recession Rate* mils/30 min	Description of Motion Picture Film Coverage
$HfB_{2.1}$ + 20% SiC (A-7)							
-26PI	3040	---	---	Oxidation	1800	---	Left edge grew hotter throughout run.
-26RII	3290	---	---	Oxidation	1800	---	Oxide formed inward from left edge.
-26RIII	3290	--	- -	Oxidation	1800	---	Left side hotter than rest of face.
-26RIV	3325	4	5	Oxidation	1400	1	No change from cycle III.
-27RI	4995	---	---	Oxidation	1800	---	Light oxide formed.
-27RII	4980	---	---	Oxidation	1800	---	No change from cycle I, slight oxide chipping.
-27RIII	4910	- -	---	Oxidation	1800	---	No change from cycle II.
-27RIV	4900	11	9	Oxidation	1800	2	No change from cycle III.
-28RI	3075	---	---	Oxidation	1800	---	Uniform heating, little activity.
-28RII	3200	--	---	Oxidation	1800	---	Uniform heating, little activity.
-28RIII	3190	---	---	Oxidation	1800	---	Uniform heating, one spot near edge oxidized.
-28RIV	3380		---	Oxidation	1800	---	Bright oxide spot near edge, patches on face.
-28RV	4720	--	---	Oxidation	1800	---	Oxide covered most of front face.
-28RVI	4825	---	---	Oxidation	1800	---	Intact from cycle V, little activity.
-28RVII	48[illegible]5	---	---	Oxidation	1800	---	Some oxide chipping, little activity.
-28RVIII	4955	---	---	Oxidation	1800	---	Intact from cycle VII, some additional oxidation.
-28RIX	5605	---	---	Oxidation	1479	---	Intact from cycle VIII, little activity.
-28RX	3300	---	---	Oxidation	1800	---	Most of oxide broke off, patchy oxide formed.
-28RXI	4730	---	---	Oxidation	1800	---	Some chipping at edges, little activity.
-28RXII	4815	---	---	Oxidation	1800	---	Intact from cycle XI, oxide covered most of face.
-28RXIII	4850	-4	15	Oxidation	1150	1	Some oxide broke off, little activity.
-29RI	3010	---	---	Oxidation	1800	---	Little activity, uniform heating.
-29RII	3290	---	---	Oxidation	1800	---	Slight hot spot at center.
-29RIII	3950	---	---	Oxidation	1800	---	Hot spot more apparent and growing.
-29RIV	4300	---	---	Oxidation	1800	---	Oxide covering most of sample.
-29RV	3790	---	---	Oxidation	1800	---	Most of oxide broke off, spotty oxide remaining.
-29RVI	4065	---	---	Oxidation	1800	---	Oxide thickest at top edge.
-29RVII	4450	---	---	Oxidation	1800	---	Some oxide broke off, surface nonuniformly oxidized.
-29RVIII	4300	---	---	Oxidation	1800	---	Some oxide broke off, surface nonuniformly oxidized.
-29RIX	4335	---	---	Oxidation	1800	---	Some oxide broke off top, heavy oxide on bottom.
-29RX	4300	---	---	Oxidation	1800	---	Bottom oxide broke off, heavier oxide remained on top.
-29RXI	3950	35	49	Oxidation	1800	4	Oxide broke away almost completely, reformed slowly.
-33R	2975	0	5	Oxidation	1542	6	Uniform heating, little activity.
-34R	5005	-13	31	Oxidation	1200	46	Slight oxide melting at edges.
-35R	5350	293	315	Melting	90	6300	Rapid melting and recession.

*Converted to 30 minutes on a linear basis.

TABLE 8

SUMMARY OF ARC PLASMA EXPOSURES OF HfB_2 + 20%SiC (A-7)

Material Sample No. Assumed Emittance at λ = 0.65μ	Mach No.	P_e atm	i_e BTU/lb	D (in)	q_{cw} BTU/ft²sec	°T R obs	q_r Surface Radiation BTU/ft²sec	ϵ_N Computed Normal Emittance	Initial Length/Thickness (mils)	Final Length*/Thickness (mils)	Exposure Time (seconds)	Calculated Temperature Ratio T(CALC)/T(OBS) Cold Wall Heat Transfer Coefficient	Fay and Riddell Heat Transfer Coefficient
$HfB_{2,1}$ + 20%SiC(A-7)													
ϵ = 0.60													
-38RH	2.2	0.128	8280	0.437	497	3015	27	0.70	1000/93**	1000/93	1800	2.03	2.23
-39RH	2.2	0.162	6540	0.437	487	3170	34	0.72	994/391**	995/390	1812	1.88	2.02
-42R	2.2	0.138	7140	0.437	498	3080	27	0.64	1001/96**	1001/96	1800	1.96	1.92
-43R	2.2	0.134	7520	0.437	503	3190	34	0.70	1001/395**	1002/394	1800	1.91	1.88
-46RS	2.2	0.169	5750	0.440	503	3680	47	0.54	1001/93**	1001/93	1200	1.60	1.53
-47RS	2.2	0.169	6290	0.440	489	3615	40	0.50	1001/399**	1009/399	1800	1.64	1.61
-48RH	2.2	0.145	7030	0.975	492	3000	25	0.65	1000/96**	1001/95	1800	2.01	1.99
-49RHS	2.2	0.162	6800	0.975	512	3280	34	0.63	1001/100**	1001/100	1800	1.85	1.82
-50RH	2.2	0.150	7250	0.975	492	3090	30	0.70	1001/399**	1001/399	1800	1.96	1.96
-51RHS	2.2	0.162	6510	0.975	497	3155	30	0.64	1000/395**	1002/393	1800	1.90	1.86
-52MI	0.25	1.03	4020	0.437	455	3850	85	0.82	692/690	----/---	1800	1.40	1.40
-52MII	0.25	1.03	4110	0.437	455	4370	152	0.88	----/---	----/---	1800	1.24	1.24
-52MIII	0.25	1.03	4140	0.437	450	5185	199	0.59	----/---	----/---	1800	1.05	1.05
-52MIV	0.26	1.03	4180	0.437	442	4830	117	0.46	----/---	----/---	1800	1.12	1.13
-52MV	0.26	1.03	4160	0.437	450	5125	163	0.50	----/---	----/---	1800	1.06	1.06
-52MVI	0.26	1.03	4350	0.437	450	5150	182	0.55	----/---	----/---	1800	1.06	1.08
-52MVII	0.26	1.03	4180	0.437	450	5215	209	0.60	----/---	----/---	1800	1.04	1.05
-52MVIII	0.26	1.03	4400	0.437	450	5170	199	0.59	----/---	----/361	1430	1.06	1.07
-38RR	2.2	0.263	7290	0.437	880	5240	227	0.64	1001/93**	----/---	1800	1.30	1.32
-39RRI	3.2	0.053	8810	0.437	885	3415	39	0.61	995/390**	----/---	1800	2.02	1.83
-39RRII	3.2	0.105	7290	0.437	937	4745	199	0.83	----/---	----/366	375	1.44	1.34
-46RR	3.2	0.109	7540	0.440	988	3570	47	0.62	1001/93**	1001/92	1800	1.94	1.65

* Final length refers to sample length prior to sectioning; thickness refers to section length.
** Nose to in-depth temperature measurement station.

Material Sample No.	°T F	Gross Recession (mil)	Material Recession (mils)	Degradation Mode	Exposure Time seconds	Recession Rate* mils/30 min	Description of Motion Picture Film Coverage
$HfB_{2,1}$ + 20%SiC(A-7)							
-38RH	2555	0	0	Oxidation	1800	0	No activity.
-39RH	2710	-1	1	Oxidation	1812	1	No activity.
-42R	2620	0	0	Oxidation	1800	0	Little visible.
-43R	2730	-1	1	Oxidation	1800	1	No activity.
-46RS	3220	0	0	Oxidation	1200	0	Little activity, hottest at sample-shroud interface.
-47RS	3155	-8	0	Oxidation	1800	0	Little activity, shroud hotter than sample.
-48RH	2540	-1	1	Oxidation	1800	1	No activity.
-49RHS	2820	0	0	Oxidation	1800	0	No activity.
-50RH	2630	0	0	Oxidation	1800	0	No activity.
-51RHS	2695	-2	2	Oxidation	1800	2	No activity
-52MI	3390	--	--	Oxidation	1800	---	Little visible, edges began to oxidize.
-52MII	3910	--	--	Oxidation	1800	---	Edge chipping and droplets, oxide buildup from edge inward.
-52MIII	4725	--	--	Oxidation	1800	---	Oxide melted, broke off, slow melting continued.
-52MIV	4370	--	--	Oxidation	1800	---	Considerable melting, solidified in sunburst.
-52MV	4665	--	--	Oxidation	1800	---	Initial melting of oxide.
-52MVI	4690	--	--	Oxidation	1800	---	Initial melting and chipping of oxide.
-52MVII	4755	--	--	Oxidation	1800	---	Intact from cycle VI, little activity.
-52MVIII	4710	--	329	Oxidation	1430	41	Intact from cycle VII, little activity.
-38RR	4780	--	--	Oxidation	1800	---	3/8" diam. hot spot oxidized at nose.
-39RRI	2955	--	--	Oxidation	1800	---	Little activity.
-39RRII	4285	--	24	Oxidation	375	115	3/8" diam. hot spot.
-46RR	3110	0	1	Oxidation	1800	1	Little activity.

*Converted to 30 minutes on a linear basis.

TABLE 9

SUMMARY OF ARC PLASMA EXPOSURES OF ZrB_2 + 20%SiC (A-8)

Material Sample No. Assumed Emittance at λ = 0.65μ	Mach No.	P_e atm	i_e BTU/lb	D (in)	q_{cw} BTU/ft²sec	T °R obs	q_r Surface Radiation BTU/ft² sec	ϵ_N Computed Normal Emittance	Initial Length/Thickness (mils)	Final Length*/Thickness (mils)	Exposure Time (seconds)	Calculated Temperature Ratio T(CALC)/T(OBS) Cold Wall Heat Transfer Coefficient	Fay and Riddell Heat Transfer Coefficient
$ZrB_{2.1}$ + 20% SiC(A-8) ε = 0.60													
-1M	0.47	1.14	5650	0.489	850	5975	293	0.49	418/410	272/255	22	1.07	1.05
-2M	0.45	1.12	5070	0.489	725	6045	306	0.49	397/397	236/212	34	1.01	1.00
-3M	0.35	1.07	4885	0.489	655	6055	363	0.57	407/393	116/86	78	0.98	0.96
-4MA	0.32	1.06	3915	0.489	515	3995	110	^.92	407/399	---/---	285	1.38	1.35
-4MB	0.32	1.06	3915	0.489	515	5905	358	0.63	---/---	271/257	42	0.93	0.91
-5M	0.62	1.25	3070	0.426	605	4935	162	0.58	880/873	698/649	1800	1.09	1.06
-6M	0.70	1.33	3320	0.426	735	5250	269	0.49	885/873	105/96	43	0.97	0.93
-7MA	0.17	1.02	3680	0.426	445	5500	258	0.60	886/880	---/---	280	0.96	0.92
-7MB	0.17	1.02	3680	0.426	445	5060	33	0.11	---/---	682/616	1520	1.05	1.00
-8M	0.10	1.01	5160	0.426	380	4640	167	0.77	852/838	854/831	1800	1.17	1.15
-9M	0.10	1.01	5230	0.426	350	3620	56	0.69	890/886	895/876	1800	1.47	1.48
-10MA	0.09	1.01	3970	0.426	240	3295	34	0.61	891/881	---/---	.200	1.45	1.47
-10MB	0.09	1.01	3970	0.426	240	3165	28	0.59	---/---	891/877	1600	1.51	1.53
-11M	0.17	1.01	3710	0.426	350	3805	61	0.62	882/879	887/869	1800	1.34	1.33
-12MA	0.76	1.35	3130	0.426	715	4945	188	0.67	891/889	---/---	660	1.12	1.08
-12MB	0.70	1.35	3130	0.426	715	5550	285	0.64	---/---	888/642	9	1.00	0.96
-13MA	0.44	1.12	3140	0.426	485	5985	278	0.46	860/852	---/---	40	0.87	0.86
-13MB	0.44	1.12	3140	0.426	485	4775	114	0.47	---/---	796/779	1760	1.10	1.08
-14MA	0.21	1.01	4490	0.426	425	5630	268	0.57	881/867	---/---	160	0.96	0.98
-14MB	0.21	1.01	4490	0.426	425	4900	159	0.59	---/---	839/787	1640	1.11	1.13
-15MI	0.13	1.00	5160	0.427	367	4810	181	0.72	788/687	---/---	1800	1.12	1.14
-15MII	0.13	1.00	4830	0.427	385	5000	199	0.68	---/---	---/---	1800	1.08	1.07
-15MIII	0.13	1.00	5260	0.427	392	5160	218	0.65	---/---	---/---	1800	1.06	1.07
-15MIV	0.13	1.00	485^	0.427	385	5000	195	0.66	---/---	---/661	1800	1.08	1.08
-17M	0.15	1.01	5700	0.427	503	5340	218	0.57	607/604	538/494	1800	1.08	1.08
-18M	0.13	1.01	6070	0.427	445	5045	185	0.61	788/681	692/654	1800	1.13	1.15
-19M	0.14	1.00	4650	0.427	350	3685	58	0.67	686/681	688/675	1800	1.43	1.45
-20M	0.15	1.00	5730	0.427	410	4720	170	0.73	687/684	701/682	1800	1.18	1.22
-25M	0.13	1.01	5280	0.426	360	3620	50	0.62	98/96**	---/88	1800	1.48	1.53
-26M	0.13	1.01	5430	0.435	370	3575	46	0.60	398/395**	---/389	1800	1.51	1.56
-29MS*	0.13	1.00	5530	0.425	358	3820	58	0.58	99/96**	---/88	1800	1.40	1.45
-30MS	0.13	1.01	4840	0.437	350	3000	29	0.76	688/395**	690/389	1800	1.76	1.79
-40M	0.46	1.13	4950	0.489	870	5975	282	0.47	323/324	189/171	28	1.05	1.00
-41M	0.42	1.10	5130	0.489	800	6055	285	0.45	305/297	155/139	29	1.03	0.99
-42M	0.35	1.07	4625	0.488	690	6090	350	0.54	306/296	248/235	40	0.98	0.94
-43MA	0.33	1.07	4255	0.489	605	4125	99	0.73	303/292	---/---	80	1.39	1.34
-43MB	0.33	1.07	4255	0.489	605	6125	366	0.55	---/---	250/234	40	0.94	0.91

* Encased in Poco (B-10) graphite shroud which ablated completely in 500 sec.

* Final length refers to sample length prior to sectioning; thickness refers to section length.
** Nose to in-depth temperature measurement station.

Material Sample No.	T °F	Gross Recession (mils)	Material Recession (mils)	Degradation Mode	Exposure Time seconds	Recession Rate* mils/30 min	Description of Motion Picture Film Coverage
$ZrB_{2.1}$ + 20% SiC(A-8)							
-1M	5515	146	155	Melting	22	12680	Large drops melting and blowing off.
-2M	5585	161	185	Melting	34	9790	Large drops melting and blowing off
-3M	5595	291	307	Melting	78	7092	Slow heatup, rapid melting
-4MA	3535	---	---	Oxidation	285	---	Slow heatup, some liquid at edges
-4MP	5445	136	142	Melting	42	6070	Rapid melting
-5M	4475	182	224	Oxidation	1800	224	Oxide melting continuously
-6M	5390	700	777	Melting	43	32526	Rapid melting
-7MA	5140	---	---	Melting	280	---	Oxide formed and melted
-7MB	4600	204	264	Oxidation	1520	264	Solidified in sunburst
-8M	4180	-2	7	Oxidation	1800	7	Little activity, some oxide melting at edges
-9M	3160	-5	10	Oxidation	1800	10	Little activity
-10MA	2835	---	---	Oxidation	200	---	Little visible
-10MB	2705	0	4	Oxidation	1600	4	Little visible
-11M	3345	-5	10	Oxidation	1800	10	Little activity, some small bubbles on surface
-12MA	4485	---	---	Oxidation	660	---	Sample loose on sting, sunburst formed
-12MB	5090	3	247	Melting	9	39600	Rapid melting
-13MA	5525	---	---	Melting	40	---	Edges melted, sunburst formation
-13MB	4315	64	73	Oxidation	1760	73	Solidified in sunburst
-14MA	5170	---	---	Melting	160	---	Melting
-14MB	4440	42	80	Oxidation	1640	80	Solidified in sunburst
-15MI	4350	---	---	Oxidation	1800	---	Edge oxide melted, central unoxidized cold spot.
-15MII	4540	---	---	Oxidation	1800	---	Slight spalling of oxide, center oxidized slowly
-15MIII	4700	---	---	Oxidation	1800	---	No change from cycle II
-15MIV	4540	---	26	Oxidation	1800	7	No change from cycle III
-17M	4880	69	110	Oxidation	1800	110	Melting, solidified in sunburst
-18M	4585	96	27	Oxidation	1800	27	Edges melted, solidified, some small bubbles
-19M	3225	-2	6	Oxidation	1800	6	Hotter at edges, some edge melting
-20M	4260	-4	2	Oxidation	1800	2	Heavy oxide formed slowly from edges to center
-25M	3160	---	8	Oxidation	1800	8	Little activity.
-26M	3115	---	6	Oxidation	1800	6	Little activity.
-29MS	3360	---	8	Oxidation	1800	8	Little activity.
-30MS	2540	-2	6	Oxidation	1800	6	Litt'; activity.
-40M	5515	134	153	Melting	28	9830	Large drops melting and blowing off
-41M	5595	150	158	Melting	29	9800	Large drops melting and blowing off
-42M	5630	58	61	Melting	40	2750	Rapid melting, large chunks flying off
-43MA	3665	---	-	Oxidation	80	---	Small bubbles, uniform heating.
-43MB	5665	53	58	Melting	40	2520	Rapid melting

*Converted to 30 minutes on a linear basis.

TABLE 10

SUMMARY OF ARC PLASMA EXPOSURES OF ZrB_2 + 20%SiC (A-8)

Material Sample No., Assumed Emittance at λ = 0.65μ	Mach No.	P_e atm	i_e BTU/lb	D (in)	q_{cw} BTU/ft^2sec	T °R obs	q_r Surface Radiation BTU/ft^2sec	ϵ_N Computed Normal Emittance	Initial Length/Thickness (mils)	Final Length*/Thickness (mils)	Exposure Time (seconds)	Calculated Temperature Ratio T(CALC)/T(OBS) Cold Wall Heat Transfer Coefficient	Fay and Riddell Heat Transfer Coefficient
$ZrB_{2.1}$ + 20%SiC(A-8) ϵ = 0.60													
-16RI	2.2	0.159	6780	0.427	452	4780	49	0.20	1001/688	---/---	1800	1.23	1.24
-16RII	2.2	0.159	6730	0.427	446	4815	155	0.61	----/---	---/---	1800	1.22	1.23
-16RIII	2.2	0.159	7170	0.427	452	4900	185	0.68	----/---	---/---	1800	1.21	1.23
-16RIV	2.2	0.159	7170	0.427	452	4400	81	0.46	----/---	1000/661	1800	1.35	1.37
-21RA	3.2	0.095	10300	0.427	575	3335	32	0.55	1144/838	---/---	400	1.93	1.91
-21RB	3.2	0.095	10300	0.427	575	5740	187	0.37	----/---	549/271	33	1.12	1.11
-22RA	3.2	0.130	8210	0.427	647	4020	61	0.50	1128/812	---/---	145	1.61	1.53
-22RB	3.2	0.130	8210	0.427	647	5525	178	0.41	----/---	659/330	55	1.17	1.12
-23RA	3.2	0.155	8140	0.427	711	4145	77	0.55	1132/822	---/---	50	1.59	1.51
-23RB	3.2	0.155	8140	0.427	711	5490	187	0.44	----/---	538/209	51	1.20	1.14
-24RA	3.2	0.170	9130	0.427	748	4145	---	----	1115/799	---/---	35	1.63	1.58
-24RB	3.2	0.170	9130	0.427	748	5715	182	0.36	----/---	466/138	55	1.16	1.15
-27R	2.2	0.117	7970	0.426	452	3335	22	0.38	1000/96**	1006/89	1800	1.80	1.81
-28R	2.2	0.111	7350	0.426	452	4080	53	0.41	1001/396**	1009/388	1810	1.46	1.43
-31RS	2.2	0.226	7390	0.440	440	3080	30	0.71	979/93**	981/90	1800	1.93	2.04
-32RS	2.2	0.228	7270	0.440	437	3225	31	0.61	1004/397**	1003/392	1800	1.83	1.94
-33R	3.2	0.057	9000	0.427	423	3190	23	0.47	938/622	941/612	1800	1.87	1.82
-34R	3.2	0.063	10160	0.427	480	4725	131	0.56	819/503	825/496	1800	1.31	1.29

* Final length refers to measurement after exposure, thickness refers to length after sectioning.
** Nose to in-depth temperature measurement station.

Material Sample No.	T °F	Gross Recession (mils)	Material Recession (mils)	Degradation Mode	Exposure Time seconds	Recession Rate* mils/30 min	Description of Motion Picture Film Coverage
$ZrB_{2.1}$ + 20%SiC(A-8)							
-16RI	4320	---	---	Oxidation	1800	---	Little activity, oxide formed on top half.
-16RII	4355	---	---	Oxidation	1800	---	Oxide broke off, spotty oxide reformed.
-16RIII	4440	---	---	Oxidation	1800	---	Oxide broke off, reformed on bottom, then top.
-16RIV	3940	1	27	Oxidation	1800	7	Intact from cycle III, oxide grew uniform, broke in spots.
-21RA	2875	---	---	Oxidation	400	---	Little activity.
-21RB	5280	595	567	Melting	33	40500	Sudden rapid melting.
-22RA	3560	--	---	Oxidation	145	---	Uniform heating, slow heatup to edge melting.
-22RB	5065	469	482	Melting	55	15700	Melted from edges to center, rapid melting.
-23RA	3685	---	---	Oxidation	50	---	Slow heatup to melting.
-23RB	5030	594	613	Melting	51	21500	Rapid melting.
-24RA	3685	---	---	Oxidation	35	---	Heated to melting.
-24RB	5255	649	661	Melting	55	21600	Rapid melting.
-27R	2875	-6	7	Oxidation	1800	7	Little activity.
-28R	3620	-8	8	Oxidation	1810	8	Oxide formed from top to center, bottom unoxidized.
-31RS	2620	-2	3	Oxidation	1800	3	Little activity, shroud slightly colder than sample.
-32RS	2765	1	5	Oxidation	1800	5	Little activity, oxidation at sample-shroud interface.
-33R	2780	-3	10	Oxidation	1800	10	Little activity.
-34R	4265	-6	7	Oxidation	1800	7	Non-uniform oxide buildup from left to right.

*Converted to 30 minutes on a linear basis

TABLE 11

SUMMARY OF ARC PLASMA EXPOSURES OF

$HfB_{2.1}$ +35 v/o SiC(A-9)

Material Sample No. Assumed Emittance at $\lambda = 0.65\mu$	Mach No.	P_e atm	i_e BTU/lb	D (in)	q_{cw} BTU/ft^2 sec	T °R obs	q_r Surface Radiation BTU/ft^2 sec	ϵ_N Computed Normal Emittance	Initial Length/thickness (mils)	Final Length*/thickness (mils)	Exposure Time (seconds)	Calculated Temperature Ratio T(CALC)/T(OBS) Cold Wall Heat Transfer Coefficient	Fay and Riddell Heat Transfer Coefficient
$HfB_{2.1}$ + 35 v/o SiC (A-9) ϵ = 0.60													
-1M	0.48	1.14	5700	0.489	910	[illegible]	327	0.51	523/505	229/222	78	1.07	1.03
-2M	0.45	1.12	4700	0.489	730	6300	369	0.50	522/510	---/279	133	0.96	0.93
-4MA	0.36	1.08	4610	0.489	645	4370	132	0.77	662/661	----/---	135	1.35	1.31
-4MB	0.36	1.08	4610	0.489	645	5870	366	0.66	----/---	----/280	118	1.00	0.98
-5M	0.33	1.07	3665	0.489	530	4000	140	0.76	575/553	544/503	1800	1.24	1.20
- 6M	0.10	1.01	4730	0.426	410	4040	65	0.52	437/424	---/418	1800	1.34	1.28
- 7M	0.13	1.01	3690	0.426	355	3860	69	0.66	436/428	438/425	1800	1.32	1.28
- 8MA	0.59	1.23	2640	0.426	530	4125	66	0.48	443/421	---/---	200	1.23	1.19
- 8MB	0.59	1.23	2640	0.426	530	3995	52	0.43	---/---	479/420	1600	1.28	1.23
- 9MA	0.10	1.01	4110	0.426	450	5525	260	0.59	433/428	---/---	360	0.98	0.90
- 9MB	0.10	1.01	4110	0.426	450	5285	134	0.37	---/---	201/183	1440	1.02	0.94
-10MA	0.27	1.05	4130	0.426	535	6010	274	0.45	432/426	---/---	75	0.93	0.91
-10MB	0.27	1.05	4130	0.426	535	5500	181	0.42	---/---	318/263	1725	1.02	1.00
-11M	0.28	1.05	5330	0.426	700	6195	279	0.40	373/367	53/ 0	142	0.99	0.97
-12M	0.10	1.01	4140	0.426	550	5825	260	0.48	431/425	87/ 51	418	0.97	0.85
-13M	0.36	1.08	3410	0.426	450	5115	138	0.43	431/421	---/297	1800	1.03	1.02
-14MA	0.21	1.02	3700	0.426	470	4370	109	0.63	435/432	---/---	200	1.23	1.18
-14MB	0.21	1.02	3700	0.426	470	5605	268	0.58	---/---	274/227	208	0.96	0.92
-15M	0.19	1.01	3520	0.426	410	4050	79	0.62	428/422	425/413	1800	1.38	1.24

*Final length is based on measurement prior to sectioning; thickness refers to length after sectioning.

Material Sample No.	T °F	Gross Recession mils	Material Recession mils	Degradation Mode	Exposure Time seconds	Recession Rate* mils/sec / mils/30 min	Description of Motion Picture Film Coverage
$HfB_{2.1}$ + 35 v/o SiC (A-9)							
-1M	5630	294	283	Melting	78	3.63/6530	immediate melting, rapid recession
-2M	5840	---	231	Melting	133	1.74/3130	slow heat-up followed by melting
-4MA	3910	---	1+	Oxidation	135	----/5+	slow heat-up, slight surface activity, then melting and rapid recession
-4MB	5410	---	380	Melting	118	3.22/5800	
-5M	3540	31	50	Oxidation	1800	----/50	slow heat-up, liquid at edges, then some melting at one edge, solidified, sunburst formed and froze, some additional surface activity
- 6M	3580	---	6	Oxidation	1800	6	Little activity, slight oxide melt at edges.
- 7M	3400	-2	3	Oxidation	1800	3	Little activity.
- 8MA	3465	---	---	Oxidation	200		Little activity, slight oxide melt at edges.
- 8MB	3535	-36	1	Oxidation	1600	1	
- 9MA	5065	---	---	Oxidation	360		Oxide melted, solidified in sunburst.
- 9MB	4825	232	245	Oxidation	1440	245	
-10MA	5550	---	---	Oxidation	75		Rapid melting of oxide, solidified in sunburst.
-10MB	5040	114	163	Oxidation	1725	163	
-11M	5735	320	347	Melting	142	[illegible]	Rapid melting and recession.
-12M	5365	344	374	Melting	418	1611	Oxide melting, considerable recession.
-13M	4655	---	124	Oxidation	1800	124	Oxide melted, solidified in sunburst.
-14MA	3910	---	---	Oxidation	200	1774	Slight edge melt, then rapid melting.
-14MB	5145	16:	205	Melting	208		
-15M	3590	0	9	Oxidation	1800	9	Little activity, hot rim around edge.

+Estimated.

+Estimated
*Recession rate converted to 30 minutes on linear basis.

TABLE 12

SUMMARY OF ARC PLASMA EXPOSURES OF ZrB_2 + 14% SiC+30%C(A-10)

Material Sample No. Assumed Emittance at λ = 0.65μ	Mach No.	P_e atm	i_e BTU/lb	D (in)	q_{cw} BTU/ft²sec	T °R obs	q_r Surface Radiation BTU/ft²sec	ϵ_N Computed Normal Emittance	Initial Length* thickness (mils)	Final Length* thickness (mils)	Exposure Time (seconds)	Calculated Temperature Ratio T(CALC)/T(OBS) Cold Wall Heat Transfer Coefficient	Calculated Temperature Ratio T(CALC)/T(OBS) Fay and Riddell Heat Transfer Coefficient
ZrB_2 + SiC + C (A-10) ε = 0.60													
-1M	0.36	1.08	5045	0.499	765	5630	300	0.64	881/876	709/696	34	1.10	1.05
-2M	0.35	1.07	4755	0.499	665	5570	315	0.70	857/848	374/346	182	1.07	1.04
-3M	0.33	1.06	3280	0.499	540	4515	104	0.53	859/849	762/735	1800	1.19	1.12
-4M	0.32	1.06	4075	0.497	620	5330	102	0.27	858/850	582/504	1800	1.07	1.02
-5M	0.36	1.08	5250	0.499	765	5570	312	0.69	857/856	195/162	162	1.11	1.07
-6M	0.31	1.06	2920	0.499	485	3425	48	0.74	861/858	883/851	1800	1.50	1.41
-7R⁺	3.2	0.025	12570	0.499	490	5430	309	0.76	1165/854	1171/827	1800	1.16	1.05
-8R⁺	3.2	0.031	13670	0.499	637	5705	283	0.57	1165/844	1025/715	1800	1.17	1.05
-9R⁺	3.2	0.222	10260	0.480	1010	5525	224	0.51	1162/852	612/277	32	1.31	1.25
-10R⁺	3.2	0.127	9290	0.497	764	5525	250	0.57	942/622	632/300	37	1.23	1.14
-11R⁺	3.2	0.084	10540	0.499	696	5535	329	0.75	1163/852	1157/816	1800	1.21	1.13
-12R⁺	3.2	0.011	14370	0.497	328	5500	336	0.78	972/647	977/636	1800	1.05	0.98
-13MA	0.21	1.02	4210	0.499	410	4025	92	0.74	855/844	-/-	1300	1.33	1.32
-13MB	0.21	1.02	4210	0.499	410	4105	120	0.90	-/-	859/840	500	1.30	1.30
-14M	0.56	1.20	3405	0.499	540	5285	240	0.65	858/851	936/825	1800	1.02	1.01
-15M	0.60	1.24	3020	0.492	580	3840	65	0.62	787/782	789/774	1800	1.38	1.33
-16MA	0.70	1.33	3240	0.499	725	5135	230	0.70	856/854	-/-	1150	1.09	1.03
-16MB	0.70	1.33	3240	0.499	725	5525	330	0.75	-/-	719/714	63	1.02	0.96
-17MA	0.24	1.03	4315	0.426	540	5850	315	0.57	824/826	-/-	100	0.97	0.94
-17MB	0.24	1.03	4315	0.426	540	4730			-/-	564/566	1700	1.19	1.16
-18MA	0.21	1.03	3560	0.426	535	5850	293	0.53	820/825	-/-	45	0.93	0.87
-18MB	0.21	1.03	3560	0.426	535	5060	163	0.53	-/-	703/685	1755	1.08	1.01
-19MA	0.18	1.01	5200	0.426	450	5390	251	0.63	824/817	-/-	38	1.04	1.06
-19MB	0.18	1.01	5200	0.426	450	5150	202	0.63	-/-	814/773	1762	1.09	1.11
-20M	0.15	1.01	4430	0.425	365	4105	105	0.79	823/822	825/816	1800	1.28	1.29
-21MA	0.75	1.36	3210	0.426	825	4240	89	0.99	815/810	-/-	45	1.35	1.27
-21MB	0.75	1.36	3210	0.426	825	5685	228	0.46	-/-	192/162	99	1.00	0.95
-22MA	0.70	1.29	3230	0.425	730	4160	91	0.65	823/818	-/-	217	1.35	1.29
-22MB	0.70	1.29	3230	0.425	730	5700	263	0.53	-/-	312/288	104	0.99	0.94

⁺Transmissivity factor equals 0.86 for sapphire window.

*Final length is based on measurement prior to sectioning; thickness refers to length after sectioning.

Material Sample No.	T °F	Gross Recession mils	Material Recession mils	Degradation Mode	Exposure Time seconds	Recession Rate* (mils/sec)/(mils/30 min)	Description of Motion Picture Film Coverage
ZrB_2 + SiC + C (A-10)							
-1M	5170	172	180	Melting	34	5.29/9520	immediate melting, sunburst late in run
-2M	5110	483	502	Melting	182	2.76/4770	immediate melting, sunburst formation
-3M	4055	97	114	Oxidation	1800	----/114	surface activity, sunburst formed and froze, little change
-4M	4870	276	346	Oxidation	1800	----/346	melting, sunburst formed and froze, some additional oxide melting
-5M	5110	662	696	Melting	162	4.30/7740	melting, rapid recession
-6M	2965	-22	7	Oxidation	1800	----/7	no film coverage
-7R	4970	-6	27	Oxidation	1800	----/27	uniform heating, some undercutting
-8R	5245	140	129	Melt + Oxid.	1800	----/129	one side heated faster, melted slightly, recession at angle, undercutting
-9R	5065	550	575	Melting	32	18.0/32,400	rapid melting and recession
-10R	5065	310	322	Melting	37	8.7/15,660	rapid melting and recession
-11R	5075	6	36	Oxidation	1800	----/36	uniform heating, some slight melting
-12R	5046	-5	11	Oxidation	1800	----/11	uniform heating, little activity
-13MA	3565			Oxidation	1300	4	Poor exposure.
-13MB	3645	- 4	4	Oxidation	500		
-14M	4825	- 78	26	Oxidation	1800	26	Initial melting, sunburst formation, oxide continued to melt.
-15M	3400	- 2	8	Oxidation	1800	8	Droplets continuously shot out from center to edges.
-16MA	4675			Oxidation	1150		Droplets formed followed by rapid melting of oxide.
-16MB	5065	137	140	Melting	63	3943	
-17MA	5390			Melting	100		Rapid melting, solidified in sunburst, little additional activity.
-17MB	4270	240	260	Oxidation	1700	260	
-18MA	5390			Melting	45		Rapid melting, solidified in sunburst, little additional activity.
-18MB	4600	117	140	Oxidation	1755	140	
-19MA	4930	---	---	Melting	38		Front face melted, solidified in sunburst, additional
-19MB	4690	10	44	Oxidation	1767	44	oxide melting.
-20M	3645	- 2	6	Oxidation	1800	6	Little activity, slight edge melt.
-21MA	3780	---	---	Oxidation	45	11782	Sample loose on sting, melting, rapid recession.
-21MB	5225	623	640	Melting	99		
-22MA	3700	---	---	Oxidation	217	9173	Sample loose on sting, melting, rapid recession.
-22MB	5240	511	530	Melting	104		

*Recession rates converted to 30 minutes on linear basis.

TABLE 13

SUMMARY OF ARC PLASMA EXPOSURES OF $ZrB_2 + 14\% SiC + 30\% C$ (A-10)

Material Sample No. Assumed Emittance at λ = 0.65μ	Mach No.	P_e atm	i_e BTU/lb	D (in)	q_{cw} BTU/ft²sec	T °R obs	q_r Surface Radiation BTU/ft² sec	ϵ_N Computed Normal Emittance	Initial Length / Thickness (mils)	Final Length* / Thickness (mils)	Exposure Time (seconds)	Calculated Temperature Ratio T(CALC)/T (OBS) Cold Wall Heat Transfer Coefficient	Fay and Riddell Heat Transfer Coefficient
ZrB_2 + SiC + C (A-10)													
ε = 0.60													
-23MI	0.21	1.02	3850	0.431	414	5090	161	0.51	822/820	---/---	1800	1.04	1.03
-23MII	0.21	1.02	4000	0.431	412	5060	158	0.51	---/---	---/---	1800	1.05	1.05
-23MIII	0.21	1.02	4150	0.431	402	5035	156	0.52	---/---	---/---	1800	1.06	1.06
-23MIV	0.21	1.02	3960	0.431	386	5035	157	0.52	---/---	822/757	1800	1.04	1.05
-24MI	0.20	1.02	4390	0.426	407	4085	75	0.57	826/825	---/---	1800	1.31	1.33
-24MII	0.20	1.02	4150	0.426	398	4710	141	0.61	---/---	---/---	1800	1.13	1.14
-24MIII	0.21	1.02	3570	0.426	396	4785	147	0.60	---/---	---/---	1800	1.08	1.07
-24MIV	0.21	1.02	4080	0.426	402	4920	170	0.62	---/---	---/---	1800	1.08	1.08
-24MV	0.21	1.02	4500	0.426	398	4865	151	0.57	---/---	---/---	1800	1.10	1.13
-24MVI	0.21	1.02	4350	0.426	394	4965	169	0.59	---/---	---/---	1800	1.07	1.10
-24MVII	0.24	1.02	4780	0.426	394	4990	175	0.60	---/---	---/---	1800	1.08	1.14
-24MVIII	0.23	1.02	4550	0.426	398	5010	169	0.57	---/---	---/---	1800	1.07	1.11
-24MIX	0.23	1.02	4150	0.426	406	5025	180	0.60	---/---	---/---	1800	1.06	1.08
-24MX	0.23	1.02	4400	0.426	394	5000	176	0.60	---/---	---/---	1800	1.07	1.10
-24MXI	0.23	1.02	3990	0.426	398	5045	187	0.61	---/---	---/---	1800	1.04	1.06
-24MXII	0.23	1.02	4310	0.426	425	5125	188	0.58	---/---	835/721	1800	1.05	1.07
-27MA	0.24	1.03	5160	0.437	511	6150	234	0.35	689/632	---/---	70	0.93	0.95
-27MB	0.24	1.03	5160	0.437	511	5535	173	0.39	---/---	574/541	1730	1.04	1.05
-28MA	0.74	1.35	3500	0.437	598	5930	181	0.31	690/685	---/---	250	0.93	0.93
-28MB	0.74	1.35	3500	0.437	598	5195	---	---	---/---	---/114	562	1.07	1.07
-34MH	0.18	1.01	3950	0.437	416	4105	68	0.51	691/103**	---/85**	1800	1.29	1.37
-35MH	0.18	1.01	3500	0.437	420	3960	62	0.54	686/393**	690/388**	1800	1.32	1.36
-38M	0.23	1.02	3870	0.437	400	3840	52	0.51	690/95**	694/89**	1800	1.37	1.37
-39M	0.21	1.02	3990	0.425	400	4740	92	0.39	692/397**	---/381**	1800	1.11	1.12
-42MS	0.21	1.03	4000	0.437	393	3020	27	0.69	693/103**	694/101	1800	1.74	1.75
-43MS	0.21	1.03	4040	0.437	403	3055	26	0.63	688/400**	693/397	1800	1.73	1.74

* Final length refers to measurement after exposure, thickness refers to length after sectioning

** Nose to in-depth temperature measurement station.

Material Sample No.	T °F	Gross Recession (mils)	Material Recession (mils)	Degradation Mode	Exposure Time seconds	Recession Rate* mils/30 min	Description of Motion Picture Film Coverage
ZrB_2 + SiC + C (A-10)							
-23MI	4630	---	---	Melt. + Oxid.	1800	---	Edges melted, sunburst formed, slight oxide melting.
-23MII	4600	---	---	Oxidation	1800	---	Intact from cycle I, little activity.
-23MIII	4575	---	---	Oxidation	1800	---	Intact from cycle II, little activity
-23MIV	4575	0	63	Oxidation	1800	16	Intact from cycle III, little activity.
-24 MI	3625	---	---	Oxidation	1800	---	Hotter at edges.
-24MII	4250	---	---	Oxidation	1800	---	Oxide formed over face, some bubbles at edge.
-24MIII	4325	---	---	Oxidation	1800	---	Heavy oxide covered face.
-24MIV	4460	---	---	Oxidation	1800	---	Little change, slight oxide melting.
-24MV	4405	---	---	Oxidation	1800	---	Little change, oxide grew heavier.
-24MVI	4505	---	---	Oxidation	1800	---	Little change, slight oxide melting.
-24MVII	4530	---	---	Oxidation	1800	---	Little change, slight oxide melting.
-24MVIII	4550	---	---	Oxidation	1800	---	Little change, oxide heavier.
-24MIX	4565	---	---	Oxidation	1800	---	Little change.
-24MX	4540	---	---	Oxidation	1800	---	Little change.
-24MXI	4585	---	---	Oxidation	1800	---	Little change.
-24MXII	4665	-9	104	Oxidation	1800	9	Little change.
-27MA	5690	---	---	Melting	70	---	Melted from edges to center
-27MB	5075	115	141	Oxidation	1730	141	Solidified in sunburst.
-28MA	5470	---	---	Melting	250	---	Small droplets, oxide melted, considerable recession.
-28MB	4735	---	571	Oxidation	562	1265	Solidified in sunburst.
-34MH	3645	---	18	Oxidation	1800	18	Hot spot 1/4" diameter at nose, little activity.
-35MH	3500	-4	5	Oxidation	1800	5	Hot spot 1/8" diameter at nose, little activity.
-38M	3380	-4	6	Oxidation	1800	6	Little visible, slightly hotter at edges.
-39M	4280	---	16	Oxidation	1800	16	Little visible, hotter at edges, oxide on front face.
-42MS	2560	-1	2	Oxidation	1800	2	Little visible.
-43MS	2595	-5	3	Oxidation	1800	3	Little visible.

*Converted to 30 minutes on a linear basis.

TABLE 14

SUMMARY OF ARC PLASMA EXPOSURES OF $ZrB_2 + 14\%SiC + 30\%C$ (A-10)

Material Sample No. Assumed Emittance at $\lambda = 0.65\mu$	Mach No.	P_e atm	i_e BTU/lb	D (in)	q_{cw} BTU/ft²sec	T °R obs	q_r Surface Radiation BTU/ft²sec	ϵ_N Computed Normal Emittance	Initial Length/Thickness (mils)	Final Length*/Thickness (mils)	Exposure Time (seconds)	Calculated Temperature Ratio T (CALC)/T (OBS) Cold Wall Heat Transfer Coefficient	Calculated Temperature Ratio T (CALC)/T (OBS) Fay and Riddell Heat Transfer Coefficient
ZrB_2 + SiC + C (A-10)													
ϵ = 0.60													
-25RI	2.2	0.117	8070	0.437	492	4865	160	0.61	1001/602	---/---	1800	1.25	1.24
-25RII	2.2	0.117	8310	0.437	498	4955	194	0.68	---/---	---/---	1800	1.24	1.23
-25RIII	2.2	0.120	7800	0.437	498	5050	214	0.70	---/---	---/---	1800	1.21	1.18
-25RIV	2.2	0.120	8160	0.437	498	5190	235	0.69	---/---	1002/688	1600	1.18	1.17
-26RI	2.2	0.242	7650	0.437	460	4595	126	0.60	1000/679	---/---	1800	1.31	1.40
-26RII	2.2	0.240	7750	0.437	452	4955	202	0.71	---/---	---/---	1800	1.21	1.30
-26RIII	2.2	0.240	7900	0.437	460	5110	216	0.67	---/---	---/---	1800	1.18	1.27
-26RIV	2.2	0.240	7900	0.437	452	5135	224	0.69	---/---	---/---	1800	1.17	1.26
-26RV	2.2	0.236	7610	0.437	460	5110	220	0.69	---/---	---/---	1800	1.17	1.25
-26RVI	2.2	0.236	7580	0.437	469	5135	227	0.70	---/---	---/---	1800	1.17	1.24
-26RVII	2.2	0.236	8140	0.437	460	5155	219	0.66	---/---	---/---	1800	1.17	1.26
-26RVIII	2.2	0.236	7570	0.437	437	5180	219	0.65	---/---	---/---	1800	1.15	1.23
-26RIX	2.2	0.236	7890	0.437	437	5190	231	0.68	---/---	---/---	1800	1.15	1.24
-26RX	2.2	0.236	7650	0.437	455	5205	229	0.66	---/---	---/---	1800	1.15	1.23
-26RXI	2.2	0.236	7580	0.437	469	5190	236	0.69	---/---	---/596	951	1.16	1.23
-30RA	3.2	0.090	10440	0.426	551	3650	33	0.40	1128/822	---/---	428	1.75	1.75
-30RB	3.2	0.090	10440	0.426	551	5455	196	0.47	---/---	1138/796	1241	1.17	1.17
-31RA	3.2	0.105	10510	0.426	596	3650	44	0.53	1128/818	---/---	300	1.78	1.78
-31RB	3.2	0.105	10510	0.426	596	4910	123	0.45	---/---	473/138	30	1.32	1.32
-32RA	3.2	0.135	9520	0.426	656	3590	64	0.82	1119/809	---/---	35	1.83	1.80
-32RB	3.2	0.135	9520	0.426	656	4605	133	0.63	---/---	434/115	40	1.43	1.41
-33RA	3.2	0.145	7950	0.426	682	5490	---	---	1128/821	---/---	30	1.19	1.13
-33RB	3.2	0.145	7950	0.426	682	4780	129	0.52	---/---	419/102	40	1.36	1.29
-36RH	2.2	0.147	7250	0.437	472	3715	69	0.77	1010/102**	1012/97	1800	1.63	1.76
-37RH	2.2	0.144	7710	0.437	482	3695	74	0.85	995/393**	996/390	1800	1.64	1.80
-40R	2.2	0.147	6320	0.437	495	4935	173	0.62	1003/95**	1004/89	1800	1.21	1.16
-41R	2.2	0.147	6460	0.425	495	5110	211	0.66	1000/399**	1014/382	1800	1.17	1.13
-44RS	2.2	0.226	7400	0.440	495	4675	125	0.56	993/96**	995/85	1800	1.30	1.35
-45RS	2.2	0.229	7470	0.440	498	5110	202	0.63	996/394**	1001/380	1800	1.19	1.24
-46RH	2.2	0.155	7220	0.975	501	3025	22	0.56	1007/105**	1007/104	1800	2.00	2.01
-47RHS	2.2	0.167	6010	0.969	507	4745	138	0.58	1004/100**	1007/87	1800	1.25	1.21
-48RH	2.2	0.155	6350	0.975	492	2970	20	0.55	1005/402**	1005/401	1800	2.01	1.97
-49RHS	2.2	0.167	6010	0.975	522	4130	99	0.73	983/391**	983/388	1800	1.45	1.40
-48RRA	3.2	0.109	6980	0.976	654	5525	286	0.65	1004/402	---/---	425	1.15	1.05
-48RRB	3.2	0.117	8040	0.976	864	5535	286	0.65	---/---	---/---	180	1.24	1.10
-48RRC	3.2	0.125	8730	0.976	871	5525	281	0.64	---/---	938/---	33	1.25	1.14

* Final length refers to measurement after exposure, thickness refers to measurement after sectioning.

** Nose to in-depth temperature measurement station

Material Sample No.	T °F	Gross Recession (mils)	Material Recession (mils)	Degradation Mode	Exposure Time seconds	Recession Rate* mils/30 min	Description of Motion Picture Film Coverage
ZrB_2 + SiC + C (A - 10)							
-25RI	4405	---	---	Oxidation	1800	----	Uniform oxide buildup, little activity.
-25RII	4495	---	---	Oxidation	1800	----	Some oxide chipping, little activity.
-25RIII	4590	---	---	Oxidation	1800	----	Oxide cracked, some chipping.
-25RIV	4730	-1	24	Oxidation	1800	6	Large pieces of oxide broke off, surface reoxidized.
-26RI	4135	---	---	Oxidation	1800	----	Spotty oxide buildup.
-26RII	4495	---	---	Oxidation	1800	----	Oxide grew more uniform.
-26RIII	4650	---	---	Oxidation	1800	----	Little change from cycle II, some chipping at edges.
-26RIV	4675	---	---	Oxidation	1800	----	Oxide chipped off center and edges.
-26RV	4650	---	---	Oxidation	1800	----	Oxide breaking off and melting.
-26RVI	4675	---	---	Oxidation	1800	----	Uniform oxide, little activity.
-26RVII	4695	---	---	Oxidation	1800	----	Some oxide broke off edges, little activity.
-26RVIII	4720	---	---	Oxidation	1800	----	Intact from cycle VII.
-26RIX	4730	---	---	Oxidation	1800	----	Intact from cycle VIII.
-26RX	4745	---	---	Oxidation	1800	----	Intact from cycle IX, some spalling of heavy oxide.
-26RXI	4730	---	83	Oxidation	951	8	Intact from cycle X.
-30RA	3190	---	---	Oxidation	428	----	Oxide formed from edges into center
-30RB	4995	-10	26	Oxidation	1241	36	Oxide covered face
-31RA	3190	---	---	Oxidation	300	----	Oxide slowly melted from edges into center
-31RB	4450	655	680	Melting	30	3710	Rapid melting
-32RA	3130	---	---	Oxidation	35	----	Heated to melting
-32RB	4145	685	694	Melting	40	16600	Rapid melting
-33RA	5030	---	---	Melting	30	----	Heated to melting
-33RB	4320	709	719	Melting	40	18400	Rapid melting
-36RH	3255	-2	5	Oxidation	1800	5	Hot spot 1/4" diam. oxidized at nose.
-37RH	3235	-1	3	Oxidation	1800	3	Hot spot 1/4" diam. oxidized at nose.
-40R	4475	-1	6	Oxidation	1800	6	Non-uniform oxide buildup, grew heavier.
-41R	4650	-14	17	Oxidation	1800	17	Speckled surface, gradual oxide buildup.
-44RS	4215	- 2	11	Oxidation	1800	11	Oxide gradually spread over sample, not shroud.
-45RS	4650	- 5	14	Oxidation	1800	14	Oxide grew over top half of shroud and most of sample.
-46RH	2565	0	1	Oxidation	1800	1	Hot spot 1/4" diam. oxidized at nose.
-47RHS	4285	- 3	13	Oxidation	1800	13	Small hot spot grew to 1/2" diam. at nose.
-48RH	2510	0	1	Oxidation	1800	1	Little activity.
-49RHS	3670	0	3	Oxidation	1800	3	Small hot spot 1/2" diam. at nose.
-48RRA	5065	---	---	Oxidation	425	----	Heavy oxide melting continuously, then solidified eventually leaving an unoxidized spot at center.
-48RRB	5065	---	---	Oxidation	180	----	
-48RRC	5065	66	---	Oxidation	33	----	

*Converted to 30 minutes on a linear basis.

TABLE 15

SUMMARY OF DEPLETION DEPTHS OBSERVED AFTER ARC PLASMA EXPOSURES OF BORIDE COMPOSITES

Material Sample No.	Temperature (°F)	Depletion Depth(mils)	Time (sec)	Depletion Rate (mils/hour)
HfB_2+20%SiC(A-4)				
-2M	5020	11	1830	22
-2-2M	3170	10	1830	20
-2-3M	4790	26	1830	51
-2-4M	5190	32	1830	63
-2-6R	5190	26	1800	52
-2-7R	5300	52	1800	104
-2-8R	5480	49	1800	98
$HfB_{2.1}$+35%SiC(A-9)				
-1M*	5630	130	78	6020
-2M*	5840	80	133	2170
-3M*	5410	70	253	996
-5M	3540	13	1800	26
-7M	3400	3	1800	6
-8M	3535	5	1800	10
-9M	4825	90	1800	180
-10M	5040	31	1800	62
-13M*	4655	41	1800	82
-14M	5145	8	408	71
-15M	3590	3	1800	6

*Melting occurred, depletion measurement unlikely to be dependable.

Material Sample No.	Temperature (°F)	Depletion Depth(mils)	Time (sec)	Depletion Rate (mils/hour)
$HfB_{2.1}$+20%SiC(A-7)				
-1M*	5760	115	56	7410
-2M	4800	80	1740	166
-3M	4880	54	1800	108
-5M*	5030	140	1750	288
-6M	5135	65	264	885
-7M	5100	80	1750	165
-23M	5060	140	7200	70
-24M	4865	130	7200	65
-25M	4945	34	19418	6
-26R	3235	2	6800	1
-27R	4945	1	7200	1
-29R	3975	2	19800	1
-30M*	4915	27	1800	54
-31M*	4190	47	1800	94
-32M*	5155	100	1800	200
-33R	2975	0	1542	0
-34R	5005	0	1200	0
-35R	5350	130	90	5200
-36MH	3910	21	1083	70
-37MH	3765	10	1080	33
-39PH	2710	0	1812	0
-40M	4205	45	1800	90
-41M	4540	39	1800	78
-42M	2610	0	1800	0
-43R	2730	0	1800	0
-52M	4400	33	14030	8

*Melting occurred, depletion measurement unlikely to be dependable.

Material Sample No.	Temperature (°F)	Depletion Depth(mils)	Time (sec)	Depletion Rate (mils/hour)
$ZrB_{2.1}$+20%SiC(A-8)				
-3M*	5585	100	34	10590
-4M*	5445	120	327	1320
-5M	4475	5	1800	10
-7M	4600	6	1800	12
-8M	4180	3	1800	6
-9M	3160	1	1800	2
-10M	2705	0	1800	0
-11M*	3345	3	1800	6
-12M*	5090	70	669	376
-13M	4315	11	1760	22
-15M	4535	3	7200	2
-16R	4265	2	7200	1
-17M	4880	20	1800	40
-18M	4585	1	1800	2
-19M	3225	3	1800	6
-20M*	4260	6	1800	12
-22R	5065	17	200	306
-25M	3160	1	1800	2
-26M	3115	1	1800	2
-27R	2875	1	1800	2
-28R	3620	1	1810	2
-29MS	3360	1	1800	2
-30MS	2540	0	1800	0
-33R	2730	1	1800	2
-34R	4265	0	1800	0

*Melting occurred, depletion measurement unlikely to be dependable.

Material Sample No.	Temperature (°F)	Depletion Depth(mils)	Time (sec)	Depletion Rate (mils/hour)
ZrB_2+SiC+C (A-10)				
-1M*	5170	5	34	530
-2M*	5110	6	182	119
-3M	4055	13	1800	26
-4M	4870	5	1800	10
-7R*	4970	42	1800	84
-8R*	5245	28	1800	56
-12P	5040	28	1800	56
-13M	3565	8	1800	16
-14M	4825	9	1800	18
-15M*	3400	8	1800	16
-16M*	5065	10	1213	30
-18M	4600	17	1755	35
-19M	4690	13	1762	27
-20M*	3645	13	1800	26
-21M*	5225	15	144	380
-22M*	5240	8	321	90
-23M	4595	20	7200	10
-24M	4410	12	21600	2
-25R	4555	14	7200	7
-26R	4420	13	18951	2
-27M	5075	8	1730	17
-28M	4735	12	562	77
-30R	4995	10	1241	29
-34MH	3645	12	1800	24
-35MH	3500	8	1800	16
-37RH	3235	0	1800	0
-38M	3380	5	1800	10
-39M	4280	11	1800	22
-40R	4475	10	1800	20
-41R	4650	6	1800	12
-42MS	2560	0	1800	0
-43MS	2595	0	1800	0
-44RS	4215	6	1800	12
-45RS	4650	7	1800	14

*Melting occurred, depletion measurement unlikely to be dependable.

TABLE 16

SUMMARY OF ARC PLASMA EXPOSURES OF RVA(B-5)

Material Sample No. Assumed Emittance at $\lambda = 0.65\mu$	Mach No.	P_e atm	i_e BTU/lb	D (in)	q_{cw} BTU/ft²sec	T °R obs	q_r Surface Radiation BTU/ft²sec	ϵ_N Computed Normal Emittance	Initial Length thickness (mils)	Final Length* thickness (mils)	Exposure Time (seconds)	Calculated Temperature Ratio T(CALC)/T(OBS) Cold Wall Heat Transfer Coefficient	Fay and Riddell Heat Transfer Coefficient
RVA(B-5)													
ϵ = 0.85 (Below 3000°F), 0.75(3000° - 3500°F), 0.65 (Above 3500°F)													
-2M	0.33	1.07	3560	0.500	550	5040	143	0.47	1016/1016	687/701	120	1.06	1.02
-3M	0.30	1.08	2745	0.500	340	4500	78	0.40	1032/1032	851/837	120	1.03	1.01
-5M	0.39	1.10	6455	0.500	1030	6180	---	----	1028/1028	822/830	58	1.05	1.00
-6M	0.49	1.15	6220	0.500	1080	6250	291	0.40	972/972	730/743	55	1.04	0.99
-7M	0.43	1.12	6225	0.500	810	5830	242	0.44	1007/1007	789/783	66	1.06	1.05
-1R+	3.20	0.187	12230	0.486	1138	5165	167*	0.49*	1053/1053	889/900	85	1.35	1.27
-2R+	3.20	0.029	9580	0.487	261	4110	57*	0.42*	1049/1049	749/741	600	1.20	1.21
-3R+	3.20	0.018	15600	0.487	487	4865	120*	0.45*	1064/1064	716/737	600	1.20	1.10
-4R+	3.20	0.163	7640	0.487	608	4665	100*	0.44*	1044/1044	687/665	300	1.26	1.21
-5R+	3.20	0.017	13570	0.486	326	4470	65*	0.34*	999/999	528/533	900	1.18	1.15
-6R+	3.20	0.016	14000	0.487	317	4570	98*	0.47*	991/991	689/690	600	1.15	1.13
-7R+	3.20	0.299	10950	0.486	979	5890	167*	0.29*	1044/1044	851/839	108	1.14	1.34
-1M°	0.35	1.08	4405	0.500	570	----	---	----	993/993	---/695	108	----	----
-4M°	0.36	1.08	5965	0.500	750	----	---	----	991/991	973/982	9	----	----
-11M	0.31	1.06	3740	0.741	455	4375	111	0.65	932/930	709/708	120	1.17	1.12
-12M	0.32	1.07	4900	0.741	529	4630	160	0.74	948/940	696/688	120	1.19	1.15
-13M	0.34	1.07	7030	0.741	640	4995	186	0.64	931/930	628/630	120	1.19	1.20
-14R+	3.2	0.012	10850	0.741	241	4010	92	0.76	1265/942	860/570	1200	1.26	1.14
-15R+	3.2	0.024	10930	0.741	455	4500	159	0.82	1262/939	841/543	900	1.30	1.11
-16R+	3.2	0.218	10060	0.739	979	5855	454	0.82	1233/929	797/490	300	1.17	1.07
-23M	0.10	1.00	2690	0.502	167	3725	58	0.64	683/679	522/521	180	1.12	1.12
-24M	0.13	1.00	3510	0.502	250	4105	89	0.67	683/680	568/561	120	1.14	1.14
-25M	0.15	1.00	2090	0.503	126	3420	41	0.64	684/678	586/584	180	1.08	1.13
-26M	0.15	1.00	1770	0.503	73	3035	27	0.68	674/670	572/573	361	1.05	1.18
-27M	0.15	1.00	1360	0.502	91	2995	27	0.71	665/663	554/534	300	1.05	1.08
-28R+	3.2	0.005	5280	0.503	34	2165	3	0.29	1000/701	971/669	1800	1.40	1.60
-29R+	3.2	0.008	11590	0.504	117	2780	20	0.71	1001/676	852/521	1800	1.50	1.63
-30R+	3.2	0.011	13950	0.502	211	3465	46	0.68	1002/680	708/387	1200	1.43	1.46
-31M	0.10	1.00	2530	0.501	135	3285	39	0.71	670/198**	534/69	240	1.15	1.18
-32M	0.10	1.00	2930	0.502	135	3475	36	0.53	671/464**	598/388	180	1.13	1.20

** Nose to in-depth temperature measurement station

+Transmissivity factor equals 0.86 for pyrex window.
*Surface radiation values may be low due to requirements for critical alignment caused by utilization of one-half inch diameter sample.
°Test terminated before temperature and surface radiation could be measured.

*Final Length is based on measurement prior to sectioning; thickness refers to length after sectioning.

Material Sample No.	T °F	Gross Recession mils	Material Recession mils	Degradation Mode	Exposure Time seconds	Recession Rate* [illegible]	Description of Motion Picture Film Coverage
RVA (B-5)							
-2M	4580	329	315	Oxidation	120	2.63/4734	uniform heating, rapid side recession
-3M	4040	181	195	Oxidation	120	1.63/2934	uniform heating, rapid side recession
-5M	5720	206	198	Oxidation	58	3.41/6138	uniform heating, rapid front and side recession
-6M	5790	242	229	Oxidation	55	4.16/7488	uniform heating, rapid front and side recession, some vibration
-7M	5370	218	224	Oxidation	66	3.39/6102	uniform heating, rapid front and side recession, some vibration
-1R	4705	164	153	Oxidation	85	1.80/3240	uniform heating and recession, rounding of edges
-2R	3650	300	308	Oxidation	600	0.51/918	
-3R	4405	348	327	Oxidation	600	0.55/990	uniform heating and recession
-4R	4205	357	379	Oxidation	300	1.26/2268	uniform heating, some side recession
-5R	4010	471	466	Oxidation	900	0.52/936	uniform heating, some side recession, rapid side recession
-6R	4110	302	301	Oxidation	600	0.50/900	uniform heating, some side recession
-7R	5430	193	205	Oxidation	108	1.90/3420	uniform heating and recession, rounding of edges
-1M	(4290)°	---	298	Oxidation	108	2.76/4968	terminated due to rapid ablation, sample blown away
-4M	(4740)°	18+	9	Oxidation	9	1.00/1800	terminated due to rapid ablation, sample blown away
-11M	3915	223	222	Oxidation	120	1.85/3330	uniform recession, slight surface activity
-12M	4170	252	252	Oxidation	120	2.10/3780	uniform recession, slight surface activity
-13M	4525	303	300	Oxidation	120	2.50/4500	uniform recession, slight surface activity
-14R	3550	405	372	Oxidation	1200	0.31/558	
-15R	4040	421	396	Oxidation	900	0.41/792	
-16R	5395	436	439	Oxidation	300	1.46/2630	Uniform recession.
-23M	3265	161	158	Oxidation	180	0.88/1580	Rough, speckled surface, uniform heating.
-24M	3645	115	119	Oxidation	120	0.99/1785	Rough, speckled surface, uniform heating.
-25M	2960	98	94	Oxidation	180	0.52/940	Rough, speckled surface, uniform heating.
-26M	2575	102	97	Oxidation	361	0.27/483	Speckled face, little visible.
-27M	2535	111	129	Oxidation	300	0.43/774	Rough, speckled surface, uniform heating.
-28R	1705	29	32	Oxidation	1800	0.018/32	Little visible.
-29R	2320	149	155	Oxidation	1800	0.086/155	Rough, speckled surface, uniform heating, gradual recession.
-30R	3005	294	293	Oxidation	1200	0.24/440	Rough surface, uniform heating, gradual recession.
-31M	2825	136	129	Oxidation	240	0.54/968	Little visible.
-32M	3015	73	76	Oxidation	180	0.42/760	Speckled heating.

+Gross recession is overestimated because of chipping or erosion of back face.
°Temperatures estimated based on Cold Wall Heat Transfer Coefficient Calculation of 5510°R and 6030°R corrected by mean ratio T(CALC)/T(OBS) of 1.16 to 4750°R and 5200°R or 4290°F and 4740°F.

*Recession rate converted to 30 minutes on linear basis.

TABLE 17

SUMMARY OF ARC PLASMA EXPOSURES OF PG(B-6)

Material Sample No. Assumed Emittance at λ = 0.65μ	Mach No.	P_e atm	i_e BTU/lb	D (in)	q_{cw} BTU/ft^{2}sec	T °R obs	q_r Surface Radiation BTU/ft^{2}sec	ϵ_N Computed Normal Emittance	Initial Length/thickness (mils)	Final Length*/thickness (mils)	Exposure Time (seconds)	Calculated Temperature Ratio T(CALC)/T(OBS): Cold Wall Heat Transfer Coefficient	Calculated Temperature Ratio T(CALC)/T(OBS): Fay and Riddell Heat Transfer Coefficient
	"C" Axis Perpendicular to Arc												
PG (B-6)													
ϵ = 0.75													
-1M	0.31	1.06	2970	0.487	390	4320	73	0.44	1160/1160	1000/1000	120	1.11	1.08
-2M	0.33	1.07	3955	0.489	540	5150	139	0.42	1154/1154	861/882	120	1.04	1.01
-3M	0.35	1.08	4580	0.489	670	4990	131	0.44	999/999	865/856	61	1.14	1.10
	Delaminated on "C" Plane after Test												
-4M	0.38	1.09	6665	0.486	810	4990	166	0.56	906/906	800/796	44	1.24	1.24
-5M	0.39	1.10	6750	0.487	980	5660	208	0.43	904/904	718/708	60	1.14	1.10
-6M	0.46	1.14	5710	0.488	940	5490	151	0.35	853/853	665/672	53	1.14	1.09
-7M	0.38	1.09	7320	0.486	870	5490	148	0.34	980/980	797/802	62	1.16	1.16
	Delaminated on "C" Plane after Test												
-1R†	3.2	0.020	15640	0.487	504	4565	87*	0.42*	1090/1090	696/704	900	1.29	1.19
-2R†	3.2	0.015	14730	0.489	330	4175	65*	0.45*	1091/1091	481/527	1200	1.27	1.24
-3R†	3.2	0.299	16380	0.488	1216	----	---	----	1078/1078	----/1069	----	----	----
	Delaminated on "C" Plane												
-4R†	3.2	0.187	8440	0.485	852	5110	75*	0.23*	1084/1084	639/628	300	1.25	1.16
-6R†	3.2	0.017	13500	0.488	328	4140	57*	0.40*	1111/1111	811/834	600	1.28	1.24
-7R†	3.2	0.187	8860	0.488	1008	----	---	----	1111/1111	----/1094	----	----	----
	Delaminated on "C" Plane												
ϵ = 0.65	"C" Axis Parallel to Arc												
-8M	0.33	1.07	3825	0.486	550	5800	173	0.32	617/456	302/230	120	0.94	0.91
-9M	0.28	1.05	2255	0.486	290	4640	79	0.36	622/465	545/387	97	0.95	0.93
-10M	0.35	1.08	4355	0.486	690	6220	228	0.32	547/390	342/227	72	0.94	0.89
-11M	0.42	1.11	5925	0.486	1170	7150	464	0.37	582/421	278/208	66	0.94	0.87
-12M	0.33	1.07	2705	0.486	530	5780	151	0 28	533/375	339/204	95	0.88	0.81
-8R†	3.2	0.030	13900	0.486	521	5555	233	0.56	619/460	462/316	300	1.13	1.06
-9R†	3.2	0.189	7190	0.486	764	5850	268	0.53	554/395	324/168	150	1.11	1.02
-10R†	3.2	0.208	9750	0.487	1013	6135	342	0.56	588/427	300/154	210	1.16	1.08
-11R†	3.2	0.228	11310	0.487	1238	6480	431	0.57	626/464	279/138	210	1.16	1.08
-12R†	3.2	0.053	8230	0.487	451	4860	143	0.58	547/357	231/97	600	1.21	1.12

†Transmissivity factor equals 0.86 for sapphire window.

*Final length is based on measurement prior to sectioning, thickness refers to length after sectioning.

*Surface radiation values may be low due to requirements for critical alignment caused by utilization of one-half inch diameter sample.

Material Sample No.	T °F	Gross Recession mils	Material Recession mils	Degradation Mode	Exposure Time seconds	Recession Rate* (mils/sec) / (mils/30 min)	Description of Motion Picture Film Coverage
PG (B-6) "A" Plane							
-1M	3860	160	160	Oxidation	120	1.33/2394	uniform heat-up, side recession observed
-2M	4690	293†	272	Oxidation	120	2.27/4086	heat-up from sides to center parallel to "A" axis, side recession observed, sample moved during test
-3M	4530	134	143	Oxid + Th. Shock	61	2.34/4212	heat-up parallel to "A" axis, side recession, some sample vibration
-4M	4530	106	110	Oxidation	44	2.50/4500	heat-up parallel to "A" axis, side recession, some sample vibration
-5M	5200	186	196	Oxidation	60	3.27/5886	heat-up parallel to "A" axis, side recession, some sample vibration
-6M	5030	188	181	Oxidation	53	3.41/6138	heat-up parallel to "A" axis, side recession, some sample vibration, indication of surface reaction nonuniformity
-7M	5030	183	178	Oxid + Th. Shock	62	2.87/5166	
-1R	4105	394	386	Oxidation	900	0.43/774	heat-up parallel to "A" axis, uniform recession, indication of liquid on top side
-2R	3715	610†	564	Oxidation	1200	0.47/846	heat-up parallel to "A" axis, uniform recession
-3R	----	---	---	Th. Shock	----	----/---	heat-up parallel to "A" axis, fracture almost immediate
-4R	4650	445	456	Oxidation	300	1.52/2736	heat-up parallel to "A" axis, uniform recession
-6R	3680	300†	277	Oxidation	600	0.46/828	heat-up parallel to "A" axis, lustrous surface, uniform recession
-7R	----	---	---	Th. Shock	----	----/----	heat-up parallel to "A" axis, thermal shock after 25 mil sector had heated up
PG (B-6) "C" Plane							
-8M	5340	315†	226	Oxidation	120	1.88/3384	uniform heating, hourglass oxidation
-9M	4180	77	78	Oxidation	97	0.80/1440	uniform heating, hourglass oxidation
-10M	5760	205	163	Oxidation	72	2.26/4068	uniform heating, hourglass oxidation
-11M	6690	304†	213	Oxidation	66	3.23/5814	uniform heating, hourglass oxidation, surface activity
-12M	5320	194†	171	Oxidation	95	1.80/3240	uniform heating, hourglass oxidation, surface activity
-8R	5095	157†	144	Oxidation	300	0.48/864	uniform recession
-9R	5390	230	227	Oxidation	150	1.51/2718	heated from edges to center, no side heating, uniform recession
-10R	5675	288	273	Oxidation	210	1.30/2340	uniform recession, little side heating
-11R	6020	347	326	Oxidation	210	1.55/2794	uniform recession, little side heating
-12R	4400	316	290	Oxidation	600	0.48/870	gradual side heat-up, hourglass recession

†Gross recession is overestimated because of chipping or erosion of back face.

*Recession rate converted to 30 minutes on linear basis.

TABLE 18

SUMMARY OF ARC PLASMA EXPOSURES OF BPG(B-7)

Material Sample No. Assumed Emittance at λ = 0.65μ	Mach No.	P_e atm	i_e BTU/lb	D (in)	q_{cw} BTU/ft²sec	T °R obs	q_r Surface Radiation BTU/ft²sec	ϵ_N Computed Normal Emittance	Initial Length thickness (mils)	Final Length* thickness (mils)	Exposure Time (seconds)	Calculated Temperature Ratio T(CALC)/T(OBS) Cold Wall Heat Transfer Coefficient	Fay and Riddell Heat Transfer Coefficient
	"C" Axis Perpendicular to Arc								"C" Axis Perpendicular to Arc				
BPG (B-7) ε = 0.75													
-1M	0.30	1.05	2955	0.487	370	4010	46	0.37	876/876	746/746	120	1.19	1.16
-2M	0.33	1.07	3965	0.486	530	5040	98	0.32	828/828	494/482	119	1.06	1.03
-3M	0.36	1.08	4745	0.483	550	5120	129	0.39	839/839	594/599	90	1.08	1.08
	Delaminated on "C" Plane after Test												
-4M	0.36	1.08	6500	0.483	760	5400	165	0.41	799/799	567/575	75	1.13	1.14
	Incipient Delamination on "C" Plane												
-1R†	3.2	0.192	8370	0.483	736	4940	102*	0.36*	874/874	482/508	300	1.25	1.20
	Delaminated on "C" Plane after Test												
-2R†	3.2	0.187	8600	0.487	852	5265	---	----	888/888	816/787	57	1.21	1.13
	Delaminated on "C" Plane after 5 Seconds												
-4R†	3.2	0.020	15200	0.487	478	4910	109*	0.39*	848/848	537/539	600	1.18	1.10
-5R†	3.2	0.022	14700	0.487	501	4920	109*	0.39*	873/873	---/120	900	1.19	1.10
-6R†	3.2	0.017	13890	0.486	321	4270	55*	0.35*	785/785	521/547	600	1.23	1.21
ε = 0.65	"C" Axis Parallel to Arc								"C" Axis Parallel to Arc				
-5M	0.33	1.07	3540	0.486	500	5690	161	0.32	501/342	329/197	82	0.93	0.90
-6M	0.28	1.05	2230	0.482	310	4695	75	0.32	500/349	392/239	120	0.95	0.92
-7M	0.35	1.08	4815	0.482	710	6300	228	0.38	495/339	275/170	70	0.94	0.91
-8M	0.38	1.09	5745	0.482	910	6405	331	0.41	489/344	229/147	64	1.00	0.95
-9M	0.32	1.06	3215	0.482	480	5610	164	0.35	506/343	307/175	96	0.92	0.88
-8R†	3.2	0.030	12000	0.486	441	5380	230	0.58	456/272	271/121	300	1.12	1.08
-9R†	3.2	0.139	7230	0.486	636	5510	210	0.48	500/347	353/195	150	1.14	1.05
-10R†	3.2	0.158	7260	0.484	781	5565	222	0.49	503/347	359/206	120	1.17	1.06
-11R†	3.2	0.208	9960	0.487	960	6290	368	0.55	431/272	259/106	120	1.12	1.06
-12R†	3.2	0.014	12340	0.486	371	5080	176	0.60	518/345	297/159	900	1.14	1.03

†Transmissivity factor equals 0.86 for pyrex window.
*Surface radiation values may be low due to requirements for critical alignment caused by utilization of one-half inch diameter sample.

*Final length is based on measurement prior to sectioning; thickness refers to length after sectioning.

Material Sample No.	T °F	Gross Recession mils	Material Recession mils	Degradation Mode	Exposure Time seconds	Recession Rate* (mils/sec) / (mils/30 min)	Description of Motion Picture Film Coverage
BPG (B-7) "A" Plane							
-1M	3550	130	130	Oxidation	120	1.08/1944	heat-up from sides to center parallel to "A" axis, side recession observed
-2M	4580	334	346	Oxidation	119	2.91/5238	heat-up from sides to center, side recession
-3M	4660	245	240	Oxid + Th. Shock	90	2.67/4806	heat-up from sides to center, side recession
-4M	4940	232	224	Oxid + Th. Shock	75	2.99/5382	heat-up from sides to center, side recession
-1R	4480	392†	366	Oxid + Th. Shock	300	1.22/2196	heat-up parallel to "A" axis, uniform recession
-2R	4805	72	101	Oxid + Th. Shock	57	1.77/3186	delaminated after 40 mil sector heated up
-4R	4450	311	309	Oxidation	600	0.52/936	heat-up parallel to "A" axis, uniform recession
-5R	4460	---	553	Oxidation	900	0.61/936	heat-up parallel to "A" axis, uniform recession, some surface activity on front face
-6R	3810	264†	238	Oxidation	600	0.40/720	heat-up parallel to "A" axis, uniform recession, bands noted on front face
BPG (B-7) "C" Plane							
-5M	5230	172†	145	Oxidation	82	1.77/3186	uniform heating, hourglass oxidation
-6M	4235	108	110	Oxidation	120	0.92/1656	no film coverage
-7M	5840	220†	169	Oxidation	70	2.41/4338	uniform heating, hourglass oxidation, speckled surface
-8M	5945	260†	197	Oxidation	64	3.09/5562	uniform heating, hourglass oxidation, speckled surface
-9M	5150	199†	168	Oxidation	96	1.75/3150	no film coverage
-8R	4920	185†	151	Oxidation	300	0.50/900	uniform heating, recession
-9R	5050	147	152	Oxidation	150	1.01/1818	little activity, uniform recession
-10R	5105	144	141	Oxidation	120	1.18/2124	little activity, uniform recession
-11R	5830	172	168	Oxidation	120	1.40/2520	uniform heating, recession
-12R	4620	221	186	Oxidation	900	0.21/372	uniform heating, recession

†Gross recession is overestimated because of chipping or erosion at back face.

*Recession rate converted to 30 minutes on linear basis.

TABLE 19

SUMMARY OF ARC PLASMA EXPOSURES OF Si/RVC(B-8)

Material Sample No. Assumed Emittance at λ = 0.65μ	Mach No.	P_e atm	i_e BTU/lb	D (in)	q_{cw} BTU/ft² sec	T °R obs	q_r Surface Radiation BTU/ft² sec	ϵ_N Computed Normal Emittance	Initial Length Thickness (mils)	Final Length* Thickness (mils)	Exposure Time (seconds)	Calculated Temperature Ratio T(CALC)/T(OBS) Cold Wall Heat Transfer Coefficient	Fay and Riddell Heat Transfer Coefficient
Si/RVC(B-8) ε = 0.70													
-1M	0.36	1.08	4670	0.503	720	6160	292*	0.42	714/717	494/489	73	0.95	0.90
-2M	0.33	1.07	4230	0.502	615	5840	257*	0.47	696/691	522/519	77	0.96	0.92
-3M	0.32	1.07	3790	0.505	555	5750	280*	0.54	715/710	541/531	75	0.94	0.90
-4M	0.31	1.06	3270	0.505	475	4230	100	0.66	731/739	729/727	240	1.21	1.16
-5MA	0.31	1.06	3720	0.503	470	4250	94*	0.62	724/729	---/---	---	1.23	1.20
	After 735 seconds, temperature and radiation changed to -5MB												
-5MB	0.31	1.06	3720	0.503	470	5370	148*	0.38	---/---	509/528	785	0.97	0.95
-6MA	0.32	1.06	3910	0.503	510	4150	90*	0.65	692/693	---/---	---	1.29	1.26
	After 90 seconds, temperature and radiation changed to -6MB												
-6MB	0.32	1.06	3910	0.503	510	5510	220*	0.51	---/---	500/520	155	0.97	0.95
-7R†	3.2	0.013	8850	0.502	210	3200	53	1.08	1031/735	1030/714	1800	1.51	1.43
-8R†	3.2	0.023	9390	0.502	415	4800	174	0.70	1041/749	701/488	500	1.18	1.03
-9R†	3.2	0.026	10090	0.505	590	5220	217	0.62	1034/725	768/451	500	1.17	0.98
-10R†	3.2	0.018	8850	0.503	310	4450	125	0.68	1031/689	747/391	750	1.19	1.07
-11R†	3.2	0.138	10170	0.503	693	5250	275	0.77	1032/720	760/435	200	1.23	1.20
-12R†	3.2	0.213	10560	0.502	968	6030	526	0.85	1027/719	679/369	160	1.16	1.11
-13MA	0.35	1.07	3260	0.507	445	4215	82	0.55	725/723	---/---	680	1.20	1.17
-13MB	0.35	1.07	3260	0.507	445	5235	128	0.36	---/---	362/335	124	0.97	0.94
-14M	0.10	1.01	5480	0.503	480	5540	196	0.44	707/708	342/335	196	1.00	0.93
-15MA	0.20	1.03	3120	0.503	295	3635	57	0.69	704/705	---/---	30	1.28	1.28
-15MB	0.20	1.03	3120	0.503	295	3530	45	0.62	---/---	704/701	1770	1.32	1.32
-16M	0.17	1.02	2520	0.504	220	3200	19	0.39	761/762	754/754	1800	1.33	1.33
-17M	0.38	1.07	2920	0.503	397	4235	90	0.60	721/729	458/349	530	1.15	1.12
-18M	0.29	1.05	3190	0.505	362	3970	59	0.77	723/728	725/718	1800	1.36	1.35
-19MA	0.18	1.02	3160	0.505	324	3730	71	0.78	716/713	---/---	100	1.28	1.24
-19MB	0.18	1.02	3160	0.503	321	4475	54	0.79	---/---	715/704	1700	1.37	1.33
-20R†	2.2	0.103	6240	0.500	227	3075	28	0.67	1054/740	1054/728	1800	1.60	1.71
-21R†	2.2	0.109	6300	0.506	262	3055	28	0.68	102 /696	1024/684	1800	1.66	1.73

* Surface radiation values might be in error since severe side erosion caused a significant change in specimen diameter.
† Transmissivity factor equals 0.86 for sapphire window.

Final length is based on measurement after exposure; thickness refers to scale length.

Material Sample No.	T °F	Gross Recession mils	Material Recession mils	Degradation Mode	Exposure Time seconds	Recession Rate* mil/sec / mils/30 min	Description of Motion Picture Film Coverage
Si/RVC(B-8)							
-1M	5720	220	228	RVC Oxidation	73	3.12/5620	Coating melted and burned off, hourglass recession.
-2M	5580	174	172	RVC Oxidation	77	2.23/4020	Coating melted and burned off, hourglass recession.
-3M	5490	171	179	RVC Oxidation	75	2.39/1290	Coating melted and burned off, hourglass recession.
-4M	3770	2	12	SiC Oxidation	240	----/90	Coating melted but remained on front face.
-5MA	3790	---	10†	SiC Oxidation	735	----/25†	Coating melted and remained, then burned off,
						----/----	hourglass recession.
-5MB	4910	215	191	RVC Oxidation	50	3.82/6876	
-6MA	3690	---	10†	SiC Oxidation	90	----/200†	Coating melted and remained, then burned off,
						----/----	Hourglass recession.
-6MB	5050	192	163	RVC Oxidation	65	2.50/4515	
-7R	2710	1	21	SiC Oxidation	1800	----/21	
-8R	3310	310	261	Oxidation	500	----/940	
-9R	3760	266	274	Oxidation	500	----/985	
-10R	3990	281	298	Oxidation	750	----/715	
-11R	3790	272	285	RVC Oxidation	200	1.38/2565	Immediate coating failure, uniform recession.
-12R	5570	318	350	RVC Oxidation	160	2.11/3938	Immediate coating failure, uniform recession.
-13MA	3755	--	---	SiC Oxidation	680	----/21	Liquid on face and edges.
-13MB	4775	363	388	RVC Oxidation	124	3.06/5516	Coating failed, rapid ablation.
-14M	5080	365	373	RVC Oxidation	196	1.86/3352	Immediate coating failure, graphite ablation.
-15MA	3175	---	---	SiC Oxidation	30	----/----	Liquid at edges.
-15MB	3070	0	4	SiC Oxidation	1770	----/4	No failure.
-16M	2710	7	8	SiC Oxidation	1800	----/8	Little visible, no failure.
-17M	3775	263	380	RVC Oxidation	530	0.70/1263	Bubbles at edges, failed near top edge and spread across face.
-18M	3110	2	10	SiC Oxidation	1800	----/10	Bubbles at edges, no failure.
-19MA	3270	---	--	SiC Oxidation	100	----/----	Small bubbles on face and edges
-19MB	3015	1	9	SiC Oxidation	1700	----/9	No failure.
-20R	2615	0	12	SiC Oxidation	1800	----/12	Little activity.
-21R	2595	1	12	SiC Oxidation	1800	----/12	Little activity.

† Estimated.

Recession rates converted to thirty minutes on linear basis.

TABLE 20

SUMMARY OF ARC PLASMA EXPOSURES OF PT0178(B-9)

Material Sample No. Assumed Emittance at $\lambda = 0.65\mu$	Mach No.	P_e atm	i_e BTU/lb	D (in)	q_{cw} BTU/ft^2 sec	T °R obs	q_r Surface Radiation BTU/ft^2 sec	ϵ_N Computed Normal Emittance	Initial Length thickness (mils)	Final Length* thickness (mils)	Exposure Time (seconds)	Calculated Temperature Ratio T(CALC)/T(OBS) Cold Wall Heat Transfer Coefficient	Fay and Riddell Heat Transfer Coefficient
PT0178 (B-9) $\epsilon = 0.75$													
-1M	0.28	1.05	1665	0.495	550	5375	193*	0.49	1083/1084	786/759	83	0.81	0.70
-2M	0.24	1.03	2285	0.495	285	4650	94*	0.43	1098/1104	832/829	100	0.93	0.90
-3M	0.29	1.05	3960	0.495	570	5410	211*	0.52	1100/1104	844/808	67	1.00	0.95
-4M	0.31	1.06	4770	0.495	780	6280	260*	0.36	1089/1091	817/815	58	0.94	0.87
-5M	0.33	1.07	5590	0.495	940	6445	375*	0.46	1078/1080	799/801	54	0.97	0.90
-6R+	3.2	0.011	12190	0.495	271	4250	133	0.87	1377/1083	909/607	1000	1.23	1.15
-7R+	3.2	0.023	10800	0.495	443	4680	197	0.87	1450/1115	978/718	550	1.24	1.10
-8R+	3.2	0.028	12990	0.495	590	5180	283	0.84	1473/1127	925/677	500	1.21	1.07
-9R+	3.2	0.030	16050	0.495	763	5500	368	0.85	1350/1091	937/675	400	1.22	1.08
-10R+	3.2	0.213	11440	0.495	1035	6355	625	0.81	1165/1096	525/260	190	1.11	1.06

*Surface radiation values might be in error since severe side erosion caused a significant change in specimen diameter.
+Transmissivity factor equals 0.86 for sapphire window.

*Final length is based on measurement prior to sectioning, thickness refers to length after sectioning.

Material Sample No.	T °F	Gross Recession mils	Material Recession mils	Degradation Mode	Exposure Time	Recession Rate* mils/sec / mils/30 min	Description of Motion Picture Film Coverage
PT0178 (B-9)							
-1M	4915	297	325	Oxidation	83	3.92/7050	rapid heat-up of entire specimen, hourglass recession
-2M	4190	266	275	Oxidation	100	2.75/4950	rapid hourglass recession
-3M	4950	256	296	Oxidation	67	4.42/7950	rapid hourglass recession
-4M	5820	272	276	Oxidation	58	4.76/8570	rapid hourglass recession
-5M	5985	279	279	Oxidation	54	5.17/9300	rapid hourglass recession
-6R	3790	468	476	Oxidation	1000	----/857	
-7R	4220	472	397	Oxidation	550	----/1298	
-8R	4720	548	450	Oxidation	500	----/1620	
-9R	5040	413	416	Oxidation	400	----/1872	
-10R	5895	640	836	Oxidation	190	4.40/7920	rounding of nose, uniform recession

*Recession rate converted to 30 minutes on linear basis.

TABLE 21

SUMMARY OF ARC PLASMA EXPOSURES OF AXF-5Q POCO (B-10) and GLASSY CARBON (B-11)

Material Sample No. Assumed Emittance at $\lambda = 0.65\mu$	Mach No.	P_e atm	i_e BTU/lb	D (in)	q_{cw} BTU/ft^2sec	T °K obs	q_r Surface Radiation BTU/ft^2sec	ϵ_N Computed Normal Emittance	Initial Length* / thickness	Final Length* / thickness	Exposure Time (seconds)	Calculated Temperature Ratio T(CALC)/T(OBS) Cold Wall Heat Transfer Coefficient	Fay and Riddell Heat Transfer Coefficient
AXF-5Q (B-10) POCO Graphite $\epsilon = 0.75$													
-1M	0.30	1.06	3485	0.501	400	4820	140	0.55	826/831	629/629	103	1.03	1.02
-2M	0.36	1.08	6370	0.501	625	6040	345	0.55	840/842	605/604	76	0.97	1.01
-3M	0.33	1.07	5180	0.501	575	5600	210	0.46	824/830	610/618	81	1.00	1.01
-4M	0.38	1.09	5210	0.501	860	6260	305	0.42	836/843	643/644	61	0.97	0.92
-5M	0.42	1.11	9195	0.501	1060	6580	515	0.59	837/841	678/679	44	1.03	1.05
-6M	0.31	1.06	3530	0.501	335	4800	120	0.48	836/843	645/646	84	1.00	1.03
-7R+	3.2	0.025	14370	0.502	638	4980	217	0.75	1179/842	619/483	800	1.28	1.13
-8R+	3.2	0.015	12760	0.500	364	4360	132	0.78	1170/830	730/386	900	1.28	1.18
-9R+	3.2	0.034	16380	0.502	902	5380	312	0.79	1163/840	681/415	550	1.29	1.12
-10R+	3.2	0.218	10890	0.502	1102	5810	487	0.91	1128/836	573/308	250	1.22	1.15
-11R+	3.2	0.220	11620	0.501	1180	6225	356	0.50	1127/836	403/118	300	1.16	1.09
-12R+	3.2	0.010	11910	0.502	184	3070	38	0.91	1133/854	750/461	1500	1.55	1.57
-13R+	3.2	0.006	10570	0.502	104	2805	20	0.69	1131/843	933/638	1800	1.59	1.57
Glassy Carbon (B-11) Grade 2000 $\epsilon = 0.55$													
-1M	0.31	1.06	3630	0.500	505	5450	193	0.46	506/135	---/---	45	1.01	0.97
-2M	0.29	1.05	3015	0.500	440	5450	219	0.53	565/135	---/31	35	0.95	0.91
-3M	0.20	1.03	3785	0.500	360	5000	147	0.50	525/135	521/10	54	1.04	1.04
-4M	0.16	1.02	3300	0.500	300	*	*	*	471/132	---/---	----	----	----

+Transmissivity factor equals 0.86 for sapphire window.
*Immediate thermal shock failure on exposure to jet.

* Final length is based on measurement prior to sectioning; thickness refers to length after sectioning.

Material Sample No.	T °F	Gross Recession mils	Material Recession mils	Degradation Mode	Exposure Time seconds	Recession Rate* mils/sec / mils/30 min	Description of Motion Picture Film Coverage
POCO Graphite							
-1M	4360	197	202	Oxidation	103	---/3531	uniform heating, slight hourglass recession
-2M	5580	235	238	Oxidation	76	---/5636	uniform heating, hourglass recession
-3M	5140	214	212	Oxidation	81	---/4710	uniform heating, slight hourglass recession
-4M	5800	193	199	Oxidation	61	---/5862	uniform heating, hourglass recession, speckled surface
-5M	6120	159	162	Oxidation	44	---/6626	rapid heating, rapid hourglass recession
-6M	4340	191	197	Oxidation	84	---/4221	uniform heating, hourglass recession, speckled surface
-7R	4520	560	359	Oxidation	800	---/808	
-8R	3900	440	444	Oxidation	900	---/888	
-9R	4920	482	425	Oxidation	550	---/1390	
-10R	5350	577	529	Oxidation	250	2.12/3816	uniform recession
-11R	5765	724	718	Ablation	300	4308	Uniform heating, recession,
-12R	2610	383	393	Ablation	1500	472	Uniform heating, recession,
-13R	2345	198	205	Ablation	1800	205	Uniform heating, recession,
Glassy Carbon (B-11) Grade 2000							
-1M	4990	---	---	Oxidation	45	----	Hourglass recession; edges melted, then rear of specimen melted, then front face melted.
-2M	4990	---	104	Oxidation	35	5349	Hourglass recession,
-3M	4540	4	125	Oxidation	54	4167	Hourglass recession,
-4M	----	---	---	Th. Shock	----	----	Thermal shocked immediately.

*Recession rates converted to 30 minutes on linear basis.

TABLE 22

SUMMARY OF ARC PLASMA EXPOSURES OF HfC + C(C-11)

Material Sample No. Assumed Emittance at λ = 0.65μ	Mach No.	P_e atm	i_e BTU/lb	D (in)	q_{cw} BTU/ft^2 sec	T $^\circ$R obs	q_r Surface Radiation BTU/ft^2 sec	ϵ_N Computed Normal Emittance	Initial Length/Thickness (mils)	Final Length*/Thickness (mils)	Exposure Time (seconds)	Calculated Temperature Ratio T(CALC)/T (OBS) Cold Wall Heat Transfer Coefficient	Calculated Temperature Ratio T(CALC)/T (OBS) Fay and Riddell Heat Transfer Coefficient
HfC + C (C-11) ϵ = 0.60													
-1M	0.35	1.07	4670	0.456	635	5710	353	0.71	407/407	486/348	1185	1.03	1.01
-2M	0.36	1.08	5320	0.456	715	5515	309	0.71	406/401	390/323	1800	1.11	1.10
-3M	0.37	1.09	5790	0.456	755	6580	538	0.61	416/408	237/208	66	0.95	0.95
-4M	0.36	1.08	5200	0.456	755	6710	465	0.49	408/404	262/256	45	0.92	0.90
-5M	0.33	1.07	3860	0.464	495	5250	244	0.68	413/412	443/362	1800	1.04	1.03
-7R	3.2	0.221	10230	0.464	889	6345	388	0.51	711/400	515/363	60	1.11	1.09
-8R	3.2	0.192	10100	0.463	801	6320	368	0.49	712/394	479/0	100	1.09	1.07
-9R	3.2	0.125	11770	0.459	709	5360	266	0.69	714/405	681/365	300	1.27	1.27
-10R	3.2	0.066	11850	0.459	614	5335	276	0.73	714/405	726/385	1800	1.24	1.19
-11R	3.2	0.011	14370	0.459	315	5240	250	0.71	714/401	724/381	1800	1.09	1.04
-12R	3.2	0.017	15420	0.459	756	6005	303	0.50	714/396	600/286	180	1.16	0.97
-13M	0.62	1.25	2590	0.456	565	4865	195	0.74	479/428	442/364	766	1.05	1.00
-14M	0.43	1.12	3490	0.455	535	5640	237	0.50	407/383	437/346	1800	0.96	0.94
-15M	0.15	1.01	2830	0.455	235	4325	65	0.39	481/415	529/368	1800	1.05	1.05
-16M	0.17	1.02	3570	0.426	310	4900	105	0.39	423/395	499/349	1800	1.01	1.02
-17M	0.14	1.01	3400	0.426	295	4820	88	0.35	439/437	481/405	1800	1.01	1.00
-18MA	0.21	1.03	6480	0.426	740	6675	409	0.44	439/438	---/---	60	0.95	0.93
-18MB	0.21	1.03	6480	0.426	740	5850	158	0.29	---/---	262/208	1740	1.08	1.06
-19R	3.2	0.029	9160	0.427	750	6055	303	0.48	752/441	734/410	45	1.11	0.89
-20R	3.2	0.180	9040	0.427	791	6175	329	0.48	751/440	523/201	120	1.10	1.07
-21M	0.27	1.04	6330	0.440	660	5800	283	0.53	451/450	431/404	1800	1.07	1.08
-22M	0.28	1.04	5960	0.439	708	5730	288	0.57	444/451	417/382	1800	1.09	1.08
-23M	0.30	1.05	6130	0.440	748	5570	240	0.53	459/453	416/374	1800	1.13	1.13
-24R	2.2	0.204	8000	0.440	633	5645	266	0.56	752/441	768/409	1800	1.14	1.13
-25R	2.2	0.204	8610	0.439	748	5690	269	0.55	753/445	746/412	1800	1.18	1.15
-26R	2.2	0.200	8340	0.439	699	5620	256	0.55	755/448	767/416	1800	1.17	1.15

* Final length refers to measurement after exposure, thickness refers to length after sectioning.

Material Sample No.	T $^\circ$F	Gross Recession (mils)	Material Recession (mils)	Degradation Mode	Exposure Time seconds	Recession Rate* mils/30 min	Description of Motion Picture Film Coverage
HfC + C (C-11)							
-1M	5250	-79	59	Melt. + Oxid.	1185	630	Melting, sunburst formed.
-2M	5055	16	78	Melt. + Oxid.	1800	78	Melting, sunburst formed at angle, some molten droplets.
-3M	6120	179	200	Melting	66	5455	Rapid melting.
-4M	6250	146	148	Melting	45	5920	Rapid melting.
-5M	4790	-30	50	Oxidation	1800	50	Heavy oxide, small sunburst, hotter at edges.
-7R	5885	196	37	Melting	60	1110	Melting throughout run.
-8R	5860	233	394	Melting	100	7092	Melting.
-9R	4900	33	40	Melt. + Oxid.	300	240	Sunburst formed, little additional activity.
-10R	4875	-12	20	Oxidation	1800	20	Slow heatup, sides grew colder as oxide thickened.
-11R	4780	-10	20	Oxidation	1800	20	Slow heatup, sides grew colder as oxide thickened.
-12R	5545	114	110	Melting	180	1100	Melting throughout run.
-13M	4405	37	64	Oxidation	766	152	Heavy oxide, some edge chipping.
-14M	5180	-30	37	Oxidation	1800	37	Heavy oxide, some edge chipping.
-15M	3865	-48	47	Oxidation	1800	47	Puffy oxide, some edge chipping.
-16M	4440	-76	46	Oxidation	1800	46	Extremely heavy oxide.
-17M	4360	-42	32	Oxidation	1800	32	Heavy oxide, some edge chipping.
-18MA	6215	...	...	Melting	60	...	Rapid melting.
-18MB	5390	177	230	Oxidation	1740	230	Solidified in sunburst, little activity.
-19R	5595	-18	31	Melt. + Oxid.	45	1240	Slow melting, sample fractured and fell.
-20R	5718	228	239	Melting	120	3585	Continuous melting.
-21M	5340	20	46	Oxidation	1800	46	Melted into sunburst, oxide continued to melt slowly.
-22M	5370	27	69	Oxidation	1800	69	Melted into sunburst, oxide continued to melt slowly.
-23M	5110	43	79	Oxidation	1800	79	Melted into sunburst, oxide continued to melt slowly.
-24R	5185	-16	32	Oxidation	1800	32	Uniform oxidation, little activity.
-25R	5230	7	32	Oxidation	1800	32	Uniform oxidation, little activity.
-26R	5160	-12	32	Oxidation	1800	32	Uniform oxidation, little activity.

* Recession rates converted to thirty minutes on linear basis.

TABLE 23

SUMMARY OF ARC PLASMA EXPOSURES OF ZrC+C(C-12)

Material Sample No. Assumed Emittance at λ = 0.65μ	Mach No.	P_e atm	i_e BTU/lb	D (in)	q_{cw} BTU/ft²sec	T °R obs	q_r Surface Radiation BTU/ft²sec	ϵ_N Computed Normal Emittance	Initial Length* thickness (mils)	Final Length* thickness (mils)	Exposure Time	Calculated Temperature Ratio T(CALC)/T(OBS) Cold Wall Heat Transfer Coefficient	Fay and Riddell Heat Transfer Coefficient
ZrC + C (C-12) ε = 0.60													
-1M	0.33	1.07	3925	0.464	500	5310	256	0.69	412/406	444/359	1800	1.03	1.02
-2M	0.34	1.07	4070	0.464	575	5480	287	0.68	406/399	414/343	1800	1.03	1.00
-3M	0.36	1.08	4580	0.464	660	6430	378	0.47	411/404	387/379	23	0.92	0.89
-4M	0.33	1.07	4330	0.464	575	5420	292	0.72	407/403	415/353	1800	1.05	1.03
-5M	0.34	1.07	4460	0.464	620	5320	280	0.74	407/407	381/341	1800	1.09	1.07
-6M	0.35	1.08	4955	0.464	625	6500	361	0.43	417/408	331/317	44	0.91	0.91
-7M	0.31	1.06	3455	0.464	430	4965	199	0.70	417/411	426/370	1800	1.05	1.04
-7R†	3.2	0.084	11100	0.463	775	5415	303	0.75	711/411	721/202	1800	1.27	1.18
-8R†	3.2	0.224	11520	0.464	1012	6125	342	0.52	710/414	---/ 0	23	1.20	1.17
-9R†	3.2	0.218	10380	0.464	870	6235	316	0.44	713/403	435/ 0	20	1.13	1.11
-10R†	3.2	0.093	11030	0.464	548	5490	319	0.75	713/404	723/372	1800	1.17	1.17
-11R†	3.2	0.011	13320	0.464	383	5225	270	0.77	713/404	723/370	1800	1.14	1.02
-12M	0.62	1.26	2720	0.425	560	5230	219	0.62	444/443	478/354	1800	0.99	0.96
-14M	0.44	1.12	3425	0.426	535	5420	252	0.62	439/428	449/386	1800	1.00	0.98
-15M	0.15	1.01	2750	0.427	235	4360	65	0.38	481/468	536/404	1800	1.03	1.04
-16MA	0.17	1.02	3490	0.426	315	4890	76	0.28	449/452	---/---	150	1.01	1.02
-16MB	0.17	1.02	3490	0.426	315	4630	48	0.22	---/---	453/422	1650	1.07	1.07
-17M	0.21	1.03	5190	0.426	700	6785	214	0.22	285/227	---/ 0	65	0.90	0.85
-18R†	3.2	0.130	12110	0.427	650	5835	255	0.47	748/442	762/393	1350	1.15	1.19

†Transmissivity factor equals 0.86 for sapphire window.

*Final length is based upon measurement prior to sectioning; thickness refers to length after sectioning.

Material Sample No.	T °F	Gross Recession mils	Material Recession mils	Degradation Mode	Exposure Time seconds	Recession Rate* (mils/sec) / (mils/30 min)	Description of Motion Picture Film Coverage
ZrC + C (C-12)							
-1M	4850	-32	47	Oxidation	1800	----/47	droplets and whiskers at edges in small sunburst, heavy oxide coating
-2M	5020	-8	56	Oxidation	1800	----/56	sunburst formation, recession at slight angle
-3M	5970	24	25	Melting	23	1.09/1960	rapid melting, specimen fell off sting
-4M	4960	-8	50	Oxidation	1800	----/50	droplets and whiskers, small sunburst
-5M	4860	26	66	Oxidation	1800	----/66	sunburst formation of droplets and whiskers
-6M	6040	86	91	Melting	44	2.07/3725	rapid melting, specimen tilted when melting began
-7M	4505	-9	41	Oxidation	1800	----/41	little activity, heavy oxide formed
-7R	4955	- 10	209*	Oxidation	1800	209	little activity
-8R	5665	---	414*	Melting	23	56000	rapid melting
-9R	5775	278	404*	Melting	20	36000	rapid melting
-10R	5030	- 10	32	Oxidation	1800	32	speckled appearance due to graphite flakes, uniform heating and recession
-11R	4765	- 10	34	Oxidation	1800	34	same as 10R
-12M	4770	- 34	89	Oxidation	1800	89	heavy oxide, sample loose on stinger, rotating and vibrating
-14M	4960	- 10	42	Oxidation	1800	42	heavy oxide, sample loose on stinger
-15M	3900	- 55	64	Oxidation	1800	64	puffy oxide formed
-16MA	4430	---	---	Oxidation	150	30	heavy oxide formed
-16MB	4170	- 4	30	Oxidation	1650		
-17M	6325	---	247	Melting	65	6286	rapid melting and recession
-18R	5375	- 14	49	Oxidation	1350	65	gradual oxide formation, little activity

*Broken specimens, could not be measured accurately.

*Recession rates converted to thirty minutes on linear basis.

TABLE 24

SUMMARY OF ARC PLASMA EXPOSURES OF JTA(D-13)

Material Sample No. Assumed Emittance at λ = 0.65μ	Mach No.	P_e atm	i_e BTU/lb	D (in)	q_{cw} BTU/ft²sec	T °R obs	q_r Surface Radiation BTU/ft²sec	ϵ_N Computed Normal Emittance	Initial Length/thickness (mils)	Final Length*/thickness (mils)	Exposure Time (seconds)	Calculated Temperature Ratio T(CALC)/T(OBS) Cold Wall Heat Transfer Coefficient	Calculated Temperature Ratio T(CALC)/T(OBS) Fay and Riddell Heat Transfer Coefficient
JTA (D-13) ε = 0.75													
-21M	0.42	1.11	2515	0.489	730	4550	54	0.26	1015/1015	1000/992	132	1.13	0.98
-22M	0.32	1.06	3075	0.486	460	4210	60	0.40	1050/1050	1048/977	1830	1.18	1.12
-23M	0.33	1.07	4510	0.486	600	----	---	----	1050/1050	----/---	6	----	----
	Four Disks Thermal Shocked Off Front								Four Disks Thermal Shocked Off Front				
-24M	0.32	1.06	4575	0.490	490	----	---	----	1032/1032	----/---	11	----	----
	Six Disks Thermal Shocked Off Front								Six Disks Thermal Shocked Off Front				
-1M	0.32	1.07	3395	0.488	450	4210	65	0.44	986/674	975/628	1830	1.20	1.16
-2M	0.34	1.07	4920	0.488	660	5450	202	0.49	997/673	547/210	274	1.05	1.03
-3M	0.38	1.09	6425	0.488	980	----	---	----	1011/693	----/---	21	----	----
	Three Disks Thermal Shocked Off Front								Three Disks Thermal Shocked Off Front				
-4M	0.36	1.08	4320	0.488	660	5020	190	0.64	998/645	466/125	214	1.12	1.07
-5M	0.38	1.09	5110	0.488	930	----	---	----	978/658	----/---	6	----	----
	Four Disks Thermal Shocked Off Front								Four Disks Thermal Shocked Off Front				
-6M	0.36	1.08	4765	0.488	810	5080	135	0.43	992/673	709/369	87	1.18	1.08
-7R+	3.2	0.074	9520	0.488	506	5125	238	0.73	1000/681	977/637	1800	1.12	1.08
-8R+	3.2	0.164	7310	0.490	770	5765	---	----	1005/713	449/132	180	1.07	0.97
-9R+	3.2	0.151	7260	0.489	771	5765	314	0.60	1003/692	425/97	180	1.07	0.96
-10R+	3.2	0.208	9110	0.488	945	6125	461	0.70	998/663	657/312	120	1.10	1.03
-31MX	0.33	1.07	5310	0.496	635	5210	170	0.49	691/682	215/198	175	1.10	1.10
-32MXA	0.33	1.07	4215	0.496	630	5215	190	0.55	688/678	---/---	300	1.07	1.02
-32MXB	0.33	1.07	4215	0.496	630	4395	---	----	---/---	118/108	1500	1.26	1.21
-33MXA	0.31	1.06	3855	0.495	540	4845	184	0.71	689/682	---/---	200	1.10	1.06
-33MXB	0.31	1.06	3855	0.495	540	4395	86	0.49	---/---	426/381	1600	1.21	1.16
-34MXA	0.31	1.06	3780	0.495	490	4705	175	0.76	689/677	---/---	300	1.11	1.08
-34MXB	0.31	1.06	3780	0.495	490	4415	99	0.55	---/---	411/395	1500	1.18	1.15
-35MXA	0.33	1.07	4250	0.495	625	5160	192	0.58	692/684	---/---	200	1.08	1.03
-35MXB	0.33	1.07	4250	0.495	625	4365	---	----	---/---	87/58	238	1.27	1.22
-36MX	0.35	1.08	4960	0.495	780	5340	164	0.43	695/686	92/82	143	1.11	1.08
-37MX	0.36	1.08	5805	0.496	860	6190	164	0.24	690/680	391/304	63	1.00	0.96
-38MX	0.35	1.08	5145	0.495	825	5435	162	0.39	693/679	127/105	132	1.11	1.05
-39MX	0.36	1.08	5505	0.495	820	5955	134	0.23	721/677	228/203	100	1.02	0.98
-40MX	0.36	1.08	5735	0.495	845	5955	114	0.19	696/687	---/246	102	1.03	0.99
-41MX**	0.36	1.08	5395	0.495	830	5310	124	0.33	693/682	---/206	111	1.14	1.09
-42M**	0.71	1.33	3100	0.435	650	6020	220	0.36	845/836	473/412	51	0.88	0.85
-43MA**	0.37	1.08	3160	0.437	445	5445	246	0.59	862/880	---/---	110	0.91	0.90
-43MB**	0.37	1.08	3160	0.437	445	4435	---	----	---/---	371/330	1690	1.12	1.10
-44MA**	0.37	1.08	3340	0.433	500	5490	215	0.57	893/896	---/---	80	0.93	0.91
-44MB**	0.37	1.08	3340	0.433	500	4480	---	----	---/---	277/246	1750	1.14	1.11
-45MA**	0.36	1.08	3060	0.435	380	4810	164	0.65	862/861	---/---	35	1.00	1.00
-45MB	0.36	1.08	3060	0.435	380	4525	---	----	---/---	717/654	1765	1.06	1.07

**Preoxidized 30 minutes at 1650°C.

+Transmissivity factor equals 0.86 for sapphire window.

*Final length is based on measurement prior to sectioning; thickness refers to length after sectioning.

Material Sample No.	T °F	Gross Recession mils	Material Recession mils	Degradation Mode	Exposure Time seconds	Recession Rate* (mils)/(30 min)	Description of Motion Picture Film Coverage
JTA (D-13)							
-21M	4090	15	23	Oxidation	132	314	no film coverage
-22M	3750	2	73	Oxidation	1830	72	no film coverage
-23M	----	---	--	Th. Shock	6	----	no film coverage
-24M	----	---	--	Th. Shock	11	----	no film coverage
-1M	3750	11	46	Oxidation	1830	45	no film coverage
-2M	4990	450	463	Oxidation	274	3042	hot liquid oxide, sunburst formation, apparent cooling of front face
-3M	----	---	---	Th. Shock	21	----	rapid oxidation, thermal shock failure
-4M	4560	532	520	Oxidation	214	4378	liquid oxide continually boiled off
-5M	----	---	---	Th. Shock	6	----	thermal shock failure
-6M	4620	283	304	Oxidation	87	6290	liquid oxide continually boiled off
-7R	4665	23	44	Oxidation	1800	44	no film coverage
-8R	5305	556	581	Oxidation	180	5810	oxide melting, rapid recession, formed rounded nose
-9R	5305	578	595	Oxidation	180	4950	oxide melting, rapid recession, formed rounded nose
-10R	5665	341	351	Oxidation	120	5265	oxide melting, rapid recession, formed rounded nose
-31MX	4750	476	484	Oxidation	175		Sunburst formation, oxide continued to melt.
-32MXA	4795	---	---	Oxidation	300	4978	Sunburst formation, slow melting of oxide
-32MXB	3935	570	570	Oxidation	1500	570	throughout run.
-33MXA	4385	---	---	Oxidation	200		Same as 32MX.
-33MXB	3935	263	301	Oxidation	1400	301	
-34MXA	4245	---	---	Oxidation	300		Same as 32MX.
-34MXB	3955	276	282	Oxidation	1500	282	
-35MXA	4700	---	---	Oxidation	200		Same as 31MX.
-35MXB	3905	605	626	Oxidation	238	2572	
-36MX	4880	603	604	Oxidation	143	7603	Front surface melted throughout run.
-37MX	5730	299	376	Oxidation	63	10742	Rapid melting.
-38MX	4975	566	574	Oxidation	132	7827	Front surface melted throughout run, recession at angle.
-39MX	5495	493	474	Oxidation	100	8532	First gradual melting of front face, then rapid melting.
-40MX	5495	---	441	Oxidation	102	7782	Same as 39MX.
-41MX	4850	---	476	Oxidation	111	7719	Same as 39MX.
-42M	5560	312	424	Melting	51	14965	Immediate melting.
-43MA	4985	---	---	Melting	110		Oxide melting, solidified in sunburst, some additional melting.
-43MB	3975	491	550	Oxidation	1690	550	
-44MA	5030	---	---	Melting	50		Oxide melting, solidified in sunburst.
-44MB	4020	616	650	Oxidation	1750	650	
-45MA	4150	---	---	Melting	35		Oxide melting, solidified in sunburst.
-45MB	4065	145	207	Oxidation	1765	207	

*Recession rate converted to 30 minutes on linear basis.

TABLE 25

SUMMARY OF ARC PLASMA EXPOSURES OF JTA(D-13)

Material Sample No. Assumed Emittance at λ = 0.65 μ	Mach No.	P_e atm	i_e BTU/lb	D (in)	q_{cw} BTU/ft^{2}sec	T °R obs	q_r Surface Radiation BTU/ft^{2}sec	ϵ_N Computed Normal Emittance	Initial Length/Thickness (mils)	Final Length*/Thickness (mils)	Exposure Time (seconds)	Calculated Temperature Ratio T(CALC)/T (OBS) Cold Wall Heat Transfer Coefficient	Fay and Riddell Heat Transfer Coefficient
JTA (D-13) ϵ = 0.75													
-48MXI	0.15	1.01	4070	0.504	380	4225	98	0.65	689/684	---/---	1800	1.19	1.15
-48MXII	0.17	1.01	4270	0.504	379	4480	122	0.64	---/---	---/---	1800	1.13	1.12
-48MXIII	0.17	1.01	4670	0.504	376	4545	139	0.69	---/---	---/---	1800	1.12	1.13
-48MXIV	0.17	1.01	4610	0.504	370	4715	143	0.62	---/---	637/566	1800	1.08	1.09
-49RXI	3.2	0.057	9590	0.503	440	4765	162	0.67	1025/685	---/---	1800	1.21	1.16
-49RXII	3.2	0.057	9600	0.503	446	4910	174	0.64	---/---	---/---	1800	1.17	1.13
-49RXIII	3.2	0.057	9700	0.503	440	4980	184	0.64	---/---	---/---	1800	1.16	1.11
-49RXIV	3.2	0.055	9420	0.503	440	4835	176	0.69	---/---	976/640	1800	1.19	1.13

Note: Samples all cut from cylindrical billet perpendicular to billet axis (pressing direction).

*Final length refers to measurement after exposure, thickness refers to length after sectioning.

Material Sample No.	T °F	Gross Recession (mils)	Material Recession (mils)	Degradation Mode	Exposure Time seconds	Recession Rate* mils/30 min	Description of Motion Picture Film Coverage
JTA (D-13)							
-48MXI	3765	---	---	Oxidation	1800	---	Oxide formed, slow melting in irregular manner.
-48MXII	4020	---	---	Oxidation	1800	---	No change from cycle I, slight oxide melting.
-48MXIII	4085	---	---	Oxidation	1800	---	No change from cycle II, slight oxide melting.
-48MXIV	4255	52	118	Oxidation	1800	30	No change from cycle III, slight oxide melting.
-49RXI	4305	---	---	Oxidation	1800	---	Slow, spotty oxide buildup to uniform layer.
-49RXII	4450	---	---	Oxidation	1800	---	No change from cycle I, some edge chipping.
-49RXIII	4520	---	---	Oxidation	1800	---	No change from cycle II, slight edge chipping.
-49RXIV	4375	49	45	Oxidation	1800	11	No change from cycle III, slight edge chipping.

*Converted to thirty minutes on a linear basis.

TABLE 26

SUMMARY OF ARC PLASMA EXPOSURES OF KT-SiC(E-14)

Material Sample No. Assumed Emittance at $\lambda = 0.65\mu$	Mach No.	P_e atm	i_e BTU/lb	D (in)	q_{cw} BTU/ft^2 sec	T °R obs	q_r Surface Radiation BTU/ft^2 sec	ϵ_N Computed Normal Emittance	Initial Length/Thickness (mils)	Final Length*/Thickness (mils)	Exposure Time (seconds)	Calculated Temperature Ratio T(CALC)/T(OBS) Cold Wall Heat Transfer Coefficient	Fay and Riddell Heat Transfer Coefficient
KT-SiC(E-14) $\epsilon = 0.70$													
-1M	0.32	1.06	3090	0.490	480	3850	55	0.53	983/983	993/983	1835	1.32	1.25
-2M	0.35	1.07	3370	0.490	348	3495	23	0.33	992/992	995/989	1800	1.39	1.43
-3M	0.39	1.10	3280	0.491	510	3740	56	0.61	984/984	994/980	656	1.39	1.33
-4M	0.33	1.07	4155	0.491	600	4130	60	0.44	841/841	840/834	1835	1.35	1.29
-5M	0.36	1.08	4910	0.490	810	4850	101	0.39	988/674	---/249	165	1.24	1.17
-6M	0.36	1.08	4285	0.490	710	4885	151	0.56	991/680	---/0	124	1.18	1.11
-7M	0.35	1.08	3130	0.490	540	4255	90	0.58	990/678	989/656	1830	1.22	1.15
	Longitudinal Crack												
-8M	0.35	1.08	4135	0.490	520	4105	88	0.66	985/678	969/644	1830	1.32	1.31
	Longitudinal Crack												
-1R+	3.2	0.075	9720	0.489	487	3325	41	0.71	991/676	985/668	1800	1.80	1.75
-2R+	3.2	0.163	7200	0.491	781	5000	183	0.62	990/669	312/15	160	1.23	1.16
-3R+	3.2	0.068	11360	0.490	607	3640	69	0.83	991/675	976/668	1800	1.74	1.65
-4R+	3.2	0.150	7690	0.487	691	4910	220	0.81	990/681	417/100	170	1.29	1.21
-5R+	3.2	0.068	11710	0.491	657	3630	66	0.81	990/672	979/656	800	1.78	1.67
-6R+	3.2	0.100	11820	0.490	697	4885	212	0.79	990/685	517/202	200	1.34	1.30
-7R+	3.2	0.097	10880	0.490	652	3500	59	0.84	990/679	979/655	1800	1.84	1.77

+Transmissivity factor equals 0.86 for sapphire window.

*Final length is based on measurement prior to sectioning; thickness refers to length after sectioning.

Material Sample No.	T °F	Gross Recession mils	Material Recession mils	Degradation Mode	Exposure Time seconds	Recession Rate* (mils)/(30 min)	Description of Motion Picture Film Coverage
KT-SiC (E-14)							
-1M	3390	-10	0	Oxidation	1835	0	liquid present, bubbling, droplets swept to outside rim
-2M	3035	-3	3	Oxidation	1800	3	no film coverage
-3M	3280	-10	4	Oxidation	656	11	liquid present, bubbling, droplets swept to outside rim
-4M	3670	1	7	Oxidation	1835	7	no film coverage
-5M	4390	---	425	Oxid + Vapor	165	4637	rapid ablation
-6M	4425	---	680	Oxid + Vapor	124	9874	surface activity, liquid oxide, rapid ablation
-7M	3795	1	22	Oxidation	1830	22	liquid oxide, bubbling due to gas evolution
-8M	3645	16	34	Oxidation	1830	35	liquid oxide, bubbling due to gas evolution
-1R	2865	6	8	Oxidation	1800	8	no film coverage
-2R	4540	678	654	Oxid + Vapor	160	7358	rapid recession
-3R	3180	15	7	Oxidation	1800	7	no film coverage
-4R	4450	573	581	Oxid + Vapor	170	6047	uniform heating, sudden brightening, then rapid vaporization
-5R	3170	11	16	Oxidation	800	36	uniform heating, little activity
-6R	4425	473	483	Oxid + Vapor	200	4347	heated from edge to center, rapid recession by vaporization
-7R	3040	11	24	Oxidation	1800	24	uniform heating, little activity

*Recession rate converted to 30 minutes on linear basis.

TABLE 27

SUMMARY OF ARC PLASMA EXPOSURES OF JT0 992(F-15)

Material Sample No. Assumed Emittance at $\lambda = 0.65\mu$	Mach No.	P_e atm	i_e BTU/lb	D (in)	q_{cw} BTU/ft^{2}sec	T °R obs	q_r Surface Radiation BTU/ft^{2}sec	ϵ_N Computed Normal Emittance	Initial Length thickness (mils)	Final Length* thickness (mils)	Exposure Time (seconds)	Calculated Temperature Ratio T(CALC)/T(OBS) Cold Wall Heat Transfer Coefficient	Calculated Temperature Ratio T(CALC)/T(OBS) Fay and Riddell Heat Transfer Coefficient
JT0992 (F-15) $\epsilon = 0.75$													
-1M	0.43	1.12	5340	0.487	870	6160	289	0.42	1038/1038	462/420	377	0.99	0.99
-2M	0.35	1.07	2105	0.486	430	3930	104	0.93	1033/1033	---/999	1173	1.15	1.06
-3M	0.40	1.10	4285	0.487	770	5390	348	0.87	1054/1054	735/692	300	1.07	1.04
-4M	0.40	1.10	4900	0.488	860	5370	227	0.58	1034/1034	618/553	480	1.12	1.09
-5M	0.49	1.14	3540	0.487	740	5030	160	0.53	1063/1063	645/619	485	1.11	1.09
-6M	0.36	1.08	4155	0.487	660	4600	242	1.14	1016/1016	970/953	161	1.22	1.17
-4R+	3.2	0.013	7380	0.489	151	4270	46*	0.29*	1010/1010	969/957	1800	1.01	0.99
-8R+	3.2	0.014	9220	0.485	218	4845	97*	0.37*	990/990	995/968	1800	0.98	0.94
-6R+	3.2	0.014	13780	0.489	308	5380	184*	0.46*	1000/1000	1000/971	1800	0.97	0.94
-5R+	3.2	0.027	14550	0.487	500	5685	213*	0.43*	988/988	860/865	1200	1.03	0.98
-1R+	3.2	0.187	9240	0.489	950	6015	114*	0.18*	1005/1005	667/668	135	1.10	1.01
-2R+	3.2	0.287	9390	0.488	1145	6090	393*	0.60*	994/994	597/594	110	1.13	1.05
-3R+	3.2	0.163	8470	0.489	790	----	---	----	971/971	---/---	----	----	----
	Four Disks Thermal Shocked Off Front												
-7R+	3.2	0.013	9600	0.488	224	----	---	----	1012/1012	---/---	----	----	----
	Two Disks Thermal Shocked Off Front												

+Transmissivity factor equals 0.86 for sapphire window.
*Surface radiation values may be low due to requirements for critical alignment caused by utilization of one-half inch diameter samples.

*Final length is based on measurement prior to sectioning, thickness refers to length after sectioning.

Material Sample No.	T °F	Gross Recession mils	Material Recession mils	Degradation Mode	Exposure Time seconds	Recession Rate* (mils) (30 min)	Description of Motion Picture Film Coverage
JT0992 (F-15)							
-1M	5700	576	618	Oxid + Melting	377	2948	liquid formation, bubbling, oxide stringers, sunburst configuration
-2M	3470	---	34	Oxidation	1173	52	oxide formation, little activity, sample vibration
-3M	4930	319	362	Oxid + Melting	300	2172	liquid oxide, stringers, sunburst configuration
-4M	4910	416	481	Oxid + Melting	480	1804	no film coverage
-5M	4570	418	444	Oxid + Melting	485	1648	no film coverage
-6M	4140	46	63	Oxid + Melting	161	1118	no film coverage
-4R	3810	41	53	Oxidation	1800	53	little activity, slight oxidation
-8R	4385	-5	22	Oxidation	1800	22	little activity, slight oxidation
-6R	4920	0	29	Oxidation	1800	29	little activity, slight oxidation
-5R	5225	128	123	Oxidation	1200	185	uniform heating, oxide melting, sunburst formation, uniform recession
-1R	5555	538	337	Oxid + Melting	135	449	oxide melting, recession
-2R	5630	397	400	Oxid + Melting	110	6544	oxide melting, recession
-3R	----	---	---	Th. Shock	----	----	delamination
-7R	----	---	---	Th. Shock	----	----	delamination

*Recession rate converted to 30 minutes on linear basis.

TABLE 28

SUMMARY OF ARC PLASMA EXPOSURES OF JT0981(F-16)

Material Sample No. Assumed Emittance at $\lambda = 0.65\mu$	Mach No	P_e atm	i_e BTU/lb	D (in)	q_{cw} BTU/ft^{2}sec	T °R obs	q_r Surface Radiation BTU/ft^{2}sec	ϵ_N Computed Normal Emittance	Initial Length/thickness (mils)	Final Length*/thickness (mils)	Exposure Time (seconds)	Calculated Temperature Ratio T(CALC)/T(OBS) Cold Wall Heat Transfer Coefficient	Fay and Riddell Heat Transfer Coefficient
JT0981 (F-16) $\epsilon = 0.75$													
-21M	0.30	1.05	2565	0.489	460	----	---	----	1077/1077	---/---	7	----	----
	One Disk Thermal Shocked Off Front												
-22M	0.32	1.06	3230	0.490	460	4330	60	0.36	1055/1055	---/---	1830	1.16	1.10
	Thermal Shocked After Test												
-23M	0.33	1.07	4510	0.489	600	----	---	----	1041/1041	---/---	6	----	----
	Five Disks Thermal Shocked Off Front												
-24M	0.33	1.07	4510	0.490	600	----	---	----	1073/1073	---/---	6	----	----
	Six Disks Thermal Shocked Off Front												
-2M	0.36	1.08	4460	0.488	710	5570	---	----	1000/662	---/162	115	1.03	0.98
	One 136 Mil Thick Disk Thermal Shocked Off Front												
-3M	0.36	1.08	3900	0.488	670	5940	187	0.32	1000/631	774/400	70	0.93	0.88
-4M	0.35	1.08	3475	0.488	640	5450	192	0.46	998/565	603/266	148	0.99	0.92
-5M	0.32	1.06	2485	0.490	390	4370	61	0.35	1000/692	900/586	1830	1.06	1.01
-6M	0.34	1.07	4730	0.490	670	----	---	----	997/675	---/---	173	----	----
	Five Disks Thermal Shocked Off Front												
-7M	0.38	1.09	6160	0.488	950	----	---	----	986/642	---/---	8	----	----
	Three Disks Thermal Shocked Off												
-8R†	3.2	0.075	9650	0.489	512	----	---	----	1017/676	---/---	13	----	----
	Thermal Shock Failure												
-9R†	3.2	0.075	9120	0.488	523	5155	251	0.75	998/696	975/655	1800	1.12	1.06
-1R†	3.2	0.179	7430	0.489	747	5525	253	0.57	1014/694	659/338	150	1.11	1.03
-10R†	3.2	0.179	7430	0.488	751	5605	274	0.59	1013/675	626/299	126	1.10	1.01
	Apparent Surface Delamination												
-11R†	3.2	0.208	9350	0.489	950	6070	395	0.62	996/667	---/---	100	1.12	1.05
	Four Disks Thermal Shocked Off Front												

†Transmissivity factor equals 0.86 for sapphire window.

*Final length is based on measurement prior to sectioning, thickness refers to length after sectioning.

Material Sample No.	T °F	Gross Recession mils	Gross Recession mils	Degradation Mode	Exposure Time seconds	Recession Rate* (mils)/(30 min)	Description of Motion Picture Film Coverage
JT0981 (F-16)							
-21M	----	---	---	Th. Shock	6		
-22M	3870	---	---	Oxid + Th. Shock	1830	----	
-23M	----	---	---	Th. Shock	6	----	no film coverage
-24M	----	---	---	Th. Shock	6	----	
-2M	5110	---	364	Th. Shock + Oxid	115	5697	thermal shock, oxidation, bubbling
-3M	5480	226	231	Oxidation	70	5939	boiling of liquid oxide
-4M	4990	395	299	Oxidation	148	3636	boiling of liquid oxide
-5M	3910	100	106	Oxidation	1830	108	no film coverage
-6M	----	---	---	Th. Shock	173	----	thermal shock
-7M	----	---	---	Th. Shock	8	----	thermal shock
-8R	----	---	---	Th. Shock	13		
-9R	4695	23	41	Oxidation	1800	41	little activity, uniform oxidation
-1R	5065	355	356	Oxid + Melting	150	4272	oxide melted, melting and rapid recession followed
-10R	5145	391	376	Oxid + Melting	126	5373	oxide melted, melting and rapid recession followed
-11R	5610	---	---	Th. Shock + Oxid + Melting	100	----	front face thermal shocked off during heat-up, but stuck to specimen, liquid formed, then front face flew off and melting continued.

*Recession rate converted to 30 minutes on linear basis.

TABLE 29

SUMMARY OF ARC PLASMA TESTS IN NITROGEN TO MEASURE THE MELTING POINTS OF MOLYBDENUM AND TUNGSTEN

Mo (Accepted Melting Point = $5220^{\circ}R$, $\epsilon_{\lambda = 0.65} = 0.30$)

Measured Value (Model 500) = $5250 + 30^{\circ}R$
Measured Value (ROVERS) = $5190 \pm 30^{\circ}R$

W (Accepted Melting Point = $6570^{\circ}R$, $\epsilon_{\lambda = 0.65} = 0.41$)

Measured Value (Model 500) = $6850 + 110^{\circ}R$
Measured Value (ROVERS) = $6710 \pm 70^{\circ}R$

TABLE 30

SUMMARY OF ARC PLASMA EXPOSURES OF WSi_2 ON W (G-18)

Material Sample No. Assumed Emittance at λ = 0.65μ	Mach No.	P_e atm	i_e BTU/lb	D (in)	q_{cw} BTU/ft²sec	T °R	q_r Surface Radiation BTU/ft²sec	ϵ_N Computed Normal Emittance	Initial Length/thickness (mils)	Final Length*/thickness (mils)	Exposure Time (seconds)	Calculated Temperature Ratio T(CALC)/T(OBS) Cold Wall Heat Transfer Coefficient	Fay and Riddell Heat Transfer Coefficient
WSi_2/W(G-18) ϵ = 0.60(below 3500°F), 0.55(above 3500°F), 0.40(bare W)													
-1M	0.28	1.05	2440	0.505	305	3435	36	0.55	761/464	768/466	1519	1.34	1.31
-2M	0.28	1.05	2330	0.504	320	3360	34	0.57	750/448	787/437	1830	1.36	1.31
-3M	0.29	1.05	2260	0.504	330	3445	38	0.53	765/449	773/447	1830	1.33	1.27
-4M	0.30	1.05	2785	0.505	460	3535	44	0.60	763/449	779/442	1830	1.43	1.34
-5M	0.28	1.05	2680	0.504	240	3085	25	0.59	754/445	758/444	1830	1.46	1.50
-6RA+	3.2	0.082	7200	0.504	498	3290	27	0.49	765/455	---/---	700	1.90	1.76
After 700 seconds arc conditions changed to 6RB													
-6RB+	3.2	0.082	8310	0.504	554	3245	27	0.52	---/---	764/437	1100	1.86	1.71
-7RA+	3.2	0.158	8020	0.505	781	4035	71	0.57	764/454	---/---	300	1.69	1.55
After 300 seconds, material began burning and conditions changed to 7RB. This may be due to burn off of the 5 mil coating of WSi_2.													
-7RB+	3.2	0.158	8020	0.505	781	5880	170	0.30	---/---	719/404	50	1.20	1.10
-8RA+	3.2	0.156	7410	0.505	775	3965	61	0.53	761/466	---/---	270	1.70	1.54
After 270 seconds, material began burning and conditions changed to 8RB. This may be due to burn off of the 5 mil coating of WSi_2.													
-8RB+	3.2	0.158	7410	0.505	775	6055	162	0.25	---/---	471/191	280	1.15	1.05
-9R+	3.2	0.033	13400	0.503	649	5975	212	0.35	756/452	548/267	800	1.23	1.10
-10RA+	3.2	0.023	11420	0.505	458	----	62	----	757/441	---/---	110	----	----
After 110 seconds, arc conditions changed to 10RB													
-10RB+	3.2	0.018	7200	0.505	224	4330	51	0.31	---/---	509/207	1090	1.28	1.19
-11M	0.36	1.08	5205	0.504	785	6375	169	0.21	471/451	---/345	77	1.05	1.01
-12M	0.34	1.07	4095	0.503	560	5510	143	0.33	487/464	---/426	29	1.10	1.07
-13M	0.30	1.06	4265	0.504	525	6310	---	----	464/437	301/278	127	0.95	0.94
-14M	0.26	1.04	3485	0.504	440	5035	82	0.27	455/452	---/---	1032	1.06	1.02
-17M	0.21	1.02	3150	0.504	320	3640	42	0.51	104/102**	---/98	1800	1.34	1.33
-18M	0.21	1.02	3280	0.504	316	3490	33	0.47	201/200**	---/199	1800	1.40	1.41
-19MS	0.21	1.02	3380	0.500	310	2880	23	0.71	440/95**	---/95	1800	1.70	1.70
-20MS	0.21	1.02	3160	0.500	306	2970	27	0.74	147/200**	---/200	1800	1.63	1.62
-21M	0.28	1.04	3600	0.503	396	3775	54	0.57	459/453	459/453	1800	1.17	1.37
-22M	0.15	1.01	4390	0.505	344	3895	66	0.61	454/448	455/448	1800	1.33	1.34
-23RA+	2.2	0.232	8180	0.505	699	3670	52	0.61	764/461	---/---	900	1.79	1.75
-23RB+	2.2	0.232	8180	0.505	699	4035	63	0.51	---/---	---/---	---	1.66	1.62
-23RC+	2.2	0.232	8180	0.505	699	4735	102	0.43	---/---	741/428	166	1.41	1.38
-24R+	2.2	0.248	7460	0.505	653	3455	41	0.61	761/450	760/449	1800	1.86	1.82

+Transmissivity factor equals 0.86 for sapphire window.

* Final length refers to measurement after exposure, thickness refers to measurement after sectioning.
** Nose to in-depth temperature measurement station

Material Sample No.	T °F	Gross Recession mils	Material Recession mils	Degradation Mode	Exposure Time seconds	Material Sample No. (mils/sec) / (mils/30 min)	Description of Motion Picture Film Coverage
WSi_2/W (G-18)							
-1M	2975	-7	-2	WSi_2-Oxid	1519	----/0	uniform oxidation, slight bubbling at edges, coating intact
-2M	2900	-7	11	WSi_2-Oxid	1830	----/11	uniform oxidation, coating intact
-3M	2985	-6	2	WSi_2-Oxid	1830	----/2	uniform oxidation, coating intact
-4M	3075	-16	7	WSi_2-Oxid	1830	----/7	uniform oxidation, coating intact
-5M	2625	-4	1	WSi_2-Oxid	1830	----/1	uniform oxidation, coating intact
-6RA	2830	1	18	WSi_2-Oxid	700	----/18	no film coverage
-6RB	2785	1	18	WSi_2-Oxid	1100	----/18	
-7RA	3575	(10)	(10)	WSi_2-Oxid	300	----/(60)°	no film coverage
-7RB	5420	35	40	W-Oxid	50	0.80/1440	
-8RA	3505	(10)	(10)	WSi_2-Oxid	270	----/(67)°	uniform heating, coating failed followed by uniform recession
-8RB	5595	380	265	W-Oxid	280	0.95/1710	
-9R	5515	208	185	W-Oxid	800	----/416	no film coverage
-10RA	----	(30)	(30)	W-Oxid	110	----/(492)°	no film coverage
-10RB	3870	118	204	W-Oxid	1090	----/337	
-11M	5915	---	106	W-Oxid	77	1.30/2480	rapid heat-up, coating burned off, hourglass recession
-12M	5050	---	38	W-Oxid	29	1.31/2360	rapid heat-up, coating burned off, hourglass recession
-13M	5850	163	168	W-Oxid	127	1.30/2340	rapid heat-up, coating burned off, hourglass recession
-14M	4575	---	---	WSi_2-Oxid	1032	----/----	coating melted, then solidified, then failed in one spot near edge which eventually spread over entire specimen
-17M	3180	...	4	WSi_2-Oxid.	1800	---/4	Little activity.
-18M	3030	...	1	WSi_2-Oxid.	1800	---/1	Little activity, some molten droplets at edge.
-19MS	2420	...	0	WSi_2-Oxid.	1800	---/0	Little visible.
-20MS	2510	...	0	WSi_2-Oxid.	1800	---/0	Little visible.
-21M	3315	0	0	WSi_2-Oxid.	1800	---/0	Some bubbling at edges, uniform heating, no coating failure.
-22M	3435	-1	0	WSi_2-Oxid.	1800	---/0	Hot spots at edge well into run, no apparent failure.
-23RA	3210	...	...	WSi_2-Oxid.	900	---/8	Little visible.
-23RB	3575	...	...	W-Oxid.	---	---/---	Probable coating failure.
-23RC	4275	23	23	W-Oxid.	166	0.13/206	Tungsten exposed.
-24R	2995	1	1	WSi_2-Oxid.	1800	---/1	Little activity.

°Recession rate converted to 30 minutes on linear basis.
°Estimated.

TABLE 31

SUMMARY OF W_5Si_3 ZONE WIDTHS FORMED ON WSi_2/W(G-18) DURING ARC PLASMA TESTS

Test	Temperature (^oF)	Time (sec)	Width (mils)
WSi_2/W(G-18)			
-1M	2975	1519	0.40
-2M	2900	1830	0.40
-3M	2985	1830	0.30
-4M	3075	1830	0.55
-5M	2625	1830	0.15
-6R	2830/2785	1800	0.40
-17M	3180	1800	1.70
-18M	3030	1800	1.15
-21MS	3315	1800	1.55
-22MS	3435	1800	3.20
-24R	2995	1800	1.20

TABLE 32

SUMMARY OF ARC PLASMA EXPOSURES OF Sn-Al ON Ta-10W (G-19)

Material Sample No. Assumed Emittance at $\lambda = 0.65\mu$	Mach No.	P_e atm	i_e BTU/lb	D (in)	q_{cw} BTU/ft^2 sec	T °R obs	q_r Surface Radiation BTU/ft^2 sec	ϵ_N Computed Normal Emittance	Initial Length/thickness (mils)	Final Length*/thickness (mils)	Exposure Time (seconds)	Calculated Temperature Ratio T(CALC)/T(OBS) Cold Wall Heat Transfer Coefficient	Calculated Temperature Ratio T(CALC)/T(OBS) Fay and Riddell Heat Transfer Coefficient
Sn-Al/Ta-W(G-19) ϵ = 0.67(Sn-Al), 0.50(Ta-W)													
-1M	0.32	1.06	2880	0.516	390	5550	194	0.44	528/368	393/244	140	0.92	0.89
	Coating Failed - Melting of Ta Observed								Coating Failed - Melting of Ta Observed				
-2M	0.24	1.04	1360	0.516	160	2565	11	0.54	512/347	518/332	1830	1.38	1.35
-3M	0.28	1.05	2135	0.516	270	3200	31	0.63	500/355	510/332	1831	1.34	1.31
-4M	0.29	1.05	2980	0.514	350	3370	39	0.64	530/378	542/367	1830	1.43	1.41
-5M	0.30	1.05	3230	0.516	460	5770	250	0.48	520/347	375/220	83	0.93	0.89
	Coating Failed - Melting of Ta Observed								Coating Failed - Melting of Ta Observed				
-6R+	3.2	0.063	8740	0.516	514	5355	67	0.17	530/371	---/258	240	1.20	1.11
	Coating Failed - Melting of Ta Observed								Coating Failed - Melting of Ta Observed				
-7R+	3.2	0.050	7100	0.516	355	3580	42	0.54	483/329	---/317	1800	1.54	1.43
-8R+	3.2	0.011	11440	0.515	208	4130	91	0.46	525/361	500/322	400	1.29	1.27
	Coating Failed - Melting of Ta Observed								Coating Failed - Melting of Ta Observed				
-9R+	3.2	0.010	10520	0.515	138	3325	35	0.61	524/362	525/342	1800	1.41	1.43
-10R+	3.2	0.011	7940	0.516	116	3075	25	0.59	516/346	519/336	1800	1.41	1.45
-11R+	3.2	0.010	7220	0.516	94	2965	21	0.58	513/351	516/338	1800	1.38	1.45
-12R+	3.2	0.011	9400	0.516	132	3230	30	0.59	529/360	532/352	1800	1.39	1.45

+Transmissivity factor equals 0.86 for sapphire window.

*Final length is based on measurements prior to sectioning; thickness refers to length after sectioning.

Material Sample No.	T °F	Gross Recession mils	Material Recession mils	Degradation Mode	Exposure Time seconds	Recession Rate* (mils/sec)/(mils/30 min)	Description of Motion Picture Film Coverage
Sn-Al on Ta-10W(G-19)							
-1M	5090	135	124	Ta-10W Melting	140	----/1595	
-2M	2105	-6	15	Sn-Al Oxid	1830	----/15	little activity, coating did not fail
-3M	2740	-10	23	Sn-Al Oxid	1831	----/23	surface activity, some liquid bubbles, no coating failure
-4M	2910	-12	11	Sn-Al Oxid	1830	----/11	surface activity, some liquid bubbles, no coating failure
-5M	5310	145	127	Ta-10W Melting	83	----/2753	coating melted 20 seconds into run, totally burned off at 30 seconds and tantalum melted severely till run ended at 83 seconds
-6R	4895	---	121	Ta-10W Melting	240	----/908	coating formed small bubble which grew, then specimen surface brightened
-7R	3120	---	12	Sn-Al Oxid	1800	----/12	little activity
-8R	3470	25	39	Ta-10W Melting	400	----/176	metal melted
-9R	2865	-1	20	Sn-Al Oxid	1800	----/20	uniform oxidation, little activity
-10R	2615	-3	10	Sn-Al Oxid	1800	----/10	little activity, uniform heating
-11R	2505	-3	13	Sn-Al Oxid	1800	----/13	little activity, uniform heating
-12R	2770	-3	16	Sn-Al Oxid	1800	----/16	little activity, uniform heating

*Recession rates converted to 30 minutes on linear basis.

TABLE 33

SUMMARY OF ARC PLASMA EXPOSURES OF W+Zr+Cu(G-20) and W+Ag(G-21)

Material Sample No. Assumed Emittance at λ = 0.65μ	Mach No.	P_s atm	i_e BTU/lb	D (in)	q_{cw} BTU/ft²sec	T °R obs	q_r Surface Radiation BTU/ft²sec	ϵ_N Computed Normal Emittance	Initial Length/thickness (mils)	Final Length*/thickness (mils)	Exposure Time (seconds)	Calculated Temperature Ratio T(CALC)/T(OBS) Cold Wall Heat Transfer Coefficient	Calculated Temperature Ratio T(CALC)/T(OBS) Fay and Riddell Heat Transfer Coefficient
W+Zr+Cu(G-20) ϵ = 0.40													
-1M	0.22	1.03	2970	0.413	315	5005	104	0.35	445/437	---/290	157	1.03	1.03
-2M	0.13	1.01	3030	0.435	170	3805	41	0.42	504/500	398/388	324	1.22	1.30
-3M	0.15	1.01	1700	0.427	95	2640	6	0.26	591/49[illegible]	404/401	1800	1.42	1.52
-4MA	0.15	1.01	1620	0.431	130	2900	18	0.54	462/458	---/---	1425	1.34	1.35
-4MB	0.15	1.01	1620	0.431	130	3420	30	0.47	---/---	408/405	182	1.14	1.15
-5MA	0.15	1.01	1670	0.412	135	3395	28	0.45	420/414	---/---	400	1.16	1.17
-5MB	0.15	1.01	1670	0.412	135	2775	---	----	---/---	340/333	1400	1.42	1.44
-6MA	0.15	1.01	1830	0.412	155	3325	31	0.54	431/427	---/---	500	1.24	1.24
-6MB	0.15	1.01	1830	0.412	155	2880	---	----	---/---	280/262	1300	1.43	1.44
-7R⁺	3.2	0.075	9280	0.412	489	5815	215	0.40	836/520	808/477	1800	1.15	1.13
-8RA⁺	3.2	0.135	11980	0.428	662	5855	406	0.74	755/438	---/---	41	1.25	1.29
-8RB⁺	3.2	0.135	11980	0.428	662	5665	442	0.91	---/---	502/181	459	1.29	1.33
-9R⁺	3.2	0.100	10680	0.425	584	5760	237	0.46	755/433	738/411	775	1.22	1.23
W+Ag(G-21) ϵ = 0.40													
-1M	0.23	1.03	2330	0.509	310	4770	81	0.33	474/466	179/0	250	1.01	0.97
-2M	0.18	1.01	2330	0.519	230	3690	43	0.49	473/461	---/300	503	1.26	1.23
-3M	0.13	1.01	2790	0.508	150	2740	15	0.56	466/455	467/452	1800	1.64	1.72
-4M	0.15	1.01	2360	0.510	210	3475	35	0.51	470/461	---/298	624	1.32	1.29
-5M	0.13	1.01	2760	0.519	210	3510	44	0.61	459/439	---/301	460	1.35	1.34
-6M	0.15	1.01	2000	0.514	160	3005	20	0.52	450/445	---/387	1800	1.41	1.40

⁺Transmissivity factor equals 0.86 for sapphire window.

*Final length is based on measurement prior to sectioning, thickness refers to length after sectioning.

Material Sample No.	T °F	Gross Recession mils	Material Recession mils	Degradation Mode	Exposure Time seconds	Material Sample No. (mils/sec)/(mils/30min)	Description of Motion Picture Film Coverage
W+Zr+Cu(G-20)							
-1M	4545	---	147	Melting	157	1685	Immediate melting of front face.
-2M	3345	106	112	Melting	324	622	Material melting out of front face, uniform melting.
-3M	2180	97	90	Oxidation	1800	90	Little visible.
-4MA	2440	---	---	Oxidation +	1425		
-4MB	2960	54	53	Melting	182	59	Little visible, some apparent melting.
-5MA	2935	---	---	Melting +	400		
-5MB	2315	80	81	Oxidation	1400	81	Little visible, some apparent melting.
-6MA	2865	---	---	Melting +	500		
-6MB	2420	151	165	Oxidation	1300	165	Little visible, some apparent melting.
-7R	5355	28	43	Oxidation	1800	43	Heavy buildup on front, some oxide chipping off.
-8RA	5395	---	---	Melting	----	925	Heavy oxide, some melting, visible recession.
-8RB	5205	253	257	Oxidation	500		
-9R	5300	17	22	Oxidation	775	51	Heavy buildup with oxide chipping off.
W+Ag(G-21)							
-1M	4310	295	466	Melting	250	3355	Little activity, rapid melting, hourglass recession.
-2M	3230	---	161	Melting	503	576	Little visible, some apparent melting.
-3M	2280	- 1	3	Oxidation	1800	3	Little visible, some apparent melting or ablation.
-4M	3015	---	163	Melt, or Ablat.	624	182	Little visible.
-5M	3050	---	138	Ablation	460	540	Little visible.
-6M	2545	---	58	Ablation	1800	58	Little visible, apparent ablation.

TABLE 34

SUMMARY OF ARC PLASMA EXPOSURES OF SiO_2+68.5 w/o W(H-22)

Material Sample No. Assumed Emittance at λ = 0.65μ	Mach No.	P_s atm	i_s BTU/lb	D (in)	q_{cw} BTU/ft^2 sec	T °R obs	q_r Surface Radiation BTU/ft^2 sec	ϵ_N Computed Normal Emittance	Initial Length/thickness (mils)	Final Length*/thickness (mils)	Exposure Time (seconds)	Calculated Temperature Ratio T(CALC)/T(OBS): Cold Wall Heat Transfer Coefficient	Calculated Temperature Ratio T(CALC)/T(OBS): Fay and Riddell Heat Transfer Coefficient
SiO_2+68.5%W(H-22) ε 0.80													
-1MA	0.32	1.06	3670	0.507	470	4700	104	0.45	679/672	---/---	250	1.08	1.06
-1MB	0.32	1.06	3670	0.507	470	4850	132	0.51	---/---	681/662	1550	1.05	1.03
-2MA	0.33	1.07	4110	0.507	580	4965	143	0.50	704/700	---/---	600	1.08	1.04
-2MB	0.33	1.07	4110	0.507	580	4785	118	0.48	---/---	692/681	957	1.13	1.08
-3MA	0.36	1.08	4730	0.507	670	5640	240	0.50	688/684	---/---	150	1.00	0.97
-3MB	0.36	1.08	4730	0.507	670	5270	181	0.50	---/---	448/428	1650	1.07	1.04
-4MA	0.36	1.08	5500	0.507	780	5665	256	0.53	680/654	---/---	65	1.05	1.01
-4MB	0.36	1.08	5500	0.507	780	5345	---	----	---/---	243/226	1735	1.11	1.07
-5MA	0.37	1.09	6170	0.507	840	5695	276	0.56	707/697	---/---	100	1.07	1.05
-5MB	0.37	1.09	6170	0.507	840	5430	---	----	---/---	0/0	931	1.13	1.10
-6MA	0.35	1.08	4690	0.507	640	5315	200	0.53	691/682	---/---	150	1.05	1.02
-6MB	0.35	1.08	4690	0.507	640	5165	172	0.51	---/---	592/574	1650	1.08	1.05
-7R+	3.2	0.086	10580	0.507	526	4635	171	0.79	993/688	493/181	230	1.28	1.27
-8R+	3.2	0.011	13780	0.507	302	4525	164	0.83	980/677	645/346	350	1.17	1.10
-9R+	3.2	0.009	9500	0.507	184	3790	79	0.81	996/670	839/535	1800	1.23	1.16
-10R+	3.2	0.009	13100	0.508	230	4210	125	0.85	973/607	609/276	600	1.18	1.14
-11R+	3.2	0.004	12440	0.508	209	4025	95	0.77	987/687	700/392	1200	1.20	1.07

+Transmissivity factor equals 0.86 for sapphire window.

*Final Length is based on measurement prior to sectioning; thickness refers to length after sectioning.

Material Sample No.	T °F	Gross Recession mils	Material Recession mils	Degradation Mode	Exposure Time seconds	Recession Rate* mils/sec / mils/30 min	Description of Motion Picture Film Coverage
SiO_2+68.5%W(H-22)							
-1MA	4240	---	---	Oxidation	250		little activity, uniform heating, small hot bursts
-1MB	4390	- 2	10	Oxid+Flow	1550	10	kept appearing on front surface
-2MA	4505	---	---	Oxidation	600		uniform heating, small hot bursts, slight melting
-2MB	4325	12	19	Oxid+Flow	957	22	at edges
-3MA	5100	---	---	Oxidation	150		uniform heating, small hot bursts, edge melting
-3MB	4810	240	256	Oxid+Flow	1650	256	
-4MA	5205	---	---	Oxidation	65		liquid around edge, visible recession
-4MB	4885	437	428	Oxid+Flow	1735	428	
-5MA	5235	---	---	Oxidation	100		liquid around edge, visible recession,
-5MB	4970	707	697	Oxid+Flow	931	1217	burned through sting hole
-6MA	4855	---	---	Oxidation	150		uniform heating, small hot bursts
-6MB	4705	99	108	Oxid+Flow	1650	108	
-7R	4175	500	507	Oxid+Flow	230	3968	rapid recession, possible melting
-8R	4065	335	331	Oxid+Flow	350	1702	slight rounding of edges, visible length recession
-9R	3330	157	135	Oxid+Flow	1800	135	slight rounding of edges, little activity
-10R	3750	364	331	Oxid+Flow	600	993	slight rounding of edges, visible length recession
-11R	3565	237	295	Oxid+Flow	1200	443	slight rounding of edges, visible length recession

*Recession rate converted to 30 minutes on linear basis.

TABLE 35

SUMMARY OF ARC PLASMA EXPOSURES OF SiO_2 + 60 w/o W(H-23)

Material Sample No. Assumed Emittance at λ = 0.65μ	Mach No.	P_e atm	i_e BTU/lb	D (in)	q_{cw} BTU/ft^{2}sec	T °R obs	q_r Surface Radiation BTU/ft^{2}sec	ϵ_N Computed Normal Emittance	Initial Length/thickness (mils)	Final Length*/thickness (mils)	Exposure Time (seconds)	Calculated Temperature Ratio T(CALC)/T(OBS): Cold Wall Heat Transfer Coefficient	Calculated Temperature Ratio T(CALC)/T(OBS): Fay and Riddell Heat Transfer Coefficient
SiO_2-60W(H-23) ϵ = 0.40													
-1M	0.32	1.07	4490	0.505	515	4860	160	0.61	703/710	686/662	1830	1.25	1.24
-2M	0.30	1.06	3380	0.505	405	4455	125	0.68	687/700	718/683	1830	1.24	1.22
-3M	0.29	1.05	3005	0.504	340	3995	75	0.63	686/690	696/688	1039	1.31	1.30
-4M	0.26	1.04	2310	0.505	200	3805	65	0.66	700/711	702/699	1065	1.19	1.22
-5M	0.37	1.08	6010	0.505	755	5520	260	0.59	688/698	563/525	1087	1.23	1.22
-6MA	0.46	1.13	5060	0.506	840	5750	285	0.55	723/724	---/---	60	1.17	1.12
	After 60 seconds, temperature and radiation changed to -6MB												
-6MB	0.46	1.13	5060	0.506	840	5095	190	0.60	---/	438/423	1740	1.32	1.27
-7MA	0.49	1.14	5230	0.506	895	5780	274	0.52	709/713	---/---	60	1.18	1.14
	After 60 seconds, temperature and radiation changed to -7MB												
-7MB	0.49	1.14	5230	0.506	895	5120	154	0.48	---/	245/217	1740	1.34	1.28
-8R$^+$	3.2	0.023	10860	0.506	475	4680	128	0.57	1006/699	634/320	325	1.44	1.27
-9R$^+$	3.2	0.014	11330	0.506	324	4590	118	0.56	1007/699	460/155	600	1.35	1.24
-10R$^+$	3.2	0.007	9260	0.506	228	3920	66	0.59	1000/707	904/593	1800	1.45	1.27
-11R$^+$	3.2	0.004	10230	0.505	156	3620	53	0.66	1008/733	990/715	1800	1.45	1.32
-12R$^+$	3.2	0.025	14830	0.506	616	4960	158	0.55	1008/697	330/19	300	1.47	1.32
-15MA	0.37	1.08	5440	0.506	855	5765	291	0.56	694/686	---/---	60	1.19	1.13
-15MB	After 60 seconds					5080	110	0.35	----/---	377/318	1226	1.35	1.23
-16MA	0.36	1.08	5150	0.506	845	5750	268	0.52	705/691	---/---	60	1.17	1.11
-16MB	After 60 seconds					5140	86	0.26	----/---	380/304	1740	1.31	1.24
-17MA	0.35	1.08	4330	0.506	700	5450	218	0.53	702/682	---/---	60	1.16	1.10
-17MB	After 60 seconds					5120	171	0.53	----/---	611/582	1740	1.24	1.17
-18MA	0.32	1.08	3670	0.505	560	4850	151	0.5?	704/692	---/---	200	1.22	1.16
-18MB	After 200 seconds					4740	136	0.58	----/---	685/663	1600	1.24	1.19
-19MA	0.33	1.07	4260	0.506	630	5190	179	0.52	688/686	---/---	100	1.19	1.14
-19MB	After 100 seconds					5020	157	0.53	----/---	627/615	1700	1.24	1.18
-20MA	0.33	1.07	3980	0.505	595	5110	170	0.53	702/698	---/---	100	1.19	1.14
-20MB	After 100 seconds					4820	135	0.53	----/---	697/647	1700	1.26	1.23
-21R$^+$	3.2	0.005	13160	0.505	173	3995	69	0.58	1009/692	715/391	1800	1.16	1.12
-22R$^+$	3.2	0.009	14120	0.504	295	4340	108	0.65	1005/689	494/169	500	1.22	1.13
-23R$^+$	3.2	0.017	13010	0.506	411	4450	111	0.60	1010/693	540/223	300	1.28	1.16
-24R$^+$	3.2	0.016	7620	0.507	218	3760	63	0.67	1000/697	954/643	1800	1.27	1.18

$^+$Transmissivity factor equals 0.86 for sapphire window.

*Final Length is based on measurement prior to sectioning; thickness refers to length after sectioning.

Material Sample No.	T °F	Gross Recession mils	Material Recession mils	Degradation Mode	Exposure Time seconds	Recession Rate* mils/sec / mils/30 min	Description of Motion Picture Film Coverage
SiO_2-60W(H-23)							
-1M	4400	17	48	Oxidation	1830	----/48	slight surface activity
-2M	3995	-31	17	Oxidation	1830	----/17	slight surface activity
-3M	3535	-10	2	Oxidation	1039	----/3	some flaking and liquid late in run
-4M	3345	-2	12	Oxidation	1065	----/21	slight bubbling at edge, little activity
-5M	5010	125	173	Oxidation	1087	----/287	uniform oxidation at angle to cylinder axis, sagging of specimen due to fracture at sting, eventually fell off
-6MA	5290	---	---	Oxidation	60		some surface activity and melting
-6MB	4635	285	301	Oxid + Flow	1740	----/301	
-7MA	5320	---	---	Oxidation	60		slight surface activity and melting
-7MB	4660	+14	496	Oxid + Flow	1740	----/496	
-8R	4220	372	379	Oxidation	325	----/2196	
-9R	4130	547	544	Oxidation	600	----/1632	
-10R	3460	96	114	Oxidation	1800	----/114	
-11R	3160	18	18	Oxidation	1800	----/18	
-12R	4600	701	678	Oxidation	300	----/4068	
-15MA	5400	---	---	Oxidation	60	----/----	melting, recession at angle
-15MB	4620	317	368	Oxid + Flow	1226	----/368	
-16MA	5295	---	---	Oxidation	60	----/----	melting, recession at angle
-16MB	4580	325	387	Oxid + Flow	1740	----/387	
-17MA	4990	---	---	Oxidation	60	----/----	no film coverage
-17MB	4660	91	100	Oxid + Flow	1740	----/100	
-18MA	4390	---	---	Oxidation	200	----/----	slight surface activity
-18MB	4280	19	29	Oxid + Flow	1600	----/29	
-19MA	4730	---	---	Oxidation	100	----/----	surface activity
-19MB	4560	61	71	Oxid + Flow	1700	----/71	
-20MA	4650	---	---	Oxidation	100	----/----	surface activity
-20MB	4360	5	51	Oxid + Flow	1700	----/51	
-21R	3535	294	301	Oxidation	1800	301	uniform heating and recession
-22R	3080	511	520	Oxidation	500	1872	uniform heating, considerable recession
-23R	3990	470	470	Oxidation	300	2820	uniform heating, considerable recession
-24R	3300	46	54	Oxidation	1800	54	uniform heating, little activity

*Recession rate converted to 30 minutes on linear basis.

TABLE 36

SUMMARY OF ARC PLASMA EXPOSURES OF Hf-20Ta-2Mo(I-23)

Material Sample No. Assumed Emittance at $\lambda = 0.65\mu$	Mach No.	P_e atm	i_e BTU/lb	D (in)	q_{cw} BTU/ft^2 sec	T °R obs	ϵ_N Surface Radiation BTU/ft^2 sec	ϵ_N Computed Normal Emittance	Initial Length thickness (mils)	Final Length* thickness (mils)	Exposure Time (seconds)	Calculated Temperature Ratio T(CALC)/T(OBS) Cold Wall Heat Transfer Coefficient	Fay and Riddell Heat Transfer Coefficient
Hf-20Ta-2Mo(I-23) $\epsilon = 0.55$													
-1M	0.35	1.08	3295	0.508	530	4655	112	0.61	880/578	889/553	1830	1.17	1.11
-2M	0.28	1.05	1725	0.509	230	3030	29	0.73	750/436	763/434	952	1.35	1.31
-3M	0.28	1.05	2585	0.514	385	4050	50	0.39	760/449	770/434	1830	1.21	1.15
-4M	0.28	1.05	2270	0.508	320	3785	50	0.52	741/428	761/416	1830	1.22	1.17
-5M	0.31	1.05	2600	0.503	400	3895	64	0.59	743/457	750/444	1830	1.27	1.20
-6M	0.30	1.05	2865	0.505	420	3715	54	0.60	720/423	729/405	1830	1.37	1.31
-7R+	3.2	0.063	7870	0.508	455	4090	72	0.55	724/414	732/402	1800	1.49	1.38
-8R+	3.2	0.151	7400	0.505	753	----	---	----	753/447	306/0	10	----	----
	Sample melted								Sample melted				
-9R+	3.2	0.022	11250	0.514	337	4855	122	0.47	744/432	719/326	1800	1.21	1.14
-10R+	3.2	0.017	9180	0.502	258	3425	62	0.96	728/424	733/402	1800	1.59	1.49
-11R+	3.2	0.017	10600	0.515	297	3860	72	0.69	753/446	764/418	1800	1.47	1.37
-12R+	3.2	0.018	12710	0.507	378	4360	112	0.66	865/560	877/534	1800	1.39	1.29
-13M	0.26	1.04	2975	0.505	585	4370	116	0.68	435/436	447/412	1830	1.16	1.11
-14M	0.29	1.05	3965	0.509	645	5290	230	0.63	442/439	---/---	30	1.09	1.07
-15M	0.32	1.06	3735	0.505	515	5320	226	0.60	430/421	370/353	1830	1.04	1.01
-21M	0.21	1.03	4790	0.742	435	4860	156	0.59	679/672	694/666	1800	1.15	1.12
-22M	0.26	1.03	4920	0.743	470	5045	177	0.58	674/666	678/640	1800	1.13	1.11
-23MA	0.24	1.03	4470	0.492	500	5070	188	0.61	445/442	---/---	40	1.12	1.10
-23MB	0.24	1.03	4470	0.492	500	5780	278	0.53	---/---	0/0	18	0.98	0.97
-24M	0.19	1.01	3990	0.487	430	5080	169	0.54	434/425	---/392	1800	1.07	1.04
-25M	0.23	1.03	5400	0.487	380	5710	251	0.50	677/650	445/407	13	1.08	1.04
-1MC	0.29	1.05	3220	0.501	425	5220	233	0.67	443/ 97	---/51	1800	1.08	0.97
-2MC	0.30	1.05	3350	0.503	505	5310	206	0.55	440/ 93	---/24	1800	1.02	0.97
-3MCA	0.31	1.06	3380	0.499	510	5415	193	0.48	441/100	---/---	1560	1.08	0.95
-3MCB	0.31	1.06	3380	0.499	510	5795	214	0.40	---/---	---/ 0	15	0.94	0.89
-4MC	0.31	1.06	3560	0.503	480	5395	212	0.53	437/ 99	---/ 0	1800	1.01	0.98

+Transmissivity factor equals 0.86 for sapphire window.

*Final Length refers to sample length prior to sectioning; thickness refers to section length.

Material Sample No.	T °F	Gross Recession mils	Material Recession mils	Degradation Mode	Exposure Time seconds	Recession Rate mils/sec / mils/30 min	Description of Motion Picture Film Coverage
Hf-20Ta-2Mo (I-23)							
-1M	4195	-9	25	Oxidation	1830	----/25	some surface activity, speckling, little oxidation
-2M	2570	-13	2	Oxidation	952	----/4	no film coverage
-3M	3590	-10	15	Oxidation	1830	----/15	little activity
-4M	3325	-20	12	Oxidation	1830	----/12	little activity
-5M	3435	-7	13	Oxidation	1830	----/13	little activity
-6M	3255	-9	8	Oxidation	1830	----/8	little activity
-7R	3630	-8	120	Oxidation	1800	----/12	uniform heating, little activity
-8R	(4460)+	447	447	Melting	10	---- /80460	
-9R	4395	25	106	Oxid + Melting	1800	----/106	began melting, then stopped and little activity followed
-10R	2965	-5	22	Oxidation	1800	----/22	
-11R	3400	-11	24	Oxidation	1800	----/24	
-12R	3900	-12	26	Oxidation	1800	----/26	
-13M	3910	-12	24	Oxidation	1830	----/24	melting at edges, sunburst formation
-14M	4830	---	---	Oxid + Th. Shock	30	----/--	rapid melting, recession, possible thermal shock
-15M	4860	60	68	Oxidation	1830	----/67	sunburst formation, oxide melting
-21M	4400	-15	6	Oxidation	1800	6	Droplets at edges, little activity.
-22M	4585	- 4	26	Oxidation	1800	26	Droplets at edges, little activity.
-23MA	4610	---	---	Oxidation	40	44200	Sunburst formed, rapid melting.
-23MB	5320	445	442	Melting	16		
-24M	4620	---	33	Oxidation	1800	[illegible]	Slow melting of oxide continuously.
-25M	5250	232	243	Melting	13	33646	Rapid melting.
-1MC	4760	---	46	Oxidation	1800	46	Sunburst formation, edges appeared hotter than center until heavy oxide built up.
-2MC	4850	---	69	Oxidation	1800	69	Sunburst formation, small spot at center and edges hotter until heavy oxide built up.
-3MCA	4955	---	---	Oxidation	1560	114	Sunburst formation, oxide melting.
-3MCB	5335	---	100	Melting	15		
-4MC	4935	---	99	Oxidation	1800	99	Sunburst formation, oxide melting.

+Temperature estimated based on Col. Wall Heat Transfer Coefficient Calculation of 6100°R corrected by mean ratio T(CALC)/T(OBS) of 1.24 to 4920°R or 4460°F.

*Recession rate converted to 30 minutes on linear basis.

TABLE 37

SUMMARY OF ARC PLASMA EXPOSURES OF Hf-20Ta-2Mo (I-23)

Material Sample No. Assumed Emittance at λ = 0.65μ	Mach No.	P_e atm	i_e BTU/lb	D (in)	q_{cw} BTU/ft^{2}sec	T °R obs	q_r Surface Radiation BTU/ft^2 sec	ϵ_N Computed Normal Emittance	Initial Length/Thickness (mils)	Final* Length/Thickness (mils)	Exposure Time (seconds)	Calculated Temperature Ratio T(CALC)/T (OBS): Cold Wall Heat Transfer Coefficient	Calculated Temperature Ratio T(CALC)/T (OBS): Fay and Riddell Heat Transfer Coefficient
Hf - 20Ta - 2Mo (I-23) ϵ = 0.55													
-26MI	0.28	1.05	3640	0.450	438	4965	152	0.53	914/914	---/---	1800	1.08	1.07
-26MII	0.29	1.05	3860	0.450	458	5265	187	0.52	---/---	---/---	1800	1.04	1.03
-26MIII	0.29	1.05	4020	0.450	462	5265	172	0.48	---/---	---/---	1800	1.05	1.05
-26MIVA	0.28	1.05	3890	0.450	450	3370	174	0.44	---/---	---/---	1350	1.02	1.01
-26MIVB	0.28	1.05	3370	0.450	386	5000	147	0.50	---/---	880/745	450	1.04	1.03
-27MI	0.30	1.05	3180	0.450	390	4065	79	0.62	948/947	---/---	1800	1.26	1.25
-27MII	0.29	1.05	3300	0.450	400	4370	130	0.7[illegible]	---/---	---/---	1800	1.19	1.18
-27MIII	0.30	1.05	3300	0.450	410	4755	180	0.75	---/---	---/---	1276	1.10	1.08
-27MIV	0.30	1.05	3510	0.450	392	3825	207	0.81	---/---	---/---	1320	1.08	1.09
-27MV	0.30	1.05	3420	0.450	430	5020	213	0.71	---/---	---/---	1800	1.05	1.04
-27MVI	0.30	1.05	3340	0.450	418	4870	168	0.63	---/---	---/---	1800	1.08	1.06
-27MVII	0.30	1.05	3300	0.450	415	4940	176	0.63	---/---	915/809	1800	1.06	1.04
-30M	0.26	1.04	4030	0.39%	470	----	---	---	706/700	---/111	9	---	----
-31M	0.21	1.02	3620	0.390	370	4665	112	0.50	693/685	701/638	1800	1.12	1.12
-32M	0.23	1.02	4080	0.395	415	4940	174	0.62	718/714	715/640	1800	1.10	1.11
-37MH	0.30	1.05	3460	0.499	648	----	---	---	665/95**	---/0	8	---	----
-38MH	0.21	1.02	3220	0.513	435	4690	101	0.44	752/398**	770/350	1800	1.12	1.05
-41M	0.28	1.04	3760	0.399	443	----	---	---	717/108**	---/ 0	8	---	----
-42M	0.31	1.05	3190	0.390	430	----	---	---	944/398**	---/350	9	---	----
-45MS	0.30	1.05	3700	0.450	445	3715	44	0.49	793/102**	804/ 91	1800	1.45	1.44
-46MS	0.30	1.05	3760	0.450	470	4210	72	0.49	794/395**	802/382	1800	1.30	1.28
-53MH	0.19	1.02	3560	0.503	452	4505	128	0.66	721/117**	725/ 60	1800	1.19	1.21
-54M	0.28	1.04	3800	0.504	455	4665	136	0.61	764/107**	779/ 65	1800	1.17	1.14
-55M	0.28	1.04	3820	0.507	455	4870	156	0.59	795/406**	812/ 370	1800	1.12	1.10

* Final length refers to measurement after exposure; thickness refers to section length.
** Nose to in-depth temperature measurement station.

Material Sample No.	T °F	Gross Recession (mils)	Material Recession (mils)	Degradation Mode	Exposure Time seconds	Recession Rate* mils/30 min	Description of Motion Picture Film Coverage
Hf-20Ta-2Mo(I-23)							
-26MI	4505	---	---	Oxid.+Melt.	1800	---	Oxidized rapidly, sunburst formed, edge melting continued.
-26MII	4805	---	---	Oxid.+Melt.	1800	---	Oxide broke off, new sunburst formed, slow melting continued.
-26MIII	4805	---	---	Oxidation	1800	---	Slight spalling, continuous slow melting.
-26MIVA	4910	---	---	Oxidation	1350	---	Slight spalling, continuous slow melting.
-26MIVB	4540	34	169	Oxidation	450	42	
-27MI	3605	---	---	Oxidation	1800	---	Edges hotter than center.
-27MII	3910	---	---	Oxidation	1800	---	Uniform oxide formed, edges melted, small sunburst.
-27MIII	4295	---	---	Oxid.+Melt.	1276	---	Oxide broke off, slowly melted into sunburst.
-27MIV	4365	---	--	Oxidation	1320	---	Slight melting of oxide, l[illegible]le change.
-27MV	4560	---	---	Oxid.+Melt.	1800	---	Most of oxide broke off, oxide melted into sunburst.
-27MVI	4410	---	---	Oxid.+Melt.	1800	---	Some oxide broke off, continuous oxide melting.
-27MVII	4480	33	138	Oxid.+Melt.	1800	21	Pieces of oxide broke off, continuous oxide melting.
-30M	---	---	589	Melting	9	117800	Rapid melting.
-31M	4205	-8	47	Oxidation	1800	47	Edge melting, sunburst formation, slow melting.
-32M	4480	3	74	Oxidation	1800	74	Edge melting, sunburst formation, slow melting.
-37MH	---	---	95	Melting	8	21400	Rapid melting.
-38MH	4230	18	48	Oxidation	1800	48	Oxidized over 3/8" diam. spot, slow melting
-41M	---	---	108	Melting	8	24300	Rapid melting.
-42M	---	---	398	Melting	9	79600	Rapid melting.
-45MS	3255	-11	11	Oxidation	1800	11	Little visible.
-46MS	3750	-8	13	Oxidation	1800	13	Little visible.
-53MH	4045	-4	57	Oxidation	1800	57	Rough, heavy oxide over entire nose.
-54M	4205	-15	42	Oxidation	1800	42	Edges melting continuously, small sunburst.
-55M	4410	-17	36	Oxidation	1800	36	Edges melting continuously, small sunburst.

*Recession rate converted to 30 minutes on linear basis.

TABLE 38

SUMMARY OF ARC PLASMA EXPOSURES OF Hf-20Ta-2Mo (I-23)

Material Sample No. Assumed Emittance at λ = 0.65μ	Mach No.	p_e atm	i_e BTU/lb	D (in)	q_{cw} BTU/ft²sec	^oT_R obs	q_r Surface Radiation BTU/ft²sec	ϵ_N Computed Normal Emittance	Initial Length/Thickness (mils)	Final Length*/Thickness (mils)	Exposure Time (seconds)	Calculated Temperature Ratio T(CALC)/T (OBS): Cold Wall Heat Transfer Coefficient	Calculated Temperature Ratio T(CALC)/T (OBS): Fay and Riddell Heat Transfer Coefficient
Hf - 20Ta - 2Mo (I-23) ϵ = 0.55													
-28RI	2.2	0.132	7590	0.451	403	4795	141	0.57	1229/910	---/---	1800	1.24	1.27
-28RII	2.2	0.132	7450	0.451	394	4715	141	0.61	---/---	---/---	1800	1.25	1.28
-28RIII	2.2	0.132	7410	0.451	394	4500	113	0.59	---/---	---/---	1820	1.31	1.34
-28RIV	2.2	0.137	7900	0.451	403	4585	126	0.61	---/---	1225/855	1800	1.30	1.35
-29RI	2.2	0.195	7400	0.451	354	4325	109	0.66	1275/951	---/---	1800	1.33	1.45
-29RII	2.2	0.195	7400	0.451	354	4455	121	0.65	---/---	---/---	1800	1.30	1.41
-29RIII	2.2	0.195	7400	0.451	354	4630	136	0.63	---/---	---/---	1800	1.25	1.36
-29RIV	2.2	0.195	7330	0.451	360	---	---	---	---/---	---/910	310	---	---
-33R	2.2	0.141	6060	0.390	360	4290	83	0.52	1027/709	1039/690	1800	1.32	1.35
-34R	2.2	0.151	8000	0.390	409	4870	130	0.49	1029/721	1056/709	1800	1.23	1.31
-35R	3.2	0.057	9580	0.391	440	4070	59	0.46	1040/728	1050/717	1800	1.51	1.49
-36RA	3.2	0.080	9150	0.391	509	3975	56	0.48	1106/787	---/---	313	1.59	1.56
-36RB	3.2	0.080	9150	0.391	509	4940	167	0.60	---/---	1121/763	380	1.28	1.26
-39RH	2.2	0.137	6740	0.504	412	4080	94	0.72	982/97**	988/75	1800	1.44	1.56
-40RH	2.2	0.132	6950	0.505	388	4070	99	0.77	1025/403**	1025/381+	1800	1.43	1.57
-43R	2.2	0.140	7690	0.400	403	4440	118	0.64	1065/109**	1087/ 83	1800	1.34	1.40
-44R	2.2	0.132	6800	0.401	403	5070	180	0.58	1276/394**	1306/365	1800	1.16	1.17
-47RS	2.2	0.222	7340	0.440	498	4735	152	0.64	1018/102**	1033/65	1800	1.31	1.35
-48RS	2.2	0.229	7090	0.440	498	4735	152	0.64	1061/399**	1078/373+	1800	1.30	1.34
-49RH	2.2	0.111	7480	1.000	408	4185	101	0.70	1167/205**	1175/182+	1800	1.42	1.44
-50RHS	2.2	0.115	5750	1.000	402	4780	106	0.67	1217/98**	1230/73+	1800	1.34	1.30
-51RH	2.2	0.114	6900	1.000	398	4255	123	0.80	1280/397**	1295/373+	1800	1.38	1.38
-52RHS	2.2	0.118	5890	1.000	398	4420	128	0.71	1348/399**	1358/373+	1803	1.30	1.27

* Final length refers to measurement after exposure; thickness refers to section length.
** Nose to in-depth temperature measurement station.
\+ Estimated.

Material Sample No.	^oF T	Gross Recession (mils)	Material Recession (mils)	Degradation Mode	Exposure Time seconds	Recession Rate* mils/30 min	Description of Motion Picture Film Coverage
Hf-20Ta - 2Mo(I-23)							
-28RI	4335	---	---	Oxidation	1800	---	Heavy oxide buildup.
-28RII	4255	---	---	Oxidation	1800	---	Some oxide broke off, reformed.
-28RIII	4040	---	---	Oxidation	1820	---	Some oxide broke off, reformed.
-28RIV	4125	4	55	Oxidation	1800	14	Some oxide broke off, reformed.
-29RI	3865	---	---	Oxidation	1800	---	Uniform oxide buildup.
-29RII	3995	---	---	Oxidation	1800	---	Oxide broke off, reformed uniformly.
-29RIII	4170	---	---	Oxidation	1800	---	Oxide broke off, reformed uniformly.
-29RIV	---	---	41	Oxidation	310	13	Oxide broke off, reformed uniformly.
-33R	3830	-12	19	Oxidation	1800	19	Slow, uniform oxidation.
-34R	4410	-27	12	Oxidation	1600	12	Some oxide melted at edges, little activity.
-35R	3610	-10	11	Oxidation	1800	11	Little activity.
-36RA	3515	---	---	Oxidation	313	---	Little activity.
-36RB	4480	-15	24	Oxidation	380	62	Oxide continuously melted at edges
-39RH	3620	-6	22	Oxidation	1800	22	Light oxide slowly formed over 1/4" diam. spot.
-40RH	3610	0	22+	Oxidation	1800	22+	Light oxide slowly formed over 1/4" diam. spot.
-43R	3980	-22	26	Oxidation	1800	26	Oxidized uniformly, little activity.
-44R	4610	-30	29	Oxidation	1800	29	Oxidized uniformly, little activity.
-47RS	4275	-15	37	Oxidation	1800	37	Shroud relatively cold, sample oxidized uniformly.
-48RS	4275	-17	26+	Oxidation	1800	26+	Shroud relatively cold, sample oxidized uniformly.
-49RH	3725	-8	23+	Oxidation	1800	23+	Light oxide formed over 1/4" diam. spot.
-50RHS	3820	-13	25+	Oxidation	1800	25+	Oxidized over 3/8" diam. spot.
-51RH	3795	-15	24+	Oxidation	1800	24+	Little visible.
-52RHS	3960	-10	26+	Oxidation	1803	26+	Oxidized over 1/2" diam. spot.

\+ Estimated.

*Recession rate converted to 30 minutes on linear basis.

\+ Estimated.

TABLE 39

SUMMARY OF ARC PLASMA EXPOSURES OF Ir ON C (I-24)

Material Sample No. Assumed Emittance at λ = 0.65μ	Mach No.	P_e atm	i_e BTU/lb	D (in)	q_{cw} BTU/ft² sec	T °R obs	q_r Surface Radiation BTU/ft² sec	ϵ_N Computed Normal Emittance	Initial Length/Thickness (mils)	Final Length*/Thickness (mils)	Exposure Time (seconds)	Calculated Temperature Ratio T(CALC)/T(OBS) Cold Wall Heat Transfer Coefficient	Fay and Riddell Heat Transfer Coefficient
Ir/Graphite (I-24) ε = 0.30													
-9M	0.31	1.06	3450	0.521	525	6455	93	0.11	702/702	393/330	105	0.93	0.89
-10MA	0.20	1.02	2985	0.521	345	4825	90	0.35	681/607	---/---	400	1.13	1.09
-10MB	0.20	1.02	2985	0.521	345	4680	61	0.27	---/---	---/**	1400	1.16	1.12
-11M	0.16	1.02	3620	0.525	310	4590	91	0.44	684/684	679/598	1800	1.22	1.21
-13M	0.16	1.02	3140	0.523	310	4995	99	0.34	695/695	---/**	1800	1.09	1.05
-16M	0.15	1.00	2185	0.521	310	4640	88	0.40	695/695	690/647	1800	1.06	0.98
-17R+	3.2	0.002	8550	0.521	98	3980	62	0.53	999/1005	1003/1005	1800	1.25	1.13
-19RA+	3.2	0.008	12260	0.519	302	5395	122	0.31	1001/1006	---/---	30	1.21	1.07
-19RB*+	3.2	0.008	12260	0.519	302	4800	197	0.79*	---/---	672/665	900	1.11	0.98
-22RA+	3.2	0.016	12980	0.525	506	5780	79	0.15	990/999	---/---	12	1.27	1.10
-22RB*+	3.2	0.016	12980	0.525	506	5100	276	0.87*	---/---	901/913	120	1.18	1.01
-24R+	3.2	0.004	9190	0.520	155	4605	98	0.46	1000/1004	995/1007	1800	1.20	1.07
-30R+	3.2	0.004	12220	0.518	194	4875	109	0.41	1019/1026	1027/1023	1800	1.22	1.10
-4M	0.18	1.02	2810	0.520	287	4810	76	0.30	695/697	692/693	600	1.09	1.06
-12M	0.17	1.01	2950	0.519	257	4575	46	0.22	701/700	699/698	1800	1.14	1.13
-18M	0.18	1.02	2930	0.521	287	4590	94	0.45	701/701	698/698	1200	1.15	1.13
-23M	0.18	1.01	2750	0.536	288	4615	98	0.46	699/698	696/694	1800	1.13	1.09
-36Mº	0.21	1.02	3450	0.520	310	4645	92	0.42	699/699	695/695	1800	1.09	1.10
-37Mº	0.27	1.04	3300	0.520	355	4835	118	0.46	688/688	694/---	1800	1.07	1.06
-3R+	2.2	0.106	6230	0.507	250	4445	69	0.38	1001/688	981/---	1800	1.34	1.40
-25R+	2.2	0.099	5650	0.515	20[illegible]	[illegible]	43	0.44	1002/702	997/897	600	1.48	1.57
-27R+	2.2	0.097	5790	0.521	196	37[illegible]	43	0.44	1002/703	1002/702	1200	1.[illegible]8	1.58
-29R+	2.2	0.097	5900	0.525	190	3820	43	0.43	1017/712	1011/705	1795	1.47	1.58
-36MRA**	0.20	1.02	3160	0.520	300	4450	103	0.56	695/695	---/---	---	1.12	1.11
-36MRB**	0.42	1.10	3250	0.520	515	5310	233	0.62	---/---	/---	889	1.03	0.99

\+ Transmissivity factor equals 0.86 for sapphire window.
* After coating burned off, pyrometer was sighting the graphite substrate. Emittance of 0.75 was used for the Poco Graphite (B-10).
º Coating composition 50% HfO_2-50% Ir, ε = 0.50 at λ = 0.65μ.
** Reruns, conditions gradually changed from (A) to (B).

** Too distorted to measure due to partial coating burn-off and irregular graphite ablation.
* Final length refers to sample length prior to sectioning; thickness refers to section length.

Material Sample No.	T °F	Gross Recession mils	Material Recession mils	Degradation Mode	Exposure Time seconds	Recession Rate* mils/30 min	Description of Motion Picture Film Coverage
Ir/Graphite(I-24)							
-9M	5995	309	372	Melting+C Ablation	105	6377	Front face melted, coating burn-off continued to sides. Some molten Ir on carbon.
-10MA	4365	---	33*	Ir Ablation	400	149	Dark spots on front face grew during run, one edge melted and formed hole which spread across front face.
-10MB	4220	---	---	C Ablation	1200		
-11M	4130	- 5	86	Oxidation	1800	86	Dark spots kept forming and disappearing except for one in center which grew near end of run.
-13M	4535	---	---	Ir+C Ablation	1600	----	Coating melted off front face in an irregular manner leaving large hole.
-16M	4180	- 5	48	Oxidation	1800	48	Dark spots formed and disappeared; center patch expanded to edge, then most of front face as coating burned off.
-17R	3520	- 4	0	Oxidation	1800	0	Uniform heating, little activity.
-19RA	4935	---	33*	Ir Melting	30	1188	Coating gradually melted off front face then sides.
-19RB	4340	329	308	C Ablation	900	616	Graphite ablation.
-22RA	5320	---	26*	Ir Melting	12	3900	Rapid melting of coating from front and sides.
-22RB	4640	89	60	C Ablation	120	900	Graphite ablation.
-24R	4145	5	- 3	Oxidation	1800	0	Uniform heating, little activity.
-30R	4415	- 8	3	Oxidation	1800	3	Uniform heating, little activity.
-4M	4350	3	4	Oxidation	600	12	Little activity.
-12M	4115	2	2	Oxidation	1800	2	Little visible, slightly mottled appearance.
-18M	4130	3	3	Oxidation	1200	4	Little activity, uniform heating.
-23M	4155	3	5	Oxidation	1600	5	Little activity, uniform heating.
-36M	4185	4	4	Oxidation	1800	4	Little activity, some roughening of surface.
-37M	4375	- 6	---	Oxidation	1800	----	Uniform heating, some roughening of surface.
-3R	3985	20	---	Melting	1800	----	Coating failed around edge, not in center.
-25R	3345	5	5	Oxidation	600	15	Uniform heating, little activity.
-27R	3335	0	1	Oxidation	1200	2	Uniform heating, little activity.
-29R	3360	6	7	Oxidation	1795	7	Uniform heating, little activity.
-36MRA	3990	---	---	Oxidation	---	----	Droplets and hot spots at edges.
-36MRA	4850	---	---	Melting	889	----	Apparent failure near edge spread inward.

*Based on original coating thickness

*Recession rate converted to 30 minutes on linear basis.

TABLE 40

SUMMARY OF IN-DEPTH TEMPERATURE EXPOSURES OF ZrB_2(A-3)

Material Sample No. Assumed Emittance at $\lambda = 0.65\mu$	Nose Thickness (Inches)	I_e BTU/lb.	q_{cw} BTU/ft^2 sec	T °R Surface	T* °R In Depth	Time (Seconds)
ZrB_2(A-3) $\epsilon = 0.57$						
-1MC	0.104	4540	475	4500	----	200
				4710	----	350
				4850	----	425
				4920	----	520
				5040	----	600
				5080	----	700
				5110	----	1300
				5150	----	1500
				5150	----	1800
-2MC	0.101	3230	365	4590	3160	130
				4560	3160	350
				4370	3130	500
				4490	3160	600
				4750	3220	900
				4770	3300	1000
				4810	3340	1350
				4790	3280	1650
				4910	3310	1750
				4930	3400	1800
-3MC	0.102	3380	460	4770	----	80
				4960	----	160
				5030	3810	600
				4980	3740	700
				5010	3700	1000
				5060	3720	1275
				5150	3740	1600
				5170	3760	1800
-4MC	0.104	4560	610	6340	4420	20
	Rapid Melting			6340	----	63.8

*Assuming ϵ = 1.00 at in-depth temperature measurement station.

TABLE 42

SUMMARY OF IN-DEPTH TEMPERATURE EXPOSURES OF $ZrB_{2.1}$+20%SiC(A-8)

Material Sample No. Assumed Emittance at $\lambda = 0.65\mu$	Nose Thickness (Inches)	I_e BTU/lb.	q_{cw} BTU/ft^2 sec	T °R Surface,	T* °R In-Depth	Time (Seconds)
$ZrB_{2.1}$+20%SiC(A-8) $\epsilon = 0.60$						
-25M	0.096	5280	360	3580	3190	367
				3620	3280	674
				3510	3270	976
				3490	3250	1255
				3470	3230	1535
				3560	3310	1735
-26M	0.395	5430	370	3560	3080	765
				3570	3070	958
				3560	3060	1275
				3580	3060	1552
				3560	3060	1748
-27R	0.102	7970	452	3050	2950	600
				3140	2960	1200
				3380	----	1800
-28R	0.400	7350	452	3010	2680	600
				3220	2680	1200
				4140	2680	1800
-29M	0.096	5330	358	3960	3350	350
				3930	3260	405
	Poco(B-10) Graphite shroud completely ablated.					500
				3790	3250	666
				3740	3290	985
				3710	3260	1268
				3710	3260	1725
-30M	0.395	4840	350	3000	2470	185
				2990	2550	649
				2975	2550	940
				2975	2550	1251
				2990	2580	1551
				2975	2570	1703
-31R	0.095	7390	440	3110	2830	600
				3110	2820	1200
				3110	2820	1800
-32R	0.399	7270	437	3260	2720	600
				3240	2720	1200
				3260	2720	1800

*Assuming ϵ = 1.00 at in-depth temperature measurement station.

TABLE 41

SUMMARY OF IN-DEPTH TEMPERATURE EXPOSURES OF $HfB_{2.1}$ + 20%SiC(A-7)

Material Sample No. Assumed Emittance at $\lambda = 0.65\mu$	Nose Thickness (Inches)	I_e BTU/lb.	q_{cw} BTU/ft^2 sec	T °R Surface	T* °R In-Depth	Time (Seconds)
$HfB_{2.1}$+20%SiC(A-7) $\epsilon = 0.60$						
-36MH	0.109	3500	513	4210	3950	249
				4370	3980	690
	Sighting hole became blocked, no further measurements.					
-37MH	0.405	3640	495	4070	3510	350
				4230	3570	671
	Sighting hole became blocked, no further measurements.					
-38RH	0.100	8280	497	3070	----	600
				3050	----	1200
				3050	----	1800
-39RH	0.401	6540	487	3230	2780	600
				3200	2880	1200
				3190	2860	1800
-40M	0.100	4390	495	4095	3620	459
				4175	3840	660
				4340	3950	985
				4580	3970	1278
				4645	3990	1555
				4670	3970	1670
-41M	0.397	4400	502	3950	3150	333
				4230	3550	651
				4565	3660	1084
				4665	3660	1259
				4870	3690	1536
				5010	3810	1695
-42R	0.102	7140	498	3110	----	600
				3110	2860	1000
				3110	2860	1500
-43R	0.400	7520	503	3230	2680	600
				3230	2690	1200
				3260	2700	1800
-44MS	0.101	4360	493	3250	3070	666
				3230	3070	958
				3230	3060	1036
				3230	3050	1273
				3230	3050	1545
				3220	3060	1727
-45MS	0.399	4580	522	3350	2780	136
				3305	2790	367
				3270	2750	678
				3260	2740	962
				3250	2750	1293
				3230	2740	1700
-46RS	0.097	5750	503	3450	3120	600
				3730	3160	1200
-47RS	0.400	6290	489	3660	2910	600
				3580	2860	1200
				3660	2830	1800
-48RH	0.100	7030	492	3030	2900	600
				3000	2850	1200
				2970	2840	1800
-50RH	0.401	7250	492	2970	2800	600
				2950	2750	1200
				2940	2780	1800
-49RHS	0.101	6800	512	3320	3000	600
				3310	3000	1200
				3310	3010	1800
-51RHS	0.399	6510	497	3200	2670	600
				3190	2660	1200
				3180	2640	1800

*Assuming ϵ = 1.00 at in-depth temperature measurement station.

TABLE 43

SUMMARY OF IN-DEPTH TEMPERATURE EXPOSURES OF ZrB_2+SiC+C(A-10)

Material Sample No. Assumed Emittance at λ = 0.65μ	Nose Thickness (Inches)	i_e BTU/lb.	q_{cw} BTU/ft^2sec	T °R Surface	T* °R In-Depth	Time (Seconds)
ZrB_2+SiC+C(A-10) ϵ = 0.60						
-34MH	0.102	3950	416	3930	3620	352
				3975	3690	658
				3910	3690	956
				4110	3770	1253
				3975	3620	1545
				3975	3630	1685
-35MH	0.391	3500	420	3840	3290	340
				3840	3270	661
				3880	3310	940
				3940	3300	1252
				3960	3330	1541
				3960	3320	1666
-36RH	0.109	7250	492	3110	2800	600
				3370	3040	1200
				3770	3280	1800
-37RH	0.393	7710	482	3160	2640	600
				3260	2900	1200
				3740	2980	1800
-38M	0.096	3870	400	3665	3480	377
				3790	3490	639
				3810	3520	950
				3840	3540	1269
				3840	3550	1571
				3840	3550	1684
-39M	0.389	3990	400	4000	3010	370
				4260	3280	665
				4150	3360	939
				4450	3430	1276
				4710	3450	1545
				4745	3440	1681
-40R	0.101	6320	495	4630	3370	600
				4840	3430	1200
				5020	3360	1800
-41R	0.400	6460	495	5130	2930	600
				5210	2930	1200
				5170	2930	1800
-42MS	0.102	4000	393	3020	2820	161
				3000	2960	480
				2990	2920	683
				3000	2930	943
				2945	2890	1264
				2930	2890	1555
				2920	2880	1700
-43MS	0.395	4040	403	2965	2540	218
				3010	2600	665
				2920	2530	961
				2965	2560	1261
				3010	2570	1545
				3060	2600	1697
-44RS	0.094	7430	495	3850	3120	600
				4670	3280	1200
				4750	3220	1800
-45RS	0.399	7470	498	3880	2880	600
				5130	2870	1200
				5210	2870	1800
-46RH	0.108	7220	501	3050	2900	600
				3060	3020	1200
				3110	3020	1800
-48RH	0.404	6350	492	3030	2740	600
				3010	2750	1200
				3000	2770	1800
-47RHS	0.103	6010	507	4060	3040	600
				4330	3180	1200
				4830	3210	1800
-49RHS	0.392	6010	522	3210	2820	600
				4150	2820	1200
				4190	2830	1800

*Assuming ϵ = 1.00 at in-depth temperature measurement station.

TABLE 44

SUMMARY OF IN-DEPTH TEMPERATURE EXPOSURES OF RVA(B-5)

Material Sample No. Assumed Emittance at λ = 0.65μ	Nose Thickness (Inches)	i_e BTU/lb.	q_{cw} BTU/ft^2sec	T °R Surface	T* °R In-Depth	Time (Seconds)
RVA(B-5) ϵ = 0.85 (Below 3000°F), 0.75(3000°-3500°F), 0.65(Above 3500°F)						
-31M	0.202	2530	135	3280	2860	75
				3320	2920	95
				3310	3000	120
				3300	3020	147
				3310	3050	165
				3310	3120	212
				3310	3100	232
-32M	0.463	2930	135	3400	2730	105
				3420	2760	115
				3440	2780	130
				3450	2815	145
				3470	2835	160
				3470	2845	170
				3480	2850	180

*Assuming ϵ = 1.00 at in-depth temperature measurement station.

TABLE 45

SUMMARY OF IN-DEPTH TEMPERATURE EXPOSURES OF WSi_2/W(G-18)

Material Sample No. Assumed Emittance at λ = 0.65μ	Nose Thickness (Inches)	i_e BTU/lb.	q_{cw} BTU/ft^2sec	T °R Surface	T* °R In-Depth	Time (Seconds)
WSi_2/W(G-18) ϵ = 0.60 (Below 3500°F)						
-17M	0.102	3150	320	3620	3160	405
				3620	3250	636
				3630	3250	941
				3650	3310	1245
				3600	3310	1545
				3600	3310	1682
-18M	0.200	3280	316	3490	2960	830
				3470	3020	1130
				3490	3070	1250
				3490	3110	1560
				3490	3110	1760
-19MS	0.096	3380	310	2880	2670	243
				2850	2760	640
				2815	2740	928
				2860	2770	1260
				2860	2770	1548
				2860	2770	1672
-20MS	0.200	3160	306	2965	2720	157
				2910	2690	359
				2850	2670	678
				2785	2640	958
				2850	2660	1263
				2770	2640	1545
				2760	2620	1707

*Assuming ϵ = 1.00 at in-depth temperature measurement station.

TABLE 46

SUMMARY OF IN-DEPTH TEMPERATURE EXPOSURES OF Hf-20Ta-2Mo(I-23)

Material Sample No. Assumed Emittance at λ = 0.65μ	Nose Thickness (Inches)	i_e BTU/lb.	q_{cw} BTU/ft^{2}sec	T °R Surface	T* °R In-Depth	Time (Seconds)
Hf-20Ta-2Mo(I-23) ϵ = 0.55						
-1MC	0.097	3220	425	3890	3400	105
				4230	3605	510
				4665	3795	750
				5085	3940	1200
				5170	3920	1400
				5220	3990	1800
-2MC	0.093	3350	505	4380	3625	150
				4695	3740	275
				4890	3740	400
				5275	3900	600
				5310	3740	800
				5335	3810	900
				5240	3760	1500
				5310	3640	1800
-3MC	0.100	3380	510	5030	3840	80
				5205	3890	380
				5335	3900	515
				5410	3920	1100
				5415	4075	1330
				5335	4280	1455**
				5340	4280	1560
				5550	4500	1565
				5670	4880	1570
				5795	(5240)+	1575
-4MC	0.099	3560	480	4770	3600	115
				5330	3820	360
				5195	3720	450
				5385	3840	800
				5265	3810	1200
				5110	3810	1560
				5195	3810	1800

*Assuming ϵ = 1.00 at in-depth temperature measurement station.

**Melting observed.

+Estimated

TABLE 47

SUMMARY OF IN-DEPTH TEMPERATURE EXPOSURES OF Hf-20Ta-2Mo(I-23)

Material Sample No. Assumed Emittance at λ = 0.65μ	Nose Thickness (Inches)	i_e BTU/lb	q_{cw} BTU/ft^{2}sec	T °R Surface	T* °R In-Depth	Time (Seconds)
Hf-20Ta-2Mo ϵ = 0.55						
-53MH	0.100	3560	452	4430	3640	319
				4490	3700	658
				4450	3690	941
				4500	3670	1240
				4460	3670	1533
				4460	3690	1718
-38MH	0.398	3220	435	4550	3390	583
				4640	3320	941
				4660	3350	1259
				4660	3320	1554
				4680	3330	1712
-39RH	0.100	6740	412	4100	3580	600
				4150	3600	1200
				4160	3680	1800
-40RH	0.410	6950	388	4060	3270	600
				4110	3285	1200
				4150	3300	1800
-54M	0.106	3800	455	4640	3510	381
				4610	3640	680
				4630	3610	1274
				4640	3550	1544
				4650	3560	1740
-55M	0.408	3820	455	4760	3250	360
				4800	3250	671
				4850	3250	946
				4870	3250	1256
				4830	3260	1549
				4800	3260	1731
-43R	0.120	7690	403	4270	3570	600
				4390	3590	1200
				4530	3560	1800
-44R	0.399	6800	403	4780	----	600
				4960	----	1200
				5190	----	1800
-45MS	0.099	3700	445	3580	3210	170
				3630	3190	660
				3650	3170	947
				3670	3160	1264
				3720	3190	1537
				3700	3170	1703
-46MS	0.393	3760	470	3920	2800	350
				3940	2790	680
				3970	2790	943
				4120	2790	1260
				4180	2790	1543
				4210	2790	1720
-47RS	0.102	7340	498	4480	3270	600
				4650	3190	1200
				4840	3160	1800
-48RS	0.400	7090	498	4900	2760	600
				4650	2760	1200
				4840	2720	1800
-49RH	0.206	7480	408	4100	3460	600
				4220	3440	1200
				4270	3460	1800
-51RH	0.400	6900	398	4230	3240	600
				4290	3240	1200
				4340	3240	1800
-50RHS	0.104	5750	402	4180	3420	600
				4310	3420	1200
				4370	3370	1800
-52RHS	0.398	5890	398	4370	2970	600
				4450	2970	1200
				4500	2980	1800

*Assuming ϵ = 1.00 at in-depth temperature measurement station.

TABLE 48

AVERAGED VALUES OF TOTAL NORMAL EMITTANCE AND RATIOS OF CALCULATED AND OBSERVED TEMPERATURES DERIVED FROM HOT GAS/COLD WALL ARC PLASMA TESTS

Material/Code		ϵ_N Computed Normal Emittance (Solid)	(Melting)	Calculated Temperature Ratio T(CALC)/T(OBS) - Cold Wall Heat Transfer Coefficient (Solid)	(Melting)
$HfB_{2.1}$	A-2	0.45	0.39	1.16	0.98
ZrB_2	A-3	0.47 (0.500")	0.39 (0.500")	1.09 (0.500")	1.08 (0.500")
ZrB_2	A-3	0.57 (0.750")	---- (0.750")	1.12 (0.750")	---- (0.750")
HfB_2 + 20 v/o SiC	A-4	0.62	0.48	1.22	1.07
Boride Z	A-5	0.75	----	1.20	----
$HfB_{2.1}$ + 20 v/o SiC	A-7	0.55	0.47	1.25	0.99
$ZrB_{2.1}$ + 20 v/o SiC	A-8	0.59	0.50	1.34	1.02
$HfB_{2.1}$ + 35 v/o SiC	A-9	0.55	0.52	1.17	0.99
ZrB_2 + 14 v/o SiC + 30 v/o C	A-10	0.62	0.55	1.20	1.11
RVA	B-5	0.52 (0.500")	0.75 (0.740")	1.17 (0.500")	1.20 (0.740")
PG	B-6	0.41 $\perp$ to C	0.41 $\parallel$ to C	1.19 $\perp$ to C	1.04 $\parallel$ to C
BPG	B-7	0.37 $\perp$ to C	0.43 $\parallel$ to C	1.18 $\perp$ to C	1.03 $\parallel$ to C
Si/RVC	B-8	0.69 Coated	0.56 Bare	1.36 Coated	1.07 Bare

TABLE 48 (CONT)

AVERAGED VALUES OF TOTAL NORMAL EMITTANCE AND RATIOS OF CALCULATED AND OBSERVED TEMPERATURES DERIVED FROM HOT GAS/COLD WALL ARC PLASMA TES[illegible]

Material/Code		ϵ_N Computed Normal Emittance (Solid)	(Melting)	Calculated Temp[illegible] T(CALC)/T(OBS)-Cold Wall Heat Transfer Coefficient (Solid)	(Melting)
PT0178	B-9	0.65	----	1.07	----
Poco Graphite	B-10	0.64	----	1.18	----
Glassy Carbon	B-11	0.50	----	1.00	----
HfC + C	C-11	0.57	0.50	1.10	1.05
ZrC + C	C-12	0.60	0.42	1.08	1.01
JTA	D-13	0.52	0.55	1.13	0.93
KT-SiC	E-14	0.63	----	1.43	----
JT0992	F-15	0.48	0.60	1.04	1.08
JT0981	F-16	0.49	0.51	1.11	1.05
WSi_2/W	G-18	0.58 Coated	0.32 Bare	1.54 Coated	1.13 Bare
Sn-Al/Ta-10W	G-19	0.59 Coated	0.44 Bare	1.4[illegible] Coated	1.09 Bare
W + Zr + Cu	G-20	0.52	0.49	1.31	1.12
W + Ag	G-21	0.54	0.33	1.35	1.01
SiO_2 + 68.5 w/o W	H-22	0.61	----	1.12	----
SiO_2 + 60 w/o W	H-23	0.56	----	1.27	----
Hf-20Ta-2Mo	I-23	0.60 (0.500") 0.59 (0.750")	0.45 (0.500") ---- (0.750")	1.20 (0.500") 1.14 (0.750")	1.00 (0.500") ---- (0.750")
Ir/C	I-24	0.36 Coated 0.51 Oxide Coated	0.83 Bare 1.06 Oxide Coated	1.21 Coated	1.15 Bare

TABLE 49

COMPUTED TEMPERATURES FOR ZrB_2 AND HfB_2 AFTER TWENTY SECONDS UNDER 10 MW ARC CONDITIONS

(i_e = 2000 BTU/lb, P_e = 4.3 atm)

Distance from Front Face mils	Cold Wall Heat Flux (BTU/ft²sec) 800	1000	1200
	ZrB_2 (density = 375 lbs/ft^3)		
Radiation Equilibrium (Eqs. 2, 3)	4530°F	4640°F	4715°F
0	3221	3498	3708
250	2557	2814	3018
500	1887	2122	2318
1000	1029	1245	1437
	HfB_2 (density = 625 lbs/ft^3)		
Radiation Equilibrium (Eqs. 2, 3)	4530°F	4640°F	4715°F
0	3298	3571	3770
250	2577	2833	3030
500	1797	2034	2224
1000	461	688	902

TABLE 50

SUMMARY OF 10 MEGAWATT ARC HIGH FLUX

EXPOSURE CONDITIONS AND RESULTS

Material Sample No. Assumed Emittance at $\lambda = 0.65\mu$ $\epsilon = 0.60$	P_{stag} atm	i_s BTU/lb	D in	q_{cw} BTU/ft^{2}sec	T_B obs	Calculated Temperature Ratio T(CALC)/T(OBS): Cold Wall Heat Trans. Coefficient	Calculated Temperature Ratio T(CALC)/T(OBS): Fay and Riddell Heat Trans. Coefficient	T_{max} °F	Exposure Time seconds	Material Recession mils	Degradation Mode	Metallographic Features (Distance of Crack from Front Face - Mils)
$HfB_{2.1}$(A-2)												
-HF-1	6.33	1965	0.875	785	4820	1.02	0.95	4360	20.1	31	Th. Shock	Large Cracks* (70)
-HF-2	6.26	1930	0.875	695	3765	1.28	1.20	3305	20.1	1	Oxidation	Fine Cracks* (90)
$HfB_{2.1}$(A-6)												
-HF-20	6.57	2235	0.875	799	4060	1.27	1.19	3600	20.1	-2	Th. Shock	Large Cracks* (380)
-HF-21	6.40	2030	0.875	733	3930	1.26	1.18	3470	20.1	-1	Oxidation	Large Cracks* (380)
$HfB_{2.1}$+20 v/o SiC(A-4)												
-HF-25A	6.76	2270	0.500	835	3700	1.41	1.37	3240	8.7	--	Oxidation	----------- (---)
-HF-25B	6.66	2300	0.500	836	4885	1.07	1.04	4425	20.0	--	Th. Shock	Large Cracks (300)
-HF-26	8.51	3895	0.500	1280	4920	1.31	1.31	4460	7.8	--	Th. Sh. + Melt	Large Cracks (160)
-HF-27A	6.73	2270	0.500	835	3670	1.42	1.38	3210	10.9	--	Oxidation	----------- (---)
-HF-27B	6.80	2270	0.500	835	4320	1.21	1.17	3860	21.0	10	Oxidation	Sound* (---)
-HF-28	7.22	2640	0.500	940	4165	1.34	1.30	3705	12.0	5	Oxidation	Sound* (---)
-HF-35	6.57	2099	0.500	773	----	----	----	----	20.4	3	Oxidation	Sound° (---)
-HF-36	7.42	2890	0.500	966	5630	1.02	1.02	5170	20.1	53	Th. Shock	Large Crack (180)
-HF-37	7.06	2540	0.500	940	5250	1.05	1.03	4790	20.2	13	Oxidation	Sound* (---)
-HF-38	7.55	3013	0.500	1197	5540	1.08	1.05	5080	19.9	36	Th. Shock	Large Crack (160)
$HfB_{2.1}$ + 20 v/o SiC(A-7)												
-HF-18	6.63	2200	0.875	787	3960	1.30	1.21	3500	20.1	5	Oxidation	Fine Cracks* (110)
-HF-19A	6.74	2338	0.875	777	4040	1.29	1.22	3580	16.2	--	Oxidation	----------- (---)
-HF-19B	6.80	2335	0.875	840	4485	1.16	1.10	4025	20.1	0	Th. Shock	Large Cracks (90)
-HF-32	7.26	2710	0.500	948	5070	1.11	1.08	4610	20.1	29	Oxidation	Sound* (---)
-HF-33	8.67	3660	0.500	1306	6240	1.04	1.03	5780	20.1	340	Th. Shock	Fine Cracks* (600)
-HF-34	6.83	2338	0.500	834	4990	1.06	1.03	4530	20.1	7	Oxidation	Sound* (---)
ZrB_2(A-3)												
-HF-5	2.67	4030	0.875	1120	6040	1.06	0.93	5580	16.2	32	Th. Sh. + Melt	Large Cracks (300)
-HF-6	2.69	4065	0.875	1120	5870	1.08	0.96	5410	20.3	64	Th. Sh. + Melt	Large Cracks (360)
-HF-7A	2.44	2235	0.875	650	----	----	----	----	17.3	--	Oxidation	----------- (---)
-HF-7B	6.95	2540	0.875	960	5830	0.95	0.88	5370	20.3	65	Th. Sh. + Melt	Large Cracks (210)
-HF-8	6.36	1968	0.875	800	4280	1.15	1.07	3820	20.3	--	Oxidation	----------- (---)
-HF-13	6.54	2030	0.875	880	5190	0.97	0.89	4730	16.6	7	Th. Shock	Large Cracks (360)
-HF-14	6.43	2030	0.875	869	----	----	----	----	20.1	1	Th. Shock	Large Cracks (180)
-HF-15	6.31	2030	0.875	880	5130	0.98	0.91	4670	17.8	30	Th. Shock	Large Cracks (90)
ZrB_2(Avco)												
-HF-17	6.37	1964	0.875	714	3885	1.26	1.18	3425	20.1	12	Oxidation	Fine Cracks* (length)
-HF-22	6.50	2130	0.875	811	4800	1.06	0.99	4340	15.6	-4	Th. Shock	Large Cracks (270)
Boride Z(A-5)												
-HF-11	6.37	1965	0.875	714	4845	1.01	0.94	4385	14.6	--	Th. Shock	Large Cracks (250)
-HF-12	6.40	1965	0.875	747	4620	1.06	0.99	4160	12.0	6	Th. Shock	Large Cracks (250)
$ZrB_{2.1}$ + 20 v/o SiC(A-8)												
-HF-23A	6.57	2200	0.875	787	4160	1.23	1.16	3700	20.1	--	Oxidation	----------- (---)
-HF-23B	6.77	2370	0.875	852	4370	1.21	1.14	3910	20.1	-6	Th. Shock	Large Cracks (length)

*Samples examined by NDT dye penetrant (Table 12) yielding results in agreement with metallographic findings.

°$HfB_{2.1}$ + 20 v/o SiC(A-4)HF-35 showed a small surface crack but was otherwise sound.

TABLE 51

SPECIFICATION OF FLUX-SIZE THRESHOLDS FOR

THERMAL SHOCK FAILURES OF BORIDE CYLINDERS

Material	No Thermal Shock Noted		Thermal Shock Occurred	
	1/2" Diam	7/8" Diam	1/2" Diam	7/8" Diam
	$(q_{cw} \frac{BTU}{ft^2 sec})$ / $(T_{max}\ ^oF)$		$(q_{cw} \frac{BTU}{ft^2 sec})$ / $(T_{max}\ ^oF)$	
HfB_2 (A-2)	----------	(695)/(3305)*	-----------	(785)/(4360)
HfB_2 (A-6)	----------	(733)/(3470)*	-----------	(799)/(3600)
HfB_2 + SiC (A-4)	(940)/(5170)	-----------	(966)/(5170)	-----------
HfB_2 + SiC (A-7)	(948)/(4610)	(787)/(3500)*	(1306)/(5780)	(840)/(4025)
ZrB_2 (A-3)	-----------	(800)/(3820)	-----------	(960)/(5370)
ZrB_2 (Avco)	-----------	(714)/(3415)*	-----------	(811)/(4340)
Boride Z (A-5)	-----------	-----------	-----------	(714)/(4380) (747)/(4160)
ZrB_2 + SiC (A-8)	-----------	(787)/(3700)	-----------	(852)/(3910)

*Cracks revealed by NDT dye penetrant test and metallographic examinations of selected samples.

TABLE 52

SUMMARY OF ARC PLASMA EXPOSURES OF PIPE SPECIMENS IN THE TEN MEGAWATT ARC FACILITY

(Mach No. = 1.73, Stagnation Pressure 6.0 Atm.)

Material Sample No.*	Position in Stream*	Enthalpy (BTU/lb)	Heat Flux (BTU/ft²sec)	Pipe Shear Stress (lbs/ft²)	°F	Emittance (λ = 0.65μ)	Sample Weight Pre-run/Post-run (grams)	Internal Diameter Pre-run/Post-run (inches)	Test Time (sec)
$HfB_{2.1}$+20%SiC(A-7)									
-1PP	UP	3960	480	26.8	***	0.60	34.44/34.46	0.608/0.610	10.00
-2PP	DOWN	3960	480	26.8	2270	0.60	36.18/36.18	0.606/0.608	10.00
-3PP	UP	3520	410	24.4	***	0.60	35.29/35.10	0.607/0.608	10.02
-4PP	DOWN	3520	410	24.4	2270	0.60	35.27/35.27	0.606/0.608	10.02
$ZrB_{2.1}$+20%SiC(A-8)									
-1PP	UP	3960	480	26.8	***	0.60	21.87/21.89	0.606/0.606	9.99
-2PP	DOWN	3960	480	26.8	2420	0.60	21.86/21.88	0.606/0.605	9.99
-3PP	UP	6000	590	26.4	***	0.60	22.08/21.98	0.606/0.610	9.61
-4PP	DOWN	6000	590	26.4	4260	0.60	21.92/21.83	0.605/0.608	9.61
ZrB_2+SiC+C(A-10)									
-1PP	UP	3960	480	26.8	***	0.60	17.94/17.94	0.606/0.605	10.05
-2PP	DOWN	3960	480	26.8	2600	0.60	18.73/18.74	0.606/0.605	10.05
-3PP	UP	6000	590	26.4	***	0.60	18.13/18.08	0.606/0.609	6.93
-4PP	DOWN	6000	590	26.4	3960	0.60	18.40/18.37	0.606/0.605	6.93
Si/RVC(B-8)									
-1PP	UP	3895	472	26.5	***	0.70	16.92/16.97	0.618/0.616	9.96
-2PP	DOWN	3895	472	26.5	3200	0.70	17.04/17.10	0.613/0.612	9.96
-3PP	UP	6000	590	26.4	***	0.70	17.59/17.53	0.611/0.616	9.96
-4PP	DOWN	6000	590	26.4	4200	0.70	17.00/16.95	0.606/0.615	9.96
KT-SiC(E-14)									
-3PP	UP	3995	485	26.9	***	0.70	12.54/12.54	0.602/0.602	10.00
-4PP	DOWN	3995	485	26.9	2420	0.70	12.49/12.50	0.601/0.604	10.00
-5PP	UP	6000	590	26.4	***	0.70	12.52/12.22	0.601/-----	9.96
-6PP	DOWN	6000	590	26.4	3920	0.70	12.48/12.26	0.602/-----	9.96
Hf-Ta-Mo(I-23)									
-1PP	UP	3960	480	26.8	***	0.55	46.78/-----	0.629/**	5.76
-2PP	DOWN	3960	180	26.8	3070	0.55	46.98/75.32*	0.629/**	5.76
-3PP	UP	3520	410	24.4	***	0.55	44.40/44.44	0.641/0.633	4.73
-4PP	DOWN	3620	410	24.4	>3000	0.55	45.50/38.71	0.632/0.623	4.73

*A single run consisted of a pair of samples denoted as "upstream" and "downstream".

* Combined weight of I-23-1PP and -2PP.
** Sample melted and distorted.
*** No measurement made upstream, pyrometer sighted on 0.10" spot 1/2" inside rear of downstream sample.

Material Sample No.	Visual Observations*	Description of Motion Picture Film Coverage**
$HfB_{2.1}$+20%SiC(A-7)		
-1PP	Series of radial cracks, longitudinal cracks 180° apart.	
-2PP	Series of radial cracks, several longitudinal cracks.	No activity visible.
-3PP	Half of sample severely cracked, half slightly cracked.	
-4PP	Cracked radially and longitudinally.	Underexposed, no activity visible.
$ZrB_{2.1}$+20%SiC(A-8)		
-1PP	Cracked longitudinally in half.	
-2PP	One quarter cracked cleanly off.	Hot spot around o-ring.
-3PP	Cracked radially and longitudinally.	
-4PP	Cracked radially and longitudinally.	Overexposed, no features visible.
ZrB_2+SiC+C(A-10)		
-1PP	No visible cracks.	
-2PP	Cracked radially in half at o-ring.	Hot spot around o-ring, some sparks blowing back.
-3PP	Cracked radially and longitudinally.	
-4PP	No visible cracks.	Some liquid droplets.
Si/RVC(B-8)		
-1PP	No visible cracks, coating inside burned off.	
-2PP	No visible cracks, streaks of silica inside.	Liquid continuously streaming back, some sparks blowing back.
-3PP	No visible cracks, coating inside burned off.	
-4PP	No visible cracks, coating inside burned off.	Liquid streaming back early in run, no activity near end.
KT-SiC(E-14)		
-3PP	Cracked longitudinally in half.	
-4PP	Cracked longitudinally in half.	Hot spot near top and around o-ring.
-5PP	Cracked longitudinally in half and radially	
-6PP	Cracked longitudinally in thirds.	Some liquid droplets, hot spot around o-ring.
Hf-Ta-Mo(I-23)		
-1PP	Burned through at o-ring, eroded behind hole.	
-2PP	Large portion melted away, o-ring area degradation.	Very hot around o-ring, then melted rapidly.
-3PP	Little damage.	
-4PP	Burned through from o-ring back.	Underexposed, no activity visible.

*Virtually all samples showed indications of heat effects where they came in contact with the o-rings of the sample holding fixture.

**Camera was sighting inside rear of downstream sample. Descriptions thus apply to this sample's behavior.

TABLE 53

SUMMARY OF MODEL DIMENSIONS BEFORE AND AFTER 15 SECOND EXPOSURE IN WAVE SUPERHEATER (HEMISPHERICAL CAPS)

Material ManLabs No/CAL No.	Sting No.	Initial Dimensions Diameter/Length/Wall mils	Final* Wall mils	Recession* Depth mils	Comments*
		TEST (67-473)			
ZrB_2(A-3)-1-2	1	492/1021/139	142	-3	No change in structure
KT-SiC(E-14)-1-8	2	488/1000/135	117	18	No change in structure
KT-SiC(E-14)-3-18	3	944/994/130	128	2	Cap fractured on cooling longitudinal crack noted in holder may be due to expansion at sting. Microstructure showed Si melted.
Hf-20Ta-2Mo(I-23)-4-19	4	997/1167/129	[illegible]	3	Melting at nose
W(G-18) Uncoated-X-11	5	491/992/152	153	-1	Nose was blue
RVA(B-5)-X-5	6	488/996/112	92	30	No change in structure
JTA(D-13)-X-7	7	489/957/125	129	-4	No change in structure
JT0992(F-15)-X-9	8	490/945/96	Thermal Shock		Shocked during exposure
		TEST (67-474)			
Hf-20Ta-2Mo(I-23)-1-12	1	491/1000/155	137	18	Light oxide coating formed
$HfB_{2.1}$(A-2)-X-1	2	491/937/144	139	5	Cap broke off at end of run
HfB_2+SiC(A-4)-X-4	3	492/963/154	159	-5	No change in structure
PG(B-6)-X-6	4	488/1061/122	104	8	"C" axis perpendicular to cylinder axis, no change in structure

TABLE 54

SUMMARY OF MODEL DIMENSIONS BEFORE AND AFTER 15 SECOND EXPOSURE IN WAVE SUPERHEATER (HEMISPHERICAL CAPS)

Material ManLabs No/CAL No.	Sting No.	Initial Dimensions Diameter/Length/Wall mils	Final* Wall mils	Recession* Depth mils	Comments*
BPG(B-7)-X-16	5	490/836/157	125	32	"C" axis perpendicular to cylinder axis, no change in structure
JT0981(F-16)-X-10	6	488/946/141	122	19	Light oxide coating formed
ZrB_2(A-3)-24-3	7	492/989/163	Thermal Shock		Shocked during exposure
Sn-Al/Ta-10W(G-19)-3-22	8	1001/1001/146	133**	13	Melted Sn at nose streamed back to sides and sting holder

*Based on metallographic analysis.
**2 mil coating on outside and 8 mil coating on inside of Ta-10W.
+8 mil coating on both sides of 130 mil Ta-10W.

TABLE 55

CAMERA SETTINGS EMPLOYED IN WAVE SUPERHEATER EXPOSURES

Run No.	Camera Number	Film Speed Frames/Sec	Focal Length of Lens	Aperature Stop	Shutter Speed Number	
-473	1	200	3 inch	f2.8	5	Ektachrome EF
	2	250	4 inch	f5.8	5	Ektachrome EF
	3	250	4 inch	f4.0	5	EF
	4	600	11 inch*	f5.6	40	ER
-474	1	200	3 inch	f4.0	5	Ektachrome ER
	2	200	4 inch	f5.6	5	Ektachrome EF
	3	200	4 inch	f8.0	5	ER
	4	600	11 inch*	----	40	ER

*Effective focal length.

TABLE 56

HEAT TRANSFER RESULTS

	Run No.	473	474
$\frac{\Delta T}{\Delta t}$	Rate of Temperature Rise - deg. F/sec	780	880
δ	Gage Thickness - in	0.1260	0.1265
T	Average Thermocouple Temp at Time of Reading - ^{o}F	360	350
c	Corresponding Specific Heat to T of Copper - BTU/lb - ^{o}F	0.096	0.096
q_w	Indicated Heat Transfer Rate - BTU/ft^2-sec	440	485
T_w	Gage Surface Temp - ^{o}F	410	395
i_w	Gage Surface Enthalpy - BTU/lb	210	205
i_s	Total Enthalpy of Stream at Time of Reading - BTU/lb	1880	1870
q_{cw}	Cold Wall Heat Transfer Rate -BTU/ft^{2}sec	495	545
i_e	Run Enthalpy - BTU/lb	2200	2180
q_{cw}	Cold Wall Heat Transfer Rate Corrected to Run Enthalpy - BTU/ft^{2}sec	580	635

TABLE 57

TEST CONDITIONS

Run No.	473	474
Rotor Total Pressure - atm	98.2	96.9
Total Temperature - ^{o}R	6740	6700
Total Enthalpy - BTU/lb	2200	2180
Tunnel Reservoir Pressure - atm	56.0	55.0
Test Section Stagnation Pressure on Model Nose - atm	1.15	1.15
Free Stream Mach Number	5.45	5.45
Free Stream Density - lbs/ft^3	8×10^{-5}	8×10^{-5}
Free Stream Pressure - psi	0.65	0.64
Free Stream Velocity - fps	9700	9700

TABLE 58

WALL TEMPERATURE AND HEAT FLUX HISTORY FOR THE STAGNATION POINT OF A 0.500-INCH RADIUS HEMISPHERICAL NOSE WITH A THICKNESS OF 0.125 INCH

Time	T_w (°R)	q_{AERO}	$-q_{RAD}$	q_{NET}
0	560	464.1	0.026	464.1
0.5	1090	431.8	0.370	431.4
1.0	1302	418.9	0.753	418.1
1.5	1481	408.0	1.26	406.7
2.0	1650	397.7	1.94	395.7
2.5	1814	387.7	2.83	384.9
3.0	1972	378.0	3.96	374.1
3.5	2126	368.6	5.35	363.3
4.0	2274	358.4	7.01	351.4
4.5	2417	348.3	8.93	339.3
5.0	2554	338.5	11.14	327.3
6.0	2813	320.0	16.39	303.6
7.0	3051	303.0	22.7	280.3
8.0	3269	287.4	29.9	257.5
9.0	3468	273.3	37.9	235.4
10.0	3648	259.8	46.4	213.4
11.0	3808	246.3	55.0	191.3
13.0	(4146)*			(146)*
15.0	(4405)*			(96)*

*Estimated by hand calculations.

TABLE 59

WALL TEMPERATURE AND HEAT FLUX HISTORY FOR THE STAGNATION POINT OF A 0.250-INCH RADIUS HEMISPHERICAL NOSE WITH A THICKNESS OF 0.125 INCH

Time	T_w (°R)	q_{AERO}	$-q_{RAD}$	q_{NET}
0	560	653.0	0.026	653.0
0.5	1293	593.1	0.732	592.4
1.0	1576	568.7	1.62	567.1
1.5	1812	548.4	2.82	545.6
2.0	2032	529.4	4.47	524.9
3.0	2441	490.1	9.29	480.8
3.5	2629	471.0	12.5	458.5
4.0	2808	453.0	16.3	436.7
4.5	2978	435.8	20.6	415.2
5.0	3139	419.6	25.4	394.2
6.0	3434	389.8	36.4	353.4
7.0	3695	361.8	48.8	313.0
8.0	3919	335.0	61.8	273.3
9.0	4113	311.9	74.9	237.0
10.0	4279	292.1	87.8	204.3
11.0	4421	275.2	100.0	175.2
12.0	(4576)*			(140)*
13.0	(4700)*			(112)*
14.0	(4800)*			(82)*
15.0	(4872)*			(67)*

*Estimated by hand calculation.

UNCLASSIFIED
Security Classification

DOCUMENT CONTROL DATA - R & D

(Security classification of title, body of abstract and indexing annotation must be entered when the overall report is classified)

1. ORIGINATING ACTIVITY (Corporate author) ManLabs, Inc. 21 Erie Street Cambridge, Massachusetts 02139	2a. REPORT SECURITY CLASSIFICATION UNCLASSIFIED 2b. GROUP N/A

3. REPORT TITLE

Stability Characterization of Refractory Materials under High Velocity Atmospheric Flight Conditions, Part III, Volume III: Experimental Results of High Velocity Hot Gas/Cold Wall Tests

4. DESCRIPTIVE NOTES (Type of report and inclusive dates)

April 1966 to July 1969

5. AUTHOR(S) (First name, middle initial, last name)

Larry Kaufman
Harvey Nesor

6. REPORT DATE February 1970	7a. TOTAL NO. OF PAGES 370	7b. NO. OF REFS 25
8a. CONTRACT OR GRANT NO. AF33(615)-3859 b. PROJECT NO. 7312 Task 731201 c. 7350 Tasks 735001 and 735002 d.	9a. ORIGINATOR'S REPORT NUMBER(S) N/A 9b. OTHER REPORT NO(S) (Any other numbers that may be assigned this report) AFML-TR-69-84, Part III, Volume III	

10. DISTRIBUTION STATEMENT

This document is subject to special export controls and each transmittal to foreign governments or foreign nationals may be made only with prior approval of the Air Force Materials Laboratory (MAMC), Wright-Patterson AFB, Ohio.

11. SUPPLEMENTARY NOTES N/A	12. SPONSORING MILITARY ACTIVITY Air Force Materials Laboratory (MAMC) Air Force Systems Command Wright-Patterson Air Force Base, Ohio

13. ABSTRACT

The oxidation of refractory borides, graphites and JT composites, hypereutectic carbide-graphite composites, refractory metals, coated refractory metals, metal oxide composites, and iridium coated graphites in air over a wide range of conditions was investigated over the spectrum of conditions encountered during reentry or high velocity atmospheric flight, as well as those employed in conventional furnace tests. Elucidation of the relationship between hot gas/cold wall (HG/CW) and cold gas/hot wall (CG/HW) surface effects in terms of heat and mass transfer rates at high temperatures was a principal goal.

Arc plasma exposures have been performed at Mach Numbers between 0.1 and 3.2 stagnation pressures between 0.01 and 1.0 atm., stagnation enthalpies up to 16,000 BTU/lb, cold wall heat flux up to 1200 BTU/ft^{2}sec, exposure times up to 23,400 seconds and surface temperatures between 2100° and 6500°F. Data include material recession, metallographic and X-ray analysis, radiated heat flux and normal total emittance. In addition, color motion picture coverage was provided. Materials forming solid oxides show lower recessions in the HG/CW tests at a stated surface temperature than in CG/HW tests. The reverse is true for ablating materials. Temperature gradients of 800° to 1500°F through 30-50 mil oxides are observed. The practical implications of this finding are substantial (if the gradients exist under free flight conditions). Long-time cyclic exposures of diboride composites in the Model 500 and ROVERS facilities for trajectories typified by FDL-7MC provide a striking illustration of the reuse capability of boride composites for lifting reentry applications.

DD FORM 1 NOV 65 1473

UNCLASSIFIED
Security Classification

UNCLASSIFIED

Security Classification

DOCUMENT CONTROL DATA - R & D

(Security classification of title, body of abstract and indexing annotation must be entered when the overall report is classified)

1. ORIGINATING ACTIVITY (Corporate author) ManLabs, Inc. 21 Erie St. Cambridge, Massachusetts 02139	2a. REPORT SECURITY CLASSIFICATION UNCLASSIFIED 2b. GROUP
3. REPORT TITLE	
4. DESCRIPTIVE NOTES (Type of report and inclusive dates)	
5. AUTHOR(S) (First name, middle initial, last name)	
6. REPORT DATE	7a. TOTAL NO. OF PAGES / 7b. NO. OF REFS
8a. CONTRACT OR GRANT NO. b. PROJECT NO. c. d.	9a. ORIGINATOR'S REPORT NUMBER(S) 9b. OTHER REPORT NO(S) (Any other numbers that may be assigned this report) AFML-TR-69-84, Part III, Volume III
10. DISTRIBUTION STATEMENT	
11. SUPPLEMENTARY NOTES	12. SPONSORING MILITARY ACTIVITY

13. ABSTRACT

This abstract is subject to special export controls and each transmittal to foreign governments or foreign nationals may be made only with prior approval of the Air Force Materials Laboratory (MAMC), Wright-Patterson AFB, Ohio.

DD FORM 1 NOV 65 1473

Security Classification

UNCLASSIFIED
Security Classification

14. KEY WORDS	LINK A		LINK B		LINK C	
	ROLE	WT	ROLE	WT	ROLE	WT
oxidation						
borides						
graphites						
JT composites						
refractory						
metal oxide composites						
reentry						
high velocity atmospheric flight						
stagnation enthalpies						
cold wall heat flux						
emittance						
temperature gradients						
trajectories						

UNCLASSIFIED
Security Classification